

UNIVERSITY OF LIÈGE
Faculty of Sciences – Department of Chemistry
Cyclotron Research Centre

Radiosynthesis of ^{18}F -Labeled Reagents
for the ^{18}F -Difluoromethylation of
Heteroarenes

Ph.D. Thesis

Agostinho LEMOS

JURY

President	Dr. Christophe DETREMBLEUR	University of Liège (ULg)
Promoter	Prof. André LUXEN	University of Liège (ULg)
Member	Prof. Guy BORMANS	Katholieke Universiteit Leuven (KUL)
Member	Dr. Thierry BILLARD	Fluorine & Medical Imaging in Lyon (FMI-Lyon)
Member	Dr. Christophe GENICOT	UCB Biopharma
Member	Dr. Patrick PASAU	UCB Biopharma
Secretary	Dr. Christian LEMAIRE	University of Liège (ULg)

ACKNOWLEDGEMENTS

This work was carried out at the GIGA Cyclotron Research Centre *In Vivo* Imaging of University of Liège under the supervision of Prof. André Luxen and at the Global Chemistry, UCB NewMedicines, UCB Biopharma in Braine l'Alleud, under the supervision of Dr. Christophe Genicot. This work was financially supported by the European Union's Horizon 2020 research and innovation programme under the Marie Skłodowska-Curie Grant agreement No 675071.

First of all, I would like to thank to my promoter, Professeur André Luxen, for allowing me to carry out this thesis on an innovative subject in his laboratory, for his level of demand, and its motivating supervision.

I would also like to thank the members of the jury for having the honor of agreeing to evaluate this work: Prof. Guy Bormans (Katholieke Universiteit Leuven (KUL)), Dr. Thierry Billard (FMI-Lyon), Dr. Christophe Genicot (UCB Biopharma), Dr. Patrick Pasau (UCB Biopharma), Dr. Christian Lemaire (University of Liège (ULg)), and Dr. Christophe Detrembleur (ULg) in the role of president of the jury.

I am particularly grateful to Dr. Christian Lemaire and Dr. Laura Trump (UCB Biopharma) for their technical support (utilization of automated synthesizers, analytical, and purification techniques), for the numerous advices, the precious reflections, and the very enriching discussions that allowed me to carry out this thesis, and to value the obtained results.

I want to thank to invited lecturers of ISOTOPICS training for contributing to enrich my theoretical knowledge in radiochemistry and medicinal chemistry fields.

I would like to thank to all my friends I met in Belgium. They were the one of the reasons why I could feel at home in Liège. And I also want to thank to all my old and new friends from Portugal, who were supporting me all this time even from such long distance.

I want to thank to my parents Luís (father) and Maria Aurora (mother), and my sister Mónica for all their love and support.

TABLE OF CONTENTS

OUTLINE OF THE THESIS.....	9
CHAPTER I: PROGRESS IN DIFLUOROALKYLATION OF ORGANIC SUBSTRATES BY VISIBLE LIGHT PHOTOREDOX CATALYSIS.....	11
1. General Introduction.....	15
2. Transition Metal Photocatalyzed Difluoroalkylation Reactions.....	20
3. Organic Photocatalyzed Difluoroalkylation Reactions.....	73
4. Concluding Remarks.....	82
References.....	83
CHAPTER II: PROGRESS IN THE SYNTHESIS OF ¹⁸F-DIFLUOROMETHYLATED MOLECULES.....	97
1. Introduction.....	101
2. Synthesis of [¹⁸ F]CHF ₂ -containing compounds <i>via</i> ¹⁸ F-fluorination....	110
3. Synthesis of [¹⁸ F]CHF ₂ -containing compounds <i>via</i> C-H ¹⁸ F-difluoromethylation.....	119
4. Concluding Remarks.....	121
References.....	122
CHAPTER III: FULLY AUTOMATED RADIOSYNTHESIS OF [¹⁸F]DIFLUOROMETHYL BENZOTHAZOLYL-SULFONE ON A GE FASTLAB™ SYNTHESIZER.....	133
1. Introduction.....	137
2. Results and Discussion.....	139
3. Material and Methods.....	154
4. Conclusions.....	160
5. Supplementary Information.....	161
References.....	175
CHAPTER IV: RADICAL C-H ¹⁸F-DIFLUOROMETHYLATION OF HETEROARENES WITH [¹⁸F]DIFLUOROMETHYL HETEROARYL-SULFONES BY VISIBLE LIGHT PHOTOREDOX CATALYSIS.....	181
1. Introduction.....	187
2. Results and Discussion.....	190
3. Material and methods.....	202
4. Conclusions.....	213
5. Supplementary Information.....	214
References.....	283

CHAPTER V: GENERAL DISCUSSION AND PERSPECTIVES.....	289
1. General Discussion and Perspectives.....	291
References.....	296
LIST OF ABBREVIATIONS.....	301
SCIENTIFIC ACTIVITY.....	303

OUTLINE OF THE THESIS

This PhD project was part of the European Union's Horizon 2020 research and innovation programme under the Marie Skłodowska-Curie grant agreement No 675071 and was conducted in collaboration with UCB Biopharma and with the PhD Laura Trump. The main objective of this work consisted on the development of a new methodology for the late-stage addition of the ^{18}F -difluoromethyl groups in *N*-containing heteroarenes typically found in medicinal chemistry, under continuous-flow conditions. This protocol relies on the use of a non-ionic ^{18}F -difluoromethylating reagent (^{18}F -difluoromethyl benzothiazolyl-sulfone) with the ability of producing CHF_2 radicals, under blue light irradiation. Inspired by the efficiency of ^{18}F -difluoromethyl benzothiazolyl-sulfone, we further studied the reactivity of structurally-related heteroaryl-sulfones toward the ^{18}F -difluoromethylation of *N*-containing heteroarenes.

The present thesis was divided into five chapters (I, II, III, IV, V).

CHAPTER I: PROGRESS IN DIFLUOROALKYLATION OF ORGANIC SUBSTRATES BY VISIBLE LIGHT PHOTOREDOX CATALYSIS

In this Chapter, we provide a thorough review concerning the synthetic methods for the visible light difluoroalkylation of organic substrates reported in the literature since 2014. To date, we have witnessed to an increasing progress in the development of transition metal-photocatalyzed methods for the introduction of difluoroalkyl motifs (CHF_2 and CF_2FG , FG = a functional group) into various building blocks using a myriad of difluoroalkylating reagents. Herein, we underlined the importance of CHF_2 and CF_2FG motifs in medicinal chemistry due to their potential to improve the biological activity of molecules. In addition, we emphasized the relevance of visible light photoredox catalysis as a sustainable approach for obtention of CF_2 -containing derivatives from the viewpoint of safety, cost, availability, and "green" chemistry.

CHAPTER II: PROGRESS IN THE SYNTHESIS OF ^{18}F -DIFLUOROMETHYLATED MOLECULES

Besides the pharmaceutical relevance of CHF_2 groups, the ^{18}F -labeling of these groups has been recently studied in radiopharmaceutical chemistry owing to the favorable nuclear and physical characteristics of fluorine-18 (^{18}F) for positron emission tomography (PET). This Chapter describes the available synthetic strategies to access ^{18}F -difluoromethylated compounds either by a stepwise (indirect) ^{18}F -difluoromethylation or by direct transfer of ^{18}F -difluoromethyl groups to adequate labeling precursors. Herein, we also describe the basic principles of PET and the applications of PET radiotracers labeled with ^{18}F in (pre)clinical research.

CHAPTER III: FULLY AUTOMATED RADIOSYNTHESIS OF [18F]DIFLUOROMETHYL BENZOTHAZOLYL-SULFONE ON A GE FASTLAB™ SYNTHESIZER

The aim of this thesis consisted in the development of novel reagents for the C-H ¹⁸F-difluoromethylation of *N*-containing heteroarenes. Based on the reactivity of the difluoromethyl benzothiazolyl-sulfone in the photoinduced difluoromethylation of substrates bearing C=C, C≡C, and C≡N bonds, we intended to perform the radiosynthesis of the [18F]difluoromethyl benzothiazolyl-sulfone as a novel labeled compound for late-stage introduction of ¹⁸F-difluoromethyl groups. The present Chapter furnishes a detailed description of the most suitable conditions for the radiosynthesis of the [18F]difluoromethyl benzothiazolyl-sulfone and the development of a fully automated process on a GE FASTlab™ synthesizer. The ¹⁸F-labeled reagent was further utilized in the late-stage C-H ¹⁸F-difluoromethylation of a wide range of *N*-containing heteroarenes, under irradiation with blue light-emitting diode (LED).

CHAPTER IV: RADICAL C-H ¹⁸F-DIFLUOROMETHYLATION OF HETEROARENES WITH [18F]DIFLUOROMETHYL HETEROARYL-SULFONES BY VISIBLE LIGHT PHOTOREDOX CATALYSIS

Taking advantage of the reactivity of the [18F]difluoromethyl benzothiazolyl-sulfone as ¹⁸F-difluoromethylating reagent, we investigated the influence of structurally-related [18F]difluoromethyl heteroaryl-sulfones in the reactivity toward the photoredox C-H ¹⁸F-difluoromethylation of *N*-containing heteroarenes under continuous-flow conditions. This Chapter is subdivided into three parts: (i) radiosynthesis of [18F]difluoromethyl heteroaryl-sulfones; (ii) investigation of their potential for C-H ¹⁸F-difluoromethylation of *N*-containing heteroarenes; (iii) radical-scavenging experiments.

CHAPTER V: GENERAL DISCUSSION AND PERSPECTIVES

This Chapter provides a general discussion of the distinct chapters and future perspectives in this research field.

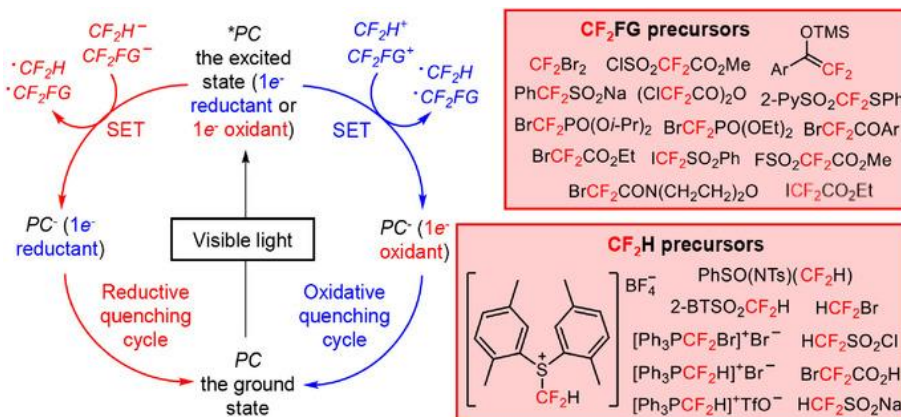
Chapter I

Progress in Difluoroalkylation of Organic Substrates by Visible Light Photoredox Catalysis

Progress in Difluoroalkylation of Organic Substrates by Visible Light Photoredox Catalysis

Agostinho Lemos,^{a,*} Christian Lemaire,^a and André Luxen^{a,*}

^a GIGA Cyclotron Research Centre *In Vivo* Imaging, University of Liège, Allée du 6 Août 8, 4000 Liège, Belgium
Fax: (+32)-4-366-2946; phone: (+32)-499-509-436; e-mail: alemos@uliege.be or aluxen@uliege.be



Chapter I

1. General Introduction.....	15
2. Transition Metal Photocatalyzed Difluoroalkylation Reactions	
2.1. Difluoroalkylation of sp ² Carbon Atoms in Unactivated Alkenes and Styrenes.....	20
2.2. Difluoroalkylation of sp ² Carbon Atoms in Enol Derivatives, α,β-Unsaturated Carboxylic Acids, and Allylic Alcohols.....	37
2.3. Difluoroalkylation of sp ² Carbon Atoms in Unsaturated Amides, Hydrazones, and Allylamines.....	45
2.4. Difluoroalkylation of sp ² Carbon Atoms in Arenes and Heteroarenes.....	55
2.5. Difluoroalkylation of sp Carbon Atoms in Alkynes and Biphenyl Isocyanides.....	64
2.6. Difluoroalkylation of SH- and OH-containing Substrates.....	70
3. Organic Photocatalyzed Difluoroalkylation Reactions.....	73
4. Concluding Remarks.....	82
References.....	83

Progress in Difluoroalkylation of Organic Substrates by Visible Light Photoredox Catalysis

Abstract: The selective incorporation of fluorinated motifs, in particular CF_2FG (FG = a functional group) and CHF_2 groups, into organic compounds has attracted increasing attention since organofluorine molecules are of the utmost importance in the areas of nuclear imaging, pharmaceutical, agrochemical, and material sciences. A variety of synthetic approaches has been employed in late-stage difluoroalkylation reactions. Visible light photoredox catalysis for the production of CF_2FG and CHF_2 radicals has provided a more sustainable alternative to other conventional radical-triggered reactions from the viewpoint of safety, cost, availability, and “green” chemistry. A wide range of difluoroalkylating reagents has been successfully implemented in these organic transformations in the presence of transition metal complexes or organic photocatalysts. In most cases, upon excitation via visible light irradiation with fluorescent light bulbs or blue light-emitting diode (LED) lamps, these photocatalysts can act as both reductive and oxidative quenchers, thus enabling the application of electron-donor or electron-acceptor difluoroalkylating reagents for the generation of CF_2FG and CHF_2 radicals. Subsequent radical addition to substrates and additional organic transformations afford the corresponding difluoroalkylated derivatives. The present review describes the distinct strategies for the transition metal- and organic-photocatalyzed difluoroalkylation of a broad range of organic substrates by visible light irradiation reported in the literature since 2014.

Keywords: C-H functionalization, difluoroalkylation, late-stage fluorination, organophotocatalysis, transition metal photocatalysis, visible light

1. General Introduction

Organic compounds containing fluorine substituents or fluoroalkyl moieties are abundant and have attracted considerable attention because of their wide applications in agrochemical [1], pharmaceutical [2,3], and material science [4] industries, and nuclear imaging [5,6]. In pharmaceutical research and drug development, the incorporation of fluoroalkyl motifs, in particular the difluoromethyl (CHF_2) group, has gained great interest for use in isostere-based drug design. As a lipophilic hydrogen-bond donor [7], the CHF_2 substitution offers a viable alternative to conventional hydrogen-bond donors [e.g., hydroxy (OH), amino (NH_2), thiol (SH), carbinol (CH_2OH), amide (CONH_2), and hydroxamic acid (CONHOH) groups] in terms of lipophilicity, cell membrane permeability, and metabolic stability, thus improving the biological activity [8,9]. Given the relevance of difluoroalkyl substituents in life sciences, the implementation of efficient approaches for the preparation of CF_2 -containing organic molecules has become a major research area in the field of organofluorine chemistry. Apart from the huge progress in the development of strategies for C-H functionalization involving fluorination and

trifluoromethylaton reactions [10-18], significant research efforts have been directed toward the late-stage introduction of CF₂FG (FG = a functional group) and CHF₂ moieties in organic skeletons *via* nucleophilic, electrophilic, and radical approaches [19-22]. Among the mentioned approaches for the difluoroalkylation process, the radical-triggered reactions *via* visible light photoredox catalysis have been the subject of intensive research by the chemistry community, owing to their unique advantages such as the use of "green" and environmentally benign reaction conditions, excellent functional group versatility, and high reactivity [23-30]. In fact, the use of photoredox catalysis has provided a powerful and versatile tool to afford a large variety of fluorinated radicals under very mild conditions, compared with conventional radical reactions that usually demand the use of high-energy ultraviolet (UV) light equipment or the employment of highly toxic radical initiators. In general, these visible light-induced chemical transformations rely on the ability of photocatalysts, such as transition metal complexes [31-33], organic dyes [34,35], or heterogeneous semiconductors [36,37] to promote single-electron transfer (SET) processes with organic molecules upon excitation with visible light. Remarkably, the lack of visible light absorbance of many organic molecules enables the application of these photocatalysts in these reactions, minimizing the occurrence of unwanted side reactions resulting from the photoexcitation and the decomposition of reaction products. Visible light irradiation is often carried out using inexpensive light sources such as blue light-emitting diode (LED) lamps and fluorescent light bulbs. A variety of transition metal photocatalysts, such as iridium ([Ir(dtbbpy)(ppy)₂][PF₆] (1), *fac*-Ir^{III}(ppy)₃ (2), and [Ir(dF(CF₃)ppy)₂(dtbbpy)][PF₆] (3)), copper ([Cu(dap)₂]Cl (4)), platinum (Pt^{II}[R(C[^]N[^]P[^]P)] (R = 4-CH₃OC₆H₄) (5)), ruthenium ([Ru(bpy)₃]Cl₂ (6)), and gold ([Au₂(μ-dppm)₂]Cl₂ (7)) complexes, and organic photocatalysts, including *N*-methyl-9-mesityl acridinium perchlorate ([Mes-Acr]ClO₄) (8), eosin Y (9), fluorescein (10), rose Bengal (RB) (11), rhodamine 6G (R6G) (12), 1,2,3,5-tetrakis-(carbazol-yl)-4,6-dicyanobenzene (4CzIPN) (13), perylene (14), and *peri*-xanthenoxanthene (PXX) (15) have been implemented in photochemistry for the difluoroalkylation of organic substrates (Figure 1). These photocatalysts are capable of absorbing light at a certain wavelength in the visible region, resulting in the generation of photoexcited species that possess the unique property of being both more oxidizing and more reducing than the species in the ground state.

The standard reduction potentials are used to quantify the redox properties of a photocatalyst in the excited state under specific standard conditions (Table 1), and describe the electrochemical potential associated with a half-reaction (E_{1/2}) of reduction. The reduction potential determines the propensity of a chemical species to be reduced. In fact, the more positive the potential values, the greater is the tendency of a molecule to be reduced. For example, *fac*-Ir^{III}(ppy)₃* is a much more potent electron donor [E_{1/2} (PC⁺/PC*) = -1.73 V *vs.* SCE] than the *fac*-Ir^{III}(ppy)₃ in the ground state [E_{1/2} (PC⁺/PC) = +0.77 V *vs.* SCE]. Reduction potentials of difluoroalkylating reagents (16-47, Figure 2) are also highlighted in this review.

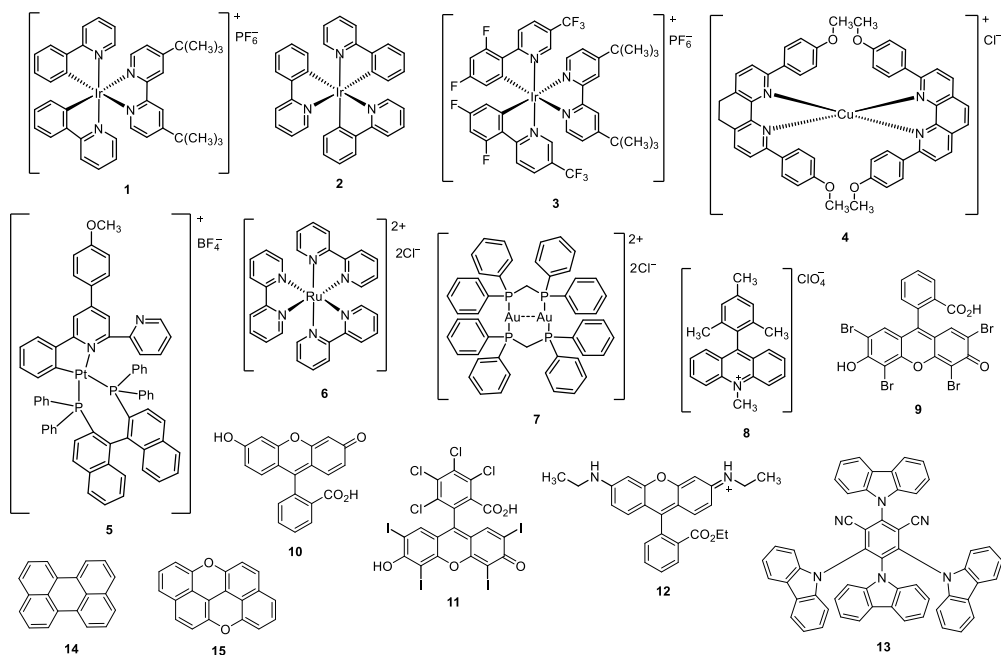


Figure 1. Transition metal (1-7) and organic photocatalysts (8-15) employed in difluoroalkylation reactions. **1** – [Ir(dtbbpy)(ppy)₂]⁺PF₆⁻; **2** – *fac*-Ir^{III}(ppy)₃; **3** – [Ir(dF(CF₃)ppy)₂(dtbbpy)]⁺PF₆⁻; **4** – [Cu(dap)₂]⁺Cl⁻; **5** – Pt^{II}[R(C^N^P^P)] (R = 4-CH₃OC₆H₄); **6** – [Ru(bpy)₃]²⁺Cl₂⁻; **7** – [Au₂(μ-dppm)]²⁺Cl₂⁻; **8** – *N*-methyl-9-mesityl acridinium perchlorate ([Mes-Acr]⁺ClO₄⁻); **9** – eosin Y; **10** – fluorescein; **11** – rose Bengal (RB); **12** – rhodamine 6G (R6G); **13** – 1,2,3,5-tetrakis-(carbazol-yl)-4,6-dicyanobenzene (4CzIPN); **14** – perylene; **15** – *perixanthenoxanthene* (PXX).

Table 1. Redox potentials and photophysical properties of transition metal (1-7) and organic photocatalysts (8-15) utilized in difluoroalkylation reactions ^{a)} (PC = a photocatalyst)

PC	E _{1/2} (PC ⁺ /PC [*])	E _{1/2} (PC [*] /PC)	E _{1/2} (PC ⁺ /PC)	E _{1/2} (PC/PC ⁻)	Excited-state lifetime τ (ns)	Excitation λ _{max} (nm)	Emission λ _{max} (nm)	Refs.
1	-0.96	+0.66	+1.21	-1.51	557	410	581	[55,56]
2	-1.73	+0.31	+0.77	-2.19	1900	375	494 ^{b)}	[50]
3	-0.89	+1.21	+1.69	-1.37	2300	380	470	[56]
4	-1.43		+0.62		270	400-600	670 ^{c)}	[72]
5	-1.90 ^{d)}	+0.82 ^{d)}	+0.61 ^{d)}	-1.69 ^{d)}	93 ^{d)}	350 ^{d)}	543 ^{d)}	[99]
6	-0.81	+0.77	+1.29	-1.33	1100	452	615	[97,98]
7	-1.63			-1.70	850	380	477	[90,91]
8		+2.06		-0.57	6.4	430	570	[167-170]
9	-1.11 ^{e)}	+0.83 ^{e)}	+0.78 ^{e)}	-1.06 ^{e)}	24000 ^{e)}	539 ^{e)}		[158]
10		+0.78		-1.27	4.1	528		[164,165]
11	-1.33	+1.18	+0.81	-0.96	0.5	549		[173,174]
12	-1.09	+1.18	+0.95	-0.86	4.1	530	548	[181]
13	-1.04	+1.35	+1.52	-1.21	5100	435	535	[177-179]
14	-2.23	+0.72	+0.61	-2.12	8.2	407,434	670	[176]
15	-2.00	+0.61			5.0	415	480	[184]

^{a)}All potentials are given in volts versus the saturated calomel electrode (SCE). Measurements were performed in MeCN at room temperature unless otherwise noted. ^{b)}Determined in 1:1 EtOH/MeOH at 77 K. ^{c)}Determined in DCM. ^{d)}Potentials are given in volts versus the ferrocene (Cp₂Fe). ^{e)}Determined in 1:1 MeCN/H₂O.

The redox potentials of both difluoroalkylating reagents and photocatalysts must be taken into consideration in order to select the most appropriate partners for the design of a photocatalytic difluoroalkylation reaction [38,39]. Subsequent addition of CF₂FG and CHF₂ radicals in *sp*²-hybridized (C=C, C=N) and *sp*-hybridized (C≡C, C≡N) carbon atoms of organic substrates and further chemical transformations would afford the corresponding CF₂FG- and CHF₂-containing products. Alternatively, the CF₂FG moiety of difluoroalkylated derivatives can be converted into other CF₂-containing functional groups, including CHF₂, under certain reaction conditions. Interestingly, the radical difluoroalkylation of key organic molecules can provide useful intermediates for the formation of structurally complex and functionalized heterocycles of pharmaceutical and medical interest.

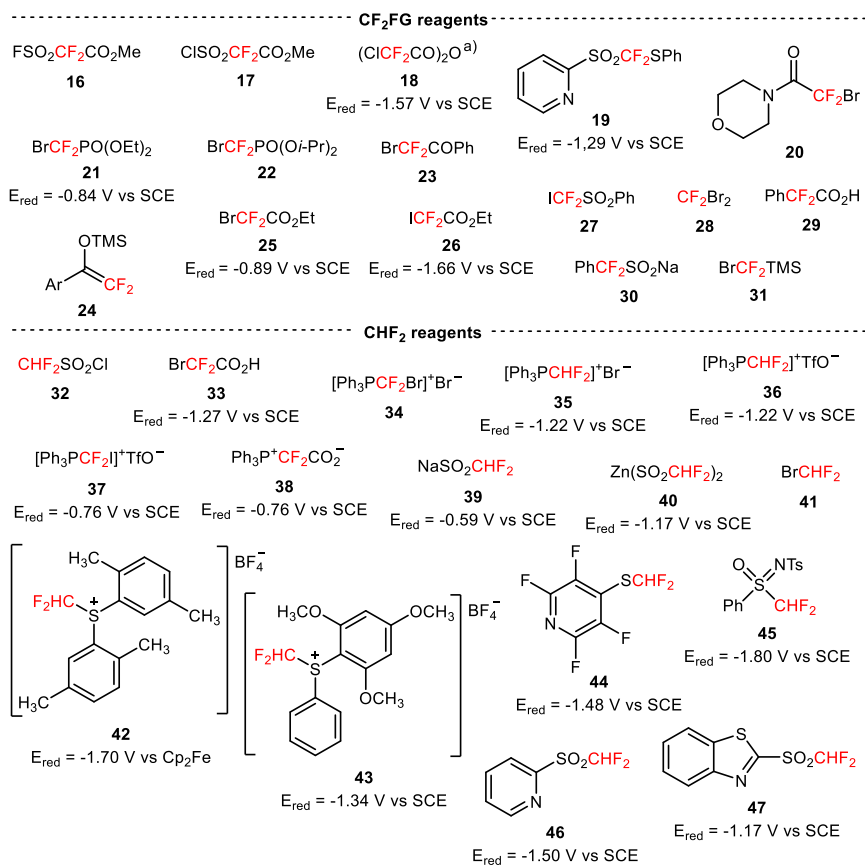


Figure 2. List of CF₂FG (16-31) and CHF₂ reagents (32-47) employed in visible light-mediated difluoroalkylation reactions and their potentials given in volts versus the saturated calomel electrode (SCE) or ferrocene (Cp₂Fe). ^{a)}Potential of 18 in combination with pyridine *N*-oxide. ^{b)}Potential of the intermediate BrCF₂CO₂Cs.

Pioneering works in fluoroalkylation chemistry *via* visible light photoredox catalysis have been reported by MacMillan, Cho, and Sanford. In 2009, MacMillan's group achieved the enantioselective α -trifluoromethylation and α -perfluoromethylation of aldehydes with trifluoroiodomethane (CF₃I) using the readily available [Ir(dtbbpy)(ppy)₂]⁺PF₆⁻ and an imidazolinone catalyst [40]. Later, in 2011, the same group developed photoredox-based protocols for the α -trifluoromethylation of enol silanes, silylketene acetals and *N,O*-acetals derived from ketones, esters, and amides using CF₃I [41] and for the trifluoromethylation of arenes as well as five-, and six-membered heteroarenes with trifluoromethanesulfonyl chloride (CF₃SO₂Cl), in the presence of [Ru(bpy)₃]²⁺Cl₂⁻ and [Ru(phen)₃]²⁺Cl₂⁻, respectively [42]. In 2012, Cho and collaborators described a procedure for the trifluoromethylation of electron-rich heterocycles *via* [Ru(bpy)₃]²⁺Cl₂⁻ photocatalysis [43]. In the same year, Sanford's group reported the trifluoromethylation and perfluoroalkylation of arylboronic acids by merging photoredox and copper catalysis [44]. Since then, photoinduced fluoroalkylation reactions have mostly relied on the incorporation of trifluoromethyl (CF₃) groups in organic substrates. Seminal works in visible light-induced difluoroalkylation chemistry were reported in 2014 and, to date, a myriad of difluoroalkylating reagents (**16-47**, Figure 2) has been successfully implemented for structurally diverse organic molecules. Remarkably, one of the most critical challenges of late-stage difluoroalkylation compared to trifluoromethylation is that the replacement of one electronegative fluorine atom in CF₃-containing reagents by a hydrogen atom or by other functional groups may induce a significant diminution of the reduction potentials. For instance, the generation of CHF₂ radicals from electrophilic CHF₂ precursors requires the use of more strongly reducing catalysts when compared with the case of CF₃ radicals.

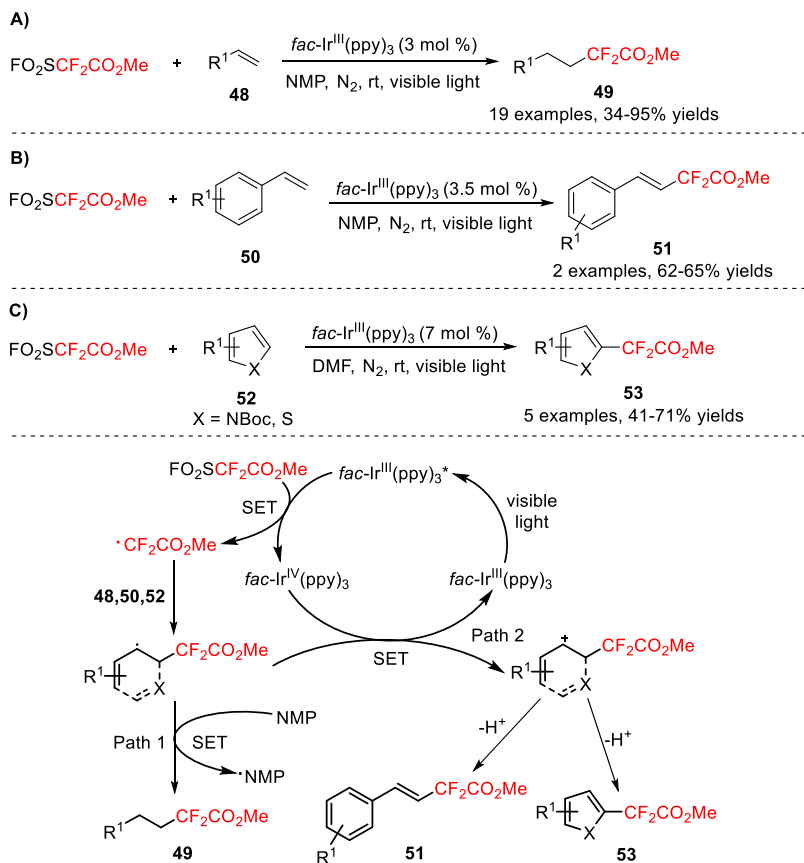
Numerous reviews in fluoroalkylation chemistry have emphasized the various synthetic approaches for visible light-mediated trifluoromethylation and other perfluoroalkylation reactions [38,39,45-47]. Although some of these reviews have covered the area of difluoroalkylation chemistry in part [46,47], a review focusing exclusively on the incorporation of CHF₂ and CF₂FG groups under visible light photoredox conditions will be convenient due to the increasing interest in the formed difluoroalkylated products in life sciences. In addition, major breakthroughs have been accomplished in this research field since the first reported works in 2014. Herein, the present review highlights the distinct synthetic strategies for transition metal- and organic-photocatalyzed difluoroalkylation of a broad range of organic substrates by visible light irradiation that have been reported in the literature since 2014. Owing to the attractive characteristics of visible light photoredox catalysis and the late-stage introduction of difluoroalkyl groups, we expect that the present review will inspire organic chemists to explore additional synthetic routes for installation of these moieties.

2. Transition Metal Photocatalyzed Difluoroalkylation Reactions

The importance of transition metal complexes as effective SET reductants and oxidants, upon excitation via irradiation with visible light, has been demonstrated by the considerable numbers of research works that were reported recently, involving the incorporation of CF₂FG and CHF₂ moieties in a variety of substrates bearing unsaturated bonds, including C=C and C=N, and the concomitant formation of new C-C bonds. In most cases, iridium transition metal complexes have proven to be privileged photocatalysts in the difluoroalkylation of unactivated alkenes, styrenes, enol derivatives, allylic alcohols, and α,β -unsaturated carboxylic acids, arenes, and heteroarenes.

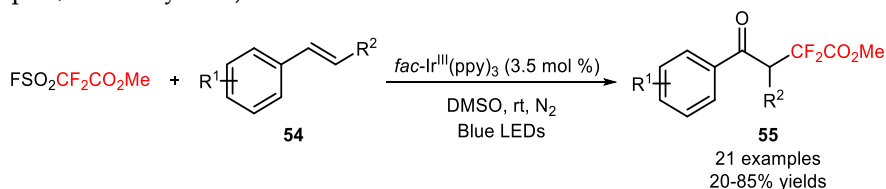
2.1. Difluoroalkylation of *sp*² Carbon Atoms in Unactivated Alkenes and Styrenes

The commercially available and easy-to-handle methyl 2,2-difluoro-2-(fluorosulfonyl)acetate (FSO₂CF₂CO₂Me, Chen's reagent, CAS number: 680-15-9) has been exclusively employed for the preparation of trifluoromethylated derivatives [48,49]. Qing and collaborators disclosed the application of FSO₂CF₂CO₂Me for the installation of CF₂CO₂Me substituents in alkenes (**49**, Scheme 1A: 19 examples, 34-95% yields), styrenes (**51**, Scheme 1B: 2 examples, 62-65% yields), and heteroarenes (**53**, Scheme 1C: 5 examples, 41-71% yields) under visible light photoredox conditions, in the presence of *fac*-Ir^{III}(ppy)₃ [50]. A plausible reaction mechanism involved the formation of CF₂CO₂Me radicals from the reduction of FO₂SCF₂CO₂Me *via* oxidative quenching of *fac*-Ir^{III}(ppy)₃* and the loss of SO₂ and F. The entrapment of these radicals by alkenes (**48**), styrenes (**50**), and heteroarenes (**52**) afforded the corresponding difluoroalkylated intermediates. The resulting radical intermediates can undergo two distinct pathways depending on the substrates. For alkenes (**48**), hydrogen abstraction of the radical intermediate from NMP gave the hydro-difluoroalkylated alkanes (**49**). For styrenes (**50**) and heteroarenes (**52**), the oxidation of the radical intermediate and subsequent deprotonation provided the methoxycarbonyldifluoromethylated products (**51** and **53**) [51].



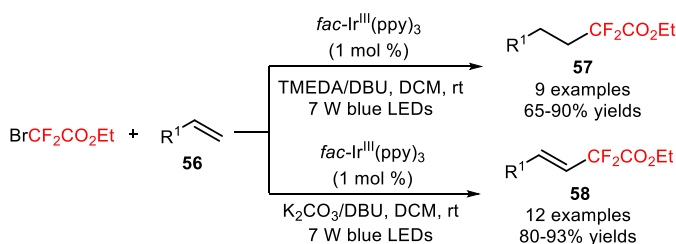
Scheme 1. Methoxycarbonyldifluoromethylation of alkenes (**48**), styrenes (**50**), and heteroarenes (**52**) by visible light photoredox catalysis and the suggested mechanism.

Chen's reagent was also utilized in the keto-difluoroalkylation of styrenes (**54**) using the DMSO as oxidant, under visible light photoredox conditions [52]. The authors hypothesized that the combination of photoredox-catalyzed difluoroalkylation and DMSO oxidation would allow the development of a facile and new approach to the direct synthesis of α -difluoroalkylated ketones without the presence of a base. A variety of α -difluoroalkylated aromatic ketones bearing electron-donating and electron-withdrawing functional groups was obtained using *fac*-Ir^{III}(ppy)₃ as a photocatalyst under blue LED irradiation (**55**, Scheme 2: 21 examples, 20-85% yields).



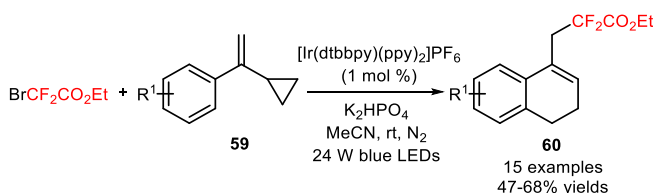
Scheme 2. Photoinduced keto-difluoroalkylation of alkenes (**54**) combining the reagent FSO₂CF₂CO₂Me with the oxidant DMSO.

The difluoroalkylating reagent ethyl 2-bromo-2,2-difluoroacetate ($\text{BrCF}_2\text{CO}_2\text{Et}$, CAS number: 565-53-7) was also implemented by Cho's group for the difluoroalkylation of unactivated alkenes (**56**) [53]. Interestingly, the authors found that the selection of the bases and solvents was critical for guiding the chemoselective synthesis of difluoroalkylated alkanes and alkenes. In fact, difluoroalkylated alkanes were preferentially obtained using a mixture of bases DBU/TMEDA in DCM (**57**, Scheme 3: 9 examples, 65-90% yields). On the other hand, the formation of difluoroalkyl-containing alkenes with high levels of regio- and *E/Z* stereoselectivity (90-97%) was achieved by complete conversion of the aliphatic alkenes and styrenes to the bromodifluoroalkylated products using the base K_2CO_3 and subsequent dehydrobromination with DBU in DMF (**58**, Scheme 3: 12 examples, 80-93% yields).



Scheme 3. Hydro-difluoroalkylation and alkenyl-difluoroalkylation of unactivated alkenes (**56**) under visible light photoredox conditions in the presence of $\text{fac-Ir}^{\text{III}}(\text{ppy})_3$.

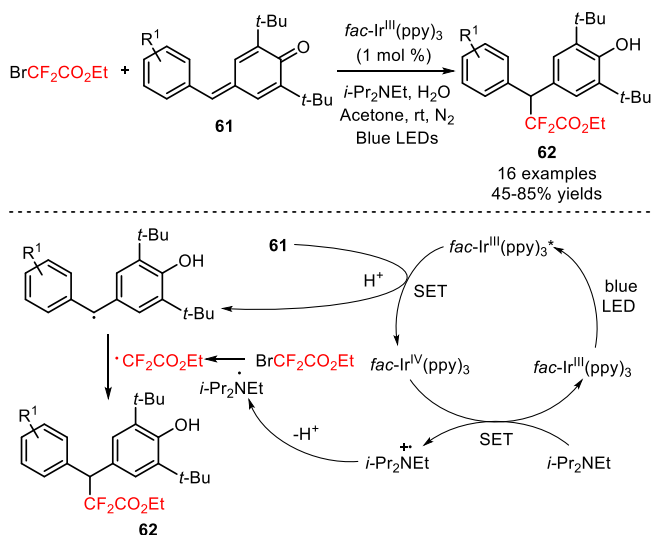
Partially hydrogenated naphthalenes and quinolines containing difluoroalkyl moieties (**60**) were efficiently prepared *via* radical difluoroalkylation of α -cyclopropylstyrenes and α -cyclopropylpyridines (**59**) with $\text{BrCF}_2\text{CO}_2\text{Et}$, respectively, opening of cyclopropyl ring, and consecutive annulation reaction [54]. In the presence of $[\text{Ir}(\text{dtbbpy})(\text{ppy})_2]\text{PF}_6$ [55,56], a wide range of α -cyclopropyl olefins bearing electron-donating and electron-withdrawing groups regioselectively afforded the corresponding products with moderate yields (**60**, Scheme 4: 15 examples, 47-68% yields). The developed methodology can be extended to other brominated compounds including bromodifluoroacetamides, ethyl 2-bromo-2-fluoroacetate ($\text{BrCHF}\text{CO}_2\text{Et}$), 2-bromoacetonitrile, and diethyl 2-bromomalonate.



Scheme 4. Photoinduced difluoroalkylation of α -cyclopropylstyrenes and α -cyclopropylpyridines (**59**).

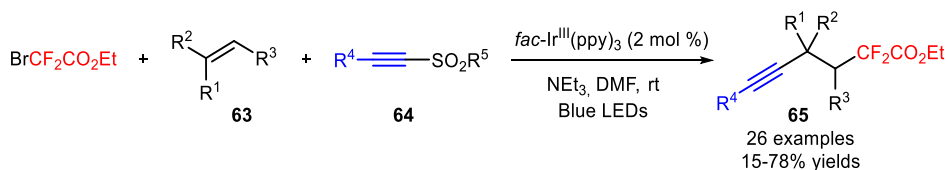
Xu and collaborators reported a new approach to access difluoroalkylated diarylmethanes (**62**) from *para*-quinone methides (**61**) and $\text{BrCF}_2\text{CO}_2\text{Et}$ *via* radical-

radical cross-coupling, under irradiation with blue LEDs [57]. In the presence of *fac*-Ir^{III}(ppy)₃, the inclusion of H₂O and the reductant (*i*-Pr)₂NEt in the reaction system was beneficial for the difluoroalkylation process. *para*-Quinone methides bearing electron-withdrawing and electron-donating groups on the aromatic ring provided the corresponding products with moderate to excellent yields. Disubstitution with chloro and methoxy groups was also well tolerated (**62**, Scheme 5: 16 examples, 45-85% yields). Remarkably, the developed strategy can be implemented using other difluoroalkylating reagents with acylamino, carbonyl, esteryl, and heteroaryl substituents. Stern-Volmer fluorescence quenching studies and radical-trapping experiments suggested the formation of diarylmethyl radicals *via* oxidative quenching of *fac*-Ir^{III}(ppy)₃* species and the CF₂CO₂Et radicals *via* oxidation of the (*i*-Pr)₂NEt radical intermediate. Cross-coupling between diarylmethyl and CF₂CO₂Et radicals afforded the difluoroalkylated diarylmethanes (**62**).



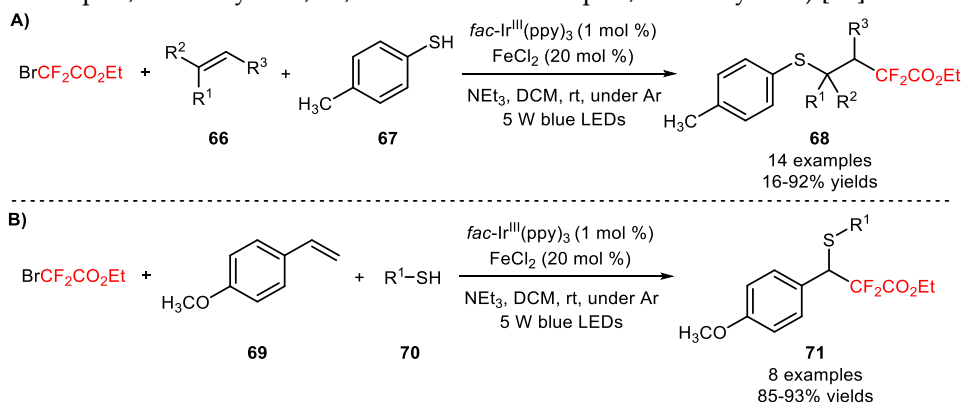
Scheme 5. Visible light-induced radical-radical cross-coupling difluoroalkylation of *para*-quinone methides (**61**).

Recently, Zhu and co-workers described a novel tactic for intermolecular alkynyl-difluoroalkylation of unactivated alkenes (**63**) via a three-component condensation with BrCF₂CO₂Et and alkynyl sulfones (**64**), under visible light photoredox conditions [58]. The combined use of *fac*-Ir^{III}(ppy)₃ with the DMF and the base NEt₃ was critical for the selective formation of β-difluoroalkylated alkynes (**65**), minimizing the unwanted bromine addition and direct difluoroalkylation of alkynyl sulfones (**64**). Terminal and internal alkenes with a variety of functional groups (**63**), and alkynyl sulfones bearing aryl and heteroaryl substituents (**64**) were all suitable substrates for the alkynyl-difluoroalkylation process (**65**, Scheme 6: 26 examples, 15-78% yields). Bromodifluoroacetamides can also provide the corresponding β-fluoroalkylated alkynes under the developed methodology.



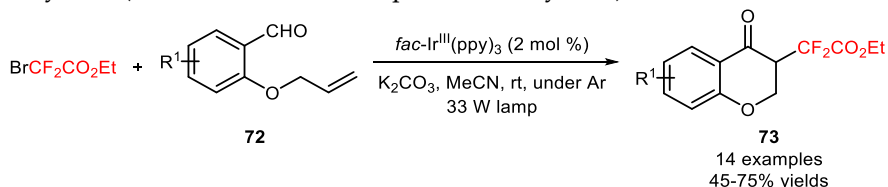
Scheme 6. Visible light-induced three-component alkynyl-difluoroalkylation of unactivated alkenes (63), BrCF₂CO₂Et, and alkynyl sulfones (64).

In 2019, Cai disclosed for the first time a three-component difluoroalkylation of alkenes (66, 69) with BrCF₂CO₂Et and subsequent thiolation with thiophenols and heteroaryl thiols (67, 70) by merging photoredox and iron catalysis (68, Scheme 7A: 14 examples, 16-92% yields; 71, Scheme 7B: 8 examples, 85-93% yields) [59].



Scheme 7. Three-component difluoroalkylation-thiolation of alkenes with BrCF₂CO₂Et and thiols by merging photoredox and iron catalysis.

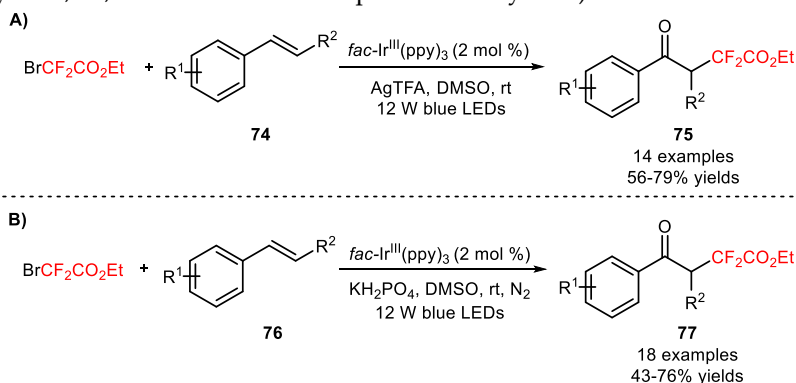
Difluoroalkylated chroman-4-ones (73) were successfully attained by Zhou and co-workers through visible light-induced difluoroalkylation of *o*-(allyloxy)arylaldehydes (72) and consecutive radical cyclization [60]. The photocatalyst *fac*-Ir^{III}(ppy)₃, the base K₂CO₃, and the solvent MeCN were determined to be the best choice for the desired organic transformation. Electron-donating and electron-withdrawing groups attached to the phenyl ring of the substrates were well tolerated with the difluoroalkylation process, affording the difluoroalkylated chroman-4-ones in good yields (73, Scheme 8: 15 examples, 45-75% yields).



Scheme 8. Synthesis of difluoroalkylated chroman-4-ones under photoredox conditions.

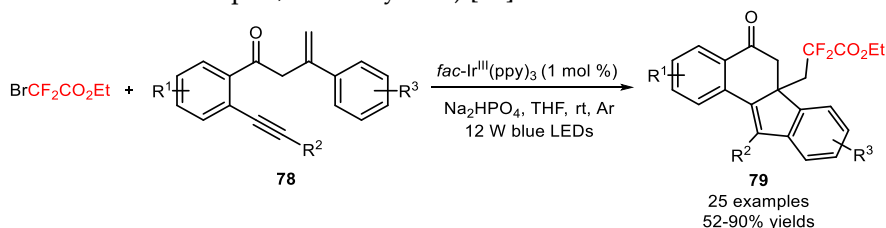
By taking advantage of the oxidative properties of DMSO, Tang [61] and Ye [62] reported the keto-difluoromethylation of styrenes (74, 76) with BrCF₂CO₂Et for C(sp³)

-CF₂CO₂Et and C(sp²)=O formation. This difunctionalization reaction was performed in DMSO with *fac*-Ir^{III}(ppy)₃ as the photocatalyst and afforded the respective keto-difluoroalkylated products in moderate to good yields (**75**, Scheme 9A: 16 examples: 56-79% yields; **77**, Scheme 9B: 18 examples: 43-76% yields).



Scheme 9. Photoinduced keto-difluoroalkylation of alkenes (**74**, **76**) combining the reagent BrCF₂CO₂Et with the oxidant DMSO reported by Tang (A) and Ye (B).

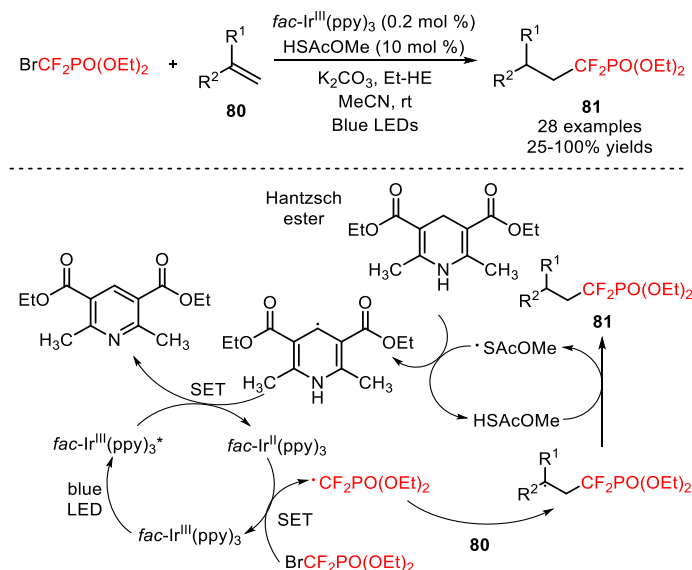
Recently, Jiang reported the preparation of difluoroalkylated benzo[*a*]fluoren-5-ones *via* *fac*-Ir^{III}(ppy)₃-catalyzed difluoroalkylation of 1,7-enynes (**78**) with BrCF₂CO₂Et, under irradiation with 12 W blue LEDs, and subsequent bicyclization (**79**, Scheme 10: 25 examples, 52-90% yields) [63].



Scheme 10. Synthesis of difluoroalkylated benzo[*a*]fluoren-5-ones under visible light photoredox conditions.

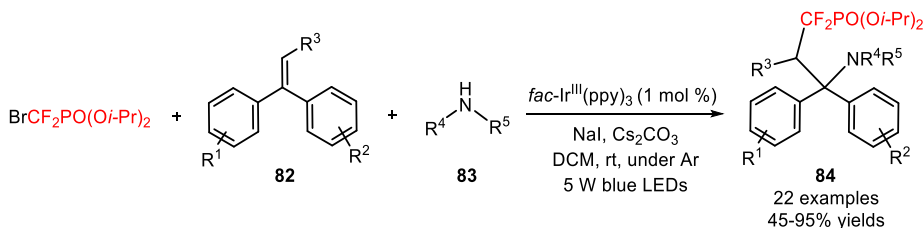
Diethyl (bromodifluoromethyl)phosphonate (BrCF₂PO(OEt)₂, CAS number: 65094-22-6) was implemented by Li and co-workers in the hydrophosphonodifluoromethylation of alkenes (**80**) using the Hantzsch ester Et-HE as a hydrogen source and the thiyl radical precursor HSAcOMe, under irradiation with blue LEDs [64]. The authors found that combining the thiyl radical-catalyzed hydrogen atom transfer ability of a HE with RQC may avoid the use of strongly basic conditions and block the undesirable halogen atom transfer addition pathway via OQC. In the presence of *fac*-Ir^{III}(ppy)₃, a diverse range of mono- and disubstituted alkenes bearing electron-rich and electron-deficient aromatic groups, heterocyclic, and aliphatic groups (**80**) were compatible substrates with the hydro-difluoroalkylation process (**81**, Scheme 11: 28 examples, 25-100% yields). This procedure was applied to the single step synthesis of the intermediate of a purine nucleoside phosphorylase (PNP) inhibitor. Mechanistic studies with radical

scavengers and alternative reductants suggested a reductive quenching of *fac*-Ir^{III}(ppy)₃^{*}, and consecutive generation of CF₂PO(OEt)₂ radicals via reduction of BrCF₂PO(OEt)₂. Radical difluoroalkylation of the alkenes (**80**) followed by hydrogen atom transfer between HSAcOMe and the difluoroalkylated radical intermediate afforded the corresponding products (**81**).



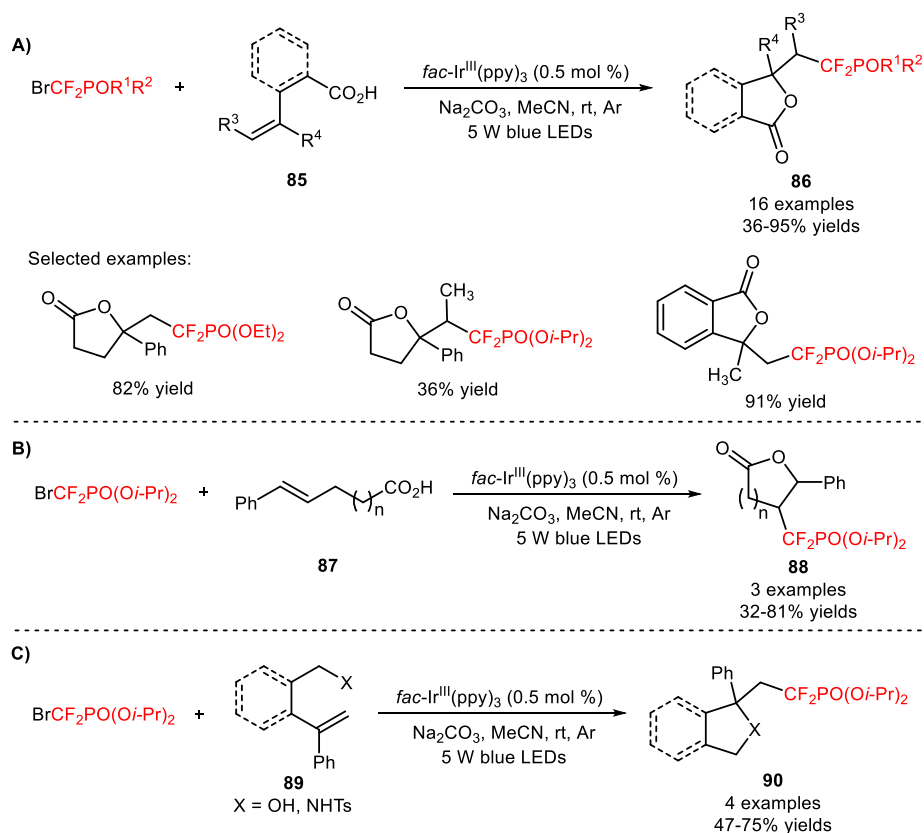
Scheme 11. Hydro-phosphonodifluoromethylation of alkenes (**80**) via a thiylyl radical/photoredox catalysis.

The synthesis of α,α -difluoro- γ -aminophosphonates (**84**) was described by Qiang and collaborators through intramolecular aminophosphonodifluoromethylation of diarylalkenes (**82**) with diisopropyl (bromodifluoromethyl)phosphonate (BrCF₂PO(Oi-Pr)₂, CAS number: 65094-24-8) under irradiation with 5 W blue LEDs [65]. A scope of electron-rich and electron-deficient diarylalkenes (**82**), and aryl amines (**83**) can be effectively converted into the difluoroalkylated products (**84**, Scheme 12: 22 examples, 45-95% yields). Interestingly, this procedure was applied to the synthesis of phosphonodifluoromethylated chiral binaphthylamines using (*R*)-(+)-1,1'-binaphthyl-2,2'-diamine ((*R*)-BINAM) and (*R*)-(+)-2'-amino-1,1'-binaphthalen-2-ol ((*R*)-NOBIN) as the substrates, and of the α,α -difluoro- γ -aminophosphoric acid. Radical-trapping and light on/off experiments suggested the intermediacy of CF₂PO(Oi-Pr)₂ radicals via oxidative quenching of *fac*-Ir^{III}(ppy)₃^{*}.



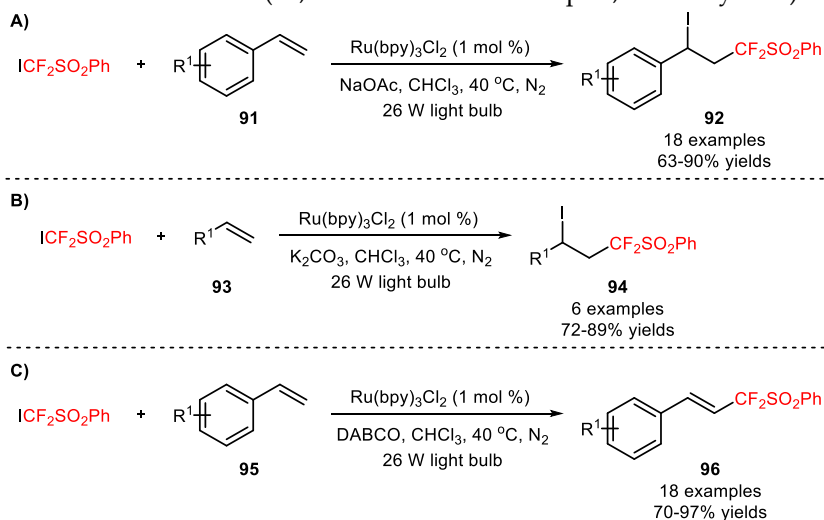
Scheme 12. Photocatalyzed intermolecular amino-phosphonodifluoromethylation of alkenes (82).

The bromodifluorophosphonate derivatives $\text{BrCF}_2\text{PO}(\text{OEt})_2$ and $\text{BrCF}_2\text{PO}(\text{O}i\text{-Pr})_2$ have recently gained a great interest by Yang and collaborators owing to their applicability to the visible light-mediated phosphonodifluoromethylation of branched (85) and linear unsaturated carboxylic acids (87), unsaturated alcohol, and unsaturated sulfonamides (89) [66]. The described protocol was employed in the synthesis of a palette of difluoroalkylated lactones (86, Scheme 13A: 16 examples, 36-95% yields), phthalides (88, Scheme 13B: 3 examples, 32-81% yields), tetrahydrofurans, and pyrrolidines (90, Scheme 13C: 4 examples, 47-75% yields).



Scheme 13. Visible light-induced phosphonodifluoromethylation of branched (85) and linear unsaturated carboxylic acids (87), unsaturated alcohol, and unsaturated sulfonamides (89) with the bromodifluorophosphonates $\text{BrCF}_2\text{PO}(\text{OEt})_2$ and $\text{BrCF}_2\text{PO}(\text{O}i\text{-Pr})_2$.

The reagent [(difluoroiodomethyl)sulfonyl]benzene ($\text{ICF}_2\text{SO}_2\text{Ph}$, CAS number: 802919-90-0) was implemented in the iodo-phenylsulfonyldifluoromethylation of unsaturated $\text{C}(sp^2)\text{-C}(sp^2)$ bonds of alkenes (**91**, **93**, **95**), in the presence of the photocatalyst $[\text{Ru}(\text{bpy})_3]\text{Cl}_2$ [67]. A variety of electron-rich and electron-poor styrenes (**91**) and aliphatic alkenes (**93**) was converted into the iodo-phenylsulfonyldifluoromethylated derivatives (**92**, Scheme 14A: 18 examples, 63-90% yields; **94**, Scheme 14B: 6 examples, 72-89% yields). The presence of the inorganic base NaOAc and K_2CO_3 was beneficial for the efficiency of difunctionalization reaction in styrenes (**91**) and aliphatic alkenes (**93**), respectively, minimizing the formation of the phenylsulfonyldifluoromethylated alkenes as by-products. On the other hand, the use of organic bases, such as DABCO, preferentially favors the synthesis of phenylsulfonyldifluoromethylated alkenes by following deprotonation instead of iodine atom transfer reaction (**96**, Scheme 14C: 18 examples, 70-97% yields).

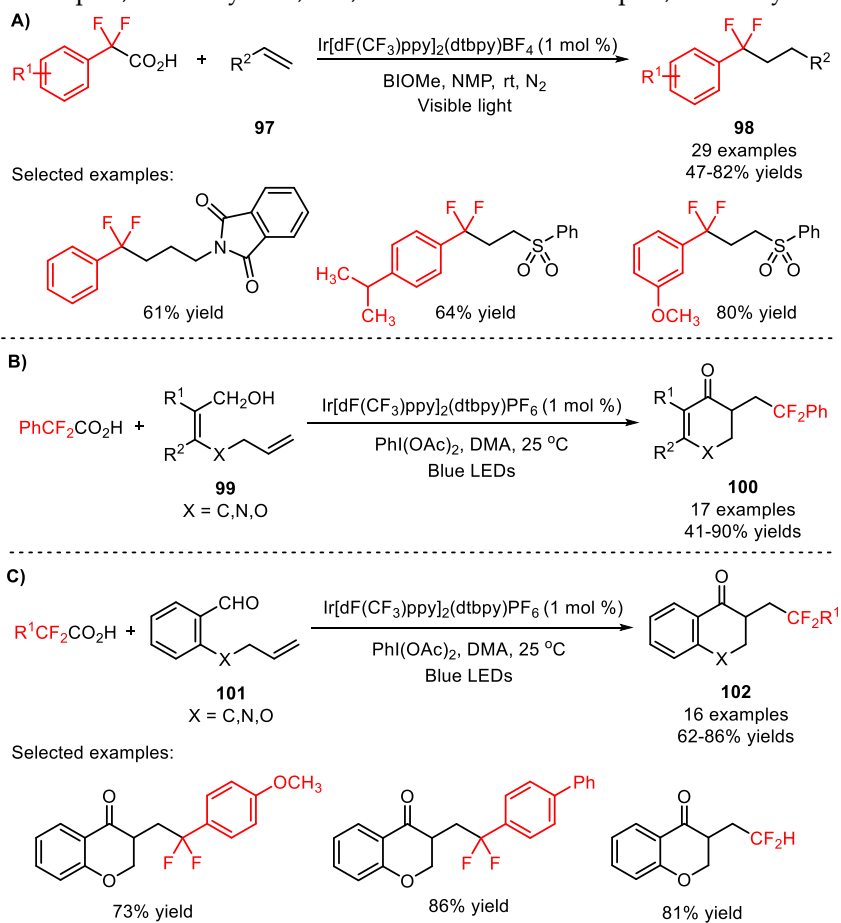


Scheme 14. A) Photoinduced iodo-phenylsulfonyldifluoromethylation of styrenes (**91**). B) Photoinduced iodo-phenylsulfonyldifluoromethylation of aliphatic alkenes (**93**). C) Photoinduced phenylsulfonyldifluoromethylation of styrenes (**95**).

Alternatively, α,α -difluoroarylacetic acids have been used as building blocks for the construction of difluoroalkylated compounds by visible light photoredox catalysis. In 2016, Qing and collaborators developed a procedure allowing the decarboxylative functionalization of α,α -difluoroarylacetic acids with alkenes (**97**) in the presence of $\text{Ir}[\text{dF}(\text{CF}_3)\text{ppy}]_2(\text{dtbpy})\text{BF}_4$ [68]. The hypervalent iodine reagent methoxybenziodoxole (BIOMe) revealed to be the most effective oxidant for decarboxylative functionalization of α,α -difluoroarylacetic acids. A wide range of alkenes underwent hydro-aryldifluoromethylation reaction to afford the corresponding products in moderate to good yields (**98**, Scheme 15A: 29 examples, 47-82% yields).

Later, Zhu and co-workers utilized α,α -difluoroarylacetic acids as building blocks for the difluoroalkylation of alkenes **99** and **101**, furnishing a range of *gem*-

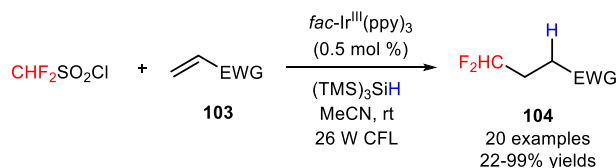
difluoroalkylated chroman-4-ones, indanones, 3,4-dihydronaphthalen-1(2*H*)-ones, 2,3-dihydroquinolin-4(1*H*)-ones, and cyclopent-2-enones, using the photocatalyst Ir[dF(CF₃)ppy]₂(dtbpy)PF₆ and the decarboxylating reagent PhI(OAc)₂ (**100**, Scheme 15B: 17 examples, 41-90% yields; **102**, Scheme 15C: 16 examples, 62-86% yields) [69].



Scheme 15. Visible light-mediated hydro-aryldifluoromethylation of alkenes **97**, **99**, and **101** with α,α -difluoroarylacetic acids.

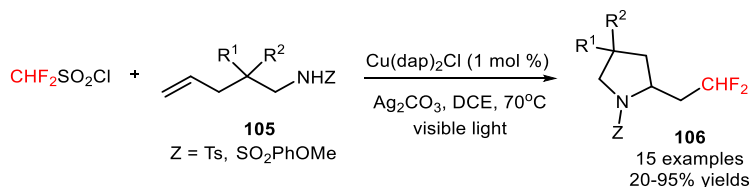
Dolbier group developed a novel strategy for hydro-difluoromethylation of alkenes (**103**) bearing a broad range of electron-withdrawing groups with the reagent difluoromethanesulfonyl chloride (HCF₂SO₂Cl, CAS number: 1512-30-7) as a source of CHF₂ radicals, under irradiation with 26 W compact fluorescent lamp (CFL) (**104**, Scheme 16: 20 examples, 22-99% yields) [70]. In addition to the photocatalyst *fac*-Ir^{III}(ppy)₃, the introduction of tris(trimethylsilyl)silane ((TMS)₃SiH) with hydrogen atom donor properties was pivotal for the direct hydro-difluoromethylation of alkenes, circumventing the formation of chloro-difluoromethylated products. Other difluoroalkylating compounds, including (bromodifluoromethyl)benzene (PhCF₂Br), 1,1-difluoroethane-1-sulfonyl chloride (CH₃CF₂SO₂Cl), and 2-azido-1,1-

difluoroethane-1-sulfonyl chloride ($\text{N}_3\text{CH}_2\text{CF}_2\text{SO}_2\text{Cl}$) can be implemented in the hydro-difluoroalkylation of the substrates, under the described reaction conditions.



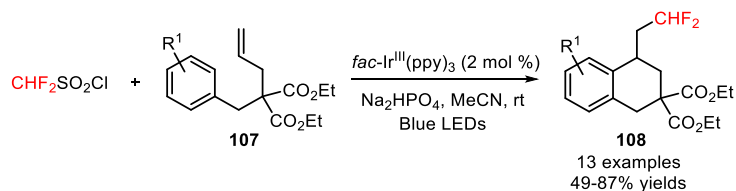
Scheme 16. Visible light-catalyzed hydro-difluoromethylation of electron-deficient alkenes (**103**) with $\text{HCF}_2\text{SO}_2\text{Cl}$.

The reagent $\text{HCF}_2\text{SO}_2\text{Cl}$ was also efficiently employed in the preparation of difluoromethylated pyrrolidines and lactones through installation of difluoromethyl groups in sulfonamides and esters (**105**), respectively, and subsequent radical cyclization by visible light photoredox catalysis (**106**, Scheme 17: 15 examples, 20-95% yields) [71]. The implementation of $[\text{Cu}(\text{dap})_2]\text{Cl}$ [72] as photocatalyst and the base Ag_2CO_3 was crucial for suppression of the chloro-difluoromethylation process.



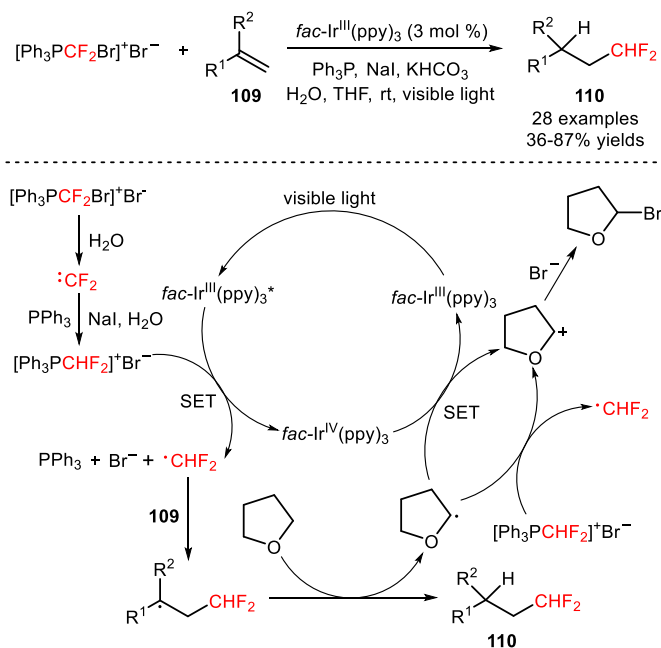
Scheme 17. Visible light-induced difluoromethylation of sulfonamides and esters (**105**) and subsequent radical cyclization in the presence of $[\text{Cu}(\text{dap})_2]\text{Cl}$.

Alkenes containing *gem*-dialkoxycarbonyl substituents (**107**) were employed as substrates for photoinduced intramolecular difluoromethylation using the reagent $\text{HCF}_2\text{SO}_2\text{Cl}$, in the presence of $\text{fac-Ir}^{\text{III}}(\text{ppy})_3$ [73]. A spectrum of difluoromethylated tetralin derivatives possessing electron-donating and electron-withdrawing groups in the aromatic ring and alkyl substituents at the β -position was efficiently obtained in moderate to good yields (**108**, Scheme 18: 13 examples, 49-87% yields). Alternative difluoroalkyl R_fX radical precursors [$\text{R}_f = \text{CF}_2\text{CH}_3$, $\text{CF}_2\text{CO}_2\text{Et}$, CF_2CONHPh , $\text{CF}_2\text{CON}(\text{CH}_2\text{CH}_2)_2\text{O}$; $\text{X} = \text{SO}_2\text{Cl}$, Br] were also compatible with the developed synthetic methodology.



Scheme 18. Visible light-catalyzed difluoromethylation/6-*exo* cyclization of unactivated alkenes (**107**) with $\text{HCF}_2\text{SO}_2\text{Cl}$.

Qing and co-workers developed a methodology for visible light-driven hydro-difluoromethylation of alkenes (**109**) with the easy-to-handle (bromodifluoromethyl)triphenylphosphonium bromide $[(\text{Ph}_3\text{PCF}_2\text{Br})^+\text{Br}^-]$, CAS number: 58201-66-4 for the insertion of CHF_2 groups, in the presence of H_2O and THF [74]. The reagent $(\text{Ph}_3\text{PCF}_2\text{Br})^+\text{Br}^-$ was recognized exclusively as a difluorocarbene precursor [75-79]. Nevertheless, the authors found that $(\text{Ph}_3\text{PCF}_2\text{Br})^+\text{Br}^-$ can be implemented as a CF_2Br donor, under visible light irradiation. The additional formation of hydro-difluoromethylated derivatives was solely observed in the presence of the photocatalyst $\text{fac-Ir}^{\text{III}}(\text{ppy})_3$. The authors suggested the formation of (difluoromethyl)triphenylphosphonium bromide $[(\text{Ph}_3\text{PCHF}_2)^+\text{Br}^-]$ resulting from the reaction between $(\text{Ph}_3\text{PCF}_2\text{Br})^+\text{Br}^-$ and H_2O to explain the unexpected hydro-difluoromethylation. Interestingly, the presence of H_2O , PPh_3 , NaI , and KHCO_3 in the reaction medium was critical for selective synthesis of hydro-difluoromethylated alkanes (**110**). Terminal and internal alkenes bearing various functional groups (**109**) were compatible with the desired organic transformation, affording the hydro-difluoromethylated products in moderate to high yields (**110**, Scheme 19: 28 examples, 36-87% yields).



Scheme 19. Hydro-difluoromethylation of unactivated alkenes (**109**) with $[\text{Ph}_3\text{PCF}_2\text{Br}]^+\text{Br}^-$ under visible light photoredox conditions.

In addition, this synthetic approach can be extended to more structurally complex substrates such as analogues of 4-methyl-umbelliferone (**111**), phthalimide (**112**), *L*-phenylalanine (**113**), and estrone (**114**), as well as to biologically active compounds, including the fungicide vinclozolin (**115**) and the two insecticides allethrin (**116**) and rotenone (**117**) (Figure 3). Isotopic mechanistic experiments

involving D₂O and THF-*d*₈ demonstrated that both H₂O and THF were the sources of hydrogen atoms for the hydro-difluoromethylation process. The authors proposed a mechanism of oxidative quenching of *fac*-Ir^{III}(ppy)₃* and concomitant reduction of (Ph₃PCHF₂)⁺Br⁻ to CHF₂ radicals. Electrophilic addition of CHF₂ radicals to the alkenes (**109**) and subsequent abstraction of a hydrogen atom from THF afforded the respective hydro-difluoromethylated derivatives (**110**).

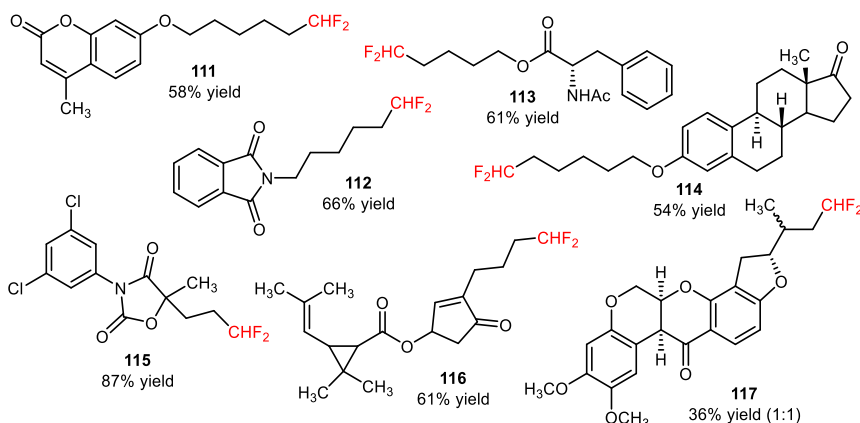
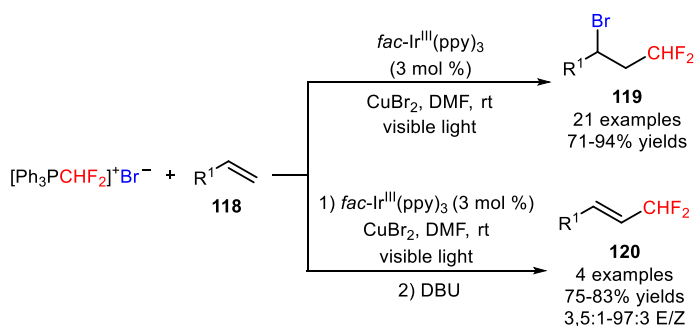


Figure 3. Chemical structures of hydro-difluoromethylated analogues of 4-methylumbelliferone (**111**), phthalimide (**112**), L-phenylalanine (**113**), and estrone (**114**), vinclozolin (**115**), allethrin (**116**), and rotenone (**117**).

Later, the same group described the application of [Ph₃PCHF₂]⁺Br⁻ in the bromo-difluoromethylation of alkenes (**118**) under visible light photoredox conditions [80]. The use of catalytic amounts of *fac*-Ir^{III}(ppy)₃ and CuBr₂ allowed the selective preparation of bromo-difluoromethylated alkanes, suppressing the unwanted hydro-difluoromethylation of the substrates (**119**, Scheme 20: 21 examples, 71-94% yields). The protocol was also applied to the direct bromo-difluoromethylation of more complex and biologically active molecules, including the fungicide vinclozolin (**121**) and the insecticides allethrin (**122**) and rotenone (**123**) (Figure 4). Difluoromethylated alkenes were achieved *via* a one-pot bromo-difluoromethylation/dehydrobromination process (**120**, Scheme 20: 4 examples, 75-83% yields).



Scheme 20. Visible light-induced photocatalytic bromo-difluoromethylation and direct difluoromethylation of alkenes (**118**) with [Ph₃PCHF₂]⁺Br⁻.

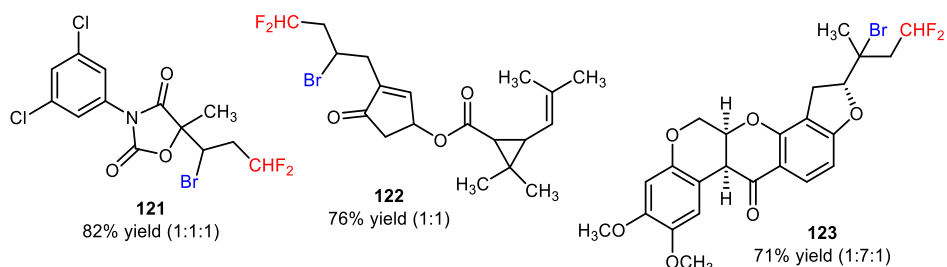
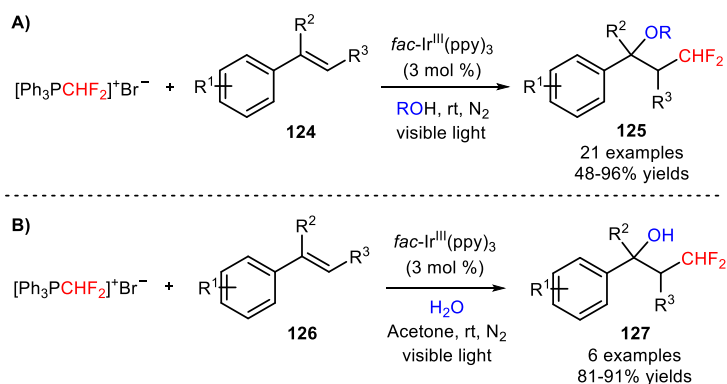


Figure 4. Chemical structures of bromo-difluoromethylated vinclizolin (**121**), allethrin (**122**), and rotenone (**123**).

Difluoromethylated ethers and alcohols were efficiently obtained *via* visible light-mediated oxy-difluoromethylation of styrenes (**124**, **126**) with the difluoromethylating reagent $[\text{Ph}_3\text{PCHF}_2]^+\text{Br}^-$ using alcohol derivatives and water, respectively, as nucleophiles (**125**, Scheme 21A: 21 examples, 48-96% yields; **127**, Scheme 21B: 6 examples, 81-91% yields) [81]. The protocol was applicable to the late-stage oxy-difluoromethylation of vinyl-*N*-benzoyl-*L*-tyrosine ethyl ester (**128**) and vinylestirine (**129**) (Figure 5).



Scheme 21. Visible light-induced oxy-difluoromethylation of styrenes with $[\text{Ph}_3\text{PCHF}_2]^+\text{Br}^-$ using alcohol derivatives (**A**) and water (**B**).

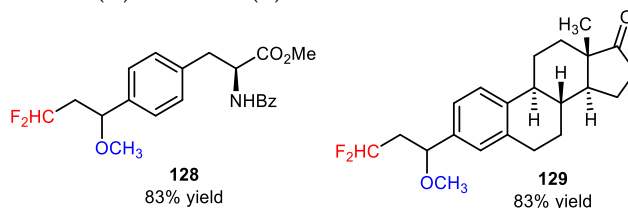
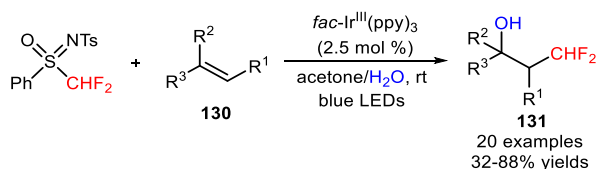


Figure 5. Chemical structures of the products of oxy-difluoromethylation of vinyl-*N*-benzoyl-*L*-tyrosine ethyl ester (**128**) and vinylestirine (**129**).

The shelf-stable and easy-to-handle *N*-tosyl-*S*-difluoromethyl-*S*-phenylsulfoximine (CAS number: 1097192-99-8, so-called Hu's reagent), with the electron-withdrawing sulfoximine group was initially conceived as a difluorocarbene

source for the introduction of CHF₂ groups to C-, N-, and S-nucleophiles [82]. Recently, it has been found that this reagent can also be implemented as a precursor of CHF₂ radicals under photoredox conditions. In fact, Akita and co-workers reported an efficient protocol to achieve the oxy-difluoromethylation of alkenes and styrenes (**130**) using *N*-tosyl-*S*-difluoromethyl-*S*-phenylsulfoximine and the nucleophile H₂O under irradiation with blue LEDs [83]. In the presence of *fac*-Ir^{III}(ppy)₃, a broad range of difluoromethylated alcohols containing electron-donating and electron-withdrawing groups was successfully synthesized (**131**, Scheme 22: 20 examples, 32–88% yields). Moreover, structurally complex alkenes, such as vinylostropane (**132**) and vinyl-*N*-benzoyl-*L*-tyrosine ethyl ester (**133**), as well as other oxygen nucleophiles, such as alcohols and carboxylic acids, were also compatible with the described oxy-difluoromethylation strategy (Figure 6). Mechanistic experiments with the radical scavenger 2,2,6,6-tetramethylpiperidine *N*-oxide (TEMPO) suggested the intermediacy of CHF₂ radicals *via* oxidative quenching of *fac*-Ir^{III}(ppy)₃*.



Scheme 22. Oxy-difluoromethylation of alkenes (**130**) using *N*-tosyl-*S*-difluoromethyl-*S*-phenylsulfoximine and H₂O in the presence of *fac*-Ir^{III}(ppy)₃.

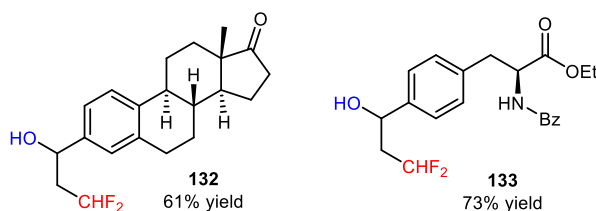
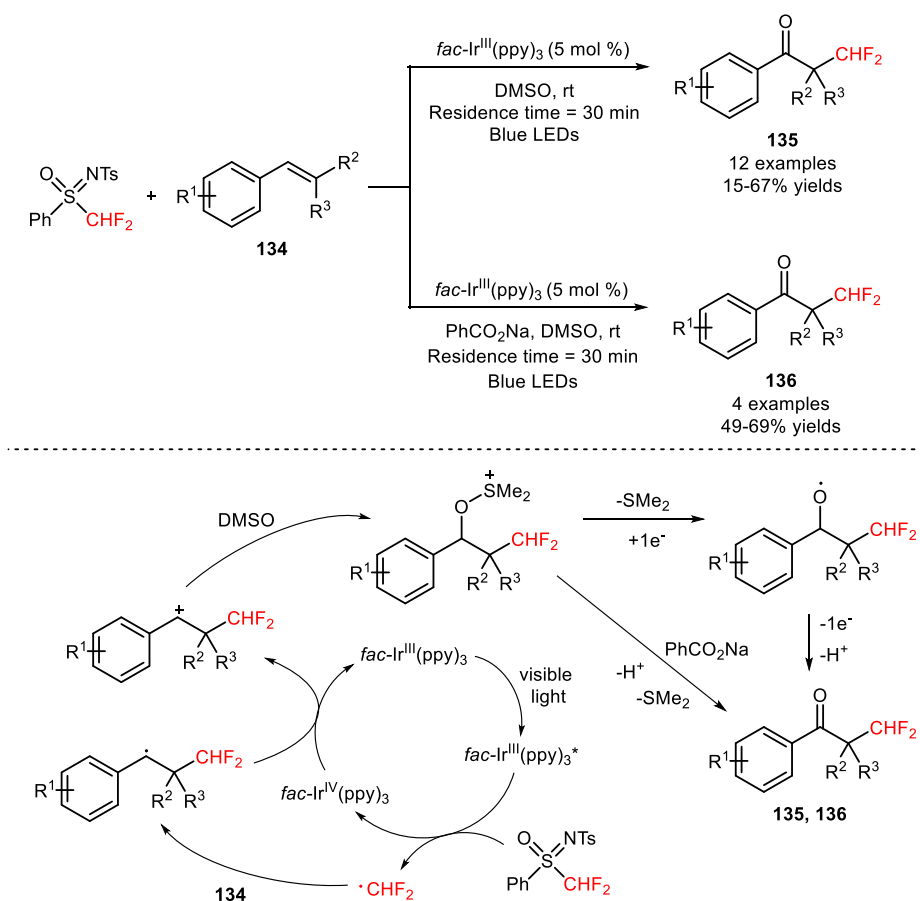


Figure 6. Chemical structures of the products of oxy-difluoromethylation of vinylostropane (**132**) and vinyl-*N*-benzoyl-*L*-tyrosine ethyl ester (**133**).

Later, Koike and Akita reported for the first time the synthesis of α -difluoromethyl-substituted ketones *via* photoredox keto-difluoromethylation of alkenes with *N*-tosyl-*S*-difluoromethyl-*S*-phenylsulfoximine and subsequent DMSO oxidation (Kornblum oxidation) in an one-pot operation [84]. Electrochemical analysis, laser flash photolysis (LFP), and density functional theory (DFT) calculations suggested that the *N*-tosyl-*S*-difluoromethyl-*S*-phenylsulfoximine is the most efficient difluoromethyl radical source compared to other sulfone-based reagents. Small scale experiments have shown that the absence of base for some substrates was beneficial for the efficiency the reaction, avoiding the deprotonation of carbocation intermediate and the formation of the difluoromethylated alkenes as by-products. For other substrates, the addition of sodium benzoate in the reaction medium minimized the generation of by-products and afforded the keto-difluoromethylated products in

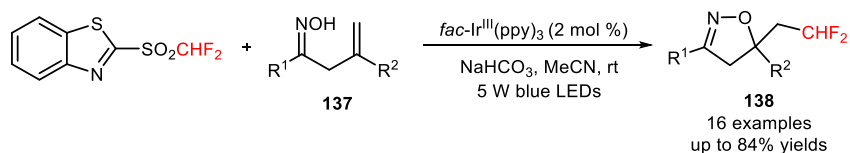
better yields. The photoredox difluoromethylation of alkenes was performed under continuous-flow conditions and gave the α -difluoromethylated ketones in the absence (**135**, Scheme 23: 12 examples, 15-67% yields) or in the presence of sodium benzoate (**136**, Scheme 23: 4 examples, 49-69% yields). The use of a flow system can shorten the residence time resulting in the prevention of dehydrofluorination reactions of α -difluoromethylated ketones, under basic conditions. Mechanistic investigations proposed that the photoredox process is mediated by the formation of a α -difluoromethyl-substituted carbocationic intermediate, which undergoes nucleophilic attack of DMSO to afford an alkoxy-sulfonium intermediate. The presence of a base can have a pivotal role in the deprotonation of that intermediate to generate the keto-difluoromethylated products. On the other hand, the deprotonation of the carbocation intermediate can give the difluoromethylated alkenes as by-products.



Scheme 23. Visible light-mediated keto-difluoromethylation of alkenes (**134**) by merging the reagent *N*-tosyl-*S*-difluoromethyl-*S*-phenylsulfonamide and the oxidant DMSO.

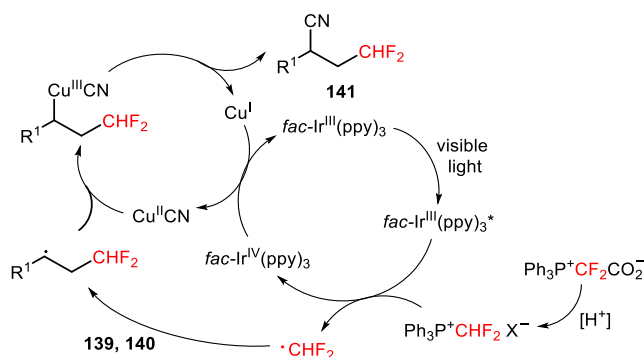
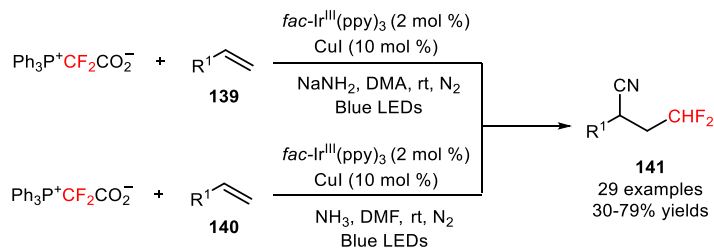
Zhu and collaborators developed a methodology enabling the use of difluoromethyl benzothiazolyl-sulfone (2-BT₂SO₂CHF₂, CAS number: 186204-66-0) for

the synthesis of difluoromethylated isoxazolines (**138**) *via* iridium-mediated difluoromethylation of β,γ -unsaturated oximes (**137**) and concomitant cyclization in MeCN at room temperature with NaHCO₃ as base (**138**, Scheme 24: 16 examples, up to 84% yields) [85].



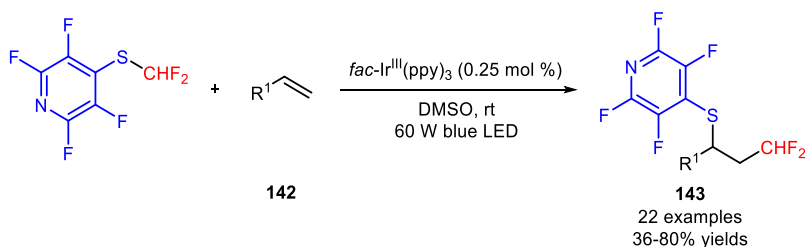
Scheme 24. Iridium-catalyzed difluoromethylation of β,γ -unsaturated oximes (**137**).

In 2019, Xiao and co-workers described the cyano-difluoromethylation of alkenes **139** and **140** with difluoromethylene phosphobetaine ($\text{Ph}_3\text{P}^+\text{CF}_2\text{CO}_2^-$, CAS number: 1449521-05-4) and NaNH₂ in DMA (or NH₃ in DMF) by combining iridium [*fac*-Ir^{III}(ppy)₃] and copper (CuI) catalysis [86]. The authors envisioned that the $\text{Ph}_3\text{P}^+\text{CF}_2\text{CO}_2^-$ could be trapped by a suitable nitrogen source to generate the cyanide anion (CN⁻) *in situ*. This procedure would avoid the use of toxic cyanation reagents for introduction of nitrile groups (CN). Under the described reaction conditions, a broad range of styrenes and aliphatic alkenes were smoothly converted into the cyano-difluoromethylated products (**141**, Scheme 25: 29 examples, 30-79% yields). Experiments with sodium picrate, an indicator of the detection of CN, demonstrated that $\text{Ph}_3\text{P}^+\text{CF}_2\text{CO}_2^-$ and NaNH₂ (or NH₃) are both carbon and nitrogen sources, respectively, for the *in situ* generated CN⁻ anion. Mechanistic investigations with radical scavengers suggested that, besides the formation of the CN⁻, the $\text{Ph}_3\text{P}^+\text{CF}_2\text{CO}_2^-$ acted as CHF₂ source by oxidative quenching of *fac*-Ir^{III}(ppy)₃^{*}.



Scheme 25. Photoredox-catalyzed cyano-difluoromethylation of alkenes **139** and **140**.

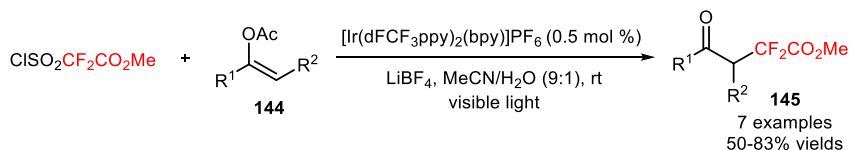
Recently, Dilman and co-workers developed a visible light-promoted difluoromethylation-thiolation of alkenes **142** using the 4-((difluoromethyl)thio)-2,3,5,6-tetrafluoropyridine (PyfSCHF₂) [87]. The authors hypothesized that the single-electron reduction of the photocatalyst triggered the cleavage of C-S bond of PyfSCHF₂ and subsequent formation of CHF₂ radicals. The resulting radical intermediate would abstract the 4-tetrafluoropyridinylthio fragment from the PyfSCHF₂. Under irradiation with 60 W blue LED, this difunctionalization reaction was carried out in DMSO at room temperature with *fac*-Ir^{III}(ppy)₃ as photocatalyst and was applied to a wide range of alkenes bearing distinct functional groups (**143**, Scheme 26: 22 examples, 36-80% yields).



Scheme 26. Visible light-induced difluoroalkylation-thiolation of alkenes (**142**) with PyfSCHF₂.

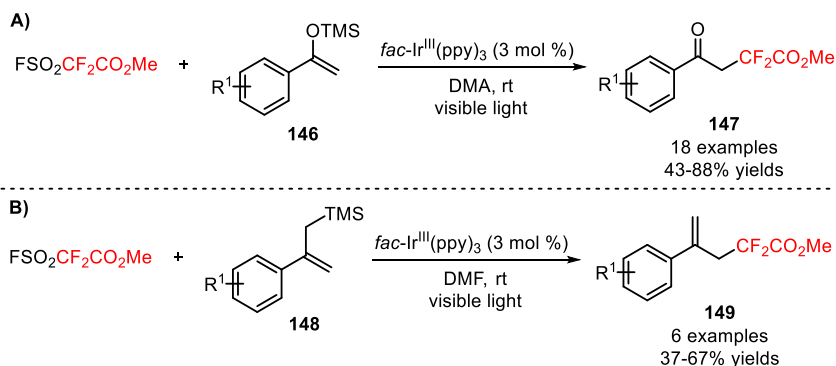
2.2. Difluoroalkylation of *sp*² Carbon Atoms in Enol Derivatives, α,β -Unsaturated Carboxylic Acids, and Allylic Alcohols

Dolbier and collaborators described a methodology for the visible light-mediated insertion of methoxycarbonyldifluoromethyl groups in enol acetates (**144**) with methyl 2,2-difluoro-2-(chlorosulfonyl)acetate (ClSO₂CF₂CO₂Me, CAS number: 18225-68-8) [88]. A wide array of 2,2-difluoro- γ -keto esters was efficiently prepared in moderate to very good yields (**145**, Scheme 27: 7 examples, 50-83% yields) using the catalyst Ir{[dF(CF₃)ppy]₂(dtbbpy)}PF₆ [56] and the additive LiBF₄ to enable removal of the acetyl groups.



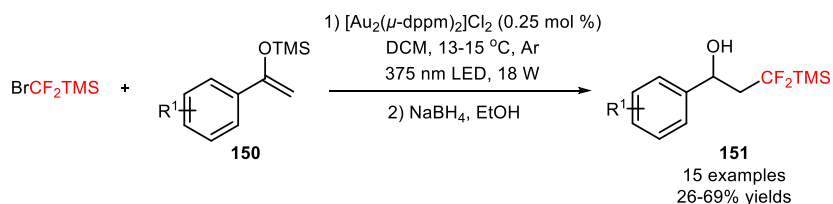
Scheme 27. Methoxycarbonyldifluoromethylation of enol acetates (**144**) by visible light photoredox catalysis.

Qing and co-workers reported the methoxycarbonyldifluoromethylation of trimethylsilyl enol ethers (**146**) and allyltrimethylsilanes (**148**) with FSO₂CF₂CO₂Me under visible light photoredox conditions [89]. The difluoroalkylation protocol was applied to silyl enol ethers and allyltrimethylsilanes with electron-donating and electron-withdrawing groups on the phenyl rings (**147**, Scheme 28A: 18 examples, 43-88% yields; **149**, Scheme 28B: 6 examples, 37-67% yields).



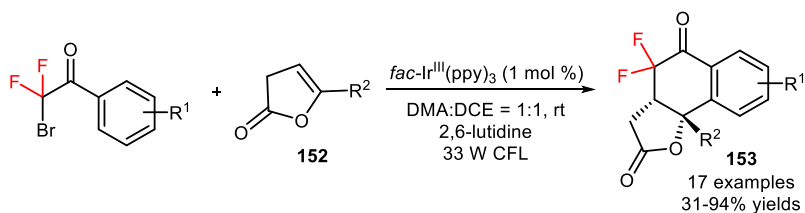
Scheme 28. Visible light-mediated methoxycarbonyldifluoromethylation of trimethylsilyl enol ethers (**146**) and allyltrimethylsilanes (**148**) with $\text{FSO}_2\text{CF}_2\text{CO}_2\text{Me}$.

Recently, the gold photocatalyst $[\text{Au}_2(\mu\text{-dppm})_2]\text{Cl}_2$ [90,91] was implemented in the silyldifluoromethylation of trimethylsilyl enol ethers (**150**) with (bromodifluoromethyl)trimethylsilane (BrCF_2TMS , CAS number: 115262-01-6) and this method was followed by a reduction of the primary difluoroalkylated products with sodium borohydride (NaBH_4) (**151**, Scheme 29: 15 examples, 25-69% yields [92]).



Scheme 29. Silyldifluoromethylation of trimethylsilyl enol ethers (**150**) with BrCF_2TMS by gold photoredox catalysis.

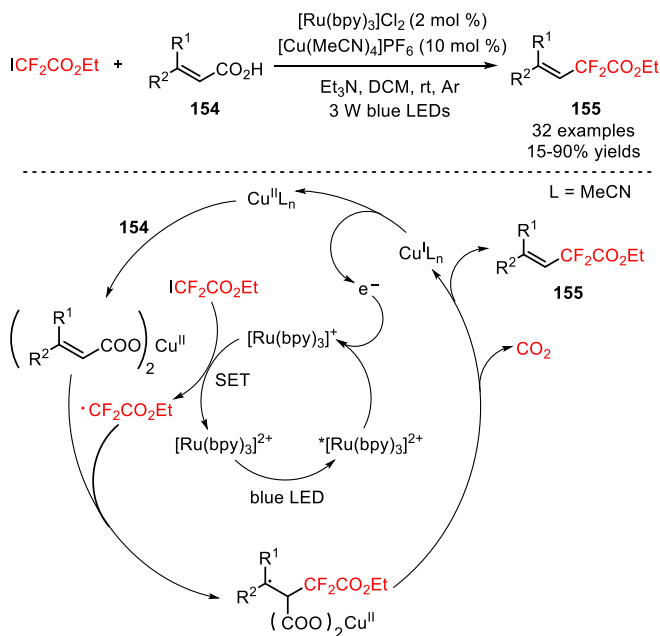
Difluoroalkylated polycyclic lactones (**153**) were synthesized by radical difluoroalkylation of 2-oxo-2,3-dihydrofuran derivatives (**152**) with α -bromo- α,α -difluoroacetophenones and a consecutive annulation reaction, under irradiation with 33 W fluorescent light bulbs [93]. The strategy of cascade difluoroalkylation/annulation was efficiently performed in the presence of $\text{fac-Ir}^{\text{III}}(\text{ppy})_3$, the base 2,6-lutidine, and using a solvent mixture of DMA and DCE in a ratio of 1:1 (Scheme 30). Alkyl-substituted enol lactones (**152**), and α -bromo- α,α -difluoroacetophenones bearing electron-rich and electron-withdrawing groups on the aromatic ring provided a wide range of annulated difluoroalkyl-containing products with an excellent diastereoselectivity (only *cis* products were generated) in moderate to excellent yields (**153**, 17 examples, 31-94% yields).



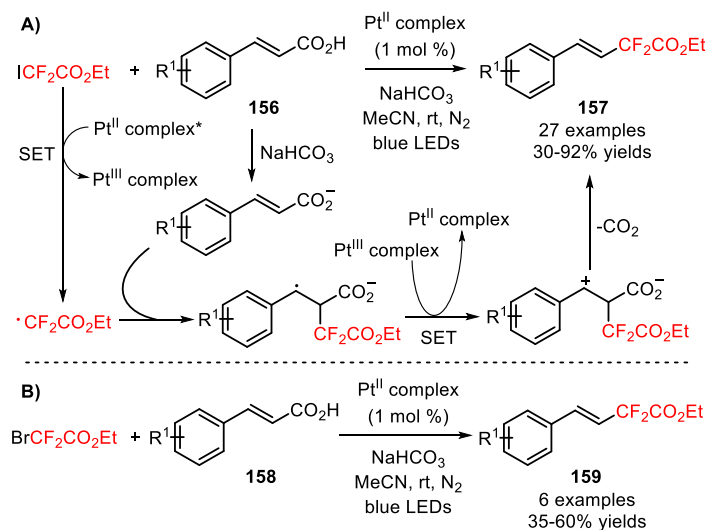
Scheme 30. Visible light-mediated photocatalytic difluoroalkylation of 2-oxo-2,3-dihydrofuran derivatives (**152**) with α -bromo- α,α -difluoroacetophenones. CFL – compact fluorescent lamp.

α,β -Unsaturated carboxylic acids have been used as substrates for decarboxylative difluoroalkylation under transition metal catalysis [94,95]. Visible light-driven methodologies using these substrates have been described by several groups. In 2016, Liu and co-workers have developed a methodology for the decarboxylative functionalization of α,β -unsaturated carboxylic acids (**154**) with the difluoroalkylating reagent ethyl 2,2-difluoro-2-iodoacetate (ICF₂CO₂Et, CAS number: 7648-30-8) by using a dual-catalytic system merging photocatalysis and copper catalysis [96]. The photocatalyst [Ru(bpy)₃]Cl₂ [97,98], the copper catalyst [Cu(MeCN)₄]PF₆, and the solvent DCM constituted the selected conditions for the difluoroalkylation reaction (Scheme 31). A wide array of α,β -unsaturated carboxylic acids possessing electron-rich and electron-deficient (hetero)aromatic groups gave the corresponding difluoroalkylated styrenes with high *E/Z* selectivity in moderate to excellent yields (**155**, 32 examples, 15-90% yields). The authors hypothesized a mechanism involving a reductive quenching of ^{*}[Ru(bpy)₃]²⁺ *via* [Cu(MeCN)₄]⁺. Subsequent reduction of ICF₂CO₂Et to CF₂CO₂Et radicals led to the regeneration of the photocatalyst in its ground state. Electrophilic radical addition to the α -position of the double bond in the substrates followed by elimination of CO₂ and [Cu(MeCN)₄]⁺ afforded the difluoroalkylated styrenes (**155**).

The application of the platinum photocatalyst Pt(II)[R(C^{^N}^P^P)] (R=4-CH₃OC₆H₄) was described as an alternative approach for the construction of *E*-difluoroalkylstyrenes from reaction between α,β -unsaturated carboxylic acids (**156**) and ICF₂CO₂Et, under irradiation with blue LEDs (**157**, Scheme 32A: 27 examples, 30-92% yields) [99]. A mechanism for the difluoroalkylation mediated by oxidation of the Pt(II) complex and formation of CF₂CO₂Et radicals was proposed along with an initial deprotonation of the α,β -unsaturated carboxylic acids (**156**) by NaHCO₃. The developed methodology for the difluoroalkylation of α,β -unsaturated carboxylic acids (**158**) can also be performed using the reagent BrCF₂CO₂Et (**159**, Scheme 32B: 6 examples, 35-60% yields). In the presence of *N,N*-diisopropylethylamine (DIPEA), the reagent ICF₂CO₂Et can also be used for the synthesis of difluoroalkyl-containing alkenyl iodides and *Z*-difluoroalkylstyrenes *via* photoinduced difluoroalkylation of terminal arylalkynes.



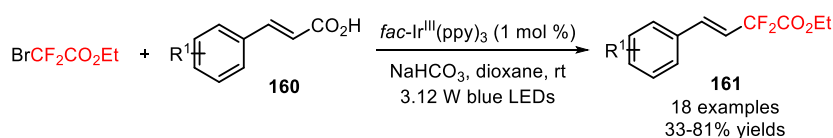
Scheme 31. Photoredox- and copper-catalyzed decarboxylative difluoroalkylation of α,β -unsaturated carboxylic acids (**154**) with $\text{ICF}_2\text{CO}_2\text{Et}$ and the proposed mechanism.



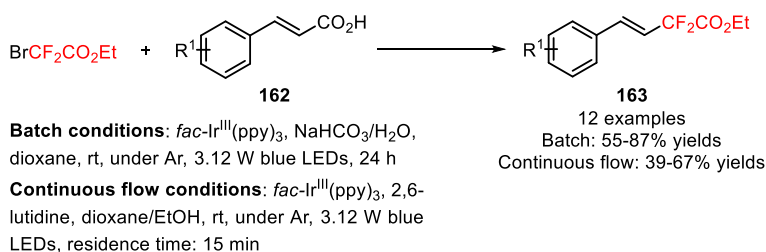
Scheme 32. Platinum-catalyzed difluoroalkylation of α,β -unsaturated carboxylic acids (**156**, **158**) with the reagents $\text{ICF}_2\text{CO}_2\text{Et}$ (**A**) and $\text{BrCF}_2\text{CO}_2\text{Et}$ (**B**).

As an alternative to $\text{ICF}_2\text{CO}_2\text{Et}$, Noël and co-workers employed the reagent $\text{BrCF}_2\text{CO}_2\text{Et}$ for the decarboxylative difluoroalkylation of α,β -unsaturated carboxylic acids (**160**) in the presence of *fac*- $\text{Ir}^{\text{III}}(\text{ppy})_3$ [100]. The developed strategy required no higher temperatures, no metal co-catalysts, or hypervalent iodine reagents to facilitate the decarboxylation process. A spectrum of *meta*- and *para*-substituted α,β -

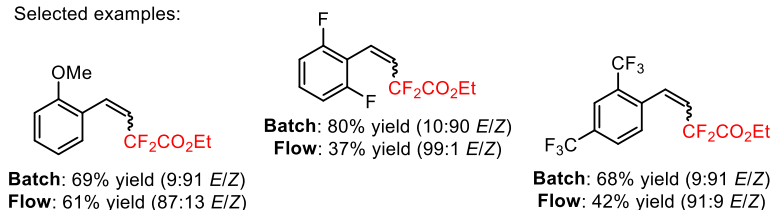
unsaturated carboxylic acids bearing electron-neutral, electron-donating, and electron-withdrawing substituents on the aromatic ring and heterocyclic substituents (pyridine and thiophene) (**160**) afforded the respective difluoroalkylated styrenes with a good to excellent *E*-stereoselectivity (**161**, Scheme 33: 18 examples, 33-81% yields). In contrast, the decarboxylative difluoroalkylation of *ortho*-substituted α,β -unsaturated carboxylic acids (**162**) provided the corresponding *Z*-products (**163**) under batch conditions. A switch in the stereoselectivity was observed when the decarboxylative functionalization of the substrates was performed under continuous-flow conditions (**163**, Scheme 34: 12 examples, batch: 55-87% yields, continuous flow: 39-67% yields). Interestingly, this methodology can be successfully applied to *ortho*-, *meta*-, *para*-substituted arylpropionic acids (**164**) for the synthesis of difluoroalkylated phenylacetylenes (**165**, Scheme 35: 12 examples, 17-62% yields).



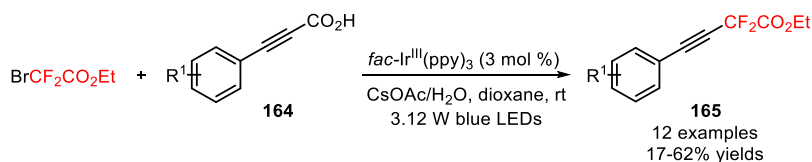
Scheme 33. Visible light-promoted photocatalytic decarboxylative difluoroalkylation of *meta*- and *para*-substituted α,β -unsaturated carboxylic acids (**160**).



Selected examples:

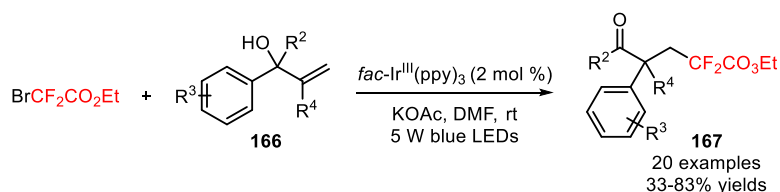


Scheme 34. Visible light-promoted photocatalytic decarboxylative difluoroalkylation of *ortho*-substituted α,β -unsaturated carboxylic acids (**162**) under batch and continuous flow conditions.



Scheme 35. Visible light-promoted photocatalytic decarboxylative difluoroalkylation of aryl propionic acids (**164**).

The synthesis of carbodifluoroalkylated ketones by visible light-promoted difunctionalization of allylic alcohols through a sequential difluoroalkylation and functional group migration process has been reported in the literature. Zhu and co-workers disclosed an efficient methodology for the carbodifluoroalkylation of α,α -diarylallylic alcohols with electron-donating and electron-withdrawing substituents (**166**) attached to the aromatic rings and a subsequent 1,2-aryl migration process, in the presence of *fac*-Ir^{III}(ppy)₃, the base KOAc, and BrCF₂CO₂Et (**167**, Scheme 36: 20 examples, 33-83% yields) [101]. The difluoroalkylation/functional group migration process was also achievable using bromodifluoroacetamides.

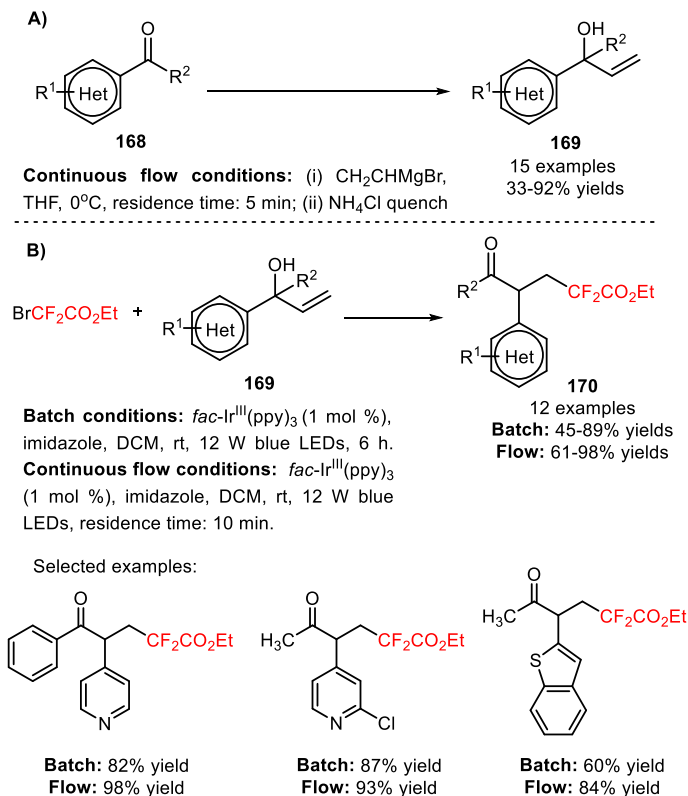


Scheme 36. Photoinduced carbodifluoroalkylation of α,α -diaryl allylic alcohols (**166**).

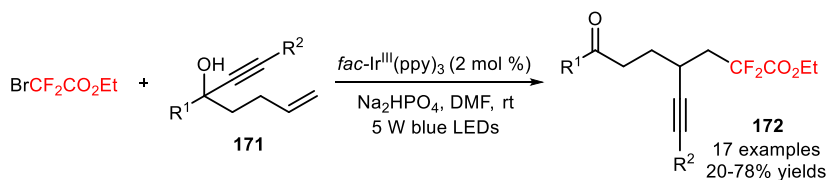
Recently, Noël's group reported a similar synthetic strategy for the difluoroalkylation of heteroaryl-containing allylic alcohols (**169**) and concomitant 1,2-heteroaryl migration with BrCF₂CO₂Et [102]. Heteroaryl-containing allylic alcohols were synthesized *via* reactions between heteroaryl ketones (**168**) and vinylmagnesium bromide, under continuous-flow conditions (**169**, Scheme 37A: 15 examples, 33-92% yields). A higher efficiency for the difluoroalkylation/1,2-heteroaryl migration process was achieved when *fac*-Ir^{III}(ppy)₃ and imidazole were chosen as photocatalyst and base, respectively. Under the optimized photochemical conditions, the 4-pyridyl, 3-pyridyl, 2-pyridyl, pyrazyl, and benzothiophenyl groups exhibited a migratory aptitude induced by incorporation of CF₂CO₂Et groups, affording the final products in good yields under batch conditions (**170**, Scheme 37B: 12 examples, batch: 45-89% yields). A switch to continuous-flow conditions enabled a reduction of the reaction time with a concomitant increase of the reaction yields (batch: 45-89% yields *vs.* continuous-flow: 61-98% yields). The radical addition of two CF₂CO₂Et groups was observed with benzofuranyl- and thiophenyl-containing substrates, yielding the respective *bis*-functionalized derivatives. Other difluoroalkyl precursors including BrCF₂PO(OEt)₂ and bromodifluoroacetamide derivatives efficiently promoted the heteroaryl migration. Mechanistic experiments with the radical scavenger 2,6-di-*tert*-butyl-4-methylphenol (BHT) corroborated the involvement of a radical-mediated difluoroalkylation.

Alkynyl-substituted difluoroalkyl ketones were achieved by photoinduced difluoroalkylation of unactivated alkenes (**171**) with BrCF₂CO₂Et and subsequent migration of the alkynyl groups (**172**, Scheme 38: 17 examples, 20-78% yields) [103]. A series of aromatic alkynyl motifs bearing electron-donating and electron-withdrawing groups exhibited this migratory aptitude. The developed methodology

can be extended to different difluoroalkyl reagents such as bromodifluoroacetamides and 2-bromo-2,2-difluoro-1-morpholinoethan-1-one.



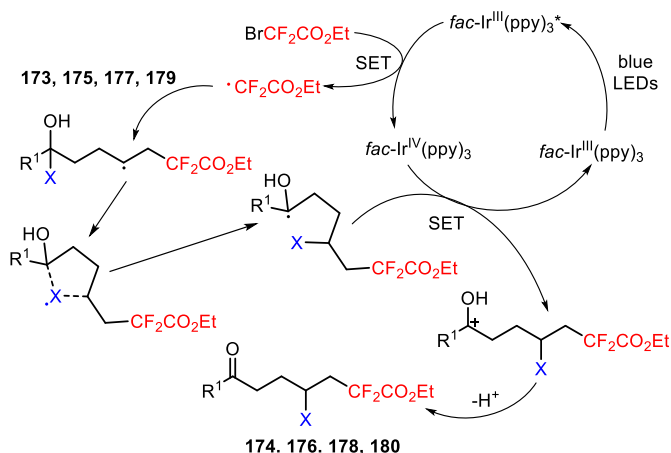
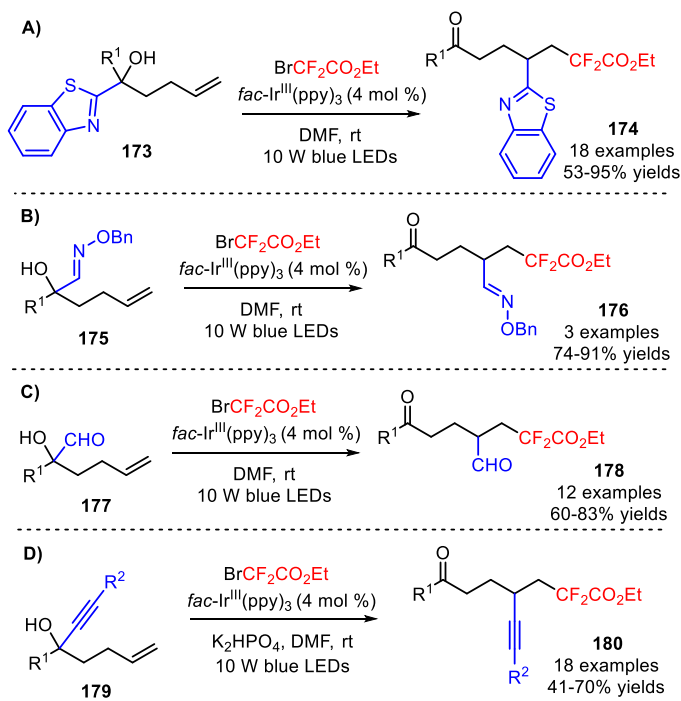
Scheme 37. Photocatalytic difluoroalkylation-induced 1,2-heteroaryl migration of allylic alcohols (**169**).



Scheme 38. Photoinduced difluoroalkylation of unactivated alkenes (**171**) in the presence of *fac*- $\text{Ir}^{\text{III}}(\text{ppy})_3$.

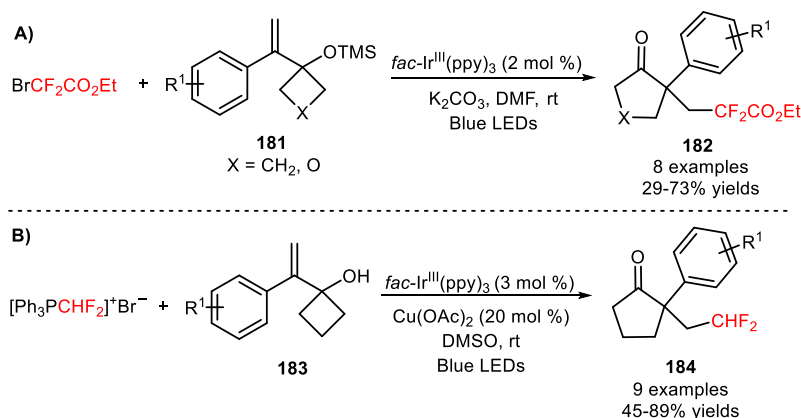
The strategy of distal functional group migration was also implemented by Zhu and collaborators for the carbodifluoroalkylation of unactivated alkenes (**173**, **175**, **177**, **179**) in combination with visible light photocatalysis [104]. For the carbodifluoroalkylation process, intramolecular migration was observed for products bearing a series of functional groups including heteroaryl (**174**, Scheme 39A: 18 examples, 53-95% yields), imino (**176**, Scheme 39B: 3 examples, 74-91% yields), formyl (**178**, Scheme 39C: 12 examples, 60-83% yields), and alkynyl groups (**180**, Scheme 39D: 18 examples, 41-70% yields), in the presence of *fac*- $\text{Ir}^{\text{III}}(\text{ppy})_3$ and $\text{BrCF}_2\text{CO}_2\text{Et}$. The

authors suggested a mechanism involving electrophilic addition of $\text{CF}_2\text{CO}_2\text{Et}$ radicals to the alkene moiety and subsequent cyclization with the radical acceptor groups (heteroaryl, imino, formyl, and alkynyl groups). Ring-opening homolysis followed by oxidation *via* $\text{fac-Ir}^{\text{IV}}(\text{ppy})_3$ and base-mediated deprotonation gave the respective difluoroalkylated ketones (**174**, **176**, **178**, **180**).



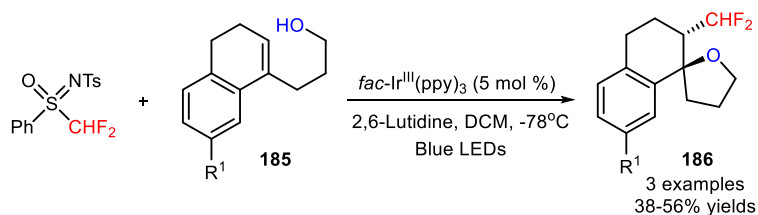
Scheme 39. Visible light-induced heteroaryl- (**173**), imino- (**175**), formyl- (**177**), and alkynyl-difluoroalkylation of unactivated alkenes (**179**) based on distal functional group migration and the proposed mechanism.

Visible light-mediated difluoroalkylation of 1-(1-arylvinyl)cyclobutanol derivatives (**181**, **183**) and ring expansion *via* 1,2 carbon migration was described by Kim and collaborators using the difluoroalkyl precursors BrCF₂CO₂Et [105] and [Ph₃PCHF₂]⁺Br⁻ [106]. A wide range of 1-(1-arylvinyl)cyclobutanols bearing electron-donating, electron-neutral, and electron-withdrawing groups furnished the difluoroalkyl-substituted cyclic ketones with moderate to good yields (**182**, Scheme 40A: 8 examples, 29-73% yields; **184**, Scheme 40B: 9 examples, 45-89% yields).



Scheme 40. Visible light-induced photocatalytic difluoroalkylation/1,2-carbon migration of 1-(1-arylvinyl)cyclobutanol derivatives (**181**, **183**) with BrCF₂CO₂Et (**A**) and [Ph₃PCHF₂]⁺Br⁻ (**B**).

The difluoromethyl precursor *N*-tosyl-*S*-difluoromethyl-*S*-phenylsulfoximine was effectively implemented in the diastereoselective synthesis of *anti*-difluoromethyl-substituted spiroethers through visible light-mediated oxy-difluoromethylation of aryl-fused cycloalkenyl alcohol derivatives (**185**) in the presence of *fac*-Ir^{III}(ppy)₃ (**186**, Scheme 41: 3 examples, 38-56% yields) [107].

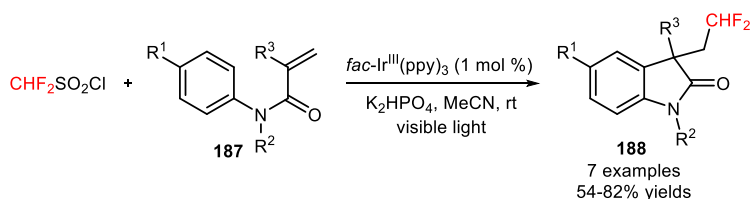


Scheme 41. Oxy-difluoromethylation of aryl-fused cycloalkenylalkanols (**185**) with *N*-tosyl-*S*-difluoromethyl-*S*-phenylsulfoximine under visible light photoredox conditions.

2.3. Difluoroalkylation of *sp*² Carbon Atoms in Unsaturated Amides, Hydrazones, and Allylamines

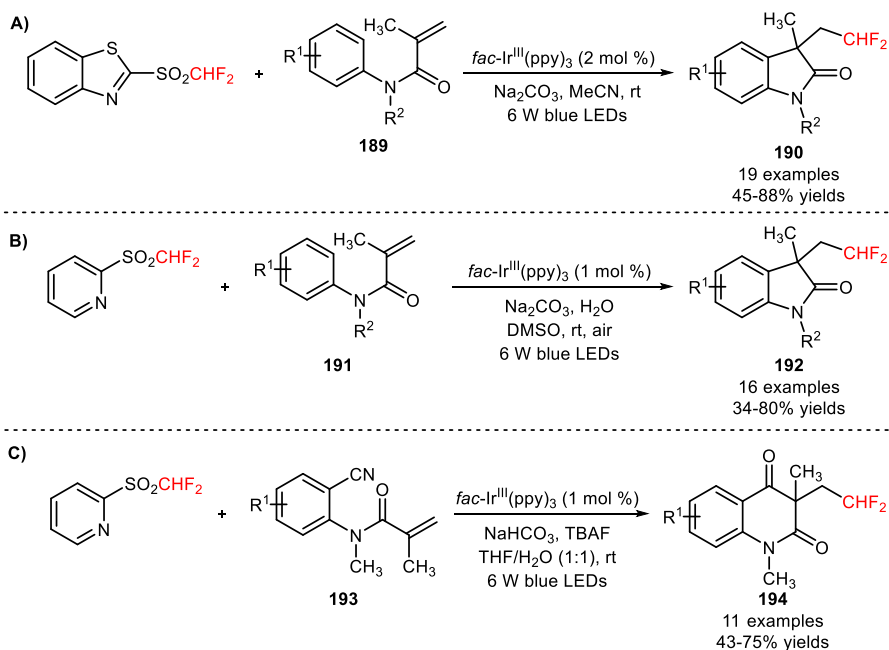
The radical difluoroalkylation of a series of unsaturated amides has been employed as an efficient strategy of producing synthetic precursors to access more complex and functionalized heterocyclic derivatives. In 2014, Dolbier and collaborators disclosed a methodology for tandem difluoromethylation of *N*-

arylacrylamides (**187**) with $\text{CHF}_2\text{SO}_2\text{Cl}$ and consecutive cyclization, under irradiation with visible light [108]. The authors found that the *fac*- $\text{Ir}^{\text{III}}(\text{ppy})_3$ was the most effective catalyst for the reduction of $\text{CHF}_2\text{SO}_2\text{Cl}$ and generation of CHF_2 radicals under mild conditions. The introduction of electron-donating and electron-withdrawing groups in the aromatic ring of *N*-arylacrylamides (**187**) was well tolerated with the desired organic transformation affording the respective difluoromethylated 3,3-disubstituted 2-oxindoles in moderate to good yields (**188**, Scheme 42: 7 examples, 54-82% yields).



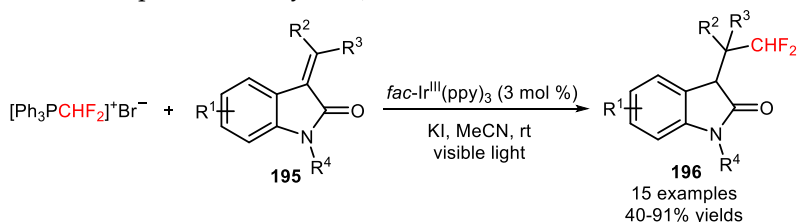
Scheme 42. Visible light-mediated tandem difluoromethylation/cyclization of *N*-arylacrylamides (**187**) with $\text{CHF}_2\text{SO}_2\text{Cl}$.

The reagents 2-BT SO_2CHF_2 and difluoromethyl pyridyl-sulfone (2-Py SO_2CHF_2 , CAS number: 1219454-89-3) were also implemented in the photocatalytic difluoromethylation of *N*-arylacrylamides (**189**, **191**, **193**) in the presence of *fac*- $\text{Ir}^{\text{III}}(\text{ppy})_3$ and a base (either Na_2CO_3 or NaHCO_3) [109,110]. This procedure allowed the access to a wide range of difluoromethylated oxindoles (**190**, Scheme 43A: 19 examples, 45-88% yields; **192**, Scheme 43B: 16 examples, 34-80% yields) and quinoline-2,4-diones (**194**, Scheme 43C: 11 examples, 43-75% yields) in moderate to good yields.



Scheme 43. Visible light-induced difluoromethylation of *N*-arylacrylamides (**189**, **191**, **193**) with the reagents 2-BT SO_2CHF_2 (A) and 2-Py SO_2CHF_2 (B, C).

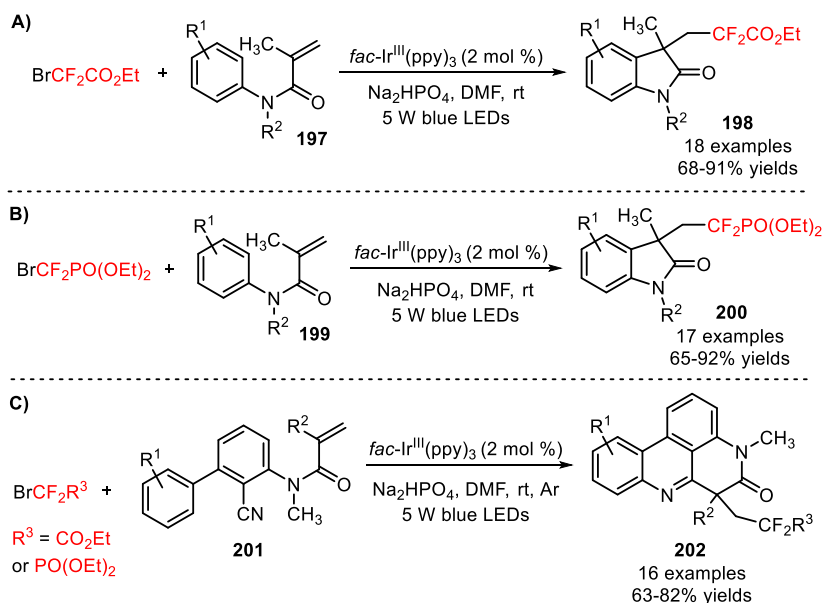
An alternative methodology for the synthesis of difluoromethylated oxindoles was developed by Qing and co-workers through the photoinduced hydro-difluoromethylation of oxindole-derived alkenes (**195**) using the difluoromethylating reagent $[\text{Ph}_3\text{PCHF}_2]^+\text{Br}^-$ [111]. In the presence of *fac*- $\text{Ir}^{\text{III}}(\text{ppy})_3$, a wide range of oxindole-derived alkenes bearing electron-donating and electron-withdrawing substituents on their aromatic ring and polysubstituted oxindole derived-alkenes afforded the hydro-difluoromethylated derivatives in moderate to high yields (**196**, Scheme 44: 15 examples, 40-91% yields).



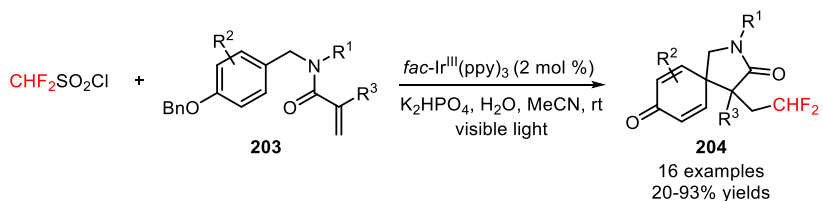
Scheme 44. Photoinduced difluoromethylation of oxindole-derived alkenes (**195**).

Other difluoroalkylating reagents, including $\text{BrCF}_2\text{CO}_2\text{Et}$ and $\text{BrCF}_2\text{PO}(\text{OEt})_2$, have been implemented in the preparation of difluoroalkylated oxindoles from *N*-arylacrylamides (**197**, **199**), in the presence of *fac*- $\text{Ir}^{\text{III}}(\text{ppy})_3$ and the base Na_2HPO_4 (**198**, Scheme 45A: 18 examples, 68-91% yields; **200**, Scheme 45B: 17 examples, 65-92% yields) [112,113]. In 2017, Sun and co-workers developed a methodology for the photoinduced difluoroalkylation with $\text{BrCF}_2\text{CO}_2\text{Et}$ and $\text{BrCF}_2\text{PO}(\text{OEt})_2$ of *N*-arylacrylamides (**201**) and consecutive intramolecular radical addition to the cyano groups and homolytic aromatic substitution [114]. A variety of *N*-arylacrylamides bearing electron-donating and electron-withdrawing groups on the aromatic ring furnished the difluoroalkylated phenanthridines (**202**, Scheme 45C: 16 examples, 63-82% yields). Alternative approaches for the synthesis of functionalized phenanthridines from biphenyl isocyanides will be discussed in Section 2.5.

Difluoromethylated 2-azaspiro[4.5]deca-6,9-diene-3,8-diones (**204**) were prepared by Dolbier and collaborators *via* the photoinduced difluoromethylation of *N*-benzylacrylamides (**203**) with $\text{HCF}_2\text{SO}_2\text{Cl}$ and subsequent 5-*exo*-cyclization [115]. Apart from the relevance of *fac*- $\text{Ir}^{\text{III}}(\text{ppy})_3$ and the base K_2HPO_4 in the difluoromethylation/5-*exo*-cyclization process, the addition of water to the reaction system influenced significantly its efficiency. A wide scope of *N*-benzylacrylamides containing *N*-substituents such as cyclohexyl, isopropyl, *n*-butyl, and *tert*-butyl, and electron-rich and electron-deficient aromatic substituents furnished the desired products (**204**, Scheme 46: 16 examples, 20-93% yields). The authors found that the steric properties of the *N*-substituents may influence the efficiency of the spirocyclization process. This synthetic approach can be extended to other fluoroalkyl radical sources, in particular $\text{BrCF}_2\text{CO}_2\text{Et}$.



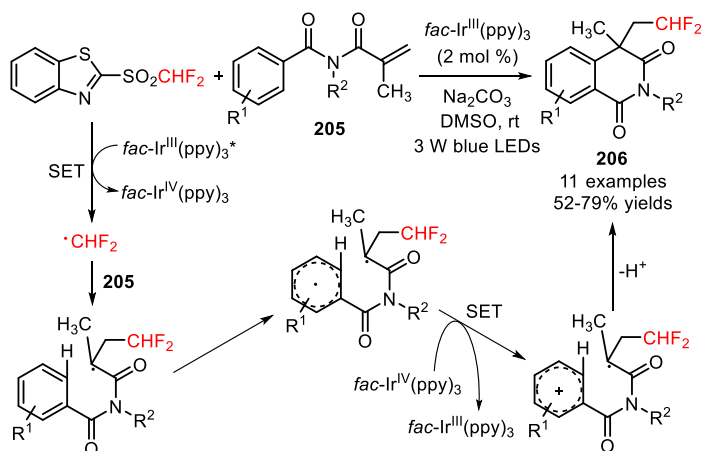
Scheme 45. Visible light-driven difluoroalkylation of *N*-arylacrylamides (**197**, **199**, **201**) with $\text{BrCF}_2\text{CO}_2\text{Et}$ (**A**), $\text{BrCF}_2\text{PO}(\text{OEt})_2$ (**B**) and both reagents (**C**).



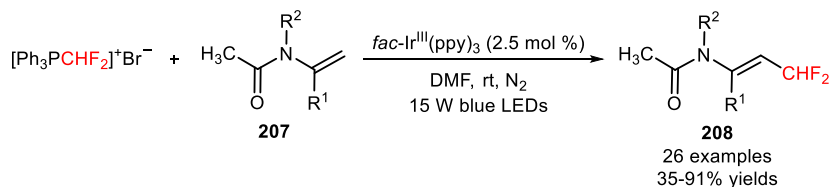
Scheme 46. Photoinduced difluoromethylation/5-*exo* radical cyclization of *N*-benzylacrylamides (**203**).

Later, Wang's group used $2\text{-BTSO}_2\text{CHF}_2$ for the radical difluoromethylation of *N*-methacryloylbenzamides (**205**) and consecutive intramolecular cyclization, under visible light photoredox conditions [116]. A palette of difluoromethylated isoquinoline-1,3(*2H,4H*)-diones bearing *N*-alkyl substituents, electron-rich, and electron-deficient aromatic substituents on the benzamide moiety was successfully obtained in moderate to good yields (**206**, Scheme 47: 11 examples, 52-79% yields). The authors suggested a mechanism involving oxidative quenching of $\text{fac-Ir}^{\text{III}}(\text{ppy})_3^*$ and reduction of $2\text{-BTSO}_2\text{CHF}_2$ to CHF_2 radicals for the preparation of the difluoromethylated products (**206**).

Under irradiation of 15 W blue LEDs, the reagent $[\text{Ph}_3\text{PCHF}_2]^+\text{Br}^-$ was implemented in the difluoromethylation of enamides (**207**) using $\text{fac-Ir}^{\text{III}}(\text{ppy})_3$ as a photocatalyst and DMF as a solvent [117]. A broad range of β -difluoromethylated enamides bearing electron-donating and electron-withdrawing substituents attached to the phenyl rings was synthesized in a stereoselective manner (*E* configuration) (**208**, Scheme 48: 26 examples, 35-91% yields).



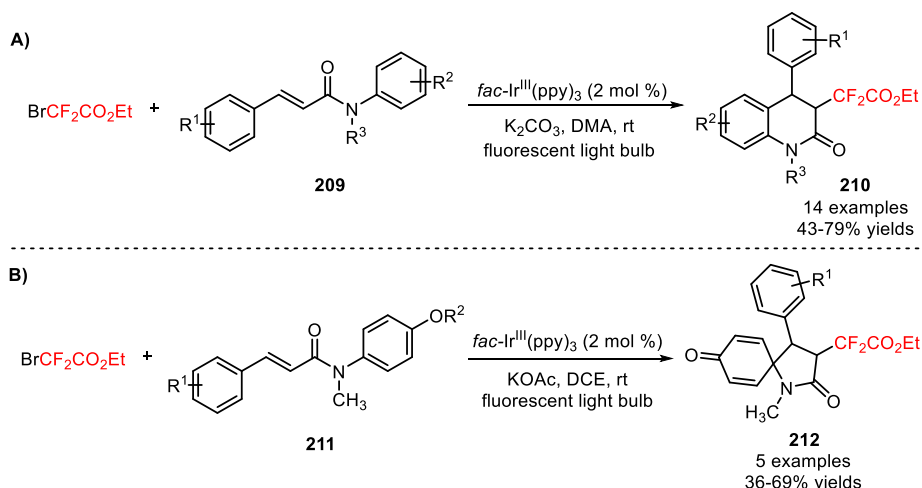
Scheme 47. Visible light-driven difluoromethylation of *N*-methacryloyl benzamides (**205**) with 2-BTSO₂CHF₂.



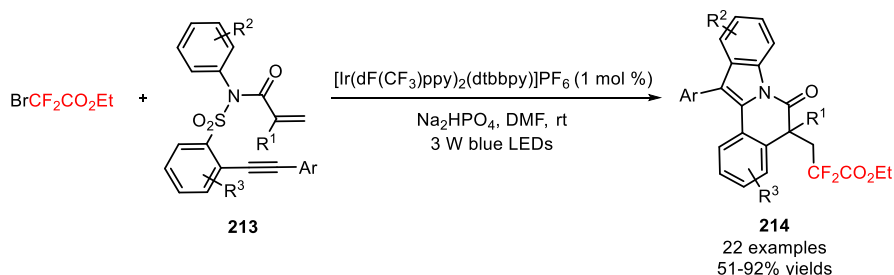
Scheme 48. Photoinduced difluoromethylation of enamides (**207**) with [Ph₃PCHF₂]⁺Br⁻.

N-Phenylcinnamamides were applied as substrates for the visible light-catalyzed difluoroalkylation using the reagent BrCF₂CO₂Et [118]. In the presence of *fac*-Ir^{III}(ppy)₃, a broad scope of *N*-phenylcinnamamides possessing bulky groups at the *N*-position and electron-withdrawing groups attached to the aromatic rings (**209**) proved to be compatible substrates for the synthesis of difluoroalkylated quinoline-2-ones after intramolecular 6-*endo* cyclization (**210**, Scheme 49A: 14 examples, 43-79% yields). A different pattern of cyclization was found when methoxy or hydroxy groups were attached to the aromatic amide moiety in the *para* position of the aromatic rings (**211**). The unexpected 5-*exo* cyclization/dearomatization process afforded the respective difluoroalkylated spiro[4.5]decanes under the defined reaction conditions (**212**, Scheme 49B: 5 examples, 36-69%).

Difluoroalkylated tetracycles embedded with indole and dihydroisoquinolinone scaffolds (**214**) were effectively constructed by the photoinduced difluoroalkylation/cyclization of 1,8-enynes (**213**) with the reagent BrCF₂CO₂Et, in the presence of [Ir(dF(CF₃)ppy)₂(dtbbpy)]PF₆ [119]. Under irradiation with 3 W blue LEDs, the combination of the selected photocatalyst with the base Na₂HPO₄ provided the best reaction conditions for the respective difluoroalkylation process (**214**, Scheme 50: 22 examples, 51-92% yields). The difluoroalkyl group of the corresponding products can undergo postfunctionalization steps and be converted into difluoroalkylated alcohol, amide or carboxylic acid derivatives.



Scheme 49. Photoinduced difluoroalkylation of *N*-phenylcinnamamides (**209**, **211**) for the regioselective synthesis of difluoroalkylated quinoline-2-ones (6-*endo* cyclization) (**210**) and 1-azaspiro[4.5]decanes (5-*exo* cyclization/dearomatization) (**212**).

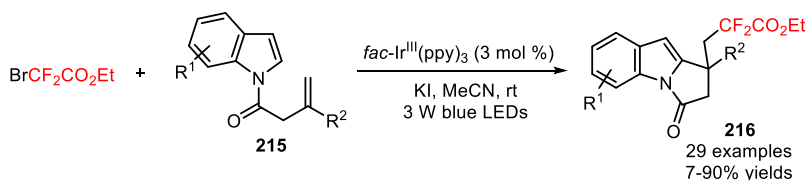


Scheme 50. Visible light-mediated radical difluoroalkylation/cyclization of 1,8-enynes (**213**).

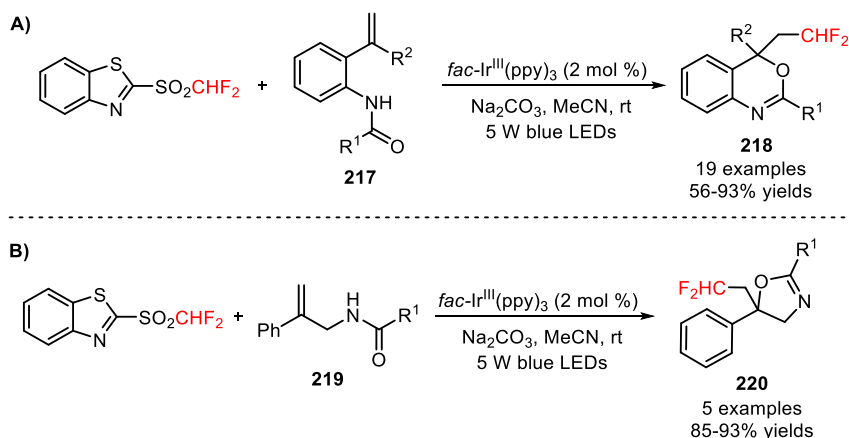
Recently, Li and co-workers applied the difluoroalkylating reagent $\text{BrCF}_2\text{CO}_2\text{Et}$ for the preparation of difluoroalkylated pyrrolo[1,2-*a*]indoles (**216**) from *N*-(but-2-enyl)indoles (**215**), under irradiation with 3 W blue LEDs [120]. The introduction of electron-donating and electron-withdrawing groups on the aromatic ring and of structurally distinct functional groups on the heteroarene ring of the indole moiety (e.g., cyano, ester, formyl, phenyl, and methyl substituents) was compatible with the desired organic transformation (**216**, Scheme 51: 29 examples, 7-90% yields). Remarkably, difluoroalkylation with alternative reagents derived from difluoroalkyl bromides, including bromoacetates, bromodifluoromethyl ketones, bromodifluoroacetamides, and $\text{BrCF}_2\text{PO}(\text{OEt})_2$ proceeded smoothly with the described methodology.

An efficient methodology involving the visible light-induced incorporation of CHF_2 groups in benzamides (**217**) with 2-BT SO_2CHF_2 and concomitant cyclization to a benzoxazine ring has been reported [121]. A variety of benzamides possessing electron-neutral, electron-donating, and electron-withdrawing groups onto the

aromatic rings, heterocyclic, and aliphatic groups (**217**) was efficiently converted into the difluoromethylated benzoxazines (**218**, Scheme 52A: 19 examples, 56-93% yields). Mechanistic experiments with radical scavengers suggested the occurrence of radical-mediated difluoromethylation process and reduction of 2-BT SO_2CHF_2 to CHF_2 radicals *via* oxidative quenching of *fac*-Ir^{III}(ppy)₃*. This protocol was expanded to the difluoromethylation of *N*-allylamides (**219**) in excellent yields (**220**, Scheme 52B: 5 examples, 85-93% yields).



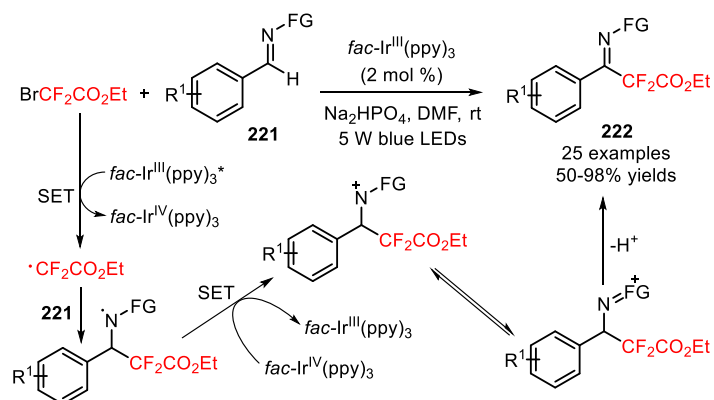
Scheme 51. Photoinduced difluoroalkylation/cyclization reaction of *N*-(but-2-enyl)indoles (**215**).



Scheme 52. Visible light-mediated radical oxy-difluoromethylation of benzamides (**217**) and *N*-allylamides (**219**) and with 2-BT SO_2CHF_2 .

Radical difluoroalkylation of the sp^2 -hybridized carbon atom of C=N bonds in aldehyde-derived hydrazones (**221**) with $\text{BrCF}_2\text{CO}_2\text{Et}$ was reported by Zhu and co-workers [122]. The selection of the photocatalyst *fac*-Ir^{III}(ppy)₃, the base Na₂HPO₄, and the use of 5 W LEDs as light source resulted in an enhanced efficiency of the difluoroalkylation process (Scheme 53). The introduction of an *N,N*-dialkyl structural motif was critical for the reactivity of *N*-substituted aldehyde-derived hydrazones. Interestingly, a large diversity of *N,N*-dialkyl aldehyde-derived hydrazones bearing electron-rich and electron-deficient aromatic groups, heteroaryl, and aliphatic groups (**221**) furnished the difluoroalkylated hydrazones with moderate to excellent yields (**222**, 25 examples, 50-98% yields). Other difluoroalkyl motifs, including bromodifluoroacetamides and phenylalanine-derived bromodifluoroamide, were also compatible with the developed difluoroalkylation procedure. Two possible reaction pathways were proposed for the formation of difluoroalkyl-containing

hydrazones (**222**): an aminyl radical/polar process and a carbon radical/polar process. Computational calculation of Gibbs free-energy profiles for both reaction pathways excluded the occurrence of a carbon radical/polar process. Therefore, the authors proposed a mechanism involving the addition of $\text{CF}_2\text{CO}_2\text{Et}$ radicals to the $\text{C}=\text{N}$ bond of the substrates (**221**) and generation of an aminyl radical intermediate. Concurrently, the aminyl radical was oxidized *via* $\text{fac-Ir}^{\text{IV}}(\text{ppy})_3$ to an aminyl cation (aminyl radical/polar cross-over step). Further tautomerization and deprotonation then furnished the corresponding difluoroalkylated products (**222**).

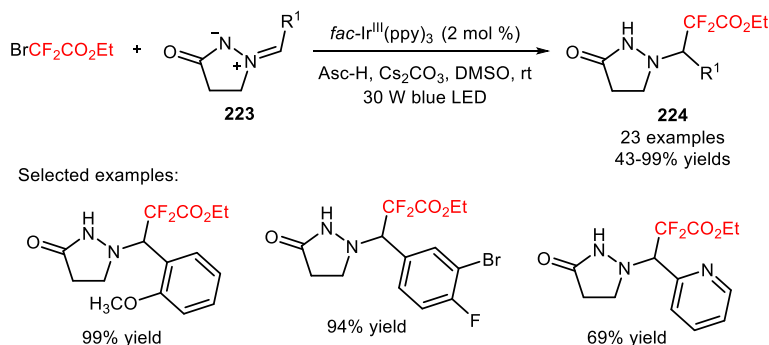


Scheme 53. Visible light-induced difluoroalkylation of aldehyde-derived hydrazones (**221**) with $\text{BrCF}_2\text{CO}_2\text{Et}$ and the proposed mechanism *via* an aminyl radical/polar pathway.

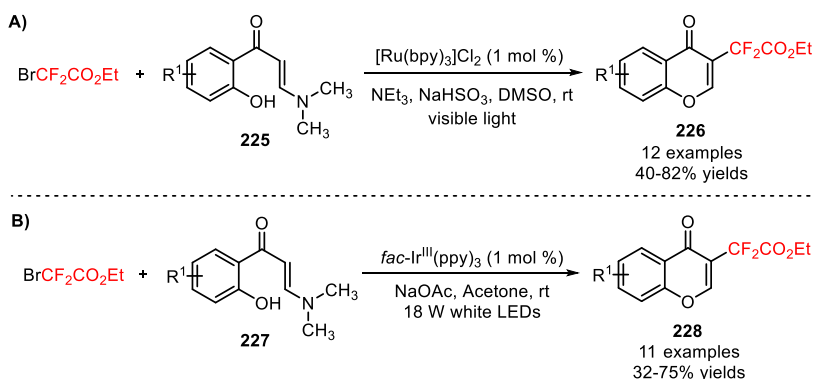
Later, Yang and collaborators developed a visible light-induced difluoroalkylation of N,N' -cyclicazomethine imines (**223**) with $\text{BrCF}_2\text{CO}_2\text{Et}$ through a radical-radical cross-coupling process [123]. Based on the reduction potential of the N,N' -cyclicazomethine imines ($E_{\text{red}} = -1.61$ V *vs.* SCE in MeCN), the photocatalyst $\text{fac-Ir}^{\text{III}}(\text{ppy})_3$ ($E_{\text{red}} = -1.73$ V *vs.* SCE in MeCN) was chosen for the difluoroalkylation process due to their ability to undergo the reduction of the substrates. The photocatalytic difluoroalkylation of the substrates was performed in DMSO using ascorbic acid as reducing agent and Cs_2CO_3 as an additive. A variety of difluoroalkylated products with electron-donating and electron-withdrawing groups attached to phenyl rings and heterocyclic rings was synthesized in moderate to excellent yields (**224**, Scheme 54: 23 examples, 43-99% yields). The developed protocol was well tolerated to bromodifluoroacetamides and 2-(bromodifluoromethyl)-benzoxazole substrates as difluoroalkylating reagents.

Apart from unsaturated amides and hydrazones, the difluoroalkylation of allylamine derivatives such as *ortho*-hydroxyaryl enaminones has also been regarded as a promising approach to access more complex heterocyclic scaffolds of biological relevance. In 2017, two independent works reported by the Zhang [124] and Yang [125] groups have described the synthesis of functionalized chromones by the visible light-mediated difluoroalkylation of *ortho*-hydroxyaryl enaminones bearing electron-donating and electron-withdrawing groups (**225**, **227**) using the reagent $\text{BrCF}_2\text{CO}_2\text{Et}$

(**226**, Scheme 55A: 12 examples, 40-82% yields; **228**, Scheme 55B: 11 examples, 32-75% yields).

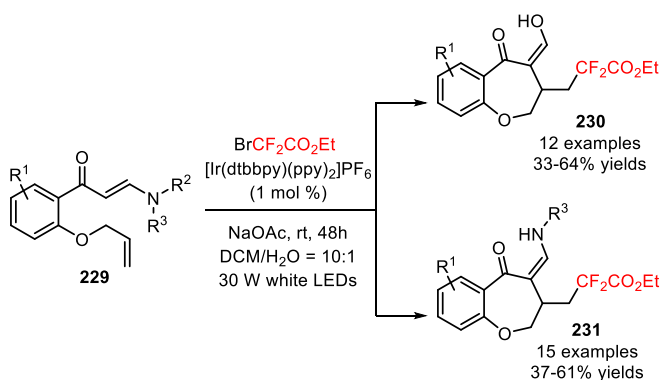


Scheme 54. Difluoroalkylation of *N,N'*-cyclicazomethine imines (**223**) with $\text{BrCF}_2\text{CO}_2\text{Et}$ under visible light photoredox conditions.



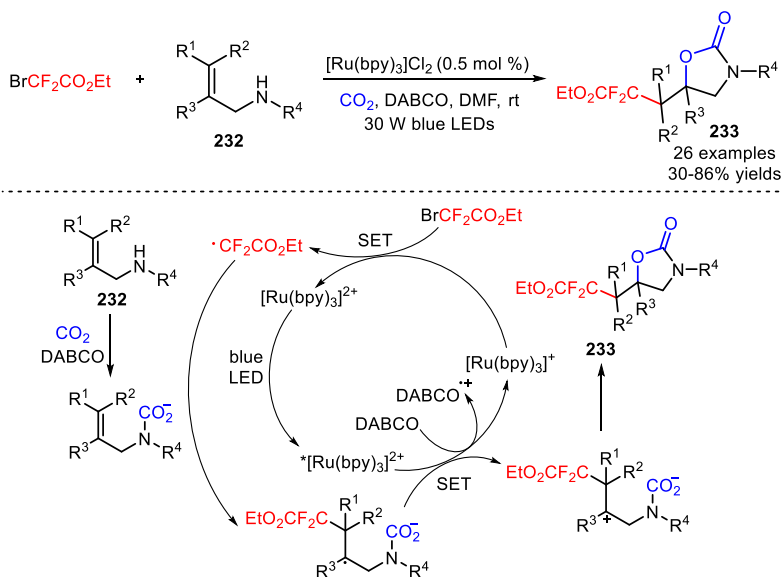
Scheme 55. Visible light-induced difluoroalkylation of *ortho*-hydroxyaryl enaminones (**225**, **227**) in the presence of $[\text{Ru}(\text{bpy})_3]\text{Cl}_2$ (**A**) and $\text{fac-Ir}^{\text{III}}(\text{ppy})_3$ (**B**).

Difluoroalkylated benzoxepines were prepared by the introduction of $\text{CF}_2\text{CO}_2\text{Et}$ groups into (*E*)-1-[2-(allyloxy)phenyl]-3-(substituted amino)prop-2-en-1-ones (**229**) under visible light photoredox conditions [126]. Yang's group envisioned that the design of a range of substrates bearing an enaminone moiety and an olefin functionality could trigger an efficient installation of difluoroalkyl moieties and simultaneous intramolecular annulation to afford seven-membered rings. The combined use of the photocatalyst $[\text{Ir}(\text{dtbbpy})(\text{ppy})_2]\text{PF}_6$ with $\text{BrCF}_2\text{CO}_2\text{Et}$, the base NaOAc , and the solvent mixture $\text{DCM}/\text{H}_2\text{O}$ (10:1) proved to be the optimal conditions for the difluoroalkyl radical-triggered annulation process (Scheme 56). Unexpectedly, the authors found that *N*-disubstituted enaminones could be hydrolyzed to the corresponding benzoxepines with a 1,3-dicarbonyl moiety. Substitution at both *meta*- and *para*-positions of the aromatic ring of *N*-disubstituted enaminones gave the corresponding products in moderate to good yields (**230**, 12 examples, 33-64% yields). In addition, *N*-monosubstituted substrates bearing structurally diverse acyclic and cyclic groups provided the desired benzoxepine derivatives without the occurrence of a deamination process (**231**, 15 examples, 37-61% yields).



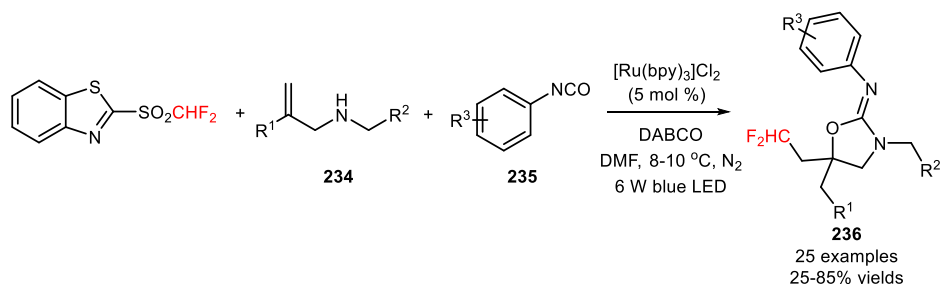
Scheme 56. Photoinduced difluoroalkylation of *N*-disubstituted and *N*-monosubstituted (*E*)-1-(2-(allyloxy)phenyl)-3-(substituted amino)prop-2-en-1-ones (**229**).

Yu and collaborators developed a novel approach for the utilization of CO_2 and $\text{BrCF}_2\text{CO}_2\text{Et}$ in the difluoroalkylation of allyl amines (**232**) and subsequent carboxylative cyclization *via* visible light photoredox catalysis, under atmospheric conditions [127]. In the presence of $[\text{Ru}(\text{bpy})_3]\text{Cl}_2$ and the base DABCO, a large variety of difluoroalkylated 2-oxazolidinones bearing electron-rich and electron-poor aromatic groups was obtained without detection of any amino-difluoroalkylated by-products (**233**, Scheme 57: 26 examples, 30-86% yields). The developed protocol was applied to the oxy-difluoroalkylation of substrates using other difluoroalkyl reagents such as $\text{BrCF}_2\text{PO}(\text{OEt})_2$, bromodifluoroacetamides, and 2-BT SO_2CHF_2 . The authors suggested a mechanism involving the intermediacy of $\text{CF}_2\text{CO}_2\text{Et}$ radicals *via* reductive quenching of $^*[\text{Ru}(\text{bpy})_3]^{2+}$ and oxidation of DABCO for the difluoroalkylation/carboxylative cyclization process.



Scheme 57. Radical difluoroalkylation/carboxylative cyclization of allylamines (**232**) with CO₂ and BrCF₂CO₂Et *via* visible light photoredox catalysis and the proposed mechanism.

Recently, Sheng and co-workers reported a synthetic method allowing the visible light promoted three-component reaction involving the reagent 2-BT₂SO₂CHF₂, aryl allylamines (**234**), and aryl isocyanates (**235**) [128]. Under irradiation with 6 W blue LED, the difluoromethylation reaction was performed in DMF with [Ru(bpy)₃]Cl₂ as a photocatalyst and DABCO as the base at 8-10 °C. Aryl allylamines and aryl isocyanates containing electron-donating and electron-withdrawing groups were compatible with the developed procedure (**236**, Scheme 58: 25 examples, 25-85% yields).



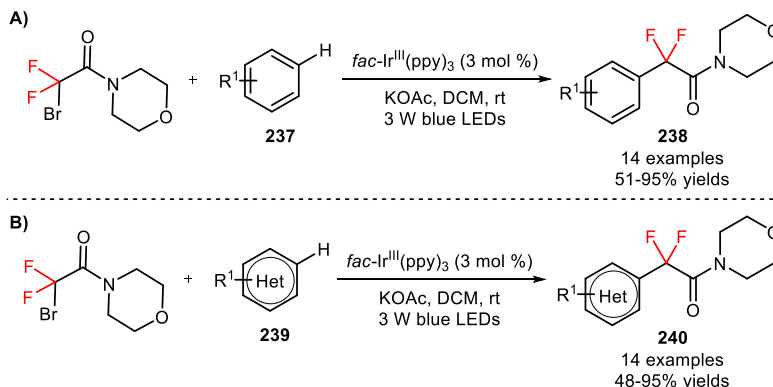
Scheme 58. Visible light-promoted three-component tandem reaction of aryl allylamines (**234**), aryl isocyanates (**235**) and the 2-BT₂SO₂CHF₂.

2.4. Difluoroalkylation of *sp*² Carbon Atoms in Arenes and Heteroarenes

Transition metal photocatalysis can also be considered as a very valuable tool in organic synthesis for the introduction of difluoroalkyl substituents in arenes and heteroarenes using various difluoroalkylating reagents.

The reagent 2-bromo-2,2-difluoro-1-morpholinoethan-1-one (CAS number: 149229-27-6) was employed by Liu and co-workers for the visible light-induced incorporation of difluoroalkyl moieties in unactivated arenes (**237**) and heteroarenes (**239**) [129]. An investigation of the reaction conditions using benzene as the organic substrate showed that the corresponding difluoroalkylated derivative was obtained in higher reaction yield when using DCM and the base KOAc, in the presence of *fac*-Ir^{III}(ppy)₃ (Scheme 59). The authors found that the difluoroalkylation procedure can be extended to a wide range of mono-, di-, and trisubstituted arenes bearing electron-donating and electron-withdrawing substituents (**238**, Scheme 59A: 14 examples, 51-95% yields) and heteroarenes (pyrazines, pyridazines, pyridines, pyrimidines, and thiophenes) (**240**, Scheme 59B: 14 examples, 48-95% yields). Alternative substrates with more complex aromatic rings such as napropamide (**241**) and pentoxifylline (**242**) can also be successfully difluoroalkylated (Figure 7). In addition, diverse bromodifluoroacetamides possessing distinct amino groups on the amide moiety, including aniline, cyclooctanamine, cyclopropylmethanamine, piperazine, piperidine, were all compatible for the desired organic transformation. A radical-

mediated mechanism was suggested by photoluminescence quenching, electron spin resonance (ESR), spin-trapping, and kinetic isotope effect (KIE) experiments.



Scheme 59. Difluoroacetamidation of unactivated arenes (**237**) and heteroarenes (**239**) with 2-bromo-2,2-difluoro-1-morpholinoethan-1-one.

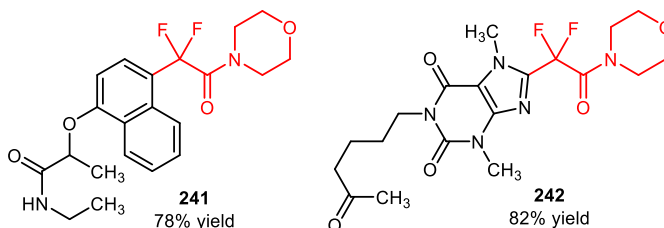
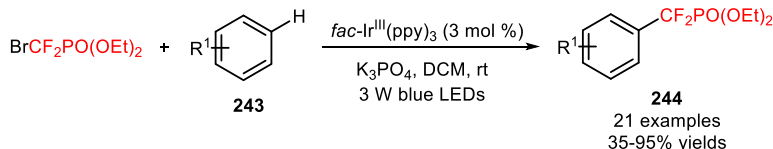


Figure 7. Chemical structures of difluoroacetamidated napropamide (**241**) and pentoxifylline (**242**).

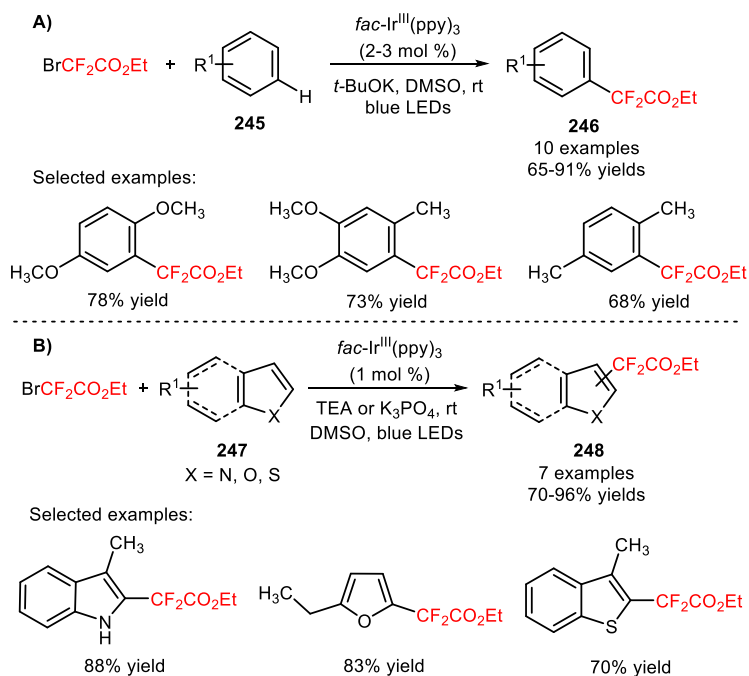
The same group implemented the reagent $\text{BrCF}_2\text{PO}(\text{OEt})_2$ for the introduction of $\text{CF}_2\text{PO}(\text{OEt})_2$ moieties in arenes and heteroarenes (**243**) under irradiation with 3 W blue LEDs [130]. Di- and trisubstituted arenes containing electron-donating and electron-withdrawing groups, and heteroarenes (benzofurans, benzothiophenes, furans, indoles, pyridines, pyrimidines, selenophenes, and thiophenes) afforded the phosphonodifluoromethylated derivatives in moderate to excellent yields (**244**, Scheme 60: 21 examples, 35-95% yields).



Scheme 60. Visible light-mediated phosphonodifluoromethylation of arenes and heteroarenes (**243**) with $\text{BrCF}_2\text{PO}(\text{OEt})_2$.

An efficient photocatalytic method for the synthesis of difluoroalkylated arenes and heteroarenes was developed by Cho's group [131]. The visible light-promoted difluoroalkylation of unactivated electron-rich arenes (**245**) was successfully achieved using $\text{BrCF}_2\text{CO}_2\text{Et}$ in the presence of $\text{fac-Ir}^{\text{III}}(\text{ppy})_3$ and the base $t\text{-BuOK}$ (**246**, Scheme

61A: 10 examples, 65-91% yields). Phosphorescence quenching experiments suggested that the difluoroalkylation process was mediated by the oxidative quenching of photoexcited *fac*-Ir^{III}(ppy)₃ and reduction of BrCF₂CO₂Et to CF₂CO₂Et radicals. Compared with electron-rich arenes, the heteroarenes (**247**) exhibited a higher reactivity, requiring a lower amount of photocatalyst and BrCF₂CO₂Et, and the weak bases TEA and K₃PO₄. Various difluoroalkylated heteroaromatics, including benzofurans, benzothiophenes, furans, indoles, pyrroles, thiophenes can be obtained using this protocol (**248**, Scheme 61B: 7 examples, 70-96% yields).

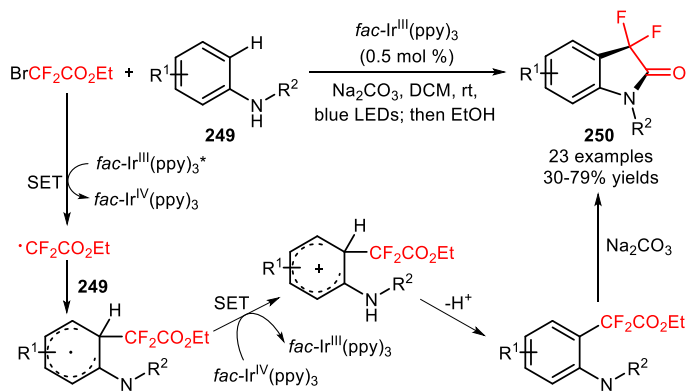


Scheme 61. Visible light-mediated difluoroalkylation of arenes (**245**) and heteroarenes (**247**) with BrCF₂CO₂Et.

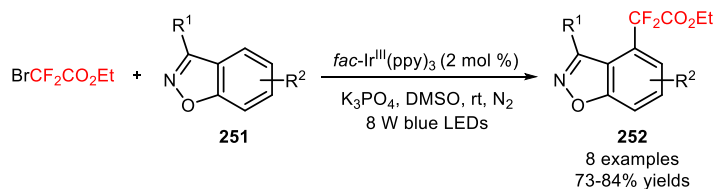
3,3-Difluoro-2-oxindoles (**250**) were successfully synthesized through *ortho*-difluoroalkylation of aniline derivatives (**249**) with BrCF₂CO₂Et and consecutive intramolecular amidation [132]. The difluoroalkylation/intramolecular amidation process exhibited an extensive substrate scope and a high functional group tolerance. In fact, the introduction of electron-neutral, electron-withdrawing, and electron-donating substituents on the aromatic ring of the aniline derivatives was well tolerated in the desired organic transformation (**250**, Scheme 62: 23 examples, 30-79% yields). Radical-trapping experiments with TEMPO suggested the intermediacy of CF₂CO₂Et radicals *via* oxidative quenching of *fac*-Ir^{III}(ppy)₃*.

Xiong and Zhang described a methodology enabling a direct difluoroalkylation of 3-substituted benzo[*d*]isoxazoles (**251**) with BrCF₂CO₂Et in DMSO with the *fac*-Ir^{III}(ppy)₃ as the photocatalyst and the K₃PO₄ as the base [133]. This procedure allowed

the regioselective synthesis of benzo[*d*]isoxazoles with difluoroalkyl groups at the C4 position (**252**, Scheme 63: 8 examples, 73-84% yields).

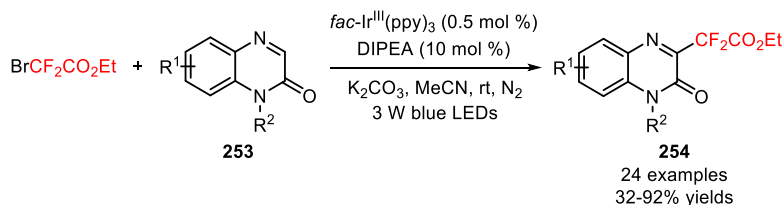


Scheme 62. Photoinduced difluoroalkylation and intramolecular amidation of anilines (**249**) with $BrCF_2CO_2Et$ and the proposed mechanism.



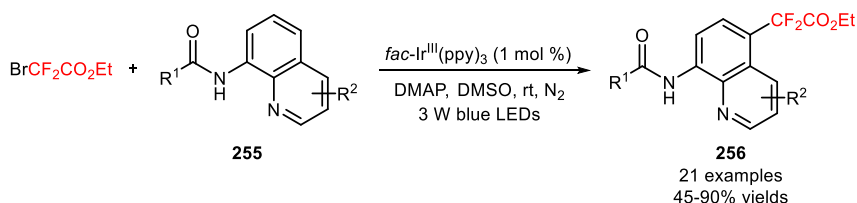
Scheme 63. Visible light-induced difluoroalkylation of 3-substituted benzo[*d*]isoxazoles (**251**) with $BrCF_2CO_2Et$.

Jin and colleagues developed an alternative approach for difluoroalkylation of quinoxalin-2(*1H*)-ones (**253**) that merges the visible light photoredox [$fac-Ir^{III}(ppy)_3$] and organoamine (DIPEA) catalysis [134]. A variety of quinoxalin-2(*1H*)-ones containing different *N*-protecting groups and bearing either electron-donating and electron-withdrawing groups attached to the phenyl rings afforded the difluoroalkylated products in satisfactory yields (**254**, Scheme 64: 24 examples, 32-92% yields). Apart from the $BrCF_2CO_2Et$, a series of bromofluoroacetamides containing aniline, dialkylamine, pyrrolidine, morpholine, thiomorpholine, and hexamethyleneimine groups can induce the difluoroalkylation of quinoxalin-2(*1H*)-ones.



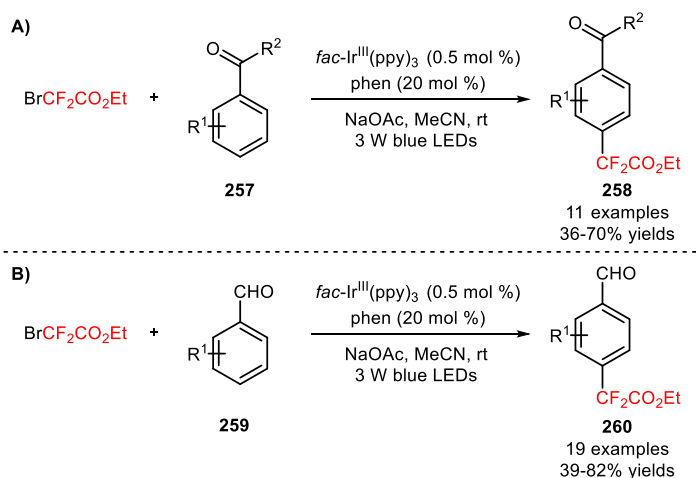
Scheme 64. Synthesis of difluoroalkylated quinoxalin-2(*1H*)-ones (**254**) under visible light photoredox conditions.

Later, Jin disclosed an efficient regioselective difluoroalkylation of 8-aminoquinolines (**255**) at C5 position with $\text{BrCF}_2\text{CO}_2\text{Et}$ in DMSO with *fac*- $\text{Ir}^{\text{III}}(\text{ppy})_3$ as the photocatalyst and the DMAP as the base [135]. A wide range of quinolines with electron-rich and electron-poor aromatic amide groups and aliphatic amide groups in C8 position was converted into the desired 5-difluoroalkylated derivatives (**256**, Scheme 65: 21 examples, 45-90% yields). Under the standard reaction conditions, the difluoroalkylation procedure can also be applied to other reagents including bromodifluoroacetamides, $\text{BrCF}_2\text{CO}_2\text{Me}$, and $\text{BrCF}_2\text{PO}(\text{OEt})_2$.



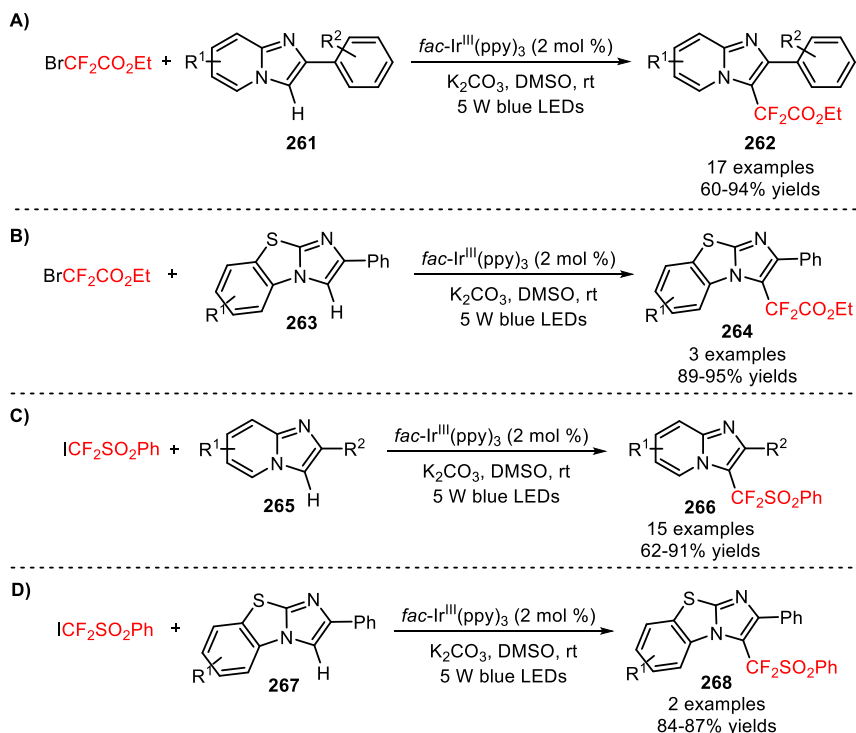
Scheme 65. Difluoroalkylation of 8-aminoquinolines (**255**) with $\text{BrCF}_2\text{CO}_2\text{Et}$ under visible light photoredox conditions.

Recently, Li and collaborators reported the use of $\text{BrCF}_2\text{CO}_2\text{Et}$ in *para*-selective difluoroalkylation of aryl ketones (**257**) and (hetero)aryl aldehydes (**259**) to give the corresponding products in good reaction yields (**258**, Scheme 66A: 11 examples, 36-70% yields; **260**, Scheme 66B: 19 examples, 39-82% yields) [136]. Under irradiation with 3 W blue LEDs, the efficiency and regioselectivity of the difluoroalkylation reaction of the carbonyl-containing substrates were mainly influenced by the presence of the photocatalyst [*fac*- $\text{Ir}^{\text{III}}(\text{ppy})_3$], the base (NaOAc), and the additive (phenanthroline). Bromodifluoroacetamides bearing distinct amine moieties such as aniline, morpholine, pyrrolidine, thiomorpholine, piperidine, and diethylamine groups were well tolerated in the difluoroalkylation of aryl aldehydes.



Scheme 66. Visible light-induced *para*-selective difluoroalkylation of aryl ketones (**A**) and (hetero)aryl aldehydes (**B**).

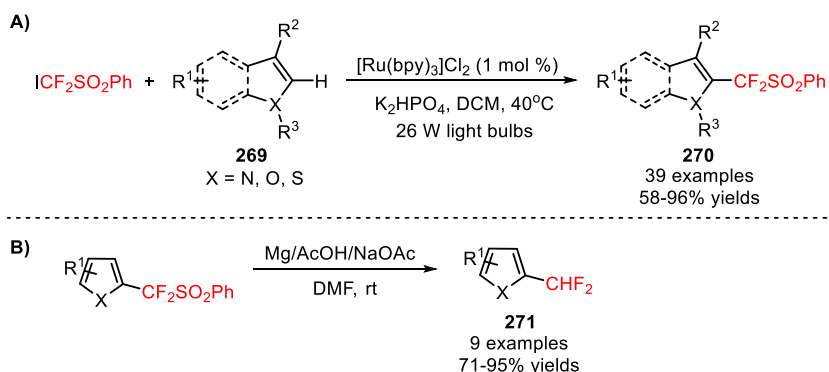
In 2017, Fu and collaborators reported two related research works concerning a methodology for the visible light difluoroalkylation of imidazo[1,2-*a*]pyridines (**261**, **265**) using the reagents BrCF₂CO₂Et (Scheme 67A) [137] and ICF₂SO₂Ph (Scheme 67C) [138], in the presence of *fac*-Ir^{III}(ppy)₃. Electron-rich, electron-neutral, and electron-deficient 2-arylimidazo[1,2-*a*]pyridines were compatible with the difluoroalkylation process using both reagents, and gave the corresponding products in moderate to excellent yields (**262**, Scheme 67A: 17 examples, 60-94% yields; **266**, Scheme 67C: 15 examples, 62-91% yields). The functionalization of benzo[*d*]-imidazo[2,1-*b*]thiazoles (**263**, **267**) was possible under the described reaction conditions (**264**, Scheme 67B: 3 examples, 89-95% yields; **268**, Scheme 67D: 2 examples, 84-87% yields).



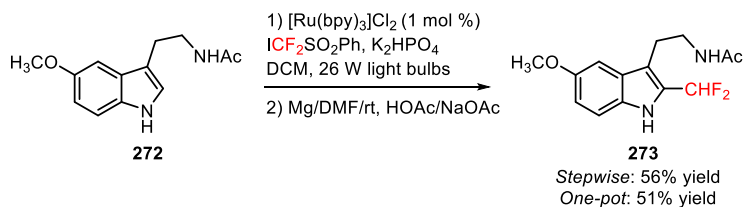
Scheme 67. Visible light-mediated difluoroalkylation of imidazo[1,2-*a*]pyridines (**261**, **265**) and benzo[*d*]-imidazo[2,1-*b*]thiazoles (**263**, **267**) with BrCF₂CO₂Et and ICF₂SO₂Ph.

The reagent ICF₂SO₂Ph was also efficiently applied in the difluoromethylation of *N*-, *O*-, and *S*-containing electron-rich heteroarenes (**269**) under irradiation with 26 W light bulbs [139]. In the presence of [Ru(bpy)₃]Cl₂, electron-rich and electron-deficient pyrroles, furans, thiophenes, indoles and other heteroarenes containing two heteroatoms furnished the respective CF₂SO₂Ph-containing heteroarenes (**270**, Scheme 68A: 39 examples, 58-96% yields). Mechanistic investigations involving radical scavengers suggested a radical-mediated difluoroalkylation process *via* oxidative quenching of *[Ru(bpy)₃]²⁺. Removal of the -SO₂Ph group through reductive desulfonylation afforded the difluoromethylated derivatives (**271**, Scheme 68B: 9

examples, 71-95% yields). Interestingly, an analogue of the natural product melatonin (**272**) can be difluoromethylated in *stepwise* and *one-pot* procedures (**273**, Scheme 69; *stepwise*: 56% yield; *one-pot*: 51% yield).

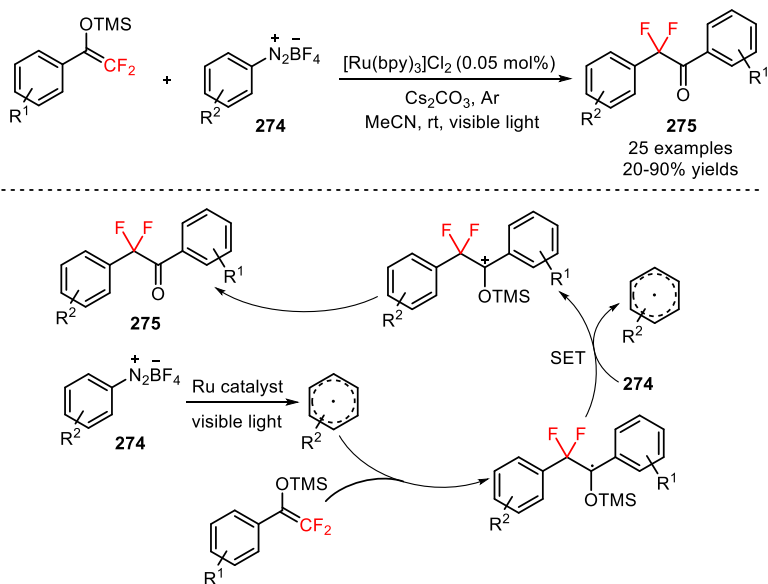


Scheme 68. A) Visible light-driven difluoroalkylation of *N*-, *O*-, and *S*-containing heteroarenes (**269**) with $\text{ICF}_2\text{SO}_2\text{Ph}$; B) Reductive desulfonation of $\text{CF}_2\text{SO}_2\text{Ph}$ -containing heteroarenes.



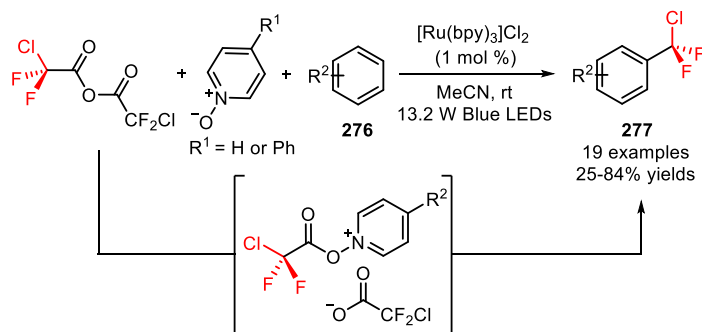
Scheme 69. Difluoromethylation of an analogue of melatonin (**272**) in *stepwise* and *one-pot* procedures.

Difluoroalkylation of arenediazonium tetrafluoroborates (**274**) was achieved using α -aryl- β,β -difluoroenol silyl ethers as the difluoroalkyl precursors under irradiation of visible light [140]. The selection of the photocatalyst $[\text{Ru}(\text{bpy})_3]\text{Cl}_2$ and the base Cs_2CO_3 was critical for preferential difluoroalkylation on the aromatic ring of the substrates and elimination of the unwanted difluoroalkylation of $\text{N}\equiv\text{N}$ bonds (Scheme 70). A wide range of arenediazonium tetrafluoroborates bearing electron-neutral and electron-withdrawing groups furnished the corresponding α -aryl- α,α -difluoro ketones in moderate to high yields (**275**, 25 examples, 20-90% yields). Quantum mechanical density functional theory calculations suggested a preferential mechanism involving the *in situ* generation of aryl radicals from arenediazonium tetrafluoroborates (**274**) via $^*[\text{Ru}(\text{bpy})_3]^{2+}$ species. Radical difluoroalkylation of aryl radicals, SET oxidation from another substrate, and abstraction of the trimethylsilyl group gave the respective α -aryl- α,α -difluoro ketones (**275**).



Scheme 70. Difluoroalkylation of arene diazonium tetrafluoroborates (**274**) under visible light photoredox conditions and the proposed mechanism.

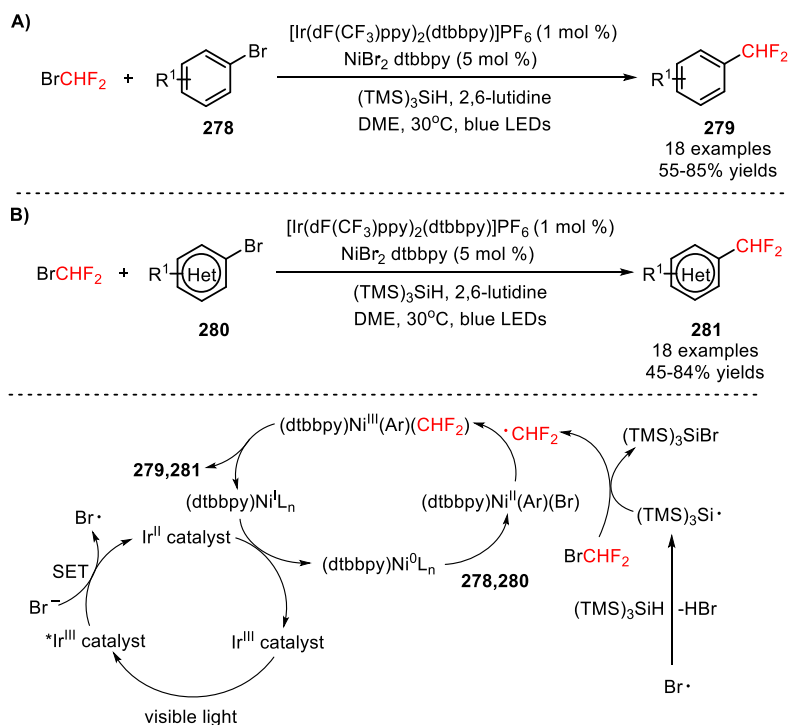
Stephenson's group achieved the radical chloro-difluoromethylation of arenes and heteroarenes (**276**) by *in situ* formation of a redox-active complex resulting from the combination of heterocyclic *N*-oxides (pyridine *N*-oxide and 4-phenylpyridine *N*-oxide) with the commercially available chlorodifluoroacetic anhydride $[(\text{ClCF}_2\text{CO})_2\text{O}]$, CAS number: 2834-23-3], in the presence of $[\text{Ru}(\text{bpy})_3]\text{Cl}_2$ [141]. Electron-rich heteroarenes and other pharmaceutically valuable agents with diverse functional groups were competent substrates for the desired organic transformation under both batch and flow conditions (**277**, Scheme 71: 19 examples, 25-84% yields). Interestingly, the chlorodifluoromethyl group-containing compounds (**277**) can be used as synthetic precursors to access electron-rich difluoromethylated arenes and heteroarenes.



Scheme 71. Photoinduced chlorodifluoromethylation of arenes and heteroarenes (**276**).

Recently, MacMillan's group reported a convenient approach for the direct difluoromethylation of aryl (**278**) and heteroaryl bromides (**280**) by combining nickel catalysis ($\text{NiBr}_2\cdot\text{dtbbpy}$) with iridium photocatalysis $\{[\text{Ir}(\text{dF}(\text{CF}_3)\text{ppy})_2(\text{dtbbpy})]\text{PF}_6\}$

[142]. Bromodifluoromethane (BrCHF_2 , CAS number: 1511-62-2) was employed as a direct source of CHF_2 radicals *via* a $(\text{TMS})_3\text{Si}$ radical-mediated halogen abstraction pathway. The authors suggested a mechanism of reductive quenching of $[\text{Ir}(\text{dF}(\text{CF}_3)\text{ppy})_2(\text{dtbbpy})]\text{PF}_6^*$ and simultaneous oxidation of the bromide anion. The resulting bromine radical can then induce the formation of $(\text{TMS})_3\text{Si}$ radicals that, in turn, can promote the bromine elimination from BrCHF_2 to afford the CHF_2 radicals. Concomitantly, an oxidative addition of the nickel catalyst to (hetero)aryl bromides and subsequent trapping of the CF_2 radicals afforded a $\text{CHF}_2\text{-Ni(II)}$ -(hetero)aryl intermediate. Reductive elimination gave the respective difluoromethylated arenes (**279**) and heteroarenes (**281**). Under irradiation with blue LEDs, a variety of aryl bromides bearing electron-withdrawing, electron neutral, and electron donating groups were compatible with the desired organic transformation (**279**, Scheme 72A: 18 examples, 55-85% yields). The developed strategy was extended to the late-stage difluoromethylation of heteroaryl bromides (**280**), including bromo-1*H*-benzoimidazoles, bromo-1*H*-indazoles, bromopyrazines, bromopyrazoles, bromopyridines, bromopyrimidines, bromoquinolines, and bromoquinoxalines (**281**, Scheme 72B: 18 examples, 45-84% yields) and analogues of sulfadimethoxine (**282**), celecoxib (**283**), indomethacin (**284**), and pomalidomide (**285**) (Figure 8).



Scheme 72. Metallaphotoredox difluoromethylation of aryl (**278**) and heteroaryl bromides (**280**) with BrCHF_2 .

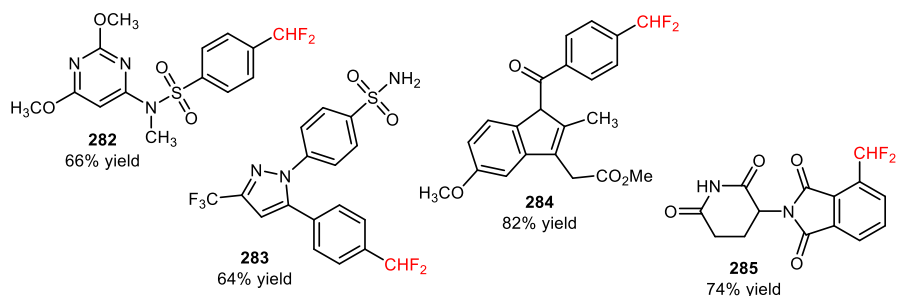
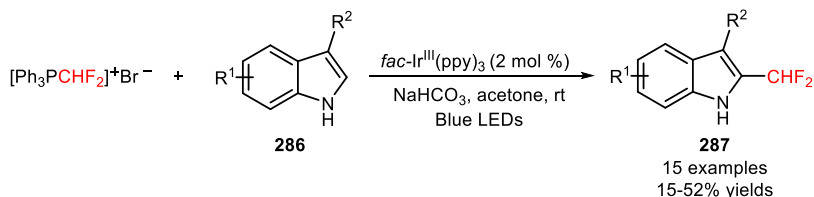


Figure 8. Chemical structures of difluoromethylated analogues of sulfadimethoxine (**282**), celecoxib (**283**), indometacin (**284**), and pomalidomide (**285**).

The reagent $[\text{Ph}_3\text{PCHF}_2]^+\text{Br}^-$ was recently applied to the visible light-induced difluoromethylation of *N*-unprotected indoles (**286**) bearing substituents on C3 position and on the phenyl ring of the indole skeleton (**287**, Scheme 73: 15 examples, 15-52% yields) [143].



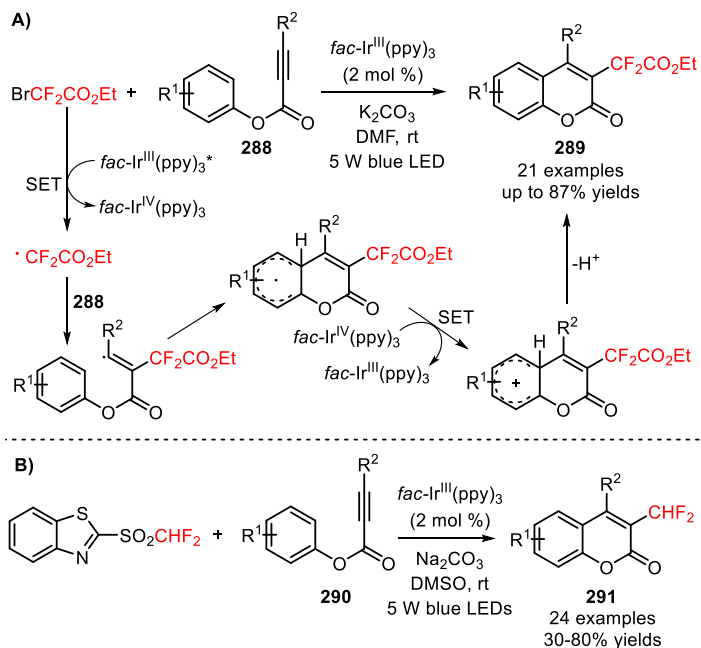
Scheme 73. Difluoromethylation of *N*-unprotected indoles (**286**) with $[\text{Ph}_3\text{PCHF}_2]^+\text{Br}^-$ by visible light photoredox catalysis.

2.5. Difluoroalkylation of *sp* Carbon Atoms in Alkynes and Biphenyl Isocyanides

Apart from the huge progress in visible light photocatalytic difluoroalkylation of sp^2 -hybridized carbon atoms in organic substrates, determined efforts have been also devoted to the exploration of efficient methodologies for the introduction of difluoroalkyl groups to *sp*-hybridized carbon atoms, including $\text{C}\equiv\text{C}$ bonds of alkynes and $\text{C}\equiv\text{N}$ bonds of biphenyl isocyanides. Direct difluoroalkylation of these substrates has been demonstrated to afford synthetically useful precursors for the construction of functionalized heterocyclic molecules, such as difluoroalkylated coumarins, quinolines, and phenanthridines, under visible light irradiation.

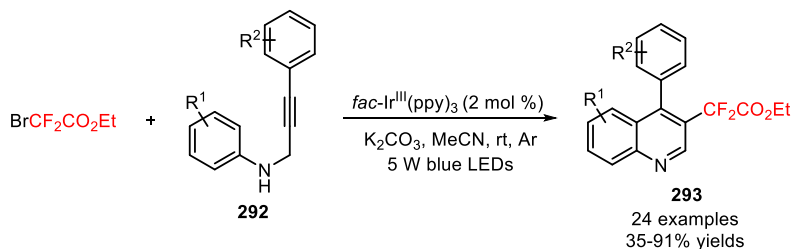
In 2015, Ji and collaborators described a protocol for the visible light-mediated difluoroalkylation of aryl 3-phenylpropiolates (**288**) with $\text{BrCF}_2\text{CO}_2\text{Et}$ and subsequent construction of a coumarin ring [144]. In the presence of $\text{fac-Ir}^{\text{III}}(\text{ppy})_3$, the radical difluoroalkylation/intramolecular annulation of a broad scope of aryl 3-phenylpropiolates bearing electron-donating and electron-withdrawing substituents in the aromatic rings gave the corresponding 3-difluoroalkylated coumarins (**289**, Scheme 74A: 21 examples, up to 87% yields). A mechanism of oxidative quenching of $\text{fac-Ir}^{\text{III}}(\text{ppy})_3^*$ and subsequent $\text{CF}_2\text{CO}_2\text{Et}$ radical-mediated difluoroalkylation of $\text{C}\equiv\text{C}$ bonds of the substrates (**288**) was proposed. Difluoromethyl-containing coumarins were also achieved *via* the photoinduced installation of CHF_2 groups in aryl 3-

phenylpropiolates (**290**) using 2-BTSO₂CHF₂ (**291**, Scheme 74B: 24 examples, 30-80% yields) [145].



Scheme 74. Visible light-mediated radical difluoroalkylation/intramolecular annulation of aryl 3-phenylpropiolates (**288**, **290**) with BrCF₂CO₂Et (**A**) and 2-BTSO₂CHF₂ (**B**).

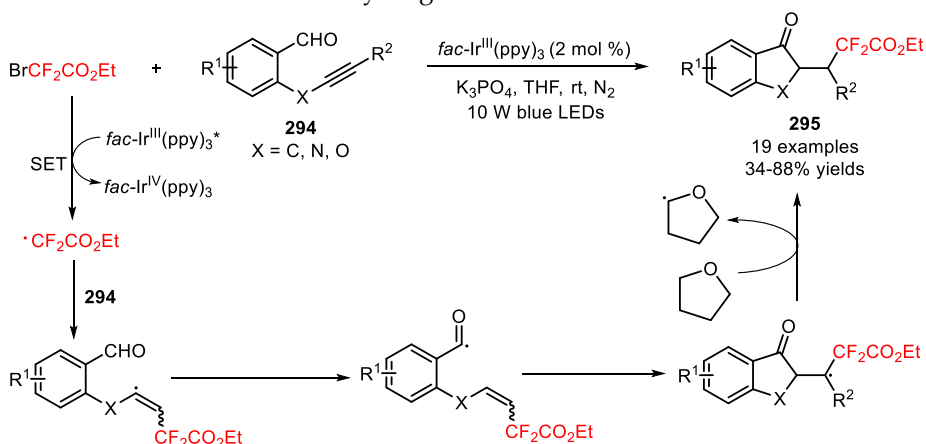
Recently, Sun and co-workers described a methodology for the visible light-induced radical difluoroalkylation of *N*-propargyl aromatic amines (**292**) with the reagent BrCF₂CO₂Et and consecutive cyclization to form a quinoline ring [146]. A large diversity of 3-difluoroalkylated quinolines bearing electron-withdrawing and electron-donating substituents on the aniline and benzene rings was effectively obtained in moderate to high yields (**293**, Scheme 75: 24 examples, 35-91% yields).



Scheme 75. Photoinduced cascade difluoroalkylation/cyclization of *N*-propargyl aromatic amines (**292**).

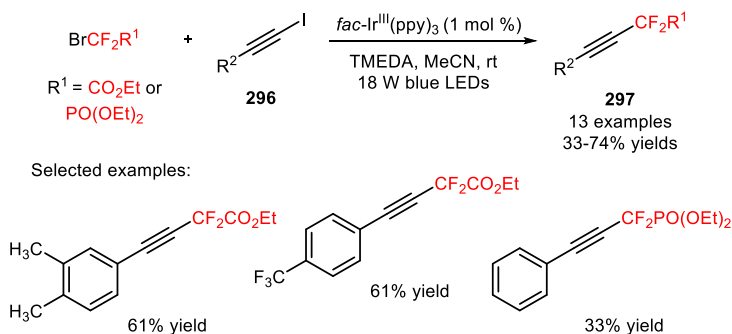
Alkynyl aldehydes (**294**) were also explored as substrates for the 1,1-hydrodifluoroalkylation and concurrent intramolecular acylation [147]. Under irradiation with 10 W blue LEDs, a range of difluoroalkylated cyclic ketones including indanones, chroman-4-ones, 2,3-dihydroquinolino-4(1*H*)-ones, and 3,4-

dihydronaphthalen-1(2*H*)-ones was synthesized in THF with the *fac*-Ir^{III}(ppy)₃ as the photocatalyst and the K₃PO₄ as the base at room temperature (**295**, Scheme 76: 19 examples, 34-88% yields). This methodology was compatible with bromodifluoroacetamides and 2-(bromodifluoromethyl)benzo[*d*]isoxazole as difluoroalkylating reagents. Experiments with radical scavengers and deuterium-labeled substrates revealed the intermediacy of CF₂CO₂Et and 2-tetrahydrofuranyl radicals, the involvement of an intramolecular hydrogen atom transfer, and the occurrence of an intermolecular hydrogen atom transfer with the THF.



Scheme 76. 1,1-Hydrodifluoroalkylation of alkynyl aldehydes (**294**) with BrCF₂CO₂Et under visible light photoredox conditions and the proposed mechanism.

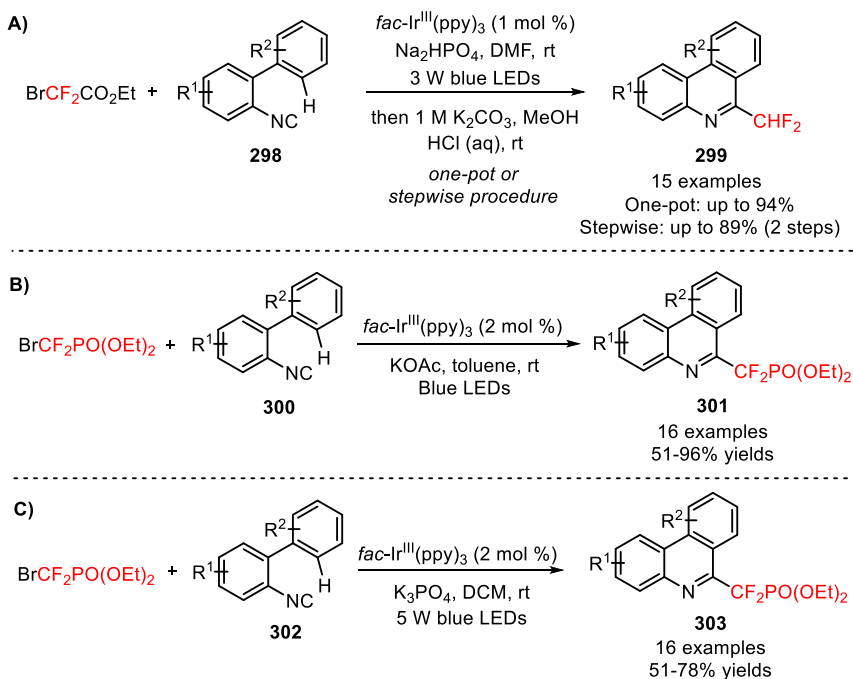
Cho and co-workers disclosed the photocatalytic difluoroalkylation of prefunctionalized alkynyl iodides (**296**) with the difluoroalkyl bromides BrCF₂CO₂Et and BrCF₂PO(OEt)₂ in the presence of *fac*-Ir^{III}(ppy)₃ [148]. Aryl-substituted alkynyl iodides containing electron-donating and electron-withdrawing groups and heteroaryl-substituted alkynyl iodides were suitable substrates for the difluoroalkylation protocol under visible light photoredox conditions (**297**, Scheme 77: 13 examples, 33-74% yields).



Scheme 77. Photoinduced difluoroalkylation of prefunctionalized alkynyl iodides (**296**) with the difluoroalkyl bromides BrCF₂CO₂Et and BrCF₂PO(OEt)₂.

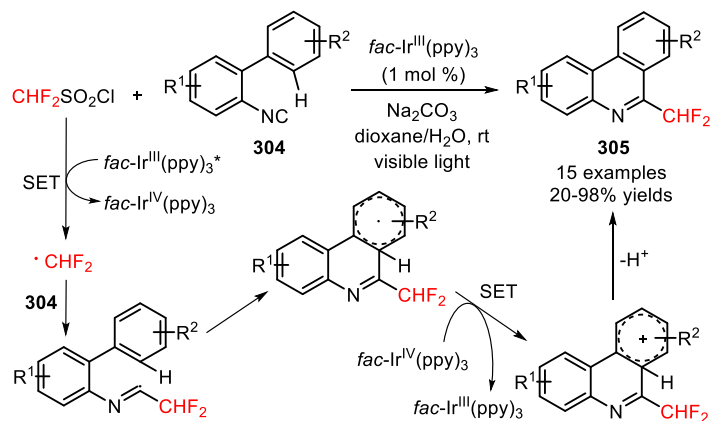
In 2014, Yu and co-workers developed a *stepwise* procedure for the preparation of difluoromethylated phenanthridine derivatives (**299**) involving the difluoroalkylation/radical cyclization of biphenyl isocyanides (**298**) with $\text{BrCF}_2\text{CO}_2\text{Et}$ and subsequent decarboxylation under basic conditions [149]. The difluoromethylation of the substrates took place upon visible light irradiation in the presence of *fac*- $\text{Ir}^{\text{III}}(\text{ppy})_3$, together with Na_2HPO_4 in DMF at room temperature. After the radical-induced difluoroalkylation, the ester functionality was removed *via* saponification and subsequent acid-mediated decarboxylation. The authors investigated the influence of a *one-pot* procedure on the overall efficiency of difluoromethylation of biphenyl isocyanides (**298**). They found that a *one-pot* procedure could afford a range of electron-deficient and electron-rich phenanthridine derivatives (**299**, Scheme 78A: 15 examples; *one-pot*: up to 94%; *stepwise*: up to 89%) with reaction yields comparable to those of the *stepwise* methodology, and could be easily scaled up.

Later, two independent research works reported by Liu [150] and Wang [151] groups have shown the successful utilization of $\text{BrCF}_2\text{PO}(\text{OEt})_2$ in the phosphonodifluoromethylation of biphenyl isocyanides (**300**, **302**) under visible light photoredox conditions. A variety of biphenyl isocyanides bearing electron-donating and electron-withdrawing substituents attached to the aromatic rings were efficiently converted into the respective phosphonodifluoromethylated phenanthridines (**301**, Scheme 78B: 16 examples, 51-96% yields; **303**, Scheme 78C: 16 examples, 51-78% yields).



Scheme 78. Visible light-mediated difluoroalkylation of biphenyl isocyanides (**298**, **300**, **302**) reported by Yu (**A**), Liu (**B**), and Wang (**C**) groups.

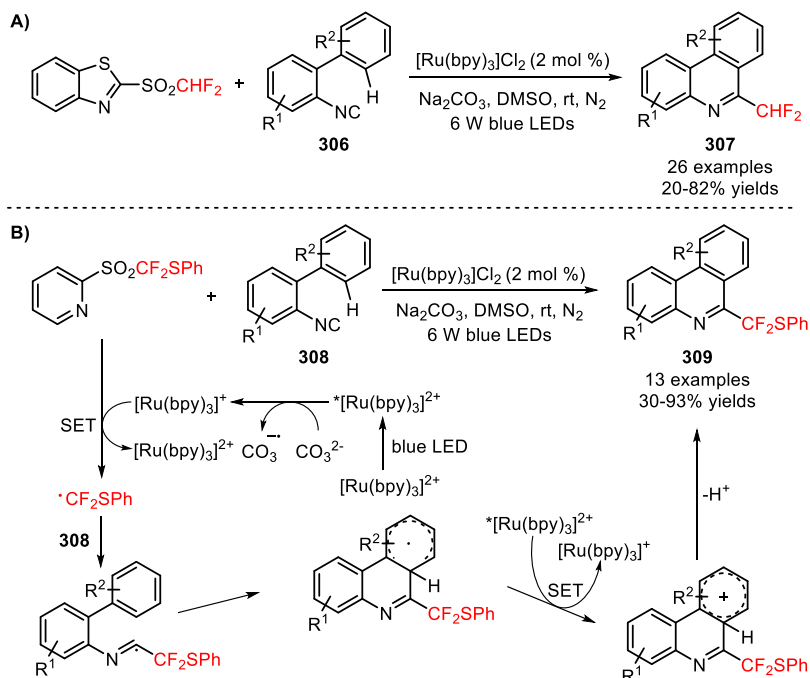
Visible light-mediated installation of CHF₂ groups in biphenyl isocyanides (**304**) was reported for the first time by Dolbier and collaborators using the reagent CHF₂SO₂Cl [152]. This method enabled the synthesis of difluoromethylated phenanthridines (**305**), excluding the need of a *stepwise* procedure involving the conversion of other *gem*-difluoroalkyl groups into a difluoromethyl group. An improved reactivity of the difluoromethylation of the substrates was accomplished using wet dioxane and K₂HPO₄, in the presence of *fac*-Ir^{III}(ppy)₃ (Scheme 79). Electron-donating and electron-withdrawing substituents in both aromatic rings were efficiently converted into the respective difluoromethylated phenanthridines (**305**, 15 examples, 20-98% yields). Other radical fluoroalkyl precursors, particularly to PhCF₂Br and CH₃CF₂SO₂Cl, were compatible with the developed methodology. The authors suggested a mechanism for the formation of phenanthridine scaffold involving the generation of CHF₂ radicals via oxidative quenching of *fac*-Ir^{III}(ppy)₃* and radical addition to the C≡N bond of biphenyl isocyanides (**304**). Subsequent cyclization onto the aromatic ring, oxidation *via* *fac*-Ir^{IV}(ppy)₃, and base-assisted deprotonation gave the final products (**305**). Similar mechanistic pathways have been proposed to the difluoroalkylation reactions described on the Scheme 78.



Scheme 79. Photoinduced difluoromethylation of biphenyl isocyanides (**304**) and the suggested mechanism.

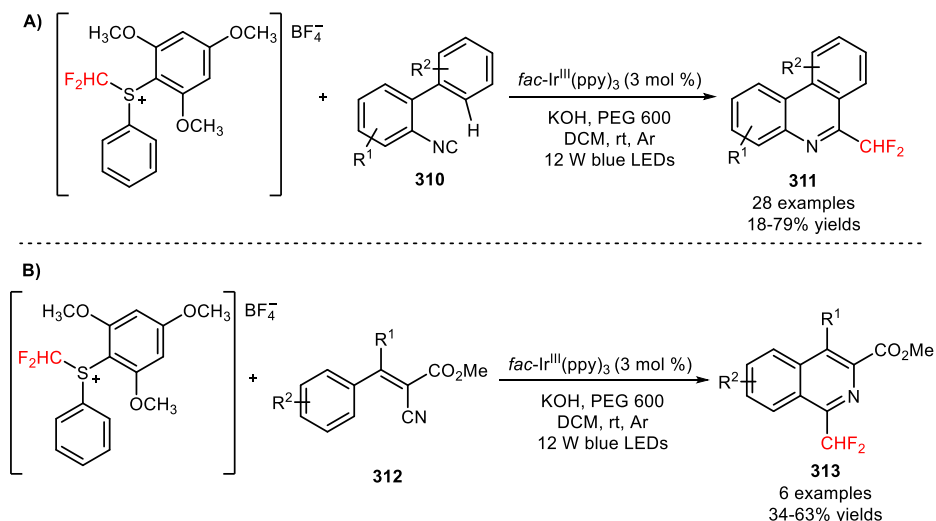
Difluoroalkyl sulfones, including 2-BT₂SO₂CHF₂ [153] and 2-PySO₂CF₂SPh [154], have also been implemented in the synthesis of difluoromethylated (**307**) and arylthio-difluoromethylated phenanthridines (**309**), respectively, from biphenyl isocyanides (**306**, **308**), under irradiation with 6 W blue LEDs. Optimal conditions for the difluoromethylation and arylthiodifluoromethylation were achieved by combining the photocatalyst [Ru(bpy)₃]Cl₂ with the base Na₂CO₃ and DMSO. Biphenyl isocyanides bearing electron-donating and electron-withdrawing substituents on the aromatic rings were suitable substrates for the desired transformation (**307**, Scheme 80A: 26 examples, 20-82% yields; **309**, Scheme 80B: 13 examples, 30-93% yields). The developed methodology was also extended to other

fluoroalkyl sulfones containing 1,1-difluoroethyl (-CF₂CH₃), (phenyl)difluoromethyl (-CF₂Ph), (benzoyl)difluoromethyl (-CF₂COPh), and arylthiodifluoromethyl (-CF₂SAr) moieties. Luminescence quenching experiments suggested a mechanism of difluoroalkylation mediated by reductive quenching of ^{*}[Ru(bpy)₃]²⁺ via oxidation of CO₃²⁻.



Scheme 80. Visible light-promoted difluoromethylation of biphenyl isocyanides (**306**, **308**) with 2-BT(SO₂)CHF₂ (**A**) and 2-Py(SO₂)CF₂SPh (**B**).

Photocatalytic difluoromethylation of biphenyl isocyanides (**310**) and 2-isocynoacrylates (**312**) was recently reported by Liu and co-workers using the bench-stable *S*-(difluoromethyl)-*S*-phenyl-*S*-(2,4,6-methoxyphenyl) sulfonium tetrafluoroborate [155]. Under irradiation with 12 W blue LEDs, the *fac*-Ir^{III}(ppy)₃-catalyzed electrophilic difluoromethylation of the substrates **310** and **312** was performed in aqueous solution of base KOH and DCM. In addition, the presence of polyethylene glycol 600 (PEG 600) found to be beneficial for the efficiency of the reaction by increasing the miscibility of KOH aqueous solution in DCM. A wide range of difluoromethylated phenanthridines with electron-rich and electron-poor aromatic groups, and heteroaryl groups, including indole, pyrrole, and thianaphthene was furnished in moderate to good reaction yields (**311**, Scheme 81A: 28 examples, 18-79% yields). The protocol was expanded to the synthesis of difluoromethylated isoquinolines furo[3,2-*c*]pyridine, and pyrido[3,4-*b*] (**313**, Scheme 81B: 6 examples, 34-63% yields), and of difluoromethylated trispheridine derivative (**314**, Figure 9).



Scheme 81. Photocatalytic difluoromethylation of biphenyl isocyanides (**310**) and 2-isocynoacrylates (**312**) with *S*-(difluoromethyl)diarylsulfonium tetrafluoroborate.

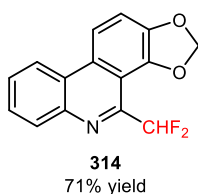


Figure 9. Chemical structure of the difluoromethylated trispheredine derivative (**314**).

2.6. Difluoroalkylation of SH- and OH-Containing Substrates

Transition metal-photoinduced difluoroalkylation of sp^2 - and sp -hybridized carbon atoms has been widely described under the scope of this review. On the other hand, the difluoroalkylation of other groups, in particular SH and OH groups, by visible light photoredox catalysis has been underdeveloped. The resulting -SCHF₂ and -OCHF₂ substituents have emerged as important functional groups in bioactive molecules, including the pyriprole (**315**), flomoxef sodium (**316**), pantoprazole (**317**), and roflumilast (**318**) (Figure 10). Just recently in 2017, the Fu and Qing groups reported on the use of fluoroalkylating agents for the synthesis of difluoroalkyl (thio)ether derivatives under photoredox conditions.

The commercially available bromodifluoroacetic acid (BrCF₂CO₂H, CAS number: 354-08-5) was employed in the difluoromethylation of phenols and thiophenols (**319**) under visible light with a 23 W CFL [156]. Screening of photocatalysts, bases, and solvents have shown that the selection of *fac*-Ir^{III}(ppy)₃, Cs₂CO₃, and DMF, respectively, was appropriate for the efficiency of difluoromethylation process (Scheme 82). A broad range of phenols and thiophenols possessing electron-donating and electron-withdrawing groups gave the corresponding difluoromethylated (thio)ethers (**320**, 32 examples, 48-97% yield). The

protocol was also applied to other substrates, such as heteroaryl alcohols and heteroaryl thiols. The authors hypothesized a mechanism of difluoromethylation involving the generation of a difluorocarbene (:CF₂) intermediate via oxidation of a radical carbanion intermediate resulting from the reaction between BrCF₂CO₂H and Cs₂CO₃, and subsequent reduction. Concurrently, the reaction of phenol and thiophenol derivatives (**319**) with Cs₂CO₃ provided the ArXC_s (X = O, S) and CsHCO₃. The reaction of ArXC_s with the :CF₂ and subsequent treatment with CsHCO₃ provided the difluoromethylated (thio)ether derivatives (**320**).

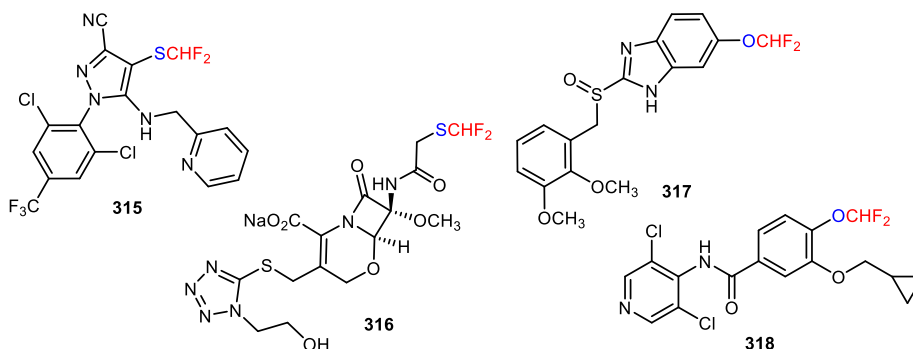
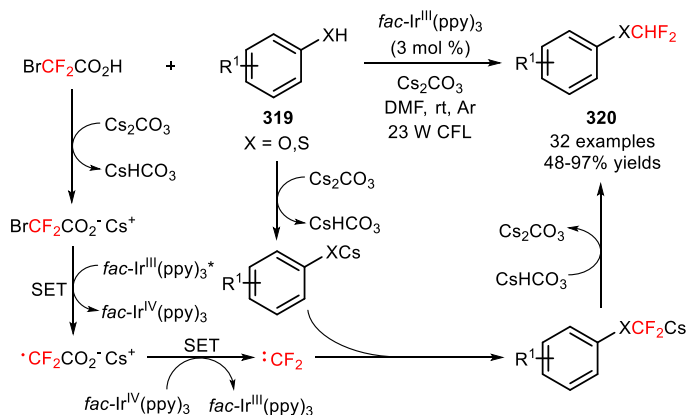


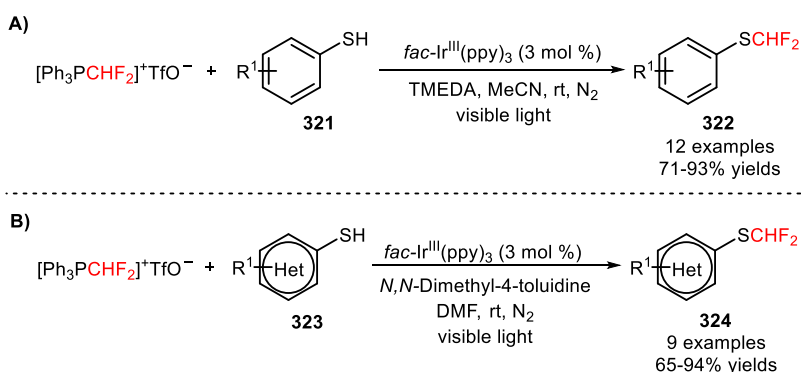
Figure 10. Chemical structures of SCHF₂- (pyriprole (**315**) and flomoxef sodium (**316**)) and OCHF₂-containing bioactive molecules (pantoprazole (**317**) and roflumilast (**318**)).



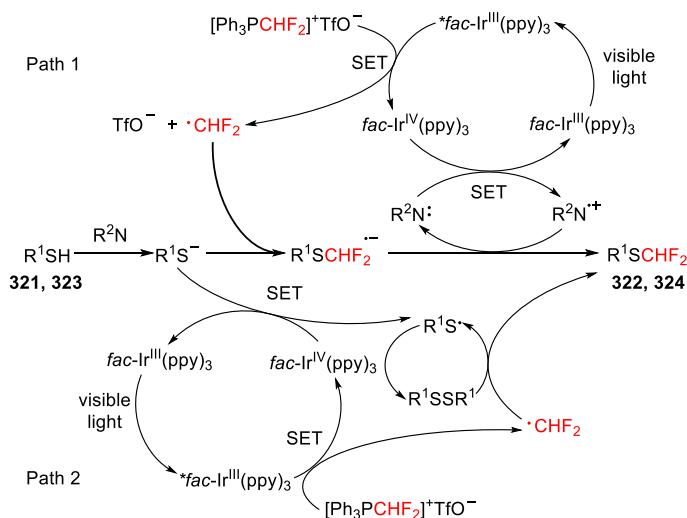
Scheme 82. Photoinduced difluoromethylation of phenols and thiophenols (**319**) with BrCF₂CO₂H in the presence of *fac*-Ir^{III}(ppy)₃ and the proposed mechanism.

In addition, the reagent (difluoromethyl)triphenylphosphonium triflate ([Ph₃PCHF₂]⁺TfO⁻) was applied to the radical difluoromethylation of thiols (**321**, **323**) under irradiation of visible light [157]. Apart from [Ph₃PCHF₂]⁺TfO⁻, the selection of photocatalyst *fac*-Ir^{III}(ppy)₃ and the base TMEDA was critical for the reactivity of difluoroalkylation reactions (Scheme 83). A large variety of thiophenols possessing electron-neutral, electron-donating, and electron-withdrawing substituents and heteroaryl thiols including benzo[*d*]thiazole-2-thiols, 2-thiopyridines, 4-

thiopyridines, and 2-thiopyrimidines yielded the corresponding difluoromethylated thioethers (**322**, Scheme 83A: 12 examples, 71-93% yields; **324**, Scheme 83B: 9 examples, 65-94% yields). Interestingly, an excellent *S*/*X* (*X* = *O*, *N*) chemoselectivity of the difluoromethylation process was observed. Two plausible pathways were proposed for the radical difluoromethylation of thiols (Scheme 84). Electrophilic addition of CHF₂ radicals to the thiolates and subsequently oxidation afforded the corresponding products (Path 1). Alternatively, the thiolate can be oxidized by *fac*-Ir^{IV}(ppy)₃ to a sulfur radical and then converted into the disulfide derivative. Difluoromethylated thioethers (**322**, **324**) are obtained from the reaction between the CHF₂ radicals and the disulfide (Path 2). The latter mechanism was considered the most likely reaction pathway due to the observed chemoselective *S*-difluoromethylation.



Scheme 83. Visible light-induced photocatalytic difluoromethylation of thiophenols (**321**) and heteroaryl thiols (**323**) using the reagent [Ph₃PCHF₂]⁺TfO⁻.

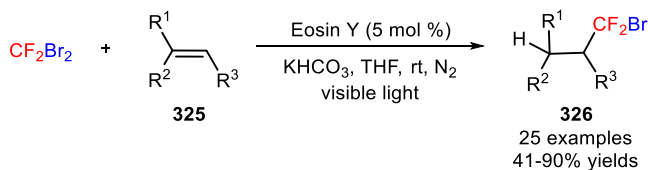


Scheme 84. Proposed mechanistic pathways for photoinduced difluoromethylation of thiophenols (**321**) and heteroaryl thiols (**323**).

3. Organic Photocatalyzed Difluoroalkylation Reactions

Over the last years, we have witnessed to promising advances in the application of transition metal photocatalysts in the late-stage difluoroalkylation of organic substrates. Nevertheless, metal-catalyzed processes usually present a number of drawbacks, including the use of expensive metal catalysts, their potential toxicity, and in few cases the problems related to the elimination of the metal catalyst at the end of a reaction [35,158,159]. The development of synthetic approaches using organic dyes and other metal-free organic compounds has been regarded an attractive alternative to transition metal complexes in photoredox catalysis. These organic photocatalysts are typically less expensive, less toxic, and easy to handle [160,161]. The development of metal-free catalyzed protocols is highly desirable to the pharmaceutical industries in order to restrict the maximal amount of transition metal impurities used in the production of pharmaceuticals. A survey of difluoroalkylation reactions that makes use of organic photocatalysts will be described in this section.

Photoinduced hydro-bromodifluoromethylation of alkenes (**325**) was reported by Qing and co-workers [162] using dibromodifluoromethane (CF₂Br₂, CAS number: 75-61-6) as difluoroalkylating reagent and eosin Y as photocatalyst [158]. Under irradiation with visible light, the combined use of THF as hydrogen atom donor with the additive KHCO₃ was appropriate to achieve the selectivity of hydro-bromodifluoromethylation process and minimize the competitive bromine trapping after the bromodifluoromethylation process (Scheme 85). A scope of mono- and disubstituted alkenes possessing a wide range of functional groups, including aldehydes, alkyl and allylic alcohols, amides, carboxylic acids, esters, ethers, halides, ketones, nitriles, nitro groups, phosphine oxides, sulfones, can be converted into the corresponding hydro-bromodifluoromethylated products (**326**, 25 examples, 41-90% yields). Remarkably, the developed protocol for hydro-bromodifluoromethylation can be extended to more complex alkenes, including a *L*-phenylalanine derivative (**327**), vinclozolin (**328**), and rotenone (**329**) (Figure 11), and alkynes **330** (**331**, Scheme 86: 4 examples, 53-55% examples). Mechanistic studies suggested the involvement of the photoexcited eosin Y in the reduction of CF₂Br₂ with concomitant generation of bromodifluoromethyl (CF₂Br) radicals. Subsequent radical addition to the alkenes (**325**) and hydrogen abstraction from THF afforded the hydro-bromodifluoromethylated products (**326**). Labeling experiments with THF-*d*s corroborated the suggested mechanism of hydrogen abstraction.



Scheme 85. Photoinduced hydro-bromodifluoromethylation of alkenes (**325**) with CF₂Br₂.

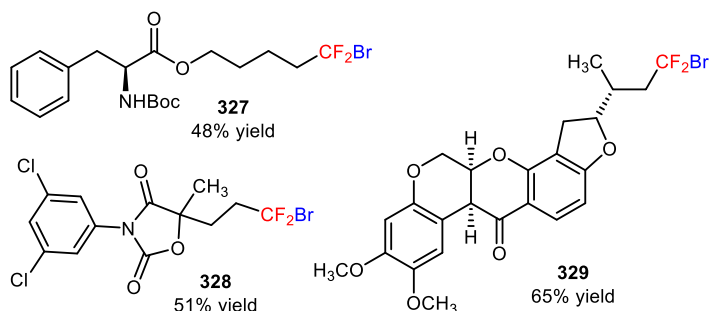
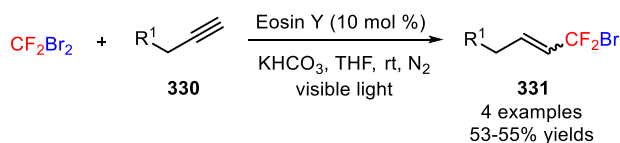


Figure 11. Chemical structures of hydro-bromodifluoromethylated *L*-phenylalanine derivative (327), vinclozolin (328), and rotenone (329).

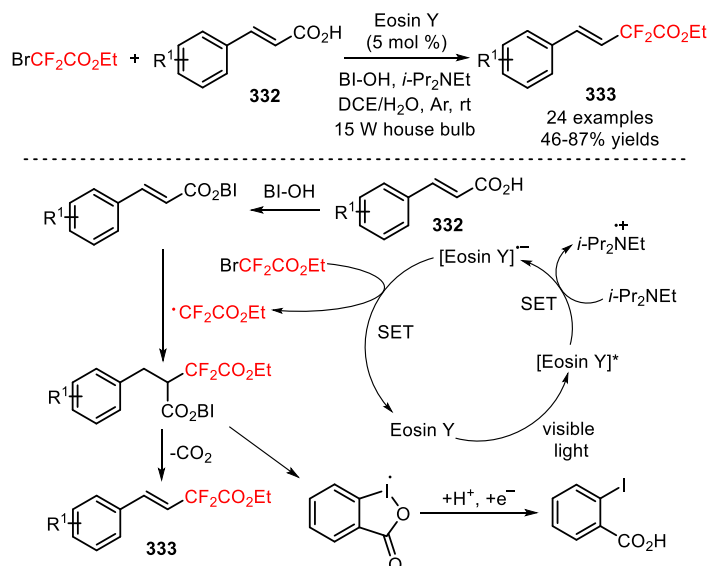


Scheme 86. Photoinduced hydro-bromodifluoromethylation of alkynes (330) with CF_2Br_2 .

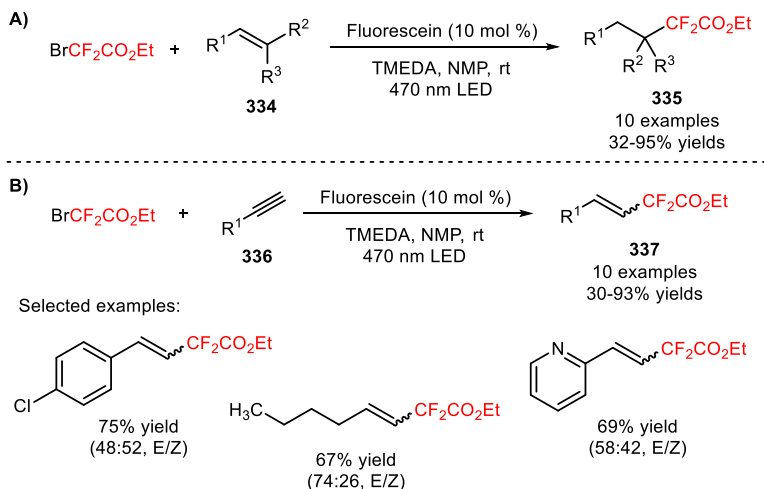
Eosin Y was also effectively employed as a metal-free photocatalytic system for the decarboxylative difluoroalkylation of α,β -unsaturated carboxylic acids (332) with $\text{BrCF}_2\text{CO}_2\text{Et}$ under mild conditions [163]. The use of the hypervalent iodine reagent 1-hydroxy-3-oxobenziodoxole (BI-OH) enabled the decarboxylative difluoromethylation of the substrates *via* activation of the carboxylic acid group. Under irradiation with a 15 W house bulb, an improved reaction efficiency was accomplished using the solvent mixture DCE/ H_2O and the reducing agent *i*- Pr_2NEt (Scheme 87). A wide range of (*E*)-difluoroalkylated styrenes possessing both electron-donating and electron-withdrawing groups at *meta*- and *para*-positions on the aromatic ring was successfully synthesized in good yields (333, 24 examples, 46-87% yields). The authors suggested a reaction mechanism involving a reductive quenching of the photoexcited eosin Y via SET oxidation of *i*- Pr_2NEt with concomitant formation of $\text{CF}_2\text{CO}_2\text{Et}$ radicals. The hypervalent iodine reagent BI-OH is incorporated into the carboxylic acid moiety of the substrates to generate a benziodoxole vinyl carboxylic acid complex. Radical difluoroalkylation to the α -carbon atoms of the benziodoxole vinyl carboxylic acid and subsequent elimination of CO_2 and benziodoxole radical provided the desired (*E*)-difluoroalkylated styrenes (333).

The reagent $\text{BrCF}_2\text{CO}_2\text{Et}$ was implemented in the difluoroalkylation of acyclic and cyclic alkenes (334) under visible light mediated reaction conditions in the presence of a suitable reducing agent and an organic photocatalyst [164,165]. Difluoroalkylated products were attained with improved reaction yields using fluorescein as a photocatalyst, the amine TMEDA as a reducing agent, and NMP as a solvent (335, Scheme 88A: 10 examples, 32-95% yields). Based on the redox potentials of fluorescein ($E_{\text{red}} = -0.78 \text{ V vs SCE}$) and of $\text{BrCF}_2\text{CO}_2\text{Et}$ ($E_{\text{red}} = -0.89 \text{ V vs SCE}$), Itoh and co-workers proposed a difluoroalkylation reaction by TMEDA-mediated reduction of the fluorescein in the photoexcited state. The same reaction conditions

were applicable to the reaction with alkynes, affording a range of difluoroalkylated alkenes with poor *E/Z* selectivity (**337**, Scheme 88B: 10 examples, 30-93% yields).



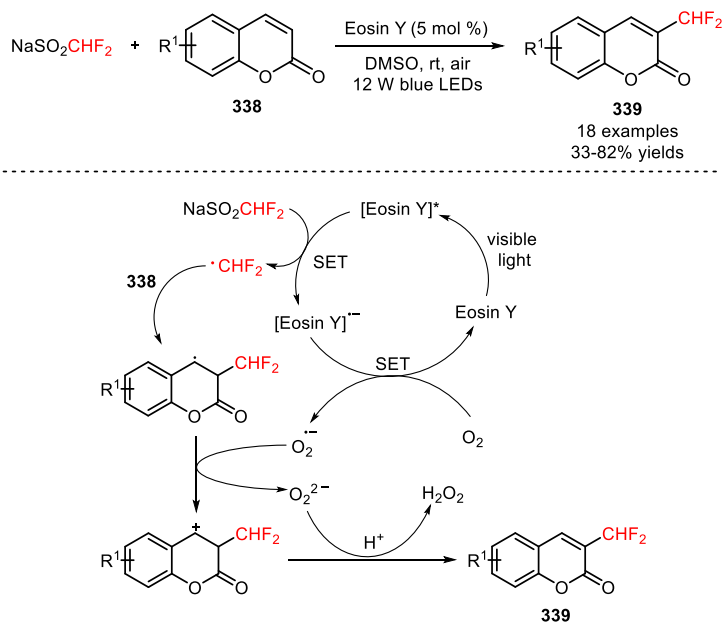
Scheme 87. Visible light-mediated decarboxylative difluoromethylation of α,β -unsaturated carboxylic acids (**332**) and the proposed mechanism.



Scheme 88. Fluorescein-mediated difluoroalkylation of alkenes (**334**) and alkynes (**336**) with $\text{BrCF}_2\text{CO}_2\text{Et}$.

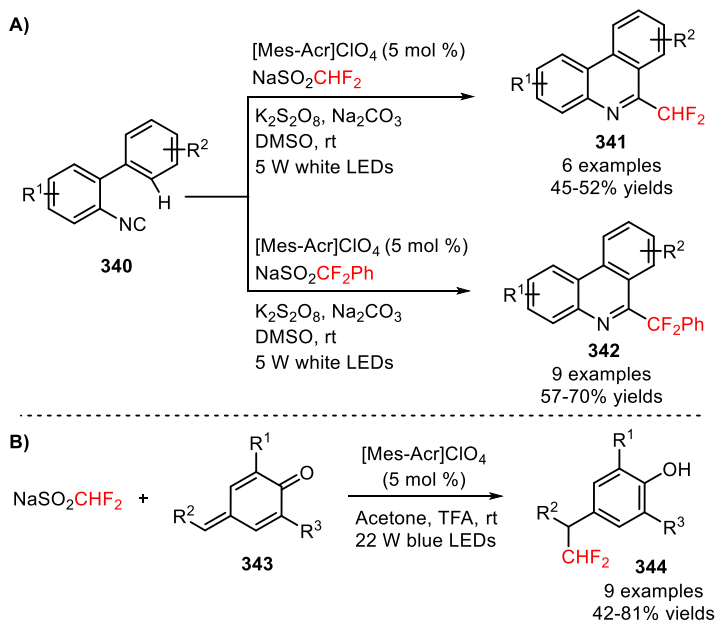
Direct difluoromethylation of coumarins (**338**) with sodium difluoromethanesulfonate ($\text{NaSO}_2\text{CHF}_2$, CAS number: 275818-95-6) was accomplished by Zhang and Deng in the presence of the organophotocatalyst eosin Y and molecular oxygen (O_2) [166]. This transition metal-free approach allowed the synthesis of difluoromethylated coumarins possessing electron-donating and electron-withdrawing groups without requiring the use of an additive (**339**, Scheme

89: 18 examples, 33-82% yields). Mechanistic studies with the radical scavengers TEMPO and 1,1-diphenylethylene and the spin trap 5,5-dimethyl-1-pyrroline-*N*-oxide (DMPO) suggested the intermediacy of the CHF₂ radicals in the difluoromethylation of the substrates and the peroxide radical anion in oxidation of the resulting difluoromethylated radical intermediates.



Scheme 89. Eosin Y-mediated difluoromethylation of coumarin derivatives with NaSO₂CHF₂.

Liu and co-workers described the successful application of the organic photocatalyst [Mes-Acr]ClO₄ [167-170] to the visible light-mediated insertion of CHF₂ and CF₂Ph radicals into biphenyl isocyanides (**340**, 6 examples, 45-52% yields) and sodium difluoro(phenyl)methanesulfinate (NaSO₂CF₂Ph, CAS number: 268730-04-7) (**342**, 9 examples, 57-70% yields), in the presence of the oxidant K₂S₂O₈ and the base Na₂CO₃ (Scheme 90A) [171]. The authors suggested a reductive quenching of the photoexcited [Mes-Acr]⁺ and the oxidation of NaSO₂CHF₂ and NaSO₂CF₂Ph *via* photoexcited [Mes-Acr] or by K₂S₂O₈ to produce the CHF₂ and CF₂Ph radicals, respectively. *Para*-quinone methides (**343**) were also difluoromethylated using the reagent NaSO₂CHF₂ and the photocatalyst [Mes-Acr]ClO₄, in the presence of TFA (Scheme 90B) [172]. Under irradiation with 9 W white LEDs, a scope of difluoromethylated derivatives were afforded in moderate to good yields (**344**, 9 examples, 42-81% yields) and no competitive nucleophilic addition of the double bond of the substrates (**343**) to the sulfonate group of the reagent was observed.

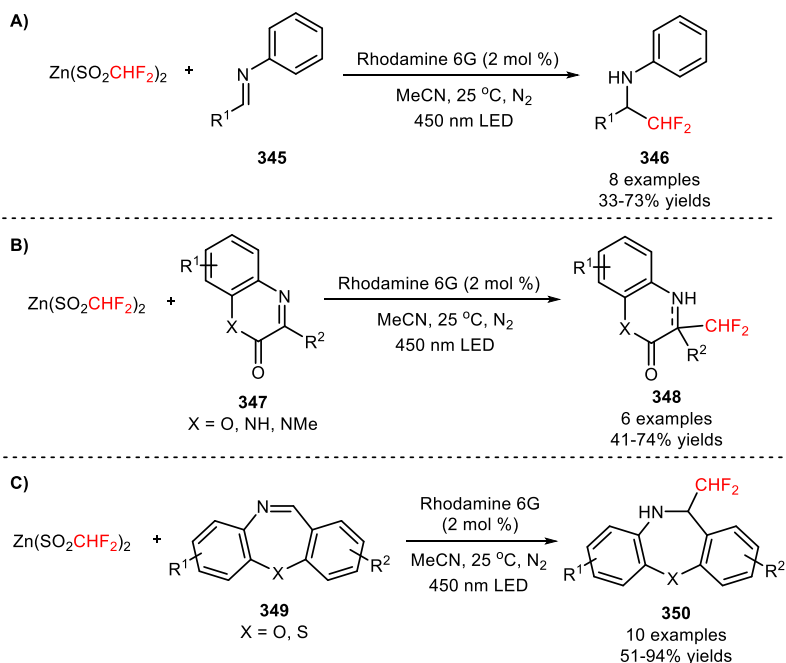


Scheme 90. Visible light-induced difluoroalkylation of biphenyl isocyanides (**340**) and *para*-quinone methides (**343**).

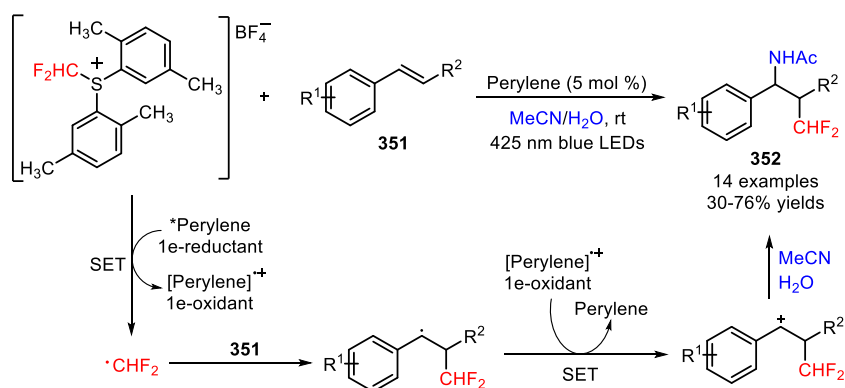
Rhodamine-6G (Rh-6G) [173,174] was employed for the first time by Maestro and Alemán in the insertion of CHF_2 groups in substrates with $\text{C}=\text{N}$ bonds (**345**, **347**, and **349**) using the commercially available zinc difluoromethanesulfinate [$\text{Zn}(\text{SO}_2\text{CHF}_2)_2$, CAS number: 1355729-38-2], under irradiation with a single 380 mW LED [175]. The developed photocatalytic difluoromethylation was compatible with several substrates featuring $\text{C}=\text{N}$ bonds, including diaryl-substituted aldimines (**346**, Scheme 91A: 8 examples, 33-73% yields), quinoxalinones (**348**, Scheme 91B: 6 examples, 41-74% yields), dibenzoxazepines and dibenzothiazepines (**350**, Scheme 91C: 10 examples, 51-94% yields). A mechanism involving the reductive quenching of the photocatalyst Rh-6G and the generation of CHF_2 radicals by oxidation of the $\text{Zn}(\text{SO}_2\text{CHF}_2)_2$ was proposed for the difluoromethylation of the $\text{C}=\text{N}$ bonds. The solvent of the reaction (MeCN) was used as proton source for the formation of the difluoromethylated products.

In 2017, Akita and collaborators described the visible light-induced amino-difluoromethylation of styrenes, using the shelf-stable and easy-to-handle difluoromethylating reagent *S*-difluoromethyl-*S*-di(*para*-xylyl)sulfonium tetrafluoroborate (CAS number: 2133476-50-1) and the photocatalyst perylene in the presence of MeCN and H_2O [176]. The presence of two methyl groups of the *para*-xylyl groups in the proximity of the sulfur atom of *S*-difluoromethyl-*S*-di(*para*-xylyl)sulfonium tetrafluoroborate confer easy-handling and stability to this reagent. The amino-difluoromethylation process exhibited a good functional group tolerance (electron-donating and electron-deficient groups) and afforded a variety of amino-difluoromethylated products in moderate to good yields (**352**, Scheme 92: 14

examples, 30-76% yields). Perylene also promoted amino- and chloro-trifluoromethylation of styrenes using Yagupolskii-Umemoto reagent and $\text{CF}_3\text{SO}_2\text{Cl}$, respectively. A plausible mechanism for amino-difluoromethylation of styrenes (**351**) involved the formation of CHF_2 radicals *via* oxidative quenching of photoexcited perylene and reductive cleavage of C-S bond of the reagent. Radical addition to styrenes, oxidation, and subsequent Ritter amination with $\text{MeCN}/\text{H}_2\text{O}$ gave the corresponding products (**352**).



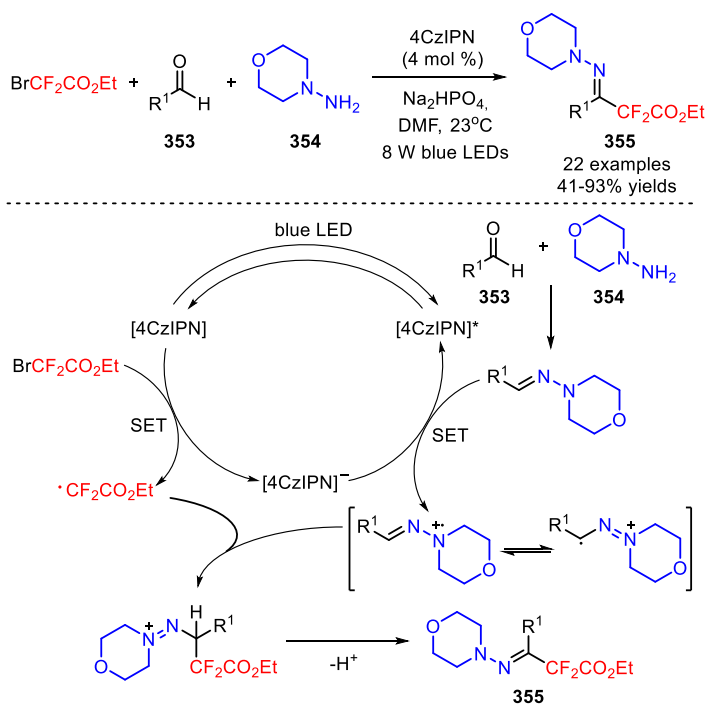
Scheme 91. Difluoromethylation of substrates featuring C=N bonds with the $\text{Zn}(\text{SO}_2\text{CHF}_2)_2$.



Scheme 92. Perylene-catalyzed amino-difluoromethylation of styrenes (**351**) with *S*-difluoromethyl-*S*-di(*para*-xylyl)sulfonium tetrafluoroborate and the proposed mechanism.

Wang and co-workers implemented the photocatalyst 4CzIPN [177-179] in the difluoroalkylation of aldehyde-derived hydrazones *via* a three-component coupling

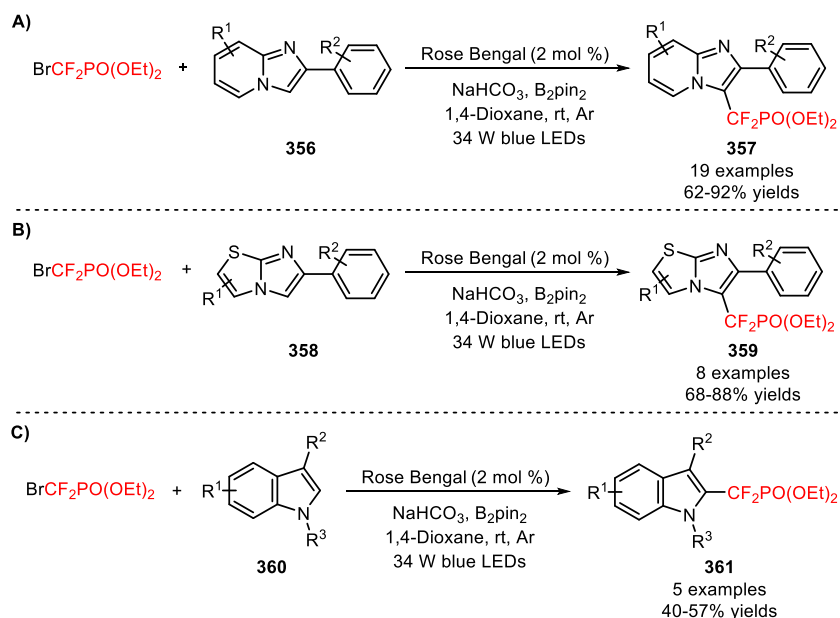
of aldehydes (**353**), hydrazines (**354**) and $\text{BrCF}_2\text{CO}_2\text{Et}$, under irradiation with 8 W blue LEDs [180]. The investigation of the substrate scope for the difluoroalkylation process demonstrated that aldehydes bearing electron-donating and electron-withdrawing substituents at *ortho*-, *meta*-, and *para*-positions on the aromatic ring, heterocyclic, and aliphatic groups were compatible substrates, providing the corresponding products in moderate to excellent yields (**355**, Scheme 93: 22 examples, 41-93% yields). This methodology can also be applied to different hydrazines and other reagents such as bromodifluoroacetamides and 2-(bromodifluoromethyl)benzoxazole. Radical trapping and fluorescence quenching experiments suggested a mechanism involving the *in situ* coupling between aldehydes (**353**) and hydrazines (**354**), the reductive quenching of the $[\text{4CzIPN}]^*$, and the intermediacy of $\text{CF}_2\text{CO}_2\text{Et}$ radicals in the difluoroalkylation process.



Scheme 93. Organic dye-catalyzed three-component coupling of aldehydes (**353**), hydrazines (**354**) and $\text{BrCF}_2\text{CO}_2\text{Et}$, under visible light photoredox conditions.

In 2019, Hajra and co-workers achieved the photocatalytic difluoroalkylation of imidazo[1,2-*a*]pyridines (**356**), imidazo[2,1-*b*]thiazoles and benzo[*d*]imidazo[2,1-*b*]thiazoles (**358**), and indoles (**360**) with the reagent $\text{BrCF}_2\text{PO}(\text{OEt})_2$ [181]. In the presence of the photocatalyst rose Bengal (RB) [182], this procedure allowed the preparation of phosphonodifluoromethylated derivatives in good yields (**357**, Scheme 94A: 19 examples, 62-92% yields; **359**, Scheme 94B: 8 examples, 68-88% yields; **361**, Scheme 94C: 5 examples, 40-57% yields). The additive bis(pinacolato)diboron (B_2pin_2) was required for the difluoroalkylation reaction, playing a key role in the

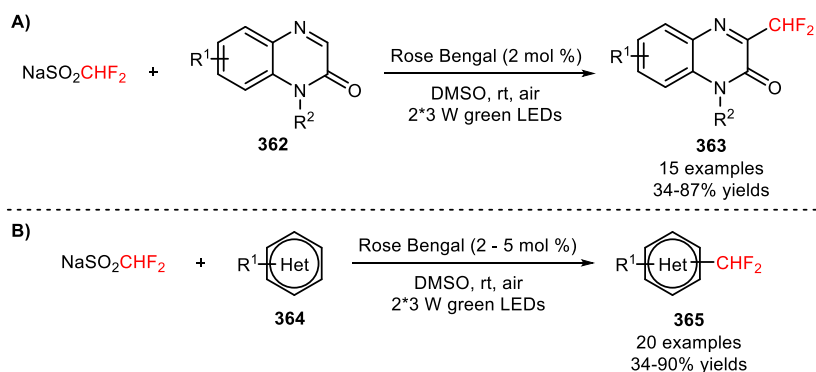
stabilization of the substrates and their activation for the coupling with the $\text{CF}_2\text{PO}(\text{OEt})_2$ radicals.



Scheme 94. Organophotocatalytic difluoroalkylation of imidazo[1,2-*a*]pyridines (**356**), imidazo[2,1-*b*]thiazoles and benzo[*d*]imidazo[2,1-*b*]thiazoles (**358**), and indoles (**360**) with $\text{BrCF}_2\text{PO}(\text{OEt})_2$.

RB was also efficiently employed in the radical difluoromethylation of quinoxalin-2(*1H*)-ones with electron-donating and electron-withdrawing groups and *N*-substituted quinoxalin-2(*1H*)-ones (**362**) using the reagent $\text{NaSO}_2\text{CHF}_2$ in combination with the oxygen under irradiation with green LEDs (**363**, Scheme 95A: 15 examples, 34-87% yields) [183]. Apart from the photocatalyst, the selection of the reaction solvent greatly influenced the efficiency of the synthesis of difluoromethylated quinoxalin-2(*1H*)-ones (**363**). The developed methodology was extended to a wide range of five- and six-membered heteroaromatics (**364**) including dimethyluracils, imidazoles, indoles, purines, pyrazines, pyridines, pyrimidines, pyrroles, quinolines, quinoxazolines, thiadiazoles, and thiophenes (**365**, Scheme 95B: 20 examples, 34-90% yields). In addition, this protocol has an important applicability to the late-stage difluoromethylation of bioactive molecules such as caffeine derivatives [caffeine (**366**, Figure 12), theophylline (**367**, Figure 12), and pentoxifylline (**368**, Figure 12)], nucleosides [deoxyuridine (**369**, Figure 12), uridine (**370**, Figure 12), and 2'-fluoro-2'-deoxyuridine (**371**, Figure 12)], drug molecules [melatonin (**372**, Figure 12), allopurinol (**373**, Figure 12), voriconazole (**374**, Figure 12), a flavorant (**375**, Figure 12), metyrapone (**376**, Figure 12), uracil (**377**, Figure 12), and an antidiabetic sulfonylurea derivative (**378**, Figure 12)]. The authors suggested a reaction mechanism involving the formation of the CHF_2 radicals by reductive quenching of

the photocatalyst RB. The oxygen is required in the difluoromethylation reaction, acting as an oxidant and in the completion of the photoredox cycle.



Scheme 95. Visible light-induced difluoromethylation of quinoxalin-2(1H)-ones (**A**) and a scope of heteroaromatics (**B**).

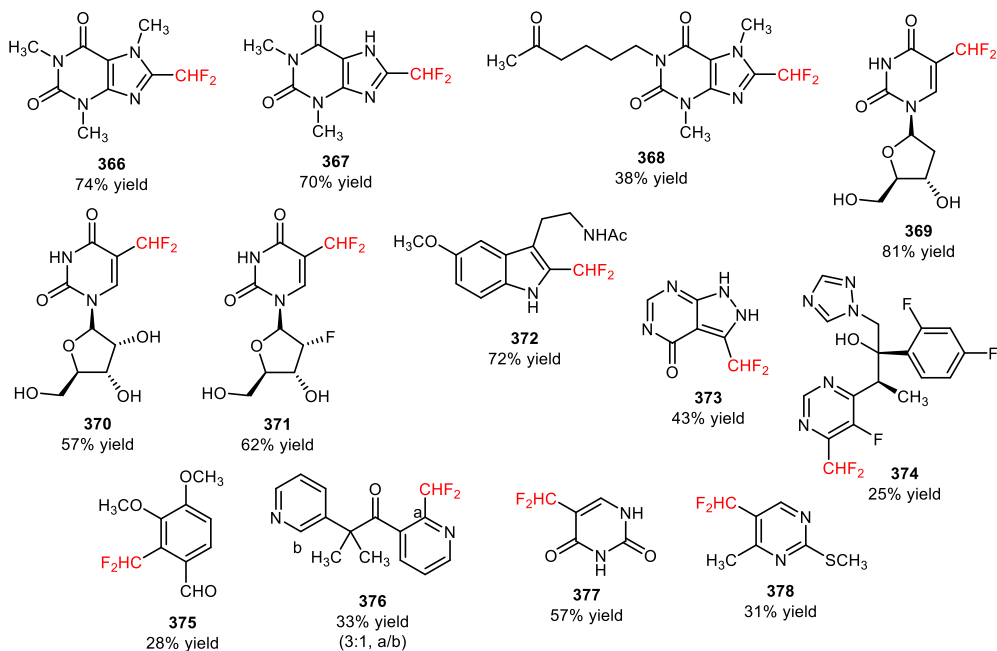
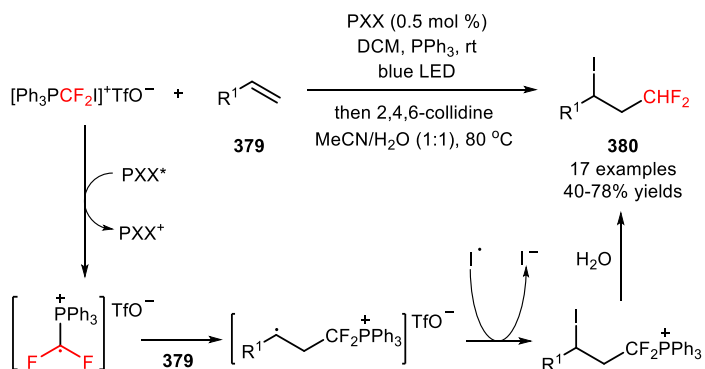


Figure 12. Chemical structure of the difluoromethylated caffeine derivatives (**366-368**), nucleosides (**369-371**), and drug molecules (**372-378**).

(Difluoroiodomethyl)triphenylphosphonium salts ($[\text{Ph}_3\text{PCF}_2\text{I}]^+\text{X}^-$) were recently explored by Dilman and co-workers in iodo-difluoromethylation of terminal alkenes (**379**) [184]. The authors found that $[\text{Ph}_3\text{PCF}_2\text{I}]^+\text{X}^-$ can generate the phosphonium-substituted radical cation *via* cleavage of the C–I bond. After radical difluoromethylation of terminal alkenes and iodine atom transfer, the iodo-difluoromethylated intermediates, which upon protodephosphorylation are

converted into the final products. The use of the reagent (difluoroiodomethyl)triphenylphosphonium triflate ($[\text{Ph}_3\text{PCF}_2\text{I}]^+\text{TfO}^-$) in combination with the organic photocatalyst *peri*-xanthenoxanthene (PXX) afforded the iodo-difluoromethylated derivatives with improved reaction yields, after protodephosphorylation reaction with 2,4,6-collidine (**380**, Scheme 96: 17 examples, 40-78% yields). The efficiency of PXX was attributed to the π - π stacking interactions between the phenyl rings of the positively charged phosphonium fragment and the electron-rich aromatic system of PXX.



Scheme 96. Visible light-induced iodo-difluoromethylation of terminal alkenes (**379**) with $[\text{Ph}_3\text{PCF}_2\text{I}]^+\text{TfO}^-$ and consecutive basic protodephosphorylation.

4. Concluding Remarks

The present review provides a general survey of visible light photoredox methodologies for the late-stage installation of CF_2FG and CHF_2 substituents into diverse families of organic substrates in the presence of distinct transition metal complexes and organic photocatalysts. In recent years, visible light photoredox catalysis has been an extensively exploited tool for promoting radical-involved transformations, including the activation of organic substrates and further construction of the corresponding difluoroalkylated products. Most of the reported photoinduced reactions are operationally simple, are efficiently performed under mild conditions, and require minimal amounts of transition metal (0.05-7 mol%) and organic photocatalyst (0.5-10 mol%).

Diverse difluoroalkylating reagents have been successfully employed in the incorporation of difluoroalkyl moieties, including $\text{CF}_2\text{CO}_2\text{Me}$, $\text{CF}_2\text{CO}_2\text{Et}$, $\text{CF}_2\text{CON}(\text{CH}_2\text{CH}_2)_2\text{O}$, CF_2COPh , $\text{CF}_2\text{PO}(\text{OEt})_2$, $\text{CF}_2\text{PO}(\text{O}i\text{-Pr})_2$, CF_2SPh , CF_2Cl , CF_2Br , and CF_2I moieties, and some of them can undergo further chemical modifications into other CF_2 -containing functional groups, including CHF_2 . Alternative difluoroalkyl precursors have enabled the direct introduction of CHF_2 substituents without the need of a post-functionalization step. Interestingly, we have witnessed a major progress in the development of photoinduced difluoroalkylation reactions involving the use of transition metal complexes as photocatalysts, in particular *fac*- $\text{Ir}^{\text{III}}(\text{ppy})_3$. In spite of the recent works regarding transition metal-free difluoroalkylation reactions

with organic photocatalysts, further research work in this field is still needed. In fact, the organophotocatalysis is a particular concern in the area of pharmaceutical industry, in order to minimize the utilization of transition metals.

The mechanistic pathway for most of the photoredox-catalyzed difluoroalkylation reactions is initiated by visible light irradiation of the transition metal or organic photosensitizer at a certain wavelength and consecutive stimulation to an excited state. Excited photosensitizers may undergo an oxidative or reductive quenching, depending on the redox potential of the difluoroalkylating reagents, thus enabling the application of electron-donor or electron-acceptor difluoroalkylating reagents for the generation of CF_2FG and CHF_2 radicals. The majority of the photoinduced difluoroalkylations reported in this review involves a mechanism of oxidative quenching of the photocatalysts and reduction of the difluoroalkylating reagents. The radical addition into carbon atoms of $\text{C}=\text{C}$, $\text{C}=\text{N}$, $\text{C}\equiv\text{C}$, $\text{C}\equiv\text{N}$ bonds and further chemical transformations (e.g., oxidation, halogen addition, cyclization) results in the formation the corresponding CF_2 -containing products. A variety of skeletons including alkenes, arenes, heteroarenes, α,β -unsaturated carboxylic acids, allylic alcohols, allylic amines, unsaturated amides, alkynes, biphenyl isocyanides, and thiols have proven to be suitable for the preparation of the corresponding difluoroalkylated compounds. Furthermore, the difluoroalkylation of structurally simple starting materials provides valuable intermediates for the synthesis of highly complex and functionalized heterocycles of potential biological interest, including benzoxazines, chromones, coumarins, oxindoles, phenanthridines, polycyclic lactones, and tetralins, in a single-step operation. Overall, the attractive characteristics of visible light photoredox reactions including environmentally benign conditions, excellent functional group versatility, and cost effectiveness will enable the application of these approaches by organic chemists in the exploration of novel methodologies for the introduction of difluoroalkyl substituents.

References

- [1] Fujiwara, T.; O'Hagan, D. Successful fluorine-containing herbicide agrochemicals. *J. Fluorine Chem.* **2014**, *167*, 16-29.
- [2] Morser, S.; Moore, P.R.; Swallow, S.; Gouverneur, V. Fluorine in medicinal chemistry. *Chem. Soc. Rev.* **2008**, *37*, 320-330.
- [3] Wang, J.; Sánchez-Roselló, M.; Aseña, J.L.; del Pozo, C.; Sorochinsky, A.E.; Fustero, S.; Soloshonok, V.A.; Liu, H. Fluorine in Pharmaceutical Industry: Fluorine-Containing Drugs Introduced to the Market in the Last Decade (2001–2011). *Chem. Rev.* **2014**, *114*, 2432-2506.
- [4] Gardiner, J. Fluoropolymers: Origin, Production, and Industrial and Commercial Applications. *Aust. J. Chem.* **2015**, *68*, 13-22.
- [5] Marsh, E.N.; Suzuki, Y. Using ^{19}F NMR to Probe Biological Interactions of Proteins and Peptides. *ACS Chem. Biol.* **2014**, *9*, 1242-1250.

- [6] Preshlock, S.; Tredwell, M.; Gouverneur, V. ^{18}F -Labeling of Arenes and Heteroarenes for Applications in Positron Emission Tomography. *Chem. Rev.* **2016**, *116*, 719-766.
- [7] Zafrani, Y.; Yeffet, D.; Sod-Mariah, G.; Berliner, A.; Amir, D.; Marciano, D.; Gershonov, E.; Saphier, S. Difluoromethyl Bioisostere: Examining the "Lipophilic Hydrogen Bond Donor" Concept. *J. Med. Chem.* **2017**, *60*, 797-804.
- [8] Hagmann, W.K. The Many Roles for Fluorine in Medicinal Chemistry. *J. Med. Chem.* **2008**, *51*, 4359-4369.
- [9] Gillis, E.P.; Eastman, K.J.; Hill, M.D.; Donnelly, D.J.; Meanwell, N.A. Applications of Fluorine in Medicinal Chemistry. *J. Med. Chem.* **2015**, *58*, 8315-8359.
- [10] Studer, A. A "Renaissance" in Radical Trifluoromethylation. *Angew. Chem. Int. Ed.* **2012**, *51*, 8950-8958.
- [11] Liu, H.; Gu, Z.; Jiang, X. Direct Trifluoromethylation of the C-H Bond. *Adv. Synth. Catal.* **2013**, *355*, 617-626.
- [12] Merino, E.; Nevado, C. Addition of CF_3 across unsaturated moieties: a powerful functionalization tool. *Chem. Soc. Rev.* **2014**, *43*, 6598-6608.
- [13] Zhang, C. Recent advances in trifluoromethylation of organic compounds using Umemoto's reagents. *Org. Biomol. Chem.* **2014**, *12*, 6580-6589.
- [14] Chu, L.; Qing, F.-L. Oxidative Trifluoromethylation and Trifluoromethylthiolation Reactions Using (Trifluoromethyl)trimethylsilane as a Nucleophilic CF_3 Source. *Acc. Chem. Res.* **2014**, *47*, 1513-1522.
- [15] Liu, X.; Xu, C.; Wang, M.; Liu, Q. Trifluoromethyltrimethylsilane: Nucleophilic Trifluoromethylation and Beyond. *Chem. Rev.* **2015**, *115*, 683-730.
- [16] Yang, X.; Wu, T.; Phipps, R.J.; Toste, F.D. Advances in Catalytic Enantioselective Fluorination, Mono-, Di-, and Trifluoromethylation, and Trifluoromethylthiolation Reactions. *Chem. Rev.* **2014**, *115*, 826-870.
- [17] Charpentier, J.; Fruh, N.; Togni, A. Electrophilic Trifluoromethylation by Use of Hypervalent Iodine Reagents. *Chem. Rev.* **2014**, *115*, 650-682.
- [18] Ni, C.; Hu, M.; Hu, J. Good Partnership between Sulfur and Fluorine: Sulfur-Based Fluorination and Fluoroalkylation Reagents for Organic Synthesis. *Chem. Rev.* **2014**, *115*, 765-825.
- [19] Belhomme, M.-C.; Besset, T.; Poisson, T.; Pannecoucke, X. Recent Progress toward the Introduction of Functionalized Difluoromethylated Building Blocks onto $\text{C}(\text{sp}^2)$ and $\text{C}(\text{sp})$ Centers. *Chem. Eur. J.* **2015**, *21*, 12836-12865.
- [20] Lu, Y.; Liu, C.; Chen, Q.-Y. Recent Advances in Difluoromethylation Reaction. *Curr. Org. Chem.* **2015**, *19*, 1638-1650.
- [21] Rong, J.; Ni, C.; Hu, J. Metal-Catalyzed Direct Difluoromethylation Reactions. *Asian J. Org. Chem.* **2017**, *6*, 139-152.
- [22] Yerier, D.E.; Barata-Vallejo, S.; Postigo, A. Difluoromethylation Reactions of Organic Compounds. *Chem. Eur. J.* **2017**, *23*, 14676-14701.
- [23] Tucker, J.W.; Zhang, Y.; Jamison, T.F.; Stephenson, C.R.J. Visible-Light Photoredox Catalysis in Flow. *Angew. Chem. Int. Ed.* **2012**, *51*, 4144-4147.

- [24] Hopkinson, M.N.; Sahoo, B.; Li, J.-L.; Glorius, F. Dual Catalysis Sees the Light: Combining Photoredox with Organo-, Acid, and Transition-Metal Catalysis. *Chem. Eur. J.* **2014**, *20*, 3874-3886.
- [25] Koike, T.; Akita, M. Visible-light radical reaction designed by Ru- and Ir-based photoredox catalysis. *Inorg. Chem. Front.* **2014**, *1*, 562-576.
- [26] Meggers, E. Asymmetric catalysis activated by visible light. *Chem. Commun.* **2015**, *51*, 3290-3301.
- [27] Cismesia, M.A.; Yoon, T.P. Characterizing chain processes in visible light photoredox catalysis. *Chem. Sci.* **2015**, *6*, 5426-5434.
- [28] Skubi, K.L.; Blum, T.R.; Yoon, T.P. Dual Catalysis Strategies in Photochemical Synthesis. *Chem. Rev.* **2016**, *116*, 10035-10074.
- [29] Shaw, M.H.; Twilton, J.; Macmillan, D.W.C. Photoredox Catalysis in Organic Chemistry. *J. Org. Chem.* **2016**, *81*, 6898-6926.
- [30] Matsui, J.K.; Lang, S.B.; Heitz, D.R.; Holander, G.A. Photoredox-Mediated Routes to Radicals: The Value of Catalytic Radical Generation in Synthetic Methods Development. *ACS Catal.* **2017**, *7*, 2563-2575.
- [31] To, W.-P.; Tong, G.S.-M.; Lu, W.; Ma, C.; Liu, J.; Chow, A.L.-F.; Che, C.-M. Luminescent Organogold(III) Complexes with Long-Lived Triplet Excited States for Light-Induced Oxidative C-H Bond Functionalization and Hydrogen Production. *Angew. Chem. Int. Ed.* **2012**, *51*, 2654-2657.
- [32] Prier, C.K.; Rankic, D.A.; Macmillan, D.W.C. Visible Light Photoredox Catalysis with Transition Metal Complexes: Applications in Organic Synthesis. *Chem. Rev.* **2013**, *113*, 5322-5363.
- [33] Revol, G.; McCallum, T.; Morin, M.; Gagosz, F.; Barriault, L. Photoredox Transformations With Dimeric Gold Complexes. *Angew. Chem. Int. Ed.* **2013**, *52*, 13342-13345.
- [34] Hari, D.P.; König, B. Eosin Y Catalyzed Visible Light Oxidative C-C and C-P bond Formation. *Org. Lett.* **2011**, *13*, 3852-3855.
- [35] Romero, N.A.; Nicewicz, D.A. Organic Photoredox Catalysis. *Chem. Rev.* **2016**, *116*, 10075-10166.
- [36] Su, F.; Matthew, S.C.; Mohlmann, L.; Antonietti, M.; Wang, X.; Blechert, S. Aerobic Oxidative Coupling of Amines by Carbon Nitride Photocatalysis with Visible Light. *Angew. Chem. Int. Ed.* **2011**, *50*, 657-660.
- [37] Li, X.-B.; Li, Z.-J.; Gao, G.Y.-J.; Meng, Q.-Y.; Yu, S.; Weiss, R.G.; Tung, C.-H.; Wu, L.-Z. Mechanistic Insights Into the Interface-Directed Transformation of Thiols Into Disulfides and Molecular Hydrogen by Visible-Light Irradiation of Quantum Dots. *Angew. Chem. Int. Ed.* **2014**, *53*, 2085-2089.
- [38] Koike, T.; Akita, M. Trifluoromethylation by Visible-Light-Driven Photoredox Catalysis. *Top. Catal.* **2014**, *57*, 967-974.
- [39] Akita, M.; Koike, T. Sunlight-driven trifluoromethylation of olefinic substrates by photoredox catalysis: A green organic process. *C. R. Chim.* **2015**, *18*, 742-751.

- [40] Nagib, D.A.; Scott, M.E.; MacMillan, D.W.C. Enantioselective α -Trifluoromethylation of Aldehydes via Photoredox Organocatalysis. *J. Am. Chem. Soc.* **2009**, *131*, 10875-10877.
- [41] Pham, P.V.; Nagib, D.A.; MacMillan, D.W.C. Photoredox Catalysis: A Mild, Operationally Simple Approach to the Synthesis of α -Trifluoromethyl Carbonyl Compounds. *Angew. Chem. Int. Ed.* **2011**, *50*, 6119-6122.
- [42] Nagib, D.A.; MacMillan, D.W.C. Trifluoromethylation of arenes and heteroarenes by means of photoredox catalysis. *Nature* **2011**, *480*, 224-228.
- [43] Iqbal, N.; Choi, S.; Ko, E.; Cho, E.J. Trifluoromethylation of heterocycles via visible light photoredox catalysis. *Tetrahedron Lett.* **2012**, *53*, 2005-2008.
- [44] Ye, Y.; Sanford, M.S. Merging Visible-Light Photocatalysis and Transition-Metal Catalysis in the Copper-Catalyzed Trifluoromethylation of Boronic Acids with CF_3I . *J. Am. Chem. Soc.* **2012**, *134*, 9034-9037.
- [45] Dagousset, G.; Carboni, A.; Masson, G.; Magnier, E. in *Modern Synthesis Processes and Reactivity of Fluorinated Compounds* (Eds.: H. Groult, F. R. Leroux, A. Tressaud), Elsevier, **2017**, pp. 389-426.)
- [46] Pan, X.; Xia, H.; Wu, J. Recent advances in photoinduced trifluoromethylation and difluoroalkylation. *Org. Chem. Front.* **2016**, *3*, 1163-1185.
- [47] Koike, T.; Akita, M. New Horizons of Photocatalytic Fluoromethylative Difunctionalization of Alkenes. *Chem* **2018**, *4*, 409-437.
- [48] Chen, Q.-Y.; Wu, S.-W. Methyl fluorosulphonyldifluoroacetate; a new trifluoromethylating agent. *J. Chem. Soc., Chem. Commun.* **1989**, *0*, 705-706.
- [49] Clarke, S.L.; McGlacken, G.P. Methyl fluorosulphonyldifluoroacetate (MFSDA): An Underutilised Reagent for Trifluoromethylation. *Chem. Eur. J.* **2017**, *23*, 1219-1230.
- [50] Flamigni, L.; Barbieri, A.; Sabatini, C.; Ventura, B.; Barigelletti, F. Photochemistry and Photophysics of Coordination Compounds: Iridium. *Top. Curr. Chem.* **2007**, *281*, 143-203.
- [51] Yu, W.; Xu, X.-H.; Qing, F.-L. Photoredox Catalysis Mediated Application of Methyl Fluorosulphonyldifluoroacetate as the $\text{CF}_2\text{CO}_2\text{R}$ Radical Source. *Org. Lett.* **2016**, *18*, 5130-5133.
- [52] Luo, X.; Fan, Z.; Zhang, B.; Chen, C.; Xi, C. Visible-light-triggered direct ketodifluoroacetylation of styrenes with (fluorosulfonyl)difluoroacetate and dimethyl sulfoxide leads to α -difluoroacetylated ketones. *Chem. Commun.* **2019**, *55*, 10980-10983.
- [53] Yu, C.; Iqbal, N.; Park, S.; Cho, E.J. Selective difluoroalkylation of alkenes by using visible light photoredox catalysis. *Chem. Commun.* **2014**, *50*, 12884-12887.
- [54] Li, J.; Chen, J.; Jiao, W.; Wang, G.; Li, Y.; Cheng, X.; Li, G. Difluoroalkylation/C-H Annulation Cascade Reaction Induced by Visible-Light Photoredox Catalysis. *J. Org. Chem.* **2016**, *81*, 9992-10001.
- [55] Slinker, J.D.; Gorodetsky, A.A.; Lowry, M.S.; Wang, J.; Parker, S.; Rohl, R.; Bernhard, S.; Malliaras, G.G. Efficient Yellow Electroluminescence from a Single Layer of a Cyclometalated Iridium Complex. *J. Am. Chem. Soc.* **2004**, *126*, 2763-2767.

- [56] Lowry, M.S.; Goldsmith, J.I.; Slinker, J.D.; Rohl, R.; Pascal, R.A.; Malliaras, G.G.; Bernhard, S. Single-Layer Electroluminescent Devices and Photoinduced Hydrogen Production from an Ionic Iridium(III) Complex. *Chem. Mater.* **2005**, *17*, 5712-5719.
- [57] Zhao, Y.-N.; Luo, Y.-C.; Wang, Z.-Y.; Xu, Z.-Y. A new approach to access difluoroalkylated diarylmethanes *via* visible-light photocatalytic cross-coupling reactions. *Chem. Commun.* **2018**, *54*, 3993-3996.
- [58] Jin, W.; Wu, M.; Xiong, Z.; Zhu, G. Visible-light induced three-component alkynyl-difluoroalkylation of unactivated alkenes. *Chem. Commun.* **2018**, *54*, 7924-7927.
- [59] Xu, R.; Cai, C. Three-Component Difluoroalkylation-Thiolation of alkenes by Iron-Facilitated Visible-light Photoredox Catalysis. *Chem. Commun.* **2019**, *53*, 4383-4386.
- [60] Zhou, N.; Wu, M.; Zhang, M.; Zhou, X. Visible-light-induced difluoroacetylation of *o*-(allyloxy)arylaldehydes: access to difluoroacetylated chroman-4-ones. *Asian J. Org. Chem.* **2019**, *8*, 2213-2217.
- [61] Li, L.; Ma, Y.-N.; Tang, M.; Guo, J.; Yang, Z.; Yan, Y.; Ma, X.; Tang, L. Photoredox-Catalyzed Oxydifluoroalkylation of Styrenes for Access to Difluorinated Ketones with DMSO as an Oxidant. *Adv. Synth. Catal.* **2019**, *361*, 3723-3728.
- [62] Xia, Z.-H.; Gao, Z.-H.; Dai, L.; Ye, S. Visible Light Promoted Oxo-Difluoroalkylation of Alkenes with DMSO as the Oxidant. *J. Org. Chem.* **2019**, *84*, 7388-7394.
- [63] Huang, M.-H.; Hao, W.-J.; Jiang, B. Iridium(III)-Catalyzed Difluoroalkylation-Bicyclization of 1,7-Enynes toward Benzo[*a*]fluoren-5-ones under Visible-Light Photoredox Conditions. *Synthesis*, **2020**, DOI: 10.1055/s-0040-1707863.
- [64] Huang, W.; Chen, J.; Hong, D.; Chen, W.; Cheng, X.; Tian, Y.; Li, G. Hydrophosphonodifluoromethylation of Alkenes *via* Thiyl-Radical/Photoredox Catalysis. *J. Org. Chem.* **2018**, *83*, 578-587.
- [65] Yang, S.-D.; Yang, Q.; Li, C.; Qi, Z.-C.; Qiang, X.-Y. Photocatalyzed Intermolecular Aminodifluoromethylphosphonation of Alkenes: Facile Synthesis of α,α -Difluoro- γ -aminophosphonates. *Chem. Eur. J.* **2018**, *24*, 14363-14367.
- [66] Yang, Q.; Lin, Q.-Q.; Xing, H.-Y.; Zhao, Z.-G. Visible-light-mediated difluoromethylphosphonation of alkenes for the synthesis of CF₂P-containing heterocycles. *Org. Chem. Front.* **2019**, *6*, 3939-3943.
- [67] Sheng, J.; Bian, K.-J.; Su, Y.-M.; Liao, G.-X.; Duan, R.; Li, C.; Liu, Z.; Wang, X.-S. Visible Light-Mediated Atom Transfer Radical Addition to Styrene: Base Controlled Selective (Phenylsulfonyl)difluoromethylation. *Org. Chem. Front.* **2020**, *6*, 617-621.
- [68] Yang, B.; Xu, X.-H.; Qing, F.-L. Synthesis of Difluoroalkylated Arenes by Hydroaryldifluoromethylation of Alkenes with α,α -Difluoroarylacetic Acids under Photoredox Catalysis. *Org. Lett.* **2016**, *18*, 5956-5959.
- [69] Zhou, Y.; Xiong, Z.; Qiu, J.; Kong, L.; Zhu, G. Visible light photocatalytic acyldifluoroalkylation of unactivated alkenes for the direct synthesis of *gem*-difluorinated ketones. *Org. Chem. Front.* **2019**, *6*, 1022-1026.

- [70] Tang, X.-J.; Zhang, Z.; Dolbier, W.R. Direct Photoredox-Catalyzed Reductive Difluoromethylation of Electron-Deficient Alkenes. *Chem. Eur. J.* **2015**, *21*, 18961-18965.
- [71] Zhang, Z.; Tang, X.; Thomason, C.S.; Dolbier, W.R. Photoredox-Catalyzed Intramolecular Aminodifluoromethylation of Unactivated Alkenes. *Org. Lett.* **2015**, *17*, 3528-3531.
- [72] Kern, J.-K.; Sauvage, J.-P. Photoassisted C–C coupling *via* electron transfer to benzylic halides by a bis(di-imine) copper(I) complex. *J. Chem. Soc., Chem. Commun.* **1987**, *0*, 546-548.
- [73] Zhang, Z.; Martinez, H.; Dolbier, W.R. Photoredox Catalyzed Intramolecular Fluoroalkylarylation of Unactivated Alkenes. *J. Org. Chem.* **2017**, *82*, 2589-2598.
- [74] Lin, Q.-Y.; Xu, X.-H.; Zhang, K.; Qing, F.-L. Visible-Light-Induced Hydrodifluoromethylation of Alkenes With a Bromodifluoromethylphosphonium Bromide. *Angew. Chem. Int. Ed.* **2016**, *55*, 1479-1483.
- [75] Burton, D.J. Preparation and synthetic utility of fluorinated phosphonium salts, bis-phosphonium salts and phosphoranium salts. *J. Fluorine Chem.* **1983**, *23*, 339-357.
- [76] Krasutsky, P.A.; Jones, M. Reaction of diphenyl- and difluorocarbenes with 3,7-dimethylenebicyclo[3.3.1]nonane. *J. Org. Chem.* **1980**, *45*, 2425-2429.
- [77] Shiue, G.-H.; Missiltz, U.; Ding, X.-t.; Jones, M.; de Meijere, A. Reaction of carbenes with bicyclo[2.1.0]pentane. *Tetrahedron Lett.* **1985**, *26*, 5399-5402.
- [78] Weber, J.; Xu, L.; Brinker, U.H. First formation of 1,1-dihalo-1,3-butadienes from reactions of dichloro- and dibromocarbenes with cyclopropenes via new addition-rearrangements. *Tetrahedron Lett.* **1992**, *33*, 4537-4540.
- [79] Flynn, R.M.; Burton, D.J.; Wiemers, D.M. Synthetic and mechanistic aspects of the reactions between bromodifluoromethyltriphenylphosphonium bromide and dibromodifluoromethyltriphenylphosphonium bromide and trialkylphosphites. *J. Fluorine Chem.* **2008**, *129*, 583-589.
- [80] Lin, Q.-Y.; Ran, Y.; Xu, X.-H.; Qing, F.-L. Photoredox-Catalyzed Bromodifluoromethylation of Alkenes with (Difluoromethyl)triphenylphosphonium Bromide. *Org. Lett.* **2016**, *18*, 2419-2422.
- [81] Ran, Y.; Lin, Q.-Y.; Xu, X.-H.; Qing, F.-L. Visible Light Induced Oxydifluoromethylation of Styrenes with Difluoromethyltriphenylphosphonium Bromide. *J. Org. Chem.* **2016**, *81*, 7001-7007.
- [82] Zhang, W.; Wang, F.; Hu, J. *N*-Tosyl-*S*-difluoromethyl-*S*-phenylsulfoximine: A New Difluoromethylation Reagent for *S*-, *N*-, and *C*-Nucleophiles. *Org. Lett.* **2009**, *11*, 2109-2112.
- [83] Arai, Y.; Tomita, R.; Ando, G.; Koike, T.; Akita, M. Oxydifluoromethylation of Alkenes by Photoredox Catalysis: Simple Synthesis of CF₂H-Containing Alcohols. *Chem. Eur. J.* **2016**, *22*, 1262-1265.
- [84] Nakayama, Y.; Ando, G.; Abe, M.; Koike, T.; Akita, M. Keto-Difluoromethylation of Aromatic Alkenes by Photoredox Catalysis: Step-Economical Synthesis of α -CF₂H-Substituted Ketones in Flow. *ACS Catal.* **2019**, *9*, 6555-6563.

- [85] Zhu, M.; Fun, W.; Guo, W.; Tian, Y.; Wang, Z.; Xu, C.; Ji, B. Visible-Light-Induced Radical Di- and Trifluoromethylation of β,γ -Unsaturated Oximes: Synthesis of Di- and Trifluoromethylated Isoxazolines. *Eur. J. Org. Chem.* **2019**, 2019, 1614-1619.
- [86] Zhang, M.; Lin, J.-H.; Xiao, J.-C. Photocatalyzed Cyanodifluoromethylation of Alkenes. *Angew. Chem. Int. Ed.* **2019**, 58, 6079-6083.
- [87] Kosobokov, M.D.; Zubkov, M.O.; Levin, V.V.; Kokorekin, V.A.; Dilman, A.D. Fluoroalkyl sulfides as photoredox-active coupling reagents for alkene difunctionalization. *Chem. Commun.* **2020**, DOI: 10.1039/D0CC04617E.
- [88] Thomason, C.S.; Dolbier, W.R. Carbomethoxydifluoromethylation of enol acetates with methyl (chlorosulfonyl)difluoroacetate using visible-light photoredox catalysis. Synthesis of 2,2-difluoro- γ -ketoesters. *J. Fluorine Chem.* **2015**, 178, 327-331.
- [89] Yu, W.; Ouyang, Y.; Xu, X.-H.; Qing, F.-L. Visible Light-Induced Methoxycarbonyldifluoromethylation of Trimethylsilyl Enol Ethers and Allyltrimethylsilanes with FSO₂CF₂CO₂Me. *Chin. J. Chem.* **2018**, 36, 1024-1030.
- [90] King, C.; Wang, J.-C.; Khan, M.N.I.; Fackler, J.P.; Jr. Luminescence and metal-metal interactions in binuclear gold(I) compounds. *Inorg. Chem.* **1989**, 28, 2145-2149.
- [91] Zidan, M.; Rohe, S.; McCallum, T.; Barriault, L. Recent advances in mono and binuclear gold photoredox catalysis. *Catal. Sci. Technol.* **2018**, 8, 6019-6028.
- [92] Supranovich, V.I.; Levin, V.V.; Dilman, A.D. Photoredox-catalyzed silyldifluoromethylation of silyl enol ethers. *Beilstein J. Org. Chem.* **2020**, 16, 1550-1553.
- [93] Qu, C.; Xu, P.; Ma, W.; Cheng, Y.; Zhu, C. A novel visible light mediated radical cyclization of enol lactones: a concise method for fluorinated polycyclic lactone scaffolds. *Chem. Commun.* **2015**, 51, 13508-13510.
- [94] Li, Z.; Cui, Z.; Liu, Z.-Q. Copper- and Iron-Catalyzed Decarboxylative Tri- and Difluoromethylation of α,β -Unsaturated Carboxylic Acids with CF₃SO₂Na and (CF₂HCO₂)₂Zn via a Radical Process. *Org. Lett.* **2013**, 15, 406-409.
- [95] Li, G.; Wang, T.; Fei, F.; Su, Y.M.; Li, Y.; Lan, Q.; Wang, X.S. Nickel-Catalyzed Decarboxylative Difluoroalkylation of α,β -Unsaturated Carboxylic Acids. *Angew. Chem. Int. Ed.* **2016**, 55, 3491-3495.
- [96] Zhang, H.-R.; Chen, D.-Q.; Han, Y.-P.; Qiu, Y.-F.; Jin, D.-P.; Liu, X.-Y. Merging photoredox with copper catalysis: decarboxylative difluoroacetylation of α,β -unsaturated carboxylic acids with ICF₂CO₂Et. *Chem. Commun.* **2016**, 52, 11827-11830.
- [97] Juris, A.; Balzani, V.; Belser, P.; von Zelewsky, A. Characterization of the Excited State Properties of Some New Photosensitizers of the Ruthenium (Polypyridine) Family. *Helv. Chim. Acta* **1981**, 64, 2175-2182.
- [98] Kalyanasundaram, K. Photophysics, photochemistry and solar energy conversion with tris(bipyridyl)ruthenium(II) and its analogues. *Coord. Chem. Rev.* **1982**, 46, 159-244.
- [99] Zhong, J.-J.; Yang, C.; Chang, X.-Y.; Zou, C.; Lu, W.; Che, C.-M. Platinum(ii) photo-catalysis for highly selective difluoroalkylation reactions. *Chem. Commun.* **2017**, 53, 8948-8951.
- [100] Wei, X.-J.; Boom, W.; Hessel, V.; Noël, T. Visible-Light Photocatalytic Decarboxylation of α,β -Unsaturated Carboxylic Acids: Facile Access to

Stereoselective Difluoromethylated Styrenes in Batch and Flow. *ACS Catal.* **2017**, *7*, 7136-7140.

[101] Xu, P.; Hu, K.; Gu, Z.; Cheng, Y.; Zhu, C. Visible light promoted carbodifluoroalkylation of allylic alcohols *via* concomitant 1,2-aryl migration. *Chem. Commun.* **2015**, *51*, 7222-7225.

[102] Wei, X.-J.; Noël, T. Visible-Light Photocatalytic Difluoroalkylation-Induced 1,2-Heteroarene Migration of Allylic Alcohols in Batch and Flow. *J. Org. Chem.* **2018**, *83*, 11377-11384.

[103] Liu, J.; Li, W.; Xie, J.; Zhu, C. Photoredox 1,2-dicarbofunctionalization of unactivated alkenes *via* tandem radical difluoroalkylation and alkynyl migration. *Org. Chem. Front.* **2018**, *5*, 797-800.

[104] Yu, J.; Wang, D.; Xu, Y.; Wu, Z.; Zhu, C. Distal Functional Group Migration for Visible-light Induced Carbo-difluoroalkylation/monofluoroalkylation of Unactivated Alkenes. *Adv. Synth. Catal.* **2018**, *360*, 744-750.

[105] Suh, C.W.; Kim, D.Y. Visible-light-mediated photocatalytic difluoroalkylation/1,2-carbon migration sequences: synthesis of difluoroalkyl-substituted cyclic ketones. *Tetrahedron Lett.* **2015**, *56*, 5661-5664.

[106] Kim, Y.J.; Kim, D.Y. Visible light photoredox-catalyzed difluoromethylation and ring expansion of 1-(1-arylvinyl)cyclobutanols. *J. Fluorine Chem.* **2018**, *211*, 119-123.

[107] Noto, N.; Koike, T.; Akita, M. Diastereoselective Synthesis of CF₃- and CF₂H-Substituted Spiroethers from Aryl-Fused Cycloalkenylalkanols by Photoredox Catalysis. *J. Org. Chem.* **2016**, *81*, 7064-7071.

[108] Tang, X.-J.; Thomason, C.S.; Dolbier, W.R. Photoredox-Catalyzed Tandem Radical Cyclization of *N*-Arylacrylamides: General Methods To Construct Fluorinated 3,3-Disubstituted 2-Oxindoles Using Fluoroalkylsulfonyl Chlorides. *Org. Lett.* **2014**, *16*, 4594-4597.

[109] Zhu, M.; You, Q.; Li, R. Synthesis of CF₂H-containing oxindoles *via* photoredox-catalyzed radical difluoromethylation and cyclization of *N*-arylacrylamides. *J. Fluorine Chem.* **2019**, DOI: 10.1016/j.jfluchem.2019.109391.

[110] Sun, H.; Jiang, Y.; Yang, Y.-S.; Li, Y.-Y.; Li, L.; Wang, W.-X.; Feng, T.; Li, Z.-H.; Liu, J.-K. Synthesis of difluoromethylated 2-oxindoles and quinoline-2,4-diones *via* visible light-induced tandem radical cyclization of *N*-arylacrylamides. *Org. Biomol. Chem.* **2019**, *17*, 6629-6638.

[111] Hu, W.-Q.; Xu, X.-H.; Qing, F.-L. Visible light induced hydrodifluoromethylation of alkenes derived from oxindoles with (difluoromethyl)triphenylphosphonium bromide. *J. Fluorine Chem.* **2018**, *208*, 73-79.

[112] Fu, W.; Zhu, M.; Zou, G.; Xu, C.; Wang, Z. Visible-Light-Mediated Radical Aryldifluoroacetylation of *N*-Arylacrylamides to give Difluoroacetylated Oxindoles. *Asian J. Org. Chem.* **2014**, *3*, 1273-1276.

[113] Yin, G.; Zhu, M.; Yang, G.; Wang, X.; Fu, W. Synthesis of difluoromethylenephosphonated oxindoles through visible-light-induced radical cyclization of *N*-arylacrylamides. *J. Fluorine Chem.* **2016**, *191*, 63-69.

- [114] Liu, X.; Wu, Z.; Zhang, Z.; Liu, P.; Sun, P. Synthesis of trifluoroalkyl or difluoroalkyl phenanthridine derivatives *via* cascade reaction using an intramolecular cyano group as a radical acceptor under photoredox catalysis. *Org. Biomol. Chem.* **2018**, *16*, 414-423.
- [115] Zhang, Z.; Tang, X.-J.; Dolbier, W.R. Photoredox-Catalyzed Intramolecular Difluoromethylation of *N*-Benzylacrylamides Coupled with a Dearomatizing Spirocyclization: Access to CF₂H-Containing 2-Azaspiro[4.5]deca-6,9-diene-3,8-diones. *Org. Lett.* **2016**, *18*, 1048-1051.
- [116] Zou, G.; Wang, X. Visible-light induced di- and trifluoromethylation of *N*-benzamides with fluorinated sulfones for the synthesis of CF₂H/CF₃-containing isoquinolinediones. *Org. Biomol. Chem.* **2017**, *15*, 8748-8754.
- [117] Zhu, T.-H.; Zhang, Z.-Y.; Tao, J.-Y.; Zhao, K.; Loh, T.-P. Regioselective and Stereoselective Difluoromethylation of Enamides with Difluoromethyltriphenylphosphonium Bromide *via* Photoredox Catalysis. *Org. Lett.* **2019**, *21*, 6155-6159.
- [118] Gu, Z.; Zhang, H.; Xu, P.; Cheng, Y.; Zhu, C. Visible-Light-Induced Radical Tandem Aryldifluoroacetylation of Cinnamamides: Access to Difluoroacetylated Quinolone-2-ones And 1-Azaspiro[4.5]decenes. *Adv. Synth. Catal.* **2015**, *357*, 3057-3063.
- [119] Huang, H.; Li, Y. Sustainable Difluoroalkylation Cyclization Cascades of 1,8-Enynes. *J. Org. Chem.* **2017**, *82*, 4449-4457.
- [120] Huang, H.; Yu, M.; Su, X.; Guo, P.; Zhao, J.; Zhou, J.; Li, Y. Sustainable Radical Cascades to Synthesize Difluoroalkylated Pyrrolo[1,2-*a*]indoles. *J. Org. Chem.* **2018**, *83*, 2425-2437.
- [121] Fu, W.; Han, X.; Zhu, M.; Xu, C.; Wang, Z.; Ji, B.; Hao, X.-Q.; Song, M.-P. Visible-light-mediated radical oxydifluoromethylation of olefinic amides for the synthesis of CF₂H-containing heterocycles. *Chem. Commun.* **2016**, *52*, 13413-13416.
- [122] Xu, P.; Wang, G.; Zhu, Y.; Li, W.; Cheng, Y.; Li, S.; Zhu, C. Visible-Light Photoredox-Catalyzed C-H Difluoroalkylation of Hydrazones through an Aminyl Radical/Polar Mechanism. *Angew. Chem. Int. Ed.* **2016**, *55*, 2939-2943.
- [123] Xia, P.-J.; Ye, Z.-P.; Song, D.; Ren, J.-W.; Wu, H.-W.; Xiao, J.-A.; Xiang, H.-Y.; Chen, X.-Q.; Yang, H. Photocatalytic reductive radical-radical coupling of *N,N'*-cyclicazomethine imines with difluorobromo derivatives. *Chem. Commun.* **2019**, *55*, 2712-2715.
- [124] Gao, H.; Hu, B.; Dong, W.; Gao, X.; Jiang, L.; Xie, X.; Zhang, Z. Synthesis of 3-CF₂-Containing Chromones *via* a Visible-Light-Induced Radical Cascade Reaction of *o*-Hydroxyaryl Enaminones. *ACS Omega* **2017**, *2*, 3168-3174.
- [125] Xiang, H.; Zhao, Q.; Tang, Z.; Xiao, J.; Xia, P.; Wang, C.; Yang, C.; Chen, X.; Yang, H. Visible-Light-Driven, Radical-Triggered Tandem Cyclization of *o*-Hydroxyaryl Enaminones: Facile Access to 3-CF₂/CF₃-Containing Chromones. *Org. Lett.* **2017**, *19*, 146-149.

- [126] Xiang, H.; Zhao, Q.-L.; Xia, P.-J.; Xiao, J.-A.; Ye, Z.-P.; Xie, X.; Sheng, H.; Chen, X.-Q.; Yang, H. Visible-Light-Induced External Radical-Triggered Annulation To Access CF₂-Containing Benzoxepine Derivatives. *Org. Lett.* **2018**, *20*, 1363-1366.
- [127] Yin, Z.-B.; Ye, J.-H.; Zhou, W.-J.; Zhang, Y.-H.; Ding, L.; Gui, Y.-Y.; Yan, S.-S.; Li, J.; Yu, D.-G. Oxy-Difluoroalkylation of Allylamines with CO₂ via Visible-Light Photoredox Catalysis. *Org. Lett.* **2018**, *20*, 190-193.
- [128] Bao, K.; Wei, J.; Yan, H.; Sheng, R. Visible-light promoted three-component tandem reaction to synthesize difluoromethylated oxazolidin-2-imine. *RSC Adv.* **2020**, *10*, 25947-25951.
- [129] Wang, L.; Wei, X.-J.; Jia, W.-L.; Zhong, J.-J.; Wu, L.-Z.; Liu, Q. Visible-Light-Driven Difluoroacetamidation of Unactive Arenes and Heteroarenes by Direct C–H Functionalization at Room Temperature. *Org. Lett.* **2014**, *16*, 5842-5845.
- [130] Wang, L.; Wei, X.-J.; Lei, W.-L.; Chen, H.; Wu, L.-Z.; Liu, Q. Direct C–H difluoromethylenephosphonation of arenes and heteroarenes with bromodifluoromethyl phosphonate *via* visible-light photocatalysis. *Chem. Commun.* **2014**, *50*, 15916-15919.
- [131] Jung, J.; Kim, E.; You, Y.; Cho, E.J. Visible Light-Induced Aromatic Difluoroalkylation. *Adv. Synth. Catal.* **2014**, *356*, 2741-2748.
- [132] Yu, L.-C.; Gu, J.-W.; Zhang, S.; Zhang, X. Visible-Light-Promoted Tandem Difluoroalkylation–Amidation: Access to Difluorooxindoles from Free Anilines. *J. Org. Chem.* **2017**, *82*, 3943-3949.
- [133] Hua, M.-Q.; Mou, F.-Y.; Wang, N.-H.; Chen, Y.; Xiong, H.-Y.; Huang, Y.; Lei, C.-L.; Zhang, Q. Visible-Light-Induced Photocatalytic Difluoroalkylation of 3-Substituted Benzo[*d*]isoxazoles *via* Direct and Regioselective C-H Functionalization. *Tetrahedron Lett.* **2018**, *59*, 4449-4453.
- [134] Jin, C.; Zhuang, X.; Sun, B.; Li, D.; Zhu, R. Merging Visible-Light Photoredox and Organoamine Catalysis for the C-3 Difluoroalkylation of Quinoxalin-2(1*H*)-Ones. *Asian J. Org. Chem.* **2019**, *8*, 1490-1494.
- [135] Jin, C.; Zhu, R.; Sun, B.; Zhang, L.; Zhuang, X.; Yu, C. Visible-Light-Induced Remote C-H Difluoroalkylation of 8-Aminoquinolines via Debrominative Coupling with Functionalized Difluoromethyl Bromides. *Asian J. Org. Chem.* **2019**, *8*, 2213-2217.
- [136] Zhou, J.; Wang, F.; Lin, Z.; Cheng, C.; Zhang, Q.; Li, J. Visible-Light-Induced *para*-Selective C(sp²)-H Difluoroalkylation of Diverse (Hetero)aromatic Carbonyls. *Org. Lett.* **2020**, *22*, 68-72.
- [137] Yin, G.; Zhu, M.; Fu, W. Visible-light-induced photocatalytic difluoroacetylation of imidazopyridines *via* direct and regioselective C-H functionalization. *J. Fluorine Chem.* **2017**, *199*, 14-19.
- [138] Yin, G.; Zhu, M.; Fu, W. in *Heterocyclic Communications, Vol. 23* (Eds.: A. L. Baumstark, J. Saczewski, C. Stephens, H. Yamada), Walter de Gruyter GmbH, Berlin/Boston, **2017**, pp. 275-279.)
- [139] Su, Y.-M.; Hou, Y.; Yin, F.; Xu, Y.-M.; Li, Y.; Zheng, X.; Wang, X.-S. Visible Light-Mediated C–H Difluoromethylation of Electron-Rich Heteroarenes. *Org. Lett.* **2014**, *16*, 2958-2961.

- [140] Wu, Y.-B.; Lu, G.-P.; Zhou, B.-J.; Bu, M.-J.; Wan, L.; Cai, C. Visible-light-initiated difluoromethylation of arene diazonium tetrafluoroborates. *Chem. Commun.* **2016**, *52*, 5965-5968.
- [141] McAtee, R.C.; Beatty, J.W.; McAtee, C.C.; Stephenson, C.R.J. Radical Chlorodifluoromethylation: Providing a Motif for (Hetero)arene Diversification. *Org. Lett.* **2018**, *20*, 3491-3495.
- [142] Bacauanu, V.; Cardinal, S.; Yamauchi, M.; Kondo, M.; Fernández, D.F.; Remy, R.; MacMillan, D.W.C. Metallaphotoredox Difluoromethylation of Aryl Bromides. *Angew. Chem. Int. Ed.* **2018**, *57*, 12543-12548.
- [143] Rubinski, M.A.; Lopez, S.E.; Dolbier Jr, W.R. Direct Access to 2-Difluoromethyl Indoles *via* Photoredox Catalysis. *J. Fluorine Chem.* **2019**, *224*, 80-88.
- [144] Fu, W.; Zhu, M.; Zou, G.; Xu, C.; Wang, Z.; Ji, B. Visible-Light-Mediated Radical Aryldifluoroacetylation of Alkynes with Ethyl Bromodifluoroacetate for the Synthesis of 3-Difluoroacetylated Coumarins. *J. Org. Chem.* **2015**, *80*, 4766-4770.
- [145] Zhu, M.; Fu, W.; Wang, Z.; Xu, C.; Ji, B. Visible-light-mediated direct difluoromethylation of alkynoates: synthesis of 3-difluoromethylated coumarins. *Org. Biomol. Chem.* **2017**, *15*, 9057-9060.
- [146] Deng, Q.; Xu, Y.; Liu, P.; Tan, L.; Sun, P. Photoredox-catalyzed cascade addition/cyclization of *N*-propargyl aromatic amines: access to 3-difluoroacetylated or 3-fluoroacetylated quinolines. *Org. Chem. Front.* **2018**, *5*, 19-23.
- [147] Wan, Y.; Shang, T.; Lu, Z.; Zhu, G. Photocatalytic 1,1-hydrofluoroalkylation of alkynes with concurrent vicinal acylation: an access to fluoroalkylated cyclic ketones. *Org. Lett.* **2019**, *21*, 4187-4191.
- [148] Iqbal, N.; Iqbal, N.; Han, S.S.; Cho, E.J. Synthesis of fluoroalkylated alkynes *via* visible-light photocatalysis. *Org. Biomol. Chem.* **2019**, *17*, 1758-1762.
- [149] Sun, X.; Yu, S. Visible-Light-Mediated Fluoroalkylation of Isocyanides with Ethyl Bromofluoroacetates: Unified Synthesis of Mono- and Difluoromethylated Phenanthridine Derivatives. *Org. Lett.* **2014**, *16*, 2938-2941.
- [150] Wang, S.; Jia, W.-L.; Wang, L.; Liu, Q. Preparation of 6-Difluoromethylphosphonated Phenanthridines by Visible-Light-Driven Radical Cyclization of 2-Isocyanobiphenyls. *Eur. J. Org. Chem.* **2015**, *2015*, 6817-6821.
- [151] Zhu, M.; Fu, W.; Zou, G.; Xu, C.; Wang, Z. Visible-light-mediated radical difluoromethylenephosphonation of 2-isocyanobiaryls with bromodifluoromethylphosphonate for the synthesis of 6-difluoromethylenephosphonyl-phenanthridines. *J. Fluorine Chem.* **2015**, *180*, 1-6.
- [152] Zhang, Z.; Tang, X.; Dolbier, W.R. Photoredox-Catalyzed Tandem Insertion/Cyclization Reactions of Difluoromethyl and 1,1-Difluoroalkyl Radicals with Biphenyl Isocyanides. *Org. Lett.* **2015**, *17*, 4401-4403.
- [153] Rong, J.; Deng, L.; Tan, P.; Ni, C.; Gu, Y.; Hu, J. Radical Fluoroalkylation of Isocyanides with Fluorinated Sulfones by Visible-Light Photoredox Catalysis. *Angew. Chem, Int. Ed.* **2016**, *55*, 2743-2747.

- [154] Wei, J.; Gu, D.; Wang, S.; Hu, J.; Dong, X.; Sheng, R. Visible-light-mediated radical arylthiodifluoromethylation of isocyanides with fluorinated 2-pyridyl sulfones. *Org. Chem. Front.* **2018**, *5*, 2568-2572.
- [155] Qin, W.-B.; Xiong, W.; Li, X.; Chen, J.-Y.; Lin, L.-T.; Wong, H.N.C.; Liu, G.-K. Visible-light-driven Difluoromethylation of Isocyanides with S-(Difluoromethyl)diarylsulfonium Salt: Access to a Wide Variety of Difluoromethylated Phenanthridines and Isoquinolines. *J. Org. Chem.* **2020**, DOI: 10.1021/acs.joc.0c00816.
- [156] Yang, J.; Jiang, M.; Jin, Y.; Yang, H.; Fu, H. Visible-Light Photoredox Difluoromethylation of Phenols and Thiophenols with Commercially Available Difluorobromoacetic Acid. *Org. Lett.* **2017**, *19*, 2758-2761.
- [157] Ran, Y.; Lin, Q.-Y.; Xu, X.-H.; Qing, F.-L. Radical Difluoromethylation of Thiols with Difluoromethylphosphonium Triflate under Photoredox Catalysis. *J. Org. Chem.* **2017**, *82*, 7373-7378.
- [158] Ravelli, D.; Fagnoni, M.; Albini, A. Photoorganocatalysis. What for? *Chem. Soc. Rev.* **2013**, *42*, 97-113.
- [159] Hari, D.P.; König, B. Synthetic applications of eosin Y in photoredox catalysis. *Chem. Commun.* **2014**, *50*, 6688-6699.
- [160] Davide, R.; Maurizio, F. Dyes as Visible Light Photoredox Organocatalysts. *ChemCatChem* **2012**, *4*, 169-171.
- [161] Nicewicz, D.A.; Nguyen, T.M. Recent Applications of Organic Dyes as Photoredox Catalysts in Organic Synthesis. *ACS Catal.* **2014**, *4*, 355-360.
- [162] Lin, Q.-Y.; Xu, X.-H.; Qing, F.-L. Visible light-induced selective hydrobromodifluoromethylation of alkenes with dibromodifluoromethane. *Org. Biomol. Chem.* **2015**, *13*, 8740-8749.
- [163] Tang, W.-K.; Feng, Y.-S.; Xu, Z.-W.; Cheng, Z.-F.; Xu, J.; Dai, J.-J.; Xu, H.-J. Visible-Light-Enabled Decarboxylative Mono- and Difluoromethylation of Cinnamic Acids under Metal-Free Conditions. *Org. Lett.* **2017**, *19*, 5501-5504.
- [164] Zhang, X.-F.; Zhang, J.; Liu, L. Fluorescence Properties of Twenty Fluorescein Derivatives: Lifetime, Quantum Yield, Absorption and Emission Spectra. *J. Fluoresc.* **2014**, *24*, 819-826.
- [165] Furukawa, Y.; Hayashi, M.; Hayase, S.; Nokami, T.; Itoh, T. Visible-Light-Driven Direct 2,2-Difluoroacetylation Using an Organic Pigment Catalyst. *ACS Sustainable Chem. Eng.* **2020**, *8*, 6533-6542.
- [166] Dai, P.; Yu, X.; Teng, P.; Zhang, W.-H.; Deng, C. Visible-light- and oxygen-promoted direct Csp³-H radical difluoromethylation of coumarins and antifungal activities. *Org. Lett.* **2018**, *20*, 6901-6905.
- [167] Fukuzumi, S.; Kotani, H.; Ohkubo, K.; Ogo, S.; Tkachenko, N.V.; Lemmetyinen, H. Electron-Transfer State of 9-Mesityl-10-methylacridinium Ion with a Much Longer Lifetime and Higher Energy Than That of the Natural Photosynthetic Reaction Center. *J. Am. Chem. Soc.* **2004**, *126*, 1600-1601.

- [168] Ohkubo, K.; Kotani, H.; Fukuzumi, S. Misleading effects of impurities derived from the extremely long-lived electron-transfer state of 9-mesityl-10-methylacridinium ion. *Chem. Commun.* **2005**, *0*, 4520-4522.
- [169] Ohkubo, K.; Mizushima, K.; Iwata, R.; Souma, K.; Suzuki, N.; Fukuzumi, S. Simultaneous production of *p*-tolualdehyde and hydrogen peroxide in photocatalytic oxygenation of *p*-xylene and reduction of oxygen with 9-mesityl-10-methylacridinium ion derivatives. *Chem. Commun.* **2010**, *46*, 601-603.
- [170] Romero, N.A.; Nicewicz, D.A. Mechanistic Insight into the Photoredox Catalysis of Anti-Markovnikov Alkene Hydrofunctionalization Reactions. *J. Am. Chem. Soc.* **2014**, *136*, 17024-17035.
- [171] Fang, J.; Shen, W.-G.; Ao, G.-Z.; Liu, F. Transition-metal-free radical fluoroalkylation of isocyanides for the synthesis of tri-/di-/monofluoromethylated phenanthridines. *Org. Chem. Front.* **2017**, *4*, 2049-2053.
- [172] Wu, Q.-Y.; Ao, G.-Z.; Liu, F. Redox-neutral tri-/difluoromethylation of *para*-quinone methides with sodium sulfonates. *Org. Chem. Front.* **2018**, *5*, 2061-2064.
- [173] Sauer, M.; Han, K.T.; Ebert, V.; Müller, R.; Schulz, A.; Seeger, S.; Wolfrum, J.; Arden-Jacob, J.; Deltau, G.; Marx, N.J.; Zander, C.; Drexhage, K.H. New fluorescent dyes in the red region for biodiagnostics. *J. Fluoresc.* **1995**, *5*, 247-261.
- [174] Dietrich, A.; Buschmann, V.; Müller, C.; Sauer, M. Fluorescence resonance energy transfer (FRET) and competing processes in donor-acceptor substituted DNA strands: a comparative study of ensemble and single-molecule data. *J. Biotechnol.* **2002**, *82*, 211-231.
- [175] Garrido-Castro, A.F.; Gini, A.; Maestro, M.C.; Alemán, J. Unlocking the Direct Photocatalytic Difluoromethylation of C=N Bonds. *Chem. Commun.* **2020**, *56*, 3769-3772.
- [176] Noto, N.; Koike, T.; Akita, M. Metal-free di- and tri-fluoromethylation of alkenes realized by visible-light-induced perylene photoredox catalysis. *Chem. Sci.* **2017**, *8*, 6375-6379.
- [177] Uoyama, H.; Goushi, K.; Shizu, K.; Nomura, H.; Adachi, C. Highly efficient organic light-emitting diodes from delayed fluorescence. *Nature* **2012**, *492*, 234-238.
- [178] Ishimatsu, R.; Matsunami, S.; Kasahara, T.; Mizuno, J.; Edura, T.; Adachi, C.; Nakano, K.; Imato, T. Electrogenerated chemiluminescence of donor-acceptor molecules with thermally activated delayed fluorescence. *Angew. Chem. Int. Ed.* **2014**, *53*, 6993-6996.
- [179] Lévêque, C.; Chenneberg, L.; Corcé, V.; Ollivier, C.; Fensterbank, L. Organic photoredox catalysis for the oxidation of silicates: applications in radical synthesis and dual catalysis. *Chem. Commun.* **2016**, *52*, 9877-9880.
- [180] Li, J.-X.; Li, L.; Zhou, M.-D.; Wang, H. Visible-light-promoted organic-dye-catalyzed three-component coupling of aldehydes, hydrazines and bromodifluorinated reagents. *Org. Chem. Front.* **2018**, *5*, 1003-1007.
- [181] Singardar, M.; Mondal, S.; Laru, S.; Hajra, A. Organophotoredox-Catalyzed C(sp²)-H Difluoromethylenephosphonation of Imidazoheterocycles. *Org. Lett.* **2019**, *21*, 5606-5610.

- [182] Shen, T.; Zhao, Z.-G.; Yu, Q.; Xu, H.-J. Photosensitized Reduction of Benzil by Heteroatom-Containing Anthracene Dyes. *J. Photochem. Photobiol., A* **1989**, *47*, 203–212.
- [183] Zhang, W.; Xiang, X.-X.; Chen, J.; Yang, C.; Pan, Y.-L.; Cheng, J.-P.; Meng, Q.; Li, X. Direct C–H difluoromethylation of heterocycles *via* organic photoredox catalysis. *Nat. Commun.* **2020**, *11*, 638, DOI: 10.1038/s41467-020-14494-8.
- [184] Trifonov, A.L.; Panferova, L.I.; Levin, V.V.; Kokorekin, V.A.; Dilman, A.D. Visible-Light-Promoted Iododifluoromethylation of Alkenes *via* (Phosphonio)difluoromethyl Radical Cation. *Org. Lett.* **2020**, *22*, 2409–2413.

Chapter II

Progress in the Synthesis of ^{18}F - Difluoromethylated Molecules

Chapter II

1. Introduction.....	101
2. Synthesis of [¹⁸ F]CHF ₂ -containing compounds <i>via</i> ¹⁸ F-fluorination.....	110
3. Synthesis of [¹⁸ F]CHF ₂ -containing compounds <i>via</i> C-H ¹⁸ F-difluoromethylation.....	119
4. Concluding Remarks.....	121
References.....	122

Progress in the Synthesis of ^{18}F -Difluoromethylated Compounds

Abstract: The suitability of the radionuclide ^{18}F in positron emission tomography (PET) has encouraged radiochemists to invest much effort in the development of ^{18}F -fluorination and ^{18}F -fluoroalkylation reactions. The difluoromethyl (CHF_2) groups are abundant and have gained a growing interest in pharmaceutical and agrochemical industries. Despite the advances in the preparation of difluoromethylated compounds, the ^{18}F -labeling of CHF_2 groups has recently received an increasing attention in radiochemistry. The present chapter summarizes all synthetic methods to access ^{18}F -difluoromethylated derivatives either by ^{18}F -fluorination or by direct transfer of ^{18}F -labeled CHF_2 groups in suitable precursors.

Keywords: positron emission tomography; fluorine-18; radiochemistry; difluoromethylation

1. Introduction

Positron emission tomography (PET) is a leading molecular imaging technique that has the ability to reveal a detailed picture of pharmacological, physiological, and biochemical processes in living subjects [1-4]. In terms of clinical diagnosis, the PET technology offers information that cannot be acquired using anatomical and structural imaging techniques such as magnetic resonance imaging (MRI), ultrasound (US), or computed tomography (CT) [1-4]. As such, PET can track biochemical and metabolic changes that may take place before the anatomical signs of a disease are detected. In combination with CT, the PET scanning is broadly used in the diagnosis and management of tumors [5-7], heart diseases [8-10], and neurological disorders [11-14]. The PET technology is highly sensitive with the quantity of radiotracer administered to living subjects by intravenous injection. In fact, only trace amounts of the radiolabeled drugs (10^{-9} - 10^{-6} grams) are needed for the PET experiments without perturbing the biological system. The application of this imaging technique relies on the use of specific radioactive probes labeled with a usually short-lived positron-emitting radionuclide such as carbon-11 (^{11}C), nitrogen-13 (^{13}N), oxygen-15 (^{15}O), and fluorine-18 (^{18}F). As some of the short-lived positron-emitting radionuclides are composed of low atomic mass elements found in drugs and biomolecules, it is possible to synthesize PET radiotracers with the identical chemical structure of the parent unlabeled molecules without interfering with their pharmacological activity. Therefore, PET radiotracers may exhibit suitable binding and physicochemical characteristics to interact with a plethora of therapeutic and biological targets, including receptors, enzymes, and ion channels [15,16].

The incorporation of the short-lived positron-emitter radionuclide ^{18}F has been largely explored in the development of ^{18}F -labeled radiotracers for imaging and quantification of biochemical and physiological processes or of specific therapeutic and biological targets, including receptors and enzymes. The 2- ^{18}F -fluoro-2-deoxy-D-glucose (^{18}F -FDG, ^{18}F 1) is an example of a PET radiotracer used as clinical

research tool and as diagnostic imaging agent in neurology and oncology [17,18]. The administration of the radiotracer [^{18}F]**1** allows the measurement of *in vivo* glucose metabolism by PET imaging. Once absorbed intracellularly, the glucose analog [^{18}F]**1** is converted into [^{18}F]FDG-6-phosphate *via* a phosphorylation reaction, inhibiting the diffusion of [^{18}F]**1** out of the cells before radioactive decay. The absence of 2-hydroxyl group prevents the phosphorylated derivative of [^{18}F]**1** to be metabolized further in the glycolytic pathway [17,18]. The PET tracer [^{18}F]fluoro-3'-deoxy-3'-L-fluorothymidine ([^{18}F]FLT, [^{18}F]**2**) is suitable for imaging and measuring cellular proliferation [19,20]. The pyrimidine analog [^{18}F]**2** is taken up by the cells and converted into [^{18}F]FLT-monophosphate by thymidine kinase 1 (TK₁). The phosphorylation of [^{18}F]**2** by TK₁ leads to an accumulation of the imaging agent within the proliferating cells [19,20]. The PET radiotracer [^{18}F]6-fluoro-L-3,4-dihydroxyphenylalanine ([^{18}F]DOPA, [^{18}F]**3**) has provided an useful research tool for the diagnosis of neuropsychiatric disorders (e.g. Parkinson's disease and schizophrenia) [21]. The [^{18}F]**3** is also an efficient radiotracer in the detection of brain tumor cells overexpressing amino acid transporters [22] and of neuroendocrine tumors [23]. Figure 1 provides a list of some ^{18}F -labeled radiopharmaceuticals as target-based imaging agents in oncology, neurologic, and heart diseases. These examples include the [^{18}F]fluoroethylflumazenil ([^{18}F]**4**) [24,25], [^{18}F]UCB-H ([^{18}F]**5**) [26-28], [^{18}F]flurpiridaz ([^{18}F]**6**) [29,30], [^{18}F]olaparib ([^{18}F]**7**) [31], [^{18}F]fallypride ([^{18}F]**8**) [32,33], [^{18}F]gefitinib ([^{18}F]**9**) [34], [^{18}F]fluciclovine ([^{18}F]**10**) [35,36], and [^{18}F]PSMA-1007 ([^{18}F]**11**) [37,38].

The mode of decay of the radionuclide ^{18}F is attractive for PET imaging. It has a clean positron profile consisting of 97% positron (β^+) emission and 3% electron capture (EC) with both modes of decay generating the stable oxygen-18 isotope (^{18}O) [39]. Furthermore, the ^{18}F emits a positron with a relatively low energy (0.635 MeV), limiting the distance of the released positron to a few millimeters in tissue (maximal positron range of 2.4 mm in water) before its annihilation event with an electron to give rise to two opposed gamma (γ) rays of 511 keV (annihilation photons). The short positron range of radionuclide ^{18}F is favorable for the acquisition of high resolution PET images [40,41]. This mode of decay of ^{18}F and other positron emitters constitutes the main basis of PET imaging (Figure 2). Compared to other positron emitter nuclides, the half life of ^{18}F ($t_{1/2} = 109.8$ min) is long enough to allow multistep synthetic labeling reactions, the transportation of the ^{18}F -labeled radiotracers over considerable distances, and the extension of PET imaging procedures over a few hours, while assuring a limited amount of radiation doses for the living subject [42]. These characteristics make ^{18}F suitable for the labeling of molecules of biological interest ranging from drug-like molecules to complex bioactive chemical structures such as proteins, oligonucleotides, and antibodies.

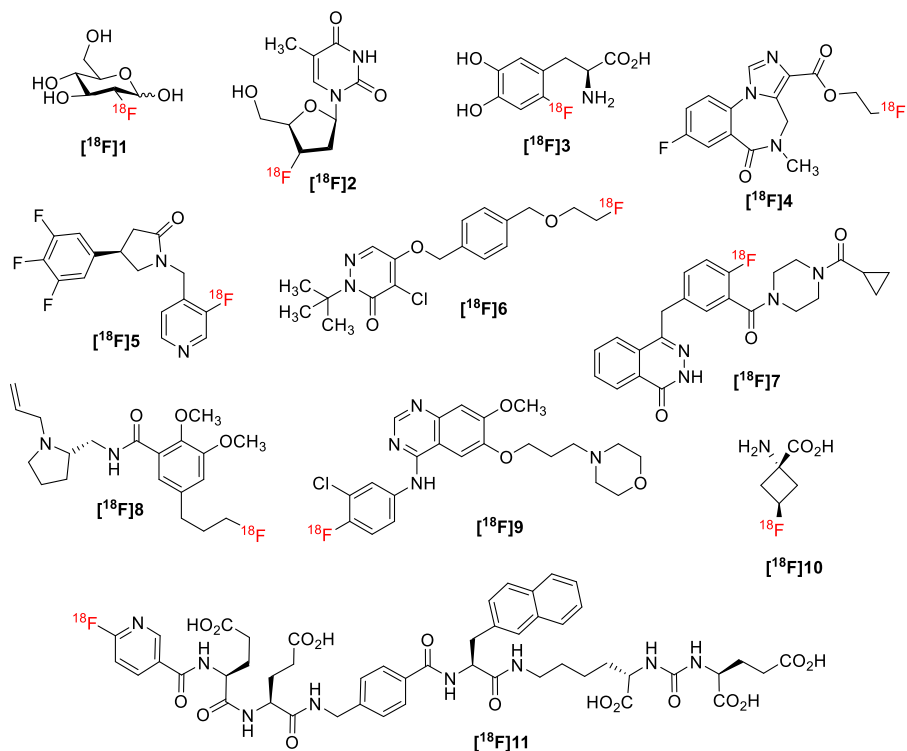


Figure 1. Chemical structures of ^{18}F -labeled radiotracers used as PET imaging agents ($[^{18}\text{F}]1$ - $[^{18}\text{F}]11$).

The production of the radionuclide ^{18}F is mainly achieved by charged particle accelerators (cyclotrons) through several nuclear reactions. The radionuclide ^{18}F can be made available to radiochemists either as gaseous $[^{18}\text{F}]\text{F}_2$ or as $[^{18}\text{F}]\text{F}^-$. The irradiation of neon-20 (^{20}Ne) with deuterons (d) [$^{20}\text{Ne}(d,\alpha)^{18}\text{F}$] and proton bombardment of the gas target $^{18}\text{O}_2$ [$^{18}\text{O}(p,n)^{18}\text{F}$] generates the gaseous $[^{18}\text{F}]\text{F}_2$. An aqueous solution of $[^{18}\text{F}]\text{F}^-$ is prepared by the efficient nuclear reaction $^{18}\text{O}(p,n)^{18}\text{F}$ to furnish a high amount of radioactivity (> 370 GBq per batch) [39].

An important difference between these production methods is the molar activity that measures the ratio of radioactivity of ^{18}F -labeled compound relative to the molar amount of the respective non-radioactive compound (the molar activity is usually expressed in $\text{Bq}\cdot\text{mol}^{-1}$). The nuclear reaction $^{18}\text{O}(p,n)^{18}\text{F}$ leads the production of no-carrier added (n.c.a.) $[^{18}\text{F}]\text{F}^-$ with a very high molar activity [43]. On the other hand, the $[^{18}\text{F}]\text{F}_2$ gas has much lower molar activity because the fluorine-19 ($[^{19}\text{F}]\text{F}_2$) gas must be added as a carrier to extract the $[^{18}\text{F}]\text{F}_2$ gas from the cyclotron target [43]. The production of ^{18}F -labeled radiopharmaceuticals with high molar activity is highly desirable for PET imaging studies, especially for targeting low-density biomacromolecules. In case of $[^{18}\text{F}]\text{F}_2$ gas, the addition of a carrier contributes to an increased molar amount of the final non-radioactive PET tracer, which may result in a saturation of the biomacromolecules and reduction of the PET signal derived from

radiotracer binding [44]. A radiopharmaceutical with high molar activity can be administered to living subjects in trace amounts, without inducing any pharmacological or toxic effects.

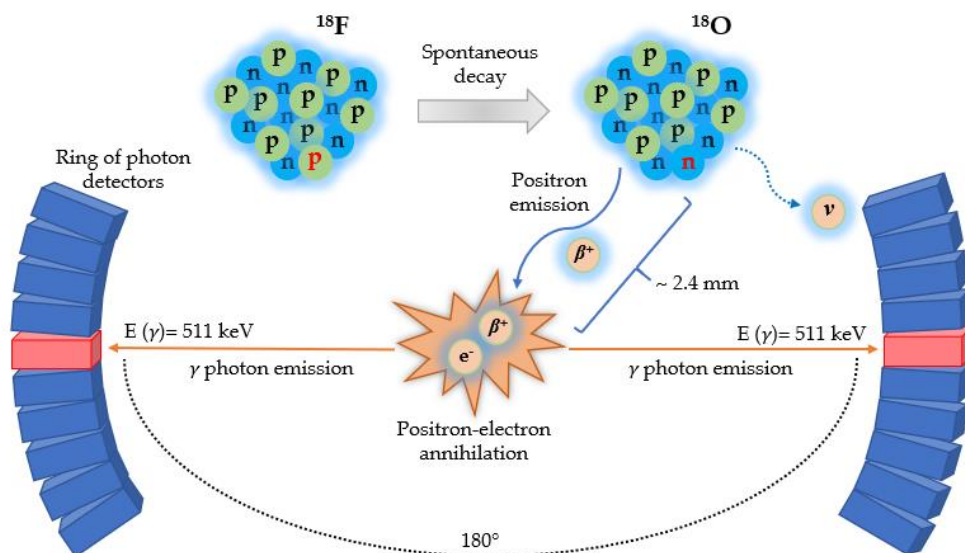


Figure 2. Schematic representation of the principal basis of PET. Once a radiotracer is administered to the subject and accumulated in the body, the radioactive isotope attached to the drug molecule decays by positron emission to a stable radioisotope. The positively charged positron interacts with surrounding tissues, progressively losing its kinetic energy and slowing down until its speed is low enough to combine with a negatively charged electron. This collision between both particles results in an annihilation event that yields two gamma (γ) rays of 511 keV (annihilation photons). To conserve momentum, the two γ rays are emitted from the site of the annihilation event in approximately opposite directions. The PET camera detects and records the arrival of coincident pairs of γ rays for the reconstruction of the three-dimensional (3D) PET images.

The selection of the methodology for the production of both forms of the radionuclide ^{18}F is dependent on the subsequent labeling reactions. The most common source of ^{18}F for electrophilic and/or radical ^{18}F -fluorination is $[^{18}\text{F}]\text{F}_2$ gas. This reagent can be used directly or derivatized into less reactive molecules. These derivatized reagents include $\{^{18}\text{F}\}$ xenon difluoride ($[^{18}\text{F}]\mathbf{12}$) [45-47], O - ^{18}F -fluorinated reagents [e.g. $[^{18}\text{F}]$ perchloryl fluoride ($[^{18}\text{F}]\mathbf{13}$) [48,49], $[^{18}\text{F}]$ trifluoromethyl hypofluorite ($[^{18}\text{F}]\mathbf{14}$) [50], and $[^{18}\text{F}]$ acetyl hypofluorite ($[^{18}\text{F}]\mathbf{15}$) [51,52]) and N - ^{18}F -fluorinated reagents [e.g. $[^{18}\text{F}]$ 1-fluoro-2-pyridone ($[^{18}\text{F}]\mathbf{16}$) [53], $[^{18}\text{F}]$ N -fluoropyridinium triflate ($[^{18}\text{F}]\mathbf{17}$) [54], $[^{18}\text{F}]$ N -fluorobenzenesulfonimide ($[^{18}\text{F}]\mathbf{18}$) [55], and $[^{18}\text{F}]$ Selectfluor *bis*(triflate) ($[^{18}\text{F}]\mathbf{19}$) [56]) (Figure 3).

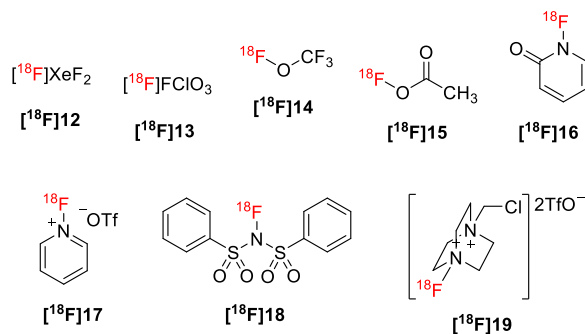


Figure 3. Electrophilic ^{18}F -fluorinating reagents employed in ^{18}F -radiochemistry.

Alternatively, the cyclotron-produced $^{18}\text{F}\text{F}^-$ is typically implemented in nucleophilic ^{18}F -fluorination reactions. The nuclear reaction $^{18}\text{O}(\text{p},\text{n})^{18}\text{F}$ delivers the aqueous $^{18}\text{F}\text{F}^-$. Although the $^{18}\text{F}\text{F}^-$ is a strong nucleophile, the ion forms hydrogen bonds with the surrounding water molecules in aqueous solution, and becomes poorly reactive toward nucleophilic ^{18}F -fluorination reactions [57]. Therefore, $^{18}\text{F}\text{F}^-$ must be adequately activated before it becomes sufficiently nucleophilic. This is accomplished with a multistep procedure starting by the trapping of the $^{18}\text{F}\text{F}^-$ on an anion-exchange cartridge [e.g. quaternary methyl ammonium (QMA) carbonate cartridge] and subsequent $^{18}\text{F}\text{F}^-$ elution using a solution of MeCN/ H_2O containing an anion exchanger, such as carbonate (CO_3^{2-}) and hydrogen carbonate ions (HCO_3^-) [58]. These anions are usually employed due to their non-nucleophilic nature and relatively low basicity, inhibiting the competitive nucleophilic substitution and elimination pathways. Potassium ions complexed with the aminopolyether cryptand Kryptofix[®] 222 ($\text{K}_{2.2.2}$) [59] and tetraalkylammonium ions [60] have been frequently used as fluoride counteranions. After the $^{18}\text{F}\text{F}^-$ elution, the solvent mixture must be evaporated in order to minimize the amount of H_2O and to furnish a more reactive $^{18}\text{F}\text{F}^-$ for nucleophilic substitution [61]. A plethora of methods describing the production of highly reactive $^{18}\text{F}\text{F}^-$ without the use of azeotropic drying was reported. The majority of these methods mainly relied on the use of alternative eluents for $^{18}\text{F}\text{F}^-$ elution: the use of strong organic bases in MeCN [62], tetraethylammonium hydrogen carbonate dissolved in polar aprotic solvents [63], alcoholic solutions of quaternary anilinium, diarylsulfonium, and triarylsulfonium precursors [64], and combination of cryptand complexes with potassium salts dissolved in protic solvents [65]. Other techniques consisted in the employment of modified anion-exchange resins such as macroporous copolymers loaded with a long alkyl chain quaternary ammonium salts [66] and phosphonium borane $[(\text{Ph}_2\text{MeP})\text{C}_6\text{H}_4(\text{BMes}_2)]^+$ [67]. In 2015, Sergeev and Dam disclosed a procedure that utilizes titanium dioxide (TiO_2) nanoparticles in as catalyst and water adsorbent allowing radiofluorination in aqueous mixtures with up to 25 vol% [68]. Pees and co-workers developed a strategy of production of reactive ^{18}F fluoride *via* formation of gaseous ^{18}F triflyl fluoride, distillation into a dry aprotic solvent, and release of ^{18}F fluoride under basic conditions [69].

The dry $[^{18}\text{F}]\text{F}^-$ must be subsequently solubilized in polar aprotic solvents prior to use for ^{18}F -labeling. The radionuclide ^{18}F can be incorporated by bimolecular nucleophilic substitution ($\text{S}_{\text{N}}2$) into alkyl-LG precursors (LG = a leaving group) or by nucleophilic aromatic substitution ($\text{S}_{\text{N}}\text{Ar}$) into aryl-LG precursors (LG = a leaving group) [70,71]. Regardless of the precursors and reaction conditions utilized in nucleophilic ^{18}F -fluorinations, the reaction time is an important parameter that should be taken into consideration, owing to the limited physical half-life of the radionuclide ^{18}F . In general, the ^{18}F -labeling reactions are performed with trace amounts of radionuclides and a large stoichiometric excess of the precursors and can reach the completion in few minutes. Other parameters such as the solvent, the temperature, and the concentration should also be explored in the optimization of the nucleophilic ^{18}F -fluorination process.

For clinical applications, the ^{18}F -radiochemistry may require the use of multiple GBq of starting radioactivity. This implies that the radiochemical reactions are carried out in computer-controlled automated synthesizers placed in shielded hotcells in order to restrict as much as possible the radiation exposure by the workers. Moreover, the automation in ^{18}F -radiochemistry may enable the preparation of ^{18}F -labeled radiopharmaceuticals in reproducible yields using the same synthetic approach [72].

The application of the ^{18}F -radiochemistry in the labeling of PET ligands presents some drawbacks. The isotopic labeling of radiotracers is restricted to biologically active molecules that possess in their structure a fluorine atom and, this is the case of ~20-30% of all molecules of therapeutic relevance [73,74]. Alternatively, the strategy of replacement of one atom of a non-fluorinated parent molecule by a fluorine atom could be used to access potential PET candidates [75]. However, the biological properties of the new fluorinated molecule need to be carefully assessed, since the introduction of a fluorine atom can significantly influence the biological and physicochemical properties of the parent molecules [76-78]. Over the last years, the increasing number of pharmaceutically relevant molecules with fluorine atoms or fluoroalkyl substituents has created the opportunity to investigate their biological and pharmacological behaviour using PET imaging.

The suitability of the ^{18}F radioisotope in PET has encouraged radiochemists to invest much effort in the development of efficient ^{18}F -fluorination and ^{18}F -fluoroalkylation strategies [39,41,79-87]. Among the existing fluorinated motifs, the difluoromethyl (CHF_2) groups has become one of the most desired functional groups in the field of organic synthesis, because of their unique characteristics that are applicable for the development of pharmaceuticals and agrochemicals (20-27, Figure 4) [88-95].

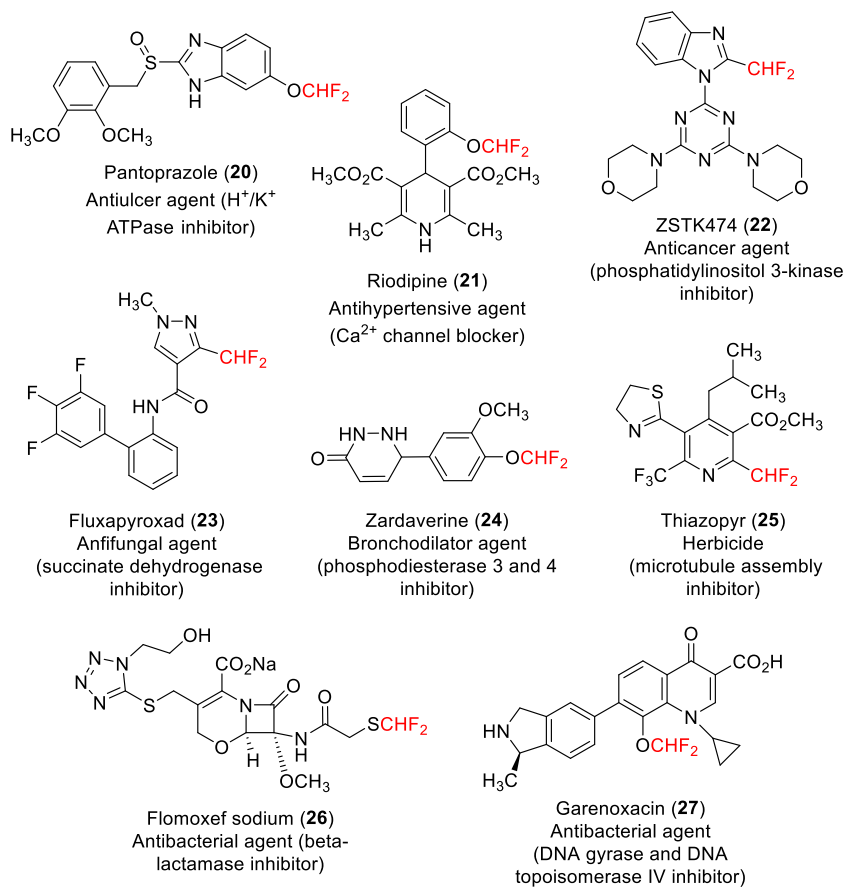


Figure 4. Chemical structure of CHF₂-containing agrochemicals and pharmaceuticals (20-27).

The biological relevance of the CHF₂ groups resides on their demonstrated involvement in hydrogen-bond donor interactions with the active site of biomacromolecules. Hartz and co-workers studied the effect of diverse substituents in the *N*³-phenylpyrazinone scaffold toward the inhibition of corticotropin-releasing factor-1 receptor (CRF₁R) [96]. Replacement of the trifluoromethoxy (-OCF₃) moiety of **28** by the difluoromethoxy group (-OCHF₂) of **29** led to an improvement of the binding affinity to CRF₁R (Figure 5A). In another study [97], the difluoromethyl-containing ketone **31** showed a greater inhibitory activity toward the G119S *Anopheles gambiae* acetylcholinesterase (G119S AgAChE) in comparison with the trifluoromethyl- and fluoromethyl-containing ketones **30** and **32**, respectively (Figure 5B). From a series of tripeptidic acylsulfonamides, Zheng and Scola found that a derivative containing a difluoromethyl cyclopropyl amino acid **35** exhibited a higher inhibitory potency to the hepatitis C virus nonstructural protein 3 (HCV NS3) protease compared to the trifluoromethylated (**33**) and trimethylated (**34**) analogues (Figure 5C) [98]. In these reported studies, the most favourable pharmacodynamic properties of the CHF₂ groups were explained by their ability to form interactions with hydrogen-bond acceptors located on the active site of the therapeutic targets.

Zafrani and collaborators also demonstrated the CHF₂ groups contained in difluoromethylated arenes, aryl/alkyl ethers, sulfides, sulfoxides, and sulfones can act as hydrogen-bond donors and their strength as hydrogen-bond donors strongly depends on the attached functional groups [99,100].

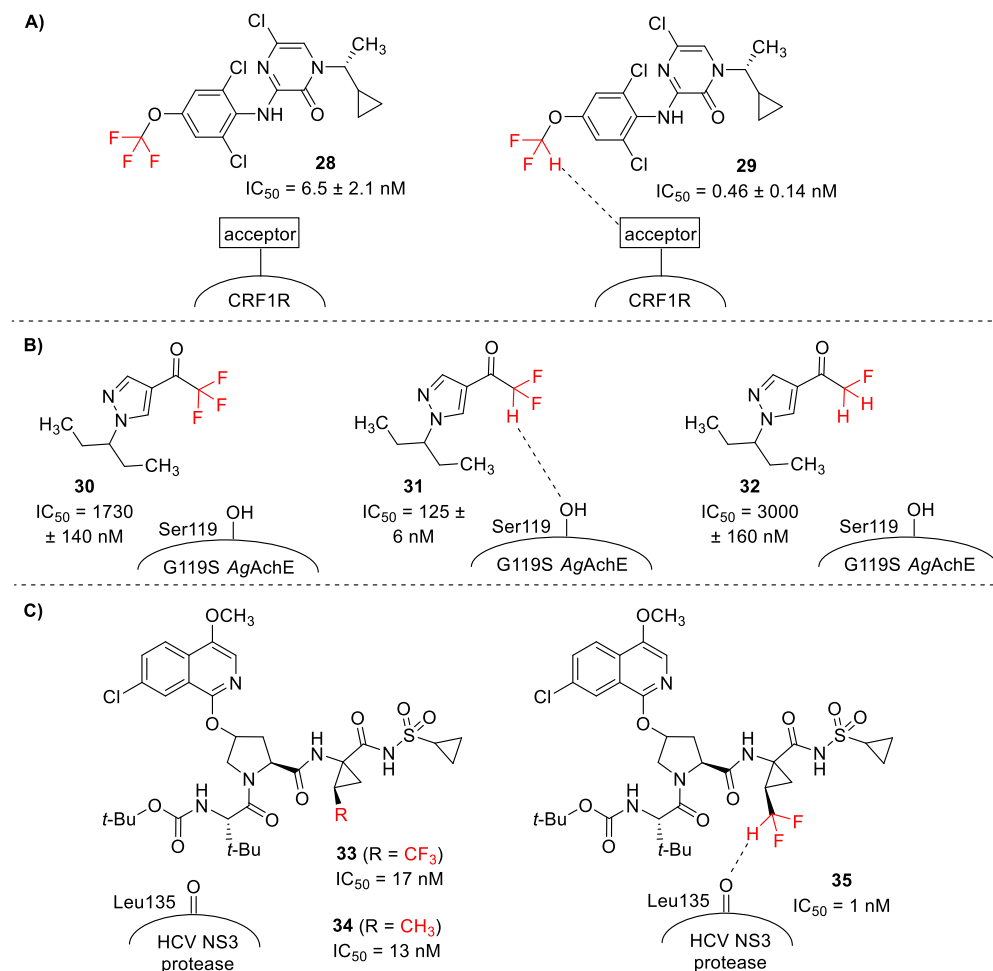


Figure 5. Examples of the influence of the hydrogen-bond donor ability of the CHF₂ groups on the pharmacodynamic properties of derivatives acting on the inhibition of the corticotropin-releasing factor-1 receptor (CRF₁R) (A), G119S *Anopheles gambiae* acetylcholinesterase (G119S AgAChE) (B), and hepatitis C virus nonstructural protein 3 (HCV NS3) protease (C).

Moreover, the replacement of a hydrogen atom by a fluorine atom can have a meaningful impact on the pK_a of bioactive molecules. As exemplified on the Table 1, a significant variation of the pK_a of ethylamines and acetic acids was observed when the hydrogen atoms of the methyl group were successively substituted by other perfluoroalkyl moieties [pK_a (CF₃-R¹) < pK_a (CHF₂-R¹) < pK_a (CHF-R¹) < pK_a (CH₃-R¹), R¹ = amine or carboxyl moiety] [101]. As the pK_a can be a very critical parameter in drug discovery, the selection of the most suitable fluoroalkyl group is a critical step.

Figure 6 demonstrates an example of two kinesin spindle protein (KSP) inhibitors, where the parent compound **36** suffered from a high efflux ratio due to high basicity of the NH₂ group [102]. This high efflux ratio limits the efficiency of the compound **36**. The introduction of a CHF₂ moiety in the α -amine position as a strategy to reduce the basicity of **36** (decrease the pKa) furnished a derivative (**37**) with a significantly lower efflux ratio.

Table 1. Influence of the fluorine substitution on the pKa of ethylamines and acetic acids [101]

Bases			
10.7	9.0	7.3	5.7
Acids			
4.8	2.6	1.3	0.5

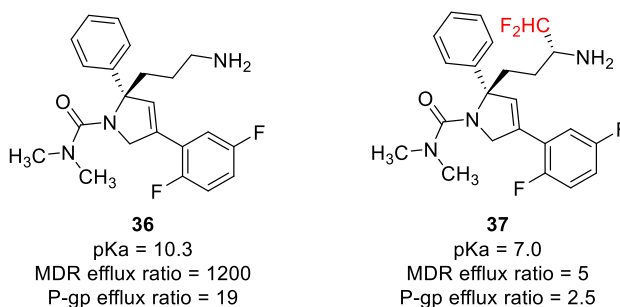
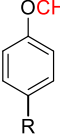
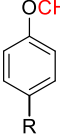
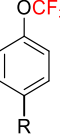
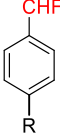
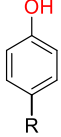
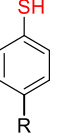
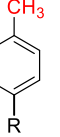


Figure 6. PKa and P-gp efflux ratio of the kinesin spindle protein (KSP) inhibitors **36** and **37**.

The CHF₂ substitution can significantly modulate the lipophilicity, i.e. the decrease or increase in octanol/water partition coefficients (log P), of the respective bioactive molecules. For instance, in a study reported by Xing and co-workers [103], the sequential replacement of a hydrogen atom by a fluorine atom led to an increment of the log P value of the anisole derivatives [$\log P$ (Ph-OCH₃) < $\log P$ (Ph-OCH₂F) < $\log P$ (Ph-OCHF₂) < $\log P$ (Ph-OCF₃)] (Table 2). Overall, the introduction of CHF₂ groups may offer a good compromise between the lower lipophilicity of the CH₂F groups and the greater lipophilicity of the CF₃ groups. Furthermore, the CHF₂ groups are considered bioisosteres of the hydroxy (OH) and the thiol (SH) groups, in terms of hydrogen-bond donor ability, and of the methyl groups (CH₃), in terms of size. Besides that, the CHF₂ substitution can also regulate the lipophilicity of OH-, SH-, and CH₃-containing bioactive molecules. As exemplified on the Table 2, the CHF₂ moiety serves as a more lipophilic bioisoster of the OH group, as a similar lipophilic bioisoster of the SH group, and as a less lipophilic bioisoster of the CH₃ group when all these groups are attached to benzene derivatives [100].

Table 2. Influence of the CHF₂ substitution on the log P of anisole and benzene derivatives

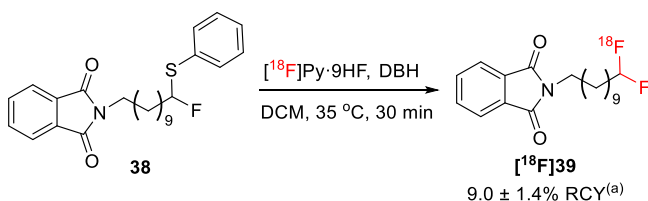
				
R=		log P		
H	2.24	2.51	3.17	
				
R=		log P		
<i>p</i> -NO ₂	2.12	1.91	2.12	2.35
H	2.40	1.46	2.50	2.52
<i>p</i> -OCH ₃	2.61	1.34	2.64	2.67

The introduction of fluorine substituents, as well as CHF₂ and CF₃ groups, may potentially increase the stability of the bioactive molecules toward the metabolism. In particular, the addition of CHF₂ moieties in critical positions of aromatic azaheterocyclic drugs has been shown to successfully reduce their susceptibility toward the metabolism by aldehyde oxidase (AO) enzymes [104].

Owing to the demonstrated benefits of CHF₂ groups in medicinal chemistry and pharmaceutical research, much effort has been made in the installation of these moieties in organic substrates. Despite the extensive development of synthetic approaches to access CHF₂-containing compounds [105-108], the ¹⁸F-labeling of CHF₂ moieties has recently received increasing attention in radiochemistry. The combination between the potential benefits of the CHF₂ moieties in drug discovery and the positron emitter function of the radionuclide ¹⁸F would improve the performance of the resulting [¹⁸F]CHF₂-containing radiotracers in PET imaging. Until the date, the radiosynthesis of these compounds would require either the ¹⁸F-fluorination of precursors or the direct introduction of [¹⁸F]CHF₂ moieties in organic substrates. This Chapter discusses all the methods available for the synthesis of the [¹⁸F]CHF₂-containing radiotracers.

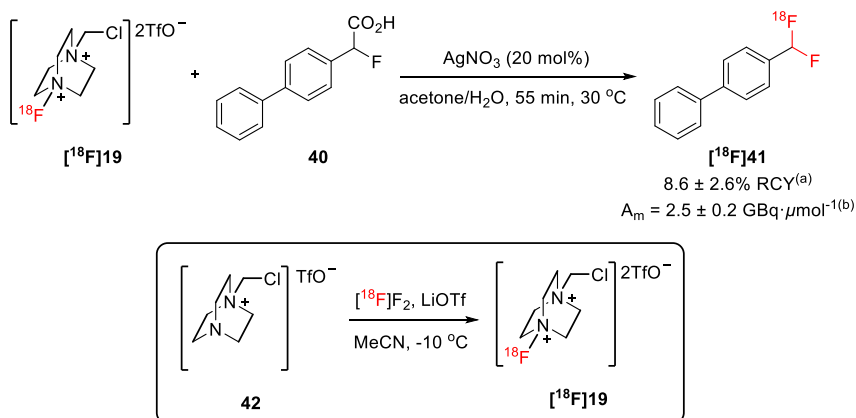
2. Synthesis of [¹⁸F]CHF₂-containing compounds *via* ¹⁸F-fluorination

The labeling of [¹⁸F]CHF₂ motifs was firstly disclosed in 2010 by Haufe and collaborators [109]. The desulfurization/¹⁸F-fluorination of the precursor 4-chlorophenyl-(1-fluoro-11-*N*-phthalimidylundec-1-yl)thioether (**38**) furnished the cartridge-purified 1,1-[¹⁸F]difluoro-11-*N*-phthalimidylundecane (**[¹⁸F]39**) in 9.0 ± 1.4% RCY (decay-corrected), by combining the carrier-added [¹⁸F]pyridinium poly(hydrogen fluoride) ([¹⁸F]Py·9HF) with the oxidant 1,3-dibromo-5,5-dimethylhydantoin (DBH).



Scheme 1. Desulfurization/ ^{18}F -fluorination of the precursor **38** with the carrier-added ^{18}F Py-9HF and DBH. ^(a)RCY of the isolated product after cartridge purification.

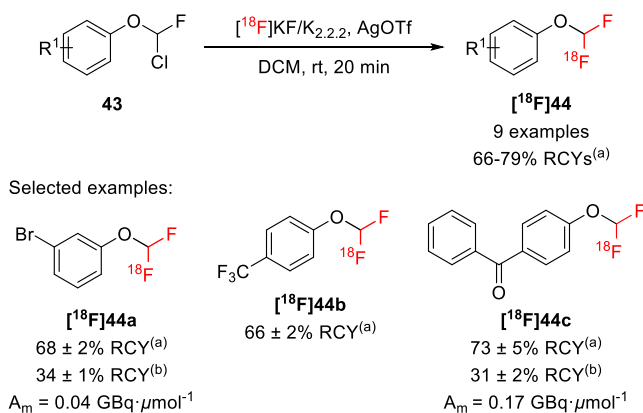
The synthesis of an ^{18}F aryl-CHF₂ derivative was described for the first time by Gouverneur and collaborators. Treatment of the readily available 2-([1,1'-biphenyl]-4-yl)-2-fluoroacetic acid (**40**) with the ^{18}F -fluorinating reagent ^{18}F Selectfluor *bis*(triflate) (^{18}F]**19**) in a mixture of acetone and H₂O provided the ^{18}F 4-(difluoromethyl)-1,1'-biphenyl (^{18}F]**41**) in $8.6 \pm 2.6\%$ RCY (Scheme 2) [110]. This ^{18}F -fluorodecarboxylation process was mediated by silver nitrate (AgNO₃) and furnished the labeled compound ^{18}F]**41** with a molar activity of $2.5 \pm 0.2 \text{ GBq}\cdot\mu\text{mol}^{-1}$ (decay-corrected at the end of the synthesis (EOS) of the ^{18}F]**19**). The reagent ^{18}F]**19** was made available by bubbling ^{18}F F₂ into a vial containing a mixture of 1-chloromethyl-4-aza-1-azoniabicyclo[2.2.2]octane triflate (**42**) and lithium triflate (LiOTf) in MeCN [56]. Until the date, the mentioned methods represent the only examples of electrophilic ^{18}F -fluorination approach to access ^{18}F CHF₂-containing compounds.



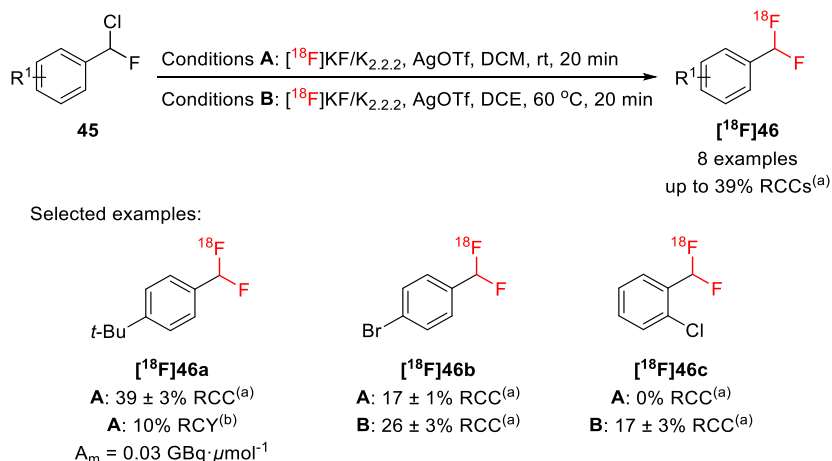
Scheme 2. Electrophilic ^{18}F -fluorination of the α -fluoroarylacetic acids (**40**) with the electrophilic ^{18}F -fluorinating reagent ^{18}F Selectfluor *bis*(triflate) (^{18}F]**19**). ^(a)Radiochemical yield (RCY) determined based on radio-TLC and radio-HPLC of the crude product ^{18}F]**41**. ^(b)Molar activity decay-corrected at the end of the synthesis (EOS) of ^{18}F]**19**.

The use of cyclotron-produced ^{18}F fluoride in the labeling of ^{18}F CHF₂ groups by nucleophilic ^{18}F -fluorination was described for the first time in 2015. Gouverneur group developed a AgOTf-mediated process that enables the preparation of a palette of ^{18}F aryl-OCHF₂ (^{18}F]**44**; Scheme 3: 9 examples, 66-79% RCY) and ^{18}F aryl-CHF₂

derivatives ($[^{18}\text{F}]\mathbf{46}$; Scheme 4: 8 examples, up to 39% RCCs) by halogen exchange of aryl-OCHFCl ($\mathbf{43}$) [111] and aryl-CHFCl precursors ($\mathbf{45}$) [112] with $[^{18}\text{F}]$ fluoride, respectively. The authors considered that the presence of the metal activation AgOTf would allow the occurrence of the ^{18}F -labeling of the precursors $\mathbf{43}$ and $\mathbf{45}$ under mild reaction conditions, avoiding the need of high temperatures for the incorporation of fluorine-18 (^{18}F). After semipreparative high performance liquid chromatography (HPLC) purification, the $[^{18}\text{F}]$ aryl-OCHF₂ $[^{18}\text{F}]\mathbf{44a}$ and $[^{18}\text{F}]\mathbf{44c}$, and the $[^{18}\text{F}]$ aryl-CHF₂ $[^{18}\text{F}]\mathbf{46a}$ were isolated in $34 \pm 1\%$, $31 \pm 2\%$, and 10% RCYs (non-decay corrected) with molar activities of $0.04 \text{ GBq}\cdot\mu\text{mol}^{-1}$, $0.17 \text{ GBq}\cdot\mu\text{mol}^{-1}$, and $0.03 \text{ GBq}\cdot\mu\text{mol}^{-1}$, respectively.

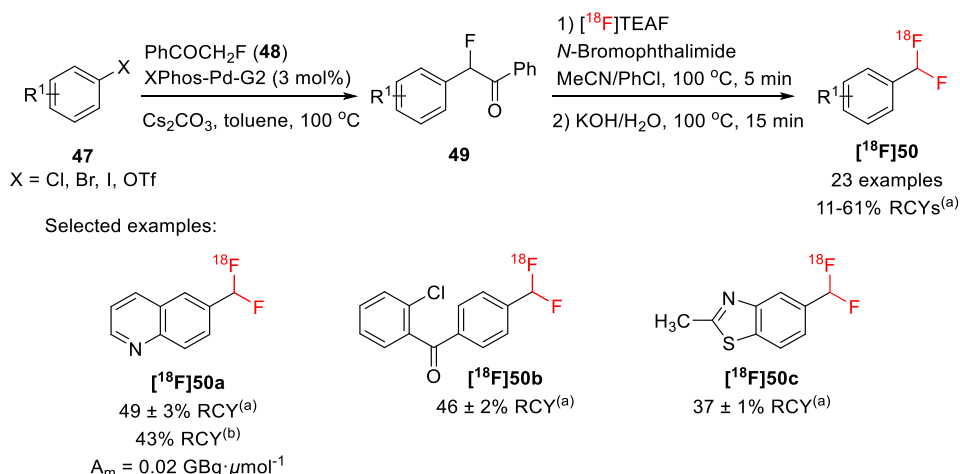


Scheme 3. Silver-mediated ^{18}F -fluorination of aryl-OCHFCl precursors ($\mathbf{43}$). ^(a)Radiochemical yield (RCY) determined by radio-TLC of the crude products. ^(b)RCY of the isolated product after HPLC purification.



Scheme 4. Silver-mediated ^{18}F -labeling of aryl-CHFCl precursors ($\mathbf{45}$). ^(a)Radiochemical conversion (RCC) determined by radio-TLC of the crude products. ^(b)RCY of the isolated product after HPLC purification.

Ritter and co-workers disclosed an alternative multi-step methodology for the radiosynthesis of [^{18}F]aryl-CHF $_2$ derivatives (**[^{18}F]50**) from aryl chlorides, bromides, iodides, and triflates (**47**) [113]. The introduction of a benzoyl group in the substrates **47** with α -fluoroacetophenone (**48**) results in the production of the aryl acetophenone intermediates (**49**) as precursors for radiofluorination. The labeling protocol comprises the C-H bromination of the intermediates **49** with *N*-bromophthalimide, the nucleophilic ^{18}F -fluorination in the presence of tetraethylammonium bicarbonate (TEAB) and [^{18}F]fluoride, and the cleavage of benzoyl groups, under basic conditions. A wide range of [^{18}F]aryl-CHF $_2$ and [^{18}F]heteroaryl-CHF $_2$ derivatives, containing 2-methylbenzo[*d*]thiazole, pyridine, and quinoline rings (**[^{18}F]50**; Scheme 5: 23 examples, 11-61% RCYs, determined after purification by solid-phase extraction (SPE)). This labeling methodology was expanded to a variety of ^{18}F -difluoromethylated derivatives of bioactive molecules including analepticon (**[^{18}F]50d**), *N*-Boc-fluoxetine (**[^{18}F]50e**), claritin (**[^{18}F]50f**), DAA1106 (**[^{18}F]50g**), estrone (**[^{18}F]50h**), fenofibrate (**[^{18}F]50i**), and SC-58125 (**[^{18}F]50j**) (Figure 7). With the objective of enhancing the molar activity of the labeled derivative **[^{18}F]50a** ($A_m = 0.02 \text{ GBq}\cdot\mu\text{mol}^{-1}$), the authors explored the identification of another labeling approach to minimize the $^{18}\text{F}/^{19}\text{F}$ isotopic exchange. The replacement of TEAB by the weaker base tetrabutylammonium methanesulfonate (TBAOMs), the additional introduction of the organic base *N,N*-diisopropylethylamine (DIPEA), the reduction of precursor's amount (from 10 μmol to 0.5 μmol) and of the labeling temperature (from 100 $^\circ\text{C}$ to 80 $^\circ\text{C}$) contributed to an improved molar activity without compromising the nucleophilicity of [^{18}F]fluoride. Starting with 1.44 GBq of [^{18}F]fluoride, the compound **[^{18}F]50a** was isolated in 8% RCY, after semi-preparative HPLC purification, with a molar activity of 3.0 GBq $\cdot\mu\text{mol}^{-1}$.



Scheme 5. Radiosynthesis of [^{18}F]aryl-CHF $_2$ and [^{18}F]heteroaryl-CHF $_2$ derivatives (**[^{18}F]50**) from aryl chlorides, bromides, iodides, and triflates (**47**). ^(a)RCY of the isolated product after solid-phase extraction (SPE) purification. ^(b)RCY of the isolated product after HPLC purification.

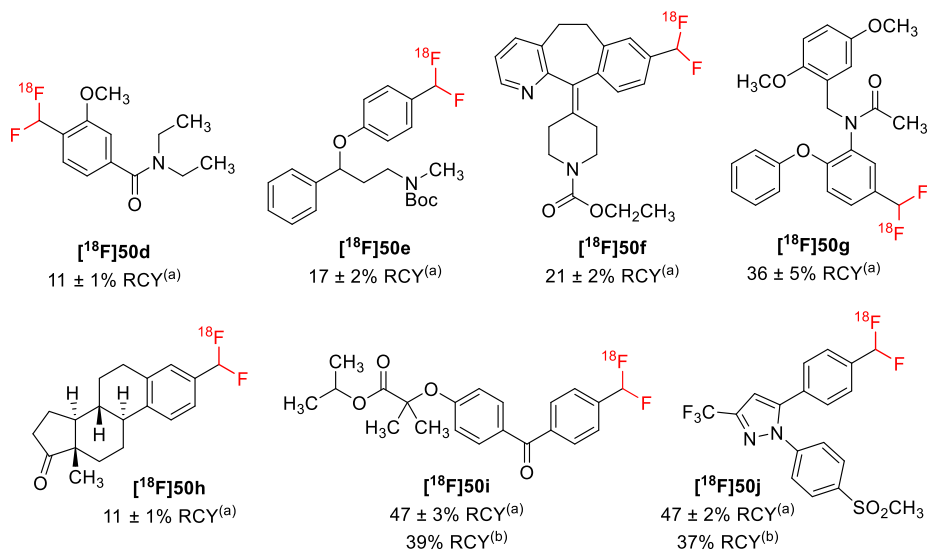
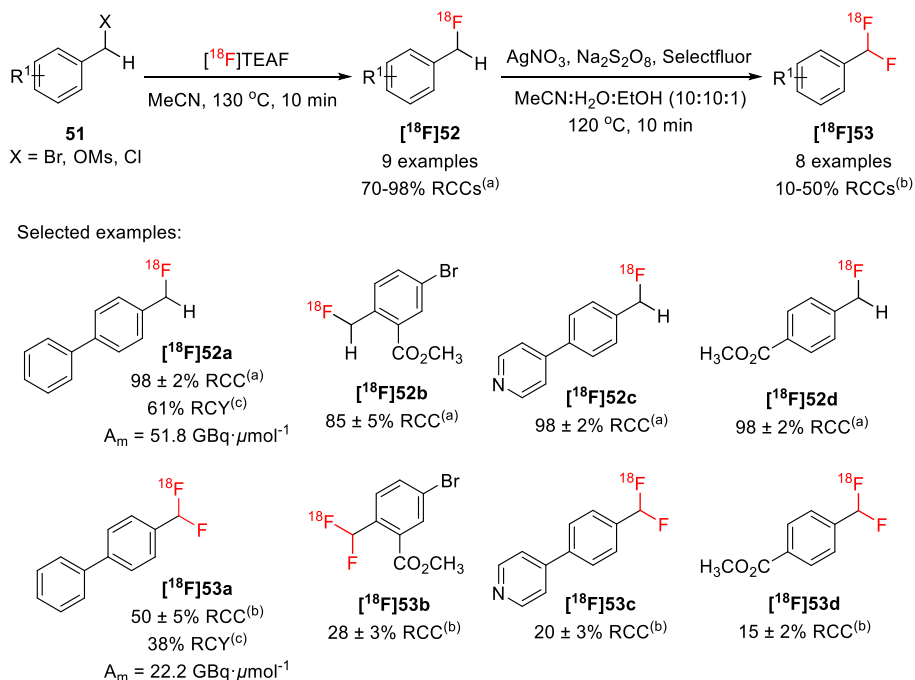


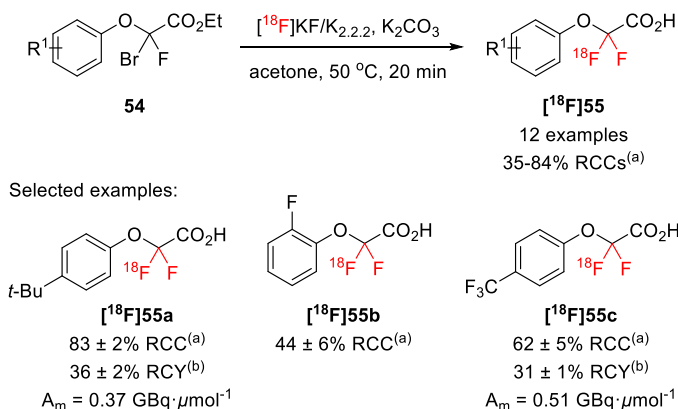
Figure 7. Chemical structures of ^{18}F -difluoromethyl-bearing analogues of bioactive molecules ($[^{18}\text{F}]\mathbf{50d}$ - $[^{18}\text{F}]\mathbf{50j}$). ^(a)RCY of the isolated product after SPE purification. ^(b)RCY of the isolated product after HPLC purification.

Later, Liang and co-workers reported a transition metal-free approach for the radiosynthesis of $[^{18}\text{F}]\text{aryl-CHF}_2$ derivatives ($[^{18}\text{F}]\mathbf{53}$), involving a two-step methodology [114]. The first step consisted in a nucleophilic ^{18}F -fluorination of benzyl (pseudo)halides ($\mathbf{51}$) with $[^{18}\text{F}]\text{fluoride}$, in the presence of TEAB, providing a series of $[^{18}\text{F}]\text{aryl-CFH}_2$ derivatives in quantitative RCCs ($[^{18}\text{F}]\mathbf{52}$; Scheme 6: 9 examples, 70-98% RCCs). The authors demonstrated that the selection and the amount of base influenced the RCC of the ^{18}F -labeling reaction. Subsequent oxidative C-H fluorination using Selectfluor and sodium peroxydisulfate ($\text{Na}_2\text{S}_2\text{O}_8$), through a radical mechanism, furnished the corresponding $[^{18}\text{F}]\text{aryl-CHF}_2$ derivatives ($[^{18}\text{F}]\mathbf{53}$; Scheme 6: 8 examples, 10-50% RCCs). Electron-neutral and electron-poor aromatic substrates were compatible with the developed radiofluorination procedure. Using the commercially available automated module GE TRACERlab™ FX_{FN}, the compound $[^{18}\text{F}]\mathbf{52a}$ was synthesized and isolated in 61% RCY [non-decay corrected (n.d.c)] with a molar activity of $51.8 \text{ GBq}\cdot\mu\text{mol}^{-1}$ at the end of the synthesis (EOS), starting from 1.7 GBq of $[^{18}\text{F}]\text{fluoride}$. Subsequent formulation of the isolated $[^{18}\text{F}]\mathbf{52a}$ on a C18 cartridge, elution with MeCN, dilution with sterile water, and oxidative C-H fluorination process enabled the synthesis of the compound $[^{18}\text{F}]\mathbf{53a}$ in 38% RCY (n.d.c.) after semi-preparative HPLC purification with a molar activity of $22.2 \text{ GBq}\cdot\mu\text{mol}^{-1}$ at the EOS.

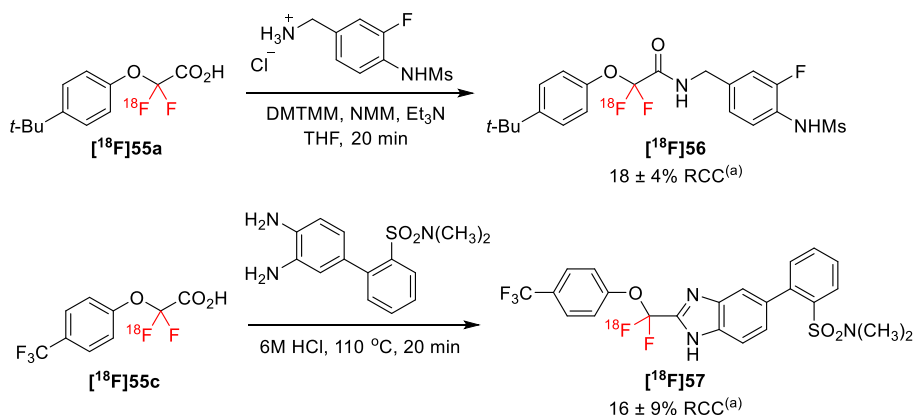


Scheme 6. Metal-free nucleophilic ¹⁸F-fluorination of aryl (pseudo)halides (**51**) and radical oxidative C-H fluorination of [¹⁸F]**52**. ^(a)RCC determined by radio-TLC. ^(b)RCC determined by radio-HPLC. ^(c)RCY of the isolated product after semi-preparative HPLC purification.

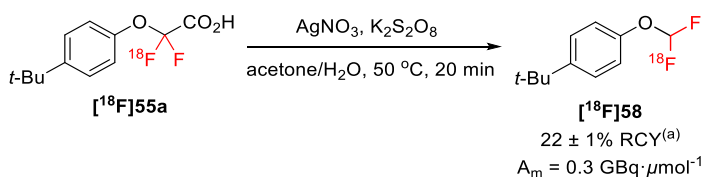
In 2017, Gouverneur group described the radiosynthesis of [¹⁸F] α,α -difluoro- α -(aryloxy)acetic acids (**[¹⁸F]55**) *via* a two-step procedure involving the halogen exchange nucleophilic radiofluorination of ethyl α -bromo- α -fluoro- α -(aryloxy)acetates (**54**) with the cyclotron-produced [¹⁸F]fluoride and consecutive hydrolysis under basic conditions [115]. The selection of the additive potassium carbonate (K₂CO₃) and the acetone was critical for the preparation of [¹⁸F] α,α -difluoro- α -(aryloxy)acetic acids (**[¹⁸F]55**) with improved RCCs. This methodology tolerated a wide range of functional groups (e.g. fluoro, ester, ketone, nitrile, trifluoromethyl, etc.) attached to the aromatic ring of the substrates (Scheme 7: 12 examples, 35-84% RCCs). The use of a higher amount of [¹⁸F]fluoride (-4 GBq) allowed the radiosynthesis of the cartridge-purified [¹⁸F]**55a** in 36 ± 2% RCY with a molar activity of 0.37 GBq·μmol⁻¹, and of the cartridge-purified [¹⁸F]**55c** in 31 ± 1% RCY with a molar activity of 0.51 GBq·μmol⁻¹. The [¹⁸F]**55a** and [¹⁸F]**55c** can be used as precursors for the preparation of the ¹⁸F-labeled transient receptor potential cation channel subfamily V member 1 (TRPV1) antagonist [¹⁸F]**56** (18 ± 4% RCC) and TRPV1 inhibitor [¹⁸F]**57** (16 ± 9% RCC), respectively, demonstrating the potential medicinal interest of the [¹⁸F]aryl-OCF₂PG motifs (PG = a protecting group) (Scheme 8). Intriguingly, a silver-mediated oxidative decarboxylation of the [¹⁸F]**55a** provided the HPLC-purified [¹⁸F]aryl-OCHF₂ [¹⁸F]**58** in 22 ± 2% RCY with a molar activity of 0.30 GBq·μmol⁻¹ (Scheme 9).



Scheme 7. ¹⁸F-Labeling of ethyl α -bromo- α -fluoro- α -(aryloxy)acetates (**54**) with [¹⁸F]fluoride and concomitant ester hydrolysis under basic conditions. ^(a)RCC determined by radio-TLC and radio-HPLC. ^(b)RCY of the isolated product after SPE purification.



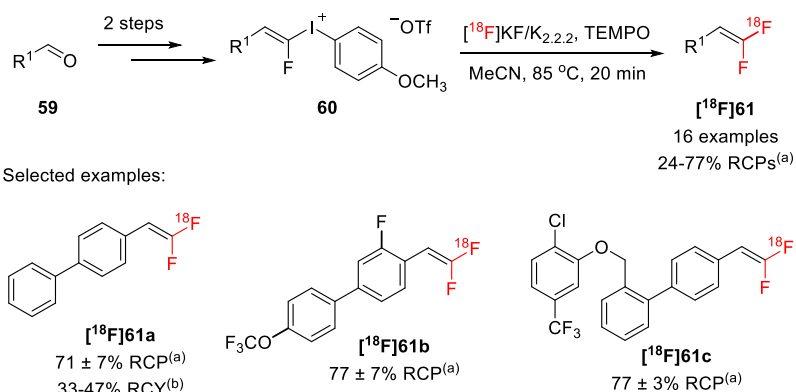
Scheme 8. Radiosynthesis of the ¹⁸F-labeled transient receptor potential cation channel subfamily V member 1 (TRPV1) antagonist [¹⁸F]**56** and of the TRPV1 inhibitor [¹⁸F]**57** from the compounds [¹⁸F]**55a** and [¹⁸F]**55c**, respectively. DMTMM: 4-(4,6-dimethoxy[1,3,5]triazin-2-yl)-4-methylmorpholinium chloride; NMM: *N*-methylmorpholine. ^(a)RCC determined by radio-TLC and radio-HPLC.



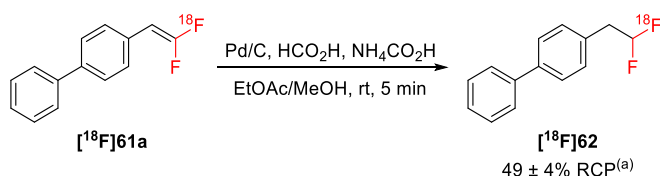
Scheme 9. Silver-mediated oxidative decarboxylation of [¹⁸F] α,α -difluoro- α -(aryloxy)acetic acid [¹⁸F]**55a**. ^(a)RCY of the isolated product after HPLC purification.

The 1,1-[¹⁸F]difluorinated alkene moiety was explored for the first time by Tredwell and co-workers [116]. The authors hypothesized that the nucleophilic ¹⁸F-fluorination of fluoroalkenyl(aryl)iodonium triflates (**60**) would afford the corresponding 1,1-[¹⁸F]difluorinated alkenes (**[¹⁸F]61**) in a regioselective manner,

minimizing the unwanted formation of [^{18}F]fluoroarenes. The precursors **60** were synthesized *via* a two-step sequence starting from the carbonylated compounds **59**. The ^{18}F -fluorination of the precursors **60** was influenced by the temperature and solvent of the reaction, and by the addition of 2,2,6,6-tetramethyl-1-piperidinyloxy (TEMPO). In the presence of TEMPO, a wide range of 1,1- ^{18}F]difluorinated alkenes (**[^{18}F]61**) were synthesized at 85 °C for 20 minutes, using MeCN as solvent for ^{18}F -labeling step (Scheme 10: 16 examples, 24-77% RCPs). The developed protocol was translated on to the commercially available synthesizer (ELIXYS FLEX/CHEM coupled to ELIXYS PURE/FORM), allowing the radiosynthesis of **[^{18}F]61a** in 33-47% RCY (determined by radio-HPLC of the crude mixture). Starting with 4 GBq of [^{18}F]fluoride, the labeled compound **[^{18}F]61a** was isolated with a molar activity of 1 GBq· μmol^{-1} , after HPLC purification and reformulation. Remarkably, the 1,1- ^{18}F]difluorinated alkene moiety of **[^{18}F]61a** can be reduced to the [^{18}F]alkyl- CHF_2 **[^{18}F]62** in $49 \pm 4\%$ RCP, using Pd/C and ammonium formate ($\text{NH}_4\text{CO}_2\text{H}$) (Scheme 11).



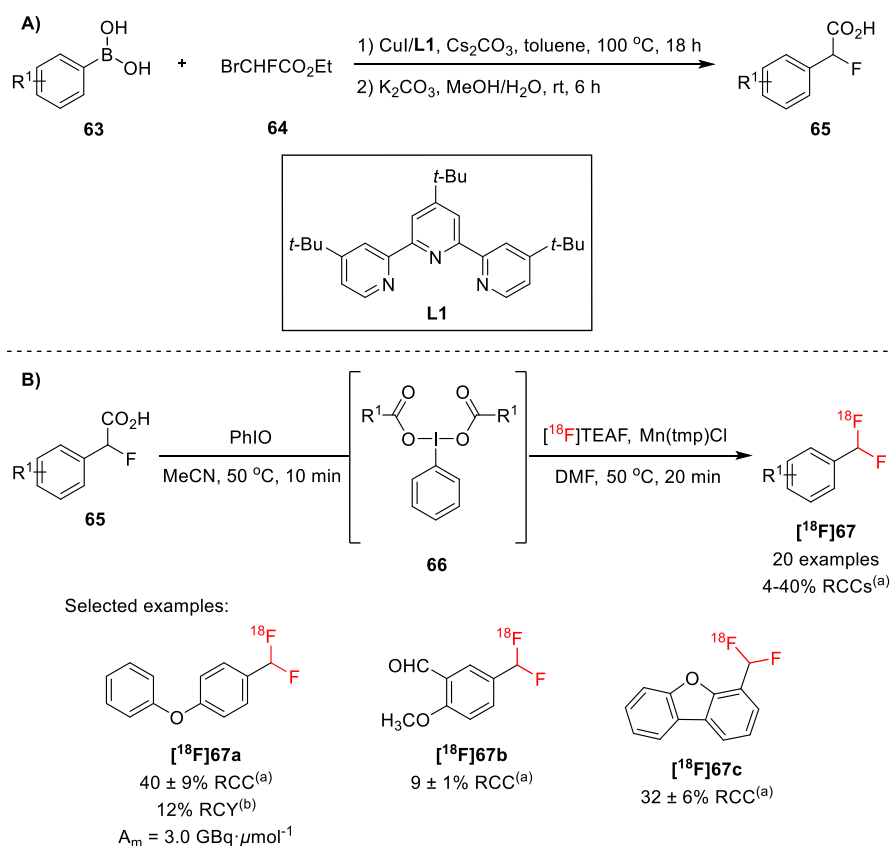
Scheme 10. Radiosynthesis of 1,1- ^{18}F]difluorinated alkenes (**[^{18}F]61**) from fluoroalkenyl(4-methoxyphenyl)iodonium triflates (**60**). ^(a)Radiochemical purities (RCPs) determined by radio-TLC. ^(b)RCY determined by radio-HPLC.



Scheme 11. Radiosynthesis of ^{18}F -difluoromethylated alkane **[^{18}F]62** *via* reduction of the 1,1- ^{18}F]difluorinated alkene **[^{18}F]61a**. ^(a)RCP determined by radio-TLC.

Inspired by the silver-mediated ^{18}F -fluorodecarboxylation procedure using [^{18}F]Selectfluor *bis*(triflate) (**[^{18}F]19**) [110] and the manganese-mediated ^{18}F -fluorodecarboxylation reaction using [^{18}F]fluoride reported by Groves and co-workers [117,118], Gouverneur group disclosed a novel methodology to afford [^{18}F]aryl- CHF_2 derivatives (**[^{18}F]67**) through ^{18}F -fluorodecarboxylation of 2-fluoro-2-arylacetic acids (**65**) with cyclotron-produced non-carrier-added (n.c.a.) [^{18}F]fluoride [119]. The 2-fluoro-2-arylacetic acids (**65**) were efficiently accessed *via* a copper-

catalyzed cross-coupling of aryl boronic acids (**63**) with ethyl bromofluoroacetate (**64**) followed by hydrolysis with K_2CO_3 (Scheme 12A). Two distinct protocols for the preparation of ^{18}F aryl- CHF_2 from the respective precursors **65** were investigated. The strategy of prior generation of a diacetoxiodobenzene complex (**66**) and subsequent incorporation of ^{18}F using ^{18}F tetraethylammonium fluoride (^{18}F TEAF) and Mn(III) *meso*-tetra(2,4,6-trimethylphenyl)porphine chloride [Mn(tmp)Cl] resulted in the radiosynthesis of a scope of ^{18}F aryl- CHF_2 compounds with improved RCCs (^{18}F **67**; Scheme 12B: 20 examples, 4-40% RCCs). Performing the ^{18}F -fluorodecarboxylation with 841 MBq of ^{18}F fluoride, the cartridge-purified ^{18}F **67a** was obtained in 12% RCY with a molar activity of $3.0 \text{ GBq}\cdot\mu\text{mol}^{-1}$, changing the precursor's amount and the solvent for the ^{18}F -labeling step (from DMF to DCE). The boronic acid derivatives of cyclooxygenase-2 (COX-2) inhibitor ZA140 and of fenofibrate were effectively converted into the ^{18}F -difluoromethylated derivatives ^{18}F **67d** and ^{18}F **67e** in $15 \pm 2\%$ and $23 \pm 4\%$ RCCs, respectively (Figure 8).



Scheme 12. (A) Copper-catalyzed cross-coupling reaction between the aryl boronic acids (**63**) and ethyl bromofluoroacetate (**64**) and subsequent hydrolysis under basic conditions. (B) Radiosynthesis of ^{18}F difluoromethylarenes (^{18}F **67**) via ^{18}F -fluorination of 2-fluoro-2-arylacetic acids (**65**) with ^{18}F fluoride. ^(a)RCC determined by radio-TLC and radio-HPLC. ^(b)RCY of the isolated product after SPE purification.

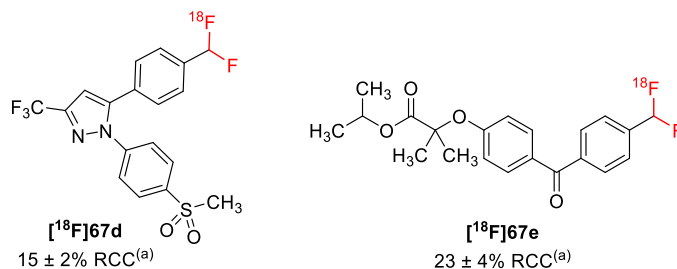
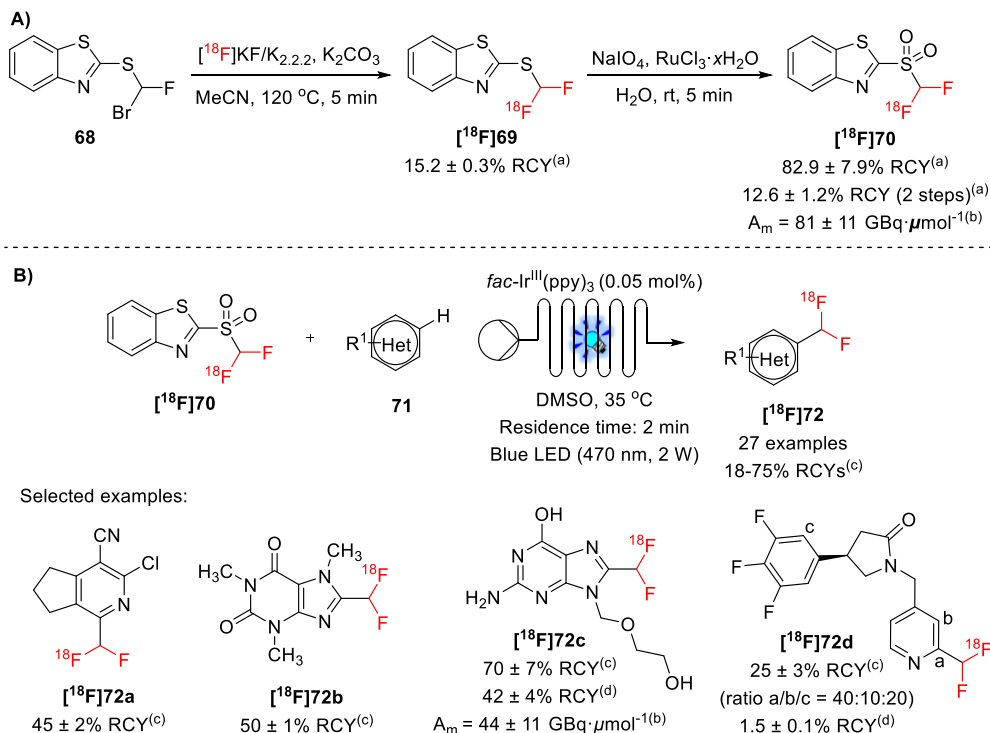


Figure 8. Chemical structures of the ^{18}F -difluoromethylated derivatives of ZA140 ($[^{18}\text{F}]\mathbf{67d}$) and fenofibrate ($[^{18}\text{F}]\mathbf{67e}$). ^(a)RCC determined by radio-TLC and radio-HPLC.

3. Synthesis of $[^{18}\text{F}]\text{CHF}_2$ -containing compounds via C-H ^{18}F -difluoromethylation

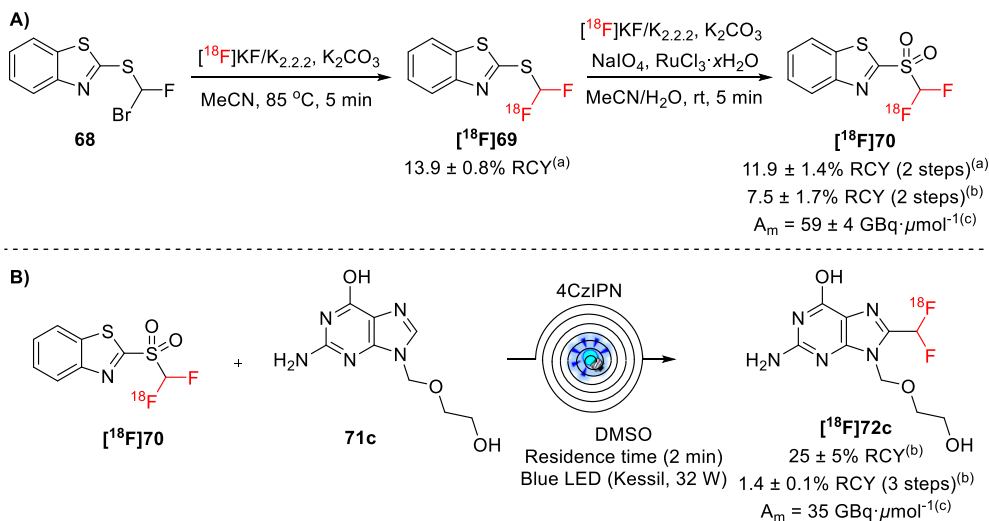
All abovementioned methods for the synthesis of $[^{18}\text{F}]\text{CHF}_2$ -containing compounds relied on the ^{18}F -fluorination of substrates with electrophilic ^{18}F -fluorinating agents [e.g. $[^{18}\text{F}]\text{Selectfluor bis(triflate)}$ ($[^{18}\text{F}]\mathbf{19}$)] and with the cyclotron-produced $[^{18}\text{F}]\text{fluoride}$. Very recently, a novel approach allowing the late-stage introduction of $[^{18}\text{F}]\text{CHF}_2$ moieties in organic substrates with ^{18}F -difluoromethylating reagents. The reagent $[^{18}\text{F}]\text{difluoromethyl benzothiazolyl-sulfone}$ ($[^{18}\text{F}]\mathbf{70}$) was initially implemented in the photoredox C-H ^{18}F -difluoromethylation of non-prefunctionalized *N*-containing heteroaromatics ($\mathbf{71}$), under continuous-flow conditions [120]. The radiosynthesis of $[^{18}\text{F}]\mathbf{70}$ was performed in a FASTlab™ synthesizer (GE Healthcare) through two reaction steps (^{18}F -labeling and oxidation). The nucleophilic ^{18}F -fluorination of bromofluoromethyl benzothiazolyl-sulfide ($\mathbf{58}$) with $[^{18}\text{F}]\text{potassium fluoride}$ ($[^{18}\text{F}]\text{KF}$) and Kryptofix® 222 ($\text{K}_{2.2.2}$) gave the cartridge-purified $[^{18}\text{F}]\text{difluoromethyl benzothiazolyl-sulfide}$ ($[^{18}\text{F}]\mathbf{69}$) in $15.2 \pm 0.3\% \text{ RCY}$, under basic conditions. Oxidation of $[^{18}\text{F}]\mathbf{69}$ provided the cartridge-purified $[^{18}\text{F}]\mathbf{70}$ in $82.9 \pm 7.9\% \text{ RCY}$ ($12.6 \pm 1.2\% \text{ RCY}$ over two steps) (Scheme 13A). After semi-preparative HPLC purification, the reagent $[^{18}\text{F}]\mathbf{70}$ was isolated with a molar activity of $81 \pm 11 \text{ GBq}\cdot\mu\text{mol}^{-1}$ [decay corrected at the end of bombardment (EOB)], starting from 125-150 GBq of $[^{18}\text{F}]\text{fluoride}$. The photoinduced C-H ^{18}F -difluoromethylation methodology with the reagent $[^{18}\text{F}]\mathbf{70}$ was optimized using the antiherpetic drug acyclovir as a model substrate and its efficiency was influenced by the selection of solvent (DMSO), the temperature (35°C), the photocatalyst *fac*- $\text{Ir}^{\text{III}}(\text{ppy})_3$, the residence time (2 min), and the light source (470 nm blue LED). This method enabled the radiosynthesis of the HPLC-purified $[^{18}\text{F}]\text{acyclovir-CHF}_2$ ($[^{18}\text{F}]\mathbf{72c}$) in $42 \pm 4\% \text{ RCY}$ and with a molar activity of $44 \pm 11 \text{ GBq}\cdot\mu\text{mol}^{-1}$. Interestingly, the C-H ^{18}F -difluoromethylation was applied to a broad scope of *N*-heteroaromatics ($\mathbf{71}$), including caffeine derivatives, nucleic bases, nucleosides, and pharmaceutical drugs ($[^{18}\text{F}]\mathbf{72}$; Scheme 13B: 27 examples, 18-75% RCYs). A mixture of structural isomers was observed in the synthesis of $[^{18}\text{F}]\mathbf{72d}$ (ratio a/b/c = 40:10:20, Scheme 13B). The ^{18}F -labeled synaptic vesicle glycoprotein 2A (SV2A) ligand (isomer b of $[^{18}\text{F}]\mathbf{72d}$) was isolated in $1.5 \pm 0.1\% \text{ RCY}$ after semi-preparative HPLC purification.



Scheme 13. (A) Radiosynthesis of the $[^{18}\text{F}]$ difluoromethyl benzothiazolyl-sulfone ($[^{18}\text{F}]\text{70}$). (B) Visible light-induced ^{18}F -difluoromethylation of heteroarenes (**71**) with the reagent $[^{18}\text{F}]\text{70}$, under continuous-flow conditions. ^(a)RCY of the isolated products after cartridge purification. ^(b)Molar activity decay-corrected at the end of bombardment (EOB). ^(c)RCY determined by radio-TLC and radio-UPLC of the crude product. ^(d)RCY of the isolated isomer b of $[^{18}\text{F}]\text{72d}$ after HPLC purification.

In 2020, Lemaire, Luxen, and Genicot described a general automated protocol for the C-H ^{18}F -difluoromethylation of the acyclovir (**71c**) on a commercially available AllInOne (AIO) synthesizer from Trasis [121]. The automated procedure entailed the radiosynthesis of the ^{18}F -difluoromethylating reagent $[^{18}\text{F}]\text{70}$ and the subsequent photoredox ^{18}F -difluoromethylation reaction, each of which requiring a HPLC purification step. Due to the limited number of free positions of the FASTlab synthesizer to introduce the additional components required for the flow ^{18}F -difluoromethylation of **71c** and the absence of an integrated purification system in the FASTlab module, the AIO synthesizer was selected for this multistep procedure. The two-step radiosynthesis of $[^{18}\text{F}]\text{70}$ was successfully transposed from the FASTlab to the AIO module and furnished the cartridge-purified $[^{18}\text{F}]\text{70}$ in $11.9 \pm 1.4\%$ RCY (decay-corrected at the SOS). No significant variation in the RCY was observed when the oxidation was performed in the AIO glass reactor [82.9% RCY (GE FASTlabTM) vs. 86.2% RCY (AIO)]. These results suggested that the presence of MeCN, K_2CO_3 , and

K_{2.2.2} has no meaningful impact on the oxidation of [¹⁸F]**1**. Starting with 165 GBq of [¹⁸F]fluoride, the reagent [¹⁸F]**70** was isolated in 7.5 ± 1.7% RCY with a molar activity of 59 ± 4 GBq·μmol⁻¹, after semi-preparative HPLC purification and reformulation on a SepPak® C18 short cartridge (Scheme 14A). The subsequent flow photoredox ¹⁸F-difluoromethylation procedure was performed in a photochemistry reactor consisting of a three-dimensional (3D)-printed with poly(ethylene terephthalate) recovered with a transparent polycarbonate (Lexan) plate and the reaction mixture was irradiated with a 32 W blue LED lamp. The replacement of *fac*-Ir^{III}(ppy)₃ by the organic photocatalyst 1,2,3,5-tetrakis(carbazol-9-yl)-4,6-dicyanobenzene (4CzIPN) demonstrated to be beneficial for the efficiency of the ¹⁸F-difluoromethylation reaction. The purification of the crude product by semipreparative HPLC afforded the [¹⁸F]acyclovir-CHF₂ [¹⁸F]**72c** in 25 ± 5% RCY. Overall, the fully automated three-step radiosynthesis of [¹⁸F]**72c** was achieved in 1.4 ± 0.1% RCY (Scheme 14B). This automated protocol can be implemented for the ¹⁸F-difluoromethylation of a wide range of *N*-heteroaromatics typically found in medicinal chemistry.



Scheme 14. Fully automated photoredox ¹⁸F-difluoromethylation of acyclovir (**71c**) in an AllInOne synthesizer, under continuous-flow conditions. ^(a)RCY of the isolated products after cartridge purification. ^(b)RCY after HPLC purification. ^(c)Molar activity decay-corrected at the end of bombardment (EOB).

4. Concluding Remarks

The ¹⁸F-radiochemistry has gained a pivotal role in the study of biochemical, physiological, and pharmacological behaviour of fluorine-containing molecules in living subjects by the application of non-invasive PET imaging techniques. The major success of PET as clinical and research tool is highly dependent on the availability of selective ¹⁸F-labeled probes. However, the development of ¹⁸F-labeled tracers still remains an important and challenging issue for radiochemists.

To date, the access to radiotracers has relied mostly on radiosynthetic methods leading to [¹⁸F]aryl-F and [¹⁸F]alkyl-F derivatives. The ¹⁸F-labeling of perfluoroalkyl motifs, such as CHF₂, has been recently explored in radiochemistry, despite the potential benefits of these functional groups in medicinal chemistry. The majority of the reported methods has been mainly focused on the late stage ¹⁸F-fluorination of preactivated precursors. The preparation of these precursors bearing suitable leaving groups requires a multistep procedure and, in some cases, may be challenging and time-consuming and can limit the number of synthetic accessibility to radiotracers. Recently, the late-stage ¹⁸F-difluoromethylation has emerged as a novel approach to expand the chemical space available for radioligand discovery.

Another critical issue in ¹⁸F-difluoromethylation chemistry resides on the fact that most protocols afforded the [¹⁸F]CHF₂-containing compounds with low-to-medium molar activities, owing to the great probability of ¹⁸F-¹⁹F isotopic dilution. This means that the synthesis of [¹⁸F]CHF₂-containing compounds must require the use of nucleophilic [¹⁸F]F⁻ with high molar activity. The production of radiotracers with high molar activity is mandatory for PET imaging studies, especially for targeting low-density biomacromolecules.

Overall, we expect that the combination of the positron emitter function of the radionuclide ¹⁸F with the CHF₂ groups could inspire other radiochemists to develop new and efficient methods to access novel PET ligands bearing ¹⁸F-difluoromethyl groups.

References

- [1] Shukla, A.K.; Kumar, U. Positron emission tomography: An overview. *J. Med. Phys.* **2006**, *31*, 13-21.
- [2] Lin, M.; Shon, I.H.; Lin, P. Positron emission tomography: Current status and future challenges. *Intern.ed. J.* **2010**, *40*, 19-29.
- [3] Vaquero, J.J.; Kinahan, P. Positron emission tomography: Current challenges and opportunities for technological advances in clinical and preclinical imaging systems. *Annu. Rev. Biomed. Eng.* **2015**, *17*, 385-414.
- [4] El-Galaly, T.C.; Gormsen, L.C.; Hutchings, M. PET/CT for staging; Past, present, and future. *Semin. Nucl. Med.* **2018**, *48*, 4-16.
- [5] Weber, W.A. Positron Emission Tomography As an Imaging Biomarker. *J. Clin. Oncol.* **2006**, *24*, 3282-3292.
- [6] Oriuchi, N.; Higuchi, T.; Ishikita, T.; Miyakubo, M.; Hanaoka, H.; Iida, Y.; Endo, K. Present role and future prospects of positron emission tomography in clinical oncology. *Cancer Sci.* **2006**, *97*, 1291-1297.
- [7] Wood, K.A.; Hoskin, P.J.; Saunders, M.I. Positron Emission Tomography in Oncology: A Review. *Clin. Oncol.* **2007**, *19*, 237-255.
- [8] Schwaiger, M.; Ziegler, S.; Nekolla, S.G. PET/CT: Challenge for Nuclear Cardiology. *J. Nucl. Med.* **2005**, *46*, 1664-1678.

- [9] Di Carli, M.F.; Dorbala, S.; Meserve, J.; El Fakhri, G.; Sitek, A.; Moore, S.C. Clinical Myocardial Perfusion PET/CT. *J. Nucl. Med.* **2007**, *48*, 783–793.
- [10] deKemp, R.A.; Yoshinaga, K.; Beanlands, S.B. Will 3-dimensional PET-CT enable the routine quantification of myocardial blood flow? *J. Nucl. Cardiol.* **2007**, *14*, 380–397.
- [11] Herholz, K.; Heiss, W.D. Positron emission tomography in clinical neurology. *Mol. Imaging Biol.* **2004**, *6*, 239–269.
- [12] Wu, C.; Pike, V.W.; Wang, Y. Amyloid Imaging: From Benchtop to Bedside. *Curr. Top. Dev. Biol.* **2005**, *70*, 171–213.
- [13] Cai, L.; Innis, R.B.; Pike, V.W. Radioligand development for PET imaging of β -amyloid ($A\beta$)-current status. *Curr. Med. Chem.* **2007**, *14*, 19–52.
- [14] Nordberg, A. PET imaging of amyloid in Alzheimer's disease. *Lancet Neurol.* **2004**, *3*, 519–527.
- [15] Liang, S.H.; Vasdev, N. Total Radiosynthesis: Thinking Outside 'the Box'. *Aust. J. Chem.* **2015**, *68*, 1319–1328.
- [16] Pike, V.W. Considerations in the Development of Reversibly Binding PET Radioligands for Brain Imaging. *Curr. Med. Chem.* **2016**, *23*, 1818–1869.
- [17] Yu, S. Review of ^{18}F -FDG Synthesis and Quality Control. *Biomed. Imaging Interv. J.* **2006**, *2*, e57.
- [18] Pauwels, E.K.; Coumou, A.W.; Kostkiewicz, M.; Kairemo, K. [^{18}F]Fluoro-2-Deoxy-D-Glucose Positron Emission Tomography/Computed Tomography Imaging in Oncology: Initial Staging and Evaluation of Cancer Therapy. *Med. Princ. Pract.* **2013**, *22*, 427–437.
- [19] Been, L.B.; Suurmeijer, A.J.H.; Cobben, D.C.P.; Jager, P.L.; Hoekstra, H.J.; Elsinga, P.H. [^{18}F]FLT-PET in Oncology: Current Status and Opportunities. *Eur. J. Nucl. Med. Mol. Imaging* **2004**, *31*, 1659–1672.
- [20] A systematic review on [^{18}F]FLT-PET uptake as a measure of treatment response in cancer patients. *Eur. J. Cancer* **2016**, *55*, 81–97.
- [21] Jauhar, S.; Veronese, M.; Rogdaki, M.; Bloomfield, M.; Natesan, S.; Turkheimer, F.; Kapur, S.; Howes, O.D. Regulation of dopaminergic function: an [^{18}F]-DOPA PET apomorphine challenge study in humans. *Transl. Psychiatry* **2017**, *7*, e1027.
- [22] Chen, W.; Silverman, D.H.; Delaloye, S.; Czernin, J.; Kamdar, N.; Pope, W.; Satyamurthy, N.; Schiepers, C.; Cloughesy, T. ^{18}F -FDOPA PET Imaging of Brain Tumors: Comparison Study with ^{18}F -FDG PET and Evaluation of Diagnostic Accuracy. *J. Nucl. Med.* **2006**, *47*, 904–911.
- [23] Becherer, A.; Szabó, M.; Karanikas, G.; Wunderbaldinger, P.; Angelberger, P.; Raderer, M.; Kurtaran, A.; Dudczak, R.; Kletter, K. Imaging of Advanced Neuroendocrine Tumors with ^{18}F -FDOPA PET. *J. Nucl. Med.* **2004**, *45*, 1161–1167.
- [24] Gründer, G.; Siessmeier, T.; Lange-Asschenfeldt, C.; Vernaleken, I.; Buchholz, H.G.; Stoeter, P.; Drzezga, A.; Lüddens, H.; Rösch, F.; Bartenstein, P. [^{18}F]Fluoroethylflumazenil: a novel tracer for PET imaging of human benzodiazepine receptors. *Eur. J. Nucl. Med.* **2001**, *28*, 1463–1470.

- [25] Levêque, P.; Labar, D.; Gallez, B. Biodistribution, binding specificity and metabolism of [¹⁸F]fluoroethylflumazenil in rodents. *Nucl. Med. Biol.* **2001**, *28*, 809-814.
- [26] Warnock, G.I.; Aerts, J.; Bahri, M.A.; Bretin, F.; Lemaire, C.; Giacomelli, F.; Mievis, F.; Mestdagh, N.; Buchanan, T.; Valade, A.; Mercier, J.; Wood, M.; Gillard, M.; Seret, A.; Luxen, A.; Salmon, E.; Plenevaux, A. Evaluation of ¹⁸F-UCB-H as a novel PET tracer for synaptic vesicle protein 2A in the brain. *J. Nucl. Med.* **2014**, *55*, 1336-1341.
- [27] Warnier, C.; Lemaire, C.; Becker, G.; Zaragoza, G.; Giacomelli, F.; Aerts, J.; Otabashi, M.; Bahri, M.A.; Mercier, J.; Plenevaux, A.; Luxen, A. Enabling Efficient Positron Emission Tomography (PET) Imaging of Synaptic Vesicle Glycoprotein 2A (SV2A) with a Robust and One-Step Radiosynthesis of a Highly Potent ¹⁸F-Labeled Ligand ([¹⁸F]UCB-H). *J. Med. Chem.* **2016**, *59*, 8955-8966.
- [28] Becker, G.; Warnier, C.; Serrano, M.E.; Bahri, M.A.; Mercier, J.; Lemaire, C.; Salmon, E.; Luxen, A.; Plenevaux, A. Pharmacokinetic Characterization of [¹⁸F]UCB-H PET Radiopharmaceutical in the Rat Brain. *Mol. Pharm.* **2017**, *14*, 2719-2725.
- [29] Yalamanchili, P.; Wexler, E.; Hayes, M.; Yu, M.; Bozek, J.; Kagan, M.; Radeke, H.S.; Azure, M.; Purohit, A.; Casebier, D.S.; Robinson, S.P. Mechanism of uptake and retention of ¹⁸F BMS-747158-02 in cardiomyocytes: A novel PET myocardial imaging agent. *J. Nucl. Cardiol.* **2007**, *14*, 782-788.
- [30] Nekolla, S.G.; Reder, S.; Saraste, A.; Higuchi, T.; Dzewas, G.; Preissel, A.; Huisman, M.; Poethko, T.; Schuster, T.; Yu, M.; Robinson, S.; Casebier, D.; Henke, J.; Wester, H.J.; Schwaiger, M. Evaluation of the novel myocardial perfusion positron-emission tomography tracer ¹⁸F-BMS-747158-02: comparison to ¹³N-ammonia and validation with microspheres in a pig model. *Circulation* **2009**, *119*, 2333-2342.
- [31] Wilson, T.C.; Xavier, M.A.; Knight, J.; Verhoog, S.; Torres, J.B.; Mosley, M.; Hopkins, S.L.; Wallington, S.; Allen, P.D.; Kersemans, V.; Hueting, R.; Smart, S.; Gouverneur, V.; Cornelissen, B. PET Imaging of PARP Expression Using ¹⁸F-Olaparib. *J. Nucl. Med.* **2019**, *60*, 504-510.
- [32] Stark, A.J.; Smith, C.T.; Petersen, K.J.; Trujillo, P.; van Wouwe, N.C.; Donahue, M.J.; Kessler, R.M.; Deutch, A.Y.; Zald, D.H.; Claassen, D.O. [¹⁸F]Fallypride characterization of striatal and extrastriatal D2/3 receptors in Parkinson's disease. *Neuroimage Clin.* **2018**, *18*, 433-442.
- [33] Huhtala, T.; Poutiainen, P.; Rytönen, J.; Lehtimäki, K.; Parkkari, T.; Kasanen, I.; Airaksinen, A.J.; Koivula, T.; Sweeney, P.; Kontkanen, O.; Wityak, J.; Dominiquez, C.; Park, L.C. Improved synthesis of [¹⁸F] fallypride and characterization of a Huntington's disease mouse model, zQ175DN KI, using longitudinal PET imaging of D2/D3 receptors. *EJNMMI Radiopharm. Chem.* **2019**, *4*, DOI: 10.1186/s41181-019-0071-6.
- [34] Su, H.; Seimbille, Y.; Ferl, G.Z.; Bodenstein, C.; Fueger, B.; Kim, K.J.; Hsu, Y.T.; Dubinett, S.M.; Phelps, M.E.; Czernin, J.; Weber, W.A. Evaluation of [¹⁸F]gefitinib as a molecular imaging probe for the assessment of the epidermal growth factor receptor status in malignant tumors. *Eur. J. Nucl. Med. Mol. Imaging* **2008**, *35*, 1089-1099.

- [35] Parent, E.E.; Schuster, D.M. Update on ^{18}F -Fluciclovine PET for Prostate Cancer Imaging. *J. Nucl. Med.* **2018**, *59*, 733-739.
- [36] Gusman, M.; Aminsharifi, J.A.; Peacock, J.G.; Anderson, S.B.; Clemenshaw, M.N.; Banks, K.P. Review of ^{18}F -Fluciclovine PET for Detection of Recurrent Prostate Cancer. *Radiographics* **2019**, *39*, 822-841.
- [37] Cardinale, J.; Schäfer, M.; Benešová, M.; Bauder-Wüst, U.; Leotta, K.; Eder, M.; Neels, O.C.; Haberkorn, U.; Giesel, F.L.; Kopka, K. Preclinical Evaluation of ^{18}F -PSMA-1007, a New Prostate-Specific Membrane Antigen Ligand for Prostate Cancer Imaging. *J. Nucl. Med.* **2017**, *58*, 425-431.
- [38] Cardinale, J.; Martin, R.; Remde, Y.; Schäfer, M.; Hienzsch, A.; Hübner, S.; Zerges, A.-M.; Marx, H.; Hesse, R.; Weber, K.; Smits, R.; Hoepfing, A.; Müller, M.; Neels, O.C.; Kopka, K. Procedures for the GMP-Compliant Production and Quality Control of [^{18}F]PSMA-1007: A Next Generation Radiofluorinated Tracer for the Detection of Prostate Cancer. *Pharmaceuticals* **2017**, *10*, 77.
- [39] Jacobson, O.; Kiesewetter, D.O.; Chen, X. Fluorine-18 Radiochemistry, Labeling Strategies and Synthetic Routes. *Bioconjug. Chem.* **2015**, *26*, 1-18.
- [40] Levin, C.S.; Hoffman, E.J. Calculation of positron range and its effect on the fundamental limit of positron emission tomography system spatial resolution. *Phys. Med. Biol.* **1999**, *44*, 781-799.
- [41] Miller, P. W.; Long, N. J.; Vilar, R.; Gee, A. D. Synthesis of ^{11}C , ^{18}F , ^{15}O , and ^{13}N Radiolabels for Positron Emission Tomography. *Angew. Chem. Int. Ed.* **2008**, *47*, 8998-9033.
- [42] Li, Z.; Conti, P.S. Radiopharmaceutical chemistry for positron emission tomography. *Adv. Drug Deliv. Rev.* **2010**, *62*, 1031-1051.
- [43] Coenen, H.H. Fluorine-18 labeling methods: features and possibilities of basic reactions. *Ernst Schering Res. Found. Workshop*, **2007**, 15-50.
- [44] Cai, L.; Lu, S.; Pike, V.W. Chemistry with [^{18}F]Fluoride Ion. *Eur. J. Org. Chem.* **2008**, *2008*, 2853-2873.
- [45] Sood, S.; Firnau, G.; Garnett, E.S. Radiofluorination with Xenon Difluoride: A New High Yield Synthesis of [^{18}F]2-Fluoro-2-deoxy-D-glucose. *Int. J. Appl. Radiat. Isot.* **1983**, *34*, 743-745.
- [46] Shiue, C.-Y.; To, K.-C.; Wolf, A.P. A Rapid Synthesis of 2-Deoxy-2-fluoro-D-glucose From Xenon Difluoride Suitable for Labelling with ^{18}F . *J. Labelled Compd. Radiopharm.* **1983**, *20*, 157-162.
- [47] Chirakal, R.; Firnau, G.; Schrobilgen, G. J.; McKay, J.; Garnett, E.S. The Synthesis of [^{18}F]Xenon Difluoride from [^{18}F]Fluorine Gas. *Int. J. Appl. Radiat. Isot.* **1984**, *35*, 401-404.
- [48] Ehrenkauf, R.E.; MacGregor, R.R. Synthesis of [^{18}F]-Perchloryl Fluoride and its Reactions with Functionalized Aryl Lithiums. *Int. J. Appl. Radiat. Isot.* **1983**, *34*, 613-615.
- [49] Hiller, A.; Ficher, C.; Jordanova, A.; Patt, J.T.; Steinbach, J. Investigations to the synthesis of n.c.a. [^{18}F]FCIO₃ as electrophilic fluorination agent. *Appl. Radiat. Isot.* **2008**, *66*, 152-157.

- [50] Neirinckx, R.D.; Lambrecht, R.M.; Wolf, A.P. Cyclotron Isotopes and Radiopharmaceuticals-XXV An Anhydrous ^{18}F -Fluorination Intermediate: Trifluoromethyl Hypofluorite. *Int. J. Appl. Radiat. Isot.* **1978**, *29*, 323–327.
- [51] Chirakal, R.; Fimau, G.; Couse, J.; Garnett, E.S. Radiofluorination with ^{18}F -labelled acetyl hypofluorite: [^{18}F]L-6-fluorodopa. *Int. J. Appl. Radiat. Isot.* **1984**, *35*, 651–653.
- [52] Adam, M.J.; Ruth, T.J.; Grierson, J.R.; Abeysekera, B.; Pate, B.D. Routine Synthesis of L- [^{18}F]6-Fluorodopa with Fluorine-18 Acetyl Hypofluorite. *J. Nucl. Med.* **1986**, *27*, 1462–1466.
- [53] Oberdorfer, F.; Hofmann, E.; Maier-Borst, W. Preparation of a New ^{18}F -Labelled precursor: 1- [^{18}F]fluoro-2-pyridone. *Appl. Radiat. Isot.* **1988**, *39*, 685–688.
- [54] Oberdorfer, F.; Hofmann, E.; Maier-Borst, W. Preparation of ^{18}F -Labelled N-Fluoropyridinium Triflate. *J. Labelled Compd. Radiopharm.* **1988**, *25*, 999–1005.
- [55] Teare, H.; Robins, E.G.; Arstad, E.; Luthra, S.K.; Gouverneur, V. Synthesis and reactivity of [^{18}F]-N-fluorobenzenesulfonimide. *Chem. Commun. (Cambridge, U.K.)*, **2007**, 2330–2332.
- [56] Teare, H.; Robins, E.G.; Kirjavainen, A.; Forsback, S.; Sanford, G.; Solin, O.; Luthra, S.K.; Gouverneur, V. Radiosynthesis and Evaluation of [^{18}F]Selectfluor bis(triflate). *Angew. Chem. Int. Ed.* **2010**, *49*, 6821–6824.
- [57] Kim, D.W.; Jeong, H.J.; Lim, S.T.; Sohn, M.H.; Katzenellenbogen, J.A.; Chi, D.Y. Facile nucleophilic fluorination reactions using *tert*-alcohols as a reaction medium: significantly enhanced reactivity of alkali metal fluorides and improved selectivity. *J. Org. Chem.* **2008**, *73*, 957–962.
- [58] Coenen, H.H. No-carrier-added ^{18}F -chemistry of radiopharmaceuticals. *Synthesis and Application of Isotopically Labeled Compounds*; Elsevier: Amsterdam, 1989; pp 433–448.
- [59] Coenen, H.H.; Klatte, B.; Knochel, A.; Schuller, M.; Stocklin, G. Preparation of n.c.a. [$^{17-18}\text{F}$]fluoroheptadecanoic acid in high yields *via* aminopolyether supported, nucleophilic fluorination. *J. Labelled Compd. Radiopharm.* **1986**, *23*, 455–467.
- [60] Gately, S.J.; Shaughnessy, W.J. Production of ^{18}F -Labeled Compounds with $^{18}\text{F}^-$ Produced with a 1-MW Research Reactor. *Int. J. Appl. Radiat. Isot.* **1982**, *33*, 1325–1330.
- [61] Zhan, C.-G.; Dixon, D.A. Hydration of the Fluoride Anion: Structures and Absolute Hydration Free Energy from First-Principles Electronic structure Calculations. *J. Phys. Chem. A* **2004**, *108*, 2020–2029.
- [62] Lemaire, C.F.; Aerts, J.J.; Voccia, S.; Libert, L.C.; Mercier, F.; Goblet, D.; Plenevaux, A.R.; Luxen, A.J. Fast Production of Highly Reactive No-Carrier Added [^{18}F]Fluoride for the Labeling of Radiopharmaceuticals. *Angew. Chem. Int. Ed.* **2010**, *49*, 3161–3164.
- [63] Brichard, L.; Aigbirhio, F.I. An Efficient Method for Enhancing the Reactivity and Flexibility of [^{18}F]Fluoride Towards Nucleophilic Substitution Using Tetraethylammonium Bicarbonate. *Eur. J. Org. Chem.* **2014**, *2014*, 6145–6149.
- [64] Richarz, R.; Krapf, P.; Zarrad, F.; Urusova, E.A.; Neumaier, B.; Zlatopolskiy, B.D. Neither azeotropic drying, nor base nor other additives: a minimalist approach to ^{18}F -labeling. *Org. Biomol. Chem.* **2014**, *12*, 8094–8099.

- [65] Lindner, S.; Rensch, C.; Neubaur, S.; Neumeier, M.; Salvamoser, R.; Samper, V.; Bartenstein, P. Azeotropic drying free [¹⁸F]FDG synthesis and its application to a lab-on-chip platform. *Chem. Commun.* **2016**, *52*, 729-732.
- [66] Aerts, J.; Voccia, S.; Lemaire, C.; Giacomelli, F.; Goblet, D.; Thonon, D.; Plenevaux, A.; Warnock, G.; Luxen, A. Fast production of highly concentrated reactive [¹⁸F]fluoride for aliphatic and aromatic nucleophilic radiolabelling. *Tetrahedron Lett.* **2010**, *51*, 64-66.
- [67] Perrio, C.; Schmitt, S.; Pla, D.; Gabbai, F.P.; Chansaenpak, K.; Mestre-Voegtle, B.; Gras, E. [¹⁸F]-Fluoride capture and release: azeotropic drying free nucleophilic aromatic radiofluorination assisted by a phosphonium borane. *Chem. Commun.* **2017**, *53*, 340-343.
- [68] Sergeev, M.E.; Morgia, F.; Lazari, M.; Wang Jr., C.; van Dam, R.M. Titania-Catalyzed Radiofluorination of Tosylated Precursors in Highly Aqueous Medium. *J. Am. Chem. Soc.* **2015**, *137*, 5686-5694.
- [69] Pees, A.; Sewing, C.; Vosjan, M.J.W.D.; Tadino, V.; Herscheid, J.D.M.; Windhorst, A.D.; Vugts, D.J. Fast and reliable generation of [¹⁸F]triflyl fluoride, a gaseous [¹⁸F]fluoride source. *Chem. Commun.* **2018**, *54*, 10179-10182.
- [70] Kim, D.W.; Jeong, H.-J.; Lim, S.T.; Sohn, M.-H. Recent trends in the nucleophilic [¹⁸F]-radiolabeling method with no-carrier-added [¹⁸F]fluoride. *Nucl. Med. Mol. Imaging* **2010**, *44*, 25-32.
- [71] Schirmmacher, R.; Wängler, B.; Bailey, J.; Bernard-Gauthier, V.; Schirmmacher, E.; Wängler, C. Small Prosthetic Groups in ¹⁸F-Radiochemistry: Useful Auxiliaries for the Design of ¹⁸F-PET Tracers. *Semin. Nucl. Med.* **2017**, *47*, 474-492.
- [72] Lemaire, C.; Libert, L.; Franci, X.; Genon, J.-L.; Kuci, S.; Giacomelli, F.; Luxen, A. Automated production at the curie level of no-carrier-added 6-[¹⁸F]fluoro-L-dopa and 2-[¹⁸F]fluoro-L-tyrosine on a FASTlab synthesizer. *J. Labelled Compd. Radiopharm.* **2015**, *58*, 281-290.
- [73] Wang, J.; Sánchez-Roselló, M.; Aceña, J.L.; del Pozo, C.; Sorochinsky, A.E.; Fustero, S.; Soloshonok, V.A.; Liu, H. Fluorine in Pharmaceutical Industry: Fluorine-Containing Drugs Introduced to the Market in the Last Decade (2001-2011). *Chem. Rev.* **2014**, *114*, 2432-2506.
- [74] Mei, H.; Han, J.; Fustero, S.; Medio-Simon, M.; Sedgwick, D.M.; Santi, C.; Ruzziconi, R.; Soloshonok, V.A. Fluorine-Containing Drugs Approved by the FDA in 2018. *Chem. Eur. J.* **2019**, *25*, 11797-11819.
- [75] Park, B.K.; Kitteringham, N.R.; O'Neill, P.M. Metabolism of Fluorine-Containing Drugs. *Annu. Rev. Pharmacol. Toxicol.* **2001**, *41*, 443-470.
- [76] Purser, S.; Moore, P.R.; Swallow, S.; Gouverneur, V. Fluorine in medicinal chemistry, *Chem. Soc. Rev.* **2008**, *37*, 320-330.
- [77] Hagmann, W.K. The Many Roles for Fluorine in Medicinal Chemistry, *J. Med. Chem.* **2008**, *51*, 4359-4369.
- [78] Wang, B.-C.; Wang, L.-J.; Jiang, B.; Wang, S.-Y.; Wu, N.; Li, X.-Q.; Shi, D.-Y. Application of Fluorine in Drug Design During 2010-2015 Years: A Mini-Review. *Mini Rev. Med. Chem.* **2017**, *17*, 683-692.

- [79] Gu, Y.; Huang, D.; Liu, Z.; Huang, J.; Zeng, W. Labeling strategies with F-18 for positron emission tomography imaging. *Med. Chem.* **2011**, *7*, 334-344.
- [80] Ying, L. ¹⁸F-Labeling techniques for positron emission tomography. *Sci. China Chem.* **2013**, *56*, 1682-1692.
- [81] Brooks, A.F.; Topczewski, J.J.; Ichiishi, N.; Sanford, M.S.; Scott, P.J.H. Late-stage [¹⁸F]fluorination: new solutions to old problems. *Chem. Sci.* **2014**, *5*, 4545-4553.
- [82] Preshlock, S.; Tredwell, M.; Gouverneur, V. ¹⁸F-Labeling of arenes and heteroarenes for applications in positron emission tomography. *Chem. Rev.* **2016**, *116*, 719-766.
- [83] Van der Born, D.; Pees, A.; Poot, A.J.; Orru, R.V.A.; Windhorst, A.D.; Vugts, D.J. Fluorine-18 labelled building blocks for PET tracer synthesis. *Chem. Soc. Rev.* **2017**, *46*, 4709-4773.
- [84] Krishnan, H.S.; Ma, L.; Vasdev, N.; Liang, S.H. ¹⁸F-Labeling of sensitive biomolecules for positron emission tomography. *Chem. Eur. J.* **2017**, *23*, 15553-15577.
- [85] Coenen, H.H.; Ermert, J. ¹⁸F-Labeling innovations and their potential for clinical application. *Clin. Transl. Imaging* **2018**, *6*, 169-193.
- [86] Krüll, J.; Heinrich, M.R. [¹⁸F]Fluorine-labeled pharmaceuticals: direct aromatic fluorination compared to multi-step strategies. *Asian J. Org. Chem.* **2019**, *8*, 576-590.
- [87] Deng, X.; Rong, J.; Wang, L.; Vasdev, N.; Zhang, L.; Josephson, L.; Liang, S.H. Chemistry for positron emission tomography: recent advances in ¹¹C-, ¹⁸F-, ¹³N-, and ¹⁵O-labeling reactions. *Angew. Chem. Int. Ed.* **2019**, *58*, 2580-2605.
- [88] Fitton, A.; Wiseman, L. Pantoprazole. A Review of Its Pharmacological Properties and Therapeutic Use in Acid-Related Disorders. *Drugs*, **1996**, *51*, 460-482.
- [89] Vilskersts, R. Vigante, B.; Neidere, Z.; Krauze, A.; Domracheva, I.; Bekere, L.; Shestakova, I.; Duburs, G.; Dambrova, M. Calcium Level Controlling Activities of Novel Derivatives of Amlodipine, Riodipine and Cerebrocrast. *Lett. Drug Des. Discov.* **2012**, *9*, 322-328.
- [90] Kong, D.-s.; Yamori, T. ZSTK474, a Novel Phosphatidylinositol 3-kinase Inhibitor Identified Using the JFCR39 Drug Discovery System. *Acta Pharmacol. Sin.* **2010**, *31*, 1189-1197.
- [91] Noh, H.H.; Lee, J.Y.; Park, H.K.; Lee, J.W.; Jo, S.H.; Lim, J.B.; Shin, H.G.; Kwon, H.; Kyung, K.S. Dissipation, persistence, and risk assessment of fluxapyroxad and penthiopyrad residues in perilla leaf (*Perilla frutescens* var. *japonica* Hara). *Plos One* **2019**, *14*, e0212209.
- [92] Schudt, C.; Winder, S.; Müller, B.; Ukena, D. Zardaverine as a selective inhibitor of phosphodiesterase isozymes. *Biochem. Pharmacol.* **1991**, *42*, 153-162.
- [93] Dellarco, V.L.; McGregor, D.; Berry, S.C.; Cohen, S.M.; Boobis, A.R. Thiazopyr and thyroid disruption: case study within the context of the 2006 IPCS Human Relevance Framework for analysis of a cancer mode of action. *Crit. Rev. Toxicol.* **2006**, *36*, 793-801.
- [94] Iwai, N.; Nakamura, H.; Miyazu, M.; Kasai, K.; Watanabe, Y.; Taneda, Y.; Ozaki, T.; Matsui, S.; Maki, T.; Tauchi, N. Laboratory and Clinical Evaluations of Flomoxef Sodium in Neonates. *Jpn. J. Antibiot.* **1991**, *44*, 1265-1285.

- [95] Takagi, H.; Tanaka, K.; Tsuda, H.; Kobayashi, H. Clinical studies of garenoxacin. *Int. J. Antimicrob. Agents* **2008**, *32*, 468-474.
- [96] Hartz, R.A.; Ahuja, V.T.; Rafalski, M.; Schmitz, W.D.; Brenner, A.B.; Denhart, D.J.; Ditta, J.L.; Deskus, J.A.; Yue, E.W.; Arvanitis, A.G.; Lelas, S.; Li, Y.W.; Molski, T.F.; Wong, H.; Grace, J.E.; Lentz, K.A.; Li, J.; Lodge, N.J.; Zaczek, R.; Combs, A.P.; Olson, R.E.; Mattson, R.J.; Bronson, J.J.; Macor, J.E. In Vitro Intrinsic Clearance-Based Optimization of *N*³-Phenylpyrazinones as Corticotropin-Releasing Factor-1 (CRF₁) Receptor Antagonists. *J. Med. Chem.* **2009**, *52*, 4161-4172.
- [97] Camerino, E.; Wong, D.M.; Tong, F.; Körber, F.; Gross, A.D.; Islam, R.; Viayna, E.; Mutunga, J.M.; Li, J.; Totrov, M.M.; Bloomquist, J.R.; Carlier, P.R. Difluoromethyl Ketones: Potent Inhibitors of Wild Type and Carbamate-Insensitive G119S Mutant Anopheles Gambiae Acetylcholinesterase. *Bioorg. Med. Chem. Lett.* **2015**, *25*, 4405-4411.
- [98] Zheng, B.; D'Andrea, S.V.; Sun, L.Q.; Wang, A.X.; Chen, Y.; Hrcnciar, P.; Friberg, J.; Falk, P.; Hernandez, D.; Yu, F.; Sheaffer, A.K.; Knipe, J.O.; Mosure, K.; Rajamani, R.; Good, A.C.; Kish, K.; Tredup, J.; Klei, H.E.; Paruchuri, M.; Ng, A.; Gao, Q.; Rampulla, R.A.; Mathur, A.; Meanwell, N.A.; McPhee, F.; Scola, P.M. Potent Inhibitors of Hepatitis C Virus NS3 Protease: Employment of a Difluoromethyl Group as a Hydrogen-Bond Donor. *ACS Med. Chem. Lett.* **2018**, *9*, 143-148.
- [99] Zafrani, Y.; Yeffet, D.; Sod-Moriah, G.; Berliner, A.; Amir, D.; Marciano, D.; Gershonov, E.; Saphier, S. Difluoromethyl Bioisostere: Examining the "Lipophilic Hydrogen Bond Donor" Concept. *J. Med. Chem.* **2017**, *60*, 797-804.
- [100] Zafrani, Y.; Sod-Moriah, G.; Yeffet, D.; Berliner, A.; Amir, D.; Marciano, D.; Elias, S.; Katalan, S.; Ashkenazi, N.; Madmon, M.; Gershonov, E.; Saphier, S. CF₂H, a Functional Group-Dependent Hydrogen-Bond Donor: Is It a More or Less Lipophilic Bioisostere of OH, SH, and CH₃? *J. Med. Chem.* **2019**, *62*, 5628-5637.
- [101] Gillis, E.P.; Eastman, K.J.; Hill, M.D.; Donnelly, D.J.; Meanwell, N.A. Applications of Fluorine in Medicinal Chemistry. *J. Med. Chem.* **2015**, *58*, 8315-8359.
- [102] Cox, C.D.; Breslin, M.J.; Whitman, D.B.; Coleman, P.J.; Garbaccio, R.M.; Fraley, M.E.; Zrada, M.M.; Buser, C.A.; Walsh, E.S.; Hamilton, K.; Lobell, R.B.; Tao, W.; Abrams, M.T.; South, V.J.; Huber, H.E.; Kohl, N.E.; Hartman, G.D. Kinesin spindle protein (KSP) inhibitors. Part V: discovery of 2-propylamino-2,4-diaryl-2,5-dihydropyrroles as potent, water-soluble KSP inhibitors, and modulation of their basicity by β -fluorination to overcome cellular efflux by P-glycoprotein. *Bioorg. Med. Chem. Lett.* **2007**, *17*, 2697-2702.
- [103] Xing, L.; Blakemore, D.C.; Narayanan, A.; Unwalla, R.; Lovering, F.; Denny, R.A.; Zhou, H.; Bunnage, M.E. Fluorine in Drug Design: A Case Study with Fluoroanisoles. *ChemMedChem* **2015**, *10*, 715-726.
- [104] O'Hara, F.; Burns, A.C.; Collins, M.R.; Dalvie, D.; Ornelas, M.A.; Vaz, A.D.N.; Fujiwara, Y.; Baran, P.S. A Simple Litmus Test for Aldehyde Oxidase Metabolism of Heteroarenes. *J. Med. Chem.* **2014**, *57*, 1616-1620.
- [105] Rong, J.; Ni, C.; Hu, J. Metal-catalyzed direct difluoromethylation reactions. *Asian J. Org. Chem.* **2017**, *6*, 139-152.

- [106] Yerien, D.E.; Barata-Vallejo, S.; Postigo, A. Difluoromethylation reactions of organic compounds. *Chem. Eur. J.* **2017**, *23*, 14676–14701.
- [107] Lemos, A.; Lemaire, C.; Luxen, A. Progress in difluoroalkylation of organic substrates by visible light photoredox catalysis. *Adv. Synth. Catal.* **2019**, *361*, 1500–1537.
- [108] Levi, N.; Amir, D.; Greshonov, E.; Zafrani, Y. Recent progress on the synthesis of CF₂H-containing derivatives. *Synthesis* **2019**, *51*, 4549–4567.
- [109] Hugenberg, V.; Wagner, S.; Kopka, K.; Schober, O.; Schäfers, M.; Haufe, G. Synthesis of geminal difluorides by oxidative desulfurization-difluorination of alkyl aryl thioethers with halonium electrophiles in the presence of fluorinating reagents and its application for ¹⁸F-radiolabeling. *J. Org. Chem.* **2010**, *75*, 6086–6095.
- [110] Mizuta, S.; Stenhagen, I.S.R.; O'Duill, M.; Wolstenhulme, J.; Kirjavainen, A.K.; Forsback, S.J.; Tredwell, M.; Sandford, G.; Moore, P.R.; Huiban, M.; Luthra, S.K.; Passchier, J.; Solin, O.; Gouverneur, V. Catalytic decarboxylative fluorination for the synthesis of tri- and difluoromethyl arenes. *Org. Lett.* **2013**, *15*, 2648–2651.
- [111] Khotavivattana, T.; Verhoog, S.; Tredwell, M.; Pfeifer, L.; Calderwood, S.; Wheelhouse, K.; Collier, T.L.; Gouverneur, V. ¹⁸F-Labeling of aryl-SCF₃, -OCF₃ and -OCHF₂ with [¹⁸F]fluoride. *Angew. Chem. Int. Ed.* **2015**, *54*, 9991–9995.
- [112] Verhoog, S.; Pfeifer, L.; Khotavivattana, T.; Calderwood, S.; Collier, T.L.; Wheelhouse, K.; Tredwell, M.; Gouverneur, V. Silver-mediated ¹⁸F-labeling of aryl-CF₃ and aryl-CHF₂ with ¹⁸F-fluoride. *Synlett* **2016**, *27*, 25–28.
- [113] Shi, H.; Braun, A.; Wang, L.; Liang, S.H.; Vasdev, N.; Ritter, T. Synthesis of ¹⁸F-difluoromethylarenes from aryl (pseudo) halides. *Angew. Chem. Int. Ed.* **2016**, *55*, 10786–10790.
- [114] Yuan, G.; Wang, F.; Stephenson, N.A.; Wang, L.; Rotstein, B.H.; Vasdev, N.; Tang, P.; Liang, S.H. Metal-free ¹⁸F-labeling of aryl-CF₂H via nucleophilic radiofluorination and oxidative C–H activation. *Chem. Commun.* **2017**, *53*, 126–129.
- [115] Khotavivattana, T.; Calderwood, S.; Verhoog, S.; Pfeifer, L.; Preshlock, S.; Vasdev, N.; Collier, T.L.; Gouverneur, V. Synthesis and reactivity of ¹⁸F-labeled α,α -difluoro- α -(aryloxy)acetic acids. *Org. Lett.* **2017**, *19*, 568–571.
- [116] Frost, A.B.; Brambilia, M.; Exner, R.M.; Tredwell, M. Synthesis and derivitization of 1,1-[¹⁸F]difluorinated alkenes. *Angew. Chem. Int. Ed.* **2019**, *58*, 472–476.
- [117] Huang, X.; Liu, W.; Ren, H.; Neelamegam, R.; Hooker, J.M.; Groves, J.T. Late stage benzylic C–H fluorination with [¹⁸F]fluoride for PET imaging. *J. Am. Chem. Soc.* **2014**, *136*, 6842–6845.
- [118] Huang, X.; Liu, W.; Hooker, J.M.; Groves, J.T. Targeted fluorination with the fluoride ion by manganese-catalyzed decarboxylation. *Angew. Chem. Int. Ed.* **2015**, *54*, 5241–5245.
- [119] Sap, J.B.I.; Wilson, T.C.; Kee, C.W.; Straathof, N.J.W.; amEnde, C.W.; Mukherjee, P.; Zhang, L.; Genicot, C.; Gouverneur, V. Synthesis of ¹⁸F-difluoromethylarenes using aryl boronic acids, ethyl bromofluoroacetate and [¹⁸F]fluoride. *Chem. Sci.* **2019**, *10*, 3237–3241.

- [120] Trump, L.; Lemos, A.; Lallemand, B.; Pasau, P.; Mercier, J.; Lemaire, C.; Luxen, A.; Genicot, C. Late-stage ^{18}F -difluoromethyl labeling of *N*-heteroaromatics with high molar activity for PET imaging. *Angew. Chem. Int. Ed.* **2019**, *58*, 13149-13154.
- [121] Trump, L.; Lemos, A.; Jacq, J.; Pasau, P.; Lallemand, B.; Mercier, J.; Genicot, C.; Luxen, A.; Lemaire, C. Development of a general automated flow photoredox ^{18}F -difluoromethylation of *N*-heteroaromatics in an AllInOne synthesizer. *Org. Process Res. Dev.* **2020**, *24*, 734-744.

Chapter III

Fully Automated Radiosynthesis of [¹⁸F]Difluoromethyl Benzothiazolyl-Sulfone on a GE FASTlab™ Synthesizer

Part of this Chapter has been included in *Angew. Chem. Int. Ed.* **2019**, 58(37),
13149-13154

Chapter III

1. Introduction.....	137
2. Results and Discussion	
2.1. Chemistry	
2.1.1. Synthesis of the Difluoromethyl Benzothiazolyl-Sulfone (1).....	139
2.2. Radiochemistry	
2.2.1. Radiosynthesis of the [¹⁸ F]Difluoromethyl Benzothiazolyl-Sulfone ([¹⁸ F]1).....	141
2.2.1.1. First Approach: Late stage ¹⁸ F-fluorination of the Bromofluoromethyl Benzothiazolyl-Sulfone (5).....	141
2.2.1.2. Second Approach: ¹⁸ F-Labeling of the Bromofluoromethyl Benzothiazolyl-Sulfide (4) and oxidation of [¹⁸ F]Difluoromethyl Benzothiazolyl-Sulfide ([¹⁸ F]2).....	144
2.2.2. Automated radiosynthesis of the sulfone [¹⁸ F]1.....	151
3. Material and Methods	
3.1. Chemistry	
3.1.1. Synthesis of 2-((Difluoromethyl)thio)benzo[<i>d</i>]thiazole (2).....	155
3.1.2. Synthesis of 2-((Bromofluoromethyl)thio)benzo[<i>d</i>]thiazole (4).....	155
3.1.3. Synthesis of 2-((Difluoromethyl)sulfonyl)benzo[<i>d</i>]thiazole (1) and 2-((Bromofluoromethyl)sulfonyl)benzo[<i>d</i>]thiazole (5).....	156
3.1.4. Synthesis of 2-((Difluoromethyl)sulfinyl)benzo[<i>d</i>]thiazole (7) and 2-((Bromofluoromethyl)sulfinyl)benzo[<i>d</i>]thiazole (6).....	157
3.2. Radiochemistry	
3.2.1. Fully Automated Radiosynthesis of 2-((Difluoromethyl)sulfonyl)benzo[<i>d</i>]thiazole ([¹⁸ F]1).....	158
3.2.2. Low-Activity ¹⁸ F-Labeling Experiments in the Precursor 4.....	159
3.2.3. Isolation and Determination of the Molar Activity of [¹⁸ F]1.....	160
4. Conclusions.....	160
5. Supplementary Information	
5.1. NMR spectra of the compounds 1, 2, 4-7.....	161
5.2. Radiochemistry	
5.2.1. Synthesis of [¹⁸ F]2-((Difluoromethyl)thio)benzo[<i>d</i>]thiazole ([¹⁸ F]2).....	170
5.2.2. Synthesis of [¹⁸ F]2-((Difluoromethyl)sulfonyl)benzo[<i>d</i>]thiazole ([¹⁸ F]1).....	172
5.3. Two-Step Radiosynthesis of the [¹⁸ F]Difluoromethyl Heteroaryl-Sulfone [¹⁸ F]1 From the Precursor 4.....	173
5.4. Fully Automated Radiosynthesis of the Labeled Compound [¹⁸ F]1.....	173
5.5. Calibration Curves of the Difluoromethyl Heteroaryl-Sulfone 1 for Determination of the Molar Activity of [¹⁸ F]1.....	174
References.....	175

Fully Automated Radiosynthesis of [¹⁸F]Difluoromethyl Benzothiazolyl-Sulfone on a GE FASTlab™ Synthesizer

Abstract: The reagent difluoromethyl benzothiazolyl-sulfone (**1**) has been extensively used in the difluoromethylation of substrates bearing C=C, C≡C, and C≡N bonds by visible light photoredox catalysis. Taking advantage of the reactivity of **1** as difluoromethylating reagent, we intended to perform the radiosynthesis the ¹⁸F-labeled compound [¹⁸F]**1** as a novel labeled compound for late-stage introduction of ¹⁸F-difluoromethyl groups. Low activity labeling experiments (150-200 MBq) were performed in order to determine the most suitable conditions for the synthesis of [¹⁸F]**1**. Our results showed that a two-step methodology consisting in the ¹⁸F-labeling of the precursor bromofluoromethyl benzothiazolyl-sulfide (**4**) and subsequent oxidation of the [¹⁸F]difluoromethyl benzothiazolyl-sulfide ([¹⁸F]**2**) afforded the cartridge-purified [¹⁸F]**1** in higher radiochemical yield (RCY). The efficiency of the ¹⁸F-labeling reaction was influenced by the following parameters: (i) the type and amount of base and phase-transfer catalyst (PTC) used in the delivery of dry [¹⁸F]fluoride ([¹⁸F]F⁻); (ii) the solvent, the temperature, and the reaction time; (iii) the type and amount of ¹⁸F-labeling precursor. The amount of the oxidizing agent sodium (meta)periodate (NaIO₄) and ruthenium (III) chloride hydrate (RuCl₃·xH₂O) had a significant impact on the oxidation of [¹⁸F]**2**. Having the optimal conditions in hand, the radiosynthesis of sulfone [¹⁸F]**1** was fully automated on a GE FASTlab™ synthesizer in conjunction with a semi-preparative high performance liquid chromatography (HPLC) purification procedure. Starting with 120-135 GBq of [¹⁸F]fluoride, the sulfone [¹⁸F]**1** was isolated in 4.5 ± 0.1% RCY [decay-corrected at the start of the synthesis (SOS)] and with a molar activity of 54 ± 7 GBq·μmol⁻¹ at the end of the synthesis (EOS).

Keywords: fluorine-18; difluoromethylation; difluoromethyl benzothiazolyl-sulfone; radiochemistry

1. Introduction

Fluorine-18 (¹⁸F) is one the most frequently used radioisotopes in positron emission tomography (PET) radiopharmaceuticals for both clinical and preclinical research [1-6]. The radioisotope ¹⁸F has unique advantages in PET radiochemistry in particular its relatively short half-life ($t_{1/2} = 109.8$ min), its favorable positron emission profile (97% β^+ emission), and its relatively low positron energy ($E = 0.635$ keV), yielding high-resolution images [7,8]. The importance of PET for *in vivo* quantification of biochemical and physiological processes, for assessment of disease state, and for drug development demanded novel and efficient approaches for the introduction of ¹⁸F-fluorinated motifs [9-14]. Until the date, the preparation of ¹⁸F-labeled compounds has relied mainly on radiosynthetic methods leading to the formation of [¹⁸F]aryl-F and [¹⁸F]alkyl-F derivatives by classical nucleophilic ¹⁸F-fluorinations. Over the last

years, the strategy of late-stage installation of ^{18}F -fluoroalkyl motifs has been reported by several groups. In fact, the use of adequate ^{18}F -labeled reagents has enabled the application of direct ^{18}F -trifluoromethylation [15-27], ^{18}F -trifluoromethylthiolation [28-30], and ^{18}F -fluoromethylation [31] procedures in late-stage functionalization of organic substrates. Alternatively, the direct introduction of ^{18}F -difluoromethyl (^{18}F -CHF₂) motifs has never been explored despite the potential benefits of these functional groups in the biological and pharmacological activity of pharmaceuticals and agrochemicals [32-37]. Performing a ^{18}F -difluoromethylation procedure requires the prior synthesis of a suitable reagent able to transfer [^{18}F]CHF₂ groups. In non-radioactive chemistry, a plethora of reagents has been employed in the difluoromethylation of organic substrates. Difluoromethyl heteroaryl-sulfones have been implemented as difluoromethylating reagents under photoredox conditions. Visible light photoredox catalysis for the production of CHF₂ radicals has provided a more sustainable alternative to other conventional radical-triggered reactions from the viewpoint of safety, cost, availability, and “green” chemistry [35,36]. The reagent difluoromethyl benzothiazolyl-sulfone (**1**) has deserved a special attention in photoredox difluoromethylation chemistry, mainly because of its ability to be reduced to CHF₂ radicals by oxidative quenching of appropriate photocatalysts in their photocatalyst state (Figure 1). Seminal works reporting the use of the reagent **1** were disclosed by Hu group in 2016 [38]. They described the application of the sulfone **1** in the visible light-mediated difluoromethylation of biphenyl isocyanides in the presence of [Ru(bpy)₃]Cl₂. This reagent was also implemented in the synthesis of difluoromethylated benzoxazines [39], oxazolines [39], and isoquinoline-1,3(2*H*,4*H*)-diones [40], under *fac*-Ir^{III}(ppy)₃ catalysis. Zhu *et al.* studied the potential of the sulfone **1** in the photoinduced difluoromethylation of alkynoates [41], β,γ -unsaturated oximes [42], and *N*-arylacrylamides [43].

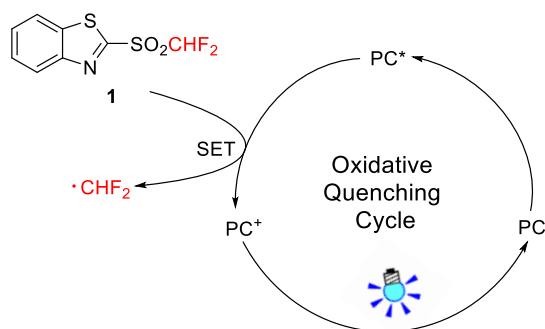


Figure 1. Generation of difluoromethyl radicals ($\cdot\text{CHF}_2$) *via* reduction of the difluoromethyl benzothiazolyl-sulfone (**1**) in the presence of a suitable photocatalyst (PC).

We hypothesized that the radiosynthesis of the [^{18}F]difluoromethyl benzothiazolyl-sulfone (**[^{18}F]**1**) would afford a novel ^{18}F -difluoromethylating reagent enabling the late-stage introduction of the ^{18}F -difluoromethyl groups in suitable substrates. Apart from its expected photoredox properties, we opted to synthesize the**

reagent [^{18}F]**1** because of its great potential for nucleophilic ^{18}F -labeling using a suitable precursor. In addition, an efficient separation and isolation of non-ionic ^{18}F -labeled reagents, such as the compound [^{18}F]**1**, by semipreparative HPLC is more easily achieved in comparison with other ionic reagents (e.g. Baran reagents). In the present work, we thoroughly describe the optimization process in the radiosynthesis of the sulfone [^{18}F]**1**. Preliminary labeling experiments with low level of radioactivity were carried out in order to determine the key parameters that may influence the effectiveness of the radiochemical process. With the optimal conditions in hand, the radiosynthesis of [^{18}F]**1** was then automated in a GE FASTlab synthesizer at high level of starting radioactivity.

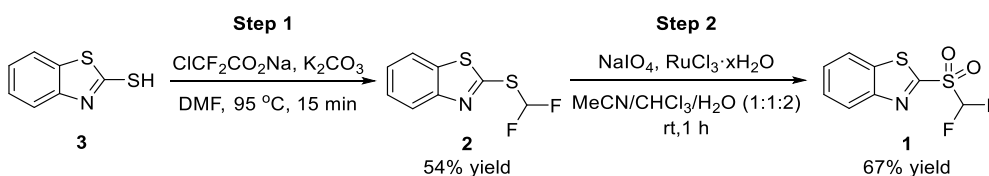
2. Results and Discussion

2.1. Chemistry

2.1.1. Synthesis of the Difluoromethyl Benzothiazolyl-Sulfone (**1**)

The synthesis of the difluoromethyl benzothiazolyl-sulfone (**1**) as non-radioactive standard was initially carried out to corroborate the identity of the ^{18}F -labeled compound [^{18}F]**1**. In order to prepare the compound **1**, we considered a two-step procedure entailing the difluoromethylation of the benzothiazolyl-thiol (**3**) and concomitant oxidation of the difluoromethyl benzothiazolyl-sulfide (**2**).

Based on the methodologies previously reported by Jubault [21] and Akita [44], the difluoromethylation of the thiol **3** using sodium chlorodifluoroacetate ($\text{ClCF}_2\text{CO}_2\text{Na}$) and potassium carbonate (K_2CO_3) furnished the corresponding sulfide **2** in 54% yield (Scheme 1, Step 1). The difluoromethyl heteroaryl-sulfone **1** was successfully accomplished by oxidation of the sulfide **2** using the oxidizing agent sodium (meta)periodate (NaIO_4) and ruthenium (III) chloride hydrate ($\text{RuCl}_3 \cdot x\text{H}_2\text{O}$) in 67% yield (Scheme 1, Step 2).



Scheme 1. Synthesis of the difluoromethyl benzothiazolyl-sulfone (**1**) through difluoromethylation of the benzothiazolyl-thiol (**3**) and subsequent oxidation of the difluoromethyl benzothiazolyl-sulfide (**2**). **Step 1:** thiol **3** (3.0 mmol), sodium chlorodifluoroacetate (6.0 mmol), K_2CO_3 (4.5 mmol), DMF (10 mL), 95 °C, 15 min. **Step 2:** sulfide **2** (1.0 mmol), sodium (meta)periodate (5.0 mmol), ruthenium (III) chloride hydrate (0.05 mmol), MeCN (2 mL), CHCl_3 (2 mL), H_2O (4 mL), rt, 1 h. All reaction yields are of isolated products.

The structure elucidation of the compounds **1** and **2** was established on the basis of high-resolution mass spectrometry (HRMS) and nuclear magnetic resonance (NMR) techniques (Figures S1–S6). Figures 1 and 2 represents the ultra performance

liquid chromatography (UPLC) UV-chromatograms of the compounds **1** and **2**, respectively.

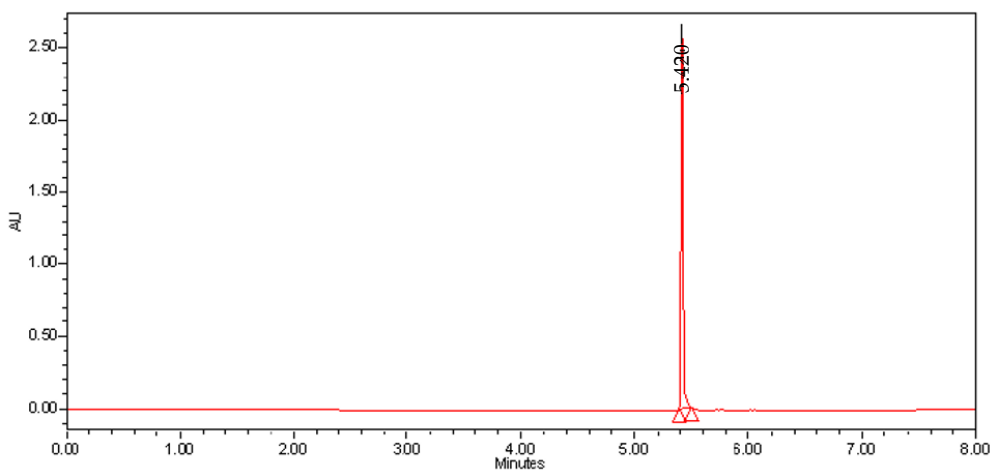


Figure 1. UPLC UV-chromatogram of the authentic reference **2** (wavelength: 254 nm). ACQUITY UPLC[®] CSH C18 column (1.7 μm , 2.1 \times 100 mm); MeCN and HCO₂H/H₂O (0.05%, v/v) in gradient mode at 0.5 mL·min⁻¹ (from 100% HCO₂H/H₂O (0.05%, v/v) to 75% MeCN + 25% HCO₂H/H₂O (0.05%, v/v) in 6 min, and from 75% MeCN + 25% HCO₂H/H₂O (0.05%, v/v) to 100% HCO₂H/H₂O (0.05%, v/v) in 2 min).

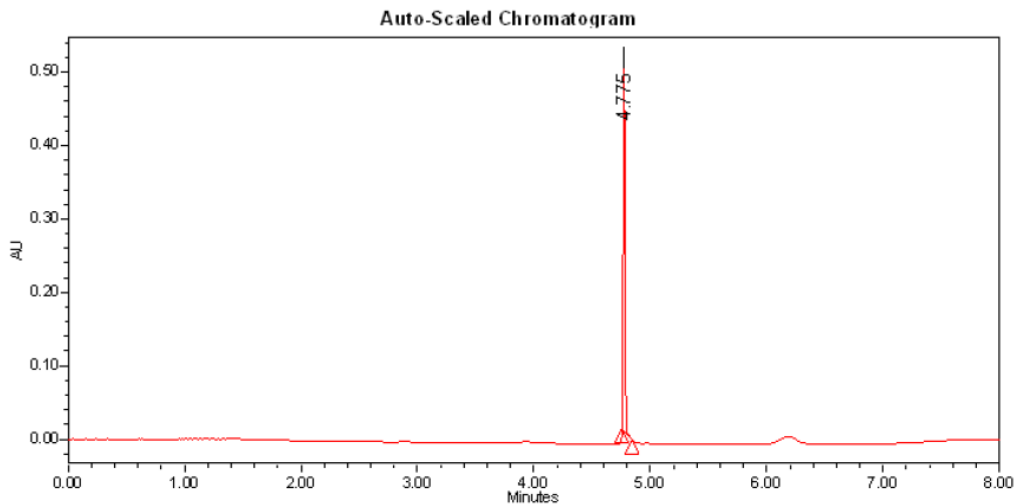


Figure 2. UPLC UV-chromatogram of the authentic reference **1** (wavelength: 254 nm). ACQUITY UPLC[®] CSH C18 column (1.7 μm , 2.1 \times 100 mm); MeCN and HCO₂H/H₂O (0.05%, v/v) in gradient mode at 0.5 mL·min⁻¹ (from 100% HCO₂H/H₂O (0.05%, v/v) to 75% MeCN + 25% HCO₂H/H₂O (0.05%, v/v) in 6 min, and from 75% MeCN + 25% HCO₂H/H₂O (0.05%, v/v) to 100% HCO₂H/H₂O (0.05%, v/v) in 2 min).

2.2. Radiochemistry

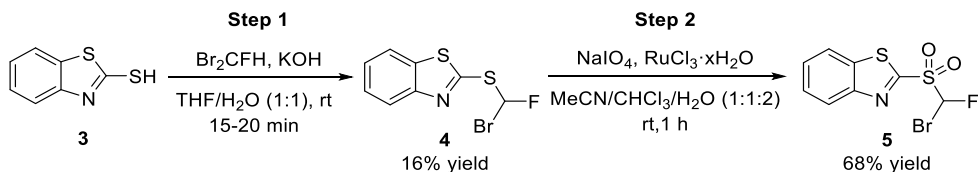
2.2.1. Radiosynthesis of the [¹⁸F]Difluoromethyl Benzothiazolyl-Sulfone ([¹⁸F]1)

Despite the recent advances in the preparation of difluoromethylated compounds, the available methods for the ¹⁸F-labeling of CHF₂ groups still remains scarce. Most of these methods relied on the introduction of the ¹⁸F radioisotope either using electrophilic ¹⁸F-fluorinating agents [e.g. [¹⁸F]Selectfluor *bis*(triflate)] or *via* nucleophilic substitution of aryl-CFXH and alkyl-CFXH precursors (X = a leaving group) with the cyclotron-produced [¹⁸F]fluoride. Since [¹⁸F]fluoride can be produced with high molar activity, the strategy of ¹⁸F-incorporation through nucleophilic substitution was implemented in the radiosynthesis of the sulfone [¹⁸F]1.

2.2.1.1. First Approach: Late stage ¹⁸F-fluorination of the Bromofluoromethyl Benzothiazolyl-Sulfone (5)

We initially hypothesized that the late-stage ¹⁸F-fluorination of the bromofluoromethyl heteroaryl-sulfone (5) would furnish the labeled compound [¹⁸F]3. The bromofluoromethylation of the thiol 3 with dibromofluoromethane (Br₂CFH) gave the bromofluoromethyl benzothiazolyl-sulfide (4) in 16% yield, in the presence of base (Scheme 2, Step 1). Subsequently, the sulfone 5 was prepared from 4 in 68% yield, under the same reaction conditions described for the oxidation of the sulfide 2 (Scheme 2, Step 2).

The structure elucidation of the compounds 4 and 5 was established on the basis of high-resolution mass spectrometry (HRMS) and nuclear magnetic resonance (NMR) techniques (Figures S7–S12).

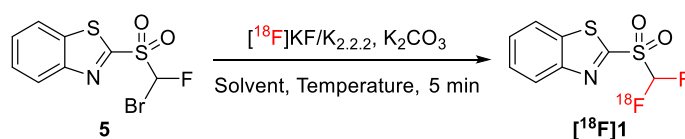


Scheme 2. Synthesis of the bromofluoromethyl benzothiazolyl-sulfone (5) through bromofluoromethylation of the thiol 3 and subsequent oxidation of the bromofluoromethyl benzothiazolyl-sulfide (4). **Step 1:** thiol 1 (3.0 mmol), dibromofluoromethane (4.8 mmol), KOH (30.0 mmol), THF (3 mL), H₂O (3 mL), rt, 15-20 min. **Step 2:** sulfide 4 (1.0 mmol), sodium (meta)periodate (5.0 mmol), ruthenium (III) chloride hydrate (0.05 mmol), MeCN (2 mL), CHCl₃ (2 mL), H₂O (4 mL), rt, 1 h. All reaction yields are of isolated products.

Low starting radioactivity experiments were performed in order to investigate the propensity of the precursor 5 to undergo the expected nucleophilic ¹⁸F-fluorination. The ¹⁸F-labeling reactions were carried out in a commercially available FASTlab™ synthesizer (GE Healthcare) placed in a shielded hotcell. An aliquot of a solution of [¹⁸F]fluoride in [¹⁸O]water ([¹⁸O]H₂O) (150-200 MBq) was passed through a quaternary methyl ammonium (QMA) carbonate cartridge for trapping of [¹⁸F]fluoride. Afterwards, the elution of [¹⁸F]fluoride with K_{2.2.2}/K₂CO₃-based eluent

and azeotropic drying in a cyclic olefin copolymer (COC) reactor provided the dry [¹⁸F]fluoride readily available for the nucleophilic ¹⁸F-fluorination. Precursor **5** solubilized in different solvents was added to the “naked” [¹⁸F]fluoride and the ¹⁸F-labeling reactions were conducted at different temperatures for 5 min (Table 1). The crude reaction mixture was pre-purified using a Sep-Pak® C18 Plus Short cartridge to remove the unreacted [¹⁸F]fluoride and other polar impurities (e.g. K₂CO₃ and K_{2.2.2}). The trapped crude product was manually eluted with MeCN and the solution was analyzed by radio-thin-layer chromatography (radio-TLC) and radio-UPLC. Our results showed that the late-stage ¹⁸F-fluorination of the precursor **5** afforded an unknown ¹⁸F-labeled compound (Figure 3) with a distinct LC retention time of the non-radioactive reference standard **1** (Figure 2), regardless the ¹⁸F-labeling temperature (85 °C or 120 °C) and the solvent (MeCN or DMF).

Table 1. ¹⁸F-Labeling of the bromofluoromethyl benzothiazolyl-sulfone (**5**)^(a)



Entry	Solvent	Temperature (°C)	RCY (%) ^(b)
1	MeCN	85	0 (n = 2)
2	MeCN	120	0 (n = 2)
3	DMF	120	0 (n = 2)

^(a) Standard conditions: **5** (0.02 mmol), [¹⁸F]KF (150–200 MBq), K₂CO₃ (0.02 mmol), K_{2.2.2} (0.02 mmol), solvent (1 mL), temperature (°C), 5 min. ^(b) All RCYs were determined based on the activity of cartridge-purified [¹⁸F]**1**, their radio-TLC and their radio-UPLC purities, and their starting radioactivity. All RCYs were decay-corrected at the start of the synthesis (SOS).

We hypothesized that the unknown ¹⁸F-labeled compound was generated from nucleophilic ¹⁸F-fluorination in the heteroaryl moiety of the precursor **5** (pathway b, Scheme 3). This heteroaromatic ¹⁸F-labeling process was corroborated by the similarity of LC retention times between the [¹⁸F]2-fluorobenzo[*d*]thiazole ([¹⁸F]**5a**) and the respective non-radioactive product **5a** (Figure 4). The cartridge-purified [¹⁸F]**5a** was afforded in 21.7 ± 1.5 RCY [decay corrected at the start of the synthesis (SOS)]. Overall, this one-step synthetic strategy revealed to be unsuccessful in the radiosynthesis of the compound [¹⁸F]**1**.

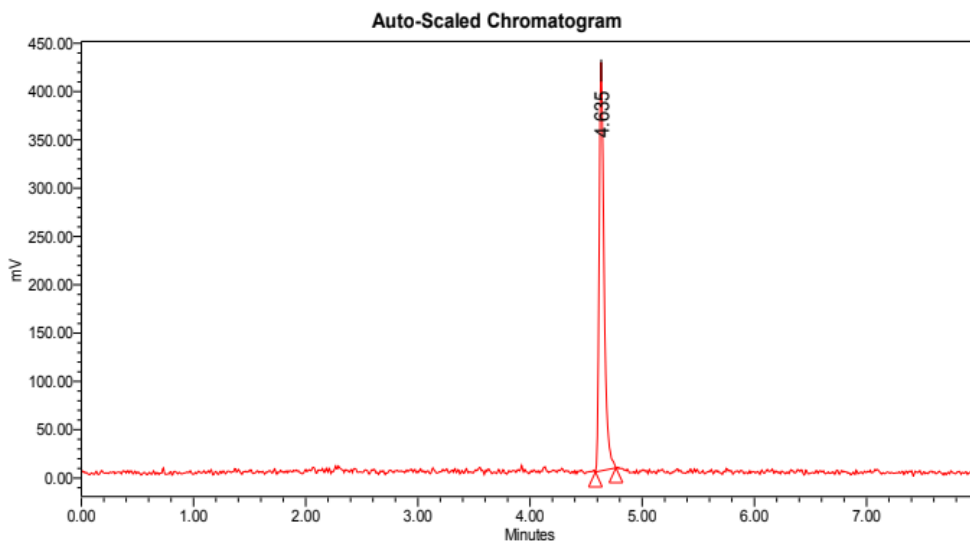
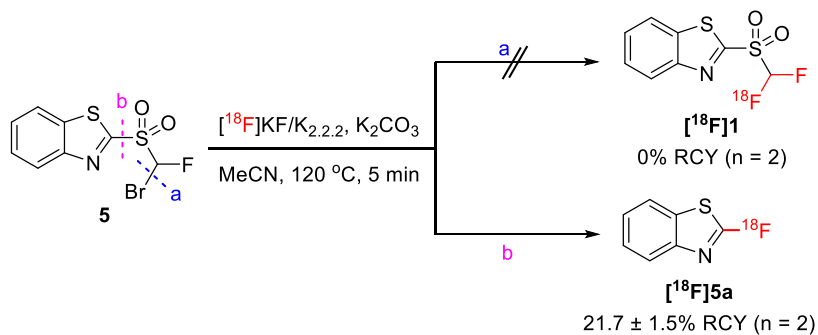


Figure 3. UPLC radio-chromatogram of the crude product resulting from the ^{18}F -labeling of the precursor **5**. ACQUITY UPLC[®] CSH C18 column (1.7 μm , 2.1 \times 100 mm); MeCN and $\text{HCO}_2\text{H}/\text{H}_2\text{O}$ (0.05%, v/v) in gradient mode at 0.5 $\text{mL}\cdot\text{min}^{-1}$ (from 100% $\text{HCO}_2\text{H}/\text{H}_2\text{O}$ (0.05%, v/v) to 75% MeCN + 25% $\text{HCO}_2\text{H}/\text{H}_2\text{O}$ (0.05%, v/v) in 6 min, and from 75% MeCN + 25% $\text{HCO}_2\text{H}/\text{H}_2\text{O}$ (0.05%, v/v) to 100% $\text{HCO}_2\text{H}/\text{H}_2\text{O}$ (0.05%, v/v) in 2 min).



Scheme 3. Plausible pathways of nucleophilic ^{18}F -fluorination of the precursor **5**: aliphatic ^{18}F -fluorination (pathway a, not observed) and heteroaromatic ^{18}F -labeling (pathway b).

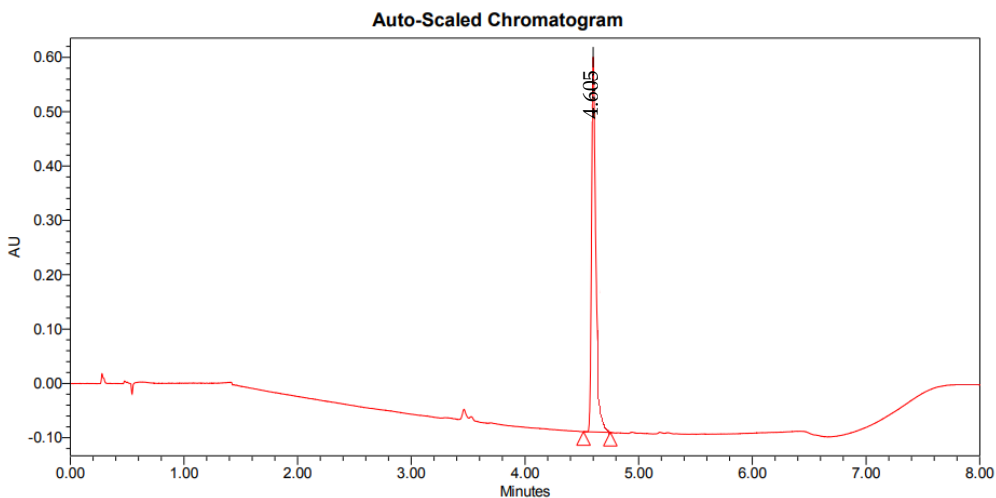


Figure 4. UPLC UV-chromatogram of the 2-fluorobenzo[*d*]thiazole (**5a**) (wavelength: 254 nm). ACQUITY UPLC® CSH C18 column (1.7 μm , 2.1 \times 100 mm); MeCN and HCO₂H/H₂O (0.05%, v/v) in gradient mode at 0.5 mL·min⁻¹ (from 100% HCO₂H/H₂O (0.05%, v/v) to 75% MeCN + 25% HCO₂H/H₂O (0.05%, v/v) in 6 min, and from 75% MeCN + 25% HCO₂H/H₂O (0.05%, v/v) to 100% HCO₂H/H₂O (0.05%, v/v) in 2 min).

2.2.1.2. Second Approach: ¹⁸F-Labeling of the Bromofluoromethyl Benzothiazolyl-Sulfide (**4**) and Oxidation of [¹⁸F]Difluoromethyl Benzothiazolyl-Sulfide ([¹⁸F]**2**)

Next, we investigated an alternative approach for the radiosynthesis of [¹⁸F]**1**. We considered a two-step methodology involving an initial ¹⁸F-labeling of a CFHX-containing benzothiazolyl sulfide (X = a leaving group) and consecutive oxidation of the [¹⁸F]difluoromethyl benzothiazolyl-sulfide ([¹⁸F]**2**).

The bromofluoromethyl derivative **4** was chosen as precursor for the ¹⁸F-labeling reaction. Using the GE FASTlab™ module, initial experiments were conducted between the precursor **4** and [¹⁸F]potassium fluoride ([¹⁸F]KF), in the presence of K₂CO₃ and Kryptofix® 222 (K_{2.2.2}), to uncover the most suitable solvent for the ¹⁸F-fluorination process. Our results showed that the precursor **4** was unreactive toward the ¹⁸F-labeling reaction when either DMSO or DCM were used as solvents (Table 2, Entries 1-2). From a survey of polar aprotic solvents (THF, DMA, NMP, DMF, nitrobenzene, propylene carbonate, DCE, acetone, and MeCN), MeCN revealed to be most efficient solvent for the ¹⁸F-labeling of the precursor **4**, furnishing the cartridge-purified [¹⁸F]**2** in 12.7 \pm 0.2% RCY (decay corrected at the SOS) (Table 2, Entries 3-11).

The UPLC retention time of the labeled compound [¹⁸F]**2** (Figure 5) was in agreement with those of the respective non-radioactive authentic reference **2** (Figure 1).

Table 2. Screening of solvents used in ^{18}F -labeling of the bromofluoromethyl benzothiazolylsulfide (**4**)^(a)

Reaction scheme: **4** $\xrightarrow[\text{Solvent, 85 } ^\circ\text{C, 5 min}]{[^{18}\text{F}]\text{KF}/\text{K}_{2.2.2}, \text{K}_2\text{CO}_3}$ **[^{18}F]**2****

Entry	Solvent	RCY (%) ^(b)
1	DMSO	0 (n = 2)
2	DCM	0 (n = 2)
3	THF	3.7 ± 1.5 (n=3)
4	DMA	4.5 ± 0.2 (n=3)
5	NMP	4.5 ± 0.4 (n=3)
6	DMF	5.3 ± 0.3 (n=3)
7	Nitrobenzene	5.6 ± 1.5 (n=3)
8	propylene carbonate	6.3 ± 0.4 (n=3)
9	DCE	7.2 ± 0.5 (n=3)
10	Acetone	9.5 ± 0.3 (n=3)
11	MeCN	12.7 ± 0.2 (n=3)

^(a) Standard conditions: **4** (0.02 mmol), ^{18}F]KF (150–200 MBq), K_2CO_3 (0.02 mmol), $\text{K}_{2.2.2}$ (0.02 mmol), solvent (1 mL), 85 °C, 5 min. ^(b) All RCYs were determined based on the activity of cartridge-purified ^{18}F]2, their radio-TLC and their radio-UPLC purities, and their starting radioactivity. All RCYs were decay-corrected at the SOS.

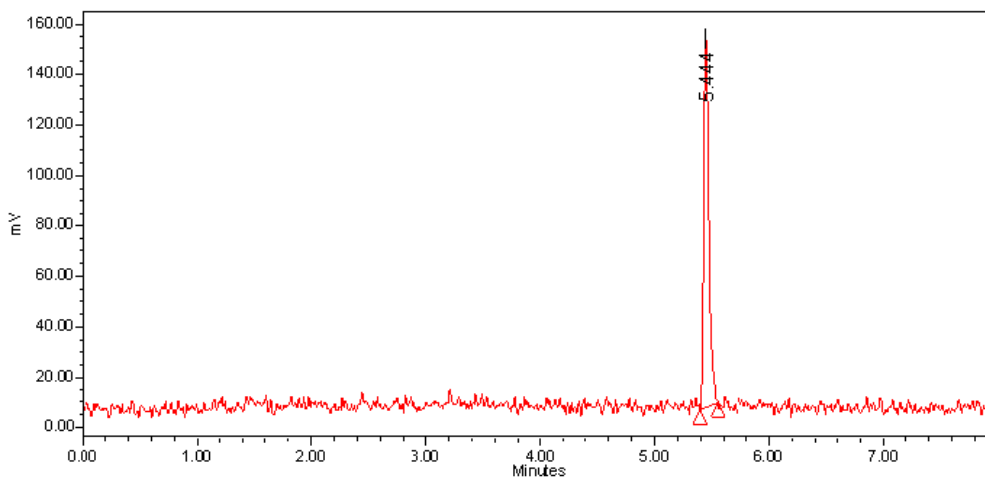
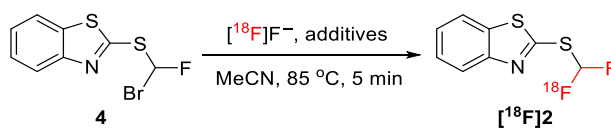


Figure 5. UPLC radio-chromatogram of the crude product ^{18}F]2. ACQUITY UPLC[®] CSH C18 column (1.7 μm , 2.1 \times 100 mm); MeCN and $\text{HCO}_2\text{H}/\text{H}_2\text{O}$ (0.05%, v/v) in gradient mode at 0.5 $\text{mL}\cdot\text{min}^{-1}$ (from 100% $\text{HCO}_2\text{H}/\text{H}_2\text{O}$ (0.05%, v/v) to 75% MeCN + 25% $\text{HCO}_2\text{H}/\text{H}_2\text{O}$ (0.05%, v/v) in 6 min, and from 75% MeCN + 25% $\text{HCO}_2\text{H}/\text{H}_2\text{O}$ (0.05%, v/v) to 100% $\text{HCO}_2\text{H}/\text{H}_2\text{O}$ (0.05%, v/v) in 2 min).

Afterwards, a screening of additives was carried out in order to enhance the RCY of the radiosynthesis of ^{18}F]2. The analysis of the Table 3 demonstrated that the

efficiency of the ^{18}F -labeling is influenced by the additives used in the elution of ^{18}F fluoride. In combination with $\text{K}_{2.2.2}$, the selection of base K_2CO_3 provided the cartridge-purified ^{18}F **2** in higher RCY (Table 3, Entry 1), in comparison with other bases such as sodium sulfite (Na_2SO_3), potassium acetate ($\text{CH}_3\text{CO}_2\text{K}$), and sodium bicarbonate (NaHCO_3) (Table 3, Entries 2-4). Other additives, such as tetrabutylammonium hydrogensulfate (TBAHS), tetrabutylammonium bromide (TBAB), tetraethylammonium bicarbonate (TEAB), and tetrabutylammonium cyanide (TBAC), were unable to improve the reactivity of the precursor **4** for the nucleophilic radiofluorination (Table 3, Entries 5-8).

Table 3. Screening of additives used in ^{18}F -labeling of the bromofluoromethyl benzothiazolylsulfide (**4**)^(a)



Entry	Additives (μmol)	RCY (%) ^(b)
1	K_2CO_3 (20), $\text{K}_{2.2.2}$ (20)	12.7 ± 0.2 (n=3)
2	Na_2SO_3 (20), $\text{K}_{2.2.2}$ (20)	6.2 ± 2.2 (n=3)
3	$\text{CH}_3\text{CO}_2\text{K}$ (20), $\text{K}_{2.2.2}$ (20)	4.6 ± 1.1 (n=3)
4	NaHCO_3 (20), $\text{K}_{2.2.2}$ (20)	3.6 ± 1.6 (n=3)
5	TBAHS (20)	7.3 ± 2.1 (n=3)
6	TBAB (20)	7.0 ± 0.9 (n=3)
7	TEAB (20)	6.7 ± 2.5 (n=3)
8	TBAC (20)	4.8 ± 1.2 (n=3)

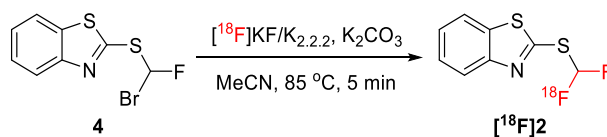
^(a) Standard conditions: **4** (0.02 mmol), ^{18}F F^- (150–200 MBq), additives (mmol), MeCN (1 mL), 85 $^\circ\text{C}$, 5 min. ^(b) All RCYs were determined based on the activity of cartridge-purified ^{18}F **2**, their radio-TLC and their radio-UPLC purities, and their starting radioactivity. All RCYs were decay-corrected at the SOS.

When the amount of K_2CO_3 was decreased from 0.02 mmol to 0.01 mmol, the cartridge-purified ^{18}F **2** was synthesized in $13.4 \pm 1.7\%$ RCY (decay corrected at the SOS) (Table 4, Entries 1-2). The reduction of the amount of K_2CO_3 in the QMA eluent was not beneficial (Table 4, Entry 3). Furthermore, no ^{18}F -labeling product formation was observed either the absence of K_2CO_3 (Table 4, Entry 4) or $\text{K}_{2.2.2}$ (Table 4, Entry 5). The latter results emphasized the importance of the base K_2CO_3 and the phase-transfer catalyst $\text{K}_{2.2.2}$ in the cartridge elution and in the reactivity of the ^{18}F fluoride in the ^{18}F -labeling of the precursor **4**.

The increase of the temperature from 85 $^\circ\text{C}$ to 120 $^\circ\text{C}$ resulting in a negligible improvement of the RCY of the ^{18}F -labeling reaction (Table 5, Entries 1-2). By raising the amount of the precursor **4** from 0.02 mmol to 0.04 mmol, the cartridge-purified ^{18}F **2** was obtained in $15.2 \pm 0.3\%$ RCY (decay corrected at the SOS) (Table 5, Entry 3). Lower RCYs were afforded either by enhancing the amount of precursor **4** to 0.06

mmol (Table 5, Entry 4) or by extending the ^{18}F -labeling reaction time from 5 min to 10 min (Table 5, Entry 5). Overall, the optimized conditions for the nucleophilic ^{18}F -fluorination with ^{18}F fluoride (150-200 MBq) were determined as: precursor (0.04 mmol), in the presence of K_2CO_3 (0.01 mmol), $\text{K}_{2.2.2}$ (0.02 mmol), with MeCN (1 mL) as solvent at 120 °C for 5 min.

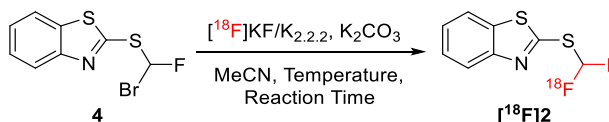
Table 4. Screening of the amount of additives used in ^{18}F -labeling of the bromofluoromethyl benzothiazolyl-sulfide (**4**)^(a)



Entry	Additives (μmol)	RCY (%) ^(b)
1	K_2CO_3 (20), $\text{K}_{2.2.2}$ (20)	12.7 ± 0.2 (n=3)
2	K_2CO_3 (10), $\text{K}_{2.2.2}$ (20)	13.4 ± 1.7 (n=3)
3	K_2CO_3 (5), $\text{K}_{2.2.2}$ (20)	9.7 ± 2.3 (n=3)
4	K_2CO_3 (0), $\text{K}_{2.2.2}$ (20)	0 (n=2)
5	K_2CO_3 (10), $\text{K}_{2.2.2}$ (0)	0 (n=2)

^(a) Standard conditions: **4** (0.02 mmol), ^{18}F KF (150–200 MBq), K_2CO_3 (mmol), $\text{K}_{2.2.2}$ (mmol), MeCN (1 mL), 85 °C, 5 min. ^(b) All RCYs were determined based on the activity of cartridge-purified ^{18}F **2**, their radio-TLC and their radio-UPLC purities, and their starting radioactivity. All RCYs were decay-corrected at the SOS.

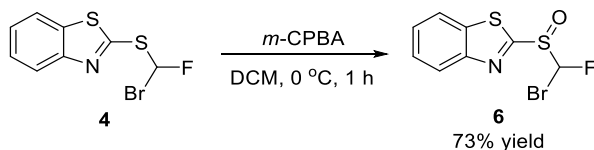
Table 5. Screening of the temperature, amount of precursor, and the reaction time for ^{18}F -labeling of the bromofluoromethyl benzothiazolyl-sulfide (**4**)^(a)



Entry	4 (mmol)	Temperature (°C)	Reaction Time (min)	RCY (%) ^(b)
1	0.02	85	5	13.4 ± 1.7 (n=3)
2	0.02	120	5	14.6 ± 0.8 (n=3)
3	0.04	120	5	15.2 ± 0.3 (n=3)
4	0.06	120	5	12.0 ± 0.7 (n=3)
5	0.04	120	10	12.9 ± 1.3 (n=3)

^(a) Standard conditions: **4** (mmol), ^{18}F KF (150–200 MBq), K_2CO_3 (0.01 mmol), $\text{K}_{2.2.2}$ (0.02 mmol), MeCN (1 mL), temperature (°C), reaction time (min). ^(b) All RCYs were determined based on the activity of cartridge-purified ^{18}F **2**, their radio-TLC and their radio-UPLC purities, and their starting radioactivity. All RCYs were decay-corrected at the SOS.

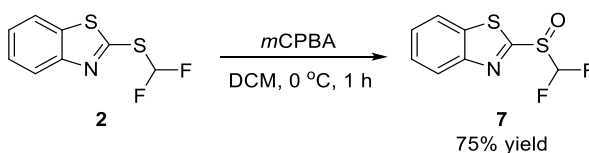
Next, we intended to explore an alternative precursor for the nucleophilic ^{18}F -fluorination, the bromofluoromethyl benzothiazolyl-sulfoxide (**6**). The oxidation of the sulfide **4** with *meta*-chloroperoxybenzoic acid (*m*CPBA) afforded the sulfoxide **6** in 73% reaction yield (Scheme 4).



Scheme 4. Synthesis of the two isomers of bromofluoromethyl benzothiazolyl-sulfoxide (**6**). Standard conditions: **4** (1.0 mmol), *meta*-chloroperoxybenzoic acid (1.1 mmol), DCM (4 mL), 0 °C, 1 h. All reaction yields of the isolated products.

In order to probe the tendency of **6** to undergo the expected nucleophilic ^{18}F -fluorination, the difluoromethyl benzothiazolyl-sulfoxide (**7**) was first synthesized as non-radioactive standard. Using the reaction conditions depicted above, the oxidation of the sulfide **2** afforded the sulfoxide **7** in 75% yield (Scheme 5).

The structure elucidation of the compounds **6** and **7** was established on the basis of high-resolution mass spectrometry (HRMS) and nuclear magnetic resonance (NMR) techniques (Figures S13–S18). Figure 6 represents UPLC UV-chromatogram of the compound **7**.



Scheme 5. Synthesis of the difluoromethyl benzothiazolyl-sulfoxide (**7**). Standard conditions: **2** (1.0 mmol), *meta*-chloroperoxybenzoic acid (1.1 mmol), DCM (4 mL), 0 °C, 1 h. All reaction yields are of isolated products.

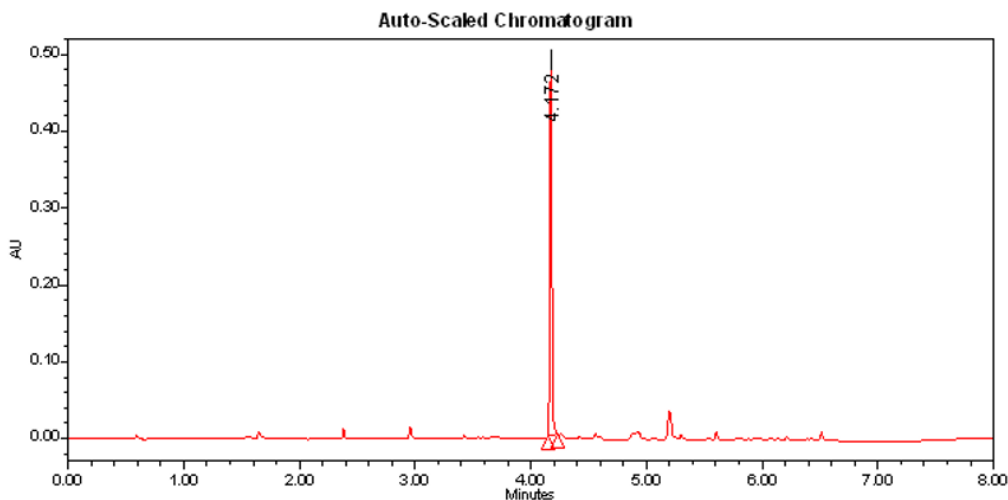
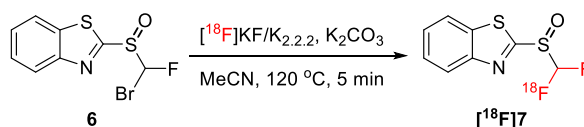


Figure 6. UPLC UV-chromatogram of the authentic reference **7** (wavelength: 254 nm). ACQUITY UPLC[®] CSH C18 column (1.7 μm , 2.1 \times 100 mm); MeCN and HCO₂H/H₂O (0.05%, v/v) in gradient mode at 0.5 mL·min⁻¹ (from 100% HCO₂H/H₂O (0.05%, v/v) to 75% MeCN + 25% HCO₂H/H₂O (0.05%, v/v) in 6 min, and from 75% MeCN + 25% HCO₂H/H₂O (0.05%, v/v) to 100% HCO₂H/H₂O (0.05%, v/v) in 2 min).

The ^{18}F -labeling of the precursor **6** in MeCN at 120 °C resulted in the formation of the cartridge-purified [^{18}F]difluoromethyl benzothiazolyl-sulfide ([^{18}F]**7**) in $3.3 \pm 0.3\%$ RCY (decay corrected at the SOS) (Table 6). The UPLC analysis of the crude product, after cartridge purification, showed the presence of a radioactive peak corresponding to [^{18}F]**7** along with an additional peak of an unknown ^{18}F -labeled compound (Figure 7). We presumed that the second peak corresponded to the by-product [^{18}F]**5a** owing the similarity of LC retention times between the ^{18}F -labeled compound [^{18}F]**5a** and the respective non-radioactive compound **5a** (Figure 4). Under the conditions, the heteroaromatic ^{18}F -labeling of precursor **6** furnished the cartridge-purified [^{18}F]**5a** was furnished in $12.3 \pm 1.3\%$ RCY (Scheme 6; decay corrected at the SOS). As the ^{18}F -labeling of the precursor **6** generated the sulfoxide [^{18}F]**7** in lower RCY, the precursor **4** was selected for the radiosynthesis of the sulfone [^{18}F]**1**.

Table 6. ^{18}F -Labeling of the bromofluoromethyl benzothiazolyl-sulfoxide (**6**)



Entry	Precursor (mmol)	RCY (%) ^(b)
1	6 (0.04)	3.3 ± 0.3 (n=2)

^(a) Standard conditions: NaIO_4 , $\text{RuCl}_3 \cdot x\text{H}_2\text{O}$, H_2O (1 mL), rt, 5 min. ^(b) All RCYs were determined based on the activity of cartridge-purified [^{18}F]**7**, their radio-TLC and their radio-UPLC purities, and their starting radioactivity. All RCYs were decay-corrected at the SOS.

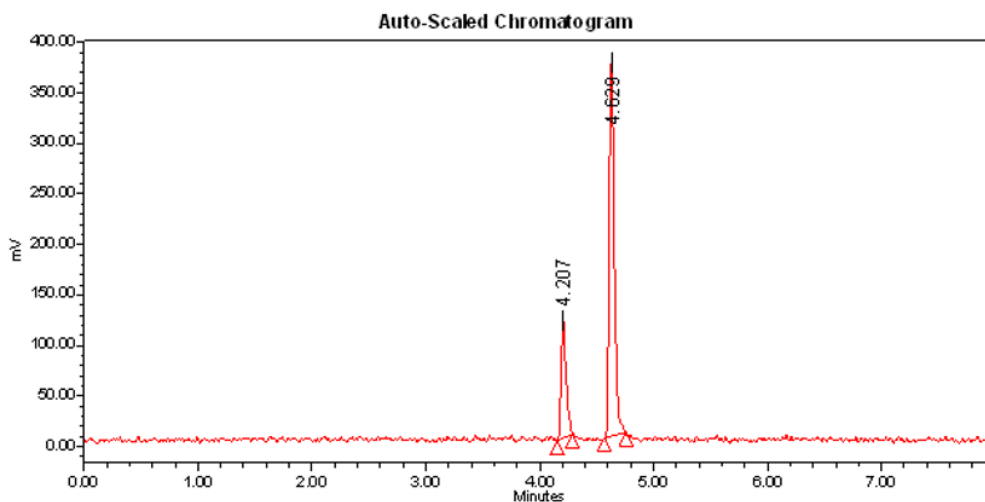
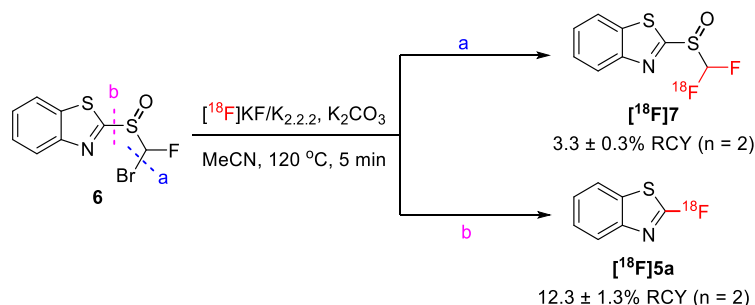


Figure 7. UPLC radio-chromatogram of the crude product [^{18}F]**7**. ACQUITY UPLC[®] CSH C18 column ($1.7 \mu\text{m}$, $2.1 \times 100 \text{ mm}$); MeCN and $\text{HCO}_2\text{H}/\text{H}_2\text{O}$ (0.05%, v/v) in gradient mode at $0.5 \text{ mL}\cdot\text{min}^{-1}$ (from 100% $\text{HCO}_2\text{H}/\text{H}_2\text{O}$ (0.05%, v/v) to 75% MeCN + 25% $\text{HCO}_2\text{H}/\text{H}_2\text{O}$ (0.05%, v/v) in 6 min, and from 75% MeCN + 25% $\text{HCO}_2\text{H}/\text{H}_2\text{O}$ (0.05%, v/v) to 100% $\text{HCO}_2\text{H}/\text{H}_2\text{O}$ (0.05%, v/v) in 2 min).



Scheme 6. Plausible pathways of nucleophilic ^{18}F -fluorination of the precursor **6**: aliphatic ^{18}F -fluorination (pathway a) and heteroaromatic ^{18}F -labeling (pathway b).

With the optimized labeling conditions for the precursor **4** in hand, we then examined the reaction of oxidation of the sulfide $[^{18}\text{F}]\text{2}$. Inspired by the oxidation of the sulfide **2** described in Scheme 1, a similar methodology was employed in the radiosynthesis of the sulfone $[^{18}\text{F}]\text{1}$. No product formation was verified in the absence of $\text{RuCl}_3 \cdot x\text{H}_2\text{O}$ (Table 7, Entry 1). This result demonstrated the importance of the pre-catalyst in the oxidation process. Gratifyingly, when the reaction was conducted in presence of NaIO_4 (0.24 mmol) and $\text{RuCl}_3 \cdot x\text{H}_2\text{O}$ (0.002 mmol) at room temperature for 5 min, the cartridge-purified $[^{18}\text{F}]\text{1}$ was afforded in $48.0 \pm 2.7\%$ RCY (decay corrected at the SOS) (Table 7, Entry 2). However, no complete conversion of the sulfide $[^{18}\text{F}]\text{2}$ was observed. Further optimization studies were conducted to achieve the complete oxidation of $[^{18}\text{F}]\text{2}$. By raising the amount of $\text{RuCl}_3 \cdot x\text{H}_2\text{O}$ to 0.008 mmol, the sulfide $[^{18}\text{F}]\text{2}$ was fully consumed and the labeled compound $[^{18}\text{F}]\text{1}$ was isolated in $82.9 \pm 7.9\%$ RCY (decay-corrected at the SOS) (Table 7, Entry 3). The reduction of the amount of NaIO_4 from 0.24 mmol to 0.06 mmol was detrimental to the oxidation efficiency (Table 6, Entry 4). Starting from 150–200 MBq of $[^{18}\text{F}]\text{fluoride}$, a two-step methodology entailing the ^{18}F -labeling and the oxidation steps generated sulfone $[^{18}\text{F}]\text{1}$ in $12.6 \pm 1.2\%$ RCY (decay-corrected at the SOS) (Table 7, Entry 3), after cartridge purification.

Table 7. Screening of the amount of NaIO_4 and $\text{RuCl}_3 \cdot x\text{H}_2\text{O}$ for oxidation of the $[^{18}\text{F}]\text{2}$

Entry	NaIO_4 (mmol)	$\text{RuCl}_3 \cdot x\text{H}_2\text{O}$ (mmol)	Conversion (%)	RCY (%) ^(b)	RCY (%) (2 steps)
1	0.24	0	0	0 ($n=2$)	-
2	0.24	0.002	61	48.0 ± 2.7 ($n=3$)	-
3	0.24	0.008	100	82.9 ± 7.9 ($n=3$)	12.6 ± 1.2 ($n=3$)
4	0.06	0.008	48	39.5 ± 8.0 ($n=3$)	-

^(a) Standard conditions: NaIO_4 (mmol), $\text{RuCl}_3 \cdot x\text{H}_2\text{O}$ (mmol), H_2O (4 mL), rt, 5 min. ^(b) All RCYs were determined based on the activity of cartridge-purified $[^{18}\text{F}]\text{1}$, their radio-TLC and their radio-UPLC purities, and their starting radioactivity. All RCYs were decay-corrected at the SOS.

The UPLC retention time of the labeled compound [^{18}F]**1** (Figure 8) was in agreement with those of the respective non-radioactive authentic reference **1** (Figure 2).

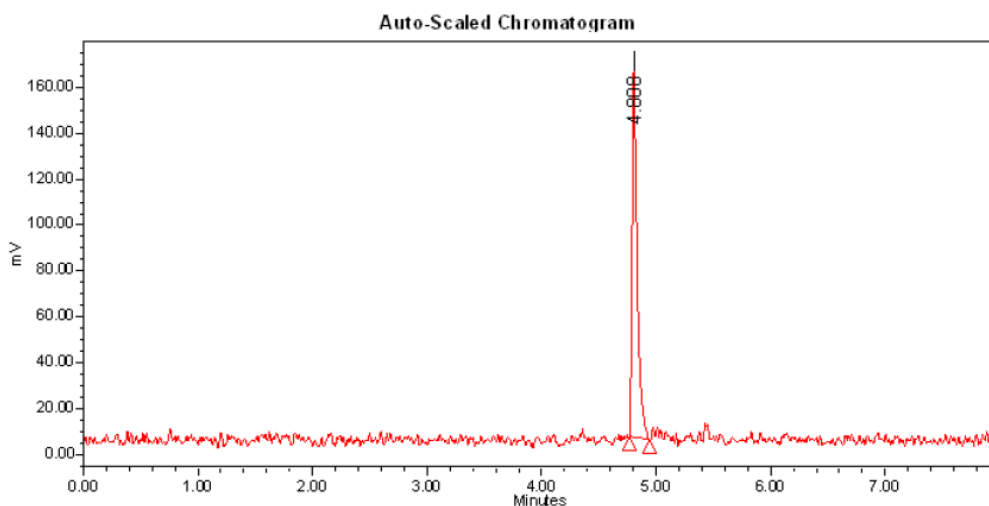


Figure 8. UPLC radio-chromatogram of the crude product [^{18}F]**1**. ACQUITY UPLC[®] CSH C18 column (1.7 μm , 2.1 \times 100 mm); MeCN and HCO₂H/H₂O (0.05%, v/v) in gradient mode at 0.5 mL \cdot min⁻¹ (from 100% HCO₂H/H₂O (0.05%, v/v) to 75% MeCN + 25% HCO₂H/H₂O (0.05%, v/v) in 6 min, and from 75% MeCN + 25% HCO₂H/H₂O (0.05%, v/v) to 100% HCO₂H/H₂O (0.05%, v/v) in 2 min).

2.2.2. Automated radiosynthesis of the sulfone [^{18}F]**1**

The automated sequence for the radiosynthesis of the sulfone [^{18}F]**1** required the following steps: (1) machine and cassette tests (presynthesis, 7 min); (2) [^{18}F]fluoride recovery, trapping, elution, and azeotropic drying (12 min); (3) transfer of the precursor **4** in MeCN to the reactor and ^{18}F -labeling (9 min); (4) dilution of the crude product [^{18}F]**2** with water, and trapping on a ^tC18 Plus Short cartridge (2 min); (5) transfer of the NaIO₄ and RuCl₃ \cdot x H₂O and oxidation on a ^tC18 cartridge at room temperature (6 min); (6) elution of the crude [^{18}F]**1** with MeCN to the reactor, dilution with water, and injection on the semi-preparative HPLC loop (4 min); (7) HPLC purification and collection of the purified [^{18}F]**1** (19 min); (8) dilution and trapping of the ^{18}F -labeled compounds on a ^tC18 Plus Short cartridge followed by elution with anhydrous dimethyl sulfoxide (DMSO) (14 min). A more detailed description of the sequence of events entailing the multi-step radiosynthesis of the [^{18}F]**1** is provided in the *Materials and Methods* section.

Figure 9 depicts the general layout of the GE FASTlab[™] cassette implemented in the radiosynthesis of the labeled compound [^{18}F]**1**. Extensive description of the cassette and of the materials used throughout the synthesis of [^{18}F]**1** may be consulted in Table 8.

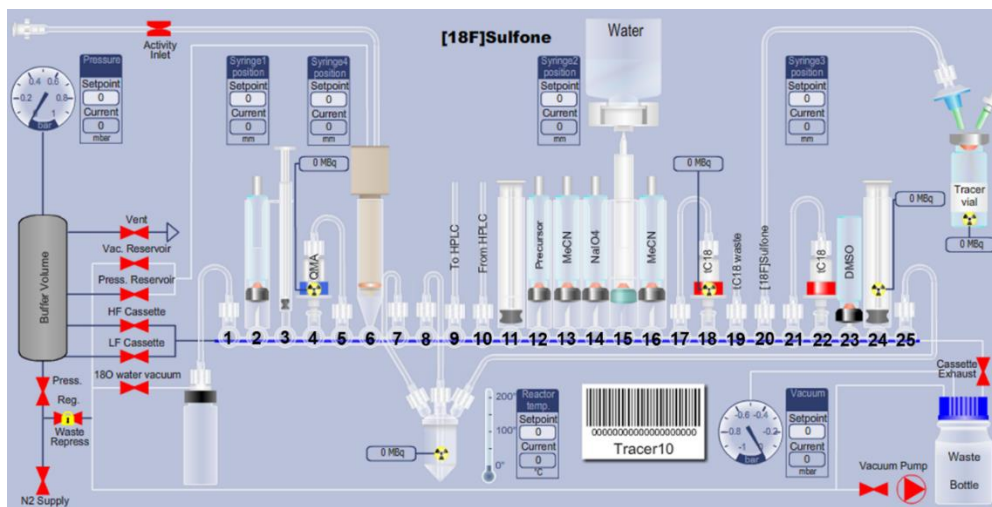


Figure 9. Layout of the GE FASTlab™ cassette for the radiosynthesis of the labeled compound [18F]1.

Table 8. Location of the reagents, solvents, and materials in the manifold of the GE FASTlab™ cassette

Manifold position	Reagents, solvents, and materials	Details
V1	Silicone tubing connected to [18O]H ₂ O recovery vial	14 cm
V2	K _{2.2.2} [®] (7.5 mg) in MeCN (600 μL) and K ₂ CO ₃ (1.4 mg) in H ₂ O (150 μL)	11 mm vial (volume = 750 μL)
V3	Syringe S1 (part of the manifold)	Maximum volume = 1 mL
V4	Sep-Pak [®] Accell™ Plus QMA Carbonate Plus Light Cartridge with silicone tubing at position V5	46 mg (40 μm) (Waters)
V5	Silicone tubing connected to the Sep-Pak [®] Accell™ Plus QMA Carbonate Plus Light Cartridge at position V4	14 cm
V6	[18O]H ₂ O/[18F]F ⁻ inlet conical reservoir (part of the manifold)	Maximum volume = 5 mL
V7	Silicone tubing connected to the cyclic olefin copolymer (COC) reactor (left-hand side)	14 cm
V8	Silicone tubing connected to the COC reactor (central port)	14 cm
V9	Outlet "to HPLC loop" <i>via</i> silicone tubing connected to a Sterifix [®] Paed filter (B. Braun)	30 cm

V10	Inlet “from HPLC loop” enabling the recovery of the purified labeled compound [¹⁸ F]1 after semi-preparative HPLC purification	30 cm
V11	Syringe S2 (part of the manifold)	Maximum volume = 6 mL
V12	Precursor 4 (11.1 mg, 40 μmol) solubilized in MeCN	11 mm vial (volume = 1 mL)
V13	MeCN	13 mm vial (volume = 4 mL)
V14	NaIO ₄ (51.3 mg) and RuCl ₃ ·xH ₂ O (1.7 mg) solubilized in H ₂ O	13 mm vial (volume = 4 mL)
V15	Water bag spike	Volume = 100 mL
V16	MeCN	13 mm vial (volume = 4 mL)
V17	Silicone tubing connected to the Sep-Pak® C18 Plus Short Cartridge at position V18	14 cm
V18	Sep-Pak® C18 Plus Short Cartridge with silicone tubing at position V17	400 mg (37-55 μm)
V19	Outlet waste bottle	21 cm
V20	Final outlet vial for collection of the labeled compound [¹⁸ F]1 after semi-preparative HPLC purification and reformulation	50 cm
V21	Silicone tubing connected to the Sep-Pak® C18 Plus Short Cartridge at position V22	14 cm
V22	Sep-Pak® C18 Plus Short Cartridge with silicone tubing at position V21	400 mg (37-55 μm)
V23	Anhydrous DMSO	13 mm vial (volume = 4 mL)
V24	Syringe S3 (part of the manifold)	Maximum volume = 6 mL
V25	Silicone tubing connected to the COC reactor (right-hand side) and vent valve for the reactor	42 cm

A reverse-phase HPLC purification procedure was implemented after the two-step radiosynthesis of the cartridge-purified sulfone [¹⁸F]1 on the GE FASTlab™ module. The selection of mobile phase of MeCN/H₂O (40/60, v/v) in isocratic mode revealed to be appropriate for the separation between the ¹⁸F-labelled compound [¹⁸F]1 and the respective UV- and radio-HPLC impurities. One of the main impurities detected in UV-HPLC profile corresponded to the product derived from the oxidation of the unreacted precursor **4** (bromofluoromethyl benzothiazolyl-sulfone, **5**) (Figure 10A). The radioactive peak corresponding to the compound [¹⁸F]1 was collected after 16 min to vial containing 30 mL of water (Figure 10B). In the reformulation step, the prior dilution of the purified [¹⁸F]1 in water was critical to assure an optimum

trapping of the labeled compound in a preconditioned Sep-Pak® Plus Short cartridge. The trapped [¹⁸F]**1** was then eluted with anhydrous DMSO using reverse flow and recovered in a 4 mL-sealed vial.

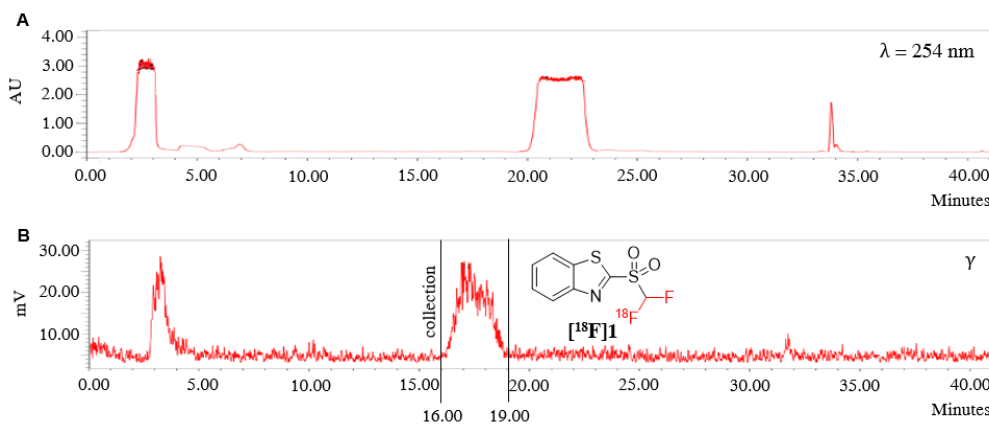


Figure 10. (A) Ultraviolet-high performance liquid chromatography (UV-HPLC) purification profile of the crude [¹⁸F]**1** (wavelength: 254 nm). (B) Radio-HPLC purification profile of the crude [¹⁸F]**1**. Note: the appearance of broad flat-topped peaks in UV-HPLC chromatogram is derived from a saturation of the UV detector by the injecting crude product [¹⁸F]**1**. XBridge® BEH C18 OBD™ Prep column (130 Å, 5 μm, 10 mm × 250 mm; Waters, Milford, MA, USA); MeCN/H₂O (40/60, v/v) in isocratic mode (flow rate: 5 mL·min⁻¹).

The full automation (¹⁸F-labeling, oxidation, HPLC purification, and formulation) enabled the radiosynthesis of [¹⁸F]**1** in 66 min. Starting with 120-135 GBq of [¹⁸F]fluoride, the labeled compound [¹⁸F]**1** was isolated in 4.5 ± 0.1% RCY (decay-corrected at the SOS) and with a molar activity of 54 ± 7 GBq·μmol⁻¹.

3. Material and Methods

3.1. Chemistry

All solvents and reagents were purchased from Sigma Aldrich (Overijse, Belgium), TCI Europe N.V. (Zwijndrecht, Belgium), abcr GmbH (Karlsruhe, Germany), or VWR (Oud-Heverlee, Belgium), and no further purification process was implemented. Solvents were evaporated using a HEI-VAP rotary evaporator (Heidolph, Germany). Thin-layer chromatography (TLC) analyses were carried out on silica gel Polygram® SIL G/UV₂₅₄ pre-coated TLC-sheets (Macherey-Nagel, Düren, Germany). Ultra-performance liquid chromatography (UPLC) analyses were carried out on a Waters system (ACQUITY UPLC® PDA UV detector (190–400 nm), Waters, Milford, MA, USA) controlled by the Empower software and with an ACQUITY UPLC® CSH C18 column (1.7 μm, 2.1 × 100 mm) (Waters, Milford, MA, USA), at 0.5 mL·min⁻¹ and 45 °C. ¹H-, ¹³C-, and ¹⁹F-nuclear magnetic resonance (NMR) spectra were recorded at room temperature on a Bruker AVANCE III UltraShield NanoBay 400 MHz NMR Spectrometer (400 MHz for ¹H, 101 MHz for ¹³C, and 376 MHz for ¹⁹F,

Bruker Biosciences Corporation, Billerica, MA, USA). The newly synthesized compounds were analyzed in DMSO-*d*⁶ at a probe temperature of 300 K. For ¹H- and ¹³C-NMR spectra, the chemical shifts (δ) were expressed in ppm downfield from tetramethylsilane (TMS) as an internal standard. For ¹⁹F-NMR spectra, the chemical shifts (δ) were given in ppm downfield from trifluoroacetic acid (TFA, $\delta = -76.50$ ppm) as internal standard. The NMR multiplicity signals were abbreviated as: s = singlet, d = doublet, t = triplet, dd = doublet of doublets, ddd = doublet of doublet of doublets, or m = multiplet. The coupling constants (*J*) were given in Hz and reported to the nearest 1 Hz. High-resolution mass spectroscopy (HRMS) spectra were measured on using a SYNAPT G2-SI Waters QTOF mass spectrometer (Waters, Milford, MA, USA). This spectrometer is equipped with an electrospray ionization (ESI) source and a Waters Acquity H-class UPLC with diode array detector (210 to 400 nm) (Waters, Milford, MA, USA). An Acquity UPLC HSS T3 C18 column (1.8 μ m, 2.1 \times 50 mm) was used. The melting points (m.p.) of the solid compounds were measured using a Büchi® melting point apparatus (model B-545, AC/DC input 230 V AC, Büchi, Flawil, Switzerland).

3.1.1. Synthesis of 2-((Difluoromethyl)thio)benzo[*d*]thiazole (2)

The difluoromethylation of benzothiazolyl-thiol (**1**) was achieved following the slightly modified protocols [21,44]. Sodium chlorodifluoroacetate (915 mg, 6.0 mmol, 2.0 equiv.) and potassium carbonate (622 mg, 4.5 mmol, 1.5 equiv.) were added to a single-neck round-bottom flask with DMF (5 mL) and the resulting suspension was stirred at room temperature for 5 minutes. Afterwards, a solution of the heteroaryl-thiol **3** (502 mg, 3.0 mmol, 1.0 equiv.) in DMF (5 mL) was slowly added. The reaction mixture was stirred at 95 °C for 15 minutes and then cooled down to room temperature. After dilution with H₂O (10 mL), the crude product was extracted with DCM (3 \times 20 mL). The organic layers were gathered and dried over anhydrous MgSO₄. After filtration, the crude product solution was concentrated under reduced pressure and further purified by flash column chromatography (SiO₂; heptane/EtOAc (95/5, v/v)) to obtain the sulfide **2** as yellow oil.

2-((Difluoromethyl)thio)benzo[*d*]thiazole (**2**). Yellow oil (350 mg, 54% yield); ¹H-NMR (DMSO-*d*⁶, 400 MHz): δ = 8.16 (1H, d, *J*_{HH} = 8.2 Hz), 8.06 (1H, d, *J*_{HH} = 8.2 Hz), 7.99 (1H, t, *J*_{HF} = 56.3 Hz), 7.60-7.56 (1H, m), 7.54-7.50 (1H, m) ppm; ¹³C-NMR (DMSO-*d*⁶, 101 MHz): δ = 155.9, 152.3, 136.0, 126.8, 125.8, 122.5, 122.1, 120.3 (t, *J*_{CF} = 275 Hz) ppm; ¹⁹F-NMR (DMSO-*d*⁶ + TFA, 376 MHz): - 94.4 (2F, d, *J*_{HF} = 54 Hz) ppm; *m/z* [C₈H₅F₂NS₂ + H]⁺ calcd. for [C₈H₅F₂NS₂]: 217.9910; found: 217.9910.

3.1.2. Synthesis of 2-((Bromofluoromethyl)thio)benzo[*d*]thiazole (4)

A solution of KOH (1.68 g, 30.0 mmol, 10.0 equiv.) in H₂O (4 mL) was placed in a single-neck round-bottom flask and stirred at 0 °C. Afterwards, a solution of the heteroaryl-thiol **1** (502 mg, 3.0 mmol, 1.0 equiv.) in THF (3 mL) was added and the

resulting mixture was allowed to stir at room temperature for 20 min. A solution of dibromofluoromethane (0.380 mL, 4.8 mmol, 1.6 equiv.) in THF (1 mL) was slowly introduced in the reaction system, and the resulting mixture was stirred at room temperature for 15–20 min. The suspension was subsequently quenched by addition of H₂O (20 mL), and the crude product was extracted with DCM (3 × 30 mL). The combined organic layers were gathered and were dried over anhydrous MgSO₄. After filtration, the solvent was removed under reduced pressure. The purification of the concentrated crude product was performed by flash chromatography (SiO₂; heptane/EtOAc (95/5, v/v)) to furnish the bromofluoromethyl heteroaryl-sulfide **4** as pure compound.

2-((Bromofluoromethyl)thio)benzo[d]thiazole (**4**). Yellow oil (130 mg, 16% yield); ¹H-NMR (DMSO-*d*₆, 400 MHz): δ = 8.47 (1H, d, *J*_{HF} = 56 Hz), 8.15 (1H, d, *J*_{HH} = 7.6 Hz), 8.06 (1H, d, *J*_{HH} = 7.6 Hz), 7.58 (1H, t, *J*_{HH} = 7.6 Hz), 7.51 (1H, t, *J*_{HH} = 7.6 Hz) ppm; ¹³C-NMR (DMSO-*d*₆, 101 MHz): δ = 199.5, 152.1, 135.8, 126.8, 125.7, 122.4, 122.1, 90.6 (d, *J*_{CF} = 295 Hz) ppm; ¹⁹F-NMR (DMSO-*d*₆ + TFA, 376 MHz): δ = -105.5 (1F, d, *J*_{HF} = 54 Hz) ppm; *m/z* [C₈H₅BrFNS₂ + H]⁺ calcd. for [C₈H₅BrFNS₂]: 277.9106; found: 277.9109.

3.1.3. Synthesis of 2-((Difluoromethyl)sulfonyl)benzo[d]thiazole (**1**) and 2-((Bromofluoromethyl)sulfonyl)benzo[d]thiazole (**5**)

To a round-bottom flask containing the difluoromethyl heteroaryl-sulfide **2** (217 mg, 1.0 mmol, 1.0 equiv.) or the bromofluoromethyl heteroaryl-sulfide **4** (278 mg, 1.0 mmol, 1.0 equiv.) in MeCN (2 mL) and CHCl₃ (2 mL), a solution of sodium (meta)periodate (NaIO₄) (1.07 g, 5.0 mmol, 5 equiv.) and ruthenium (III) chloride hydrate (RuCl₃·*x*H₂O) (10 mg, 0.05 mmol, 0.05 equiv.) in H₂O (4 mL) was added to the reaction system. The resulting reaction mixture was stirred at room temperature for 1 h. After the completion of the reaction, the suspension was diluted with H₂O (5 mL) and the crude product was extracted with DCM (3 × 25 mL). The combined organic layers were washed with saturated aqueous solution of NaHCO₃ and subsequently dried over anhydrous MgSO₄. After filtration, the solvent was evaporated under reduced pressure. The resulting crude product was then purified by flash chromatography (SiO₂; heptane/EtOAc (90/10, v/v)) to afford the sulfones **1** and **5** as pure compounds.

2-((Difluoromethyl)sulfonyl)benzo[d]thiazole (**1**). White solid (170 mg, 67% yield); *m.p.* 155–156 °C; ¹H-NMR (DMSO-*d*₆, 400 MHz): δ = 8.47–8.41 (2H, m), 7.83–7.81 (2H, m), 7.73 (1H, t, *J*_{HF} = 53 Hz) ppm; ¹³C-NMR (DMSO-*d*₆, 101 MHz): δ = 159.0, 152.4, 137.5, 129.2, 128.6, 125.5, 123.7, 115.0 (t, *J*_{CF} = 282 Hz) ppm; ¹⁹F-NMR (DMSO-*d*₆ + TFA, 376 MHz): -124.0 (2F, d, *J*_{HF} = 53 Hz) ppm.

2-((Bromofluoromethyl)sulfonyl)benzo[d]thiazole (**5**). White solid (210 mg, 68% yield); *m.p.* 129–131 °C; ¹H-NMR (DMSO-*d*₆, 400 MHz): δ = 8.31–8.26 (1H, m), 8.09–8.04 (1H,

m), 7.74-7.62 (2H, m), 7.37 (1H, d, $J_{HF} = 48$ Hz) ppm; ^{13}C -NMR (DMSO- d_6 , 101 MHz): $\delta = 158.7, 152.3, 137.3, 128.5, 127.8, 125.5, 121.9, 95.4$ (d, $J_{CF} = 293$ Hz) ppm; ^{19}F -NMR (DMSO- d_6 + TFA, 376 MHz): -140.2 ppm.

3.1.4. Synthesis of 2-((Bromofluoromethyl)sulfinyl)benzo[d]thiazole (6) and 2-((Difluoromethyl)sulfinyl)benzo[d]thiazole (7)

Meta-chloroperoxybenzoic acid (*m*CPBA) (190 mg, 1.1 mmol, 1.1 equiv.) was slowly added at 0 °C to a stirred solution of difluoromethyl benzothiazolyl-sulfide **2** (217 mg, 1.0 mmol, 1.0 equiv.) or bromofluoromethyl benzothiazolyl-sulfide **4** (278 mg, 1.0 mmol, 1.0 equiv.) in DCM (2 mL). The reaction mixture was stirred at 0 °C for 4 h. After the completion of the reaction, the crude product was extracted with a saturated solution of NaHCO₃ (2 × 25 mL) and with DCM (3 × 25 mL). The organic layers were gathered and subsequently dried over anhydrous MgSO₄. After filtration, the solution was concentrated under reduced pressure and the resulting crude products were further purified by flash chromatography (SiO₂; heptane/EtOAc (95/5, v/v)) to furnish the heteroaryl-sulfoxides **6** and **7** as pure compounds.

2-((Bromofluoromethyl)sulfinyl)benzo[d]thiazole (**6**). Light yellow solid (215 mg, 73% yield); m.p. 100-102 °C; ^1H -NMR (DMSO- d_6 , 400 MHz): $\delta = 8.34$ -8.31 (1H, m), 8.21-8.18 (1H, m), 8.13 (1H, d, $J_{FH} = 47.3$ Hz), 7.70-7.61 (2H, m) ppm; ^{13}C -NMR (DMSO- d_6 , 101 MHz): $\delta = 171.6$ (d, $J_{CF} = 8.9$ Hz), 152.9, 135.6, 127.5, 127.0, 124.0, 123.3, 105.3 (d, $J_{CF} = 290.7$ Hz) ppm; ^{19}F -NMR (DMSO- d_6 + TFA, 376 MHz): -142.7 (1F, d, $J_{FH} = 47.3$ Hz), -147.2 (1F, d, $J_{FH} = 47.3$ Hz) ppm.

2-((Difluoromethyl)sulfinyl)benzo[d]thiazole (**7**). White solid (174 mg, 75% yield); m.p. 135-137 °C; ^1H -NMR (DMSO- d_6 , 400 MHz): $\delta = 8.35$ -8.32 (1H, m), 8.21-8.18 (1H, m), 7.70-7.62 (2H, m), 7.37 (1H, dd, $J_{HF} = 53.4$ and 53.4 Hz) ppm; ^{13}C -NMR (DMSO- d_6 , 101 MHz): $\delta = 170.7$ -170.6 (m), 153.1, 135.5, 127.5, 127.0, 124.0, 123.3, 120.2 (dd, $J_{CF} = 293.4$ and 289.5 Hz) ppm; ^{19}F -NMR (DMSO- d_6 + TFA, 376 MHz): -121.2 (1F, dd, $J_{FH} = 251.2$ and 53.4 Hz), -124.0 (1F, dd, $J_{FH} = 251.2$ and 53.4 Hz) ppm.

3.2. Radiochemistry

Semi-preparative high performance liquid chromatography (HPLC) purification was conducted on a XBridge® BEH C18 OBD™ Prep column (130 Å, 5 μm, 10 mm × 250 mm; Waters, Milford, MA, USA) with a mixture of MeCN/H₂O (40/60, v/v) in isocratic mode (flow rate: 5 mL·min⁻¹). The radio-HPLC profiles were monitored with a custom homemade Geiger-Muller (GM) radioactivity detector (Thermo Fisher Scientific, Waltham, MA, USA), connected to the semi-preparative HPLC system. Ultra performance liquid chromatography (UPLC) analyses were performed at 45 °C using an ACQUITY UPLC® CSH™ C18 column (2.1 × 100 mm, 1.7 μm; Waters, Milford, MA, USA) on an ACQUITY UPLC® system with a mobile phase of MeCN and HCO₂H/H₂O (0.05%, v/v) in gradient mode at 0.5 mL·min⁻¹ (from 100%

HCO₂H/H₂O (0.05%, v/v) to 75% MeCN + 25% HCO₂H/H₂O (0.05%, v/v) in 6 min, and from 75% MeCN + 25% HCO₂H/H₂O (0.05%, v/v) to 100% HCO₂H/H₂O (0.05%, v/v) in 2 min). The UV signal of the newly synthesized ¹⁸F-labeled compounds was measured at 254 nm with a photodiode array (PDA) UV detector (190–400 nm) controlled by the Empower software and connected to the UPLC system. A thallium-activated sodium iodide (NaI(Tl)) scintillation detector from Eberline (Eberline Instruments Corp, Miami, FL, USA) was used to monitor the radio-UPLC elution profile of the newly synthesized ¹⁸F-labeled compounds. TLC analyses were carried out on silica gel Polygram[®] SIL G/UV₂₅₄ pre-coated TLC-sheets (TLC eluent: *n*-hexane/ethyl acetate, 1:1) (Macherey-Nagel, Düren, Germany). The TLC profile of ¹⁸F-labeled compounds was then analyzed with a BertHold TLC scanner model AR2000 (BertHold, Bad Wildbad, Germany).

The radiosyntheses of the ¹⁸F-labeled compounds were achieved using the commercially available FASTlab[™] synthesizer (GE Healthcare, Chicago, IL, USA). The SepPak[®] cartridges (SepPak[®] Accell[™] Plus QMA Carbonate Plus Light Cartridge (46 mg, 40 μm) and SepPak[®] ¹⁸C18 Plus Short Cartridge (400 mg, 37–55 μm) were purchased from Waters (Milford, MA, USA). No-carrier-added [¹⁸F]fluoride was prepared from the ¹⁸O-enriched water ([¹⁸O]H₂O) *via* the ¹⁸O(p,n)¹⁸F nuclear reaction with a Cyclone 18/9 from IBA (Louvain-la-Neuve, Belgium). [¹⁸O]H₂O was purchased from Cambridge Isotope Laboratories (Tewksbury, MA, USA). At the end of bombardment (EOB), the activity was transferred to the hot lab cell with helium pressure through Teflon tubing (~ 50 m).

3.2.1. Fully Automated Radiosynthesis of 2-((Difluoromethyl)sulfonyl)benzo[*d*]thiazole ([¹⁸F]**1**)

The fully automated radiosynthesis of the labeled compound [¹⁸F]**1** was conducted in a FASTlab[™] synthesizer (GE Healthcare, Chicago, IL, USA). The reagents and solvents used in the radiosynthesis of [¹⁸F]**1** was placed in 11 mm- and 13 mm-sealed vials and positioned in the FASTlab[™] manifold as depicted in Table 8 and illustrated in Figure 9.

The no-carrier-added (n.c.a.) [¹⁸F]fluoride in [¹⁸O]H₂O was transferred from the cyclotron target onto the FASTlab[™] synthesizer *via* the [¹⁸F]fluoride inlet conical reservoir (V6). The [¹⁸F]fluoride was trapped on an ion-exchange resin (Sep-Pak[®] Accell[™] Plus QMA Carbonate Plus Light Cartridge; Waters, Milford, MA, USA; from V5 to V4) and the [¹⁸O]H₂O was recovered in a separate vial (V1). The trapped [¹⁸F]fluoride was eluted into the cyclic olefin copolymer (COC) reactor through a central tubing (V8) with a solution of Kryptofix[®] 222 (K_{2.2.2}; 7.5 mg in 600 μL of MeCN) and K₂CO₃ (1.4 mg in 150 μL of H₂O). The eluent was azeotropically evaporated under vacuum and nitrogen flow by heating at 105 °C and 120 °C for 8 min. Subsequently, a solution of the precursor **4** (11.1 mg, 0.04 mmol) solubilized in MeCN (1.0 mL) was transferred to the dry [¹⁸F]potassium fluoride/Kryptofix[®] 222 ([¹⁸F]KF/K_{2.2.2}) complex *via* the central tubing of the reactor (V8) and heated to 120 °C for 5 min. After the ¹⁸F-

labeling of **4**, the reaction mixture was diluted two times with H₂O (~ 12 mL) (V15), and the labeled compound [¹⁸F]**2** was trapped on a ¹C18 cartridge (Sep-Pak® C18 Plus Short Cartridge; Waters, Milford, MA, USA; from V17 to V18). The COC reactor was subsequently washed with H₂O (~ 4 mL), and the crude solution was passed through the ¹C18 cartridge. A solution containing NaIO₄ (51.3 mg, 0.024 mmol) and RuCl₃·xH₂O (1.7 mg, 0.008 mmol) in H₂O (4.0 mL) was transferred to the ¹C18 cartridge and the oxidation of the labeled compound [¹⁸F]**2** was carried out on the solid-phase for 5 min at room temperature. Afterwards, the crude product [¹⁸F]**1** was eluted (from V18 to V17; reverse flow elution) with MeCN (2 mL; syringe S3, V24) and recovered into the reactor through its central tubing. After dilution with H₂O (~ 4 mL) using the syringe S2 (V11), the resulting mixture was conducted to the semi-preparative HPLC loop (V9; 6 mL) *via* a Sterifix® Paed filter (B. Braun, Melsungen, Germany; 0.2 μm). The COC reactor was subsequently washed with H₂O (~ 2 mL) and this solution was also transferred into the HPLC loop. The semi-preparative HPLC purification of [¹⁸F]**1** was accomplished with a mixture of MeCN/H₂O (40/60, v/v) in isocratic mode at 5 mL·min⁻¹. The HPLC peak corresponding to the [¹⁸F]**1** were collected (retention time of [¹⁸F]**1**: 16-19 min) in a sealed vial containing H₂O (~ 30 mL). Subsequently, the purified compound [¹⁸F]**1** was pumped (from V10), 6 mL by 6 mL, with the syringe S2 (V11) and further conducted to a preconditioned ¹C18 cartridge (from V21 to V22). Finally, [¹⁸F]**1** was eluted into the outlet vial (V20) with reverse flow of DMSO (1 mL, syringe S3 (V24)).

3.2.2. Low-Activity ¹⁸F-Labeling Experiments in the Precursor **4**

Using the GE FASTlab™ synthesizer, an aliquot of [¹⁸F]fluoride (100–150 MBq) was trapped on a Sep-Pak® Accell™ Plus QMA Carbonate Plus Light cartridge (Waters, Milford, MA, USA) and eluted with a solution of Kryptofix® 222 (K_{2.2.2}; 7.5 mg in 600 μL of MeCN) and K₂CO₃ (1.4 mg in 150 μL of H₂O). Upon azeotropic drying, a solution of the precursor **4** (11.1 mg, 0.04 mmol) in MeCN (1 mL) was transferred to the dry [¹⁸F]potassium fluoride/Kryptofix® 222 ([¹⁸F]KF/K_{2.2.2}) complex and heated to 120 °C. After 5 min of ¹⁸F-labeling and dilution of the reaction mixture with H₂O, the labeled compound [¹⁸F]**2** was trapped on a Sep-Pak® C18 Plus Short cartridge (Waters, Milford, MA, USA). Subsequently, the ¹C18 cartridge was removed and the trapped crude product [¹⁸F]**2** was recovered to a 4 mL-vial *via* manual elution with MeCN (1 mL). The radiochemical yield (RCY) of the ¹⁸F-labeling step was determined based on the activity of the recovered crude product [¹⁸F]**2**, on their radio-TLC and radio-UPLC purities, and the starting radioactivity, according to the following equation:

$$RCY (\%, d. c.) = \frac{\text{radioTLC purity} (\%) \times \text{radioUPLC purity} (\%) \times \text{activity of } [^{18}\text{F}]\mathbf{2} (d. c.)}{\text{starting radioactivity} \times 100}$$

A solution containing NaIO₄ (51.3 mg, 0.024 mmol) and RuCl₃·xH₂O (1.7 mg, 0.008 mmol) in H₂O (1 mL) was transferred to the ¹C18 cartridge and the oxidation of the trapped crude product [¹⁸F]**2** (10–20 MBq) was carried out in solid-phase for 5 min at room temperature. Afterwards, the corresponding [¹⁸F]difluoromethyl heteroaryl-

sulfone [¹⁸F]**1** was manually eluted from the C18 cartridge with MeCN (1 mL) to a 4 mL-vial. The RCY of the oxidation step was determined based on the activity of the crude products [¹⁸F]**1** and [¹⁸F]**2**, and on their radio-TLC and radio-UPLC purities, according to the following equation:

$$RCY (\%, d. c.) = \frac{\text{radioTLC purity (\%)} \times \text{radioUPLC purity (\%)} \times \text{activity of } [^{18}\text{F}]\mathbf{1} (d. c.)}{\text{activity of } [^{18}\text{F}]\mathbf{2} \times 100}$$

The RCYs of ¹⁸F-labeling and oxidation steps were decay-corrected at the SOS.

3.2.3. Isolation and Determination of the Molar Activity of [¹⁸F]**1**

The fully automated radiosynthesis of the sulfone [¹⁸F]**1** was accomplished on a commercially available FASTlab™ synthesizer (GE Healthcare, Chicago, IL, USA), using the optimized conditions for the labeling of the precursor **4** (11.1 mg, 0.04 mmol), and for the oxidation of the labeled compound [¹⁸F]**2**. The molar activity of the sulfone [¹⁸F]**1** was determined using an aliquot of the reformulated solution (3 μL). After UPLC injection, the radioactive peak of [¹⁸F]**1** associated to the non-radioactive sulfone **1** was collected and counted in an ionization chamber. The PDA UV area under the peak of the non-radioactive sulfone **1** at 239 nm enabled the determination of the corresponding amount (in μmol) of the **1** using the calibration curves described in the Supplementary Information (Figure S18). The molar activity of [¹⁸F]**1** was determined on the basis of the following equation:

$$\text{Molar activity (GBq} \cdot \mu\text{mol}^{-1}) = \frac{\text{activity of the collected UPLC peak of } [^{18}\text{F}]\mathbf{1}}{\text{amount of } \mathbf{1} \text{ associated to the radioactive peak}}$$

4. Conclusions

From the investigated synthetic approaches, a two-step methodology involving an initial ¹⁸F-labeling of the bromofluoromethyl-sulfide derivative **4** with [¹⁸F]KF/K_{2.2.2} and subsequent oxidation of the ¹⁸F-difluoromethyl-containing derivative [¹⁸F]**2** was selected for the synthesis of [¹⁸F]**1**. Our results showed that the efficiency of the nucleophilic ¹⁸F-fluorination was mainly influenced by the solvent, the temperature, the reaction time, the amount of precursor, and the type of base used for elution of [¹⁸F]fluoride from a QMA cartridge. Under optimal conditions, the cartridge-purified [¹⁸F]**2** was afforded in 15.2 ± 0.3% RCY (decay-corrected at the SOS). Regarding the oxidation step, the amount of NaIO₄ and RuCl₃·xH₂O had an impact on the conversion of the sulfide [¹⁸F]**2** into the sulfone [¹⁸F]**1**. This ¹⁸F-labeled product was isolated in 82.9 ± 7.9% RCY (decay-corrected at the SOS).

The two-step radiosynthesis of the [¹⁸F]difluoromethyl heteroaryl-sulfone [¹⁸F]**1** was fully automated in the GE FASTlab™ module. In conjunction with a semi-preparative HPLC purification procedure and formulation in a preconditioned Sep-Pak® C18 Plus Short Cartridge, the reagent [¹⁸F]**1** was isolated in reproducible 4.5 ± 0.1% RCY (decay-corrected at the SOS).

Obtaining a high molar activity still persists a challenging task in the radiosynthesis of ^{18}F CHF₂-bearing compounds, due to the unwanted ^{18}F - ^{19}F isotopic exchange reactions. In fact, the reported ^{18}F -labeling methods enabled the access to ^{18}F CHF₂-bearing compounds with low-to-medium molar activity (up to 22 GBq· μmol^{-1}) [45-49]. The production of radiotracers with high molar activity is mandatory for PET imaging studies, especially for targeting low-density biomacromolecules. Starting with 120-135 GBq of ^{18}F fluoride, the labeled compound ^{18}F **1** was obtained with a molar activity of 54 ± 7 GBq· μmol^{-1} at the EOS.

The reagent ^{18}F **1** was further utilized in the late-stage C-H ^{18}F -difluoromethylation of a wide range of *N*-containing heteroarenes, in particular of drugs, nucleosides, and nucleic bases, under irradiation with blue light-emitting diode (LED) (470 nm, 2 W) [50]. The C-H ^{18}F -difluoromethylation reactions performed in continuous-flow using an easy-to-use platform equipped with a 100 μL microreactor made from glass and a syringe that continuously pumps the reaction mixture into the microreactor at a given flow rate (FlowStart Evo, FutureChemistry, Nijmegen, The Netherlands). This method may enable the access to novel ^{18}F -difluoromethyl-containing PET ligands with improved molar activities.

5. Supplementary Information

5.1. NMR spectra of the compounds **1**, **2**, and **4-7**

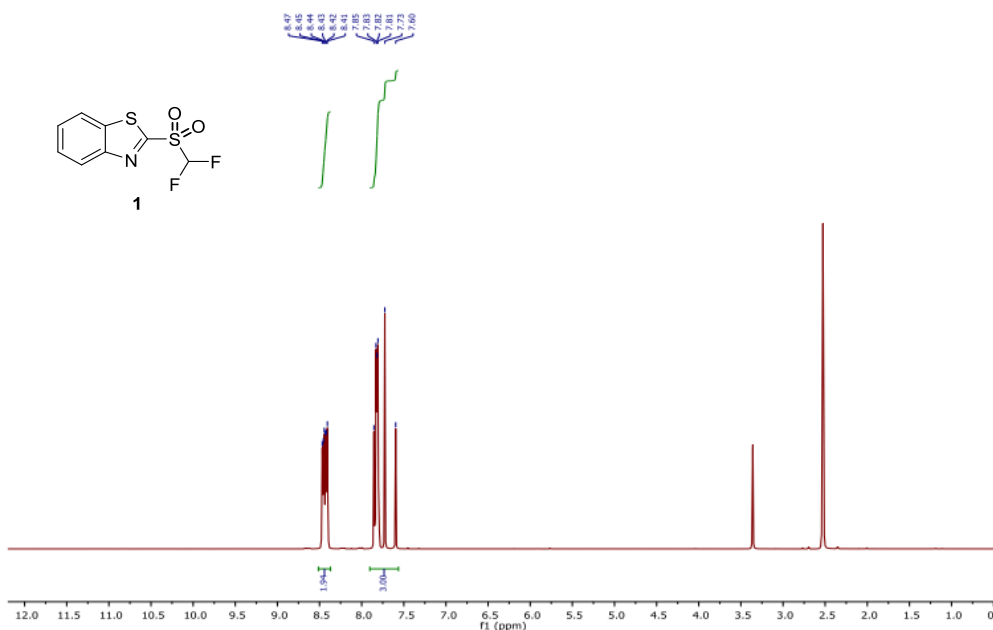


Figure S1. ¹H-NMR spectrum of **1**.

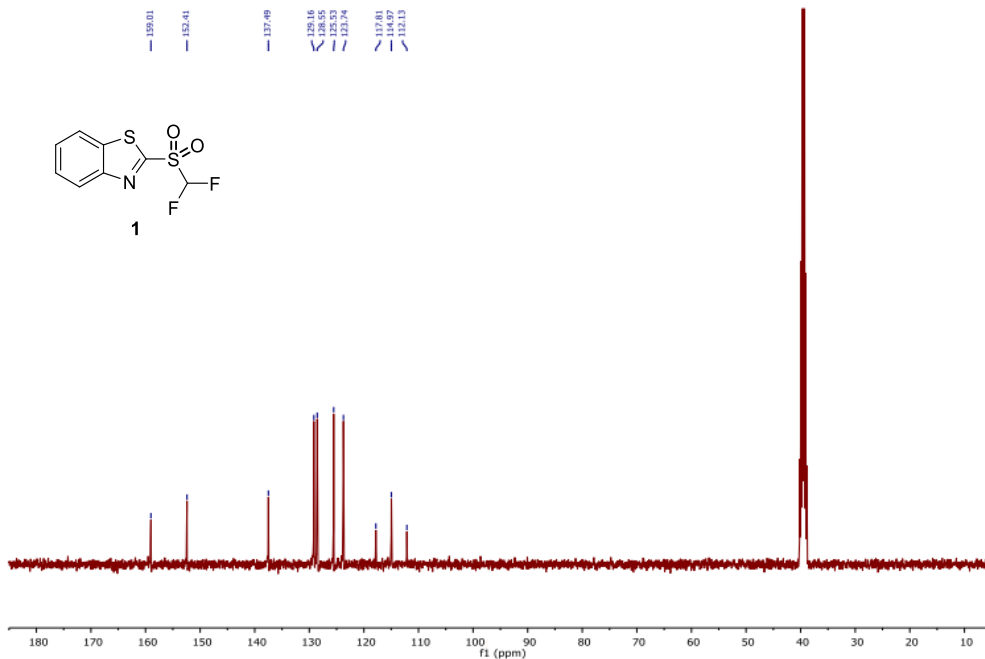


Figure S2. ¹³C-NMR spectrum of **1**.

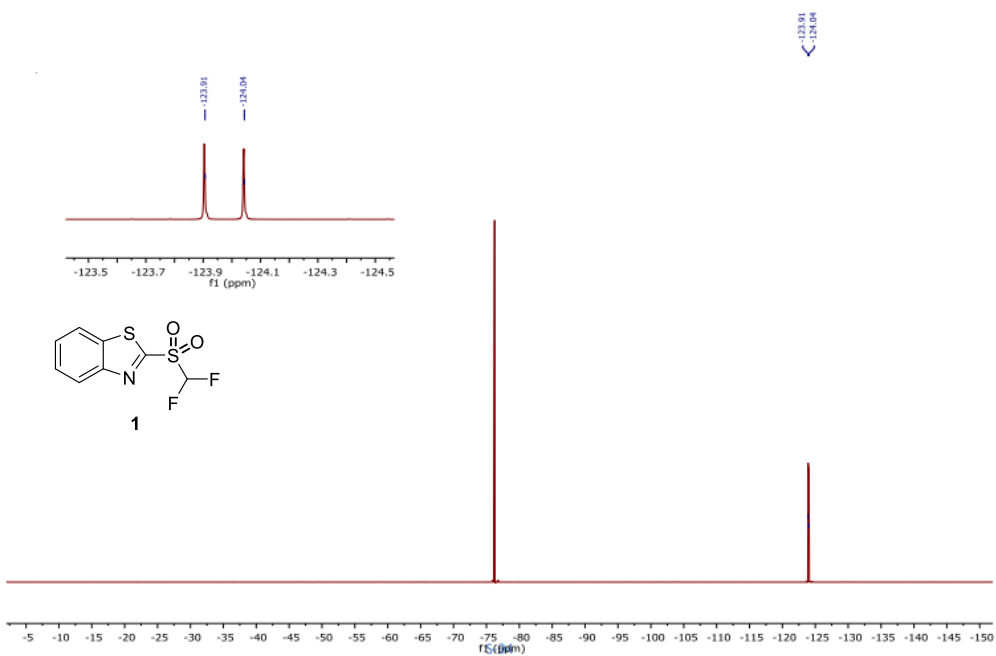


Figure S3. ¹⁹F-NMR spectrum of **1**.

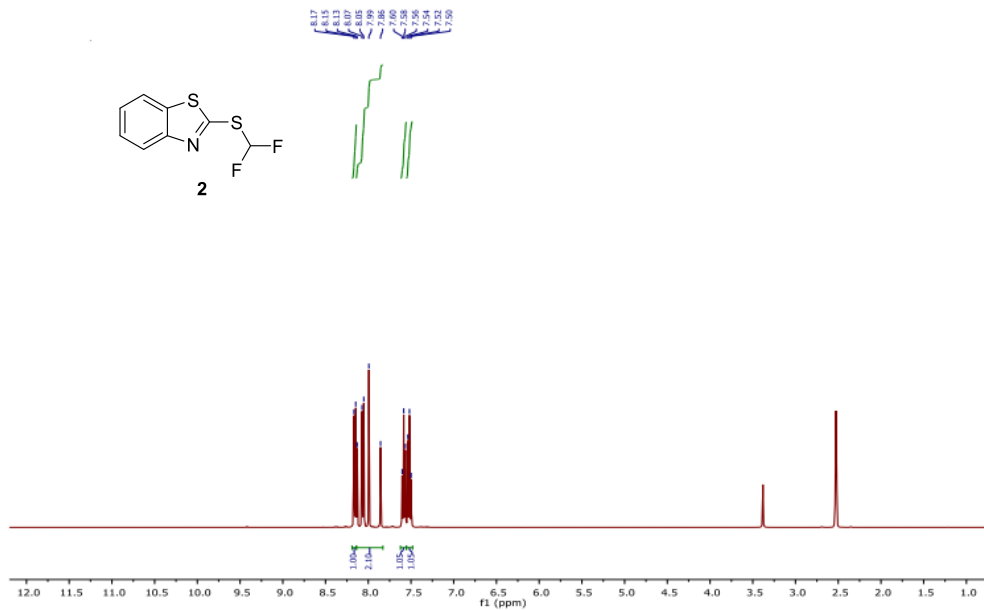


Figure S4. ¹H-NMR spectrum of **2**.

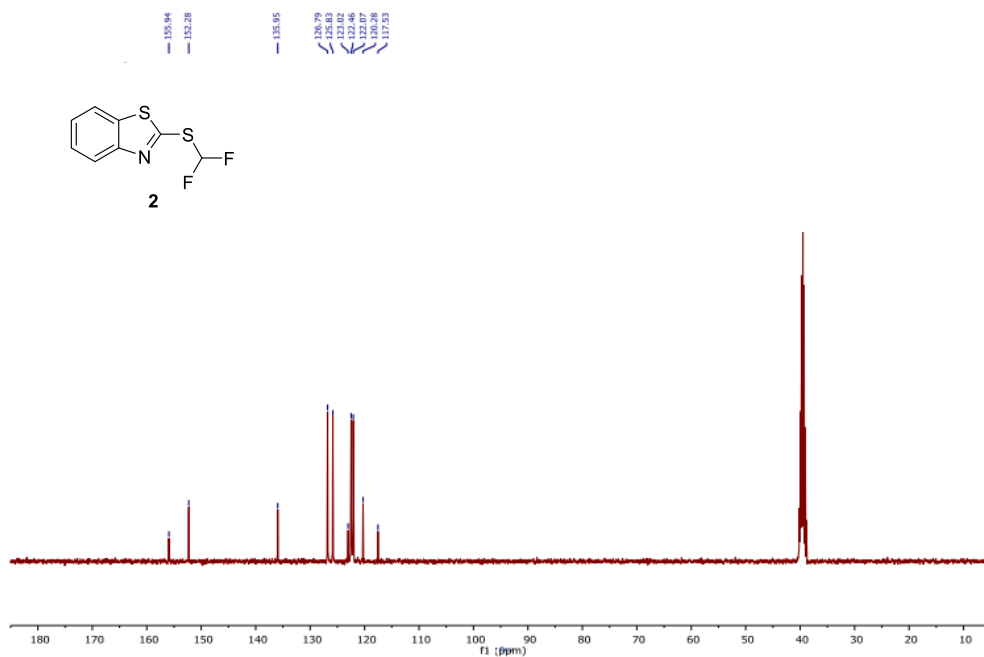


Figure S5. ¹³C-NMR spectrum of **2**.

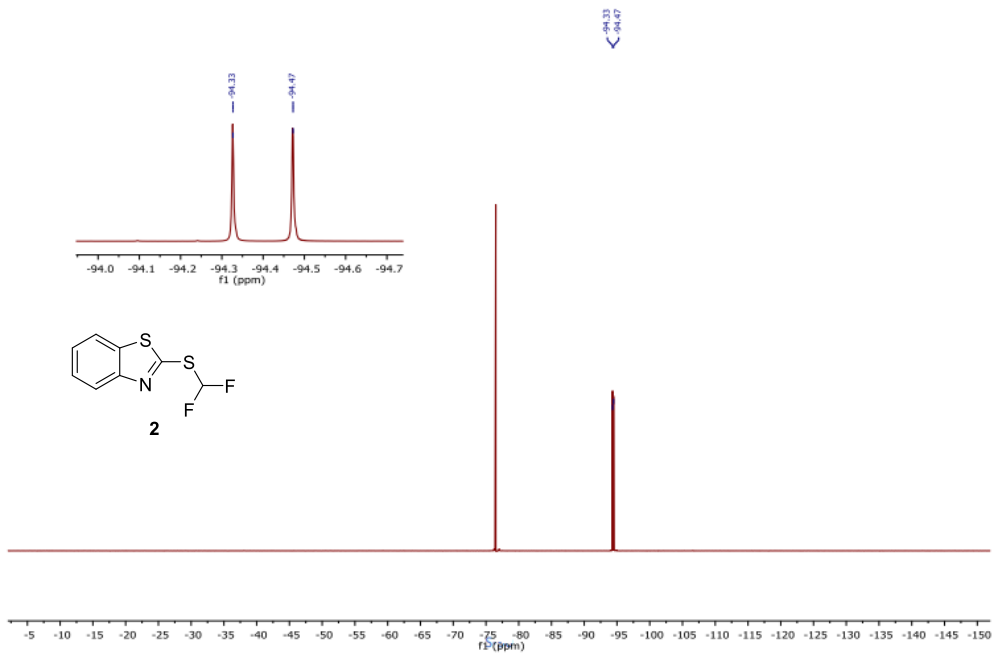


Figure S6. ¹⁹F-NMR spectrum of **2**.

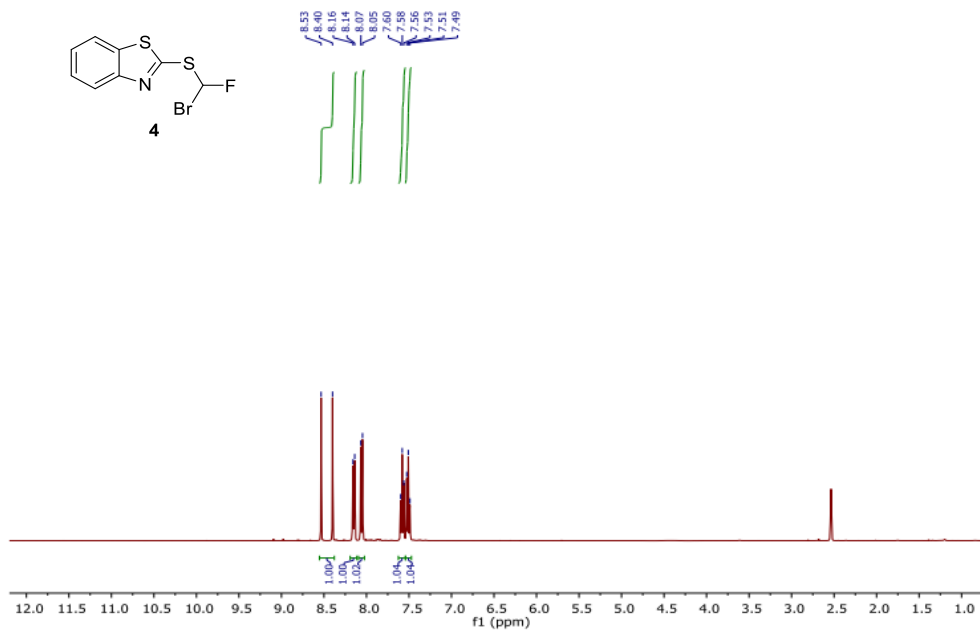


Figure S7. ¹H-NMR spectrum of **4**.

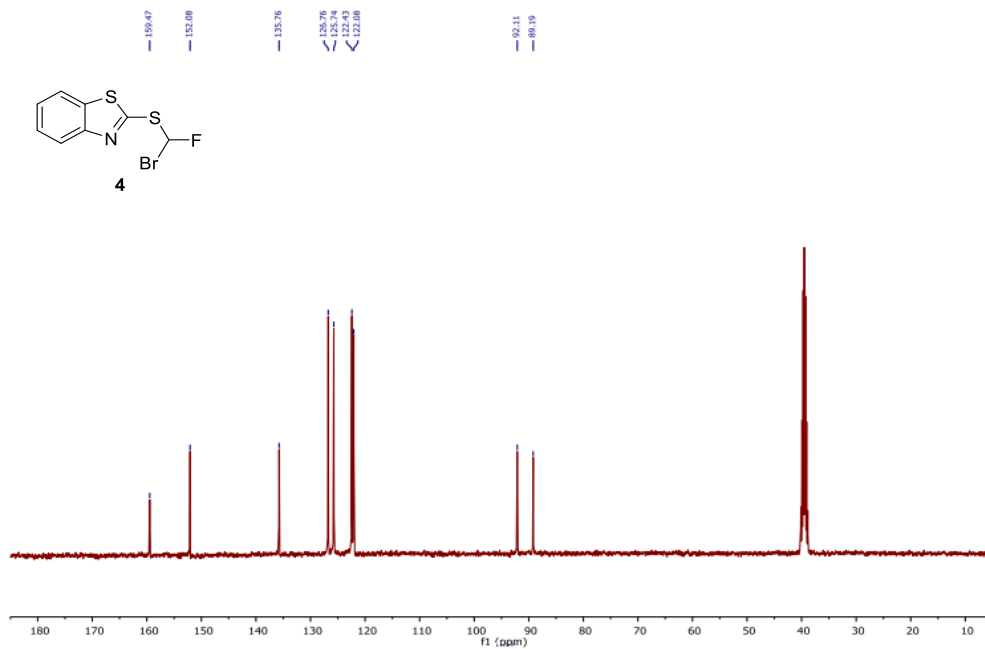


Figure S8. ¹³C-NMR spectrum of 4.

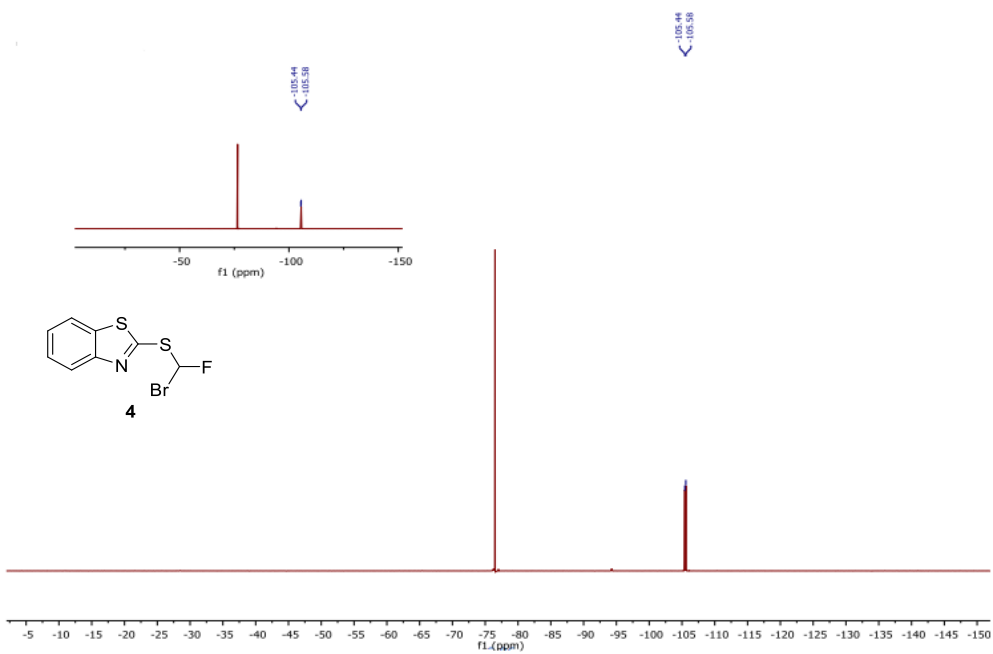


Figure S9. ¹⁹F-NMR spectrum of 4.

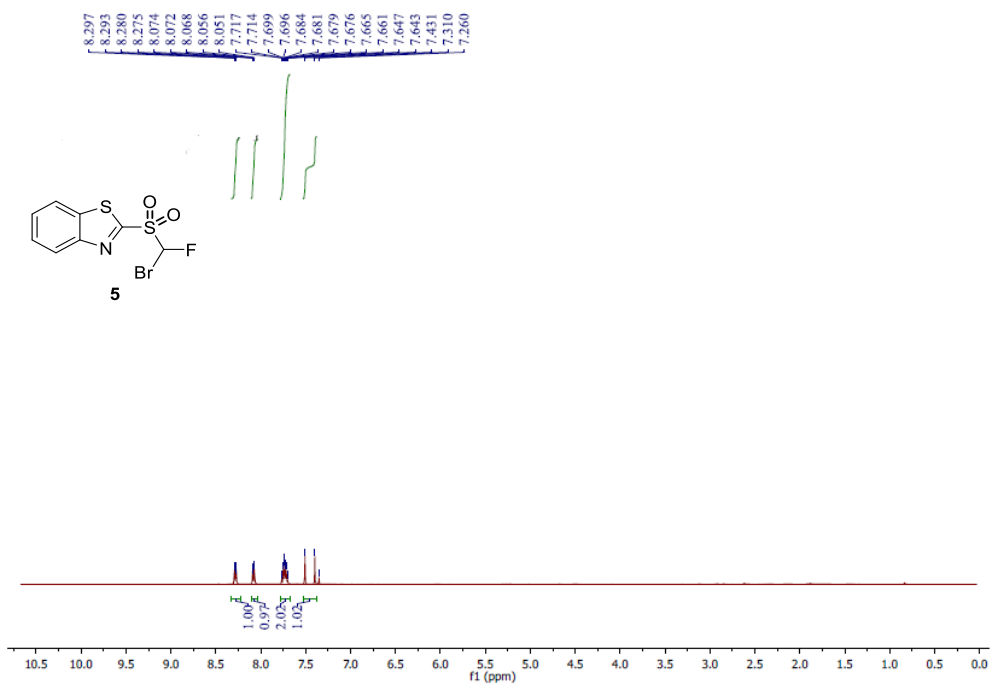


Figure S10. ¹H-NMR spectrum of 5.

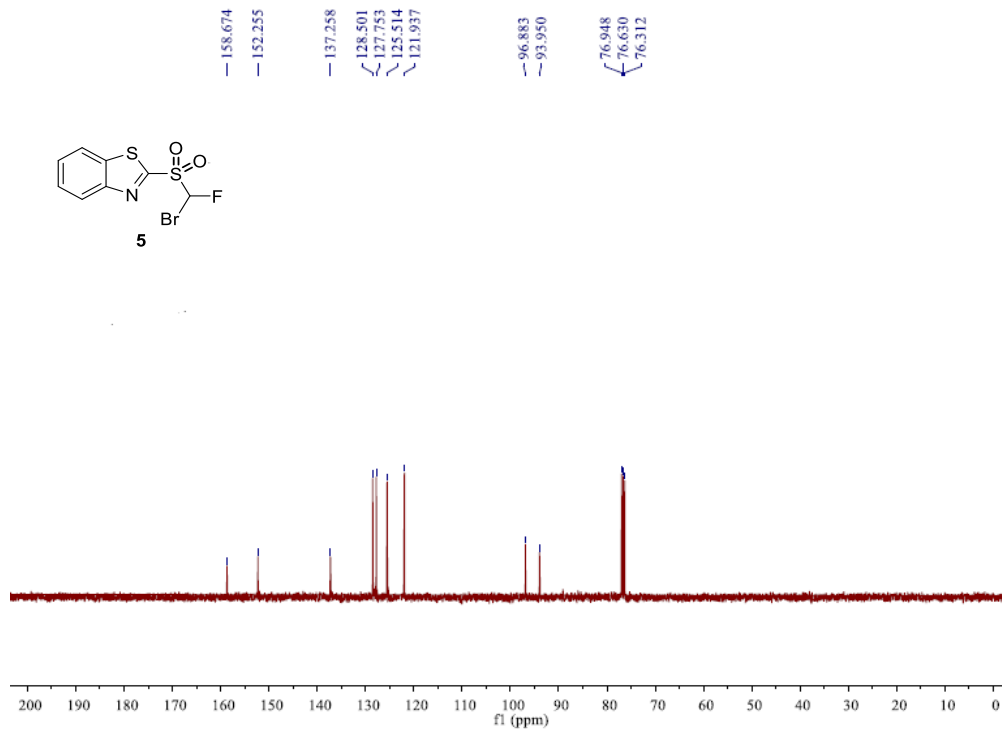


Figure S11. ¹³C-NMR spectrum of 5.

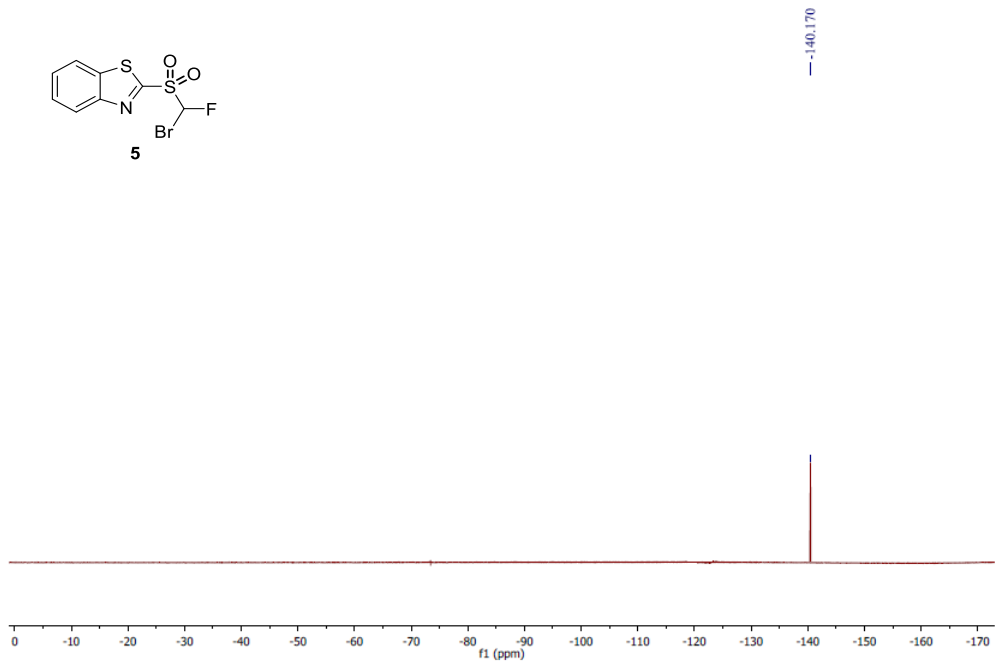


Figure S12. ^{19}F -NMR spectrum of **5**.

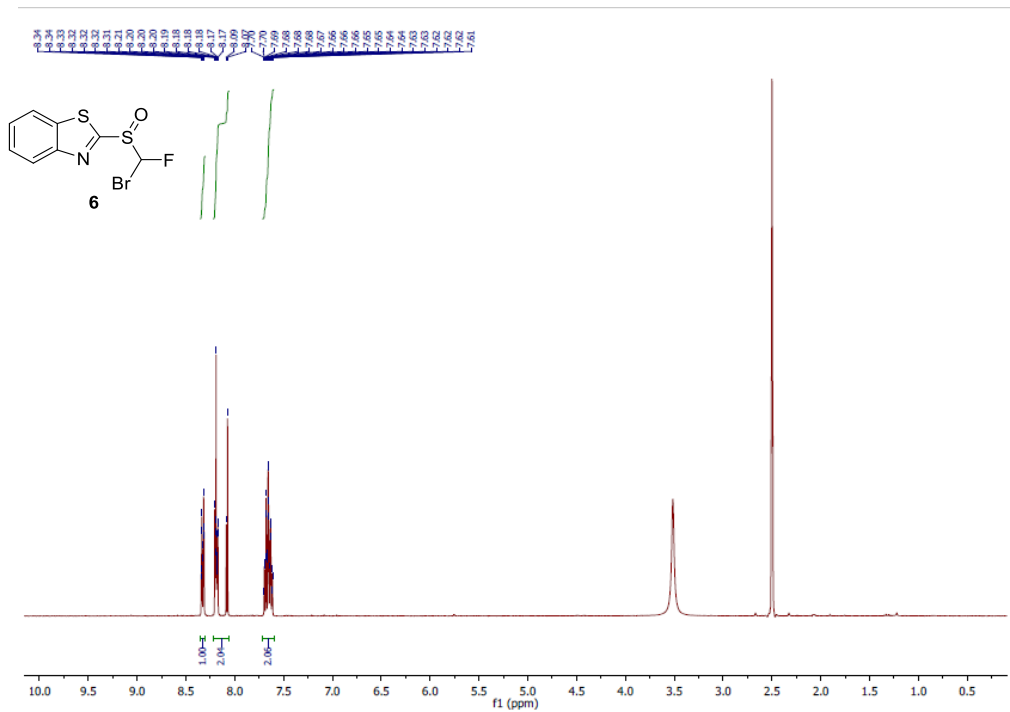


Figure S13. ^1H -NMR spectrum of **6**.

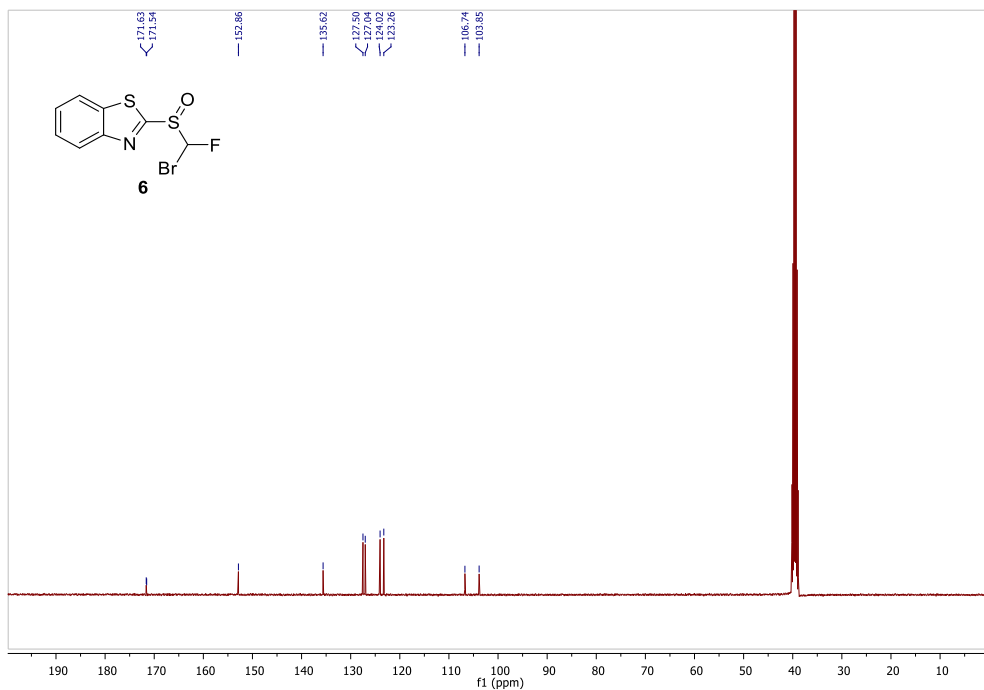


Figure S14. ¹³C-NMR spectrum of **6**.

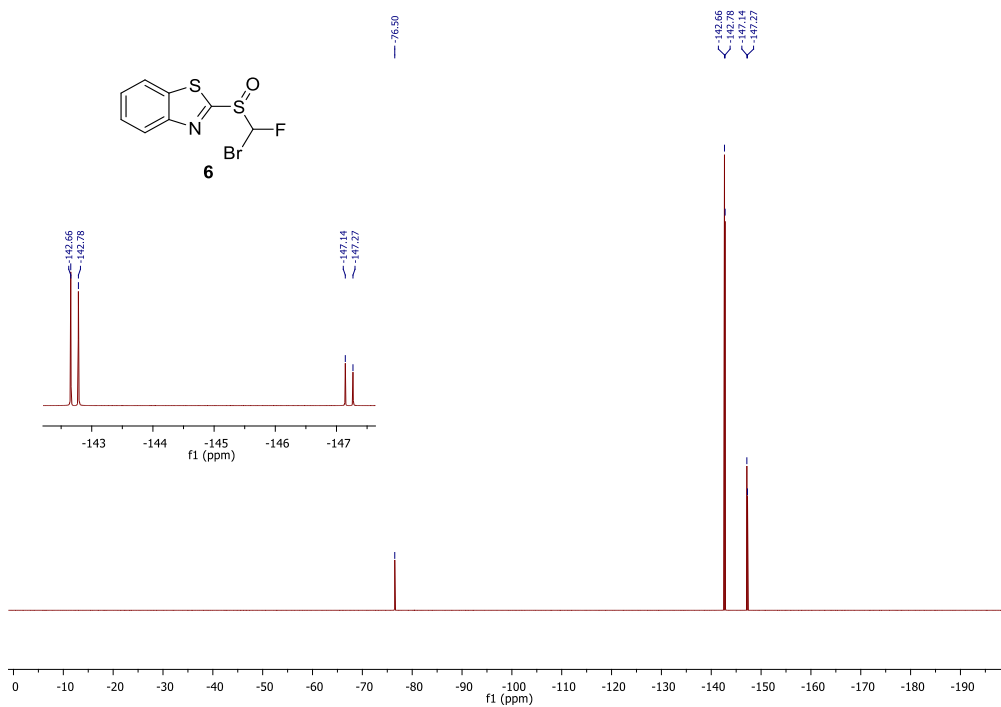


Figure S15. ¹⁹F-NMR spectrum of **6**.

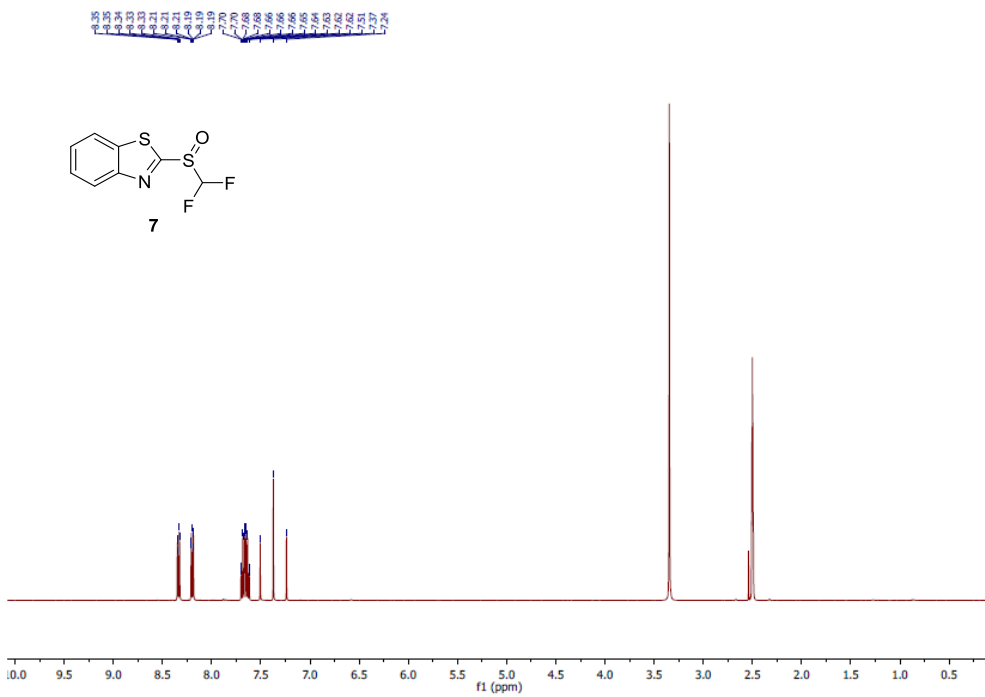


Figure S16. ¹H-NMR spectrum of 7.

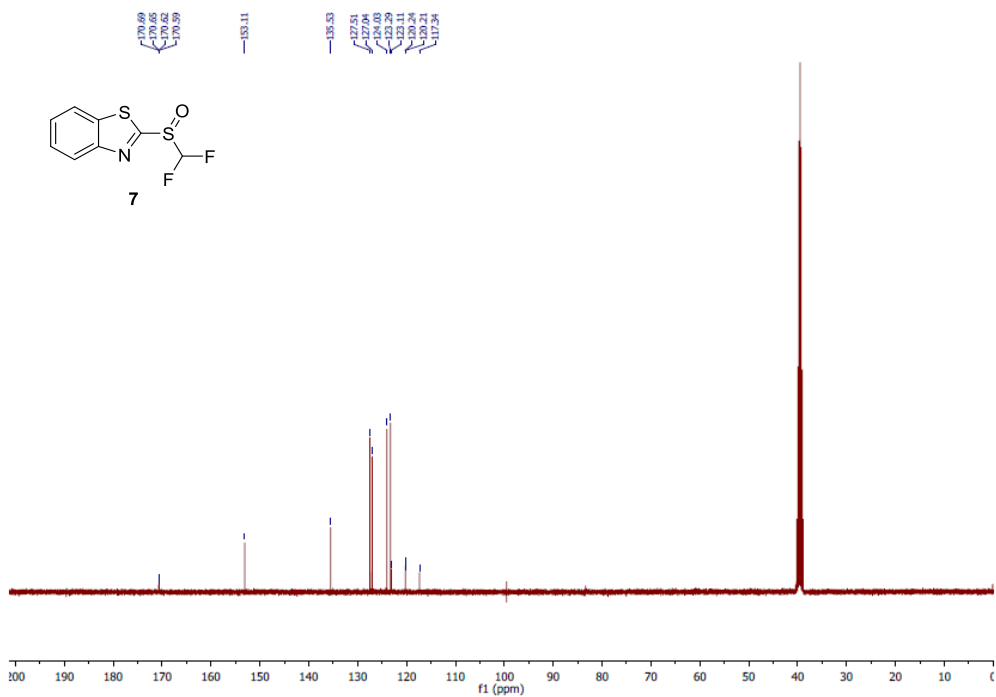


Figure S17. ¹³C-NMR spectrum of 7.

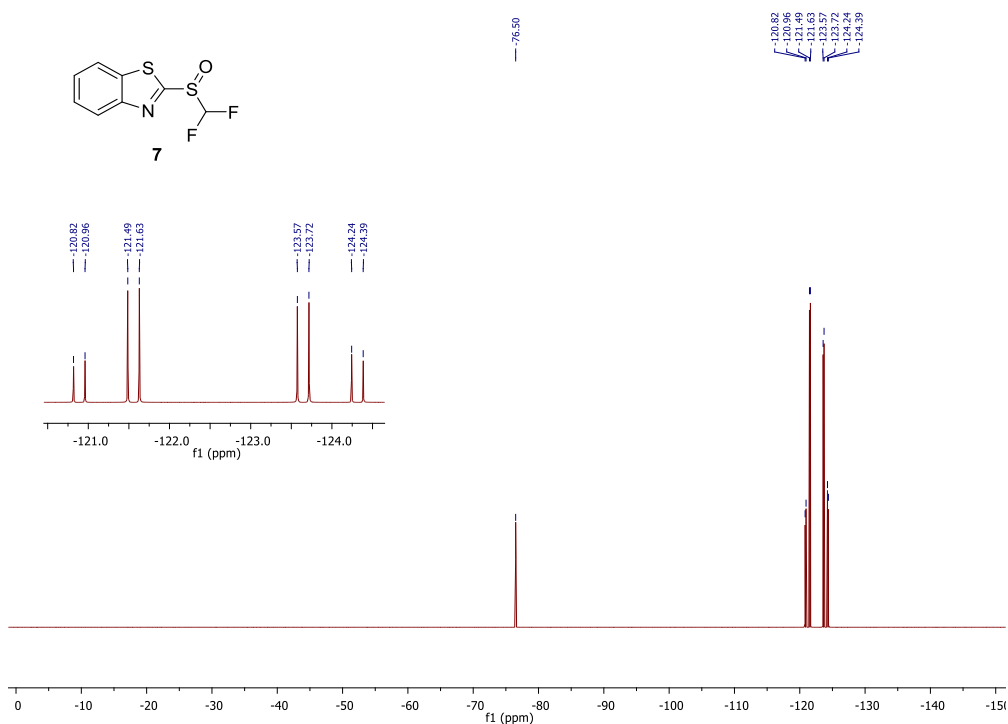


Figure S18. ^{19}F -NMR spectrum of **7**.

5.2. Radiochemistry

The UPLC gradient used for the analyses of the crude products are depicted in Table S1.

Table S1. UPLC gradient for the analysis of the crude products

Time (min)	$\text{HCO}_2\text{H}/\text{H}_2\text{O}$ (0.05%, v/v)	MeCN	Flow rate ($\text{mL}\cdot\text{min}^{-1}$)
0	100	0	0.5
6	25	75	0.5
8	100	0	0.5

5.2.1. Synthesis of [^{18}F]2-((Difluoromethyl)thio)benzo[*d*]thiazole ([^{18}F]2)

The implementation of the general procedure 3.2.2. for the ^{18}F -labeling of 2-((bromofluoromethyl)thio)benzo[*d*]thiazole (**4**) (11.1 mg, 0.04 mmol) provided the labeled compound [^{18}F]2 in $15.2 \pm 0.3\%$ RCY (d.c. at the SOS).

The radiochemical yield (RCY) of the ^{18}F -labeling step was determined based on the activity of the recovered crude product [^{18}F]2, on their radio-TLC and radio-UPLC purities, and the starting radioactivity, according to the following formula:

$$\text{RCY (\%, d. c.)} = \frac{\text{radioTLC purity (\%)} \times \text{radioUPLC purity (\%)} \times \text{activity of } [^{18}\text{F}]\mathbf{2} \text{ (d. c.)}}{\text{starting radioactivity} \times 100}$$

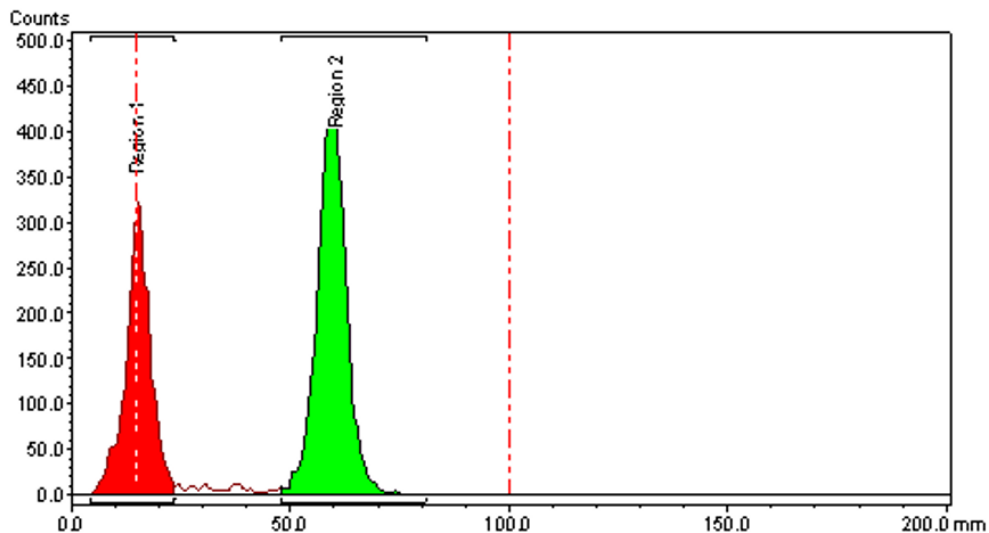


Figure S19. TLC radio-chromatogram of the crude product $[^{18}\text{F}]\mathbf{2}$ (eluent: *n*-hexane/ethyl acetate, 1:1).

Table S2. Determination of the radio-TLC purity of the crude product $[^{18}\text{F}]\mathbf{2}$

Retention factor (R_f , mm)	Ratio (%)
0.03	37 (impurity/by-product)
0.59	63 (desired crude product)

$$RCY (\%, d.c.) = \frac{\text{radioTLC purity (\%)} \times \text{radioUPLC purity (\%)} \times \text{activity of } [^{18}\text{F}]\mathbf{1} (d.c.)}{\text{starting radioactivity} \times 100}$$

$$RCY (\%, d.c.) = \frac{63 \times 100 \times 35.4}{144.7 \times 100}$$

$$RCY (\%, d.c.) = 15.4 \%$$

Table S3 furnishes more details of the RCY determination. The UPLC radio-chromatogram of the crude product $[^{18}\text{F}]\mathbf{2}$ is depicted in Figure 5. Figure 1 represents the UPLC UV-chromatogram of the non-radioactive reference **2**.

Table S3. Determination of the radiochemical yield (%) of the synthesis of $[^{18}\text{F}]\mathbf{2}$

Reaction	Starting activity (MBq)	Activity of the crude product $[^{18}\text{F}]\mathbf{2}$ (MBq, d.c.)	Radio-TLC purity (%)	Radio-UPLC purity (%)	Radiochemical Yield (%)
1	126.8	30.4	63	100	15.1
2	132.2	30.3	65	100	14.9
3	144.7	35.4	63	100	15.4
Radiochemical Yield (%) \pm Deviation					15.2 \pm 0.3

5.2.2. Synthesis of [¹⁸F]2-((Difluoromethyl)sulfonyl)benzo[*d*]thiazole ([¹⁸F]1)

The implementation of the general procedure 3.2.2. for the oxidation of [¹⁸F]2-((difluoromethyl)thio)benzo[*d*]thiazole ([¹⁸F]2) (10-20 MBq) provided the labeled compound [¹⁸F]1 in 82.9 ± 7.9% RCY (d.c. at the SOS).

The RCY of the oxidation step was determined based on the activity of the crude products [¹⁸F]1 and [¹⁸F]2, and on their radio-TLC and radio-UPLC purities, according to the following equation:

$$RCY (\%, d. c.) = \frac{\text{radioTLC purity (\%)} \times \text{radioUPLC purity (\%)} \times \text{activity of } [^{18}\text{F}]\mathbf{1} (d. c.)}{\text{activity of } [^{18}\text{F}]\mathbf{2} \times 100}$$

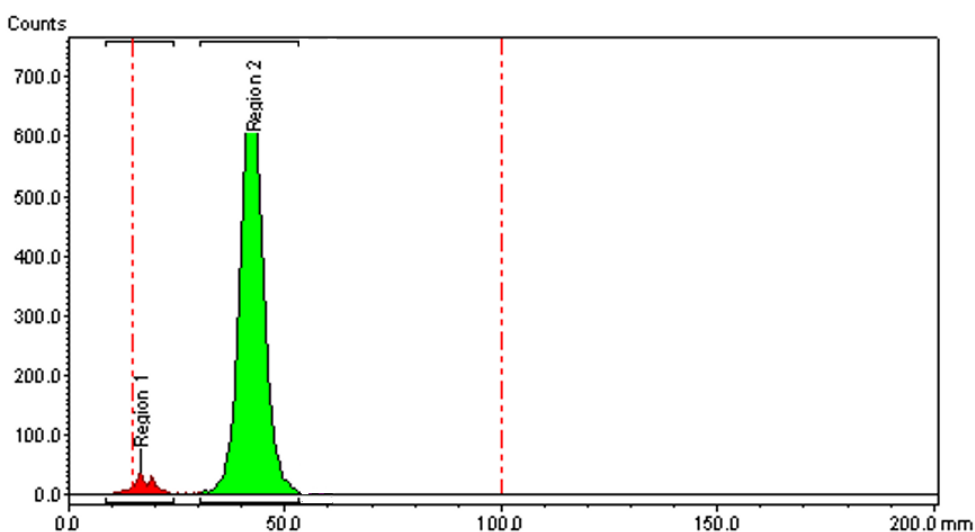


Figure S20. TLC radio-chromatogram of the crude product [¹⁸F]1 (eluent: *n*-hexane/ethyl acetate, 1:1).

Table S4. Determination of the radio-TLC purity of the crude product [¹⁸F]1

Retention factor (<i>R_f</i> , mm)	Ratio (%)
0.03	4 (impurity/by-product)
0.49	96 (desired crude product)

$$RCY (\%, d. c.) = \frac{\text{radioTLC purity (\%)} \times \text{radioUPLC purity (\%)} \times \text{activity of } [^{18}\text{F}]\mathbf{1} (d. c.)}{\text{activity of } [^{18}\text{F}]\mathbf{2} (d. c.) \times 100}$$

$$RCY (\%, d. c.) = \frac{100 \times 92 \times 12.0}{15.6 \times 100}$$

$$RCY (\%, d. c.) = 70.6 \%$$

Table S5 furnishes more details of the RCY determination. The UPLC radio-chromatogram of the crude product [¹⁸F]**1** is depicted in Figure 8. Figure 2 represents the UPLC UV-chromatogram of the non-radioactive reference **1**.

Table S5. Determination of the radiochemical yield (%) of the synthesis of [¹⁸F]**1**

Reaction	Activity of the crude product [¹⁸ F] 2 (MBq)	Activity of the crude product [¹⁸ F] 1 (MBq, d.c.)	Radio-TLC purity (%)	Radio-UPLC purity (%)	Radiochemical Yield (%)
1	13.8	12.1	96	100	83.9
2	15.3	11.6	96	100	72.8
3	15.1	14.5	96	100	92
Radiochemical Yield (%) ± Deviation					82.9 ± 7.9

5.3. Two-Step Radiosynthesis of the [¹⁸F]Difluoromethyl Heteroaryl-Sulfone [¹⁸F]**1** From the Precursor **4**

The overall RCY of the ¹⁸F-labeling step of **4** and the oxidation of [¹⁸F]**2** was determined based on the activity of the recovered crude product [¹⁸F]**1**, on their radio-TLC and radio-UPLC purities, and the starting radioactivity, according to the following formula:

$$RCY (\%, d. c.) = \frac{\text{radioTLC purity} (\%) \times \text{radioUPLC purity} (\%) \times \text{activity of } [^{18}\text{F}]\mathbf{1} (d. c.)}{\text{starting radioactivity} \times 100}$$

Table S6 furnishes more details of the RCY determination of the radiosynthesis of the [¹⁸F]difluoromethyl heteroaryl-sulfone [¹⁸F]**1** from the precursor **4**.

Table S6. Determination of the radiochemical yield (%) of the synthesis of [¹⁸F]**1** from the precursor **4**

Reaction	Starting activity (MBq)	Activity of the crude product [¹⁸ F] 1 (MBq, d.c.)	Radio-TLC purity (%)	Radio-UPLC purity (%)	Radiochemical Yield (%)
1	158.5	22.2	93	100	13.0
2	117.0	16.8	96	100	13.8
3	118.4	13.7	95	100	11
Radiochemical Yield (%) ± Deviation					12.6 ± 1.2

5.4. Fully Automated Radiosynthesis of the Labeled Compound [¹⁸F]**1**

The RCY of the fully automated radiosynthesis of the [¹⁸F]difluoromethyl heteroaryl-sulfone [¹⁸F]**1** was determined based on the radioactivity of the [¹⁸F]**1**

present in DMSO solution and the radioactivity trapped on the QMA carbonate cartridge, according to the following formula:

$$RCY (\%, d. c.) = \frac{\text{activity of the solution of } [^{18}\text{F}]\mathbf{1} \text{ in DMSO (d. c.)}}{\text{activity trapped on the QMA carbonate cartridge} \times 100}$$

Table S7 provide more details of the RCY determination of the radiosynthesis of the [¹⁸F]difluoromethyl heteroaryl-sulfone [¹⁸F]**1** from the precursor **4**.

Table S7. Determination of the radiochemical yield (%) of the synthesis of [¹⁸F]**1** from the precursor **4**

Reaction	Starting activity (GBq)	Activity of the isolated product [¹⁸ F] 1 (GBq, d.c.)	Radiochemical Yield (%)
1	125.3	5.8	4.6
2	134.7	6.3	4.7
3	126.7	5.7	4.5
4	123.3	5.3	4.3
Radiochemical Yield (%) ± Deviation			4.5 ± 0.1

5.5. Calibration Curves of the Difluoromethyl Heteroaryl-Sulfone **1** for Determination of the Molar Activity of [¹⁸F]**1**

The fully automated radiosynthesis of the sulfone [¹⁸F]**1** was performed on a commercially available FASTlab™ synthesizer (GE Healthcare), using the optimized conditions for the labeling of the precursor **1** (11.1 mg, 0.04 mmol) and the oxidation of the labeled compound [¹⁸F]**2**. The molar activity of the [¹⁸F]difluoromethyl heteroaryl-sulfone [¹⁸F]**1** was determined using an aliquot of each reformulated solution (3 μL). After injection of an aliquot in UPLC, the radioactive peak of [¹⁸F]**1** associated to the non-radioactive sulfone **1** was collected and counted in an ionization chamber. The PDA UV area under the peak of the non-radioactive sulfone **1** at 239 nm enabled the determination of the corresponding amount (in μmol) of the difluoromethyl heteroaryl-sulfone using the calibration curve described in Figure S21. The molar activity was calculated by the ratio between the radioactivity of the [¹⁸F]**1** and the corresponding amount of non-radioactive compound, according to the following formula:

$$\text{Molar activity (GBq} \cdot \mu\text{mol}^{-1}\text{)} = \frac{\text{activity of the UPLC peak of } [^{18}\text{F}]\mathbf{1}}{\text{amount of } \mathbf{1} \text{ associated to the radioactive peak}}$$

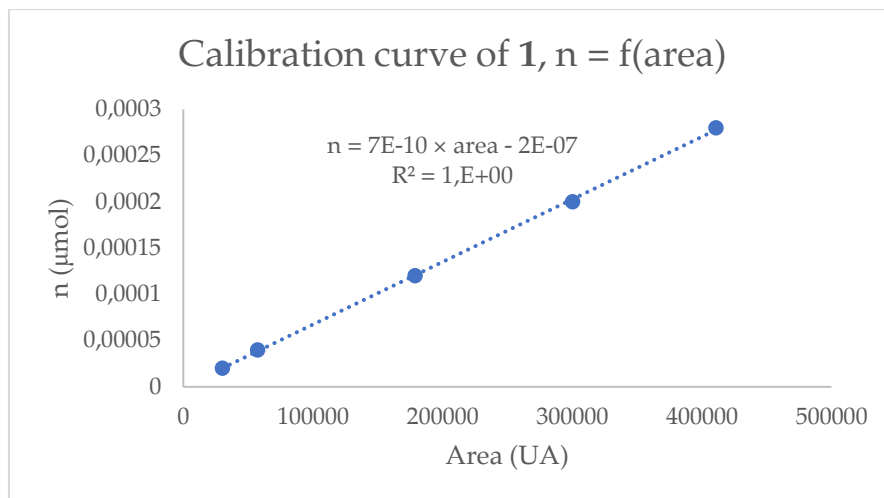


Figure S21. Calibration curve of the difluoromethyl heteroaryl-sulfone **1** (wavelength: 239 nm).

Table S8. Determination of the molar activity of [^{18}F]**1**

Reaction	Activity of the radioactive peak of [^{18}F] 1 (GBq)	Area under the peak of 1 (UA) at 239 nm	Amount of 1 (μmol)	Molar activity (GBq·μmol $^{-1}$)
1	1.781×10^{-2}	537563	3.634×10^{-4}	49
2	1.146×10^{-2}	360606	2.437×10^{-4}	47
3	1.152×10^{-2}	309991	2.095×10^{-4}	55
4	1.713×10^{-2}	396010	2.677×10^{-4}	64
Molar activity (GBq·μmol$^{-1}$) ± Deviation				54 ± 7

The sulfone [^{18}F]**1** was isolated with a molar activity of 54 ± 7 GBq·μmol $^{-1}$ at the EOS.

References

- [1] Le Bars, D. Fluorine-18 and medical imaging: Radiopharmaceuticals for positron emission tomography. *J. Fluorine Chem.* **2006**, *127*, 1488–1493.
- [2] Even-Sapir, E.; Mishani, E.; Flusser, G.; Metser, U. ^{18}F -Fluoride positron emission tomography and positron emission tomography/computed tomography. *Semin. Nucl. Med.* **2007**, *37*, 462–469.
- [3] Banister, S.; Roeda, D.; Dollé, F.; Kassiou, M. Fluorine-18 chemistry for PET: A concise introduction. *Curr. Radiopharm.* **2010**, *3*, 68–80.
- [4] Miller, P.W.; Long, N.J.; Vilar, R.; Gee, A.D. Synthesis of ^{11}C , ^{18}F , ^{15}O , and ^{13}N radiolabels for positron emission tomography. *Angew. Chem. Int. Ed.* **2008**, *47*, 8998–9033.
- [5] Gu, Y.; Huang, D.; Liu, Z.; Huang, J.; Zeng, W. Labeling strategies with F-18 for positron emission tomography imaging. *Med. Chem.* **2011**, *7*, 334–344.
- [6] Ying, L. ^{18}F -Labeling techniques for positron emission tomography. *Sci. China Chem.* **2013**, *56*, 1682–1692.

- [7] Varlow, C.; Szames, D.; Dahl, K.; Bernard-Gauthier, V.; Vasdev, N. Fluorine-18: An untapped resource in inorganic chemistry. *Chem. Commun.* **2018**, *54*, 11835–11842.
- [8] Brooks, A.F.; Topczewski, J.J.; Ichiishi, N.; Sanford, M.S.; Scott, P.J.H. Late-stage [¹⁸F]fluorination: New solutions to old problems. *Chem. Sci.* **2014**, *5*, 4545–4553.
- [9] Jacobson, O.; Kiesewetter, D.O.; Chen, X. Fluorine-18 radiochemistry, labeling strategies and synthetic routes. *Bioconjugate Chem.* **2015**, *26*, 1–18.
- [10] Preshlock, S.; Tredwell, M.; Gouverneur, V. ¹⁸F-Labeling of arenes and heteroarenes for applications in positron emission tomography. *Chem. Rev.* **2016**, *116*, 719–766.
- [11] Van der Born, D.; Pees, A.; Poot, A.J.; Orru, R.V.A.; Windhorst, A.D.; Vugts, D.J. Fluorine-18 labelled building blocks for PET tracer synthesis. *Chem. Soc. Rev.* **2017**, *46*, 4709–4773.
- [12] Coenen, H.H.; Ermert, J. ¹⁸F-Labeling innovations and their potential for clinical application. *Clin. Transl. Imaging* **2018**, *6*, 169–193.
- [13] Krüll, J.; Heinrich, M.R. [¹⁸F] Fluorine-labeled pharmaceuticals: Direct aromatic fluorination compared to multi-step strategies. *Asian, J. Org. Chem.* **2019**, *8*, 576–590.
- [14] Deng, X.; Rong, J.; Wang, L.; Vasdev, N.; Zhang, L.; Josephson, L.; Liang, S.H. Chemistry for positron emission tomography: Recent advances in ¹¹C-, ¹⁸F-, ¹³N-, and ¹⁵O-labeling reactions. *Angew. Chem. Int. Ed.* **2019**, *58*, 2580–2605.
- [15] Van der Born, D.; Herscheid, J.D.M.; Orru, R.V.A.; Vugts, D.J. Efficient synthesis of [¹⁸F]trifluoromethane and its application in the synthesis of PET tracers. *Chem. Commun.* **2013**, *49*, 4018–4020.
- [16] Huiban, M.; Tredwell, M.; Mizuta, S.; Wan, Z.; Zhang, X.; Collier, T.L.; Gouverneur, V.; Passchier, J. A broadly applicable [¹⁸F]trifluoromethylation of aryl and heteroaryl iodides for PET imaging. *Nat. Chem.* **2013**, *5*, 941–944.
- [17] Rühl, T.; Rafique, W.; Lien, V.T.; Riss, P.J. Cu(I)-mediated ¹⁸F-trifluoromethylation of arenes: Rapid synthesis of ¹⁸F-labeled trifluoromethyl arenes. *Chem. Commun.* **2014**, *50*, 6056–6059.
- [18] Ivashkin, P.; Lemonnier, G.; Cousin, J.; Grégoire, V.; Labar, D.; Jubault, P.; Pannecoucke, X. [¹⁸F]CuCF₃: A [¹⁸F]trifluoromethylating agent for arylboronic acids and aryl iodides. *Chem. Eur. J.* **2014**, *20*, 9514–9518.
- [19] Van der Born, D.; Sewing, C.; Herscheid, J.D.M.; Windhorst, A.D.; Orru, R.V.A.; Vugts, D.J. A universal procedure for the [¹⁸F]trifluoromethylation of aryl iodides and aryl boronic acids with highly improved specific activity. *Angew. Chem. Int. Ed.* **2014**, *53*, 11046–11050.
- [20] Huiban, M.; Coello, C.; Wu, K.; Xu, Y.; Lewis, Y.; Brown, A.P.; Buraglio, M.; Guan, C.; Shabbir, S.; Fong, R.; Passchier, J.; Rabiner, E.A.; Lockhart, A. Investigation of the brain biodistribution of the lipoprotein-associated phospholipase A₂ (Lp-PLA₂) inhibitor [¹⁸F]GSK2647544 in healthy male subjects. *Mol. Imaging Biol.* **2017**, *19*, 153–161.
- [21] Carbonnel, E.; Besset, T.; Poisson, T.; Labar, D.; Pannecoucke, X.; Jubault, P. ¹⁸F-Fluoroform: a ¹⁸F-trifluoromethylating agent for the synthesis of SCF₂¹⁸F-aromatic derivatives. *Chem. Commun.* **2017**, *53*, 5706–5709.

- [22] Verhoog, S.; Kee, C.W.; Wang, Y.; Khotavivattana, T.; Wilson, T.C.; Kersemans, V.; Smart, S.; Tredwell, M.; Davis, B.G.; Gouverneur, V. ^{18}F -Trifluoromethylation of unmodified peptides with 5- ^{18}F -(trifluoromethyl)dibenzothiophenium trifluoromethanesulfonate. *J. Am. Chem. Soc.* **2018**, *140*, 1572-1575.
- [23] King, A.; Doepner, A.; Turton, D.; Ciobota, D.M.; Pieve, C.D.; Fong, A.-C.W.T.; Kramer-Marek, A.; Chung, Y.-L.; Smith, G. Radiosynthesis of the anticancer nucleoside analogue Trifluridine using an automated ^{18}F -trifluoromethylation procedure. *Org. Biomol. Chem.* **2018**, *16*, 2986-2996.
- [24] Kim, H.Y.; Lee, J.Y.; Lee, Y.-S.; Jeong, J.M. Design and synthesis of enantiopure ^{18}F -labelled [^{18}F]trifluoromethyltryptophan from 2-halotryptophan derivatives via copper(I)-mediated [^{18}F]trifluoromethylation and evaluation of its *in vitro* characterization for the serotonergic system imaging. *J. Label. Compd. Radiopharm.* **2019**, *62*, 566-579.
- [25] Fu, Z.; Lin, Q.; Hu, B.; Zhang, Y.; Chen, W.; Zhu, J.; Zhao, Y.; Choi, H.S.; Shi, H.; Cheng, D. P2X7 radioligand ^{18}F -PTTP for the differentiation of lung tumor and inflammation. *J. Nucl. Med.* **2019**, *60*, 930-936.
- [26] Yang, B.Y.; Telu, S.; Haskali, M.B.; Morse, C.L.; Pike, V.W. A gas route to [^{18}F]fluoroform with limited molar activity dilution. *Sci. Rep.* **2019**, *9*, 14835.
- [27] Kee, C.W.; Tack, O.; Guibbal, F.; Wilson, T.C.; Isenegger, P.G.; Imiołek, M.; Verhoog, S.; Tilby, M.; Boscutti, G.; Ashworth, S.; Chupin, J.; Kashani, R.; Poh, A.W.J.; Sosabowski, J.K.; Macholi, S.; Plisson, C.; Cornelissen, B.; Willis, M.C.; Passchier, J.; Davis, B.G.; Gouverneur, V. ^{18}F -Trifluoromethanesulfinate enables direct C-H ^{18}F -trifluoromethylation of native aromatic residues in peptides. *J. Am. Chem. Soc.* **2020**, *142*, 1180-1185.
- [28] Zheng, J.; Wang, L.; Lin, J.-H.; Xiao, J.-C.; Liang, S.H. Difluorocarbene-derived trifluoromethylthiolation and [^{18}F]trifluoromethylthiolation of aliphatic electrophiles. *Angew. Chem. Int. Ed.* **2015**, *54*, 13236-13240.
- [29] Zheng, J.; Cheng, R.; Lin, J.-H.; Yu, D.-H.; Ma, L.; Jia, L.; Zhang, L.; Wang, L.; Xiao, J.-C.; Liang, S.L. An unconventional mechanistic insight into SCF_3 formation from difluorocarbene: Preparation of ^{18}F -labeled α - SCF_3 carbonyl compounds. *Angew. Chem. Int. Ed.* **2017**, *56*, 3196-3200.
- [30] Liu, S.; Ma, H.; Zhang, Z.; Lin, L.; Yuan, G.; Tang, X.; Nie, D.; Jiang, S.; Yang, G.; Tang, G. Synthesis of enantiopure ^{18}F -trifluoromethyl cysteine as a structure-mimetic amino acid tracer for glioma imaging. *Theranostics* **2019**, *9*, 1144-1153.
- [31] Lu, Y.; Choi, J.-Y.; Kim, S.E.; Lee, B.C. HPLC-free *in situ* ^{18}F -fluoromethylation of bioactive molecules by azidation and MTBD scavenging. *Chem. Commun.* **2019**, *55*, 11798-11801.
- [32] Rong, J.; Ni, C.; Hu, J. Metal-catalyzed direct difluoromethylation reactions. *Asian J. Org. Chem.* **2017**, *6*, 139-152.
- [33] Yerien, D.E.; Barata-Vallejo, S.; Postigo, A. Difluoromethylation reactions of organic compounds. *Chem. Eur. J.* **2017**, *23*, 14676-14701.

- [34] Feng, Z.; Xiao, Y.-L.; Zhang, X. Transition-metal (Cu, Pd, Ni)-catalyzed difluoroalkylation via cross-coupling with difluoroalkyl halides. *Acc. Chem. Res.* **2018**, *51*, 2264-2278.
- [35] Lemos, A.; Lemaire, C.; Luxen, A. Progress in difluoroalkylation of organic substrates by visible light photoredox catalysis. *Adv. Synth. Catal.* **2019**, *361*, 1500-1537.
- [36] Koike, T.; Akita, M. Recent progress in photochemical radical di- and mono-fluoromethylation. *Org. Biomol. Chem.* **2019**, *17*, 5413-5419.
- [37] Levi, N.; Amir, D.; Greshonov, E.; Zafrani, Y. Recent progress on the synthesis of CF₂H-containing derivatives. *Synthesis* **2019**, *51*, 4549-4567.
- [38] Rong, J.; Deng, L.; Tan, P.; Ni, C.; Gu, Y.; Hu, J. Radical fluoroalkylation of isocyanides with fluorinated sulfones by visible-light photoredox catalysis. *Angew. Chem. Int. Ed.* **2016**, *55*, 2743-2747.
- [39] Fu, W.; Han, X.; Zhu, M.; Xu, C.; Wang, Z.; Ji, B.; Hao, X.-Q.; Song, M.-P. Visible-light-mediated radical oxydifluoromethylation of olefinic amides for the synthesis of CF₂H-containing heterocycles. *Chem. Commun.* **2016**, *52*, 13413-13416.
- [40] Zou, G.; Wang, X. Visible-light induced di- and trifluoromethylation of *N*-benzamides with fluorinated sulfones for the synthesis of CF₂H/CF₃-containing isoquinolinediones. *Org. Biomol. Chem.* **2017**, *15*, 8748-8751.
- [41] Zhu, M.; Fu, W.; Wang, Z.; Xu, C.; Ji, B. Visible-light-mediated direct difluoromethylation of alkynoates: synthesis of 3-difluoromethylated coumarins. *Org. Biomol. Chem.* **2017**, *15*, 9057-9060.
- [42] Zhu, M.; Fu, W.; Guo, W.; Tian, Y.; Wang, Z.; Xu, C.; Ji, B. Visible-light-induced radical di- and trifluoromethylation of β , γ -unsaturated oximes: synthesis of di- and trifluoromethylated isoxazolines. *Eur. J. Org. Chem.* **2019**, *2019*, 1614-1619.
- [43] Zhu, M.; You, Q.; Li, R. Synthesis of CF₂H-containing oxindoles *via* photoredox-catalyzed radical difluoromethylation and cyclization of *N*-arylacrylamides. *J. Fluorine Chem.* **2019**, DOI: 10.1016/j.jfluchem.2019.109391.
- [44] Arai, Y.; Tomita, R.; Ando, G.; Koike, T.; Akita, M. Oxydifluoromethylation of alkenes by photoredox catalysis: simple synthesis of CF₂H-containing alcohols. *Chem. Eur. J.* **2016**, *22*, 1262-1265.
- [45] Mizuta, S.; Stenhagen, I.S.R.; O'Duill, M.; Wolstenhulme, J.; Kirjavainen, A.K.; Forsback, S.J.; Tredwell, M.; Sandford, G.; Moore, P.R.; Huiban, M.; Luthra, S.K.; Passchier, J.; Solin, O.; Gouverneur, V. Catalytic decarboxylative fluorination for the synthesis of tri- and difluoromethyl arenes. *Org. Lett.* **2013**, *15*, 2648-2651.
- [46] Verhoog, S.; Pfeifer, L.; Khotavivattana, T.; Calderwood, S.; Collier, T.L.; Wheelhouse, K.; Tredwell, M.; Gouverneur, V. Silver-mediated ¹⁸F-labeling of aryl-CF₃ and aryl-CHF₂ with ¹⁸F-fluoride. *Synlett* **2016**, *27*, 25-28.
- [47] Shi, H.; Braun, A.; Wang, L.; Liang, S.H.; Vasdev, N.; Ritter, T. Synthesis of ¹⁸F-difluoromethylarenes from aryl (pseudo) halides. *Angew. Chem. Int. Ed.* **2016**, *55*, 10786-10790.
- [48] Yuan, G.; Wang, F.; Stephenson, N.A.; Wang, L.; Rotstein, B.H.; Vasdev, N.; Tang, P.; Liang, S.H. Metal-free ¹⁸F-labeling of aryl-CF₂H *via* nucleophilic radiofluorination and oxidative C-H activation. *Chem. Commun.* **2017**, *53*, 126-129.

[49] Sap, J.B.I.; Wilson, T.C.; Kee, C.W.; Straathof, N.J.W.; amEnde, C.W.; Mukherjee, P.; Zhang, L.; Genicot, C.; Gouverneur, V. Synthesis of ^{18}F -difluoromethylarenes using aryl boronic acids, ethyl bromofluoroacetate and ^{18}F fluoride. *Chem. Sci.* **2019**, *10*, 3237-3241.

[50] Trump, L.; Lemos, A.; Lallemand, B.; Pasau, P.; Mercier, J.; Lemaire, C.; Luxen, A.; Genicot, C. Late-stage ^{18}F -difluoromethyl labeling of *N*-heteroaromatics with high molar activity. *Angew. Chem. Int. Ed.* **2019**, *58*, 13149-13154.

Chapter IV

Radical C-H ^{18}F -Difluoromethylation of
Heteroarenes with [^{18}F]Difluoromethyl
Heteroaryl-Sulfones by Visible Light
Photoredox Catalysis

Article

Radical C–H ^{18}F -Difluoromethylation of Heteroarenes with [^{18}F]Difluoromethyl Heteroaryl-Sulfones by Visible Light Photoredox Catalysis

Agostinho Luís Pereira Lemos ^{1,*†}, Laura Trump ^{1,2,†}, Bénédicte Lallemand ², Patrick Pasau ², Joël Mercier ², Christian Lemaire ¹, Jean-Christophe Monbaliu ³, Christophe Genicot ^{2,*} and André Luxen ^{1,*}

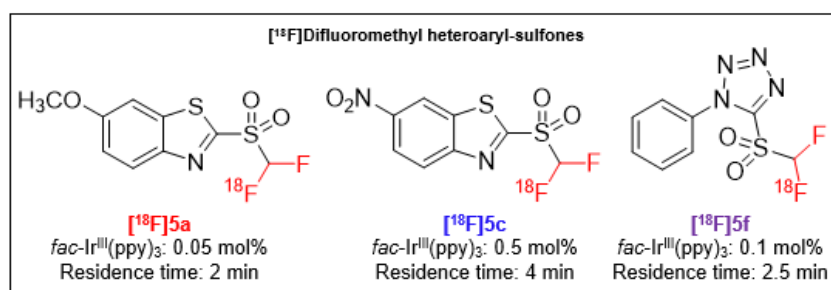
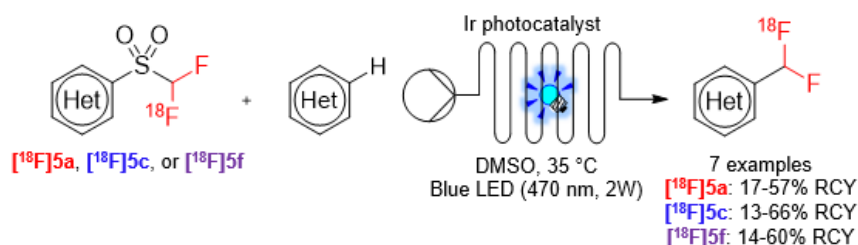
¹ GIGA-Cyclotron Research Centre In Vivo Imaging, University of Liège, 8 Allée du Six Août, Building B30, Sart Tilman, 4000 Liège, Belgium; laura.trump@ucb.com (L.T.); christian.lemaire@uliege.be (C.L.)

² Global Chemistry, UCB NewMedicines, UCB Biopharma SPRL, 1420 Braine-l'Alleud, Belgium; benedicte.lallemand@ucb.com (B.L.); patrick.pasau@ucb.com (P.P.); joel.mercier@ucb.com (J.M.)

³ Center for Integrated Technology and Organic Synthesis, Research Unit MolSys, University of Liège, (Sart Tilman), B-4000, Liège, Belgium; jc.monbaliu@uliege.be

* Correspondence: agostinholemos43@gmail.com (A.L.P.L.); christophe.genicot@ucb.com (C.G.); aluxen@uliege.be (A.L.)

† The authors contributed equally to this work



Chapter IV

1. Introduction.....	187
2. Results and Discussion	
2.1. Chemistry	
2.1.1. Synthesis of the Difluoromethyl Heteroaryl-Sulfones 5a–5f	190
2.2. Radiochemistry	
2.2.1. Radiosyntheses of the [¹⁸ F]Difluoromethyl Heteroaryl-Sulfones [¹⁸ F] 5a– [¹⁸ F] 5f	191
2.2.2. Automated Radiosyntheses of the [¹⁸ F]Difluoromethyl Heteroaryl-Sulfones [¹⁸ F] 5a , [¹⁸ F] 5c , and [¹⁸ F] 5f	194
2.2.3. ¹⁸ F-Difluoromethylation of Heteroarenes with Sulfones [¹⁸ F] 5a , [¹⁸ F] 5c , and [¹⁸ F] 5f	198
3. Material and methods	
3.1. Chemistry.....	202
3.1.1. General Procedure for the Synthesis of Difluoromethyl Heteroaryl-Sulfides (4a–4f).....	203
3.1.2. General Procedure for the Synthesis of Difluoromethyl Heteroaryl-Sulfones (5a–5f).....	205
3.1.3. General Procedure for the Synthesis of Bromofluoromethyl Heteroaryl- Sulfides (6a–6f).....	206
3.1.4. General Procedure for the Synthesis of the Difluoromethylated Heteroarenes (8a–8g).....	208
3.2. Radiochemistry.....	208
3.2.1. Fully Automated Radiosyntheses of 2-[¹⁸ F]((difluoromethyl)sulfonyl)-6- methoxybenzo[<i>d</i>]thiazole ([¹⁸F]5a), 2-[¹⁸ F]((difluoromethyl)sulfonyl)-6- nitrobenzo[<i>d</i>]thiazole ([¹⁸F]5c), and 5-[¹⁸ F]((difluoromethyl)sulfonyl)-1-phenyl- 1 <i>H</i> -tetrazole ([¹⁸F]5f).....	209
3.2.2. Low-Activity ¹⁸ F-Labeling Experiments in the Precursors 6a–6f	211
3.2.3. Isolation and Determination of the Molar Activity of [¹⁸ F] 5a , [¹⁸ F] 5c , and [¹⁸ F] 5f	212
3.2.4. General Procedure for the C–H ¹⁸ F-Difluoromethylation of the Heteroarenes 7a–7g with the [¹⁸ F]Difluoromethyl Heteroaryl-Sulfones [¹⁸ F] 5a , [¹⁸ F] 5c , and [¹⁸ F] 5f	212
4. Conclusions.....	213
5. Supplementary Information	
5.1. NMR spectra of the compounds 4a–4f , 5a–5f , and 6a–6f	214
5.2. Radiochemistry.....	241
5.2.1. Synthesis of [¹⁸ F]2-((Difluoromethyl)thio)-6-methoxybenzo[<i>d</i>]thiazole ([¹⁸F]4a).....	241
5.2.2. Synthesis of [¹⁸ F]2-((Difluoromethyl)thio)-5-methoxybenzo[<i>d</i>]thiazole ([¹⁸F]4b).....	244

5.2.3. Synthesis of [¹⁸ F]2-((Difluoromethyl)thio)-6-nitrobenzo[<i>d</i>]thiazole ([¹⁸F]4c).....	245
5.2.4. Synthesis of [¹⁸ F]2-((Difluoromethyl)thio)-5-nitrobenzo[<i>d</i>]thiazole ([¹⁸F]4d).....	246
5.2.5. Synthesis of [¹⁸ F]2-((Difluoromethyl)thio)-1-methyl-1 <i>H</i> -benzo[<i>d</i>]imidazole ([¹⁸F]4e).....	248
5.2.6. Synthesis of [¹⁸ F]5-((Difluoromethyl)thio)-1-phenyl-1 <i>H</i> -tetrazole ([¹⁸F]4f).....	249
5.2.7. Synthesis of [¹⁸ F]2-((Difluoromethyl)sulfonyl)-6-methoxybenzo[<i>d</i>]thiazole ([¹⁸F]5a).....	250
5.2.8. Synthesis of [¹⁸ F]2-((Difluoromethyl)sulfonyl)-5-methoxybenzo[<i>d</i>]thiazole ([¹⁸F]5b).....	253
5.2.9. Synthesis of [¹⁸ F]2-((Difluoromethyl)sulfonyl)-6-nitrobenzo[<i>d</i>]thiazole ([¹⁸F]5c).....	255
5.2.10. Synthesis of [¹⁸ F]2-((Difluoromethyl)sulfonyl)-5-nitrobenzo[<i>d</i>]thiazole ([¹⁸F]5d).....	256
5.2.11. Synthesis of [¹⁸ F]2-((Difluoromethyl)sulfonyl)-1-methyl-1 <i>H</i> -benzo[<i>d</i>]imidazole ([¹⁸F]5e).....	257
5.2.12. Synthesis of [¹⁸ F]5-((Difluoromethyl)sulfonyl)-1-phenyl-1 <i>H</i> -tetrazole ([¹⁸F]5f).....	259
5.3. Two-Step Radiosynthesis of the [¹⁸ F]Difluoromethyl Heteroaryl-Sulfones [¹⁸F]5a - [¹⁸F]5f from the Precursors 6a - 6f	260
5.4. Fully Automated Radiosynthesis of the Labeled Compounds [¹⁸F]5a , [¹⁸F]5c , and [¹⁸F]5f	262
5.5. Calibration Curves of the Difluoromethyl Heteroaryl-Sulfones 5a , 5c , and 5f for Determination of the Molar Activity of [¹⁸F]5a , [¹⁸F]5c , and [¹⁸F]5f	263
5.6. Photocatalytic C-H ¹⁸ F-Difluoromethylation of Heteroarenes with the Reagents [¹⁸F]5a , [¹⁸F]5c , and [¹⁸F]5f	266
5.6.1. Synthesis of [¹⁸ F]2-Amino-8-(difluoromethyl)-9-((2-hydroxyethoxy)methyl)-9 <i>H</i> -purin-6-ol ([¹⁸F]8e).....	267
5.6.2. Synthesis of [¹⁸ F]2-(Difluoromethyl)-4-methyl-1 <i>H</i> -pyrrolo[2,3- <i>b</i>]pyridine ([¹⁸F]8aa) and [¹⁸ F]6-(Difluoromethyl)-4-methyl-1 <i>H</i> -pyrrolo[2,3- <i>b</i>]pyridine ([¹⁸F]8ab).....	270
5.6.3. Synthesis of [¹⁸ F]3-(Difluoromethyl)-6-methyl-1 <i>H</i> -pyrazolo[3,4- <i>b</i>]pyridine ([¹⁸F]8ba) and [¹⁸ F]4-(Difluoromethyl)-6-methyl-1 <i>H</i> -pyrazolo[3,4- <i>b</i>]pyridine ([¹⁸F]8bb).....	272
5.6.4. Synthesis of [¹⁸ F]4-(Difluoromethyl)-2-methyl-5,8-dihydropyrido[2,3- <i>d</i>]pyrimidin-7(6 <i>H</i>)-one ([¹⁸F]8c).....	275
5.6.5. Synthesis of [¹⁸ F]Ethyl 2-(difluoromethyl)isonicotinate ([¹⁸F]8da) and [¹⁸ F]Ethyl 3-(difluoromethyl)isonicotinate ([¹⁸F]8db).....	277
5.6.6. Synthesis of [¹⁸ F]4-Chloro-2-(difluoromethyl)- <i>N</i> -(4,5-dihydro-1 <i>H</i> -imidazol-2-yl)-6-methoxypyrimidin-5-amine ([¹⁸F]8f).....	279

5.6.7. Synthesis of [¹⁸ F]8-(Difluoromethyl)-3,7-dimethyl-1-(5-oxohexyl)-3,7-dihydro-1 <i>H</i> -purine-2,6-dione ([¹⁸F]8g).....	281
References.....	283

Radical C-H ¹⁸F-Difluoromethylation of Heteroarenes with [¹⁸F]Difluoromethyl Heteroaryl-Sulfones by Visible Light Photoredox Catalysis

Abstract: The ¹⁸F-labeling of CHF₂ groups has been recently studied in radiopharmaceutical chemistry owing to the favorable nuclear and physical characteristics of the radioisotope ¹⁸F for positron emission tomography (PET). Following up on the reported efficiency of the [¹⁸F]difluoromethyl benzothiazolyl-sulfone (**[¹⁸F]1**) as a ¹⁸F-difluoromethylating reagent, we investigated the influence of structurally-related [¹⁸F]difluoromethyl heteroaryl-sulfones in the reactivity toward the photoredox C–H ¹⁸F-difluoromethylation of heteroarenes under continuous-flow conditions. In the present work, six new [¹⁸F]difluoromethyl heteroaryl-sulfones **[¹⁸F]5a**–**[¹⁸F]5f** were prepared and, based on the overall radiochemical yields (RCYs), three of these reagents (**[¹⁸F]5a**, **[¹⁸F]5c**, and **[¹⁸F]5f**) were selected for the fully automated radiosynthesis on a FASTlab™ synthesizer (GE Healthcare) at high level of starting radioactivity. Subsequently, their efficiency as ¹⁸F-difluoromethylating reagents was evaluated using the antiherpetic drug acyclovir as a model substrate. Our results showed that the introduction of molecular modifications in the structure of **[¹⁸F]1** influenced the amount of *fac*-Ir^{III}(ppy)₃ and the residence time needed to ensure a complete C–H ¹⁸F-difluoromethylation process. The photocatalytic C–H ¹⁸F-difluoromethylation reaction with the reagents **[¹⁸F]5a**, **[¹⁸F]5c**, and **[¹⁸F]5f** was extended to other heteroarenes. Radical-trapping experiments demonstrated the likely involvement of radical species in the C–H ¹⁸F-difluoromethylation process.

Keywords: fluorine-18; difluoromethylation; heteroarenes; visible light; photocatalysis

1. Introduction

The fluorine-18 (¹⁸F) isotope has been regarded the “radionuclide of choice” due to its suitable physical and nuclear features for *in vivo* positron emission tomography (PET) imaging in living subjects [1–4]. The unique sensitivity of PET makes this technique appropriate for the study of absorption, distribution, metabolism, and excretion (ADME) properties of radiopharmaceuticals and the evaluation of their pharmacodynamic profile. In addition, PET technology has proven highly valuable in the observation of biochemical and physiological changes that may take place before the anatomical alterations of a certain disease are detected [5–8]. The suitability of the ¹⁸F radioisotope in PET has encouraged radiochemists to invest much effort in the development of efficient ¹⁸F-fluorination and ¹⁸F-fluoroalkylation strategies [9–19].

Among the existing fluorinated motifs, the difluoromethyl (CHF₂) group has recently attracted considerable attention in medicinal chemistry due to its lipophilic hydrogen-bond donor properties [20–24]. The CHF₂ substitution may offer a viable alternative to conventional hydrogen-bond donors (e.g., hydroxy (OH) and thiol (SH) groups) in terms of lipophilicity, cell membrane permeability, and metabolic stability,

thus modulating the pharmacological activity of pharmaceuticals and agrochemicals [25–31]. Despite the recent progresses in the preparation of CHF₂-containing derivatives in organofluorine chemistry, methodologies for the ¹⁸F-labeling of CHF₂ groups are still relatively scarce. Most labeling strategies relied on the radiosynthesis of [¹⁸F]aryl-CHF₂ derivatives *via* ¹⁸F-fluorination of suitable precursors with the electrophilic reagent [¹⁸F]Selectfluor *bis*(triflate) [32] or with the cyclotron-produced [¹⁸F]fluoride by aliphatic nucleophilic substitution [33–36]. Furthermore, the resulting [¹⁸F]aryl-CHF₂ derivatives are afforded in low-to-moderate molar activities (up to 22 GBq·μmol⁻¹). The production of radiotracers with high molar activity is mandatory for PET imaging studies, especially for targeting low-density biomacromolecules. Recently, we disclosed an innovative method reporting the photoredox late-stage C–H ¹⁸F-difluoromethylation of *N*-containing heteroarenes with the [¹⁸F]difluoromethyl benzothiazolyl-sulfone ([¹⁸F]**1**) with improved molar activity [*A*_m (**1**)] = 54 ± 7 GBq·μmol⁻¹] [37,38] (Figure 1A).

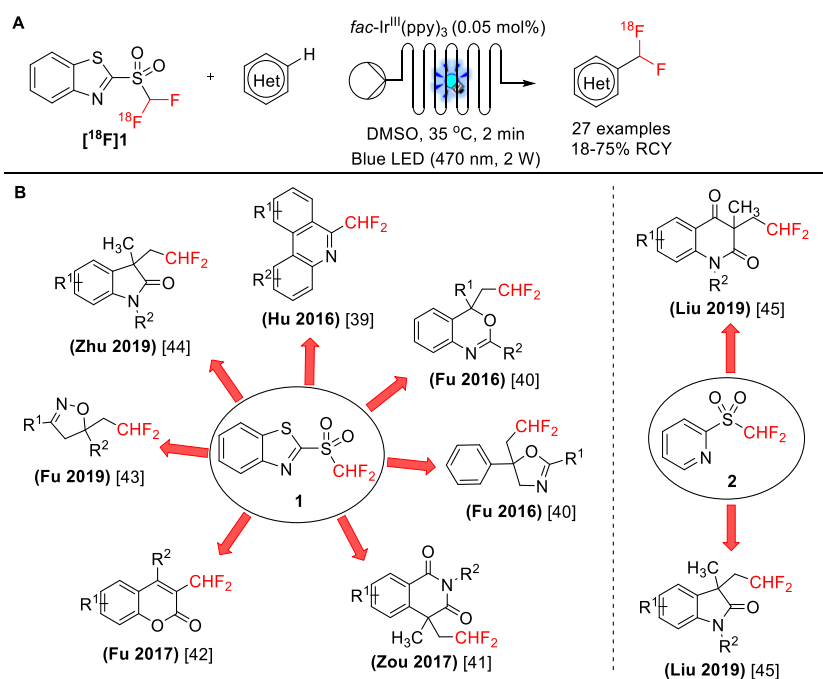


Figure 1. (A) Photoredox C–H ¹⁸F-difluoromethylation of *N*-containing heteroarenes with [¹⁸F]difluoromethyl benzothiazolyl-sulfone (**1**), under continuous-flow conditions [37,38]. (B) Application of the difluoromethyl sulfones **1** and **2** in the preparation of heterocycles of biological relevance, under visible light photoredox catalysis [39–45].

In non-radioactive chemistry, difluoromethyl heteroaryl-sulfones have been widely implemented in photoredox catalyzed C–H difluoromethylation processes because of the ability of these compounds to be reduced to CHF₂ radicals in the presence of appropriate photocatalysts in their photoexcited state. In 2016, Hu and Fu reported the use of difluoromethyl benzothiazolyl-sulfone (**1**) in the radical difluoromethylation of biphenyl isocyanides [39] and olefinic amides [40],

respectively. The reagent **1** was also employed in the preparation of CHF₂-substituted heterocycles of biological relevance, including isoquinolinediones [41], coumarins [42], isoxazolines [43], and oxindoles [44]. In 2019, Liu and co-workers developed a procedure for difluoromethylation of *N*-arylacrylamides with the reagent difluoromethyl pyridyl-sulfone (**2**), under visible light photoredox conditions [45] (Figure 1B). Based on the effectiveness of the sulfone [¹⁸F]**1** as ¹⁸F-difluoromethylating reagent [37,38], we intended to study the influence of certain molecular modifications in the structure of [¹⁸F]**1** on the reactivity towards the C–H ¹⁸F-difluoromethylation of *N*-heteroarenes. The molecular modifications consisted in the introduction of a single electron-donating (OCH₃) (Figure 2A) or electron-withdrawing (NO₂) (Figure 2B) substituent (Figure 2B) either at position 5 or 6 of the benzothiazolyl ring and in the alteration of the original benzothiazolyl moiety to other heteroaryl rings (*N*-methylbenzimidazolyl and *N*-phenyl-tetrazolyl rings) (Figure 2C). In this work, we opted to perform the radiosyntheses of structurally-related [¹⁸F]difluoromethyl heteroaryl-sulfones and subsequently evaluate their efficiency in the photoredox C–H ¹⁸F-difluoromethylation of heteroarenes, under continuous-flow conditions as reported previously [37]. To the best of our knowledge, the effectiveness of the non-radioactive references of these novel [¹⁸F]difluoromethyl heteroaryl-sulfones in photoredox C–H difluoromethylation has never been described in the literature.

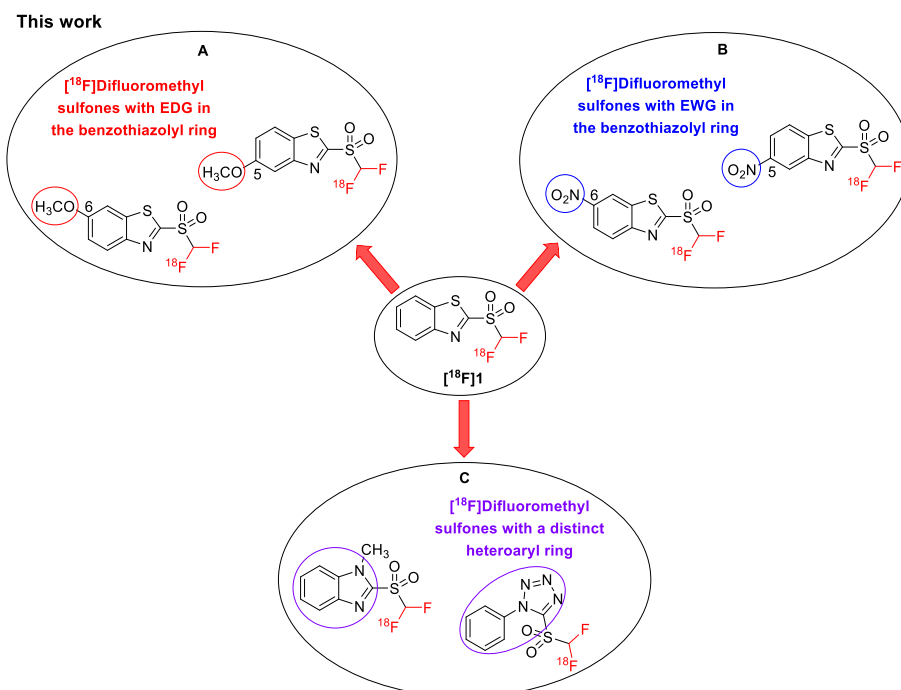


Figure 2. Molecular modifications performed on [¹⁸F]**1**: introduction of a single electron-donating (OCH₃) (**A**) or electron-withdrawing (NO₂) (**B**) substituent either at position 5 or 6 of the benzothiazolyl ring, and modification of the original benzothiazolyl moiety to other heteroaryl rings (**C**).

2. Results and Discussion

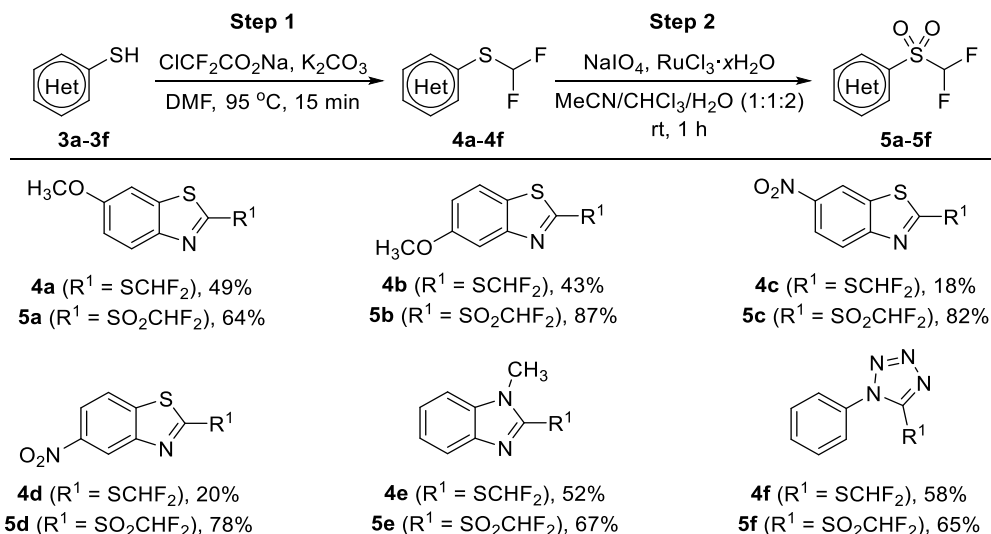
2.1. Chemistry

2.1.1. Synthesis of the Difluoromethyl Heteroaryl-Sulfones 5a–5f

We initially performed the organic synthesis of the difluoromethyl heteroaryl-sulfones **5a–5f** as non-radioactive standards for confirmation of the identity of the ^{18}F -labeled compounds. In order to prepare the difluoromethyl heteroaryl-sulfones **5a–5f**, we considered a two-step procedure involving the difluoromethylation of the heteroaryl-thiols **3a–3f** to afford the difluoromethyl heteroaryl-sulfides **4a–4f**. Oxidation of the sulfides **4a–4f** would lead to the sulfones **5a–5f** (Scheme 1).

Inspired by the methodologies formerly described by Akita [46] and Jubault [47], the difluoromethylation of the heteroaryl-thiols **3a–3f** using sodium chlorodifluoroacetate ($\text{ClCF}_2\text{CO}_2\text{Na}$) and potassium carbonate (K_2CO_3) provided the corresponding sulfides **4a–4f** in moderate yields (Scheme 1, 18–58% yields). The difluoromethyl heteroaryl-sulfones **5a–5f** were successfully achieved by oxidation of the sulfides **4a–4f** using the oxidizing agent sodium (meta)periodate (NaIO_4) and ruthenium (III) chloride hydrate ($\text{RuCl}_3 \cdot x\text{H}_2\text{O}$) (Scheme 1, 64–87% yields).

The structure elucidation of the compounds **4a–4f** and **5a–5f** was established on the basis of high-resolution mass spectrometry (HRMS) and nuclear magnetic resonance (NMR) techniques (Figures S1–S36).

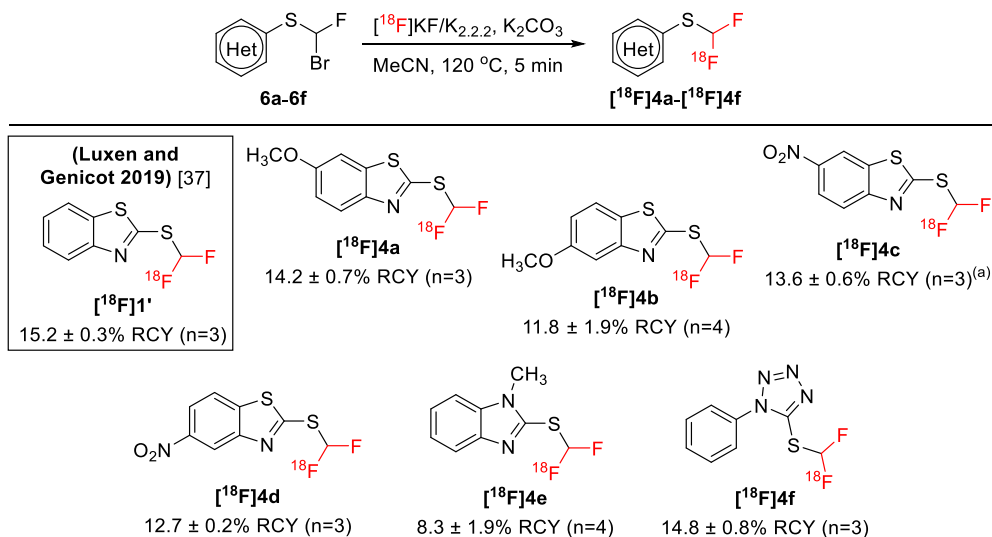


Scheme 1. Synthesis of the difluoromethyl heteroaryl-sulfides **4a–4f** and the heteroaryl-sulfones **5a–5f**. **Step 1:** **3a–3f** (3.0 mmol), sodium chlorodifluoroacetate (6.0 mmol), K_2CO_3 (4.5 mmol), DMF (10 mL), 95 °C, 15 min. **Step 2:** **4a–4f** (1.0 mmol), sodium (meta)periodate (5.0 mmol), ruthenium (III) chloride hydrate (0.05 mmol), MeCN (2 mL), CHCl_3 (2 mL), H_2O (4 mL), rt, 1 h. All reaction yields are of isolated products.

2.2. Radiochemistry

2.2.1. Radiosyntheses of the [¹⁸F]Difluoromethyl Heteroaryl-Sulfones [¹⁸F]5a–[¹⁸F]5f

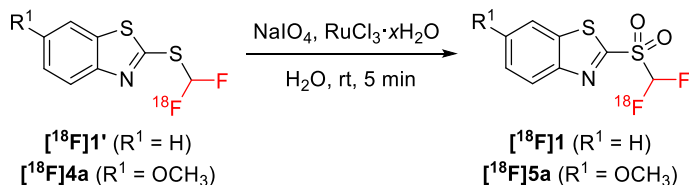
We planned the radiosyntheses of the sulfones [¹⁸F]5a–[¹⁸F]5f following a two-step methodology previously described in the literature [37]. This multi-step strategy involved the initial nucleophilic ¹⁸F-fluorination of the bromofluoromethyl heteroaryl-sulfides **6a–6f** and subsequent oxidation of the [¹⁸F]difluoromethyl heteroaryl-sulfides [¹⁸F]4a–[¹⁸F]4f. The precursors **6a–6f** were prepared by a one-step bromofluoromethylation of the heteroaryl-thiols **3a–3f** with dibromofluoromethane (Br₂CFH), under basic conditions (see *Materials and Methods* section for more details). The structure elucidation of the compounds **6a–6f** was established on the basis of HRMS and NMR techniques (Figures S37-S54). Low starting radioactivity experiments were performed in order to investigate the propensity of the newly synthesized precursors to undergo the expected nucleophilic ¹⁸F-fluorination, under the same ¹⁸F-labeling conditions used to prepare the [¹⁸F]difluoromethyl benzothiazolyl-sulfide ([¹⁸F]1') [37]. To minimize the radiation exposure, the ¹⁸F-labeling reactions were conducted in a commercially available FASTlab™ module (GE Healthcare) placed in a shielded hotcell. An aliquot of a solution of [¹⁸F]fluoride in [¹⁸O]water ([¹⁸O]H₂O) (150-200 MBq) was passed through a quaternary methyl ammonium (QMA) carbonate cartridge for [¹⁸F]fluoride trapping. Subsequent elution of the [¹⁸F]fluoride using K_{2.2.2}/K₂CO₃-based eluent and azeotropic drying in a cyclic olefin copolymer (COC) reactor furnished the “naked” [¹⁸F]fluoride readily available for the nucleophilic ¹⁸F-fluorination. Precursors **6c** (0.02 mmol) and **6a**, **6b**, **6d–6f** (0.04 mmol) in acetonitrile (MeCN, 1 mL) were added to the dry [¹⁸F]fluoride and the ¹⁸F-labeling reaction was conducted at 120 °C for 5 min. The crude reaction mixture was pre-purified using a Sep-Pak® C18 Plus Short cartridge to eliminate the unreacted [¹⁸F]fluoride and other polar impurities. Only for RCY determination, the cartridge-purified [¹⁸F]4a–[¹⁸F]4f were then eluted with MeCN [Scheme 2: 6 examples, 8.3-14.8% RCY (decay-corrected at the start-of-synthesis (SOS))]. No significant differences in RCYs of the radiosyntheses of the cartridge-purified [¹⁸F]1' and [¹⁸F]4a–[¹⁸F]4f were remarked. These results suggest that the introduction of either electron-donating or electron-withdrawing groups on the benzothiazolyl ring, or the alteration of the original benzothiazolyl moiety to other heteroaryl rings did not have a meaningful impact in the reactivity of the precursors towards the ¹⁸F-labeling reaction.



Scheme 2. Radiosyntheses of [¹⁸F]difluoromethyl heteroaryl-sulfides (**[¹⁸F]4a–[¹⁸F]4f**). Standard conditions: **6a**, **6b**, **6d–6f** (0.04 mmol), [¹⁸F]KF (150–200 MBq), K₂CO₃ (0.01 mmol), K_{2.2.2} (0.02 mmol), MeCN (1 mL), 120 °C, 5 min. ^(a) ¹⁸F-Labeling reaction of **6c** was performed on a 0.02 mmol scale. All radiochemical yields (RCYs) were determined based on the activity of cartridge-purified [¹⁸F]4a–[¹⁸F]4f, their radio-thin layer chromatography (radio-TLC) and their radio-ultra performance liquid chromatography (radio-UPLC) purities, and the starting radioactivity. All RCYs were decay-corrected at the start-of-synthesis (SOS).

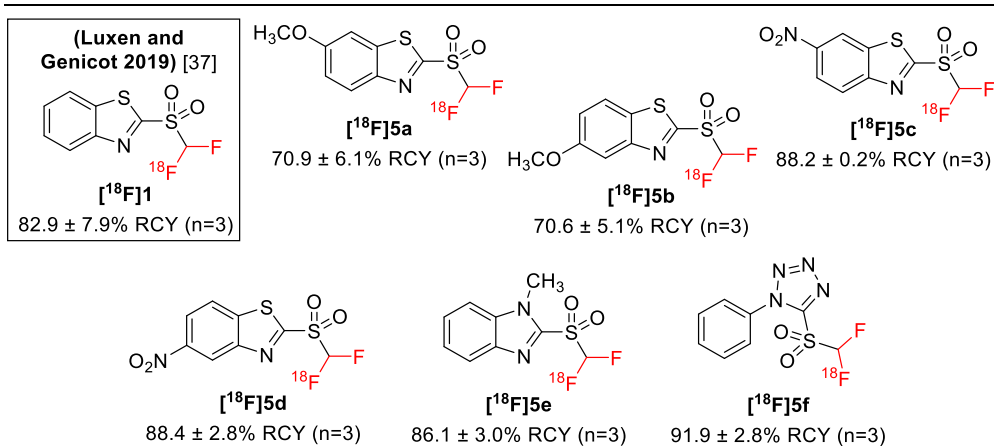
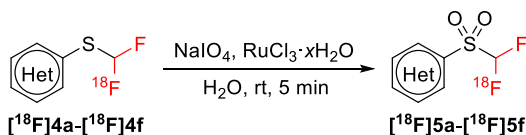
Afterward, the oxidation of the cartridge-purified [¹⁸F]4a–[¹⁸F]4f was undergone in the Sep-Pak® C18 Plus Short cartridge, upon the addition of an aqueous solution of the NaIO₄ and RuCl₃·xH₂O, at room temperature for 5 min. Based on the previously reported oxidation conditions for the radiosynthesis of [¹⁸F]1 (Table 1, Entry 1) [37], the labeled compound [¹⁸F]5a was synthesized from the cartridge-purified [¹⁸F]4a in 32.1% RCY (Table 1, Entry 2). However, no complete conversion of [¹⁸F]4a was observed. Optimization studies were then conducted to uncover the most suitable reaction conditions to achieve the complete oxidation of [¹⁸F]4a. A two-fold increase in the amount of RuCl₃·xH₂O resulted in a significant improvement of the oxidation efficiency (Table 1, Entry 3). By raising the amount of NaIO₄ from 0.24 mmol to 0.72 mmol, the [¹⁸F]4a was fully consumed and the labeled compound [¹⁸F]5a was isolated in 70.9 ± 6.1% RCY, after cartridge purification (Table 1, Entry 4).

With the optimized conditions in hand, the oxidation protocol was extended to the other [¹⁸F]difluoromethyl heteroaryl-sulfides (**[¹⁸F]4b–[¹⁸F]4f**), furnishing the labeled compounds **[¹⁸F]5b–[¹⁸F]5f** in good-to-excellent RCY (70.6–91.9% RCY, Scheme 3). The ultra performance liquid chromatography (UPLC) retention times of the labeled compounds [¹⁸F]4a–[¹⁸F]4f (Figures S56–S67) and [¹⁸F]5a–[¹⁸F]5f (Figures S69–S80) were compliant with those of the respective non-radioactive authentic references.

Table 1. Optimization of the oxidation conditions of the [^{18}F]4a^(a)

Entry	Substrate	NaIO ₄ (mmol)	RuCl ₃ ·xH ₂ O (mmol)	Conversion (%) ^(b)	RCY (%) ^(c)
1	[^{18}F]1'	0.24	0.008	100	82.9 ± 7.9 (n = 3)
2	[^{18}F]4a	0.24	0.008	35	32.1
3	[^{18}F]4a	0.24	0.016	64	59.6
4	[^{18}F]4a	0.72	0.016	100	70.9 ± 6.1 (n = 3)

^(a) Standard conditions: NaIO₄, RuCl₃·xH₂O, H₂O (1 mL), rt, 5 min. ^(b) UPLC conversion of the substrate [^{18}F]4a. ^(c) All RCYs were determined based on the activity of cartridge-purified [^{18}F]4a and [^{18}F]5a, their radio-TLC and their radio-UPLC purities. All RCYs were decay-corrected at the SOS.

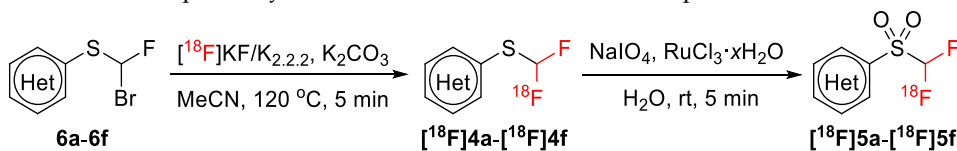


Scheme 3. Radiosyntheses of [^{18}F]difluoromethyl heteroaryl-sulfones ($[\text{}^{18}\text{F}]\mathbf{5a}$ – $[\text{}^{18}\text{F}]\mathbf{5f}$). Standard conditions: [$^{18}\text{F}]\mathbf{4a}$ – $[\text{}^{18}\text{F}]\mathbf{4f}$ (10–20 MBq), sodium (meta)periodate (0.72 mmol), ruthenium (III) chloride hydrate (0.016 mmol), H₂O (1 mL), rt, 5 min. All RCYs were determined based on the activity of cartridge-purified [$^{18}\text{F}]\mathbf{4a}$ – $[\text{}^{18}\text{F}]\mathbf{4f}$ and [$^{18}\text{F}]\mathbf{5a}$ – $[\text{}^{18}\text{F}]\mathbf{5f}$, their radio-TLC and their radio-UPLC purities. All RCYs were decay-corrected at the SOS.

According to the results presented in Table 2, the best RCYs for the two-step radiosyntheses of the cartridge-purified [$^{18}\text{F}]\mathbf{5a}$ – $[\text{}^{18}\text{F}]\mathbf{5f}$ at low level of starting radioactivity (90–150 MBq) were attained with the electron-rich benzothiazolyl

derivative [^{18}F]**5a** [RCY (^{18}F]**5a**) > RCY (^{18}F]**5b**), Table 2], the electron-poor derivative [^{18}F]**5c** [RCY (^{18}F]**5c**) > RCY (^{18}F]**5d**), Table 2], and the *N*-phenyl-tetrazolyl derivative [^{18}F]**5f** [RCY (^{18}F]**5f**) > RCY (^{18}F]**5e**), Table 2]. These compounds were then selected for the investigation of their reactivity towards the photocatalytic ^{18}F -difluoromethylation of *N*-containing heteroarenes. In order to circumvent any potential radioprotection issues, a fully automated process involving the two-step radiosyntheses of [^{18}F]**5a**, [^{18}F]**5c**, or [^{18}F]**5f** and a high performance liquid chromatography (HPLC) purification was implemented on a FASTlab™ synthesizer (GE Healthcare) for the preparation of the purified ^{18}F -labeled compounds.

Table 2. Two-step radiosyntheses of the [^{18}F]**5a**–[^{18}F]**5f** from the precursors **6a–6f**.



Entry	[^{18}F]Difluoromethyl heteroaryl-sulfones	RCY (%) ^(a)
1	[^{18}F] 5a	10.1 ± 0.8 (n = 3)
2	[^{18}F] 5b	8.3 ± 0.6 (n = 3)
3	[^{18}F] 5c	12 ± 0.5 (n = 3)
4	[^{18}F] 5d	11.2 ± 0.3 (n = 3)
5	[^{18}F] 5e	7.2 ± 0.2 (n = 3)
6	[^{18}F] 5f	13.6 ± 0.4 (n = 3)

^(a) All RCYs were determined based on the activity of cartridge-purified [^{18}F]**5a**–[^{18}F]**5f**, their radio-TLC, their radio-UPLC purities, and the starting radioactivity. All RCYs were decay-corrected at the SOS.

2.2.2. Automated Radiosyntheses of the [^{18}F]Difluoromethyl Heteroaryl-Sulfones [^{18}F]**5a**, [^{18}F]**5c**, and [^{18}F]**5f**

The automated sequence for the radiosyntheses of [^{18}F]**5a**, [^{18}F]**5c**, and [^{18}F]**5f** involved the following steps: (1) machine and cassette tests (presynthesis, 7 min); (2) [^{18}F]fluoride recovery, trapping, elution, and azeotropic drying (12 min); (3) transfer of the precursors **6a**, **6c**, and **6f** to the reactor and ^{18}F -labeling (9 min); (4) dilution of the crude product [^{18}F]**4a**, [^{18}F]**4c**, and [^{18}F]**4f** with water, and trapping on a 'C18 Plus Short cartridge (2 min); (5) transfer of the NaIO_4 and $\text{RuCl}_3 \cdot x\text{H}_2\text{O}$ and oxidation on a 'C18 cartridge (6 min); (6) elution of the crude [^{18}F]**5a**, [^{18}F]**5c**, and [^{18}F]**5f** with MeCN to the reactor, dilution with water, and injection on the semi-preparative HPLC loop (4 min); (7) HPLC purification and collection of the purified [^{18}F]**5a** (26 min), [^{18}F]**5c** (23 min), and [^{18}F]**5f** (18 min); (8) dilution and trapping of the ^{18}F -labeled compounds on a 'C18 Plus Short cartridge followed by elution with anhydrous dimethyl sulfoxide (DMSO) (14 min). A more detailed description of the sequence of events comprising the multi-step radiosyntheses of the [^{18}F]**5a**, [^{18}F]**5c**, and [^{18}F]**5f** is provided in the

Materials and Methods section. The reagents and materials used throughout the radiochemical process were prepared and positioned in the FASTlab™ manifold as depicted in Table S23 and illustrated in Figure 3.

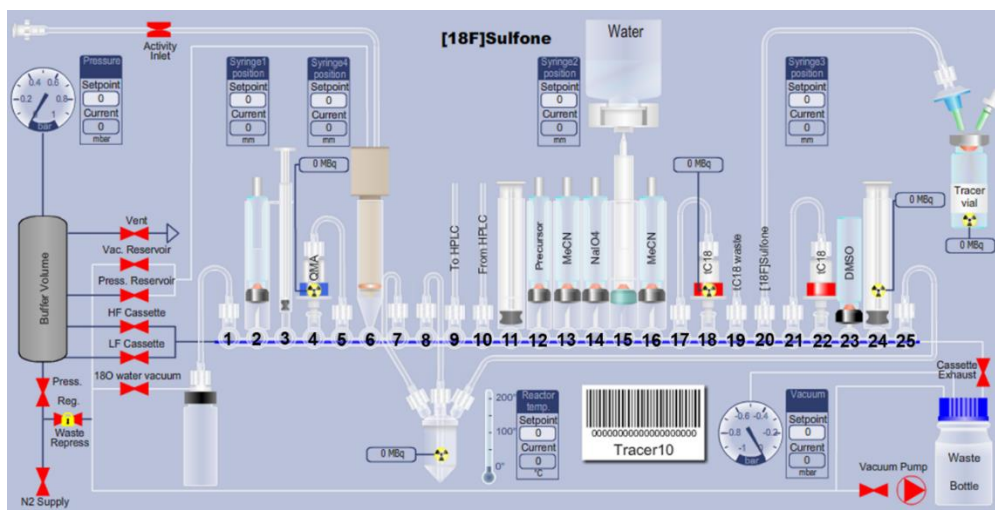
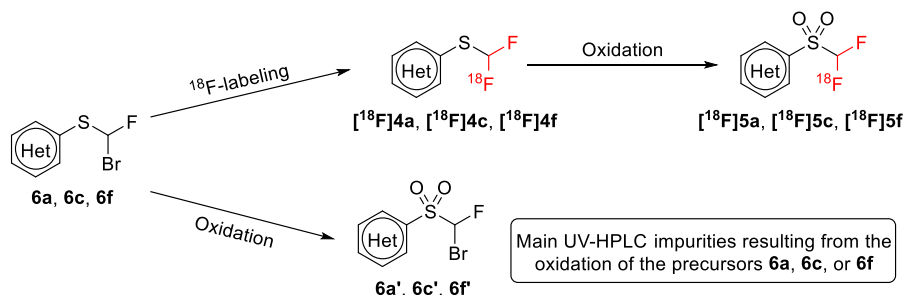


Figure 3. Layout of the FASTlab™ cassette for the radiosyntheses of the labeled compounds $[^{18}\text{F}]5\text{a}$, $[^{18}\text{F}]5\text{c}$, and $[^{18}\text{F}]5\text{f}$.

A HPLC purification of the crude $[^{18}\text{F}]5\text{a}$, $[^{18}\text{F}]5\text{c}$, and $[^{18}\text{F}]5\text{f}$ was implemented on a reverse-phase HPLC column. The purity of these newly synthesized compounds revealed to be critical for the examination of their efficiency towards the following photocatalytic ^{18}F -difluoromethylation reaction. In fact, during the radiosyntheses of the sulfones $[^{18}\text{F}]5\text{a}$, $[^{18}\text{F}]5\text{c}$, and $[^{18}\text{F}]5\text{f}$, the oxidation of the precursors **6a**, **6c**, and **6f** represented an important side reaction, leading to the formation of the corresponding bromofluoromethyl heteroaryl-sulfones (**6a'**, **6c'**, and **6f'**, Scheme 4).



Scheme 4. Formation of the by-products **6a'**, **6c'**, and **6f'** by oxidation of the precursors **6a**, **6c**, and **6f**, respectively.

The use of a mobile phase of MeCN/H₂O (40/60, v/v) in isocratic mode enabled an effective separation between the radiotracers $[^{18}\text{F}]5\text{a}$, $[^{18}\text{F}]5\text{c}$, and $[^{18}\text{F}]5\text{f}$ and the respective UV by-products, particularly the bromofluoromethyl heteroaryl-sulfones **6a'**, **6c'**, and **6f'**. The radioactive peaks corresponding to the radiotracers $[^{18}\text{F}]5\text{a}$,

[¹⁸F]5c, and [¹⁸F]5f were collected after 22 min (Figure 4), 19 min (Figure 5), and 15 min (Figure 6), respectively, and formulated on the same FASTlab™ cassette by using a preconditioned Sep-Pak® C18 Plus Short cartridge. The trapped [¹⁸F]5a, [¹⁸F]5c, and [¹⁸F]5f were then eluted with anhydrous DMSO using reverse flow and recovered in a 4 mL-sealed vial.

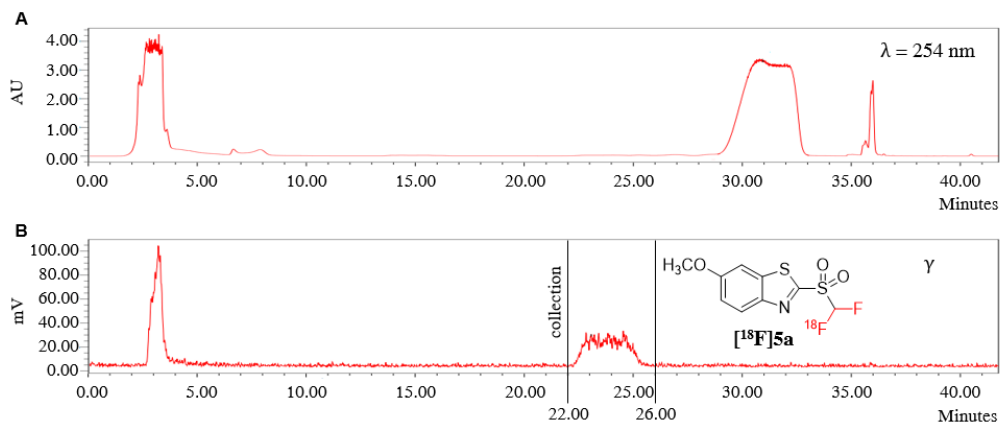


Figure 4. (A) Ultraviolet-high performance liquid chromatography (UV-HPLC) purification profile of the crude [¹⁸F]5a. (B) Radio-HPLC purification profile of the crude [¹⁸F]5a. Note: the appearance of broad flat-topped peaks in UV-HPLC chromatogram is derived from a saturation of the UV detector by the injecting crude product [¹⁸F]5a. XBridge® BEH C18 OBD™ Prep column (130 Å, 5 μm, 10 mm × 250 mm; Waters, Milford, MA, USA); MeCN/H₂O (40/60, v/v) in isocratic mode (flow rate: 5 mL·min⁻¹).

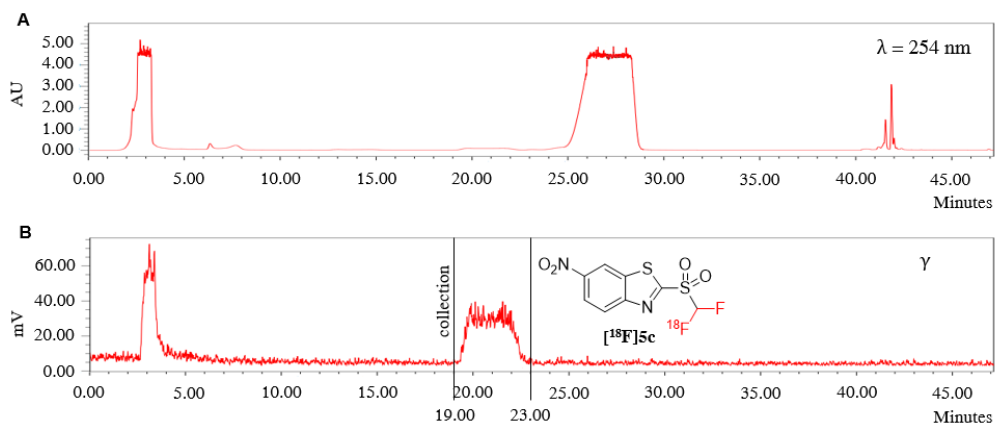


Figure 5. (A) UV-HPLC purification profile of the crude [¹⁸F]5c. (B) Radio-HPLC purification profile of the crude [¹⁸F]5c. Note: the appearance of broad flat-topped peaks in UV-HPLC chromatogram is derived from a saturation of the UV detector by the injecting crude product [¹⁸F]5c. XBridge® BEH C18 OBD™ Prep column (130 Å, 5 μm, 10 mm × 250 mm; Waters, Milford, MA, USA); MeCN/H₂O (40/60, v/v) in isocratic mode (flow rate: 5 mL·min⁻¹).

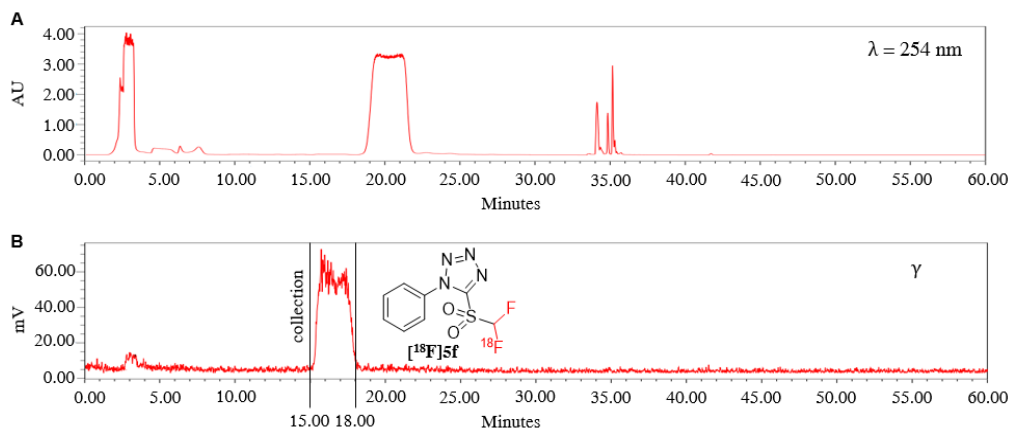


Figure 6. (A) UV-HPLC purification profile of the crude $[^{18}\text{F}]\mathbf{5f}$. (B) Radio-HPLC purification profile of the crude $[^{18}\text{F}]\mathbf{5f}$. Note: the appearance of broad flat-topped peaks in UV-HPLC chromatogram is derived from a saturation of the UV detector by the injecting crude product $[^{18}\text{F}]\mathbf{5f}$. XBridge[®] BEH C18 OBD[™] Prep column (130 Å, 5 μm , 10 mm \times 250 mm; Waters, Milford, MA, USA); MeCN/H₂O (40/60, v/v) in isocratic mode (flow rate: 5 mL \cdot min⁻¹).

The fully automated radiosyntheses of $[^{18}\text{F}]\mathbf{5a}$, $[^{18}\text{F}]\mathbf{5c}$, and $[^{18}\text{F}]\mathbf{5f}$ (^{18}F -labeling, oxidation, HPLC purification, and formulation) were performed in 73 min, 70 min, and 65 min, respectively. Starting from 125-150 GBq of $[^{18}\text{F}]\text{fluoride}$, the labeled compounds $[^{18}\text{F}]\mathbf{5a}$, $[^{18}\text{F}]\mathbf{5c}$, and $[^{18}\text{F}]\mathbf{5f}$ were isolated in $2.9 \pm 0.1\%$, $5.7 \pm 0.5\%$, and $8.0 \pm 0.9\%$ RCYs (decay-corrected at the SOS), respectively (Table 3). The RCY of each automated radiosynthesis was determined based on the ratio between the radioactivity of the $[^{18}\text{F}]\mathbf{5a}$, $[^{18}\text{F}]\mathbf{5c}$, or $[^{18}\text{F}]\mathbf{5f}$ present in the DMSO solution (decay-corrected at the SOS) and the radioactivity trapped on the QMA carbonate cartridge at the SOS.

Obtaining a high molar activity still constitutes a major challenge for the radiosyntheses of $[^{18}\text{F}]\text{CHF}_2$ -bearing compounds, due to the unwanted ^{18}F - ^{19}F isotopic exchange reactions. This fully automated methodology allowed the preparation of the $[^{18}\text{F}]\mathbf{5a}$, $[^{18}\text{F}]\mathbf{5c}$, and $[^{18}\text{F}]\mathbf{5f}$ with improved molar activities in comparison with the sulfone $[^{18}\text{F}]\mathbf{1}$ [A_m ($[^{18}\text{F}]\mathbf{5a}$) = 139 ± 17 GBq $\cdot\mu\text{mol}^{-1}$ > A_m ($[^{18}\text{F}]\mathbf{5f}$) = 113 ± 17 GBq $\cdot\mu\text{mol}^{-1}$ > A_m ($[^{18}\text{F}]\mathbf{5c}$) = 62 ± 12 GBq $\cdot\mu\text{mol}^{-1}$ > A_m ($[^{18}\text{F}]\mathbf{1}$) = 54 ± 7 GBq $\cdot\mu\text{mol}^{-1}$, all A_m values in Table 3 were determined at the end of the synthesis (EOS)].

Table 3. Radiochemical yields and molar activities of the reagents $[^{18}\text{F}]\mathbf{5a}$, $[^{18}\text{F}]\mathbf{5c}$, and $[^{18}\text{F}]\mathbf{5f}$.

Reagents	$[^{18}\text{F}]\mathbf{5a}$	$[^{18}\text{F}]\mathbf{5c}$	$[^{18}\text{F}]\mathbf{5f}$
Duration of the radiosynthesis (min)	73	70	65
RCY (%) ^(a)	2.9 ± 0.1	5.7 ± 0.5	8.0 ± 0.9
Molar activity (GBq $\cdot\mu\text{mol}^{-1}$) ^(b)	139 ± 17	62 ± 12	113 ± 17

^(a) All RCYs were determined based on the radioactivity of the $[^{18}\text{F}]\mathbf{5a}$, $[^{18}\text{F}]\mathbf{5c}$, or $[^{18}\text{F}]\mathbf{5f}$ present in the dimethyl sulfoxide (DMSO) solution (decay-corrected at the SOS) and the radioactivity trapped on the QMA carbonate cartridge at the SOS. ^(b) Molar activities were determined at the end of the synthesis (EOS).

2.2.3. ^{18}F -Difluoromethylation of Heteroarenes with Sulfones $[^{18}\text{F}]\mathbf{5a}$, $[^{18}\text{F}]\mathbf{5c}$, and $[^{18}\text{F}]\mathbf{5f}$

Next, we evaluated the tendency of the newly synthesized $[^{18}\text{F}]$ difluoromethyl heteroaryl-sulfones $[^{18}\text{F}]\mathbf{5a}$, $[^{18}\text{F}]\mathbf{5c}$, and $[^{18}\text{F}]\mathbf{5f}$ towards the C–H ^{18}F -difluoromethylation of *N*-containing heteroarenes, under irradiation with blue light-emitting diode (LED) (470 nm, 2 W). The C–H ^{18}F -difluoromethylation reactions were performed in continuous-flow using an easy-to-use platform equipped with a 100 μL microreactor made from glass and a syringe that continuously pumps the reaction mixture into the microreactor at a given flow rate (FlowStart Evo, FutureChemistry, Nijmegen, The Netherlands) (Figure S84). The use of a continuous-flow system assures an efficient irradiation of the reaction mixture during the photocatalytic processes and can potentially lead to an enhanced productivity in significantly reduced reaction times [37]. The reaction time is a relevant parameter in ^{18}F -radiochemistry. We initially explored the reactivity of the sulfones $[^{18}\text{F}]\mathbf{5a}$, $[^{18}\text{F}]\mathbf{5c}$, and $[^{18}\text{F}]\mathbf{5f}$ for the C–H ^{18}F -difluoromethylation of the antiherpetic drug acyclovir (**7e**) [48] under the reaction conditions recently reported in our laboratories (Table 4, Entry 1) [37]. The visible light-mediated C–H ^{18}F -difluoromethylation of **7e** with the sulfones $[^{18}\text{F}]\mathbf{5a}$, $[^{18}\text{F}]\mathbf{5c}$, and $[^{18}\text{F}]\mathbf{5f}$ was conducted at 35 °C in DMSO, in the presence of the photocatalyst *fac*- $\text{Ir}^{\text{III}}(\text{ppy})_3$ (0.05 mol %), and with a residence time of 2 min (flow rate = 50 $\mu\text{L}\cdot\text{min}^{-1}$). Under these conditions, the reagents $[^{18}\text{F}]\mathbf{5a}$, $[^{18}\text{F}]\mathbf{5c}$, and $[^{18}\text{F}]\mathbf{5f}$ revealed to be competent substrates for the C–H ^{18}F -difluoromethylation of **7e**, affording the $[^{18}\text{F}]$ acyclovir- CHF_2 ($[^{18}\text{F}]\mathbf{8e}$) in $57 \pm 7\%$ (Table 4, Entry 2), $14 \pm 1\%$ (Table 4, Entry 3), and $48 \pm 8\%$ RCYs (Table 4, Entry 6), respectively. Regardless of the employed ^{18}F -difluoromethylating reagent, the labeled compound $[^{18}\text{F}]\mathbf{8e}$ was furnished in lower RCYs, in comparison with the sulfone $[^{18}\text{F}]\mathbf{1}$ (Table 4, Entry 1). Among the tested reagents, only $[^{18}\text{F}]\mathbf{5a}$ was fully consumed after the present photocatalytic reaction. Raising the amount of *fac*- $\text{Ir}^{\text{III}}(\text{ppy})_3$ and the residence time demonstrated to be beneficial for the efficiency of the sulfones $[^{18}\text{F}]\mathbf{5c}$ and $[^{18}\text{F}]\mathbf{5f}$ toward the C–H ^{18}F -difluoromethylation of **7e**. Regarding the sulfone $[^{18}\text{F}]\mathbf{5c}$, a ten-fold increase of the amount of photocatalyst (0.5 mol%) led to the formation of the product $[^{18}\text{F}]\mathbf{8e}$ in $26 \pm 3\%$ RCY (Table 4, Entry 4). The duplication of the residence time (flow rate = 25 $\mu\text{L}\cdot\text{min}^{-1}$) allowed a full consumption of $[^{18}\text{F}]\mathbf{5c}$ in the photochemical process and the obtention of $[^{18}\text{F}]\mathbf{8e}$ in $51 \pm 7\%$ RCY (Table 4, Entry 5). Changing the amount of photocatalyst from 0.05 mol% to 0.1 mol % and the residence time from 2 min (flow rate = 50 $\mu\text{L}\cdot\text{min}^{-1}$) to 2.5 min (flow rate = 40 $\mu\text{L}\cdot\text{min}^{-1}$) enabled the complete consumption of the reagent $[^{18}\text{F}]\mathbf{5f}$ and resulted in the production of $[^{18}\text{F}]\mathbf{8e}$ in $56 \pm 1\%$ RCY (Table 4, Entry 8). These results demonstrated that a single introduction of the $-\text{NO}_2$ group (an electron-withdrawing substituent) at position 6 and the alteration of the benzothiazolyl ring of $[^{18}\text{F}]\mathbf{1}$ to the *N*-phenyl-tetrazolyl moiety yielded ^{18}F -difluoromethylating reagents with lower reactivity for the C–H ^{18}F -difluoromethylation of **7e** in comparison with the sulfone $[^{18}\text{F}]\mathbf{1}$. Overall, the introduction of molecular modifications in the structure of $[^{18}\text{F}]\mathbf{1}$ can modulate the

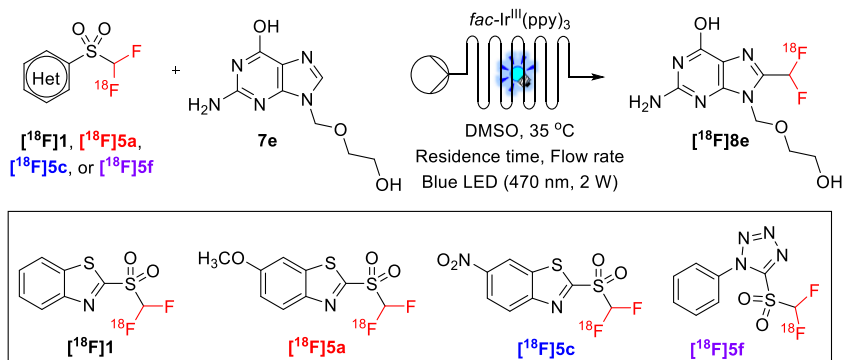
reactivity of the resulting ^{18}F -difluoromethylating reagents, influencing the amount of the photocatalyst $\text{fac-Ir}^{\text{III}}(\text{ppy})_3$ and the residence time necessary to assure a complete C–H ^{18}F -difluoromethylation reaction.

Having identified the optimal conditions for the photoredox C–H ^{18}F -difluoromethylation with ^{18}F 5a, ^{18}F 5c, and ^{18}F 5f, we then investigated the scope of the developed photochemical process (Scheme 5). Gratifyingly, the C–H ^{18}F -difluoromethylation of a series of structurally-diverse heteroarenes such as 4-methyl-1*H*-pyrrolo[2,3-*b*]pyridine (7a), 6-methyl-1*H*-pyrazolo[3,4-*b*]pyridine (7b), 2-methyl-5,8-dihydropyrido[2,3-*d*]pyrimidin-7(6*H*)-one (7c), and ethyl isonicotinate (7d) successfully afforded the corresponding products ^{18}F 8a– ^{18}F 8d in 17–57%, 13–66%, and 14–57% RCYs, using the reagents ^{18}F 5a, ^{18}F 5c, and ^{18}F 5f, respectively. A mixture of structural isomers was observed after the C–H ^{18}F -difluoromethylation of the heteroarenes 7a (^{18}F 8aa and ^{18}F 8ab), 7b (^{18}F 8ba and ^{18}F 8bb), and 7d (^{18}F 8da and ^{18}F 8db). Regardless of the employed ^{18}F -difluoromethylating reagent, the ratio between the distinct isomers was not significantly changed. Besides the antihypertensive drug 7e [48], the C–H ^{18}F -difluoromethylation procedure was also extended to other heteroarenes of medicinal relevance, in particular to the demethylated derivative of the antihypertensive drug moxonidine (7f) [49] and to the xanthine derivative pentoxifylline (7g) [50]. The respective ^{18}F heteroaryl–CHF₂ derivatives ^{18}F 8f and ^{18}F 8g were attained in 21–52%, 17–30%, and 35–60% RCYs from the reagents ^{18}F 5a, ^{18}F 5c, and ^{18}F 5f, respectively. The UPLC radio-chromatogram retention times of the ^{18}F heteroaryl–CHF₂ derivatives ^{18}F 8a– ^{18}F 8g were in agreement with those of the respective non-radioactive authentic references (Figures S87–S103).

To gain insights into the mechanism, the C–H ^{18}F -difluoromethylation of the substrate 7e was examined. The addition of the radical scavenger 2,2,6,6-tetramethyl-1-piperidinyloxy (TEMPO) to the reaction system completely inhibited the C–H ^{18}F -difluoromethylation of the substrate 7e, in the presence of the sulfones ^{18}F 5a, ^{18}F 5c, and ^{18}F 5f (Scheme 6, Entry 1). Furthermore, when the model reaction was performed without blue light irradiation (Scheme 6, Entry 2) and photocatalyst (Scheme 6, Entry 3), no desired product ^{18}F 8e was formed. These results suggest the involvement of radical intermediates in the present photocatalytic C–H ^{18}F -difluoromethylation reaction. On the basis of these observations and previous research works reporting photoredox difluoromethylation reactions with the sulfones 1 [39–44] and 2 [45], a general and simplified reaction mechanism is shown in Figure 7.

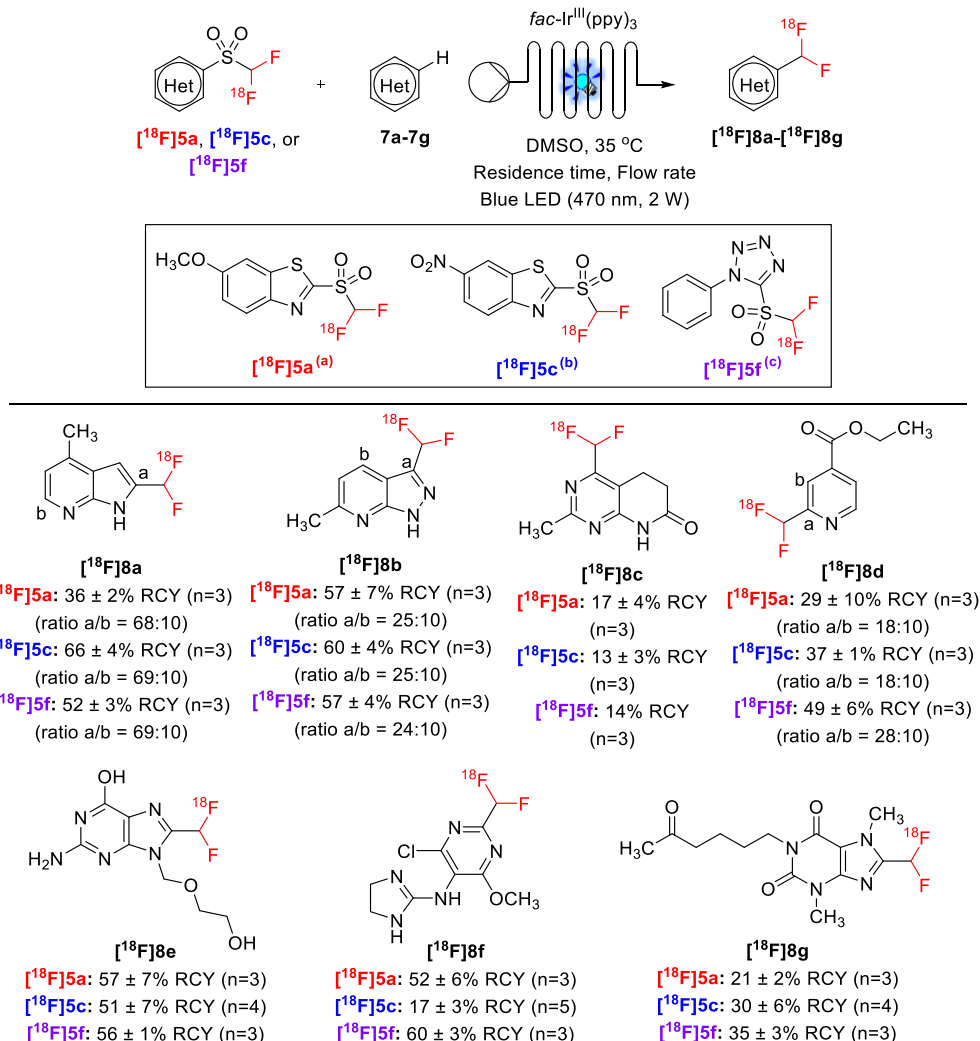
The proposed mechanism for the C–H ^{18}F -difluoromethylation of heteroarenes 7a–7g involved the reduction of the ^{18}F difluoromethyl heteroaryl sulfones (^{18}F 5a, ^{18}F 5c, and ^{18}F 5f), *via* an oxidative quenching of the photoexcited $\text{fac-Ir}^{\text{III}}(\text{ppy})_3$, to generate the ^{18}F CHF₂ radicals. The radical C–H ^{18}F -difluoromethylation of the substrates 7a–7g in favourable reaction site(s) would result in the formation of ^{18}F heteroaryl–CHF₂ radical intermediates. Subsequent oxidation by $\text{fac-Ir}^{\text{IV}}(\text{ppy})_3$ and deprotonation would afford the corresponding ^{18}F heteroaryl–CHF₂ derivatives ^{18}F 8a– ^{18}F 8g.

Table 4. Optimization of the conditions for the C–H ¹⁸F-difluoromethylation of acyclovir (**7e**) with the reagents [¹⁸F]**1**, [¹⁸F]**5a**, [¹⁸F]**5c**, and [¹⁸F]**5f**^(a).

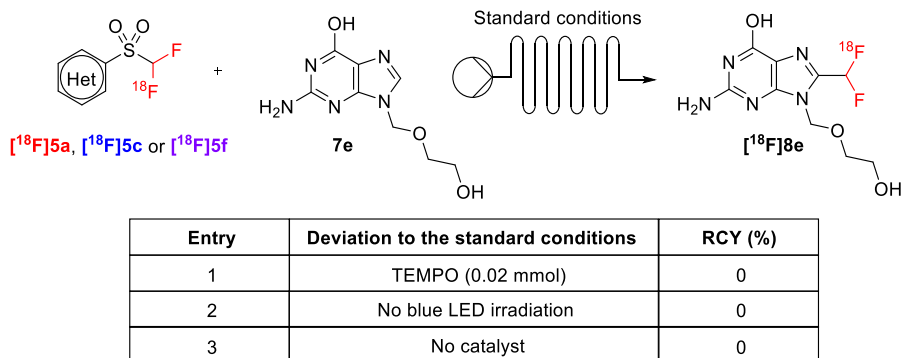


Entry	Reagents	<i>fac</i> -Ir ^{III} (ppy) ₃ (mol%)	Residence time (min)	Flow rate (μL·min ⁻¹)	Conversion (%) ^(b)	RCY (%) ^(c)
1	[¹⁸ F] 1	0.05	2	50	100	70 ± 7 (n = 4)
2	[¹⁸ F] 5a	0.05	2	50	100	57 ± 7 (n = 3)
3	[¹⁸ F] 5c	0.05	2	50	17	14 ± 1 (n = 3)
4	[¹⁸ F] 5c	0.5	2	50	36	26 ± 3 (n = 3)
5	[¹⁸ F] 5c	0.5	4	25	100	51 ± 7 (n = 4)
6	[¹⁸ F] 5f	0.05	2	50	73	48 ± 8 (n = 3)
7	[¹⁸ F] 5f	0.1	2	50	98	55 ± 1 (n = 3)
8	[¹⁸ F] 5f	0.1	2.5	40	100	56 ± 1 (n = 3)

^(a) Standard reaction conditions for the photoredox C–H ¹⁸F-difluoromethylation: substrate **7e** (0.02 mmol), [¹⁸F]**5a**, [¹⁸F]**5c**, or [¹⁸F]**5f** (30–40 MBq), *fac*-Ir^{III}(ppy)₃ (mol %), residence time (min), flow rate (μL·min⁻¹), DMSO (250 μL), 35 °C, blue light-emitting diode (LED) (470 nm, 2 W). ^(b) UPLC conversion of the reagents [¹⁸F]**5a**, [¹⁸F]**5c**, or [¹⁸F]**5f**. ^(c) All RCYs were determined based on the radio-TLC and radio-UPLC purities of the crude product [¹⁸F]**8e**.



Scheme 5. Scope of [¹⁸F]heteroaryl-CHF₂ derivatives [¹⁸F]8a–[¹⁸F]8g. Reactions were conducted on a 0.02 mmol scale. ^(a) Conditions: [¹⁸F]5a (30–40 MBq), *fac*-Ir^{III}(ppy)₃ (0.05 mol %), residence time (2 min), flow rate (50 μL·min⁻¹), DMSO (250 μL), 35 °C, blue LED (470 nm, 2 W). ^(b) Conditions: [¹⁸F]5c (30–40 MBq), *fac*-Ir^{III}(ppy)₃ (0.5 mol %), residence time (4 min), flow rate (25 μL·min⁻¹), DMSO (250 μL), 35 °C, blue LED (470 nm, 2 W). ^(c) Conditions: [¹⁸F]5f (30–40 MBq), *fac*-Ir^{III}(ppy)₃ (0.1 mol %), residence time (2.5 min), flow rate (40 μL·min⁻¹), DMSO (250 μL), 35 °C, blue LED (470 nm, 2 W). All RCYs were determined based on the radio-TLC and radio-UPLC purities of the crude products [¹⁸F]8a–[¹⁸F]8g.



Scheme 6. Control experiments with the radical scavenger 2,2,6,6-tetramethyl-1-piperidinyloxy (TEMPO) (Entry 1), in the absence of blue light irradiation (Entry 2), and in the absence of photocatalyst (Entry 3). Reactions were conducted on a 0.02 mmol scale. Standard conditions: (i) $[^{18}\text{F}]\mathbf{5a}$ (30–40 MBq), $\text{fac-Ir}^{\text{III}}(\text{ppy})_3$ (0.05 mol %), residence time (2 min), flow rate ($50 \mu\text{L}\cdot\text{min}^{-1}$), DMSO (250 μL), 35 $^\circ\text{C}$, blue LED (470 nm, 2 W); (ii) $[^{18}\text{F}]\mathbf{5c}$ (30–40 MBq), $\text{fac-Ir}^{\text{III}}(\text{ppy})_3$ (0.5 mol %), residence time (4 min), flow rate ($25 \mu\text{L}\cdot\text{min}^{-1}$), DMSO (250 μL), 35 $^\circ\text{C}$, blue LED (470 nm, 2 W); (iii) $[^{18}\text{F}]\mathbf{5f}$ (30–40 MBq), $\text{fac-Ir}^{\text{III}}(\text{ppy})_3$ (0.1 mol %), residence time (2.5 min), flow rate ($40 \mu\text{L}\cdot\text{min}^{-1}$), DMSO (250 μL), 35 $^\circ\text{C}$, blue LED (470 nm, 2 W).

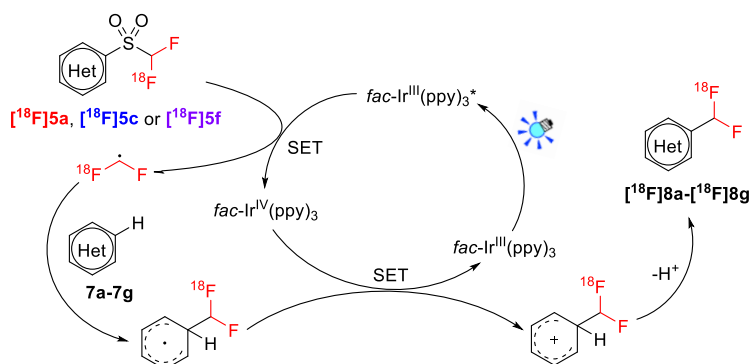


Figure 7. A general and simplified mechanism for the C–H ^{18}F -difluoromethylation of $\mathbf{7a-7g}$ with the sulfones $[^{18}\text{F}]\mathbf{5a}$, $[^{18}\text{F}]\mathbf{5c}$, and $[^{18}\text{F}]\mathbf{5f}$.

3. Materials and Methods

3.1. Chemistry

All solvents and reagents were purchased from Sigma Aldrich (Overijssel, Belgium), TCI Europe N.V. (Zwijndrecht, Belgium), abcr GmbH (Karlsruhe, Germany), or VWR (Oud-Heverlee, Belgium), and no further purification process was implemented. Solvents were evaporated using a HEI-VAP rotary evaporator (Heidolph, Germany). Thin-layer chromatography (TLC) analyses were carried out on silica gel Polygram[®] SIL G/UV₂₅₄ pre-coated TLC-sheets (Macherey-Nagel, Düren, Germany). Ultra-performance liquid chromatography (UPLC) analyses were carried out on a Waters system (ACQUITY UPLC[®] PDA UV detector (190–400 nm), Waters,

Milford, MA, USA) controlled by the Empower software and with an ACQUITY UPLC® CSH C18 column (1.7 μm , 2.1 \times 100 mm) (Waters, Milford, MA, USA), at 0.5 mL \cdot min $^{-1}$ and 45 $^{\circ}\text{C}$. Purifications by flash chromatography were carried out automatically by a CombiFlash® system (Teledyne Isco, San Diego, CA, USA) with RediSep® Rf Normal Phase Silica columns (sizes: 24 g, 40 g, and 80 g). ^1H -, ^{13}C -, and ^{19}F -nuclear magnetic resonance (NMR) spectra were recorded at room temperature on a Bruker AVANCE III UltraShield NanoBay 400 MHz NMR Spectrometer (400 MHz for ^1H , 101 MHz for ^{13}C , and 376 MHz for ^{19}F , Bruker Biosciences Corporation, Billerica, MA, USA). The newly synthesized compounds were analyzed in DMSO- d_6 and CDCl_3 at a probe temperature of 300 K. For ^1H - and ^{13}C -NMR spectra, the chemical shifts (δ) were expressed in ppm downfield from tetramethylsilane (TMS) as an internal standard. For ^{19}F -NMR spectra, the chemical shifts (δ) were given in ppm downfield from trifluoroacetic acid (TFA, $\delta = -76.50$ ppm) as internal standard. The NMR multiplicity signals were abbreviated as: s = singlet, d = doublet, t = triplet, dd = doublet of doublets, ddd = doublet of doublet of doublets, or m = multiplet. The coupling constants (J) were given in Hz and reported to the nearest 1 Hz. High-resolution mass spectroscopy (HRMS) spectra were measured on using a SYNAPT G2-SI Waters QTOF mass spectrometer (Waters, Milford, MA, USA). This spectrometer is equipped with an electrospray ionization (ESI) source and a Waters Acquity H-class UPLC with diode array detector (210 to 400 nm) (Waters, Milford, MA, USA). An Acquity UPLC HSS T3 C18 column (1.8 μm , 2.1 \times 50 mm) was used. The melting points (m.p.) of the solid compounds were measured using a Büchi® melting point apparatus (model B-545, AC/DC input 230 V AC, Büchi, Flawil, Switzerland).

3.1.1. General Procedure for the Synthesis of Difluoromethyl Heteroaryl-Sulfides (**4a–4f**)

The difluoromethylation of heteroaryl-thiols (**3a–3f**) was achieved following the slightly modified protocols [46,47]. Sodium chlorodifluoroacetate (915 mg, 6.0 mmol, 2.0 equiv.) and potassium carbonate (622 mg, 4.5 mmol, 1.5 equiv.) were added to a single-neck round-bottom flask with DMF (5 mL) and the resulting suspension was stirred at room temperature for 5 minutes. Afterwards, a solution of the heteroaryl-thiols **3a–3f** (3.0 mmol, 1.0 equiv.) in DMF (5 mL) was slowly added. The reaction mixture was stirred at 95 $^{\circ}\text{C}$ for 15 minutes and then cooled down to room temperature. After dilution with H_2O (10 mL), the crude product was extracted with DCM (3 \times 20 mL). The organic layers were gathered and dried over anhydrous MgSO_4 . After filtration, the solution was concentrated under reduced pressure and the resulting crude product was purified by flash chromatography as described below.

2-((Difluoromethyl)thio)-6-methoxybenzo[d]thiazole (**4a**). Purified by flash chromatography (SiO_2 ; heptane/EtOAc (95/5, v/v)). Yellow oil (363 mg, 49% yield); ^1H -NMR (DMSO- d_6 , 400 MHz): $\delta = 7.95$ (1H, dd, $J_{\text{HH}} = 9.0$ and 0.4 Hz), 7.87 (1H, t, $J_{\text{HF}} = 54.9$

Hz), 7.73 (1H, d, $J_{HH} = 2.6$ Hz), 7.17 (1H, dd, $J_{HH} = 9.0$ and 2.6 Hz), 3.84 (3H, s) ppm; ^{13}C -NMR (DMSO- d_6 , 101 MHz): $\delta = 157.8, 151.6$ (t, $J_{CF} = 3.9$ Hz), 147.0, 138.1, 123.3, 120.3 (t, $J_{CF} = 276.1$ Hz), 116.3, 104.5, 55.8 ppm; ^{19}F -NMR (DMSO- d_6 + TFA, 376 MHz): $\delta = -95.8$ (2F, d, $J_{HF} = 54.9$ Hz) ppm; m/z [$\text{C}_9\text{H}_7\text{F}_2\text{NOS}_2 + \text{H}$] $^+$ calcd. for [$\text{C}_9\text{H}_8\text{F}_2\text{NOS}_2$]: 248.0015; found: 248.0018.

2-((Difluoromethyl)thio)-5-methoxybenzo[*d*]thiazole (**4b**). Purified by flash chromatography (SiO₂; heptane/EtOAc (95/5, v/v)). White powder (317 mg, 43% yield); m.p. 48-49 °C; ^1H -NMR (DMSO- d_6 , 400 MHz): $\delta = 8.01$ (1H, dd, $J_{HH} = 8.9$ and 0.3 Hz), 7.93 (1H, t, $J_{HF} = 54.8$ Hz), 7.59 (1H, d, $J_{HH} = 2.4$ Hz), 7.15 (1H, dd, $J_{HH} = 9.0$ and 2.4 Hz), 3.85 (3H, s) ppm; ^{13}C -NMR (DMSO- d_6 , 101 MHz): $\delta = 158.9, 156.5$ (t, $J_{CF} = 3.7$ Hz), 153.8, 127.8, 122.4, 120.3 (t, $J_{CF} = 275.7$ Hz), 115.8, 105.2, 55.6 ppm; ^{19}F -NMR (DMSO- d_6 + TFA, 376 MHz): $\delta = -96.1$ (2F, d, $J_{HF} = 54.5$ Hz) ppm; m/z [$\text{C}_9\text{H}_7\text{F}_2\text{NOS}_2 + \text{H}$] $^+$ calcd. for [$\text{C}_9\text{H}_8\text{F}_2\text{NOS}_2$]: 248.0015; found: 248.0025.

2-((Difluoromethyl)thio)-6-nitrobenzo[*d*]thiazole (**4c**). Purified by flash chromatography (SiO₂; heptane/DCM (60/40, v/v)). Light yellow powder (139 mg, 18% yield); m.p. 96-97 °C; ^1H -NMR (DMSO- d_6 , 400 MHz): $\delta = 9.18$ (1H, d, $J_{HH} = 2.4$ Hz), 8.34 (1H, dd, $J_{HH} = 9.0$ and 2.4 Hz), 8.18 (1H, d, $J_{HH} = 9.0$ Hz), 8.06 (1H, t, $J_{HF} = 54.4$ Hz) ppm; ^{13}C -NMR (DMSO- d_6 , 101 MHz): $\delta = 164.6$ (t, $J_{CF} = 3.7$ Hz), 155.6, 144.5, 136.2, 122.6, 122.1, 120.2 (t, $J_{CF} = 276.2$ Hz), 119.2 ppm; ^{19}F -NMR (DMSO- d_6 + TFA, 376 MHz): $\delta = -95.2$ (2F, d, $J_{HF} = 54.4$ Hz) ppm; m/z [$\text{C}_8\text{H}_4\text{F}_2\text{N}_2\text{O}_2\text{S}_2 + \text{H}$] $^+$ calcd. for [$\text{C}_8\text{H}_5\text{F}_2\text{N}_2\text{O}_2\text{S}_2$]: 262.976; found: 262.976.

2-((Difluoromethyl)thio)-5-nitrobenzo[*d*]thiazole (**4d**). Purified by flash chromatography (SiO₂; heptane/DCM (60/40, v/v)). Light yellow powder (155 mg, 20% yield); m.p. 79-80 °C; ^1H -NMR (DMSO- d_6 , 400 MHz): $\delta = 8.77$ (1H, d, $J_{HH} = 2.2$ Hz), 8.42 (1H, d, $J_{HH} = 8.9$ Hz), 8.32 (1H, dd, $J_{HH} = 8.9$ and 2.3 Hz), 8.03 (1H, t, $J_{HF} = 54.4$ Hz) ppm; ^{13}C -NMR (DMSO- d_6 , 101 MHz): $\delta = 161.7$ (t, $J_{CF} = 3.6$ Hz), 151.7, 146.7, 142.5, 123.5, 120.2 (t, $J_{CF} = 276.2$ Hz), 119.9, 117.2 ppm; ^{19}F -NMR (DMSO- d_6 + TFA, 376 MHz): $\delta = -94.8$ (2F, d, $J_{HF} = 54.4$ Hz) ppm; m/z [$\text{C}_8\text{H}_4\text{F}_2\text{N}_2\text{O}_2\text{S}_2 + \text{H}$] $^+$ calcd. for [$\text{C}_8\text{H}_5\text{F}_2\text{N}_2\text{O}_2\text{S}_2$]: 262.976; found: 262.976.

2-((Difluoromethyl)thio)-1-methyl-1*H*-benzo[*d*]imidazole (**4e**). Purified by flash chromatography (SiO₂; heptane/EtOAc (95/5, v/v)). Light yellow powder (333 mg, 52% yield); m.p. 44-45 °C; ^1H -NMR (DMSO- d_6 , 400 MHz): $\delta = 7.78$ (1H, t, $J_{HF} = 55.4$ Hz), 7.69-7.67 (1H, m), 7.63-7.61 (1H, m), 7.35-7.32 (1H, m), 7.29-7.25 (1H, m), 3.83 (3H, s) ppm; ^{13}C -NMR (DMSO- d_6 , 101 MHz): $\delta = 142.7, 141.7$ (t, $J_{CF} = 4.7$ Hz), 136.3, 123.2, 122.4, 120.9 (t, $J_{CF} = 275.1$ Hz), 118.9, 110.7, 30.8 ppm; ^{19}F -NMR (DMSO- d_6 + TFA, 376 MHz): $\delta = -93.6$ (2F, d, $J_{HF} = 55.4$ Hz) ppm; m/z [$\text{C}_9\text{H}_8\text{F}_2\text{N}_2\text{S} + \text{H}$] $^+$ calcd. for [$\text{C}_9\text{H}_9\text{F}_2\text{N}_2\text{S}$]: 215.0455; found: 215.0455.

5-((Difluoromethyl)thio)-1-phenyl-1H-tetrazole (**4f**). Purified by flash chromatography (SiO₂; heptane/EtOAc (95/5, v/v)). Yellow oil (395 mg, 58% yield); ¹H-NMR (CDCl₃, 400 MHz): δ = 7.73 (1H, t, *J*_{HF} = 55.9 Hz), 7.63–7.60 (3H, m), 7.53–7.50 (2H, m) ppm; ¹³C-NMR (CDCl₃, 101 MHz): δ = 148.3 (t, *J*_{CF} = 5.0 Hz), 132.9, 131.1, 130.2, 124.3, 119.5 (t, *J*_{CF} = 279.8 Hz) ppm; ¹⁹F-NMR (CDCl₃ + TFA, 376 MHz): δ = -92.6 (2F, d, *J*_{HF} = 55.4 Hz) ppm; *m/z* [C₈H₆F₂N₄S + H]⁺ calcd. for [C₈H₇F₂N₄S]: 229.0359; found: 229.0362.

3.1.2. General Procedure for the Synthesis of Difluoromethyl Heteroaryl-Sulfones (**5a–5f**)

To a round-bottom flask containing the difluoromethyl heteroaryl-sulfides **4a–4f** (1.0 mmol, 1.0 equiv.) in MeCN (2 mL) and CHCl₃ (2 mL), a solution of sodium (meta)periodate (NaIO₄) (1.07 g, 5.0 mmol, 5 equiv.) and ruthenium (III) chloride hydrate (RuCl₃·*x*H₂O) (10 mg, 0.05 mmol, 0.05 equiv.) in H₂O (4 mL) was added to the reaction system. The resulting reaction mixture was stirred at room temperature for 1 h. After the completion of the reaction, the suspension was diluted with H₂O (5 mL) and the crude product was extracted with DCM (3 × 25 mL). The combined organic layers were washed with saturated aqueous solution of NaHCO₃ and subsequently dried over anhydrous MgSO₄. After filtration, the solvent was evaporated under reduced pressure. The resulting crude product was then purified by flash chromatography (SiO₂; heptane/EtOAc (90/10, v/v)) to afford the difluoromethyl heteroaryl-sulfones **5a–5f** as pure compounds.

2-((Difluoromethyl)sulfonyl)-6-methoxybenzo[*d*]thiazole (**5a**). Light yellow powder (121 mg, 87% yield); m.p. 129–130 °C; ¹H-NMR (DMSO-*d*⁶, 400 MHz): δ = 8.27 (1H, d, *J*_{HH} = 9.2 Hz), 7.96 (1H, d, *J*_{HH} = 2.6 Hz), 7.65 (1H, t, *J*_{HF} = 51.6 Hz), 7.38 (1H, dd, *J*_{HH} = 9.2 and 2.6 Hz), 3.91 (3H, s) ppm; ¹³C-NMR (DMSO-*d*⁶, 101 MHz): δ = 160.1, 155.0, 147.1, 140.0, 126.4, 119.4, 114.9 (t, *J*_{CF} = 284.9 Hz), 104.8, 56.1 ppm; ¹⁹F-NMR (DMSO-*d*⁶ + TFA, 376 MHz): δ = -126.0 (2F, d, *J*_{HF} = 51.7 Hz) ppm; *m/z* [C₉H₇F₂NO₃S₂ + H]⁺ calcd. for [C₉H₈F₂NO₃S₂]: 279.9914; found: 279.9915.

2-((Difluoromethyl)sulfonyl)-5-methoxybenzo[*d*]thiazole (**5b**). Yellow powder (89 mg, 64% yield); m.p. 110–111 °C; ¹H-NMR (DMSO-*d*⁶, 400 MHz): δ = 8.29 (1H, d, *J*_{HH} = 9.1 Hz), 7.90 (1H, d, *J*_{HH} = 2.4 Hz), 7.67 (1H, t, *J*_{HF} = 51.5 Hz), 7.43 (1H, dd, *J*_{HH} = 9.2 and 2.5 Hz), 3.91 (3H, s) ppm; ¹³C-NMR (DMSO-*d*⁶, 101 MHz): δ = 160.0, 159.2, 154.1, 129.9, 124.1, 120.4, 115.0 (t, *J*_{CF} = 285.4 Hz), 106.6, 55.9 ppm; ¹⁹F-NMR (DMSO-*d*⁶ + TFA, 376 MHz): δ = -125.9 (2F, d, *J*_{HF} = 51.7 Hz) ppm; *m/z* [C₉H₇F₂NO₃S₂ + H]⁺ calcd. for [C₉H₈F₂NO₃S₂]: 279.9914; found: 279.9917.

2-((Difluoromethyl)sulfonyl)-6-nitrobenzo[*d*]thiazole (**5c**). Light yellow powder (115 mg, 78% yield); m.p. 161–162 °C; ¹H-NMR (DMSO-*d*⁶, 400 MHz): δ = 9.46 (1H, d, *J*_{HH} = 2.4 Hz), 8.62 (1H, d, *J*_{HH} = 9.1 Hz), 8.54 (1H, dd, *J*_{HH} = 9.2 and 2.4 Hz), 7.76 (1H, t, *J*_{HF} = 51.4 Hz) ppm; ¹³C-NMR (DMSO-*d*⁶, 101 MHz): δ = 165.0, 155.4, 146.6, 137.9, 126.5, 123.3,

121.1, 115.1 (t, $J_{CF} = 285.5$ Hz) ppm; ^{19}F -NMR (DMSO- d^6 + TFA, 376 MHz): $\delta = -123.9$ (2F, d, $J_{HF} = 51.5$ Hz) ppm; m/z [$\text{C}_8\text{H}_4\text{F}_2\text{N}_2\text{O}_4\text{S}_2 + \text{H}$] $^+$ calcd. for [$\text{C}_8\text{H}_5\text{F}_2\text{N}_2\text{O}_4\text{S}_2$]: 294.9659; found: 294.9671.

2-((Difluoromethyl)sulfonyl)-5-nitrobenzo[d]thiazole (**5d**). White powder (120 mg, 82% yield); m.p. 168–169 °C; ^1H -NMR (DMSO- d^6 , 400 MHz): $\delta = 9.23$ (1H, dd, $J_{HH} = 2.2$ and 0.4 Hz), 8.70 (1H, dd, $J_{HH} = 9.1$ and 0.4 Hz), 8.57 (1H, dd, $J_{HH} = 9.1$ and 2.2 Hz), 7.74 (1H, t, $J_{HF} = 51.3$ Hz) ppm; ^{13}C -NMR (DMSO- d^6 , 101 MHz): $\delta = 163.3, 151.8, 147.7, 143.4, 125.5, 122.9, 121.0, 115.1$ (t, $J_{CF} = 286.0$ Hz) ppm; ^{19}F -NMR (DMSO- d^6 + TFA, 376 MHz): $\delta = -123.9$ (2F, d, $J_{HF} = 51.4$ Hz) ppm; m/z [$\text{C}_8\text{H}_4\text{F}_2\text{N}_2\text{O}_4\text{S}_2 + \text{H}$] $^+$ calcd. for [$\text{C}_8\text{H}_5\text{F}_2\text{N}_2\text{O}_4\text{S}_2$]: 294.9659; found: 294.966.

2-((Difluoromethyl)sulfonyl)-1-methyl-1H-benzo[d]imidazole (**5e**). White powder (82 mg, 67% yield); m.p. 134–135 °C; ^1H -NMR (DMSO- d^6 , 400 MHz): $\delta = 7.94$ – 7.92 (1H, m), 7.88– 7.86 (1H, m), 7.61 (1H, t, $J_{HF} = 51.9$ Hz), 7.62– 7.58 (1H, m), 7.50– 7.46 (1H, m), 4.14 (3H, s) ppm; ^{13}C -NMR (DMSO- d^6 , 101 MHz): $\delta = 141.1, 140.9, 136.7, 127.0, 124.7, 121.4, 114.8$ (t, $J_{CF} = 283.9$ Hz), 112.4, 32.1 (t, $J_{CF} = 0.8$ Hz) ppm; ^{19}F -NMR (DMSO- d^6 + TFA, 376 MHz): $\delta = -125.6$ (2F, d, $J_{HF} = 51.9$ Hz) ppm; m/z [$\text{C}_9\text{H}_8\text{F}_2\text{N}_2\text{O}_2\text{S} + \text{H}$] $^+$ calcd. for [$\text{C}_9\text{H}_9\text{F}_2\text{N}_2\text{O}_2\text{S}$]: 247.0352; found: 247.0353.

5-((Difluoromethyl)sulfonyl)-1-phenyl-1H-tetrazole (**5f**). White powder (85 mg, 65% yield); m.p. 68–69 °C; ^1H -NMR (CDCl_3 , 400 MHz): $\delta = 7.72$ – 7.59 (5H, m), 6.83 (1H, t, $J_{HF} = 52.9$ Hz) ppm; ^{13}C -NMR (CDCl_3 , 101 MHz): $\delta = 132.5, 132.2, 130.1, 125.4, 114.2$ (t, $J_{CF} = 289.3$ Hz), 104.9 ppm; ^{19}F -NMR (CDCl_3 + TFA, 376 MHz): $\delta = -124.1$ (2F, d, $J_{HF} = 52.9$ Hz) ppm; m/z [$\text{C}_8\text{H}_6\text{F}_2\text{N}_4\text{O}_2\text{S} + \text{H}$] $^+$ calcd. for [$\text{C}_8\text{H}_7\text{F}_2\text{N}_4\text{O}_2\text{S}$]: 261.0258; found: 261.0257.

3.1.3. General Procedure for the Synthesis of Bromofluoromethyl Heteroaryl-Sulfides (**6a–6f**)

The bromofluoromethylation of heteroaryl-thiols (**3a–3f**) was carried out on the basis of a previously described procedure [37] with slight modifications. A solution of KOH (1.68 g, 30.0 mmol, 10.0 equiv.) in H_2O (4 mL) was placed in a single-neck round-bottom flask and stirred at 0 °C. Afterwards, a solution of the heteroaryl-thiols **3a–3f** (3.0 mmol, 1.0 equiv.) in THF (3 mL) was added and the resulting mixture was allowed to stir at room temperature for 20 min. A solution of dibromofluoromethane (0.713 mL, 9.0 mmol, 3.0 equiv.) in THF (1 mL) was slowly introduced in the reaction system, and the resulting mixture was stirred at room temperature for 15–20 min. The suspension was subsequently quenched by addition of H_2O (20 mL), and the crude product was extracted with DCM (3 × 30 mL). The combined organic layers were gathered and were dried over anhydrous MgSO_4 . After filtration, the solvent was removed under reduced pressure. The purification of the concentrated crude product was performed by flash chromatography (SiO_2 ; heptane/EtOAc (95/5, v/v)) to furnish the bromofluoromethyl heteroaryl-sulfides **6a–6f** as pure compounds.

2-((Bromofluoromethyl)thio)-6-methoxybenzo[d]thiazole (**6a**). Yellow powder (182 mg, 20% yield); m.p. 53-55 °C; ¹H-NMR (DMSO-*d*₆, 400 MHz): δ = 8.35 (1H, d, *J*_{HF} = 53.7 Hz), 7.94 (1H, d, *J*_{HH} = 9.0 Hz), 7.73 (1H, d, *J*_{HH} = 2.6 Hz), 7.16 (1H, dd, *J*_{HH} = 9.0 and 2.6 Hz), 3.84 (3H, s) ppm; ¹³C-NMR (DMSO-*d*₆, 101 MHz): δ = 157.8, 155.3 (d, *J*_{CF} = 2.8 Hz), 146.8, 137.9, 123.3, 116.4, 104.6, 91.2 (d, *J*_{CF} = 294.5 Hz), 55.8 ppm; ¹⁹F-NMR (DMSO-*d*₆ + TFA, 376 MHz): δ = -105.0 (1F, d, *J*_{HF} = 53.8 Hz) ppm; *m/z* [C₉H₈BrFNOS₂ + H]⁺ calcd. for [C₉H₈BrFNOS₂]: 307.9214; found: 307.9218.

2-((Bromofluoromethyl)thio)-5-methoxybenzo[d]thiazole (**6b**). Yellow oil (166 mg, 18% yield); ¹H-NMR (DMSO-*d*₆, 400 MHz): δ = 8.39 (1H, d, *J*_{HF} = 53.8 Hz), 8.01 (1H, d, *J*_{HH} = 9.0 Hz), 7.58 (1H, d, *J*_{HH} = 2.5 Hz), 7.14 (1H, dd, *J*_{HH} = 9.0 and 2.5 Hz), 3.85 (3H, s) ppm; ¹³C-NMR (DMSO-*d*₆, 101 MHz): δ = 160.1 (d, *J*_{CF} = 2.8 Hz), 159.0, 153.6, 127.7, 122.5, 115.8, 105.3, 90.8 (d, *J*_{CF} = 293.3 Hz), 55.6 ppm; ¹⁹F-NMR (DMSO-*d*₆ + TFA, 376 MHz): δ = -105.6 (1F, d, *J*_{HF} = 54.1 Hz) ppm; *m/z* [C₉H₇BrFNOS₂ + H]⁺ calcd. for [C₉H₈BrFNOS₂]: 307.9214; found: 307.9223.

2-((Bromofluoromethyl)thio)-6-nitrobenzo[d]thiazole (**6c**). Light yellow powder (105 mg, 11% yield); m.p. 115-117 °C; ¹H-NMR (DMSO-*d*₆, 400 MHz): δ = 9.20 (1H, dd, *J*_{HH} = 2.4 and 0.4 Hz), 8.53 (1H, d, *J*_{HF} = 53.8 Hz), 8.35 (1H, dd, *J*_{HH} = 9.0 and 2.4 Hz), 8.17 (1H, dd, *J*_{HH} = 9.0 and 0.4 Hz) ppm; ¹³C-NMR (DMSO-*d*₆, 101 MHz): δ = 167.9 (d, *J*_{CF} = 3.0 Hz), 155.6, 144.4, 136.2, 122.6, 122.1, 119.4, 90.1 (d, *J*_{CF} = 293.5 Hz) ppm; ¹⁹F-NMR (DMSO-*d*₆ + TFA, 376 MHz): δ = -107.5 (1F, d, *J*_{HF} = 54.1 Hz) ppm; *m/z* [C₈H₅BrFN₂O₂S₂ + H]⁺ calcd. for [C₈H₅BrFN₂O₂S₂]: 322.896; found: 322.8952.

2-((Bromofluoromethyl)thio)-5-nitrobenzo[d]thiazole (**6d**). Orange powder (88 mg, 9% yield); m.p. 93-95 °C; ¹H-NMR (DMSO-*d*₆, 400 MHz): δ = 8.76 (1H, d, *J*_{HH} = 2.2 Hz), 8.50 (1H, d, *J*_{HF} = 53.6 Hz), 8.43 (1H, d, *J*_{HH} = 9.0 Hz), 8.31 (1H, dd, *J*_{HH} = 9.0 and 2.2 Hz) ppm; ¹³C-NMR (DMSO-*d*₆, 101 MHz): δ = 165.1 (d, *J*_{CF} = 2.9 Hz), 151.6, 146.7, 142.4, 123.6, 119.9, 117.2, 90.3 (d, *J*_{CF} = 293.4 Hz) ppm; ¹⁹F-NMR (DMSO-*d*₆ + TFA, 376 MHz): δ = -106.7 (1F, d, *J*_{HF} = 53.6 Hz) ppm; *m/z* [C₈H₄BrFN₂O₂S₂ + H]⁺ calcd. for [C₈H₅BrFN₂O₂S₂]: 322.896; found: 322.8964.

2-((Bromofluoromethyl)thio)-1-methyl-1H-benzo[d]imidazole (**6e**). Light yellow powder (214 mg, 26% yield); m.p. 79-80 °C; ¹H-NMR (DMSO-*d*₆, 400 MHz): δ = 8.19 (1H, d, *J*_{HF} = 54.0 Hz), 7.70-7.68 (1H, m), 7.64-7.62 (1H, m), 7.36-7.32 (1H, m), 7.30-7.26 (1H, m), 3.83 (3H, s) ppm; ¹³C-NMR (DMSO-*d*₆, 101 MHz): δ = 144.7 (d, *J*_{CF} = 1.8 Hz), 142.4, 136.1, 123.4, 122.5, 118.9, 110.9, 91.5 (d, *J*_{CF} = 294.9 Hz), 30.8 ppm; ¹⁹F-NMR (DMSO-*d*₆ + TFA, 376 MHz): δ = -104.6 (2F, d, *J*_{HF} = 53.8 Hz). HRMS (ESI⁺) ppm; *m/z* [C₉H₈BrFN₂S + H]⁺ calcd. for [C₉H₉BrFN₂S]: 274.9654; found: 274.9662.

5-((Bromofluoromethyl)thio)-1-phenyl-1H-tetrazole (**6f**). Yellow oil (171 mg, 20% yield); ¹H-NMR (DMSO-*d*₆, 400 MHz): δ = 8.16 (1H, d, *J*_{HF} = 52.8 Hz), 7.72-7.67 (5H, m) ppm;

^{13}C -NMR (DMSO- d_6 , 101 MHz): 149.7 (d, $J_{\text{CF}} = 3.0$ Hz), 132.9, 131.0, 129.9, 125.4, 89.9 (d, $J_{\text{CF}} = 295.9$ Hz) ppm; ^{19}F -NMR (DMSO- d_6 + TFA, 376 MHz): $\delta = -105.3$ (1F, d, $J_{\text{HF}} = 53.0$ Hz) ppm; m/z [$\text{C}_6\text{H}_5\text{BrFN} + \text{H}$] $^+$ calcd. for [$\text{C}_6\text{H}_6\text{BrFN}$]: 288.9559; found: 288.9563.

3.1.4. General Procedure for the Synthesis of the Difluoromethylated Heteroarenes (8a–8g)

The difluoromethylated heteroarenes **8a–8g** were synthesized from the heteroarenes **7a–7g** and characterized according to the formerly reported procedures [37,51].

3.2. Radiochemistry

Semi-preparative high performance liquid chromatography (HPLC) purification was conducted on a XBridge[®] BEH C18 OBD[™] Prep column (130 Å, 5 μm , 10 mm \times 250 mm; Waters, Milford, MA, USA) with a mixture of MeCN/H₂O (40/60, v/v) in isocratic mode (flow rate: 5 mL·min⁻¹). The radio-HPLC profiles were monitored with a custom homemade Geiger-Muller (GM) radioactivity detector (Thermo Fisher Scientific, Waltham, MA, USA), connected to the semi-preparative HPLC system. Ultra performance liquid chromatography (UPLC) analyses were performed at 45 °C using an ACQUITY UPLC[®] CSH[™] C18 column (2.1 \times 100 mm, 1.7 μm ; Waters, Milford, MA, USA) on an ACQUITY UPLC[®] system with a mobile phase of MeCN and HCO₂H/H₂O (0.05%, v/v) in gradient mode at 0.5 mL·min⁻¹ (gradient A: from 100% HCO₂H/H₂O (0.05%, v/v) to 75% MeCN + 25% HCO₂H/H₂O (0.05%, v/v) in 6 min, and from 75% MeCN + 25% HCO₂H/H₂O (0.05%, v/v) to 100% HCO₂H/H₂O (0.05%, v/v) in 2 min; gradient B: from 100% HCO₂H/H₂O (0.05%, v/v) to 100% MeCN in 6 min, and from 100% MeCN to 100% HCO₂H/H₂O (0.05%, v/v) in 2 min). The UV signal of the newly synthesized ^{18}F -labeled compounds was measured at 254 nm with a photodiode array (PDA) UV detector (190–400 nm) controlled by the Empower software and connected to the UPLC system. A thallium-activated sodium iodide (NaI(Tl)) scintillation detector from Eberline (Eberline Instruments Corp, Miami, FL, USA) was used to monitor the radio-UPLC elution profile of the newly synthesized ^{18}F -labeled compounds. TLC analyses were carried out on silica gel Polygram[®] SIL G/UV₂₅₄ pre-coated TLC-sheets (TLC eluent: methanol) (Macherey-Nagel, Düren, Germany). The TLC profile of ^{18}F -labeled compounds was then analyzed with a BertHold TLC scanner model AR2000 (BertHold, Bad Wildbad, Germany).

The radiosyntheses of the ^{18}F -labeled compounds were achieved using the commercially available FASTlab[™] synthesizer (GE Healthcare, Chicago, IL, USA). The SepPak[®] cartridges (SepPak[®] Accell[™] Plus QMA Carbonate Plus Light Cartridge (46 mg, 40 μm) and SepPak[®] $^t\text{C}18$ Plus Short Cartridge (400 mg, 37–55 μm) were purchased from Waters (Milford, MA, USA). No-carrier-added [^{18}F]fluoride was prepared from the ^{18}O -enriched water ([^{18}O]H₂O) *via* the $^{18}\text{O}(\text{p},\text{n})^{18}\text{F}$ nuclear reaction with a Cyclone 18/9 from IBA (Louvain-la-Neuve, Belgium). [^{18}O]H₂O was purchased from Cambridge Isotope Laboratories (Tewksbury, MA, USA). At the end of

bombardment (EOB), the activity was transferred to the hot lab cell with helium pressure through Teflon tubing (~ 50 m).

3.2.1. Fully Automated Radiosyntheses of 2-[¹⁸F]((Difluoromethyl)Sulfonyl)-6-Methoxybenzo[*d*]thiazole (**[¹⁸F]5a**), 2-[¹⁸F]((Difluoromethyl)sulfonyl)-6-nitrobenzo[*d*]thiazole (**[¹⁸F]5c**), and 5-[¹⁸F]((Difluoromethyl)Sulfonyl)-1-Phenyl-1*H*-Tetrazole (**[¹⁸F]5f**)

The fully automated radiosyntheses of the labeled compounds **[¹⁸F]5a**, **[¹⁸F]5c**, and **[¹⁸F]5f** were conducted in a FASTlab™ synthesizer (GE Healthcare, Chicago, IL, USA) according to a radiochemical process previously reported in the literature [37,52]. The reagents and solvents used in the radiosyntheses of **[¹⁸F]5a**, **[¹⁸F]5c**, and **[¹⁸F]5f** were placed in 11 mm- and 13 mm-sealed vials and positioned in the FASTlab™ manifold as depicted in Table 5 and illustrated in Figure 3.

The no-carrier-added (n.c.a.) [¹⁸F]fluoride in [¹⁸O]H₂O was transferred from the cyclotron target onto the FASTlab™ synthesizer *via* the [¹⁸F]fluoride inlet conical reservoir (V6). The [¹⁸F]fluoride was trapped on an ion-exchange resin (Sep-Pak® Accell™ Plus QMA Carbonate Plus Light Cartridge; Waters, Milford, MA, USA; from V5 to V4) and the [¹⁸O]H₂O was recovered in a separate vial (V1). The trapped [¹⁸F]fluoride was eluted into the cyclic olefin copolymer (COC) reactor through a central tubing (V8) with a solution of Kryptofix® 222 (K_{2.2.2}; 7.5 mg in 600 μL of MeCN) and K₂CO₃ (1.4 mg in 150 μL of H₂O). The eluent was azeotropically evaporated under vacuum and nitrogen flow by heating at 105 °C and 120 °C for 8 min. Subsequently, a solution of the precursors **6a** (12.3 mg, 0.04 mmol), **6c** (6.5 mg, 0.02 mmol), or **6f** (11.6 mg, 0.04 mmol) solubilized in MeCN (1.0 mL) was transferred to the dry [¹⁸F]potassium fluoride/Kryptofix® 222 ([¹⁸F]KF/K_{2.2.2}) complex *via* the central tubing of the reactor (V8) and heated to 120 °C for 5 min. After the ¹⁸F-labeling of **6a**, **6c**, or **6f**, the reaction mixture containing the [¹⁸F]**4a**, [¹⁸F]**4c**, or [¹⁸F]**4f**, respectively, was diluted two times with H₂O (~ 12 mL) (V15), and the labeled compounds [¹⁸F]**4a**, [¹⁸F]**4c**, or [¹⁸F]**4f** were trapped on a ¹⁸C18 cartridge (Sep-Pak® C18 Plus Short Cartridge; Waters, Milford, MA, USA; from V17 to V18). The COC reactor was subsequently washed with H₂O (~ 4 mL), and the crude solution was passed through the ¹⁸C18 cartridge. A solution containing NaIO₄ (153.9 mg, 0.072 mmol) and RuCl₃·*x*H₂O (3.4 mg, 0.016 mmol) in H₂O (4.0 mL) was transferred to the ¹⁸C18 cartridge and the oxidation of the labeled compounds [¹⁸F]**4a**, [¹⁸F]**4c**, or [¹⁸F]**4f** was carried out on the solid-phase for 5 min at room temperature. Afterwards, the crude products [¹⁸F]**5a**, [¹⁸F]**5c**, or [¹⁸F]**5f** were eluted (from V18 to V17; reverse flow elution) with MeCN (2 mL; syringe S3, V24) and recovered into the reactor through its central tubing. After dilution with H₂O (~ 4 mL) using the syringe S2 (V11), the resulting mixture was conducted to the semi-preparative HPLC loop (V9; 6 mL) *via* a Sterifix® Paed filter (B. Braun, Melsungen, Germany; 0.2 μm). The COC reactor was subsequently washed with H₂O (~ 2 mL) and this solution was also transferred into the HPLC loop. The semi-preparative HPLC purification of [¹⁸F]**5a**, [¹⁸F]**5c**, or [¹⁸F]**5f** was accomplished

with a mixture of MeCN/H₂O (40/60, v/v) in isocratic mode at 5 mL·min⁻¹. The HPLC peaks corresponding to the [¹⁸F]5a, [¹⁸F]5c, or [¹⁸F]5f were collected (retention time of [¹⁸F]5a: 22-26 min; retention time of [¹⁸F]5c: 19–23 min; retention time of [¹⁸F]5f: 15–18 min) in a sealed vial containing H₂O (~ 30 mL). Subsequently, the purified compounds [¹⁸F]5a, [¹⁸F]5c, or [¹⁸F]5f were pumped (from V10), 6 mL by 6 mL, with the syringe S2 (V11) and further conducted to a preconditioned ¹C18 cartridge (from V21 to V22). Finally, [¹⁸F]5a, [¹⁸F]5c, or [¹⁸F]5f were eluted into the outlet vial (V20) with reverse flow of DMSO (1 mL, syringe S3 (V24)).

Table 5. Location of the reagents, solvents, and materials in the manifold of the FASTlab™ cassette

Manifold position	Reagents, solvents, and materials	Details
V1	Silicone tubing connected to [¹⁸ O]H ₂ O recovery vial	14 cm
V2	K _{2.2.2} [®] (7.5 mg) in MeCN (600 μL) and K ₂ CO ₃ (1.4 mg) in H ₂ O (150 μL)	11 mm vial (volume = 750 μL)
V3	Syringe S1 (part of the manifold)	Maximum volume = 1 mL
V4	Sep-Pak [®] Accell™ Plus QMA Carbonate Plus Light Cartridge with silicone tubing at position V5	46 mg (40 μm) (Waters)
V5	Silicone tubing connected to the Sep-Pak [®] Accell™ Plus QMA Carbonate Plus Light Cartridge at position V4	14 cm
V6	[¹⁸ O]H ₂ O/[¹⁸ F]F ⁻ inlet conical reservoir (part of the manifold)	Maximum volume = 5 mL
V7	Silicone tubing connected to the cyclic olefin copolymer (COC) reactor (left-hand side)	14 cm
V8	Silicone tubing connected to the COC reactor (central port)	14 cm
V9	Outlet “to HPLC loop” <i>via</i> silicone tubing connected to a Sterifix [®] Paed filter (B. Braun)	30 cm
V10	Inlet “from HPLC loop” enabling the recovery of the purified labeled compounds [¹⁸ F]5a, [¹⁸ F]5c, and [¹⁸ F]5f after semi-preparative HPLC purification	30 cm
V11	Syringe S2 (part of the manifold)	Maximum volume = 6 mL
V12	Precursors 6a (12.3 mg, 40 μmol), 6c (6.5 mg, 20 μmol), or 6f (11.6 mg, 40 μmol) solubilized in MeCN	11 mm vial (volume = 1 mL)

V13	MeCN	13 mm vial (volume = 4 mL)
V14	NaIO ₄ (153.9 mg) and RuCl ₃ ·xH ₂ O (3.4 mg) solubilized in H ₂ O	13 mm vial (volume = 4 mL)
V15	Water bag spike	Volume = 100 mL
V16	MeCN	13 mm vial (volume = 4 mL)
V17	Silicone tubing connected to the Sep-Pak® C18 Plus Short Cartridge at position V18	14 cm
V18	Sep-Pak® C18 Plus Short Cartridge with silicone tubing at position V17	400 mg (37-55 μm)
V19	Outlet waste bottle	21 cm
V20	Final outlet vial for collection of the labeled compounds [¹⁸ F]5a, [¹⁸ F]5c, and [¹⁸ F]5f after semi-preparative HPLC purification and reformulation	50 cm
V21	Silicone tubing connected to the Sep-Pak® C18 Plus Short Cartridge at position V22	14 cm
V22	Sep-Pak® C18 Plus Short Cartridge with silicone tubing at position V21	400 mg (37-55 μm)
V23	Anhydrous DMSO	13 mm vial (volume = 4 mL)
V24	Syringe S3 (part of the manifold)	Maximum volume = 6 mL
V25	Silicone tubing connected to the COC reactor (right-hand side) and vent valve for the reactor	42 cm

3.2.2. Low-Activity ¹⁸F-Labeling Experiments in the Precursors **6a–6f**

Using the GE FASTlab™ synthesizer, an aliquot of [¹⁸F]fluoride (150–200 MBq) was trapped on a Sep-Pak® Accell™ Plus QMA Carbonate Plus Light cartridge (Waters, Milford, MA, USA) and eluted with a solution of Kryptofix® 222 (K_{2.2.2}; 7.5 mg in 600 μL of MeCN) and K₂CO₃ (1.4 mg in 150 μL of H₂O). Upon azeotropic drying, a solution of the precursors **6a** (12.3 mg, 0.04 mmol), **6b** (12.3 mg, 0.04 mmol), **6c** (6.5 mg, 0.02 mmol), **6d** (12.9 mg, 0.04 mmol), **6e** (11.0 mg, 0.04 mmol), or **6f** (11.6 mg, 0.04 mmol) in MeCN (1 mL) was transferred to the dry [¹⁸F]potassium fluoride/Kryptofix® 222 ([¹⁸F]KF/K_{2.2.2}) complex and heated to 120 °C. After 5 min of ¹⁸F-labeling and dilution of the reaction mixture with H₂O, the labeled compounds [¹⁸F]4a–[¹⁸F]4f were trapped on a Sep-Pak® C18 Plus Short cartridge (Waters, Milford, MA, USA). Subsequently, the C18 cartridge was removed and the trapped crude products [¹⁸F]4a–[¹⁸F]4f were recovered to a 4 mL-vial *via* manual elution with MeCN (1 mL). The radiochemical yield (RCY) of the ¹⁸F-labeling step was determined based on the activity of the recovered crude products [¹⁸F]4a–[¹⁸F]4f, on their radio-TLC and radio-UPLC purities, and the starting radioactivity, according to the following equation:

$$RCY (\%, d. c.) = \frac{\text{radioTLC purity (\%)} \times \text{radioUPLC purity (\%)} \times \text{activity of } [^{18}\text{F}]\mathbf{4a}\text{--}[^{18}\text{F}]\mathbf{4f} (d. c.)}{\text{starting radioactivity} \times 100}$$

A solution containing NaIO₄ (153.9 mg, 0.072 mmol) and RuCl₃·xH₂O (3.4 mg, 0.016 mmol) in H₂O (1 mL) was transferred to the ¹C18 cartridge and the oxidation of the trapped crude products [¹⁸F]**4a**–[¹⁸F]**4f** (10–20 MBq) was carried out in solid-phase for 5 min at room temperature. Afterwards, the corresponding [¹⁸F]difluoromethyl heteroaryl-sulfones [¹⁸F]**5a**–[¹⁸F]**5f** were manually eluted from the ¹C18 cartridge with MeCN (1 mL) to a 4 mL-vial. The RCY of the oxidation step was determined based on the activity of the crude products [¹⁸F]**4a**–[¹⁸F]**4f** and [¹⁸F]**5a**–[¹⁸F]**5f**, and on their radio-TLC and radio-UPLC purities, according to the following equation:

$$RCY (\%, d. c.) = \frac{\text{radioTLC purity (\%)} \times \text{radioUPLC purity (\%)} \times \text{activity of } [^{18}\text{F}]\mathbf{5a}\text{--}[^{18}\text{F}]\mathbf{5f} (d. c.)}{\text{activity of } [^{18}\text{F}]\mathbf{4a}\text{--}[^{18}\text{F}]\mathbf{4f} \times 100}$$

The RCYs of ¹⁸F-labeling and oxidation steps were decay-corrected at the SOS.

3.2.3. Isolation and Determination of the Molar Activity of [¹⁸F]**5a**, [¹⁸F]**5c**, and [¹⁸F]**5f**

The fully automated radiosyntheses of the sulfones [¹⁸F]**5a**, [¹⁸F]**5c**, or [¹⁸F]**5f** were accomplished on a commercially available FASTlab™ synthesizer (GE Healthcare, Chicago, IL, USA), using the optimized conditions for the labeling of precursors **6a** (12.3 mg, 0.04 mmol), **6c** (6.5 mg, 0.02 mmol), or **6f** (11.6 mg, 0.04 mmol), and for the oxidation of the labeled compounds [¹⁸F]**4a**, [¹⁸F]**4c**, and [¹⁸F]**4f**. The molar activities of the sulfones [¹⁸F]**5a**, [¹⁸F]**5c**, and [¹⁸F]**5f** were determined using an aliquot of each reformulated solution (3 μL). After UPLC injection, the radioactive peak of [¹⁸F]**5a**, [¹⁸F]**5c**, and [¹⁸F]**5f** associated to the non-radioactive sulfones **5a**, **5c**, and **5f**, respectively, were collected and counted in an ionization chamber. The PDA UV area under the peak of the non-radioactive sulfones **5a**, **5c**, and **5f** at 258 nm, 290 nm, and 244 nm, respectively, enabled the determination of the corresponding amount (in μmol) of the **5a**, **5c**, and **5f** using the calibration curves described in the Supplementary Information (Figures S82–S84). The molar activities of [¹⁸F]**5a**, [¹⁸F]**5c**, and [¹⁸F]**5f** were determined on the basis of the following equation:

$$\text{Molar activity (GBq} \cdot \mu\text{mol}^{-1}\text{)} = \frac{\text{activity of the collected UPLC peak of } [^{18}\text{F}]\mathbf{5a}, [^{18}\text{F}]\mathbf{5c}, \text{ or } [^{18}\text{F}]\mathbf{5f}}{\text{amount of } \mathbf{5a}, \mathbf{5c}, \text{ or } \mathbf{5f} \text{ associated to the radioactive peak}}$$

3.2.4. General Procedure for the C–H ¹⁸F-Difluoromethylation of the Heteroarenes **7a**–**7g** with the [¹⁸F]Difluoromethyl Heteroaryl-Sulfones [¹⁸F]**5a**, [¹⁸F]**5c**, and [¹⁸F]**5f**

A solution of the heteroarenes (0.02 mmol) and *fac*-Ir^{III}(ppy)₃ (0.05 mol% for [¹⁸F]**5a**; 0.5 mol % for [¹⁸F]**5c**; 0.1 mol % for [¹⁸F]**5f**) in DMSO (200 μL) was prepared in a 4 mL-vial. Next, a solution of [¹⁸F]**5a**, [¹⁸F]**5c**, or [¹⁸F]**5f** in DMSO (30–40 MBq, 50 μL) was added. The resulting mixture was injected in a 100 μL-microchip pumped with

DMSO at a flow rate of 50 $\mu\text{L}\cdot\text{min}^{-1}$ (residence time: 2 min for [^{18}F]5a), 25 $\mu\text{L}\cdot\text{min}^{-1}$ (residence time: 4 min for [^{18}F]5c) or 40 $\mu\text{L}\cdot\text{min}^{-1}$ (residence time: 2.5 min for [^{18}F]5f) and irradiated under blue LED (470 nm, 2 W), at a temperature of 35 °C. An aliquot of the reaction mixture containing the crude products [^{18}F]8a–[^{18}F]8g was then analyzed by radio-TLC and radio-UPLC for RCY determination, according to the following equation:

$$\text{RCY (\%)} = \frac{\text{radioTLC purity (\%)} \times \text{radioUPLC purity (\%)}}{100}$$

4. Conclusions

In the present work, the two-step radiosyntheses of the [^{18}F]difluoromethyl heteroaryl-sulfones [^{18}F]5a, [^{18}F]5c, [^{18}F]5f was fully automated in the GE FASTlab™ module. In conjunction with a semi-preparative HPLC purification procedure and formulation in a preconditioned Sep-Pak® C18 Plus Short Cartridge, the reagents [^{18}F]5a, [^{18}F]5c, [^{18}F]5f were isolated in reproducible 2.9 \pm 0.1%, 5.7 \pm 0.5%, and 8.0 \pm 0.9% RCYs, respectively (decay-corrected at the SOS). The use of automated synthesizers in radiochemical processes involving the production of multiple GBq of labeled compounds is required to assure the minimization of the radiation exposure to workers.

The great probability of $^{18}\text{F}/^{19}\text{F}$ isotopic exchange still constitutes a major limitation in the preparation of [^{18}F]CHF₂-bearing compounds with high molar activity. The production of radiotracers with high molar activity is mandatory for PET imaging studies, especially for targeting low-density biomacromolecules. Starting from 125–150 GBq of [^{18}F]fluoride, this fully automated methodology enabled the preparation of the labeled compounds [^{18}F]5a, [^{18}F]5c, and [^{18}F]5f with improved molar activities (139 \pm 17 GBq· μmol^{-1} for [^{18}F]5a, 62 \pm 12 GBq· μmol^{-1} for [^{18}F]5c, and 113 \pm 17 GBq· μmol^{-1} for [^{18}F]5f).

Interestingly, these newly synthesized compounds were revealed to be competent reagents for the C–H ^{18}F -difluoromethylation of the antiherpetic drug 7e under the reaction conditions recently reported in our laboratories [37]. Still, none of the new reagents performed as good as the original sulfone [^{18}F]1 in the radiosynthesis of the labeled compound [^{18}F]8e. Additionally, the sulfones [^{18}F]5c and [^{18}F]5f exhibited a lower reactivity towards the C–H ^{18}F -difluoromethylation of 7e, in comparison with the sulfone [^{18}F]1. Overall, the introduction of molecular modifications in the structure of [^{18}F]1 can modulate the reactivity of the resulting ^{18}F -difluoromethylating reagents, influencing the amount of photocatalyst and the residence time necessary to assure a complete C–H ^{18}F -difluoromethylation process. Delightfully, the labeled compounds [^{18}F]5a, [^{18}F]5c, and [^{18}F]5f were suitable for the developed flow photoredox C–H ^{18}F -difluoromethylation of a scope of heteroarenes, demanding a low amount of *fac*-Ir^{III}(ppy)₃ (0.05–0.5 mol %) and short residence times (2–4 min). Radical-scavenging experiments suggested the participation of radical intermediates in the present photocatalytic C–H ^{18}F -difluoromethylation reaction. To

the best of our knowledge, the effectiveness of the non-radioactive references of [^{18}F]5a, [^{18}F]5c, and [^{18}F]5f as difluoromethylating reagents has never been described in visible light photoredox catalysis. This study clearly demonstrates that the great potential of [^{18}F]difluoromethyl heteroaryl-sulfones toward the C-H functionalization of heteroarenes. Taking into consideration the reactivity of the sulfones **1** and **2** [39-45], the newly synthesized [^{18}F]difluoromethyl heteroaryl-sulfones can also be explored in the photoredox ^{18}F -difluoromethylation of substrates bearing C=C, C \equiv C, and C \equiv N bonds. Alternatively, Hu and co-workers recently reported the employment of the sulfone **1** in the metal-free insertion of difluoromethylthio (-SCF $_2$ H) groups in indoles [53]. The sulfone **2** is widely described as a reagent for difluoroolefination of aldehydes and ketones [54-58]. Late-stage ^{18}F -difluoromethylthiolation and ^{18}F -difluoroolefination of organic substrates has never been reported in the literature. Thus, the use of [^{18}F]difluoromethyl heteroaryl-sulfones in these organic transformations would enable the direct transfer [^{18}F]SCF $_2$ H and [^{18}F]CF $_2$ groups in adequate precursors.

Overall, we expect that the potential versatility of newly synthesized [^{18}F]difluoromethyl heteroaryl-sulfones [^{18}F]5a, [^{18}F]5c, and [^{18}F]5f may contribute to the development of novel radioactive probes for PET imaging with improved molar activities.

5. Supplementary Information

5.1. NMR spectra of the compounds 4a-4f, 5a-5f, and 6a-6f

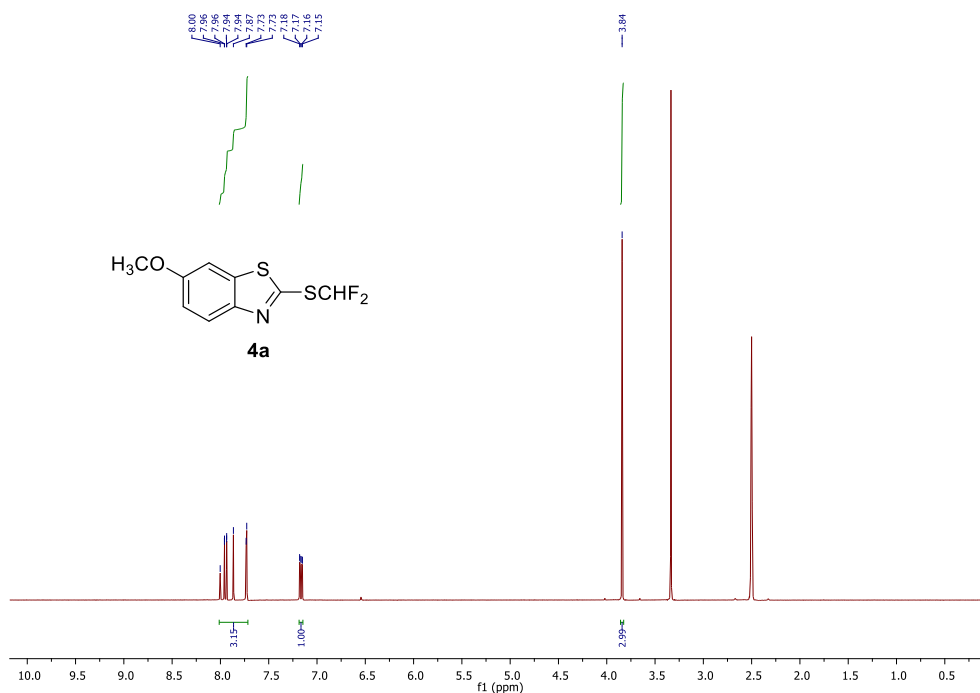


Figure S1. ^1H -NMR spectrum of **4a**.

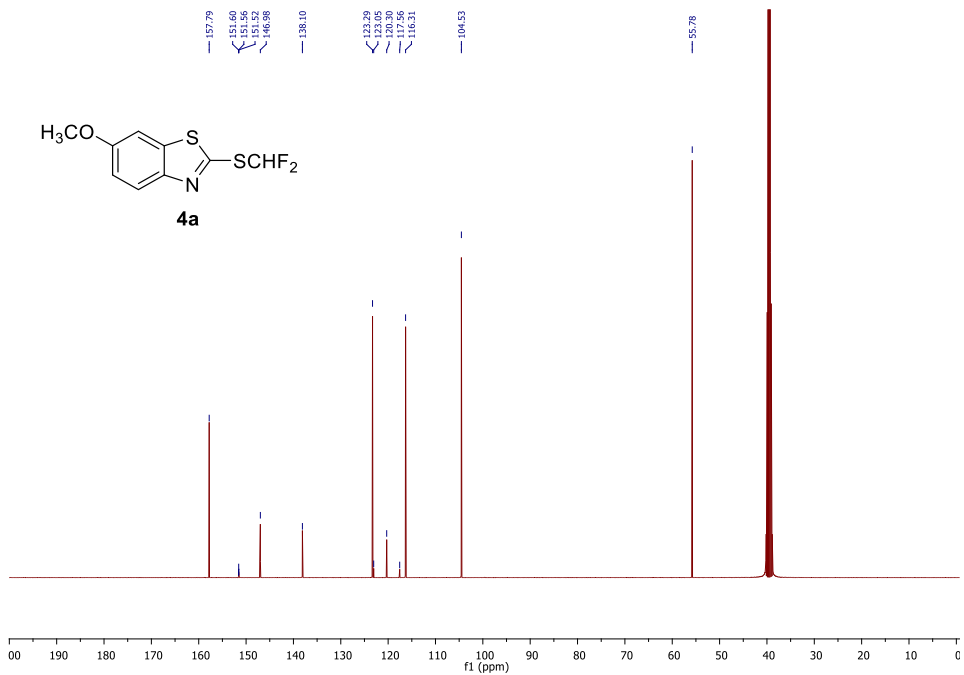


Figure S2. ¹³C-NMR spectrum of 4a.

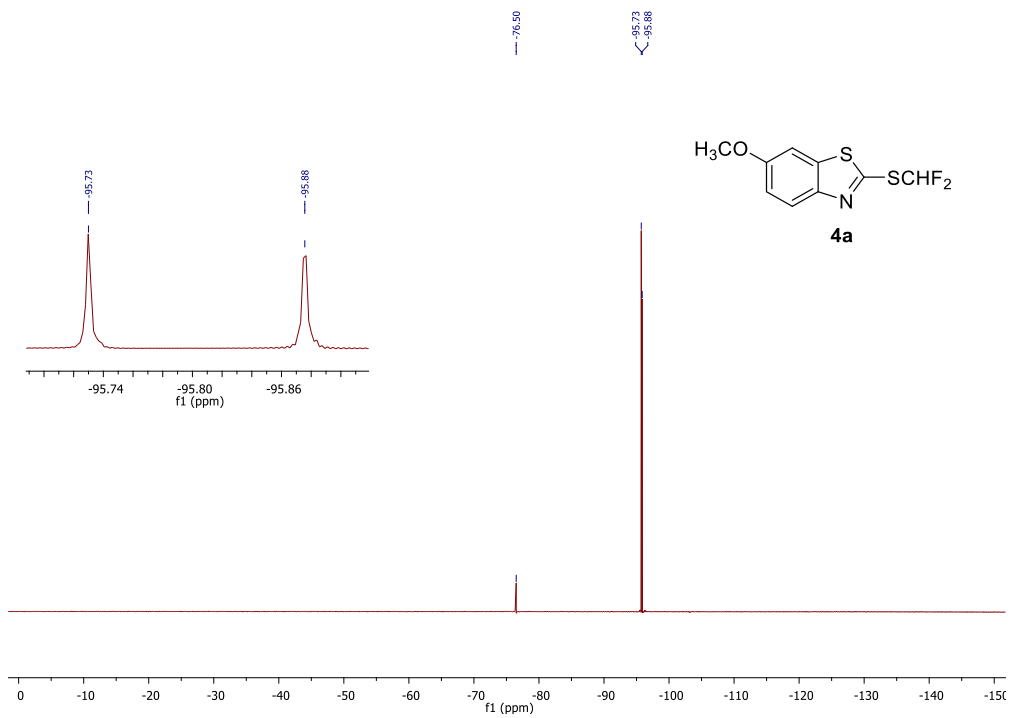


Figure S3. ¹⁹F-NMR spectrum of 4a.

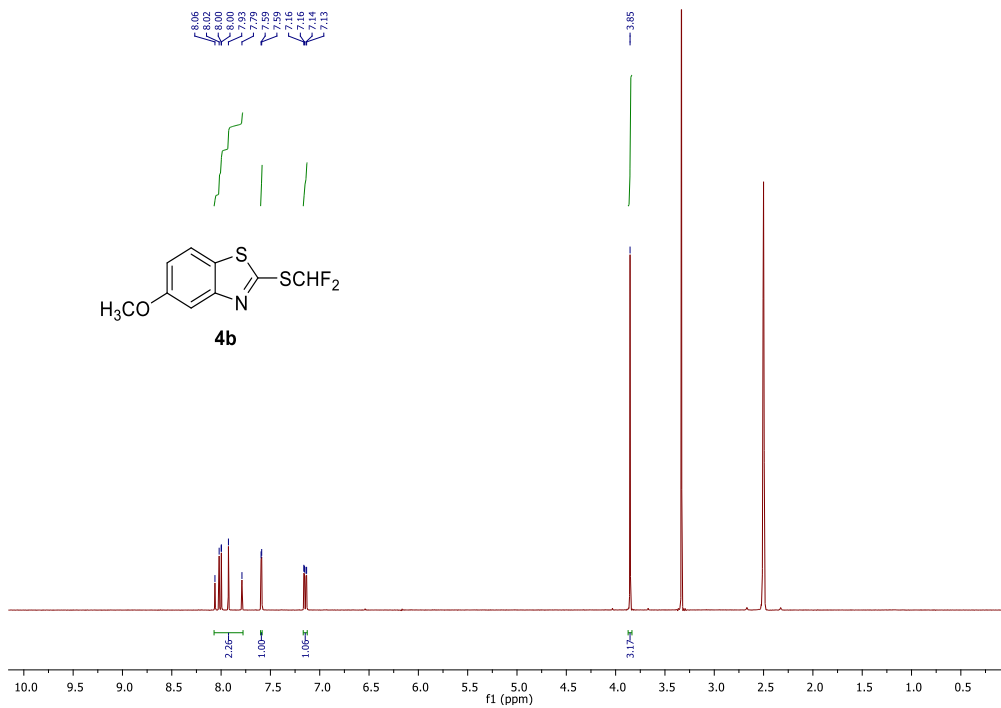


Figure S4. ¹H-NMR spectrum of **4b**.

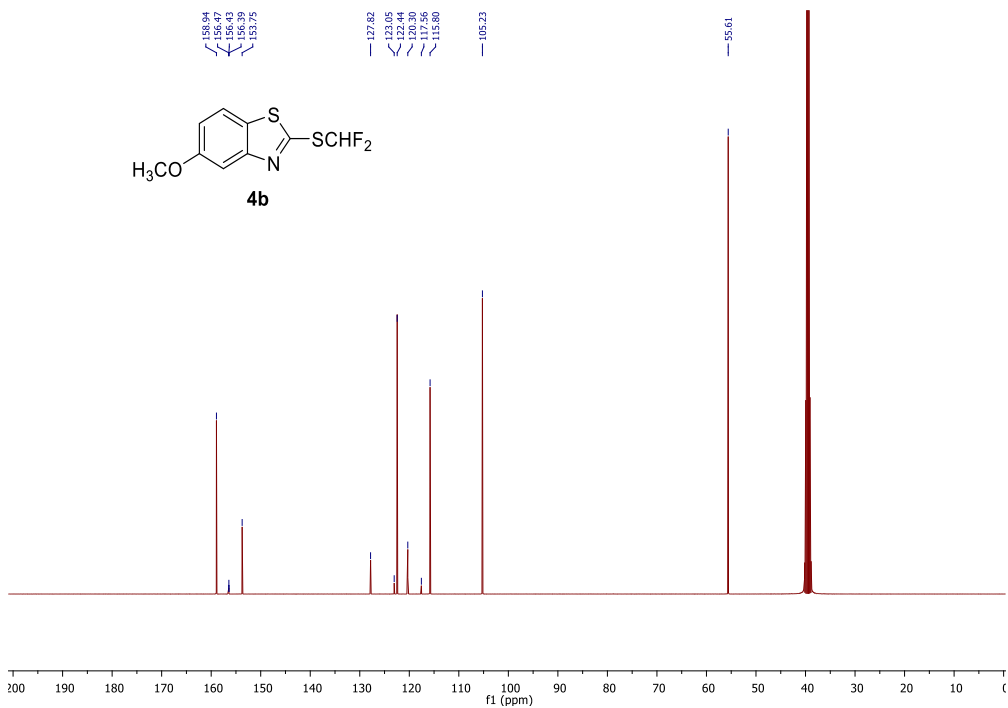
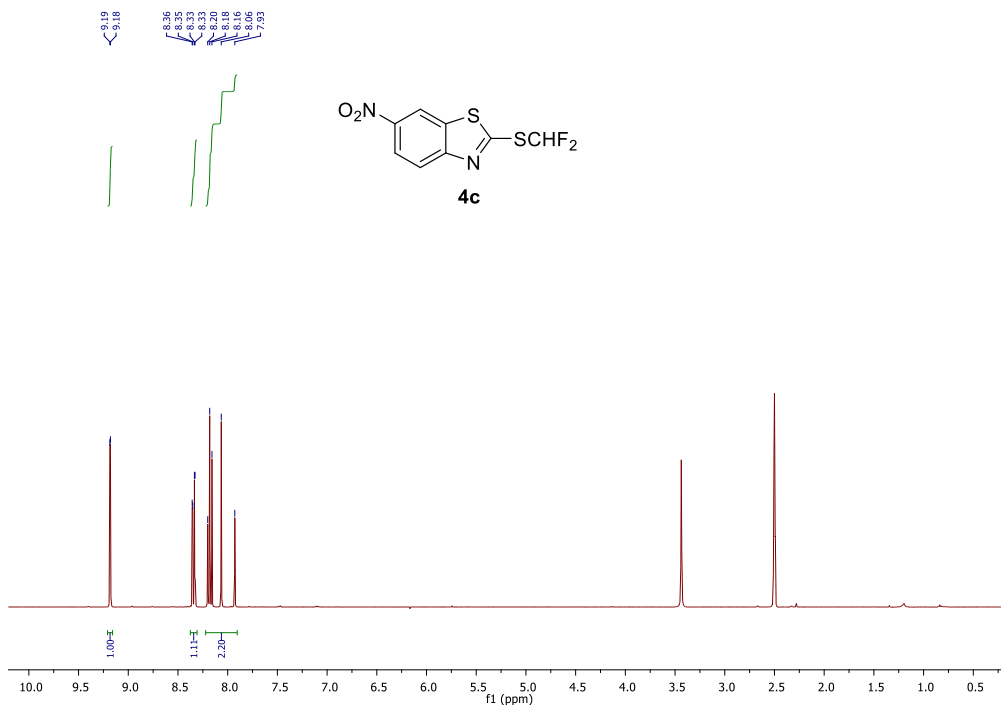
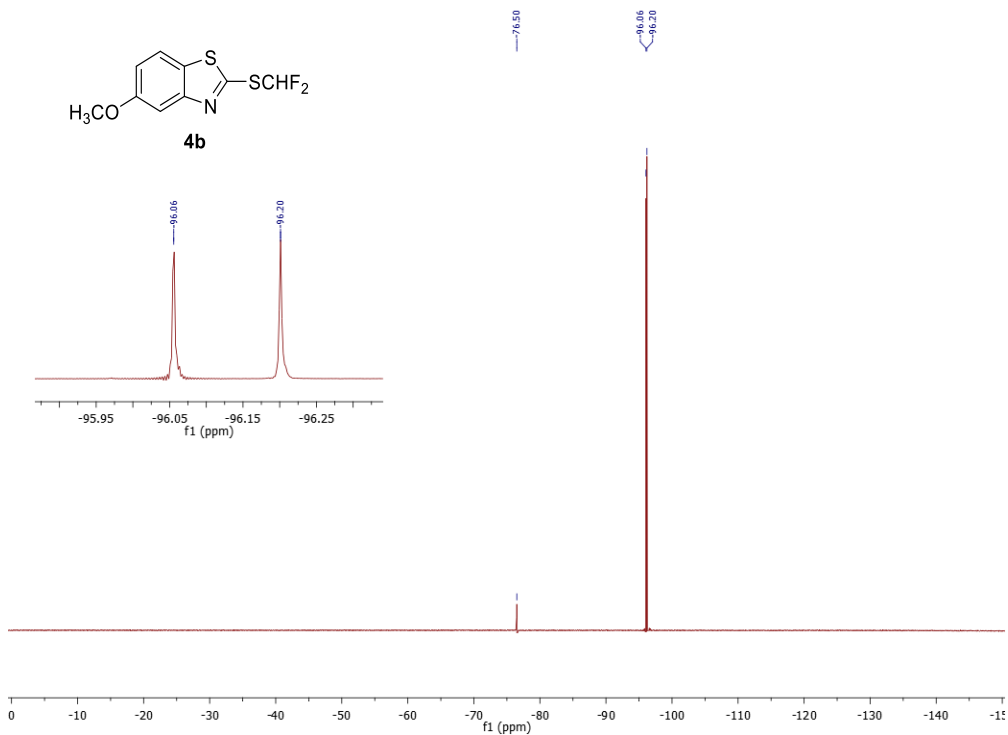


Figure S5. ¹³C-NMR spectrum of **4b**.



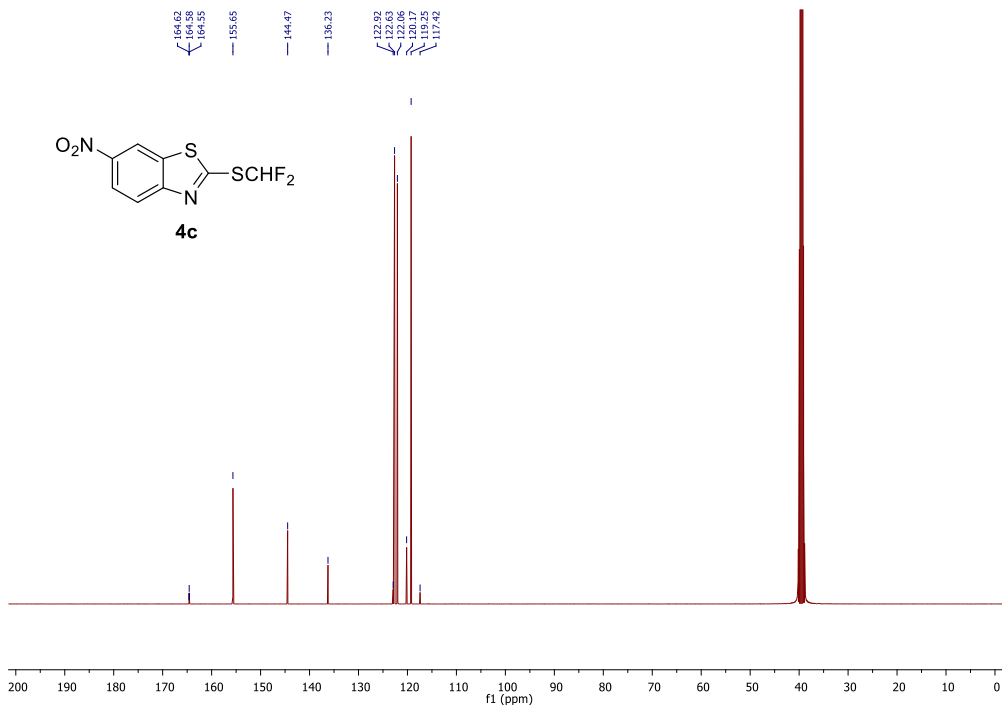


Figure S8. ¹³C-NMR spectrum of **4c**.

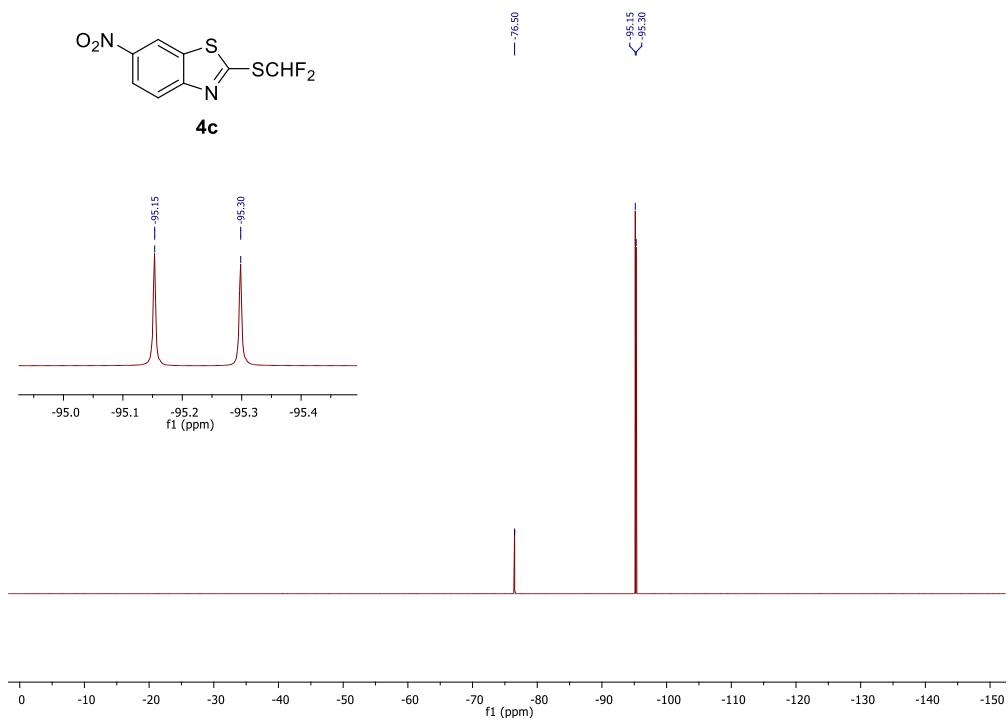


Figure S9. ¹⁹F-NMR spectrum of **4c**.

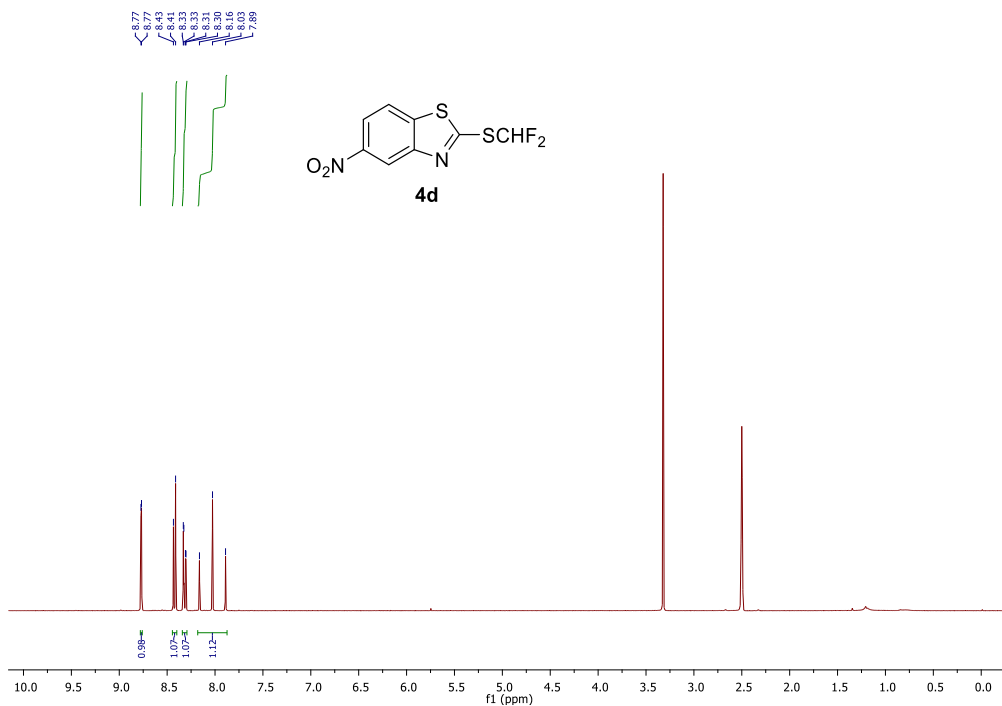


Figure S10. ¹H-NMR spectrum of **4d**.

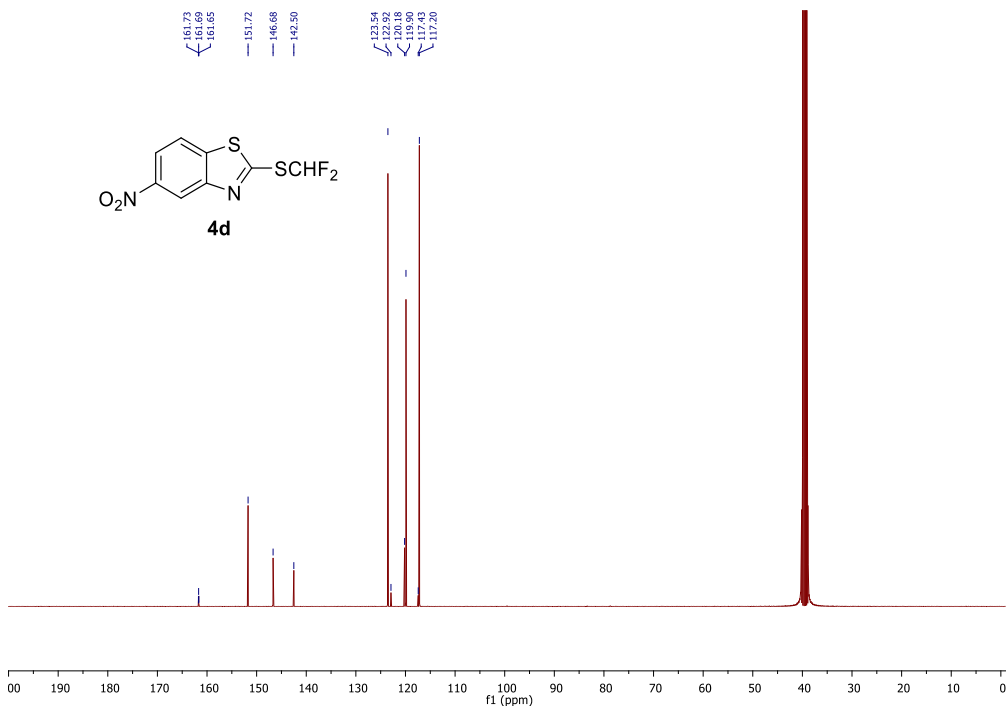


Figure S11. ¹³C-NMR spectrum of **4d**.

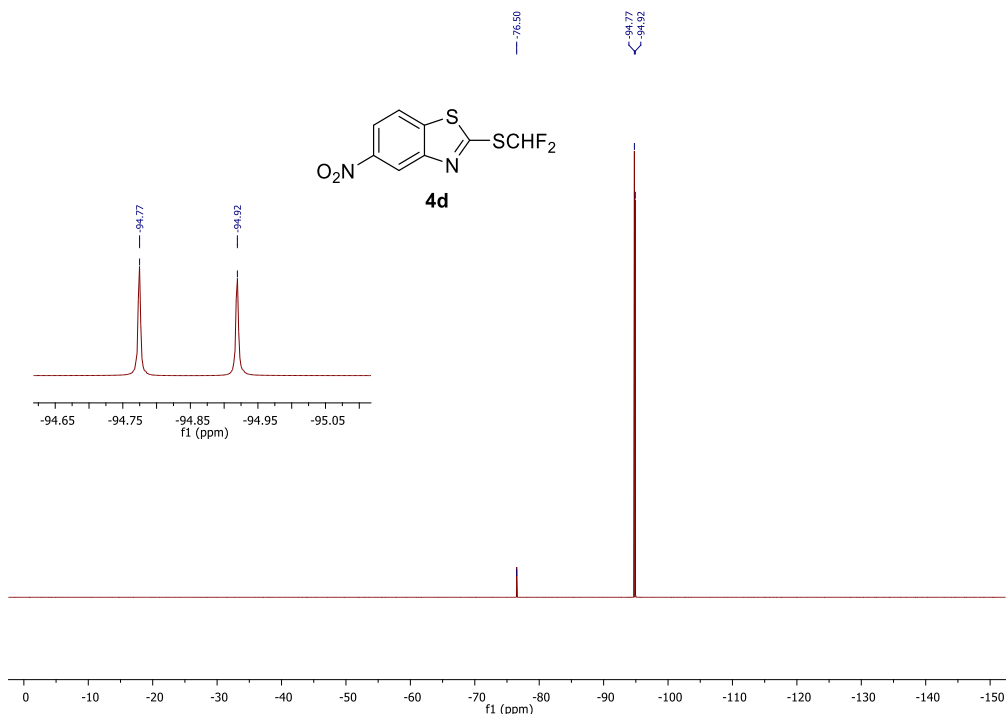


Figure S12. ¹⁹F-NMR spectrum of **4d**.

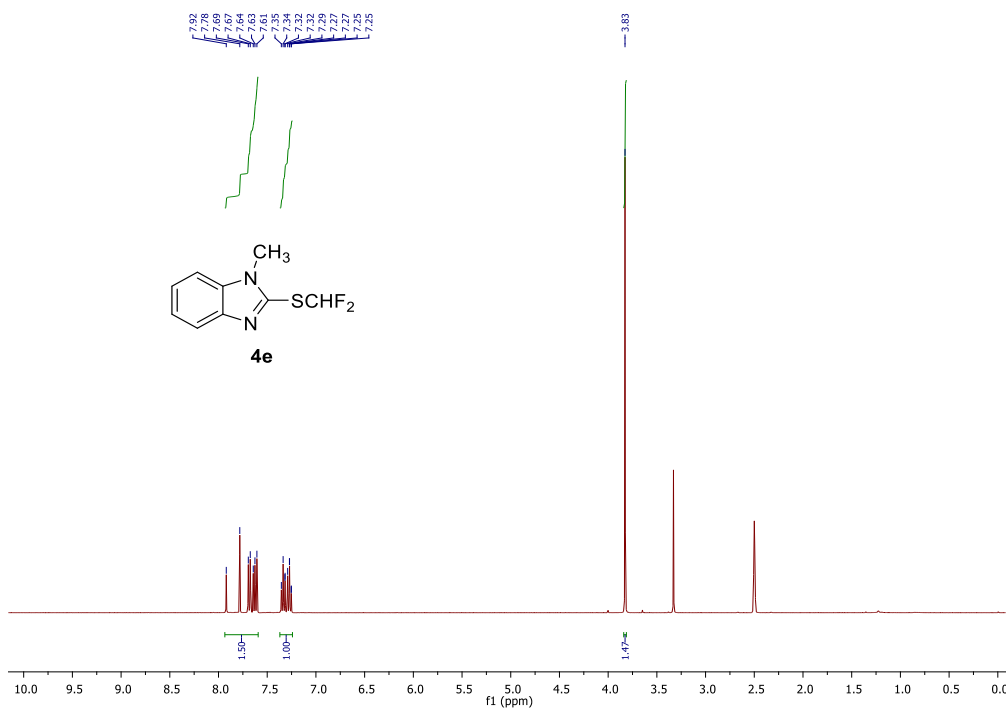


Figure S13. ¹H-NMR spectrum of **4e**.

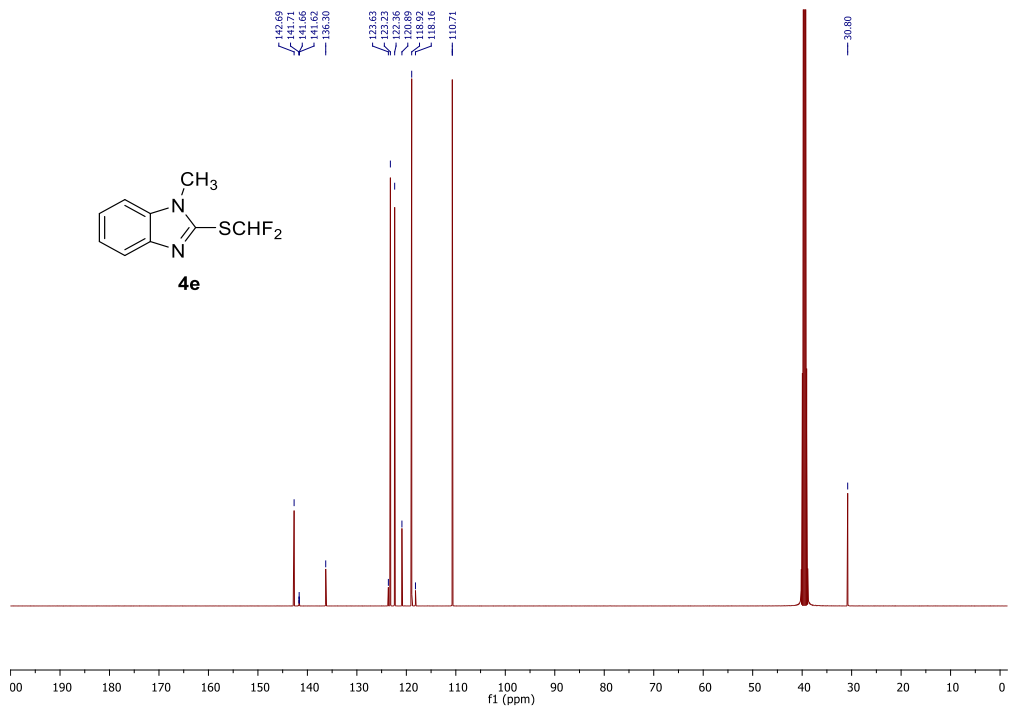


Figure S14. ¹³C-NMR spectrum of **4e**.

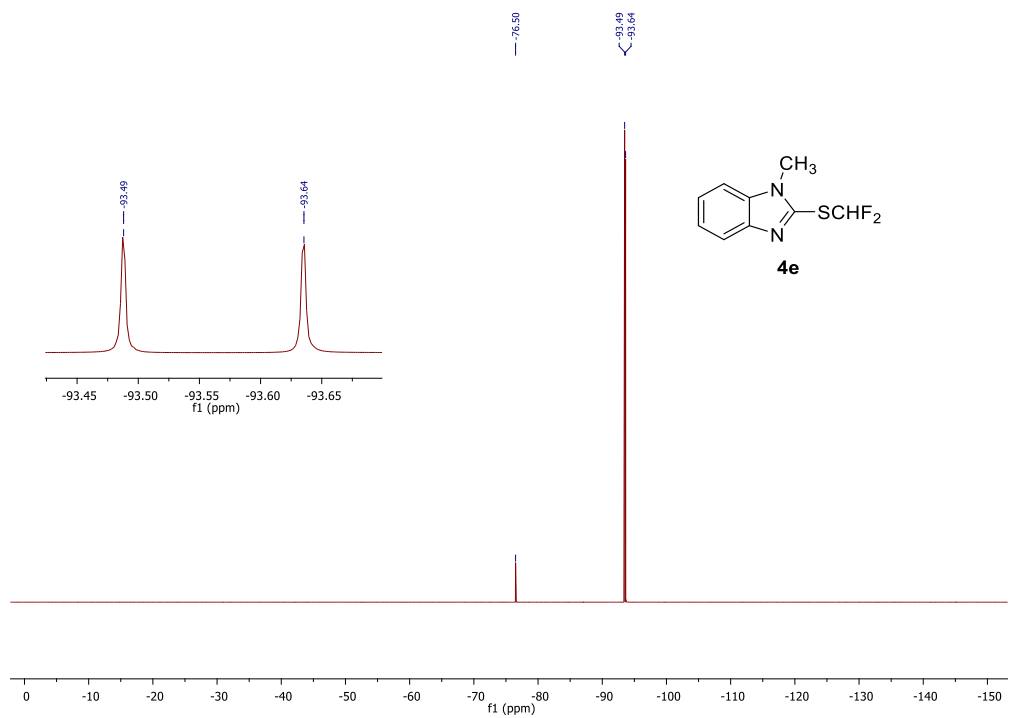


Figure S15. ¹⁹F-NMR spectrum of **4e**.

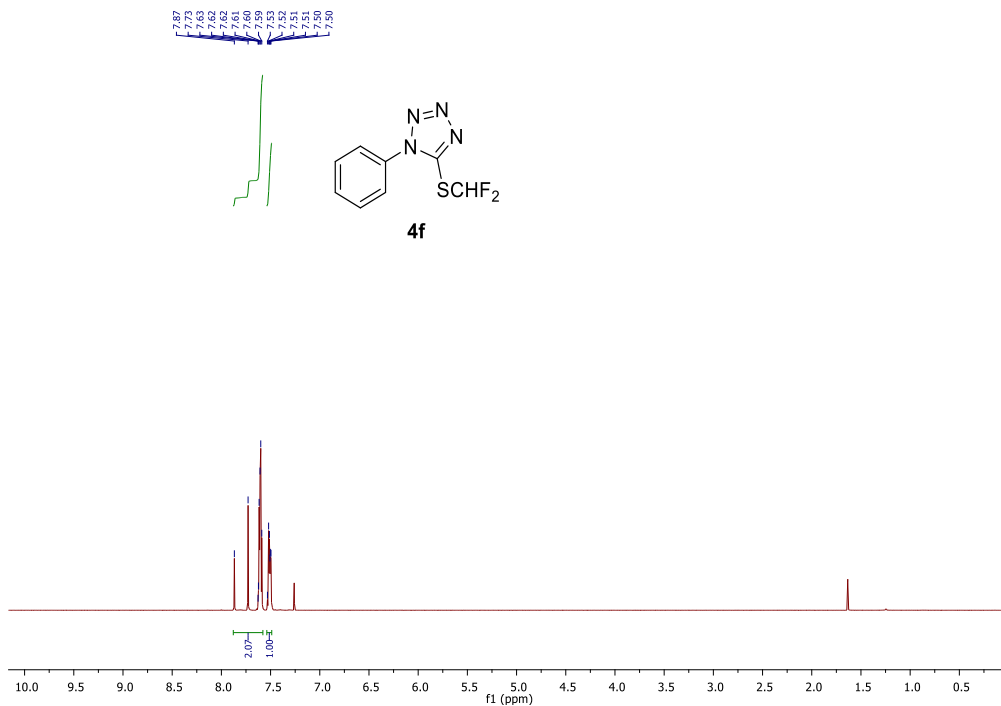


Figure S16. ^1H -NMR spectrum of **4f**.

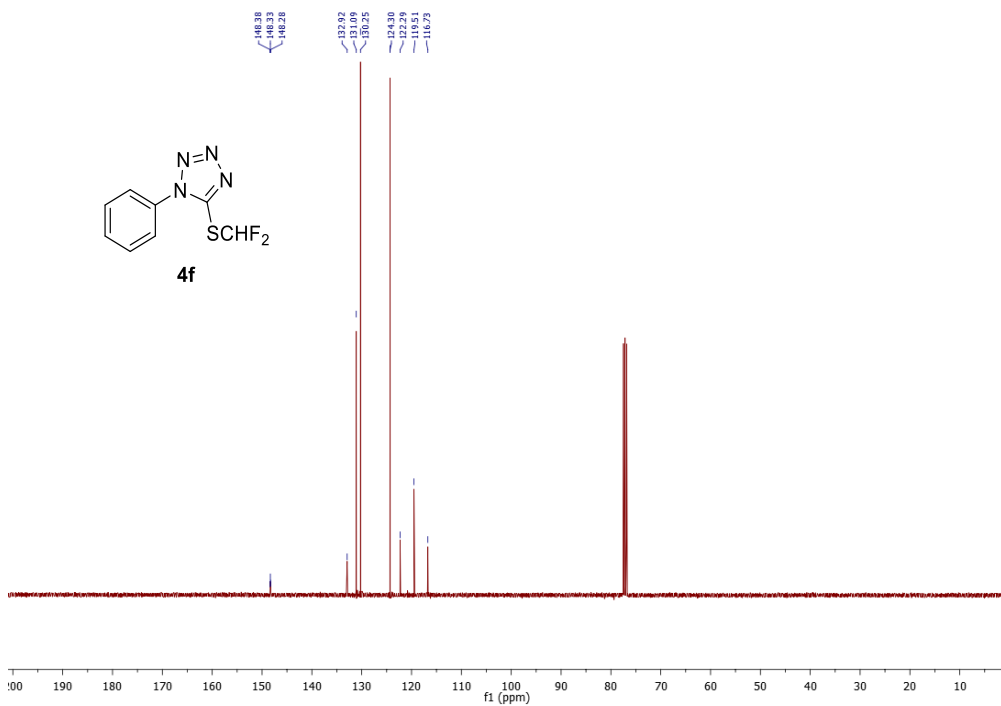
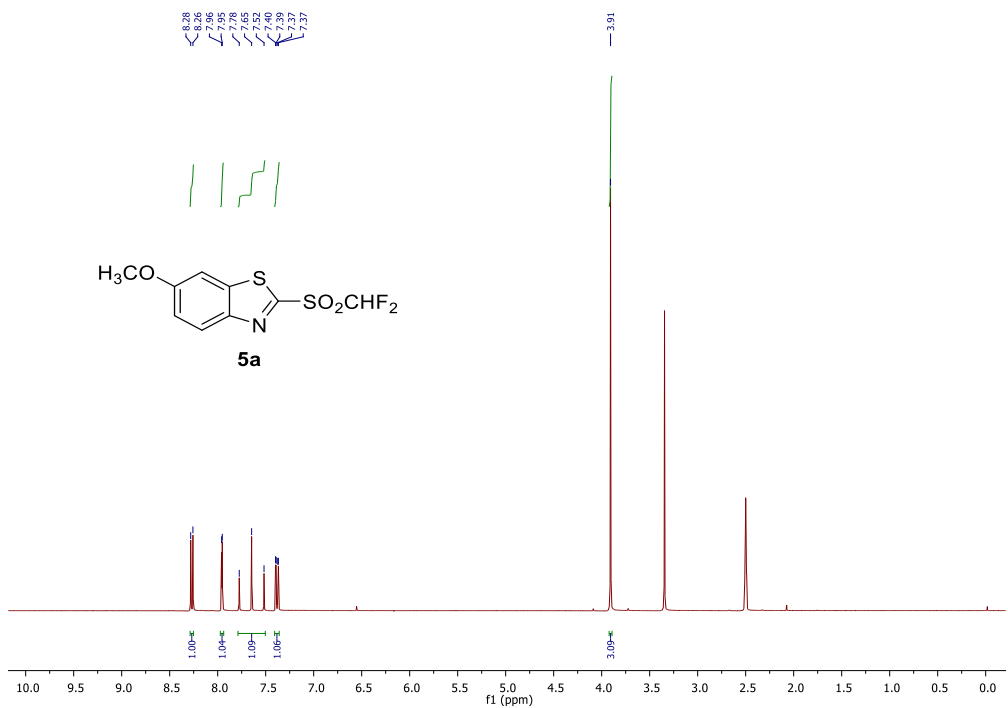
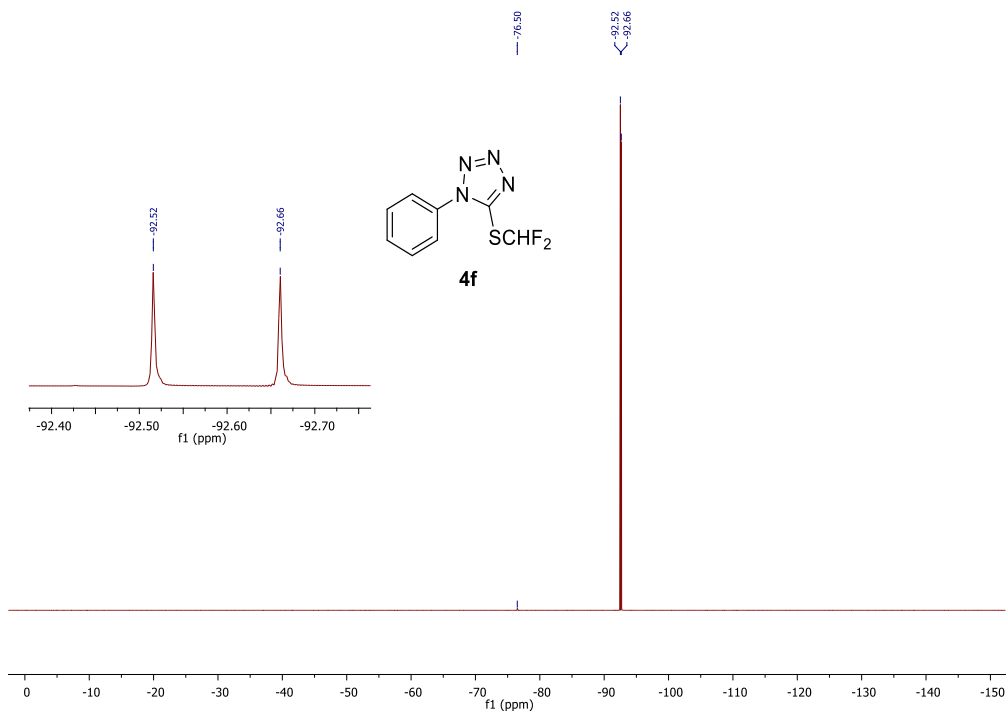


Figure S17. ^{13}C -NMR spectrum of **4f**.



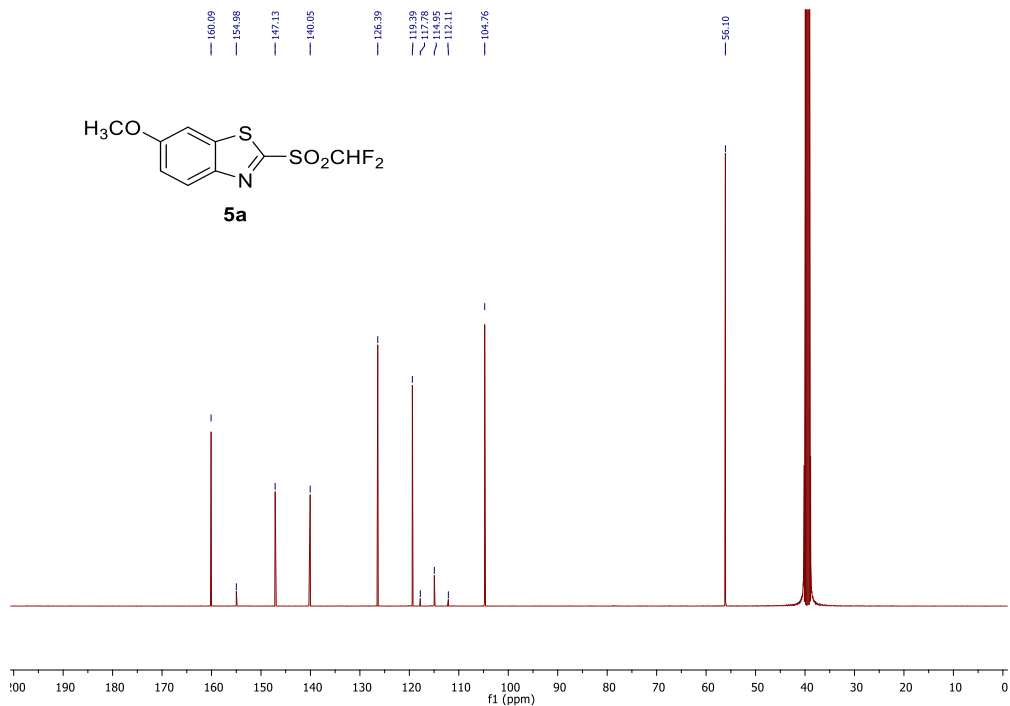


Figure S20. ¹³C-NMR spectrum of **5a**.

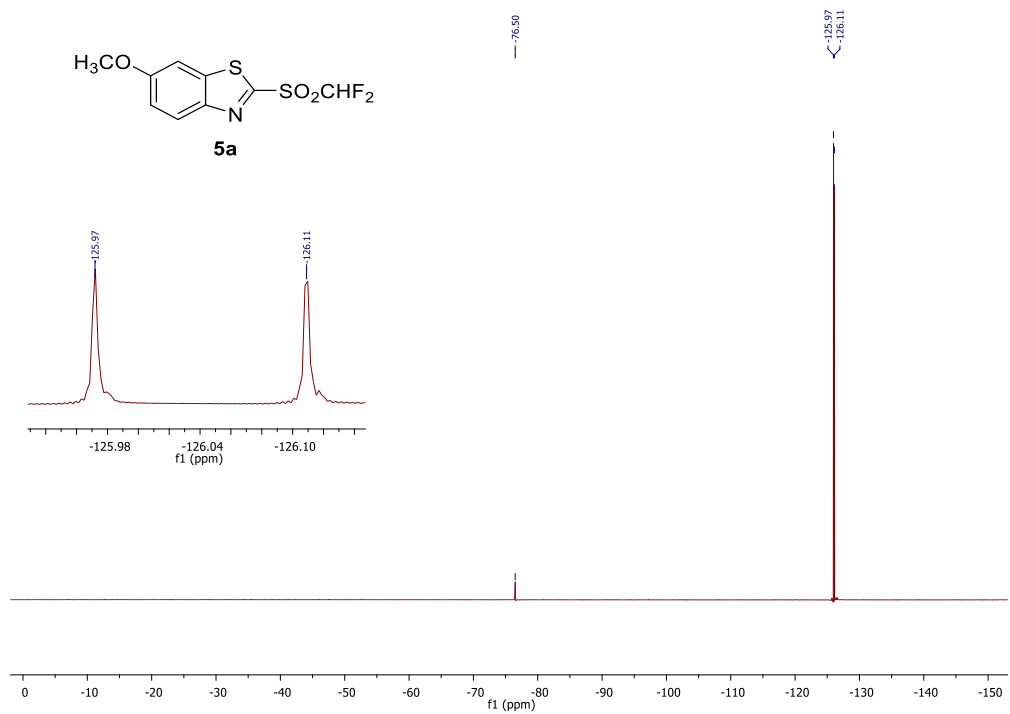


Figure S21. ¹⁹F-NMR spectrum of **5a**.

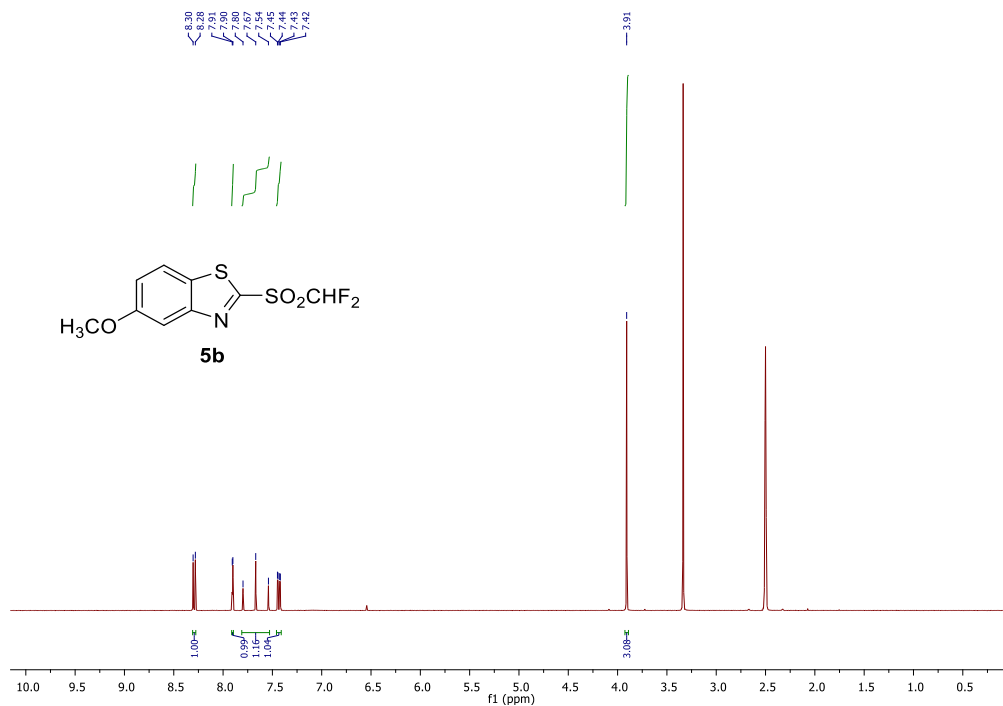


Figure S22. ¹H-NMR spectrum of **5b**.

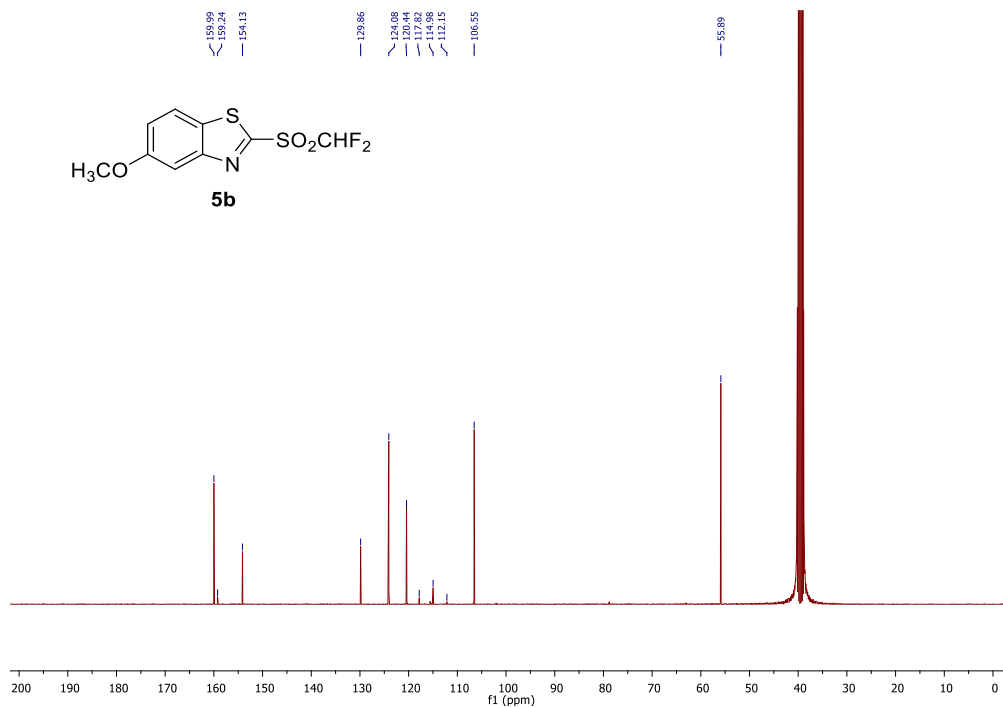


Figure S23. ¹³C-NMR spectrum of **5b**.

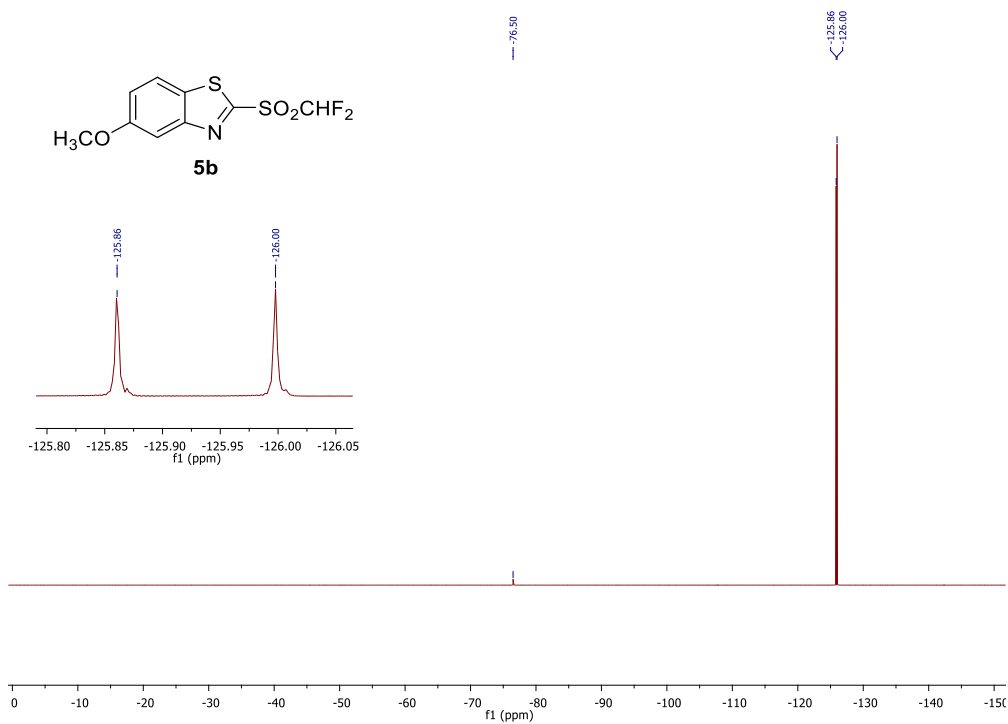


Figure S24. ^{19}F -NMR spectrum of **5b**.

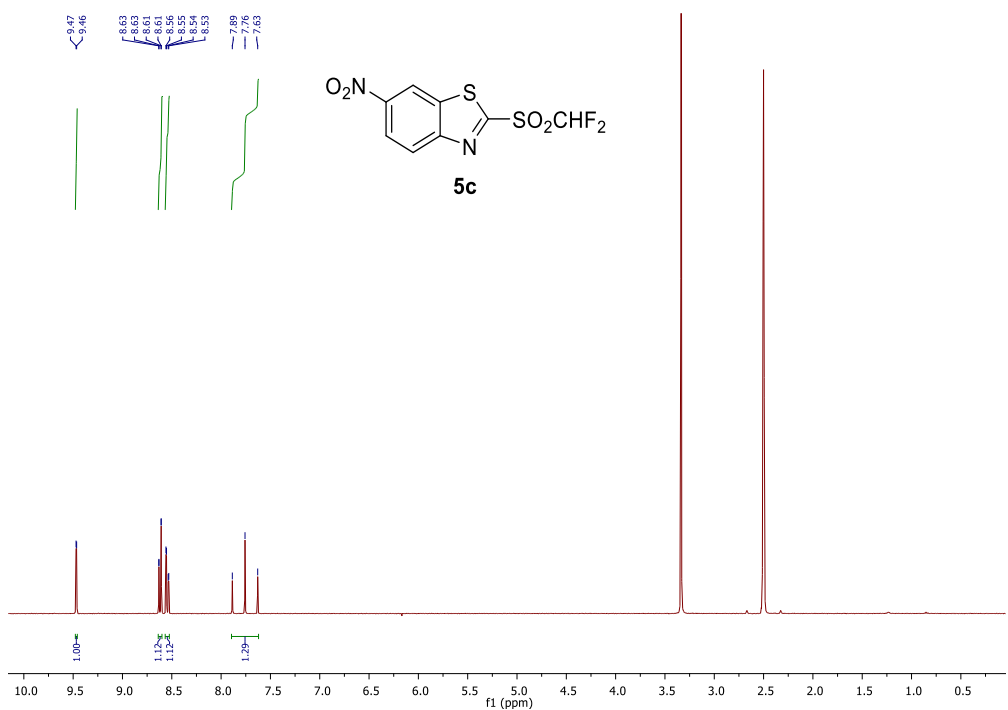


Figure S25. ^1H -NMR spectrum of **5c**.

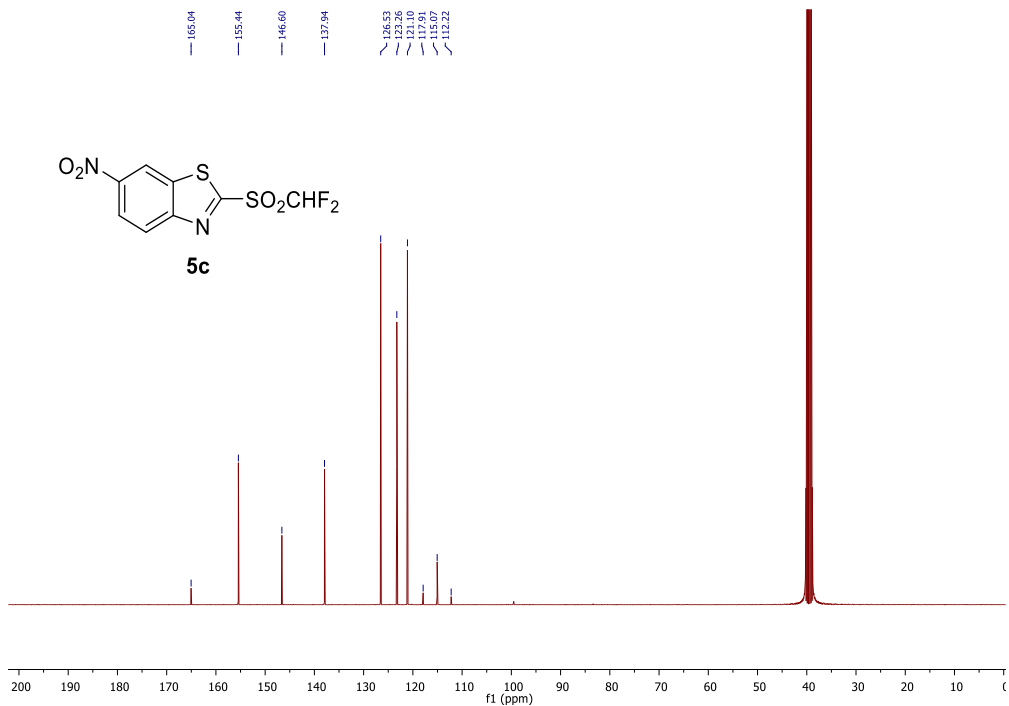


Figure S26. ¹³C-NMR spectrum of **5c**.

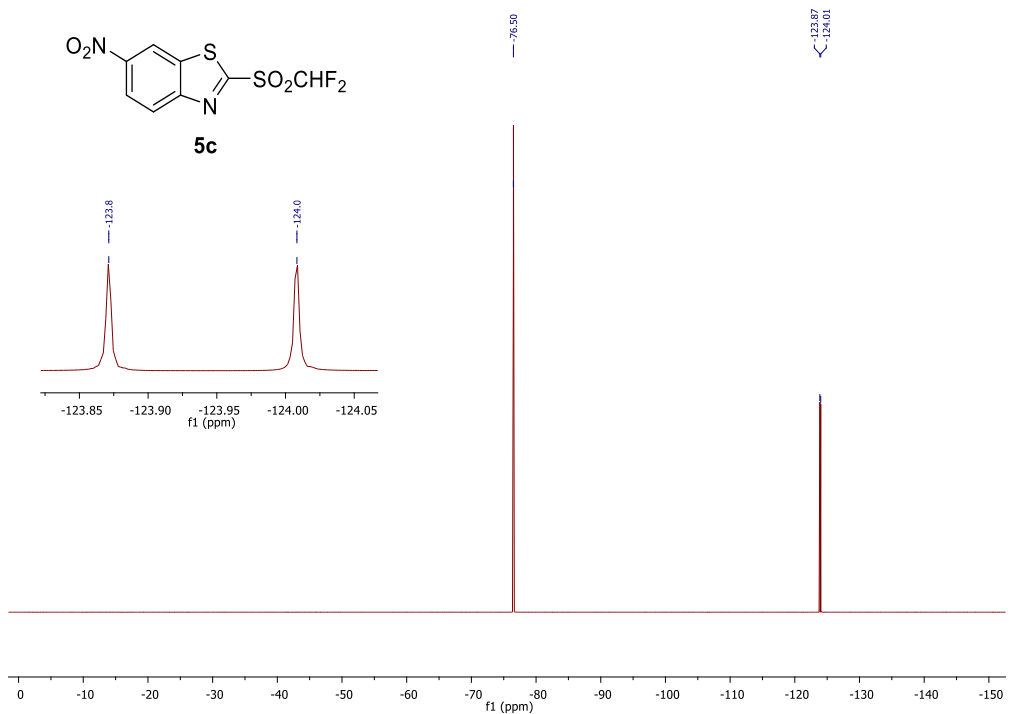


Figure S27. ¹⁹F-NMR spectrum of **5c**.

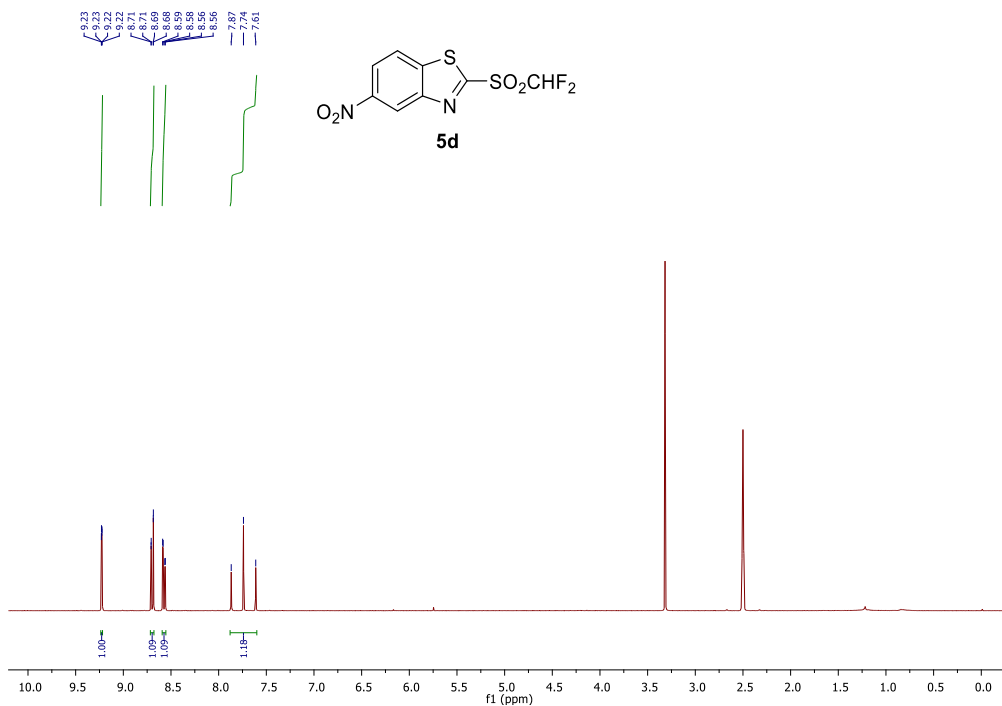


Figure S28. ¹H-NMR spectrum of **5d**.

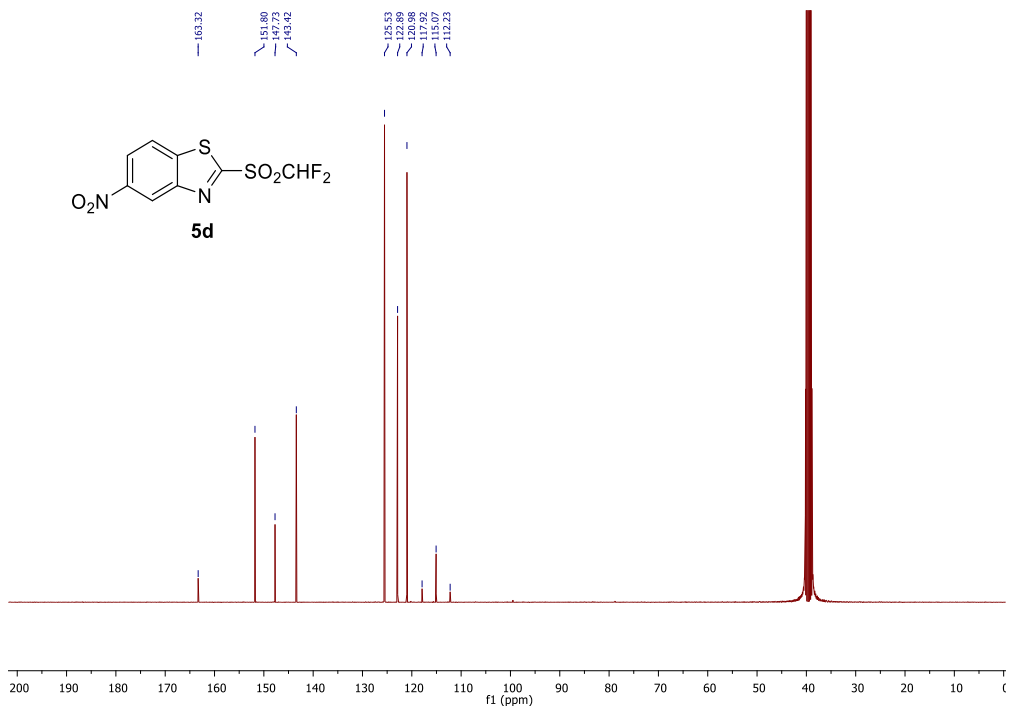


Figure S29. ¹³C-NMR spectrum of **5d**.

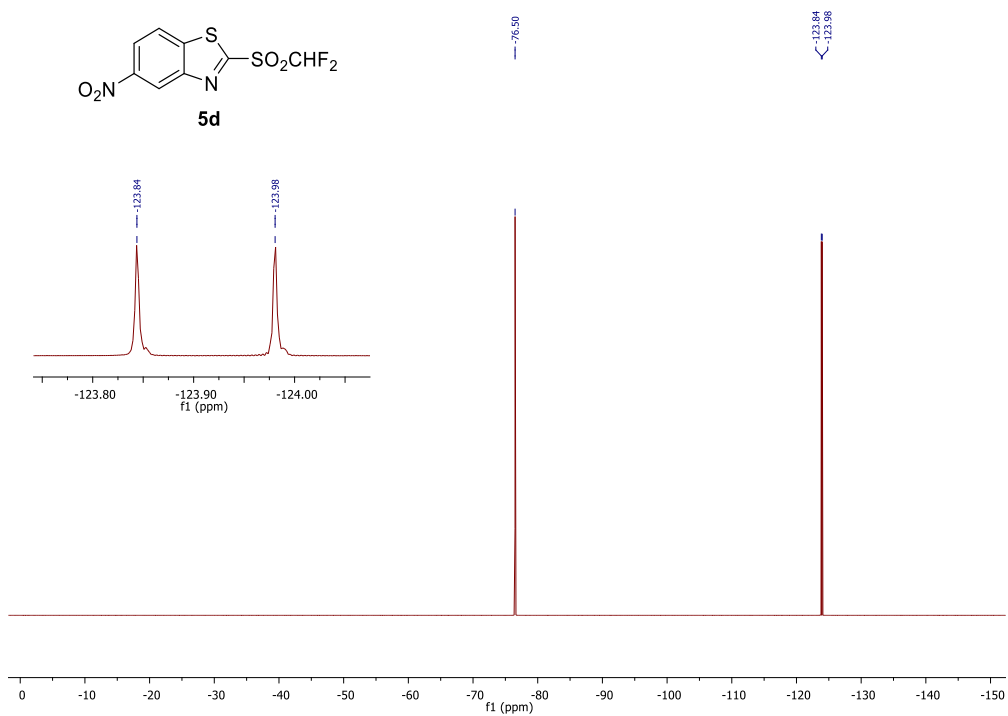


Figure S30. ^{19}F -NMR spectrum of **5d**.

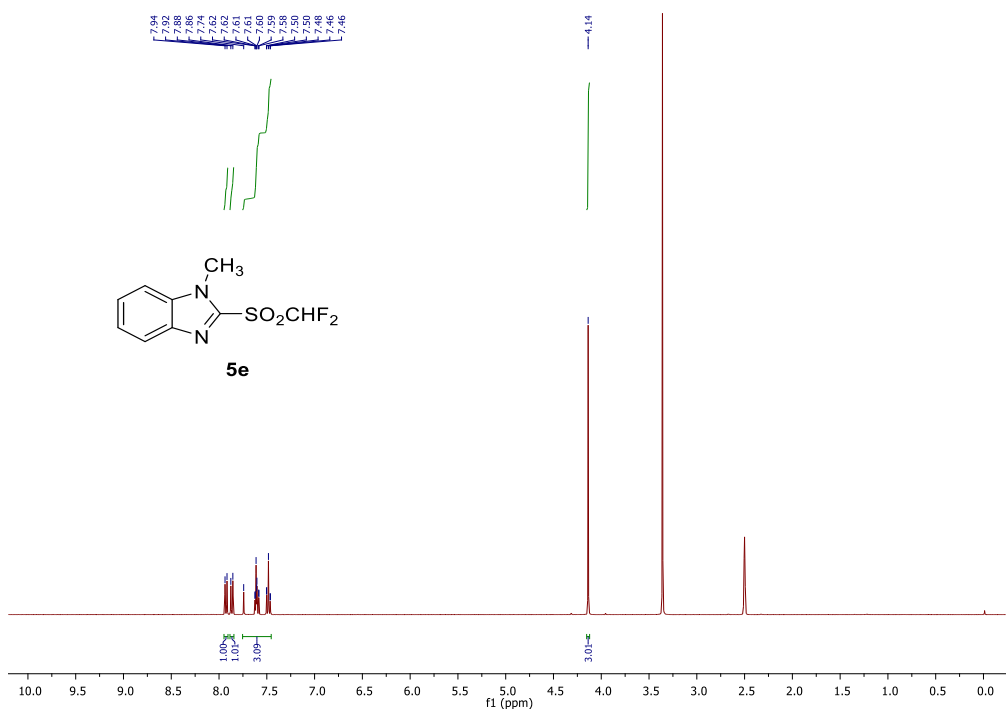


Figure S31. ^1H -NMR spectrum of **5e**.

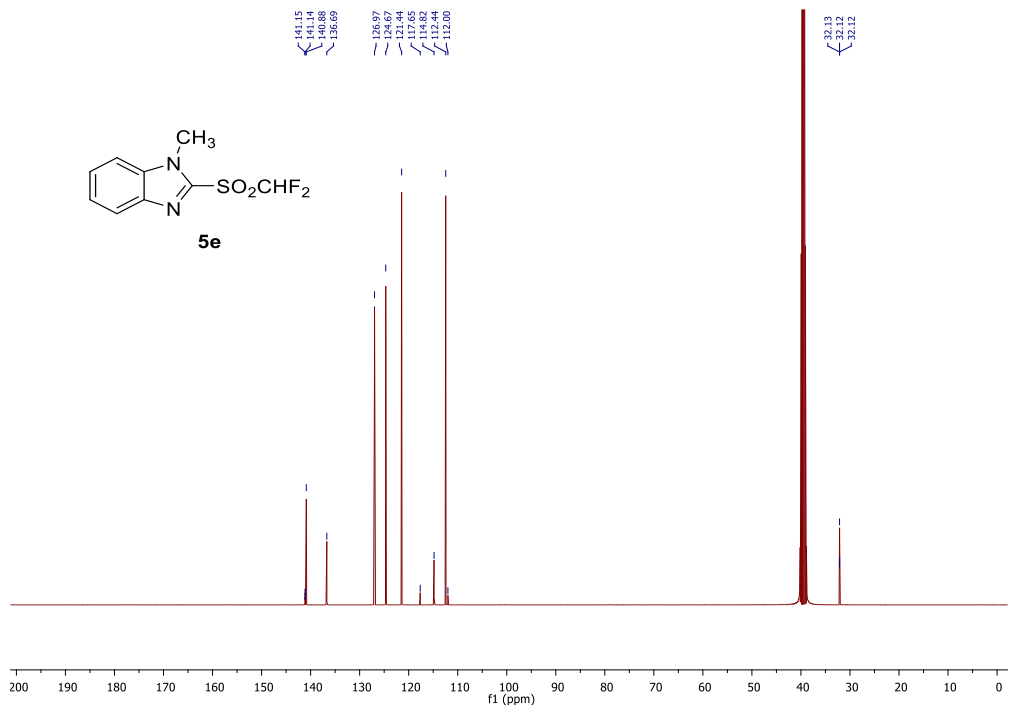


Figure S32. ^{13}C -NMR spectrum of **5e**.

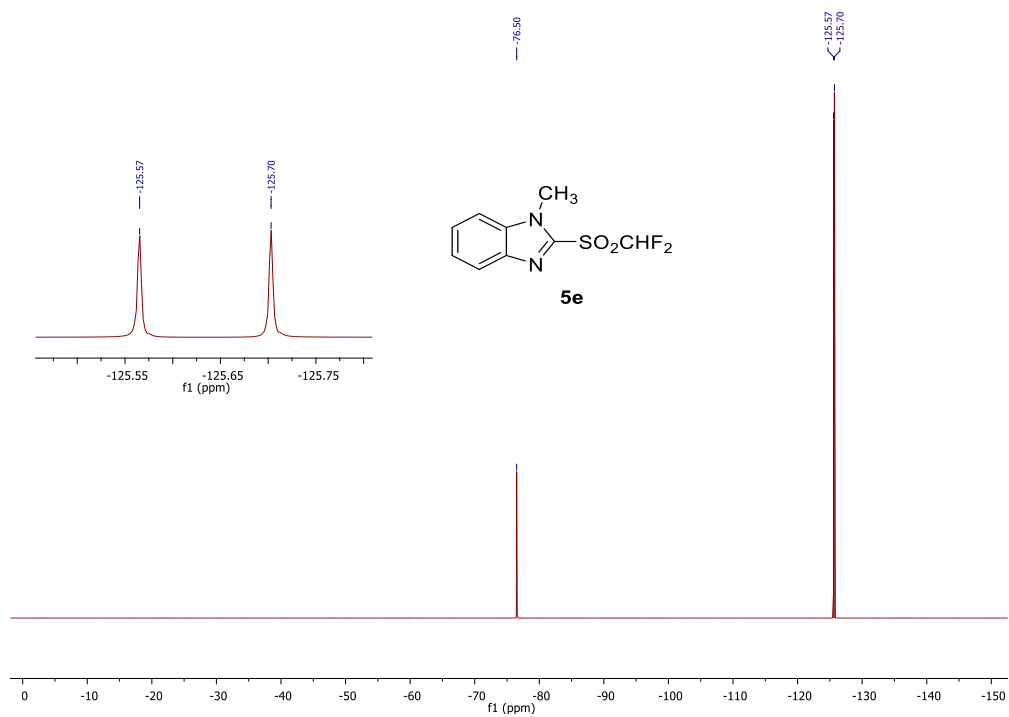


Figure S33. ^{19}F -NMR spectrum of **5e**.

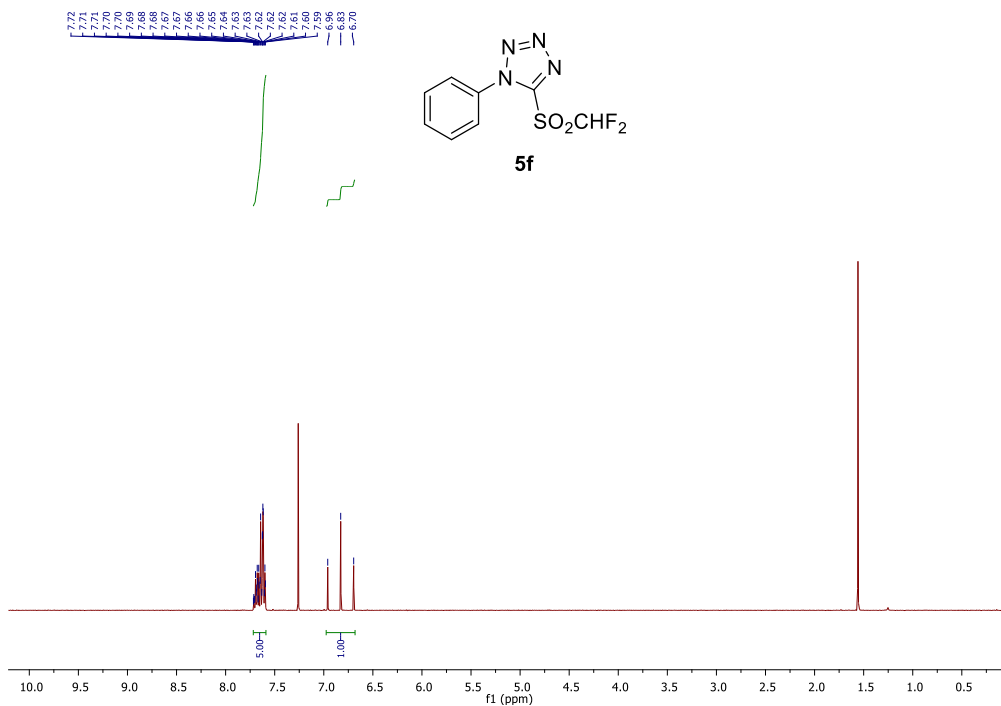


Figure S34. ¹H-NMR spectrum of **5f**.

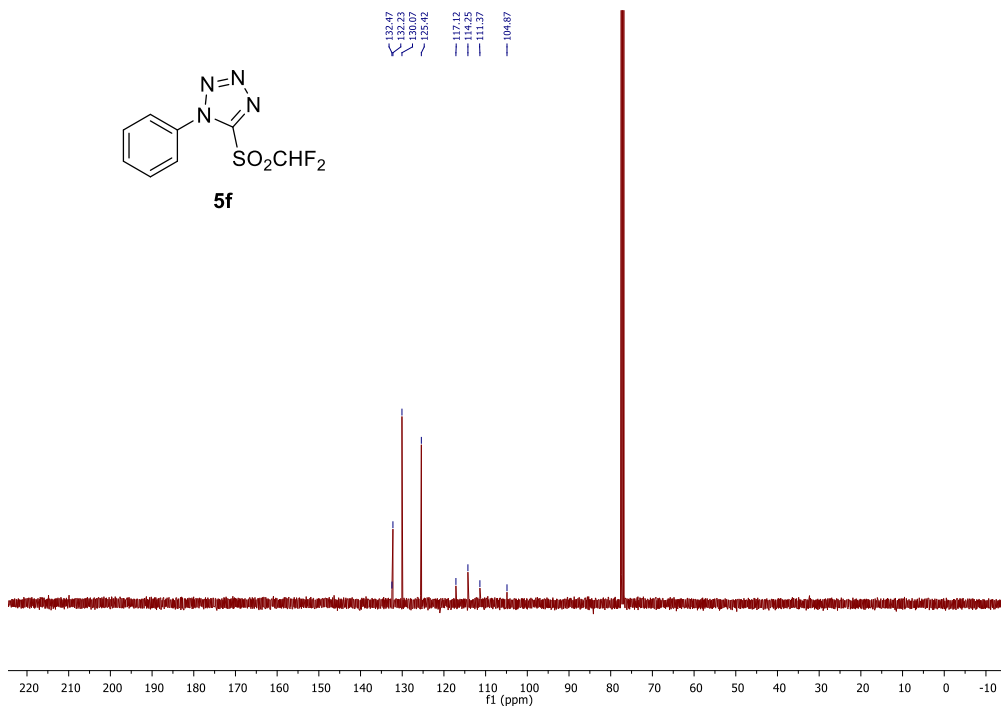


Figure S35. ¹³C-NMR spectrum of **5f**.

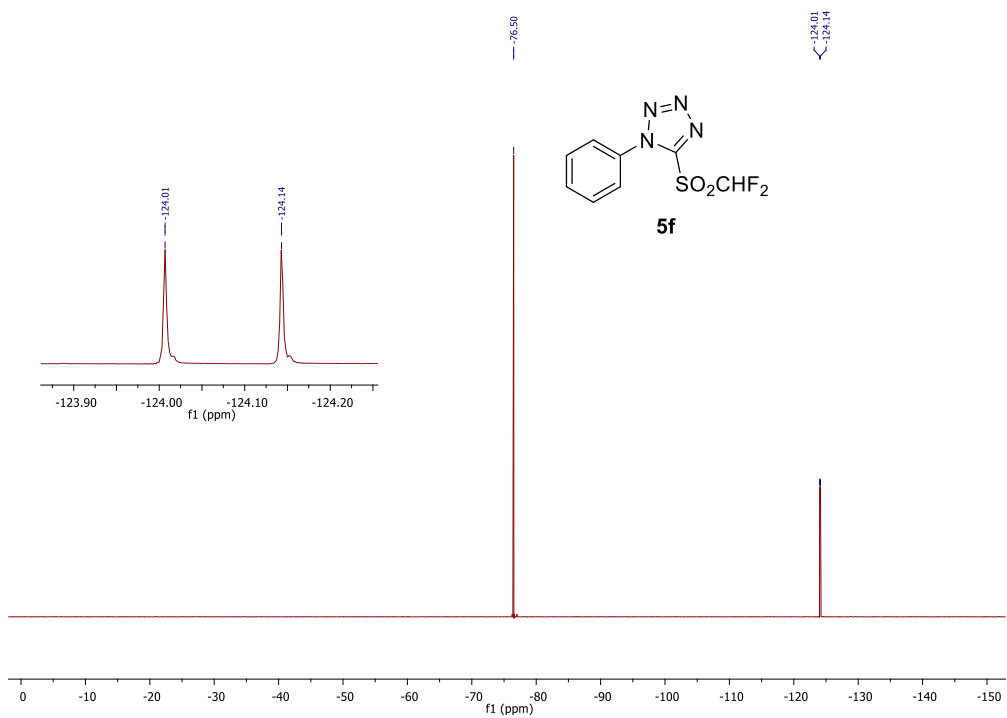


Figure S36. ^{19}F -NMR spectrum of **5f**.

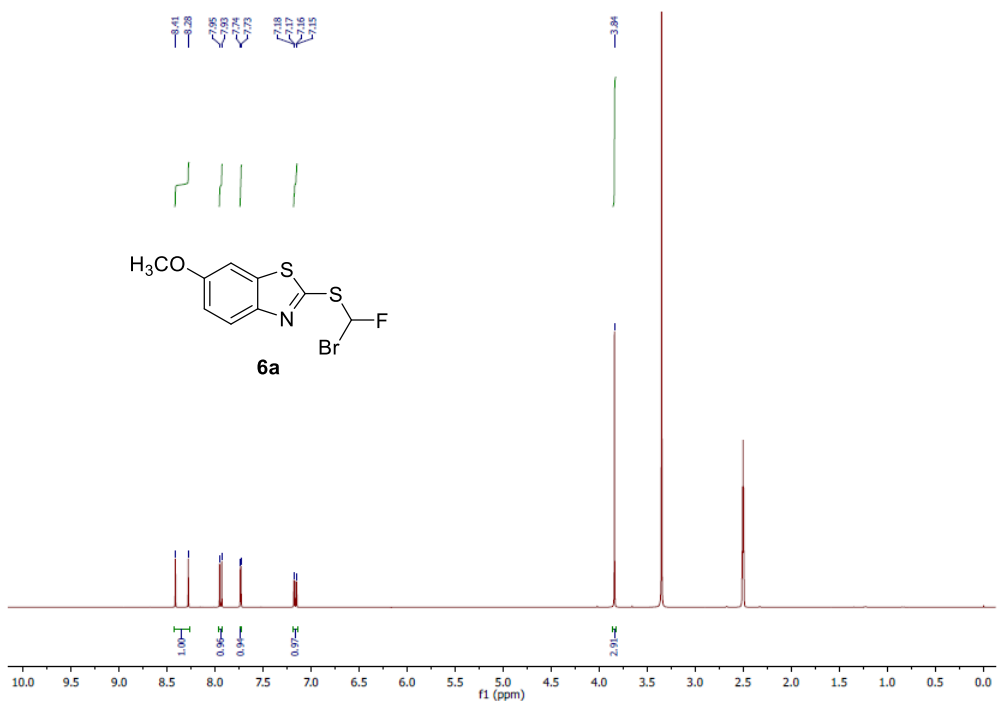


Figure S37. ^1H -NMR spectrum of **6a**.

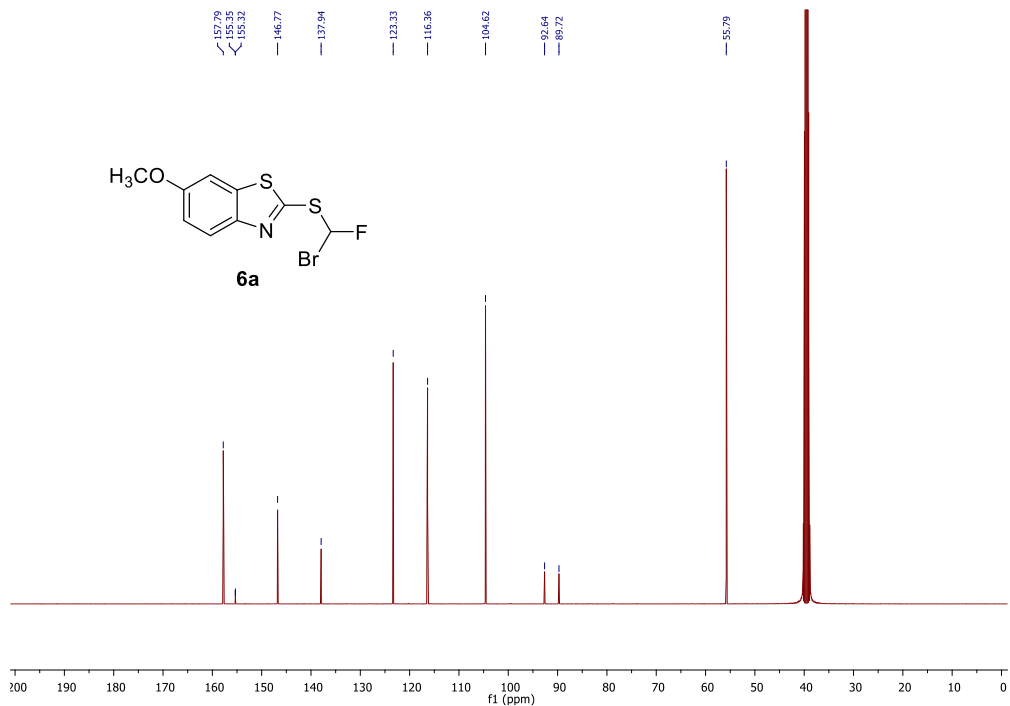


Figure S38. ¹³C-NMR spectrum of **6a**.

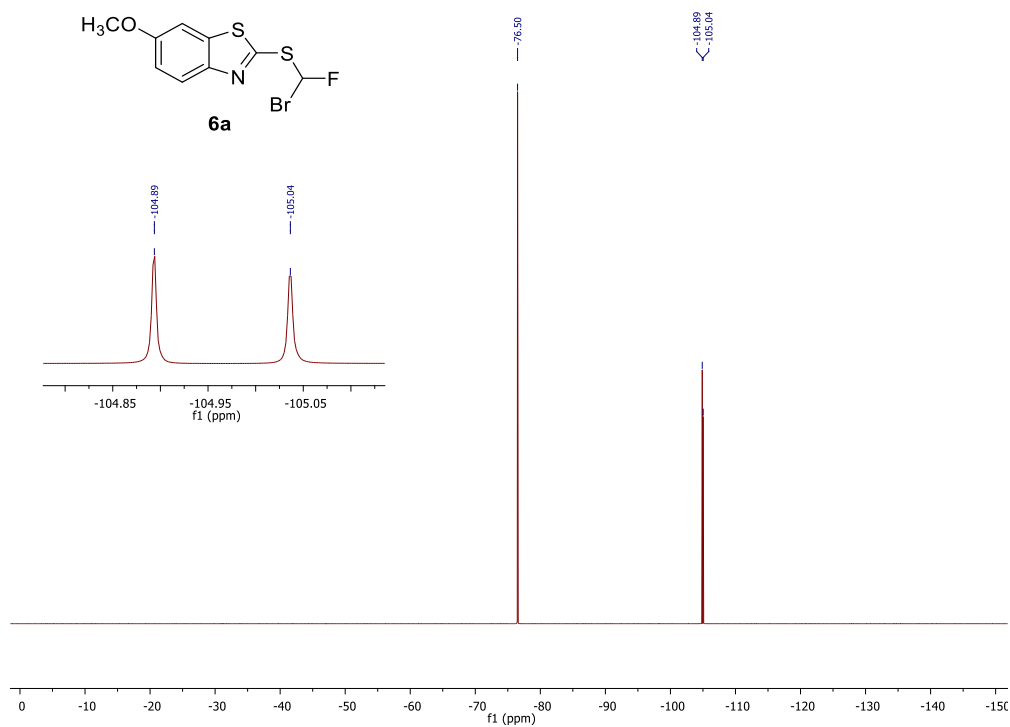


Figure S39. ¹⁹F-NMR spectrum of **6a**.

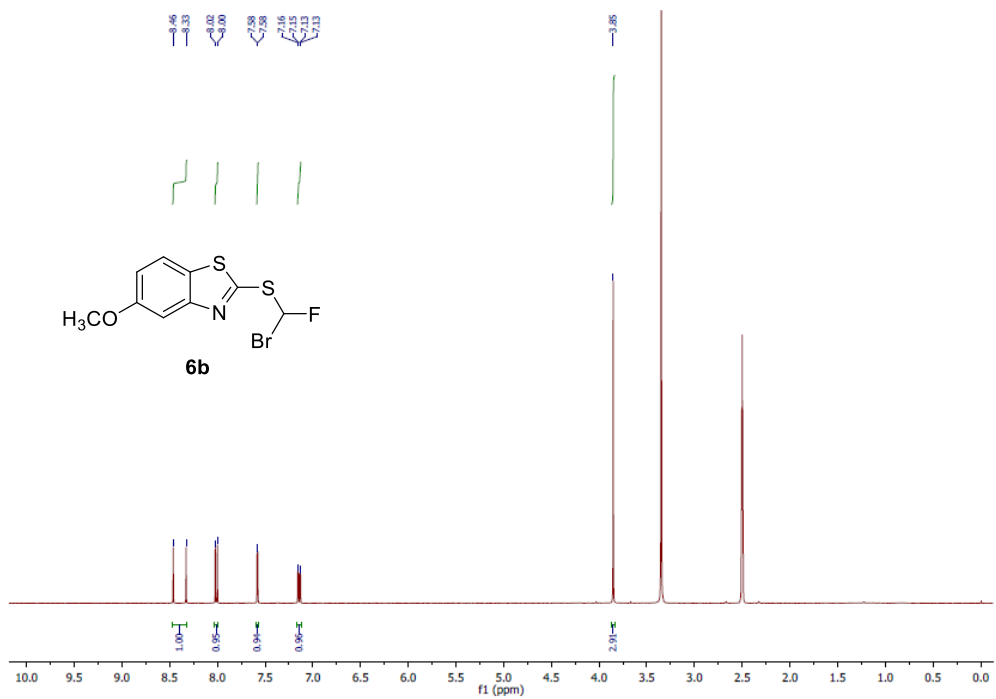


Figure S40. ¹H-NMR spectrum of **6b**.

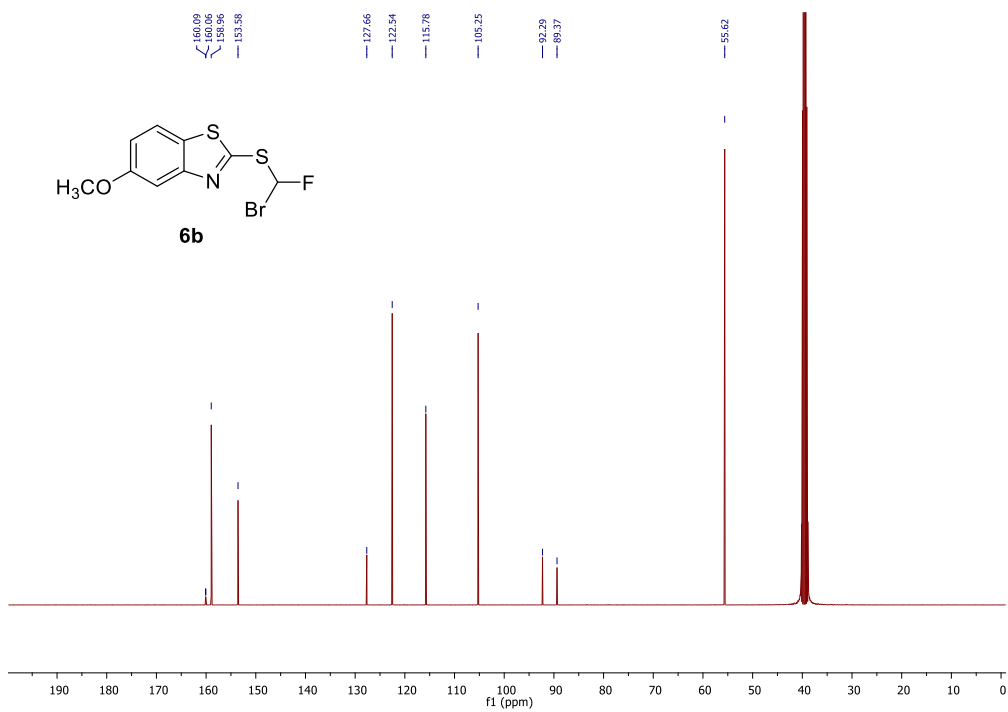


Figure S41. ¹³C-NMR spectrum of **6b**.

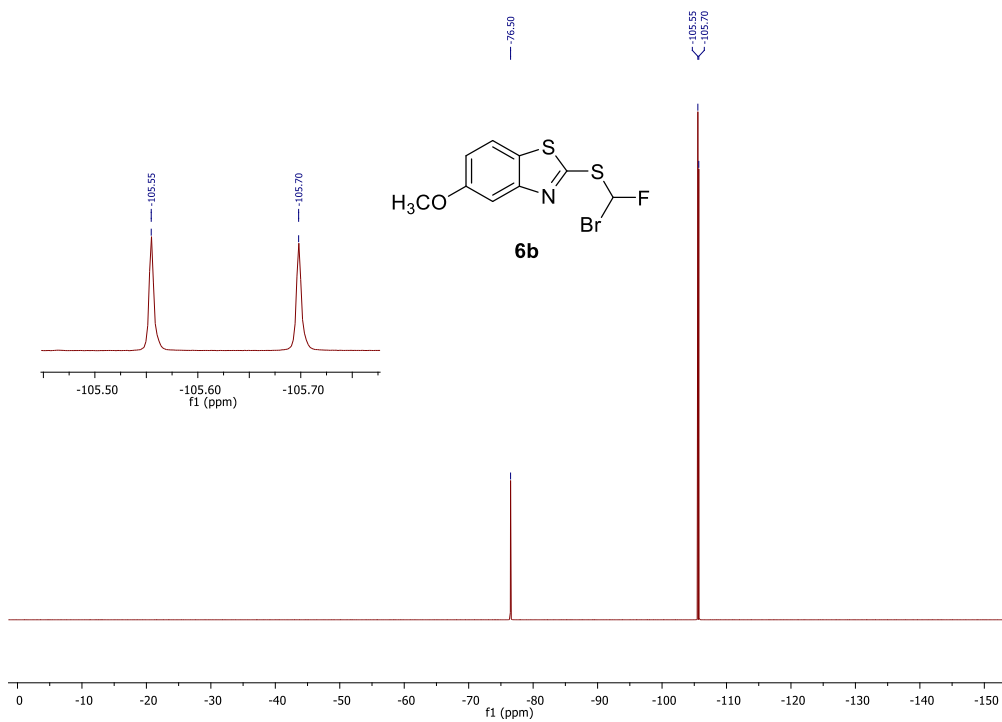


Figure S42. ¹⁹F-NMR spectrum of **6b**.

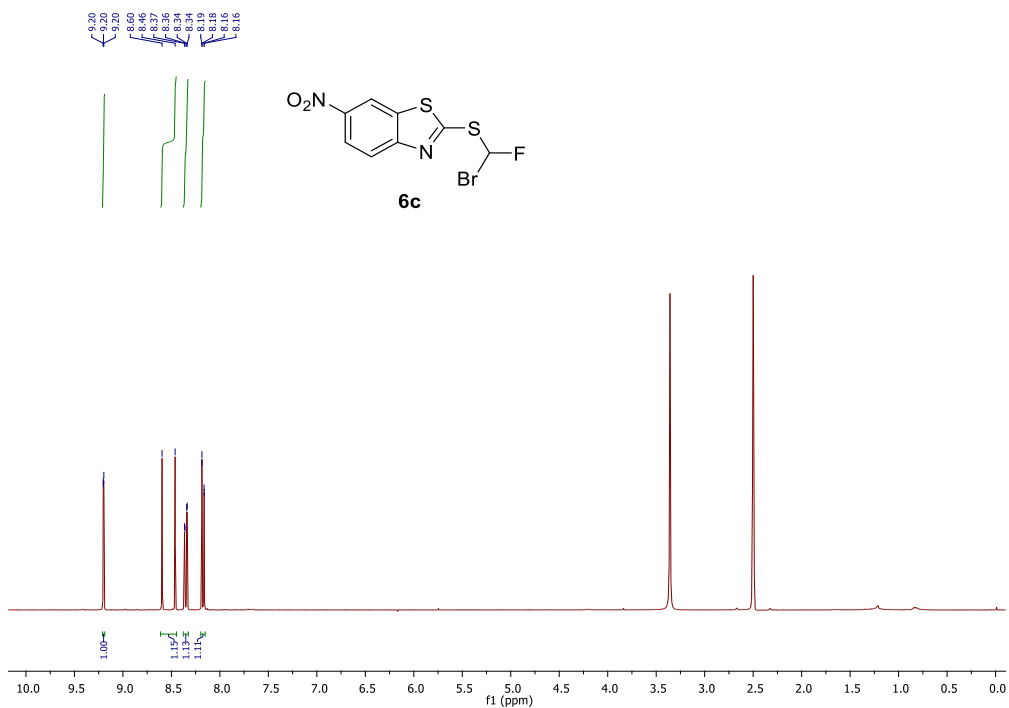


Figure S43. ¹H-NMR spectrum of **6c**.

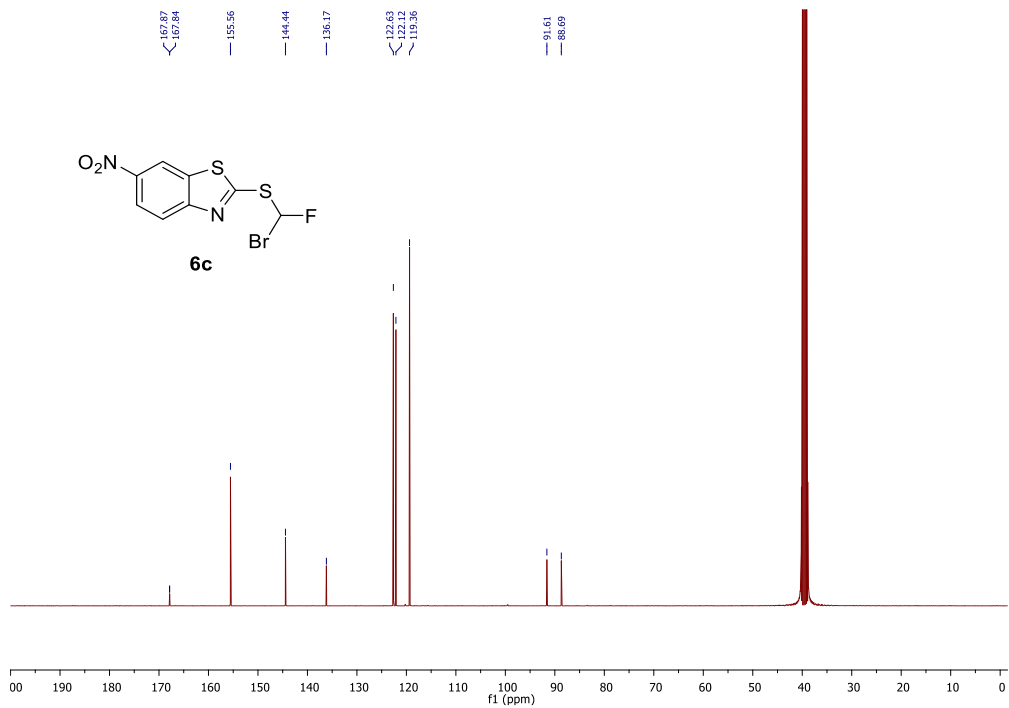


Figure S44. ¹³C-NMR spectrum of **6c**.

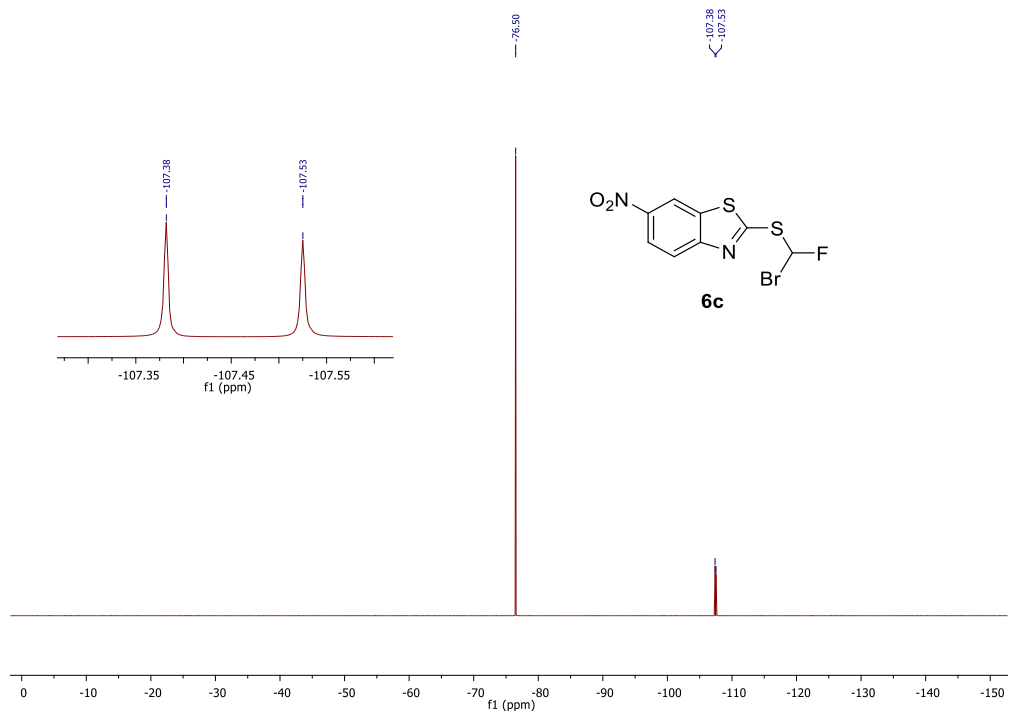


Figure S45. ¹⁹F-NMR spectrum of **6c**.

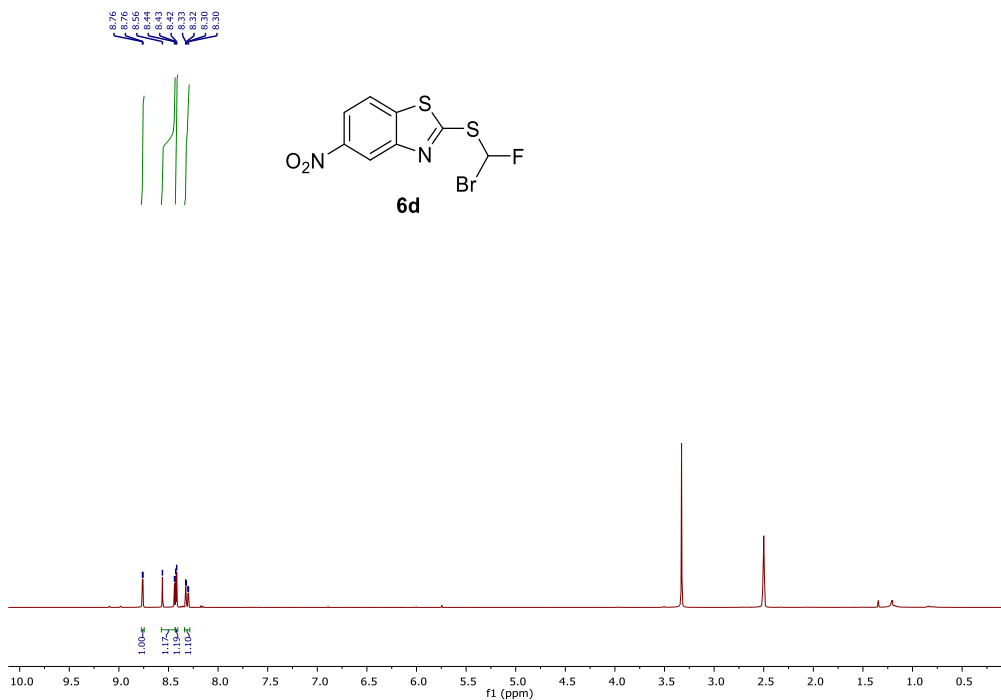


Figure S46. ¹H-NMR spectrum of **6d**.

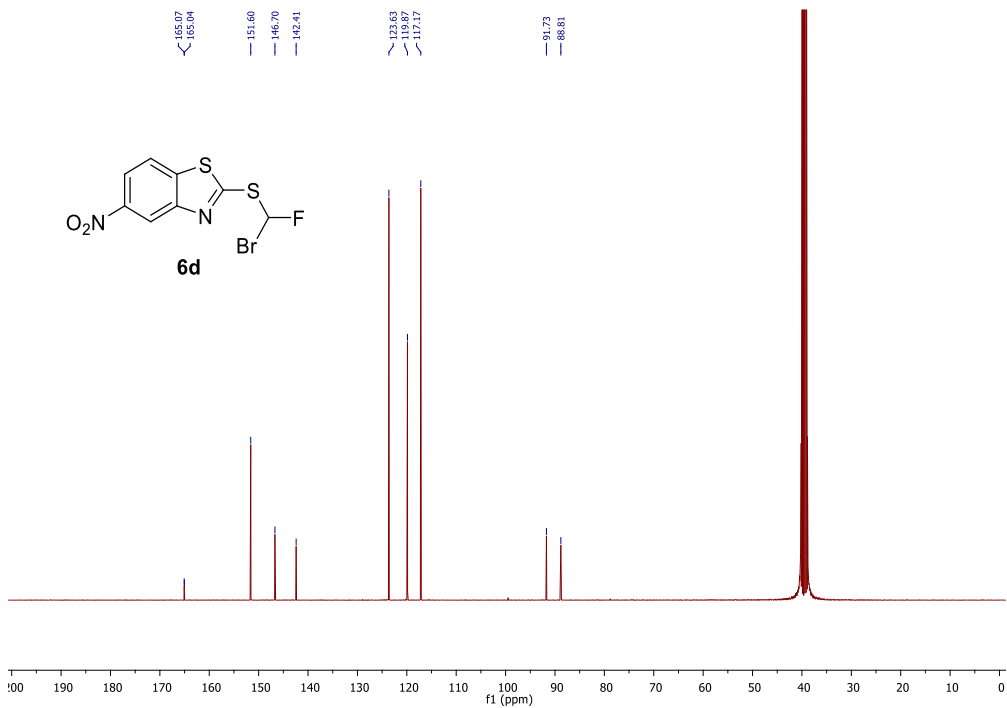


Figure S47. ¹³C-NMR spectrum of **6d**.

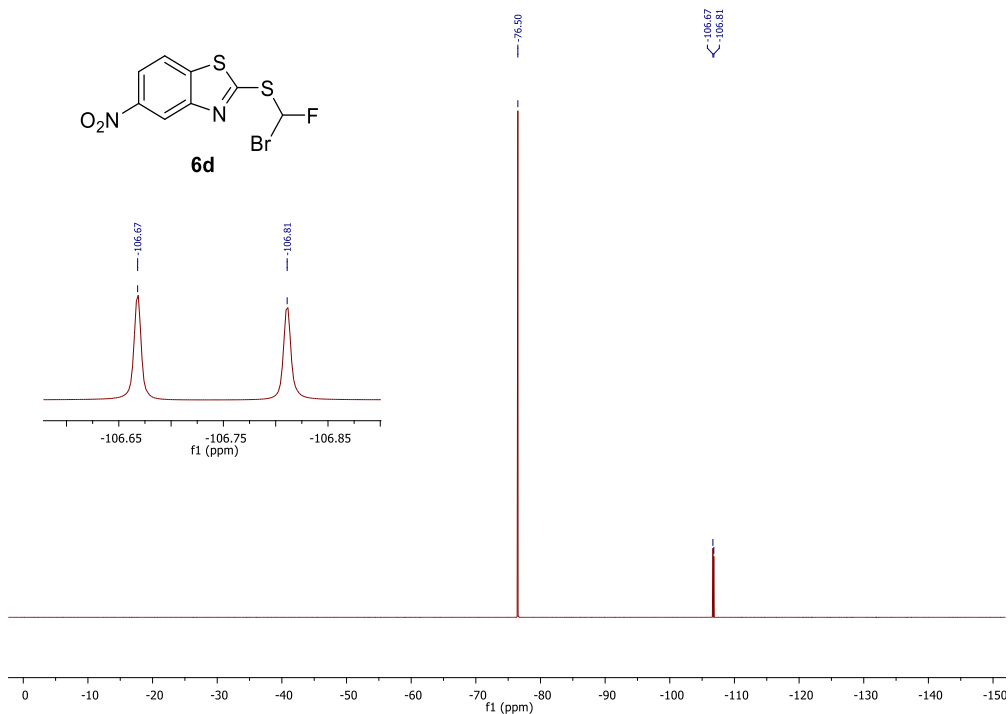


Figure S48. ^{19}F -NMR spectrum of **6d**.

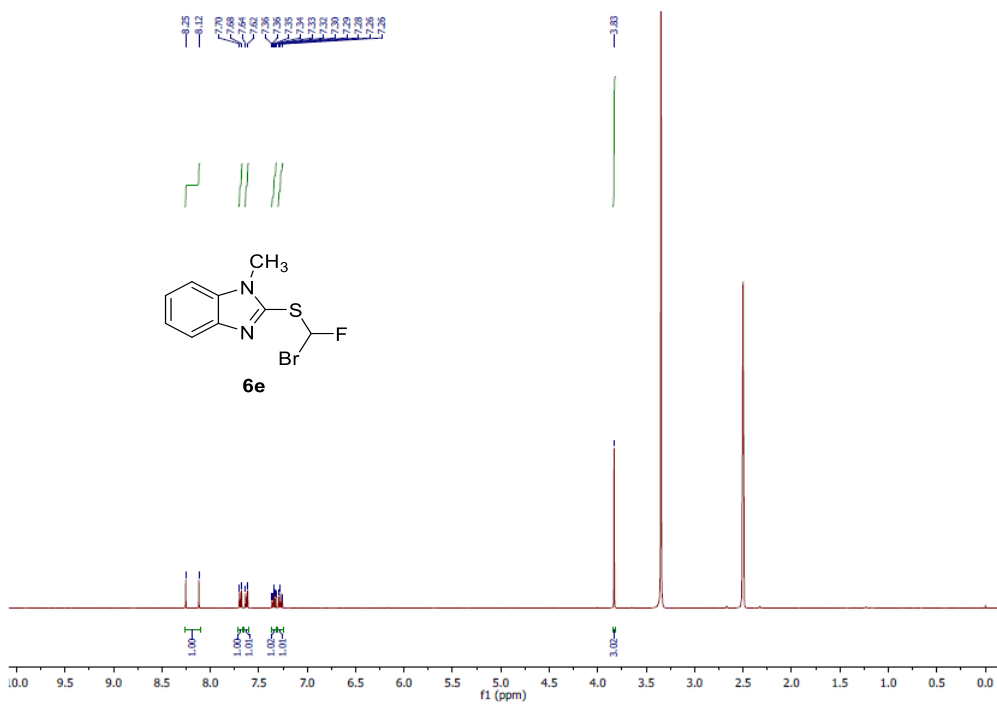


Figure S49. ^1H -NMR spectrum of **6e**.

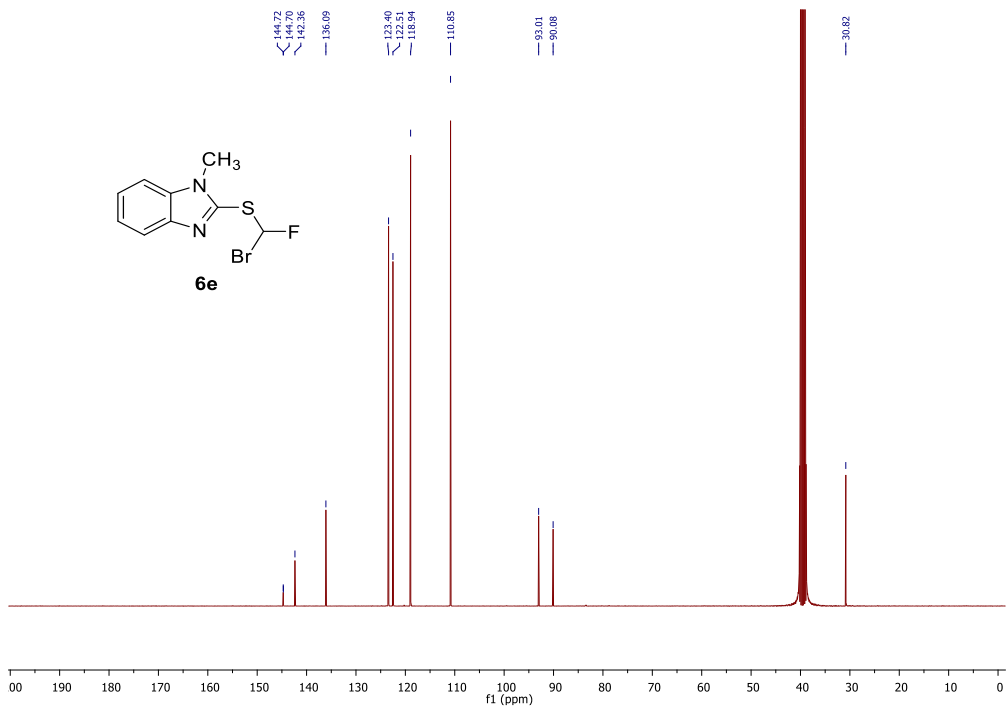


Figure S50. ¹³C-NMR spectrum of **6e**.

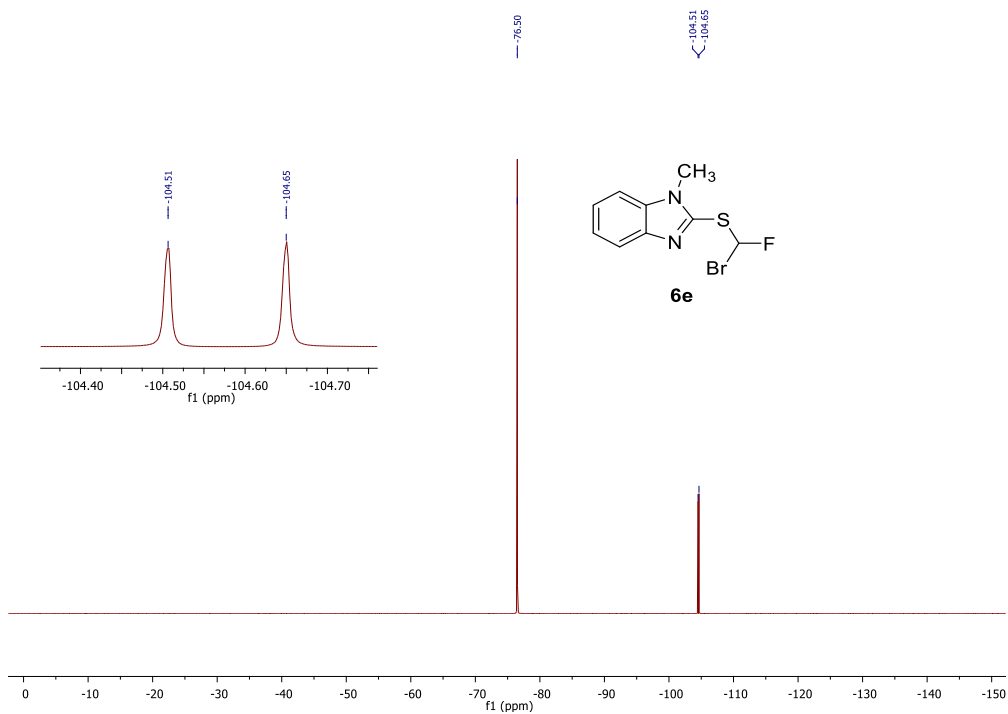


Figure S51. ¹⁹F-NMR spectrum of **6e**.

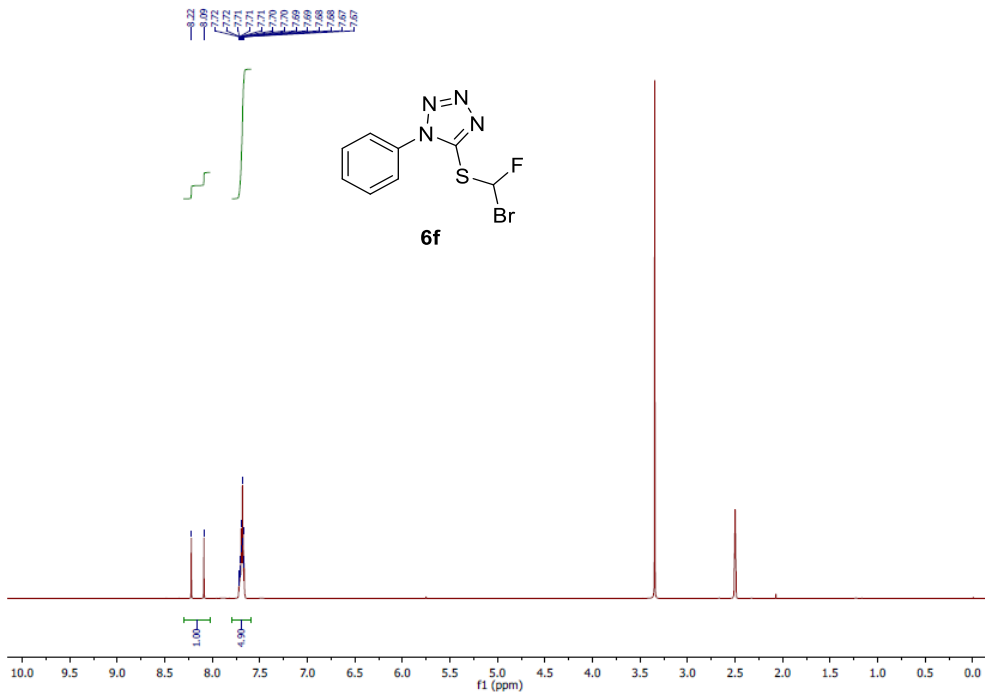


Figure S52. ¹H-NMR spectrum of **6f**.

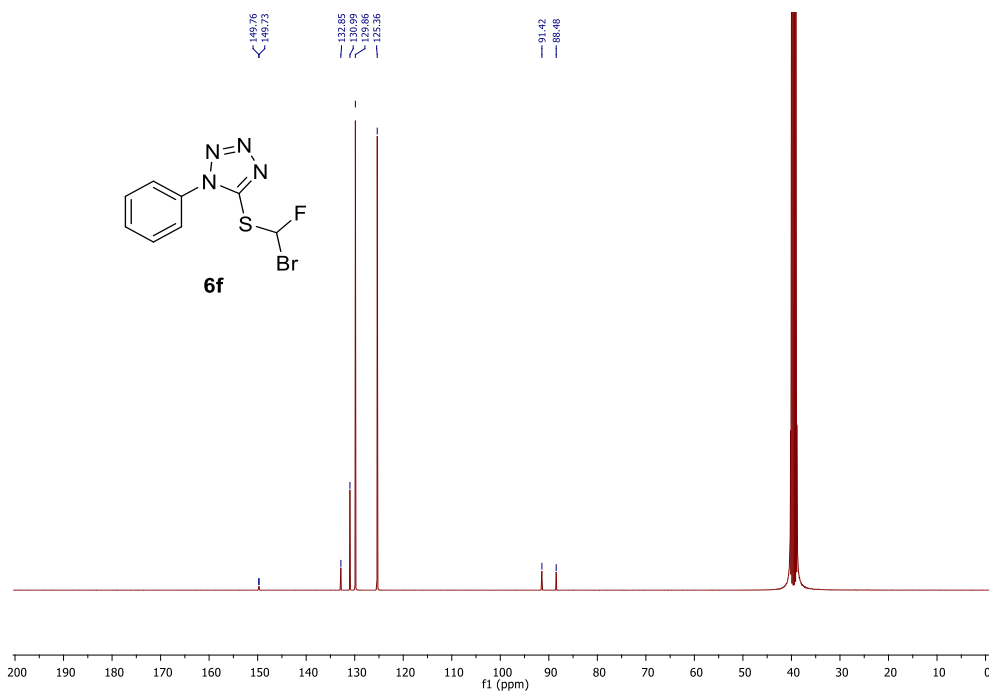


Figure S53. ¹³C-NMR spectrum of **6f**.

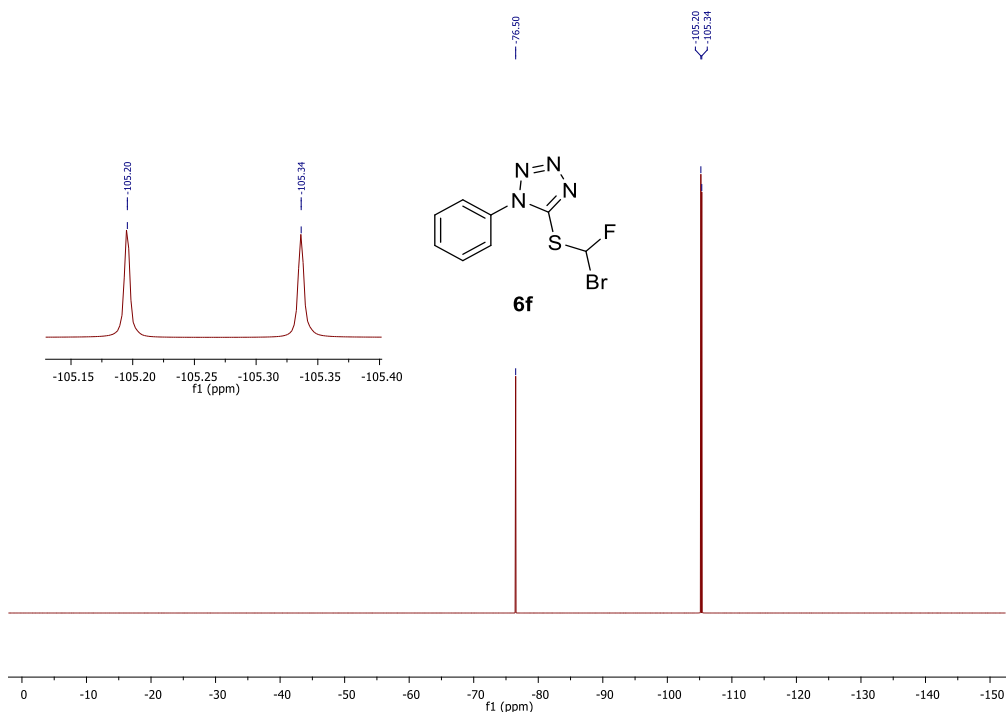


Figure S54. ^{19}F -NMR spectrum of **6f**.

5.2. Radiochemistry

The UPLC gradients used for the analyses of the crude products [^{18}F]**4a**-[^{18}F]**4f**, [^{18}F]**5a**-[^{18}F]**5f**, and [^{18}F]**8a**-[^{18}F]**8g** are depicted in Tables S1 and S2.

Table S1. UPLC gradient for the analysis of the crude products [^{18}F]**4a**-[^{18}F]**4f** and [^{18}F]**5a**-[^{18}F]**5f** (gradient A)

Time (min)	$\text{HCO}_2\text{H}/\text{H}_2\text{O}$ (0.05%, v/v)	MeCN	Flow rate ($\text{mL}\cdot\text{min}^{-1}$)
0	100	0	0.5
6	25	75	0.5
8	100	0	0.5

Table S2. UPLC gradient for the analysis of the crude products [^{18}F]**8a**-[^{18}F]**8g** (gradient B)

Time (min)	$\text{HCO}_2\text{H}/\text{H}_2\text{O}$ (0.05%, v/v)	MeCN	Flow rate ($\text{mL}\cdot\text{min}^{-1}$)
0	100	0	0.5
6	0	100	0.5
8	100	0	0.5

5.2.1. Synthesis of [^{18}F]2-((Difluoromethyl)thio)-6-methoxybenzo[*d*]thiazole ([^{18}F]**4a**)

The implementation of the general procedure 3.2.2. for the ^{18}F -labeling of 2-((bromofluoromethyl)thio)-6-methoxybenzo[*d*]thiazole (**6a**) (12.3 mg, 0.04 mmol) provided the labeled compound [^{18}F]**4a** in $14.2 \pm 0.7\%$ RCY (d.c. at the SOS).

The radiochemical yield (RCY) of the ^{18}F -labeling step was determined based on the activity of the recovered crude product [^{18}F]**4a**, on their radio-TLC and radio-UPLC purities, and the starting radioactivity, according to the following formula:

$$RCY (\%, d. c.) = \frac{\text{radioTLC purity (\%)} \times \text{radioUPLC purity (\%)} \times \text{activity of } [^{18}\text{F}]\mathbf{4a} (d. c.)}{\text{starting radioactivity} \times 100}$$

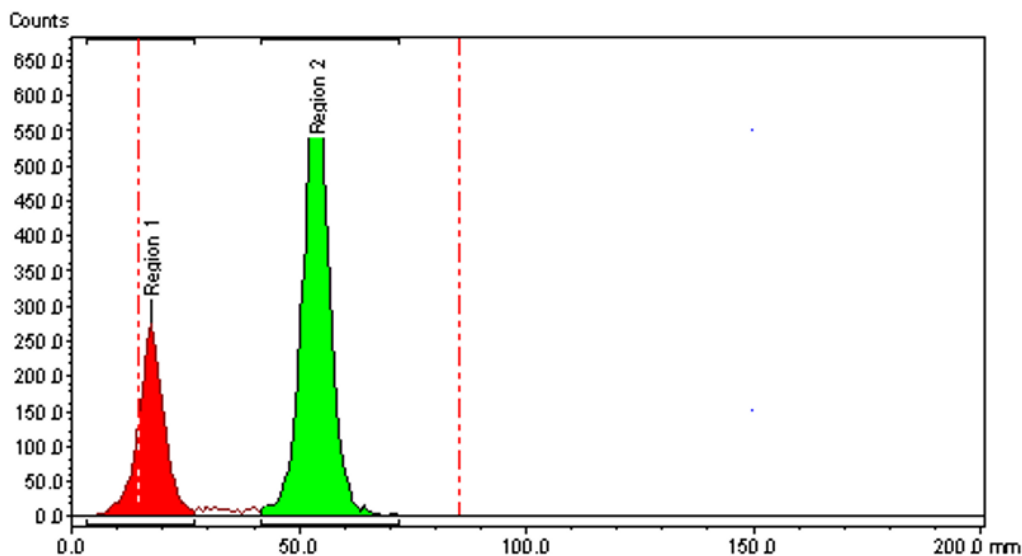


Figure S55. TLC radio-chromatogram of the crude product [^{18}F]**4a** (eluent: methanol).

Table S3. Determination of the radio-TLC purity of the crude product [^{18}F]**4a**

Retention factor (R_f , mm)	Ratio (%)
0.03	29 (impurity/by-product)
0.67	71 (desired crude product)

$$RCY (\%, d. c.) = \frac{\text{radioTLC purity (\%)} \times \text{radioUPLC purity (\%)} \times \text{activity of } [^{18}\text{F}]\mathbf{4a} (d. c.)}{\text{starting radioactivity} \times 100}$$

$$RCY (\%, d. c.) = \frac{71 \times 92 \times 37.0}{169.4 \times 100}$$

$$RCY (\%, d. c.) = 14.3 \%$$

Table S4 furnishes more details of the RCY determination. The UPLC radio-chromatogram of the crude product [^{18}F]**4a** is depicted in Figure S56. Figure S57 represents the UPLC UV-chromatogram of the non-radioactive reference **4a**.

Table S4. Determination of the radiochemical yield (%) of the synthesis of [¹⁸F]4a

Reaction	Starting activity (MBq)	Activity of the crude product [¹⁸ F]4a (MBq, d.c.)	Radio-TLC purity (%)	Radio-UPLC purity (%)	Radiochemical Yield (%)
1	169.4	37.0	71	92	14.3
2	144.4	28.8	74	90	13.3
3	187.9	50.9	55	100	14.9
Radiochemical Yield (%) ± Deviation					14.2 ± 0.7

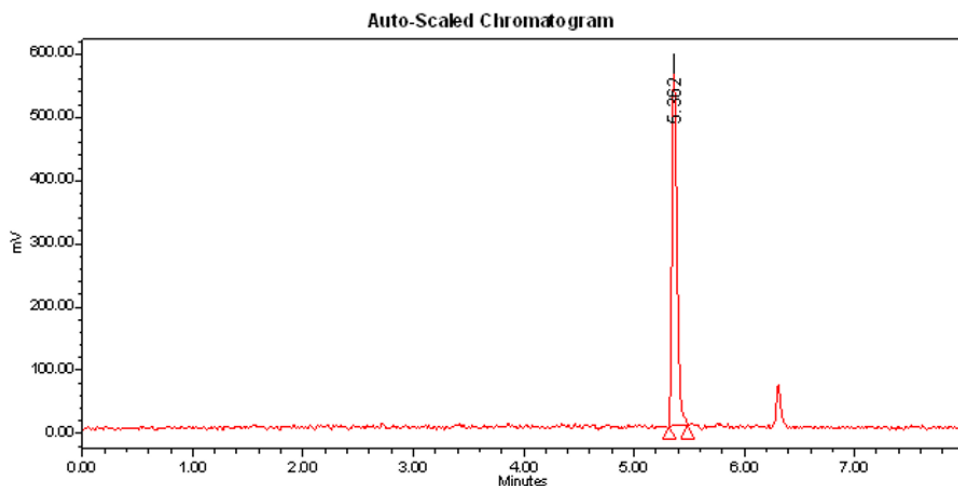


Figure S56. UPLC radio-chromatogram of the crude product [¹⁸F]4a. ACQUITY UPLC® CSH C18 column (1.7 μm, 2.1 × 100 mm); MeCN and HCO₂H/H₂O (0.05%, v/v) in gradient mode at 0.5 mL·min⁻¹ (from 100% HCO₂H/H₂O (0.05%, v/v) to 75% MeCN + 25% HCO₂H/H₂O (0.05%, v/v) in 6 min, and from 75% MeCN + 25% HCO₂H/H₂O (0.05%, v/v) to 100% HCO₂H/H₂O (0.05%, v/v) in 2 min).

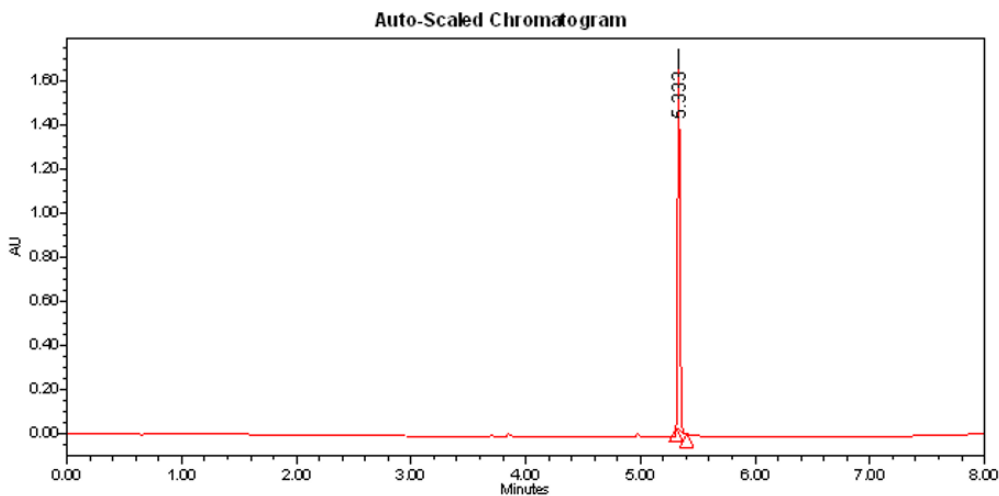


Figure S57. UPLC UV-chromatogram of the authentic reference **4a** (wavelength: 254 nm). ACQUITY UPLC® CSH C18 column (1.7 μm , 2.1 \times 100 mm); MeCN and HCO₂H/H₂O (0.05%, v/v) in gradient mode at 0.5 mL·min⁻¹ (from 100% HCO₂H/H₂O (0.05%, v/v) to 75% MeCN + 25% HCO₂H/H₂O (0.05%, v/v) in 6 min, and from 75% MeCN + 25% HCO₂H/H₂O (0.05%, v/v) to 100% HCO₂H/H₂O (0.05%, v/v) in 2 min).

5.2.2. Synthesis of [¹⁸F]2-((Difluoromethyl)thio)-5-methoxybenzo[*d*]thiazole ([¹⁸F]**4b**)

The implementation of the general procedure 3.2.2. for the ¹⁸F-labeling of 2-((bromofluoromethyl)thio)-5-methoxybenzo[*d*]thiazole (**6b**) (12.3 mg, 0.04 mmol) provided the labeled compound [¹⁸F]**4b** in 11.8 \pm 1.9% RCY (d.c. at the SOS). Table S5 furnishes more details of the RCY determination. The UPLC radio-chromatogram of the crude product [¹⁸F]**4b** is depicted in Figure S58. Figure S59 represents the UPLC UV-chromatogram of the non-radioactive reference **4b**.

Table S5. Determination of the radiochemical yield (%) of the synthesis of [¹⁸F]**4b**

Reaction	Starting activity (MBq)	Activity of the crude product [¹⁸ F] 4b (MBq, d.c.)	Radio-TLC purity (%)	Radio-UPLC purity (%)	Radiochemical Yield (%)
1	187.5	41.5	42	100	9.3
2	142.2	24.2	68	100	11.6
3	173.4	30.5	67	100	11.8
4	167.4	34.2	73	97	14.5
Radiochemical Yield (%) \pm Deviation					11.8 \pm 1.9

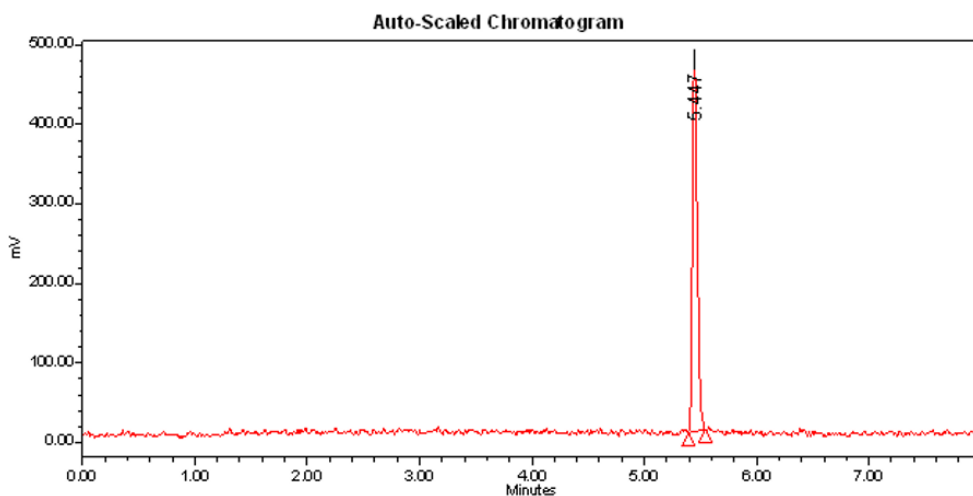


Figure S58. UPLC radio-chromatogram of the crude product [¹⁸F]**4b**. ACQUITY UPLC® CSH C18 column (1.7 μm , 2.1 \times 100 mm); MeCN and HCO₂H/H₂O (0.05%, v/v) in gradient mode at 0.5 mL·min⁻¹ (from 100% HCO₂H/H₂O (0.05%, v/v) to 75% MeCN + 25% HCO₂H/H₂O (0.05%,

v/v) in 6 min, and from 75% MeCN + 25% HCO₂H/H₂O (0.05%, v/v) to 100% HCO₂H/H₂O (0.05%, v/v) in 2 min).

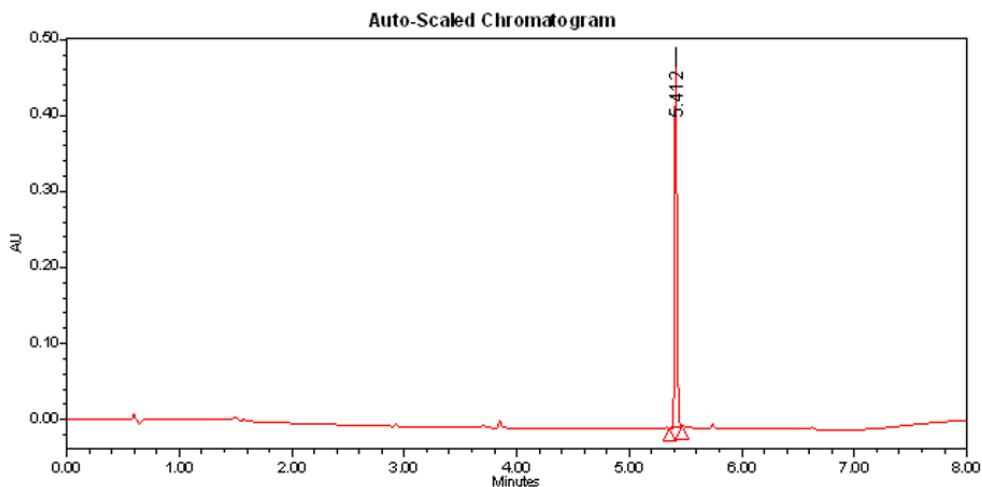


Figure S59. UPLC UV-chromatogram of the authentic reference **4b** (wavelength: 254 nm). ACQUITY UPLC[®] CSH C18 column (1.7 μ m, 2.1 \times 100 mm); MeCN and HCO₂H/H₂O (0.05%, v/v) in gradient mode at 0.5 mL·min⁻¹ (from 100% HCO₂H/H₂O (0.05%, v/v) to 75% MeCN + 25% HCO₂H/H₂O (0.05%, v/v) in 6 min, and from 75% MeCN + 25% HCO₂H/H₂O (0.05%, v/v) to 100% HCO₂H/H₂O (0.05%, v/v) in 2 min).

5.2.3. Synthesis of [¹⁸F]2-((Difluoromethyl)thio)-6-nitrobenzo[*d*]thiazole ([¹⁸F]**4c**)

The implementation of the general procedure 3.2.2. for the ¹⁸F-labeling of 2-((bromofluoromethyl)thio)-6-nitrobenzo[*d*]thiazole (**6c**) (6.5 mg, 0.02 mmol) provided the labeled compound [¹⁸F]**4c** in 13.6 \pm 0.6% RCY (d.c. at the SOS). Table S6 furnishes more details of the RCY determination. The UPLC radio-chromatogram of the crude product [¹⁸F]**4c** is depicted in Figure S60. Figure S61 represents the UPLC UV-chromatogram of the non-radioactive reference **4c**.

Table S6. Determination of the radiochemical yield (%) of the synthesis of [¹⁸F]**4c**

Reaction	Starting activity (MBq)	Activity of the crude product [¹⁸ F] 4c (MBq, d.c.)	Radio-TLC purity (%)	Radio-UPLC purity (%)	Radiochemical Yield (%)
1	150.9	32.6	75	82	13.3
2	173.1	36.1	81	86	14.5
3	196.1	37.8	70	97	13.1
Radiochemical Yield (%) \pm Deviation					13.6 \pm 0.6

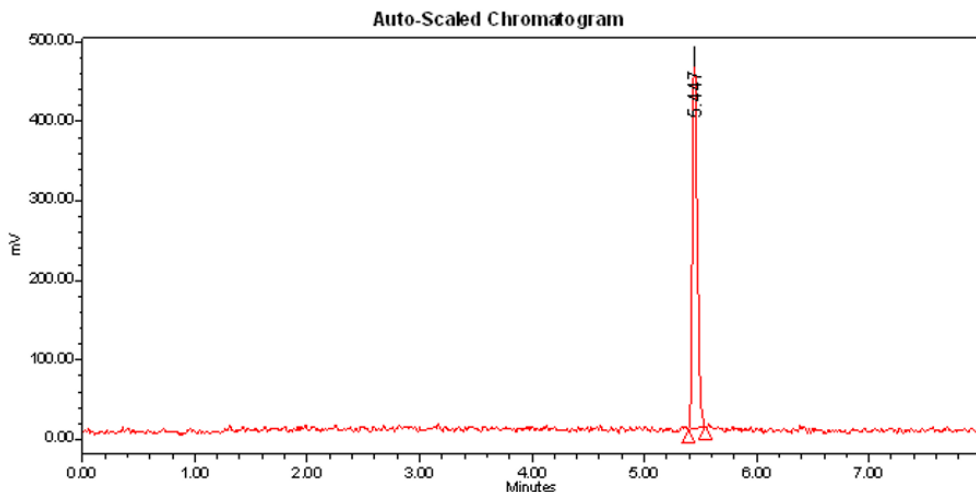


Figure S60. UPLC radio-chromatogram of the crude product $[^{18}\text{F}]\mathbf{4c}$. ACQUITY UPLC[®] CSH C18 column (1.7 μm , 2.1 \times 100 mm); MeCN and HCO₂H/H₂O (0.05%, v/v) in gradient mode at 0.5 mL·min⁻¹ (from 100% HCO₂H/H₂O (0.05%, v/v) to 75% MeCN + 25% HCO₂H/H₂O (0.05%, v/v) in 6 min, and from 75% MeCN + 25% HCO₂H/H₂O (0.05%, v/v) to 100% HCO₂H/H₂O (0.05%, v/v) in 2 min).

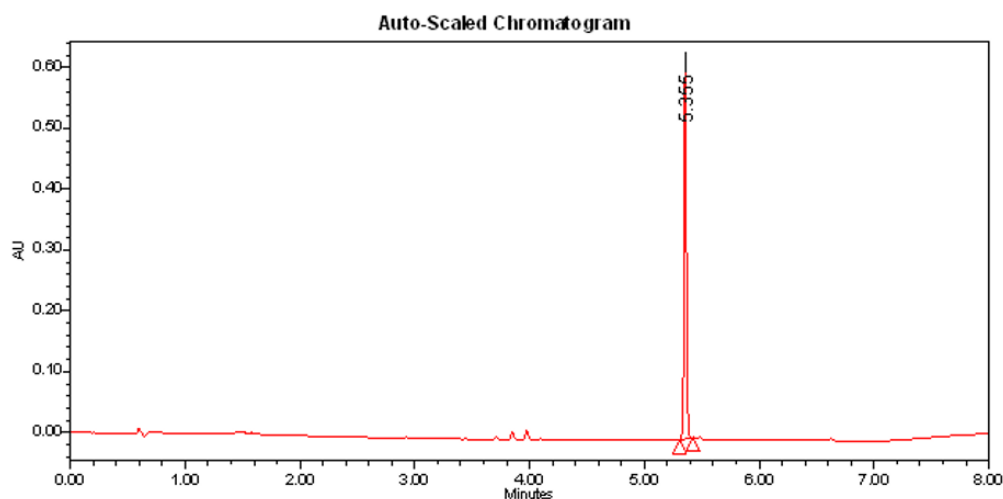


Figure S61. UPLC UV-chromatogram of the authentic reference $\mathbf{4c}$ (wavelength: 254 nm). ACQUITY UPLC[®] CSH C18 column (1.7 μm , 2.1 \times 100 mm); MeCN and HCO₂H/H₂O (0.05%, v/v) in gradient mode at 0.5 mL·min⁻¹ (from 100% HCO₂H/H₂O (0.05%, v/v) to 75% MeCN + 25% HCO₂H/H₂O (0.05%, v/v) in 6 min, and from 75% MeCN + 25% HCO₂H/H₂O (0.05%, v/v) to 100% HCO₂H/H₂O (0.05%, v/v) in 2 min).

5.2.4. Synthesis of $[^{18}\text{F}]2$ -((Difluoromethyl)thio)-5-nitrobenzo[*d*]thiazole ($[^{18}\text{F}]\mathbf{4d}$)

The implementation of the general procedure of the ¹⁸F-labeling of 2-((bromofluoromethyl)thio)-5-nitrobenzo[*d*]thiazole ($\mathbf{6d}$) (12.9 mg, 0.04 mmol) provided the labeled compound $[^{18}\text{F}]\mathbf{4d}$ in 12.7 \pm 0.2% RCY (d.c. at the SOS). Table S7

furnishes more details of the RCY determination. The UPLC radio-chromatogram of the crude product [^{18}F]**4d** is depicted in Figure S62. Figure S63 represents the UPLC UV-chromatogram of the non-radioactive reference **4d**.

Table S7. Determination of the radiochemical yield (%) of the synthesis of [^{18}F]**4d**

Reaction	Starting activity (MBq)	Activity of the crude product [^{18}F] 4d (MBq, d.c.)	Radio-TLC purity (%)	Radio-UPLC purity (%)	Radiochemical Yield (%)
1	196.8	62.1	46	86	12.5
2	161.4	38.7	67	79	12.7
3	180.6	34.9	75	89	12.9
Radiochemical Yield (%) \pm Deviation					12.7 \pm 0.2

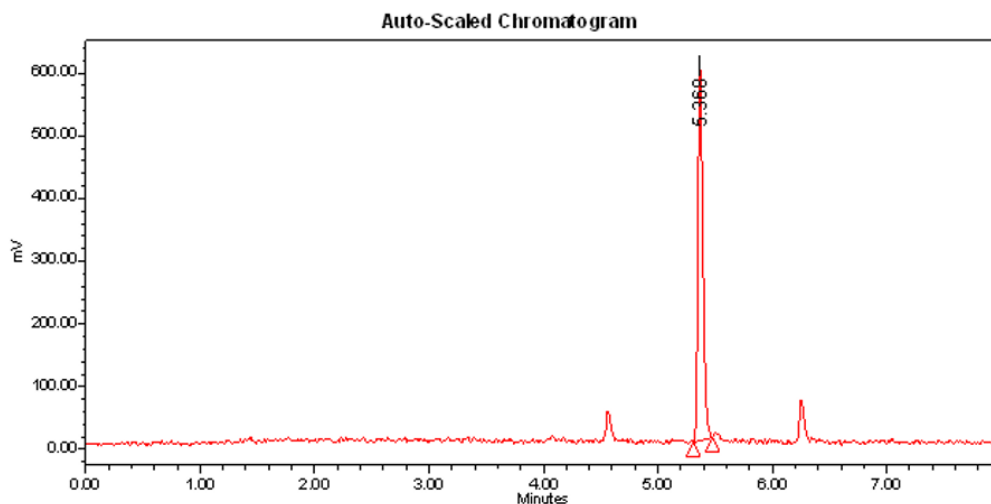


Figure S62. UPLC radio-chromatogram of the crude product [^{18}F]**4d**. ACQUITY UPLC[®] CSH C18 column (1.7 μm , 2.1 \times 100 mm); MeCN and HCO₂H/H₂O (0.05%, v/v) in gradient mode at 0.5 mL·min⁻¹ (from 100% HCO₂H/H₂O (0.05%, v/v) to 75% MeCN + 25% HCO₂H/H₂O (0.05%, v/v) in 6 min, and from 75% MeCN + 25% HCO₂H/H₂O (0.05%, v/v) to 100% HCO₂H/H₂O (0.05%, v/v) in 2 min).

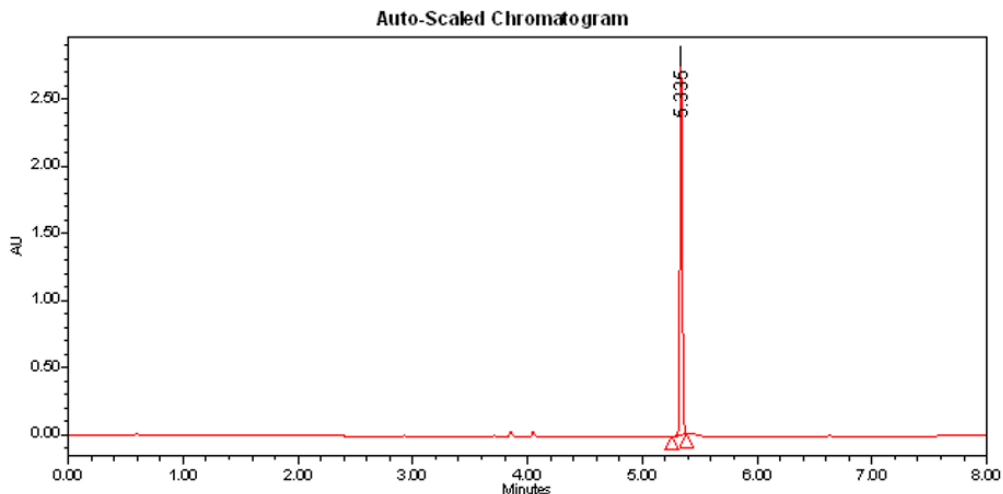


Figure S63. UPLC UV-chromatogram of the authentic reference **4d** (wavelength: 254 nm). ACQUITY UPLC® CSH C18 column (1.7 μm , 2.1 \times 100 mm); MeCN and HCO₂H/H₂O (0.05%, v/v) in gradient mode at 0.5 mL·min⁻¹ (from 100% HCO₂H/H₂O (0.05%, v/v) to 75% MeCN + 25% HCO₂H/H₂O (0.05%, v/v) in 6 min, and from 75% MeCN + 25% HCO₂H/H₂O (0.05%, v/v) to 100% HCO₂H/H₂O (0.05%, v/v) in 2 min).

5.2.5. Synthesis of [¹⁸F]2-((Difluoromethyl)thio)-1-methyl-1*H*-benzo[*d*]imidazole ([¹⁸F]**4e**)

The implementation of the general procedure 3.2.2. for the ¹⁸F-labeling of 2-((bromofluoromethyl)thio)-1-methyl-1*H*-benzo[*d*]imidazole (**6e**) (11.0 mg, 0.04 mmol) provided the labeled compound [¹⁸F]**4e** in 8.3 \pm 1.9% RCY (d.c. at the SOS). Table S8 furnishes more details of the RCY determination. The UPLC radio-chromatogram of the crude product [¹⁸F]**4e** is depicted in Figure S64. Figure S65 represents the UPLC UV-chromatogram of the non-radioactive reference **4e**.

Table S8. Determination of the radiochemical yield (%) of the synthesis of [¹⁸F]**4e**

Reaction	Starting activity (MBq)	Activity of the crude product [¹⁸ F] 4e (MBq, d.c.)	Radio-TLC purity (%)	Radio-UPLC purity (%)	Radiochemical Yield (%)
1	182.4	33	32	100	5.8
2	154.6	16.8	69	100	7.5
3	169.8	25.7	58	100	8.8
4	187.4	30.5	71	95	11.0
Radiochemical Yield (%) \pm Deviation					8.3 \pm 1.9

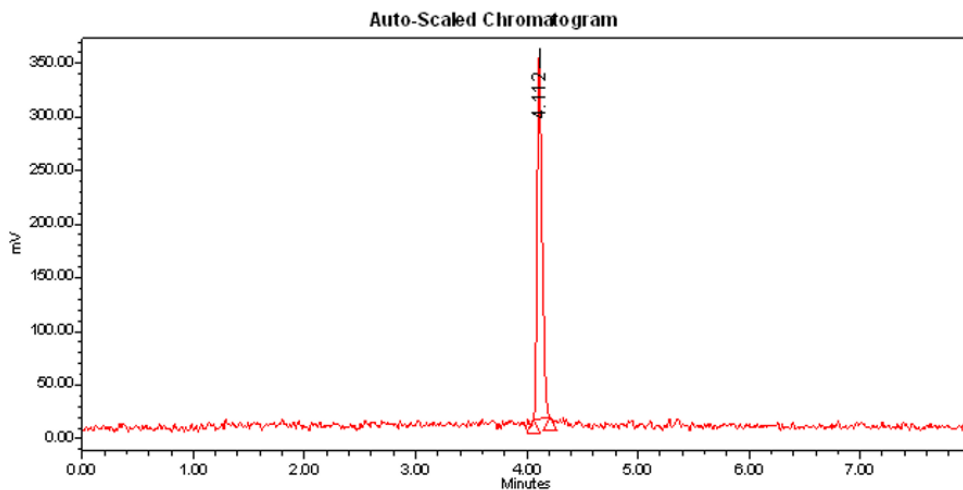


Figure S64. UPLC radio-chromatogram of the crude product $[^{18}\text{F}]\mathbf{4e}$. ACQUITY UPLC[®] CSH C18 column ($1.7\ \mu\text{m}$, $2.1 \times 100\ \text{mm}$); MeCN and $\text{HCO}_2\text{H}/\text{H}_2\text{O}$ (0.05%, v/v) in gradient mode at $0.5\ \text{mL}\cdot\text{min}^{-1}$ (from 100% $\text{HCO}_2\text{H}/\text{H}_2\text{O}$ (0.05%, v/v) to 75% MeCN + 25% $\text{HCO}_2\text{H}/\text{H}_2\text{O}$ (0.05%, v/v) in 6 min, and from 75% MeCN + 25% $\text{HCO}_2\text{H}/\text{H}_2\text{O}$ (0.05%, v/v) to 100% $\text{HCO}_2\text{H}/\text{H}_2\text{O}$ (0.05%, v/v) in 2 min).

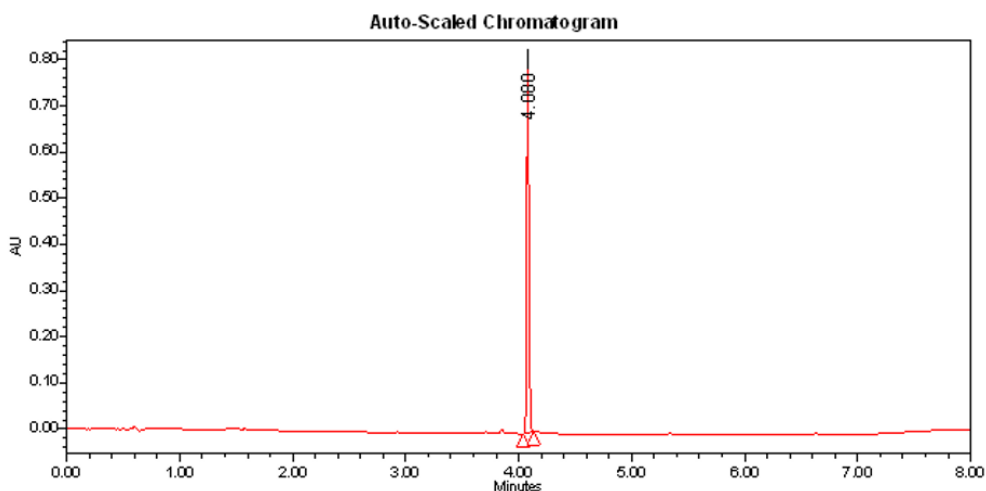


Figure S65. UPLC UV-chromatogram of the authentic reference $\mathbf{4e}$ (wavelength: 254 nm). ACQUITY UPLC[®] CSH C18 column ($1.7\ \mu\text{m}$, $2.1 \times 100\ \text{mm}$); MeCN and $\text{HCO}_2\text{H}/\text{H}_2\text{O}$ (0.05%, v/v) in gradient mode at $0.5\ \text{mL}\cdot\text{min}^{-1}$ (from 100% $\text{HCO}_2\text{H}/\text{H}_2\text{O}$ (0.05%, v/v) to 75% MeCN + 25% $\text{HCO}_2\text{H}/\text{H}_2\text{O}$ (0.05%, v/v) in 6 min, and from 75% MeCN + 25% $\text{HCO}_2\text{H}/\text{H}_2\text{O}$ (0.05%, v/v) to 100% $\text{HCO}_2\text{H}/\text{H}_2\text{O}$ (0.05%, v/v) in 2 min).

5.2.6. Synthesis of $[^{18}\text{F}]\mathbf{5}$ -((Difluoromethyl)thio)-1-phenyl-1*H*-tetrazole ($[^{18}\text{F}]\mathbf{4f}$)

The implementation of the general procedure 3.2.2. for the ^{18}F -labeling of 5-((bromofluoromethyl)thio)-1-phenyl-1*H*-tetrazole ($\mathbf{6f}$) (11.6 mg, 0.04 mmol) provided the labeled compound $[^{18}\text{F}]\mathbf{4f}$ in $14.8 \pm 0.8\%$ RCY (d.c. at the SOS). Table S9 furnishes

more details of the RCY determination. The UPLC radio-chromatogram of the crude product [¹⁸F]4f is depicted in Figure S66. Figure S67 represents the UPLC UV-chromatogram of the non-radioactive reference 4f.

Table S9. Determination of the radiochemical yield (%) of the synthesis of [¹⁸F]4f

Reaction	Starting activity (MBq)	Activity of the crude product [¹⁸ F]4f (MBq, d.c.)	Radio-TLC purity (%)	Radio-UPLC purity (%)	Radiochemical Yield (%)
1	130.2	26.8	81	96	16.0
2	190.4	38.4	74	95	14.2
3	195.8	39.3	75	95	14.3
Radiochemical Yield (%) ± Deviation					14.8 ± 0.8

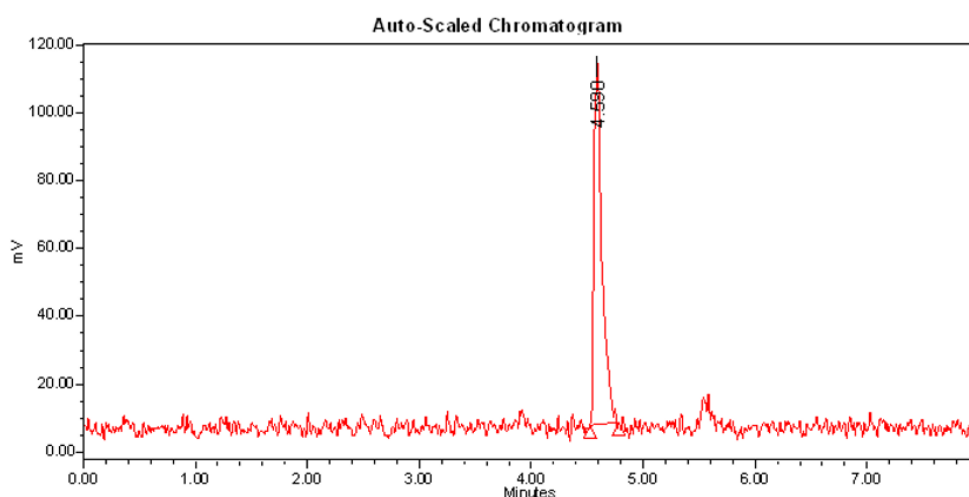


Figure S66. UPLC radio-chromatogram of the crude product [¹⁸F]4f. ACQUITY UPLC® CSH C18 column (1.7 μm, 2.1 × 100 mm); MeCN and HCO₂H/H₂O (0.05%, v/v) in gradient mode at 0.5 mL·min⁻¹ (from 100% HCO₂H/H₂O (0.05%, v/v) to 75% MeCN + 25% HCO₂H/H₂O (0.05%, v/v) in 6 min, and from 75% MeCN + 25% HCO₂H/H₂O (0.05%, v/v) to 100% HCO₂H/H₂O (0.05%, v/v) in 2 min).

5.2.7. Synthesis of [¹⁸F]2-((Difluoromethyl)sulfonyl)-6-methoxybenzo[*d*]thiazole ([¹⁸F]5a)

The implementation of the general procedure 3.2.3. for the oxidation of [¹⁸F]2-((difluoromethyl)thio)-6-methoxybenzo[*d*]thiazole ([¹⁸F]4a) (10-20 MBq) provided the labeled compound [¹⁸F]5a in 70.9 ± 6.1% RCY (d.c. at the SOS).

The RCY of the oxidation step was determined based on the activity of the crude products [¹⁸F]4a and [¹⁸F]5a, and on their radio-TLC and radio-UPLC purities, according to the following equation:

$$RCY (\%, d. c.) = \frac{\text{radioTLC purity} (\%) \times \text{radioUPLC purity} (\%) \times \text{activity of } [^{18}\text{F}]\mathbf{5a} (d. c.)}{\text{activity of } [^{18}\text{F}]\mathbf{4a} \times 100}$$

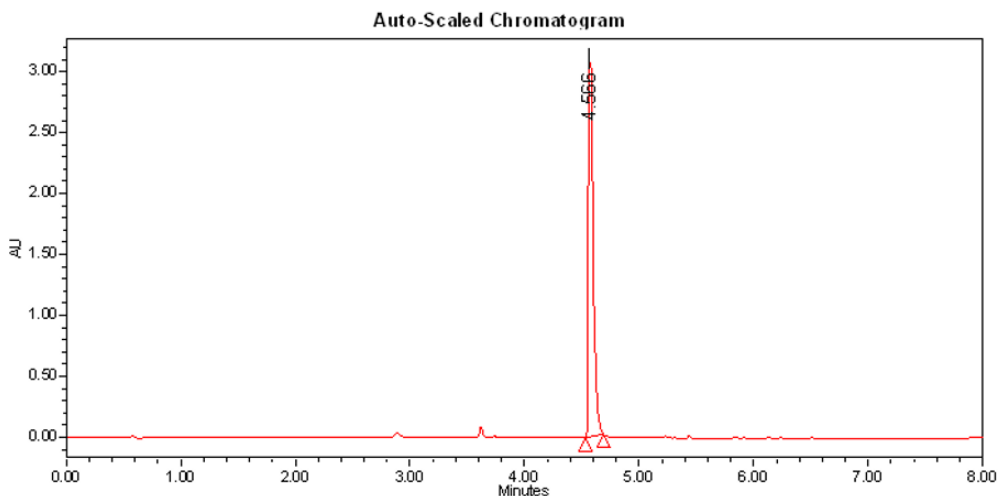


Figure S67. UPLC UV-chromatogram of the authentic reference **4f** (wavelength: 254 nm). ACQUITY UPLC® CSH C18 column (1.7 μm , 2.1 \times 100 mm); MeCN and HCO₂H/H₂O (0.05%, v/v) in gradient mode at 0.5 mL·min⁻¹ (from 100% HCO₂H/H₂O (0.05%, v/v) to 75% MeCN + 25% HCO₂H/H₂O (0.05%, v/v) in 6 min, and from 75% MeCN + 25% HCO₂H/H₂O (0.05%, v/v) to 100% HCO₂H/H₂O (0.05%, v/v) in 2 min).

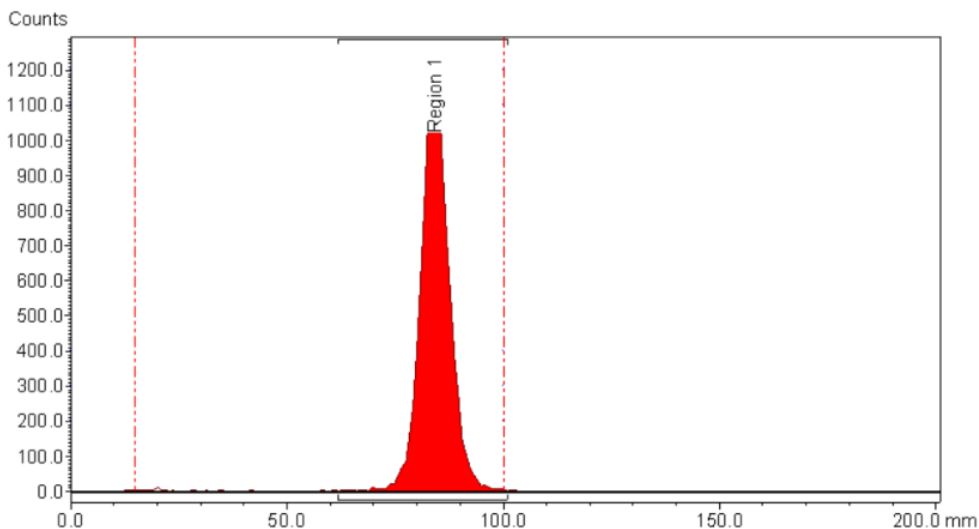


Figure S68. TLC radio-chromatogram of the crude product [¹⁸F]**5a** (eluent: methanol).

Table S10. Determination of the radio-TLC purity of the crude product [¹⁸F]**5a**

Retention factor (R _f , mm)	Ratio (%)
0	0 (impurity/by-product)
0.78	100 (desired crude product)

$$RCY (\%, d. c.) = \frac{\text{radioTLC purity (\%)} \times \text{radioUPLC purity (\%)} \times \text{activity of } [^{18}\text{F}]\mathbf{5a} (d. c.)}{\text{activity of } [^{18}\text{F}]\mathbf{4a} (d. c.) \times 100}$$

$$RCY (\%, d. c.) = \frac{100 \times 92 \times 12.0}{15.6 \times 100}$$

$$RCY (\%, d. c.) = 70.6 \%$$

Table S11 furnishes more details of the RCY determination. The UPLC radio-chromatogram of the crude product $[^{18}\text{F}]\mathbf{5a}$ is depicted in Figure S69. Figure S70 represents the UPLC UV-chromatogram of the non-radioactive reference $\mathbf{5a}$.

Table S11. Determination of the radiochemical yield (%) of the synthesis of $[^{18}\text{F}]\mathbf{5a}$

Reaction	Activity of the crude product $[^{18}\text{F}]\mathbf{4a}$ (MBq)	Activity of the crude product $[^{18}\text{F}]\mathbf{5a}$ (MBq, d.c.)	Radio-TLC purity (%)	Radio-UPLC purity (%)	Radiochemical Yield (%)
1	15.6	12.0	100	92	70.6
2	12.7	10.3	99	98	78.5
3	13.6	11.5	100	75	63.6
Radiochemical Yield (%) \pm Deviation					70.9 \pm 6.1

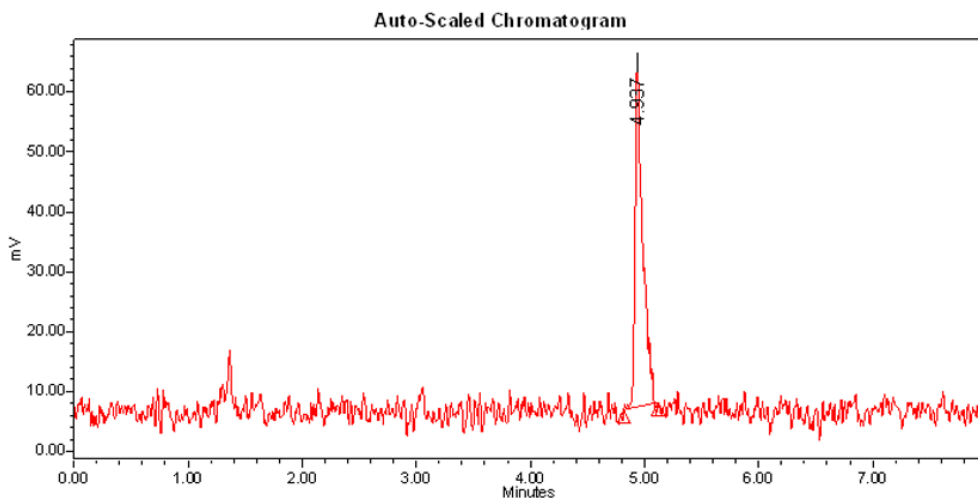


Figure S69. UPLC radio-chromatogram of the crude product $[^{18}\text{F}]\mathbf{5a}$. ACQUITY UPLC[®] CSH C18 column (1.7 μm , 2.1 \times 100 mm); MeCN and HCO₂H/H₂O (0.05%, v/v) in gradient mode at 0.5 mL \cdot min⁻¹ (from 100% HCO₂H/H₂O (0.05%, v/v) to 75% MeCN + 25% HCO₂H/H₂O (0.05%, v/v) in 6 min, and from 75% MeCN + 25% HCO₂H/H₂O (0.05%, v/v) to 100% HCO₂H/H₂O (0.05%, v/v) in 2 min).

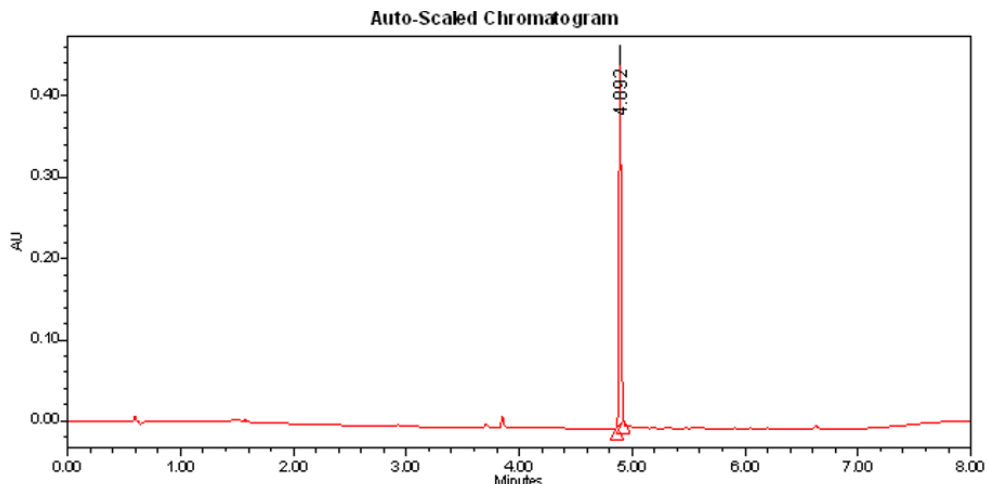


Figure S70. UPLC UV-chromatogram of the authentic reference **5a** (wavelength: 254 nm). ACQUITY UPLC® CSH C18 column (1.7 μm , 2.1 \times 100 mm); MeCN and HCO₂H/H₂O (0.05%, v/v) in gradient mode at 0.5 mL·min⁻¹ (from 100% HCO₂H/H₂O (0.05%, v/v) to 75% MeCN + 25% HCO₂H/H₂O (0.05%, v/v) in 6 min, and from 75% MeCN + 25% HCO₂H/H₂O (0.05%, v/v) to 100% HCO₂H/H₂O (0.05%, v/v) in 2 min).

5.2.8. Synthesis of [¹⁸F]2-((Difluoromethyl)sulfonyl)-5-methoxybenzo[*d*]thiazole ([¹⁸F]**5b**)

The implementation of the general procedure 3.2.3. for the oxidation of [¹⁸F]2-((difluoromethyl)thio)-5-methoxybenzo[*d*]thiazole ([¹⁸F]**4b**) (10-20 MBq) provided the labeled compound [¹⁸F]**5b** in 70.6 \pm 5.1% RCY (d.c. at the SOS). Table S12 furnishes more details of the RCY determination. The UPLC radio-chromatogram of the crude product [¹⁸F]**5b** is depicted in Figure S71. Figure S72 represents the UPLC UV-chromatogram of the non-radioactive reference **5b**.

Table S12. Determination of the radiochemical yield (%) of the synthesis of [¹⁸F]**5b**

Reaction	Activity of the crude product [¹⁸ F] 4b (MBq)	Activity of the crude product [¹⁸ F] 5b (MBq, d.c.)	Radio-TLC purity (%)	Radio-UPLC purity (%)	Radiochemical Yield (%)
1	17.4	13.1	99	85	63.5
2	16.2	13.7	99	87	72.9
3	14.9	11.2	100	100	75.4
Radiochemical Yield (%) \pm Deviation					70.6 \pm 5.1

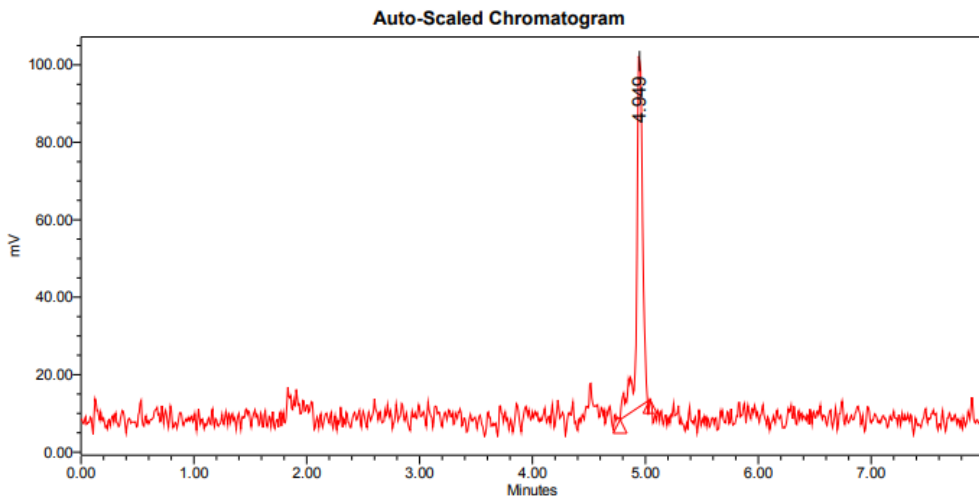


Figure S71. UPLC radio-chromatogram of the crude product [^{18}F]**5b**. ACQUITY UPLC[®] CSH C18 column (1.7 μm , 2.1 \times 100 mm); MeCN and HCO₂H/H₂O (0.05%, v/v) in gradient mode at 0.5 mL·min⁻¹ (from 100% HCO₂H/H₂O (0.05%, v/v) to 75% MeCN + 25% HCO₂H/H₂O (0.05%, v/v) in 6 min, and from 75% MeCN + 25% HCO₂H/H₂O (0.05%, v/v) to 100% HCO₂H/H₂O (0.05%, v/v) in 2 min).

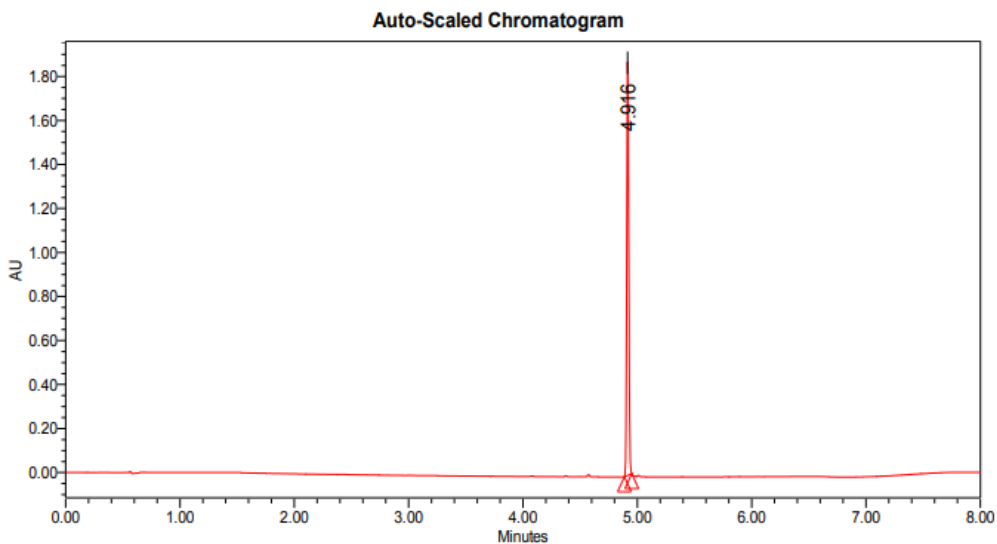


Figure S72. UPLC UV-chromatogram of the authentic reference **5b** (wavelength: 254 nm). ACQUITY UPLC[®] CSH C18 column (1.7 μm , 2.1 \times 100 mm); MeCN and HCO₂H/H₂O (0.05%, v/v) in gradient mode at 0.5 mL·min⁻¹ (from 100% HCO₂H/H₂O (0.05%, v/v) to 75% MeCN + 25% HCO₂H/H₂O (0.05%, v/v) in 6 min, and from 75% MeCN + 25% HCO₂H/H₂O (0.05%, v/v) to 100% HCO₂H/H₂O (0.05%, v/v) in 2 min).

5.2.9. Synthesis of [¹⁸F]2-((Difluoromethyl)sulfonyl)-6-nitrobenzo[d]thiazole ([¹⁸F]5c)

The implementation of the general procedure 3.2.3. for the oxidation of [¹⁸F]2-((difluoromethyl)thio)-6-nitrobenzo[d]thiazole ([¹⁸F]4c) (10-20 MBq) provided the labeled compound [¹⁸F]5c in 88.2 ± 0.2% RCY (d.c. at the SOS). Table S13 furnishes more details of the RCY determination. The UPLC radio-chromatogram of the crude product [¹⁸F]5c is depicted in Figure S73. Figure S74 represents the UPLC UV-chromatogram of the non-radioactive reference 5c.

Table S13. Determination of the radiochemical yield (%) of the synthesis of [¹⁸F]5c

Reaction	Activity of the crude product [¹⁸ F]4c (MBq)	Activity of the crude product [¹⁸ F]5c (MBq, d.c.)	Radio-TLC purity (%)	Radio-UPLC purity (%)	Radiochemical Yield (%)
1	15.9	14.1	100	100	88.4
2	14.2	12.6	100	99	88
3	14.8	13.4	100	97	88.1
Radiochemical Yield (%) ± Deviation					88.2 ± 0.2

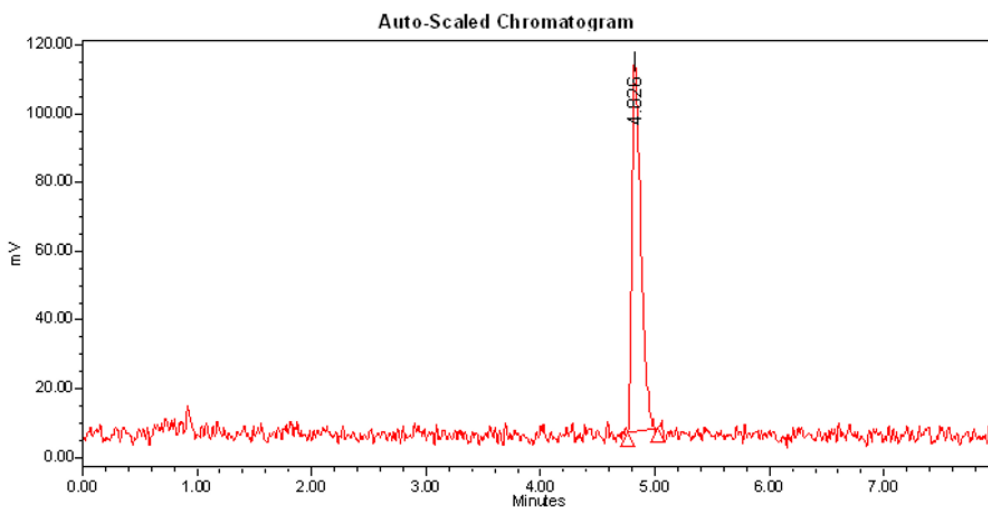


Figure S73. UPLC radio-chromatogram of the crude product [¹⁸F]5c. ACQUITY UPLC® CSH C18 column (1.7 μm, 2.1 × 100 mm); MeCN and HCO₂H/H₂O (0.05%, v/v) in gradient mode at 0.5 mL·min⁻¹ (from 100% HCO₂H/H₂O (0.05%, v/v) to 75% MeCN + 25% HCO₂H/H₂O (0.05%, v/v) in 6 min, and from 75% MeCN + 25% HCO₂H/H₂O (0.05%, v/v) to 100% HCO₂H/H₂O (0.05%, v/v) in 2 min).

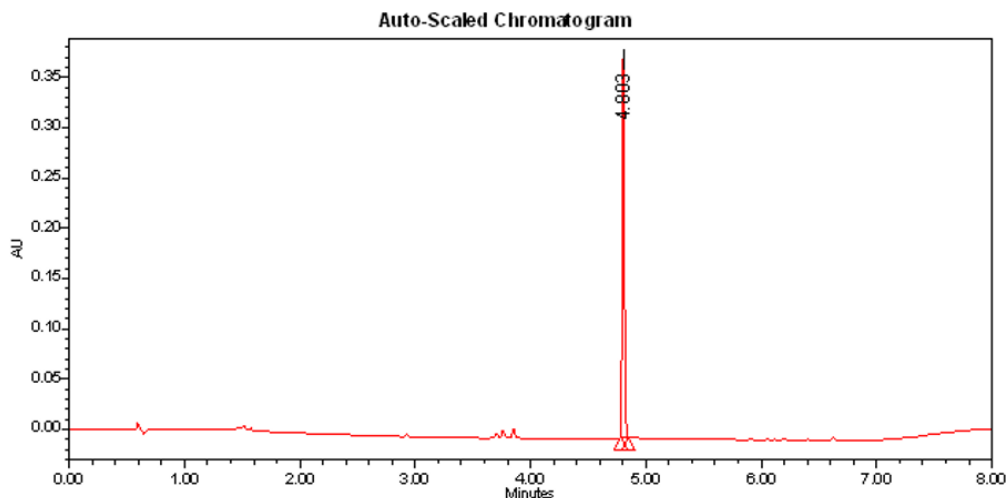


Figure S74. UPLC UV-chromatogram of the authentic reference **5c** (wavelength: 254 nm). ACQUITY UPLC® CSH C18 column (1.7 μm , 2.1 \times 100 mm); MeCN and HCO₂H/H₂O (0.05%, v/v) in gradient mode at 0.5 mL·min⁻¹ (from 100% HCO₂H/H₂O (0.05%, v/v) to 75% MeCN + 25% HCO₂H/H₂O (0.05%, v/v) in 6 min, and from 75% MeCN + 25% HCO₂H/H₂O (0.05%, v/v) to 100% HCO₂H/H₂O (0.05%, v/v) in 2 min).

5.2.10. Synthesis of [¹⁸F]2-((Difluoromethyl)sulfonyl)-5-nitrobenzo[*d*]thiazole ([¹⁸F]**5d**)

The implementation of the general procedure 3.2.3. for the oxidation of [¹⁸F]2-((difluoromethyl)thio)-5-nitrobenzo[*d*]thiazole ([¹⁸F]**4d**) (10-20 MBq) provided the labeled compound [¹⁸F]**5d** in 88.4 \pm 2.8% RCY (d.c. at the SOS). Table S14 furnishes more details of the RCY determination. The UPLC radio-chromatogram of the crude product [¹⁸F]**5d** is depicted in Figure S75. Figure S76 represents the UPLC UV-chromatogram of the non-radioactive reference **5d**.

Table S14. Determination of the radiochemical yield (%) of the synthesis of [¹⁸F]**5d**

Reaction	Activity of the crude product [¹⁸ F] 4d (MBq)	Activity of the crude product [¹⁸ F] 5d (MBq, d.c.)	Radio-TLC purity (%)	Radio-UPLC purity (%)	Radiochemical Yield (%)
1	13.9	13.3	99	97	92.1
2	15.0	14.6	99	89	85.6
3	15.9	15.1	99	93	87.6
Radiochemical Yield (%) \pm Deviation					88.4 \pm 2.8

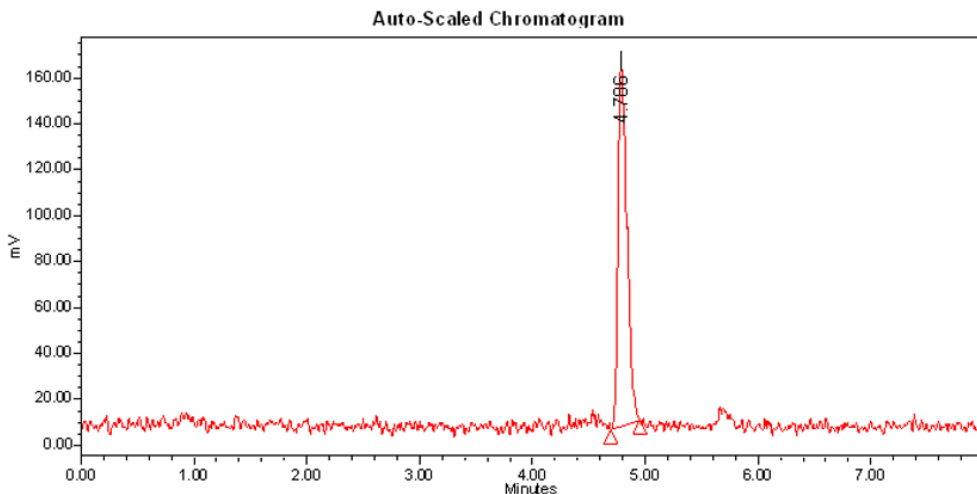


Figure S75. UPLC radio-chromatogram of the crude product $[^{18}\text{F}]\mathbf{5d}$. ACQUITY UPLC[®] CSH C18 column ($1.7\ \mu\text{m}$, $2.1 \times 100\ \text{mm}$); MeCN and $\text{HCO}_2\text{H}/\text{H}_2\text{O}$ (0.05%, v/v) in gradient mode at $0.5\ \text{mL}\cdot\text{min}^{-1}$ (from 100% $\text{HCO}_2\text{H}/\text{H}_2\text{O}$ (0.05%, v/v) to 75% MeCN + 25% $\text{HCO}_2\text{H}/\text{H}_2\text{O}$ (0.05%, v/v) in 6 min, and from 75% MeCN + 25% $\text{HCO}_2\text{H}/\text{H}_2\text{O}$ (0.05%, v/v) to 100% $\text{HCO}_2\text{H}/\text{H}_2\text{O}$ (0.05%, v/v) in 2 min).

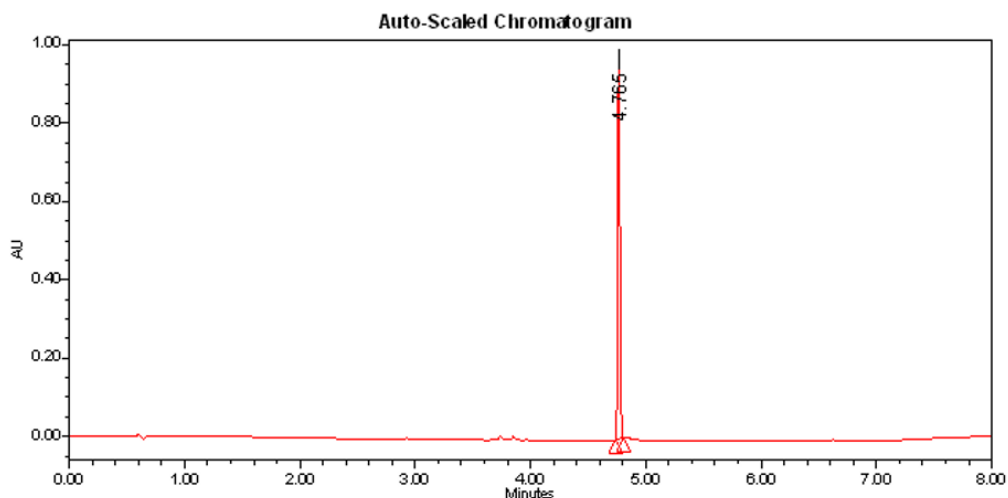


Figure S76. UPLC UV-chromatogram of the authentic reference $\mathbf{5d}$ (wavelength: 254 nm). ACQUITY UPLC[®] CSH C18 column ($1.7\ \mu\text{m}$, $2.1 \times 100\ \text{mm}$); MeCN and $\text{HCO}_2\text{H}/\text{H}_2\text{O}$ (0.05%, v/v) in gradient mode at $0.5\ \text{mL}\cdot\text{min}^{-1}$ (from 100% $\text{HCO}_2\text{H}/\text{H}_2\text{O}$ (0.05%, v/v) to 75% MeCN + 25% $\text{HCO}_2\text{H}/\text{H}_2\text{O}$ (0.05%, v/v) in 6 min, and from 75% MeCN + 25% $\text{HCO}_2\text{H}/\text{H}_2\text{O}$ (0.05%, v/v) to 100% $\text{HCO}_2\text{H}/\text{H}_2\text{O}$ (0.05%, v/v) in 2 min).

5.2.11. Synthesis of $[^{18}\text{F}]\mathbf{2}$ -((Difluoromethyl)sulfonyl)-1-methyl-1*H*-benzo[*d*]imidazole ($[^{18}\text{F}]\mathbf{5e}$)

The implementation of the general procedure 3.2.3. for the oxidation of $[^{18}\text{F}]\mathbf{2}$ -((difluoromethyl)thio)-1-methyl-1*H*-benzo[*d*]imidazole ($[^{18}\text{F}]\mathbf{4e}$) (10-20 MBq)

provided the labeled compound [^{18}F]5e in $86.1 \pm 3.0\%$ RCY (d.c. at the SOS). Table S15 furnishes more details of the RCY determination. The UPLC radio-chromatogram of the crude product [^{18}F]5e is depicted in Figure S77. Figure S78 represents the UPLC UV-chromatogram of the non-radioactive reference 5e.

Table S15. Determination of the radiochemical yield (%) of the synthesis of [^{18}F]5e

Reaction	Activity of the crude product [^{18}F]4e (MBq)	Activity of the crude product [^{18}F]5e (MBq, d.c.)	Radio-TLC purity (%)	Radio-UPLC purity (%)	Radiochemical Yield (%)
1	13.7	12.4	100	100	90.2
2	17.4	16.0	93	97	83.1
3	14.7	13.2	100	95	85
Radiochemical Yield (%) \pm Deviation					86.1 \pm 3.0

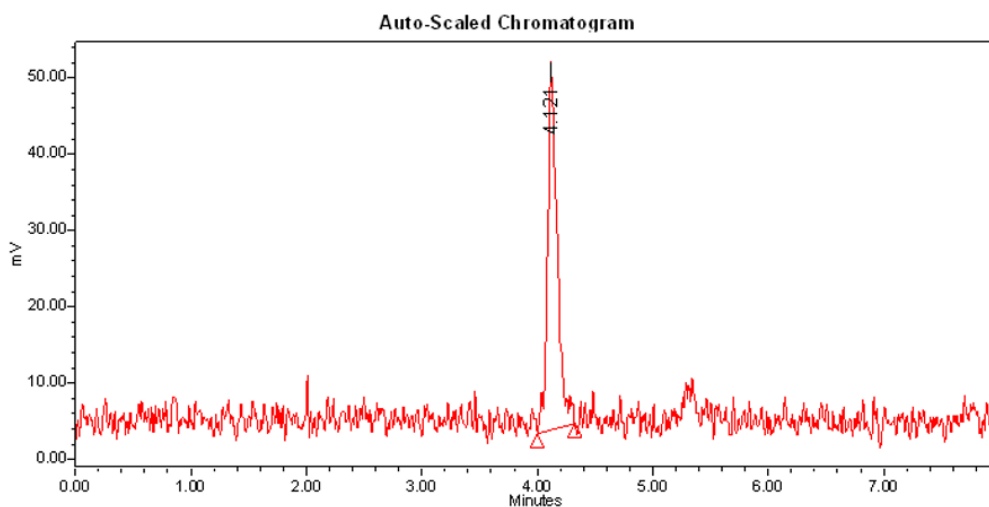


Figure S77. UPLC radio-chromatogram of the crude product [^{18}F]5e. ACQUITY UPLC[®] CSH C18 column (1.7 μm , 2.1 \times 100 mm); MeCN and HCO₂H/H₂O (0.05%, v/v) in gradient mode at 0.5 mL \cdot min⁻¹ (from 100% HCO₂H/H₂O (0.05%, v/v) to 75% MeCN + 25% HCO₂H/H₂O (0.05%, v/v) in 6 min, and from 75% MeCN + 25% HCO₂H/H₂O (0.05%, v/v) to 100% HCO₂H/H₂O (0.05%, v/v) in 2 min).

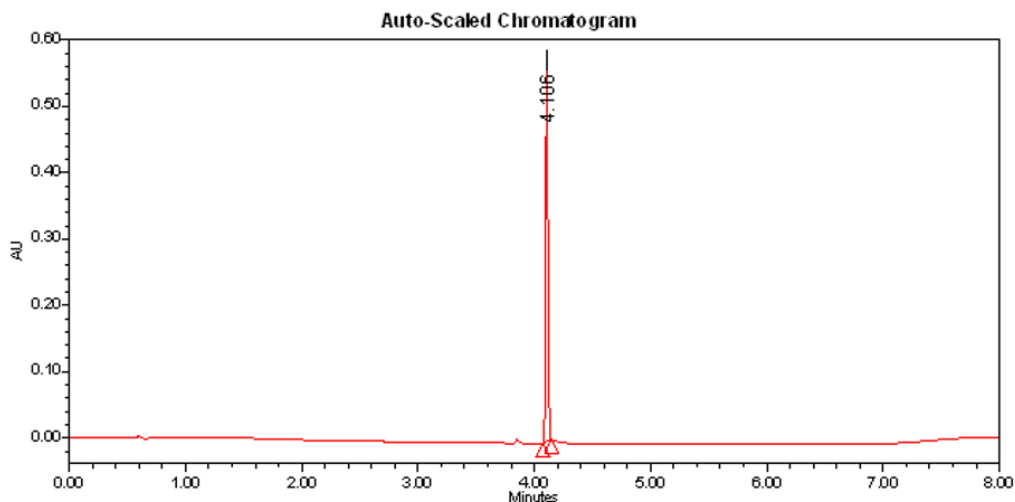


Figure S78. UPLC UV-chromatogram of the authentic reference **5e** (wavelength: 254 nm). ACQUITY UPLC[®] CSH C18 column (1.7 μm , 2.1 \times 100 mm); MeCN and HCO₂H/H₂O (0.05%, v/v) in gradient mode at 0.5 mL·min⁻¹ (from 100% HCO₂H/H₂O (0.05%, v/v) to 75% MeCN + 25% HCO₂H/H₂O (0.05%, v/v) in 6 min, and from 75% MeCN + 25% HCO₂H/H₂O (0.05%, v/v) to 100% HCO₂H/H₂O (0.05%, v/v) in 2 min).

5.2.12. Synthesis of [¹⁸F]5-((Difluoromethyl)sulfonyl)-1-phenyl-1*H*-tetrazole ([¹⁸F]**5f**)

The implementation of the general procedure 3.2.3. for the oxidation of [¹⁸F]5-((difluoromethyl)thio)-1-phenyl-1*H*-tetrazole ([¹⁸F]**4f**) (10-20 MBq) provided the labeled compound [¹⁸F]**5f** in 91.9 \pm 2.8% RCY (d.c. at the SOS). Table S16 furnishes more details of the RCY determination. The UPLC radio-chromatogram of the crude product [¹⁸F]**5f** is depicted in Figure S79. Figure S80 represents the UPLC UV-chromatogram of the non-radioactive reference **5f**.

Table S16. Determination of the radiochemical yield (%) of the synthesis of [¹⁸F]**5f**

Reaction	Activity of the crude product [¹⁸ F] 4f (MBq)	Activity of the crude product [¹⁸ F] 5f (MBq, d.c.)	Radio-TLC purity (%)	Radio-UPLC purity (%)	Radiochemical Yield (%)
1	15.4	13.7	100	100	88.7
2	16.1	14.7	100	100	91.4
3	15.7	15.0	100	100	95.6
Radiochemical Yield (%) \pm Deviation					91.9 \pm 2.8

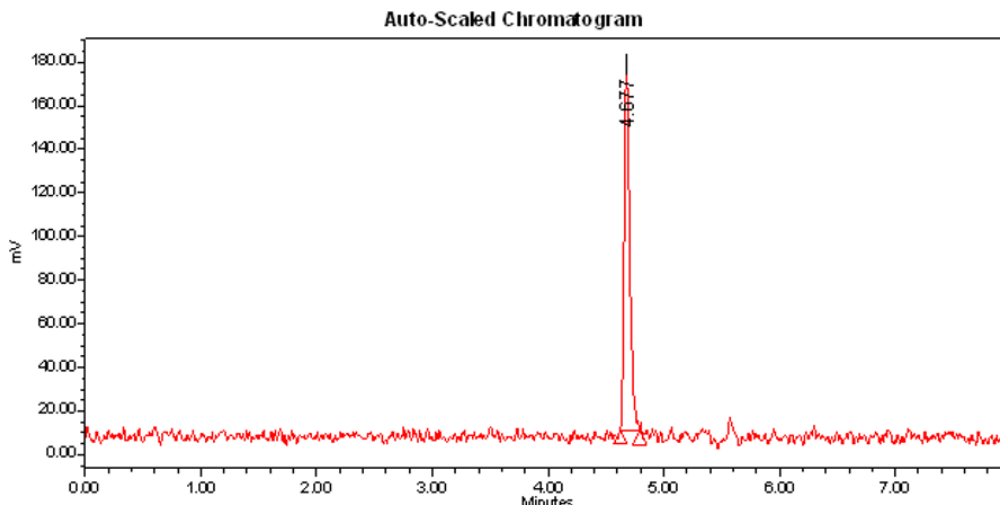


Figure S79. UPLC radio-chromatogram of the crude product $[^{18}\text{F}]\mathbf{5f}$. ACQUITY UPLC[®] CSH C18 column (1.7 μm , 2.1 \times 100 mm); MeCN and HCO₂H/H₂O (0.05%, v/v) in gradient mode at 0.5 mL·min⁻¹ (from 100% HCO₂H/H₂O (0.05%, v/v) to 75% MeCN + 25% HCO₂H/H₂O (0.05%, v/v) in 6 min, and from 75% MeCN + 25% HCO₂H/H₂O (0.05%, v/v) to 100% HCO₂H/H₂O (0.05%, v/v) in 2 min).

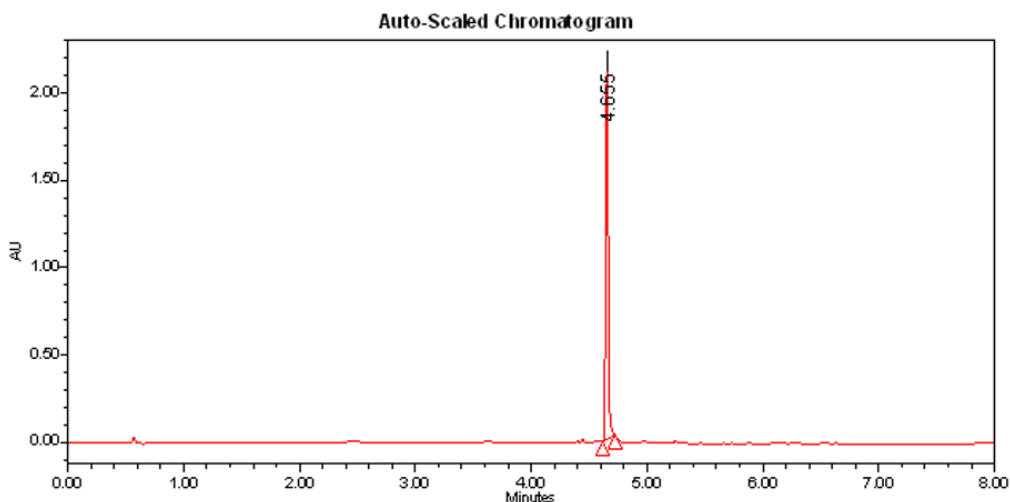


Figure S80. UPLC UV-chromatogram of the authentic reference $\mathbf{5f}$ (wavelength: 254 nm). ACQUITY UPLC[®] CSH C18 column (1.7 μm , 2.1 \times 100 mm); MeCN and HCO₂H/H₂O (0.05%, v/v) in gradient mode at 0.5 mL·min⁻¹ (from 100% HCO₂H/H₂O (0.05%, v/v) to 75% MeCN + 25% HCO₂H/H₂O (0.05%, v/v) in 6 min, and from 75% MeCN + 25% HCO₂H/H₂O (0.05%, v/v) to 100% HCO₂H/H₂O (0.05%, v/v) in 2 min).

5.3. Two-Step Radiosynthesis of the $[^{18}\text{F}]$ Difluoromethyl Heteroaryl-Sulfones $[^{18}\text{F}]\mathbf{5a}$ - $[^{18}\text{F}]\mathbf{5f}$ from the Precursors $\mathbf{6a-6f}$

The overall RCY of the ^{18}F -labeling step of $\mathbf{6a-6f}$ and the oxidation of $[^{18}\text{F}]\mathbf{4a-4f}$ was determined based on the activity of the recovered crude products $[^{18}\text{F}]\mathbf{5a-5f}$.

[¹⁸F]5f, on their radio-TLC and radio-UPLC purities, and the starting radioactivity, according to the following formula:

$$RCY (\%, d. c.) = \frac{\text{radioTLC purity (\%)} \times \text{radioUPLC purity (\%)} \times \text{activity of } [^{18}\text{F}]5\text{a} - [^{18}\text{F}]5\text{f (d. c.)}}{\text{starting radioactivity} \times 100}$$

Tables S17-S22 furnishes more details of the RCY determination of the radiosynthesis of the [¹⁸F]difluoromethyl heteroaryl-sulfones [¹⁸F]5a-[¹⁸F]5f from the precursors 6a-6f.

Table S17. Determination of the radiochemical yield (%) of the synthesis of [¹⁸F]5a from the precursor 6a

Reaction	Starting activity (MBq)	Activity of the crude product [¹⁸ F]5a (MBq, d.c.)	Radio-TLC purity (%)	Radio-UPLC purity (%)	Radiochemical Yield (%)
1	100	11.0	98	93	10.0
2	98.6	11.8	98	95	11.1
3	131.8	13.6	99	89	9.1
Radiochemical Yield (%) ± Deviation					10.1 ± 0.8

Table S18. Determination of the radiochemical yield (%) of the synthesis of [¹⁸F]5b from the precursor 6b

Reaction	Starting activity (MBq)	Activity of the crude product [¹⁸ F]5b (MBq, d.c.)	Radio-TLC purity (%)	Radio-UPLC purity (%)	Radiochemical Yield (%)
1	92.2	9.3	98	87	8.6
2	112.0	10.1	98	85	7.5
3	110.0	11.5	99	86	8.9
Radiochemical Yield (%) ± Deviation					8.3 ± 0.6

Table S19. Determination of the radiochemical yield (%) of the synthesis of [¹⁸F]5c from the precursor 6c

Reaction	Starting activity (MBq)	Activity of the crude product [¹⁸ F]5c (MBq, d.c.)	Radio-TLC purity (%)	Radio-UPLC purity (%)	Radiochemical Yield (%)
1	112.8	14.6	100	99	12.8
2	101.3	12.1	100	98	11.7
3	122.9	14.5	100	98	11.6
Radiochemical Yield (%) ± Deviation					12 ± 0.5

Table S20. Determination of the radiochemical yield (%) of the synthesis of [¹⁸F]5d from the precursor 6d

Reaction	Starting activity (MBq)	Activity of the crude product [¹⁸ F]5d (MBq, d.c.)	Radio-TLC purity (%)	Radio-UPLC purity (%)	Radiochemical Yield (%)
1	115.1	12.9	100	97	10.9
2	108.9	12.5	100	97	11.1
3	98.2	11.7	100	98	11.7
Radiochemical Yield (%) ± Deviation					11.2 ± 0.3

Table S21. Determination of the radiochemical yield (%) of the synthesis of [¹⁸F]5e from the precursor 6e

Reaction	Starting activity (MBq)	Activity of the crude product [¹⁸ F]5e (MBq, d.c.)	Radio-TLC purity (%)	Radio-UPLC purity (%)	Radiochemical Yield (%)
1	106.8	8.2	100	98	7.5
2	99.1	7.4	99	96	7.1
3	105.3	7.6	99	96	6.9
Radiochemical Yield (%) ± Deviation					7.2 ± 0.2

Table S22. Determination of the radiochemical yield (%) of the synthesis of [¹⁸F]5f from the precursor 6f

Reaction	Starting activity (MBq)	Activity of the crude product [¹⁸ F]5f (MBq, d.c.)	Radio-TLC purity (%)	Radio-UPLC purity (%)	Radiochemical Yield (%)
1	116.8	15.8	100	100	13.5
2	111.3	14.6	100	100	13.1
3	110.6	15.6	100	100	14.1
Radiochemical Yield (%) ± Deviation					13.6 ± 0.4

5.4. Fully Automated Radiosynthesis of the Labeled Compounds [¹⁸F]5a, [¹⁸F]5c, and [¹⁸F]5f

The RCY of the fully automated radiosynthesis of the [¹⁸F]difluoromethyl heteroaryl-sulfones [¹⁸F]5a, [¹⁸F]5c, and [¹⁸F]5f was determined based on the radioactivity of the [¹⁸F]5a, [¹⁸F]5c, or [¹⁸F]5f present in DMSO solution and the radioactivity trapped on the QMA carbonate cartridge, according to the following formula:

$$RCY (\%, d. c.) = \frac{\text{activity of the solution of } [^{18}\text{F}]5a, [^{18}\text{F}]5c, \text{ or } [^{18}\text{F}]5f \text{ in DMSO (d. c.)}}{\text{activity trapped on the QMA carbonate cartridge}} \times 100$$

Tables S23-S25 provide more details of the RCY determination of the radiosynthesis of the [¹⁸F]difluoromethyl heteroaryl-sulfones [¹⁸F]5a, [¹⁸F]5c, and [¹⁸F]5f from the precursors 6a, 6c, and 6f, respectively.

Table S23. Determination of the radiochemical yield (%) of the synthesis of [¹⁸F]5a from the precursor 6a

Reaction	Starting activity (GBq)	Activity of the isolated product [¹⁸ F]5a (GBq, d.c.)	Radiochemical Yield (%)
1	135.0	4.0	3.0
2	137.3	3.7	2.7
3	148.9	4.3	2.9
Radiochemical Yield (%) ± Deviation			2.9 ± 0.1

Table S24. Determination of the radiochemical yield (%) of the synthesis of [¹⁸F]5c from the precursor 6c

Reaction	Starting activity (GBq)	Activity of the isolated product [¹⁸ F]5c (GBq, d.c.)	Radiochemical Yield (%)
1	134.3	6.3	4.7
2	146.9	8.5	5.8
3	135.3	8.2	6.1
4	127.6	7.5	5.9
5	147.6	9.0	6.1
Radiochemical Yield (%) ± Deviation			5.7 ± 0.5

Table S25. Determination of the radiochemical yield (%) of the synthesis of [¹⁸F]5f from the precursor 6f

Reaction	Starting activity (GBq)	Activity of the isolated product [¹⁸ F]5a (GBq, d.c.)	Radiochemical Yield (%)
1	140.1	10.2	7.3
2	130.9	9.7	7.4
3	124.9	11.6	9.3
Radiochemical Yield (%) ± Deviation			8.0 ± 0.9

5.5. Calibration Curves of the Difluoromethyl Heteroaryl-Sulfones 5a, 5c, and 5f for Determination of the Molar Activity of [¹⁸F]5a, [¹⁸F]5c, and [¹⁸F]5f

The fully automated radiosynthesis of the sulfones [¹⁸F]5a, [¹⁸F]5c, or [¹⁸F]5f was performed on a commercially available FASTlab™ synthesizer (GE Healthcare), using the optimized conditions for the labeling of precursors 6a (12.3 mg, 0.04 mmol), 6c (6.5 mg, 0.02 mmol), or 6f (11.6 mg, 0.04 mmol), and the oxidation of the labeled compounds [¹⁸F]4a, [¹⁸F]4c, and [¹⁸F]4f. The molar activity of the [¹⁸F]difluoromethyl heteroaryl-sulfones was determined using an aliquot of each reformulated solution (3 μL). After injection of an aliquot in UPLC, the radioactive peak of [¹⁸F]5a, [¹⁸F]5c, and [¹⁸F]5f associated to the non-radioactive sulfones 5a, 5c, and 5f, respectively, were

collected and counted in an ionization chamber. The PDA UV area under the peak of the non-radioactive sulfones **5a**, **5c**, and **5f** at 258 nm, 290 nm, and 244 nm, respectively, enabled the determination of the corresponding amount (in μmol) of the difluoromethyl heteroaryl-sulfones using the calibration curves described in Figures S81-S83. The molar activity was calculated by the ratio between the radioactivity of the [^{18}F]**5a**, [^{18}F]**5c**, and [^{18}F]**5f** and the corresponding amount of non-radioactive compound, according to the following formula:

$$\text{Molar activity (GBq} \cdot \mu\text{mol}^{-1}) = \frac{\text{activity of the UPLC peak of } [^{18}\text{F}]\mathbf{5a}, [^{18}\text{F}]\mathbf{5c}, \text{ or } [^{18}\text{F}]\mathbf{5f}}{\text{amount of } \mathbf{5a}, \mathbf{5c}, \text{ or } \mathbf{5f} \text{ associated to the radioactive peak}}$$

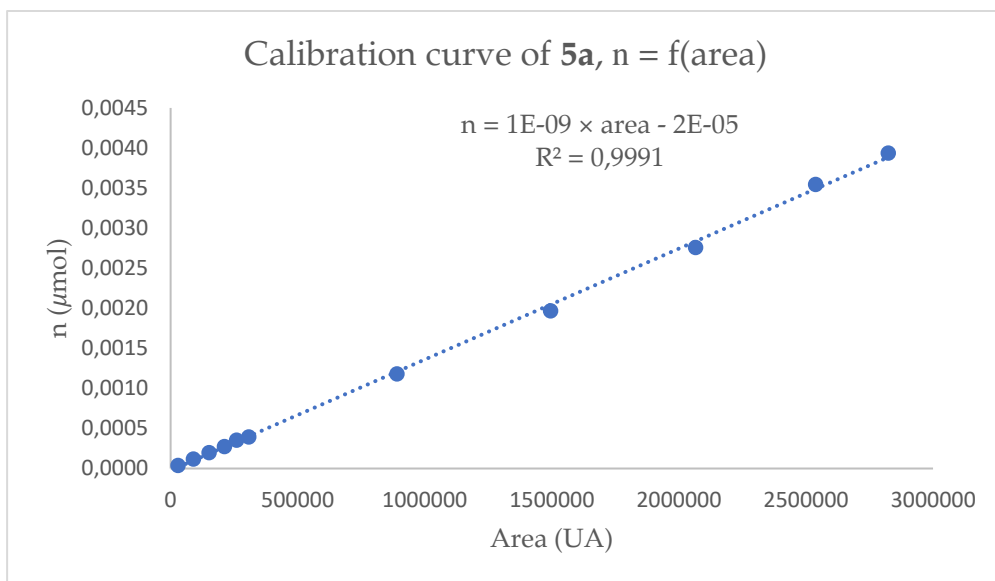


Figure S81. Calibration curve of the difluoromethyl heteroaryl-sulfone **5a** (wavelength: 258 nm).

Table S26. Determination of the molar activity of [^{18}F]**5a**

Reaction	Activity of the radioactive peak of [^{18}F] 5a (GBq)	Area under the peak of 5a (UA) at 258 nm	Amount of 5a (μmol)	Molar activity ($\text{GBq} \cdot \mu\text{mol}^{-1}$)
1	4.552×10^{-3}	40425	3.146×10^{-5}	145
2	4.454×10^{-3}	38473	2.876×10^{-5}	155
3	5.175×10^{-3}	50000	4.471×10^{-5}	116
Molar activity ($\text{GBq} \cdot \mu\text{mol}^{-1}$) \pm Deviation				139 ± 17

The sulfone [^{18}F]**5a** was isolated with a molar activity of $139 \pm 17 \text{ GBq} \cdot \mu\text{mol}^{-1}$ at the EOS.

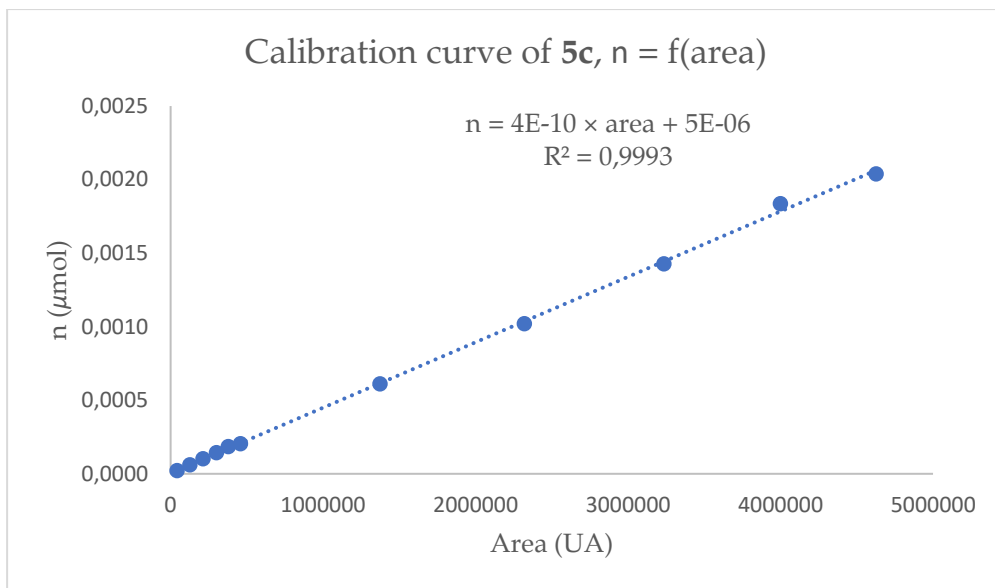


Figure S82. Calibration curve of the difluoromethyl heteroaryl-sulfone **5c** (wavelength: 290 nm).

Table S27. Determination of the molar activity of [^{18}F]**5c**

Reaction	Activity of the radioactive peak of [^{18}F] 5c (GBq)	Area under the peak of 5c (UA) at 290 nm	Amount of 5c (μmol)	Molar activity (GBq· μmol^{-1})
1	4.863×10^{-3}	247987	1.150×10^{-4}	42
2	2.662×10^{-3}	90325	4.489×10^{-5}	59
3	8.242×10^{-3}	244309	1.134×10^{-4}	73
4	2.038×10^{-3}	65547	3.387×10^{-5}	60
5	2.524×10^{-3}	66094	3.412×10^{-5}	74
Molar activity (GBq·μmol^{-1}) \pm Deviation				62 ± 12

The sulfone [^{18}F]**5c** was isolated with a molar activity of 62 ± 12 GBq· μmol^{-1} at the EOS.

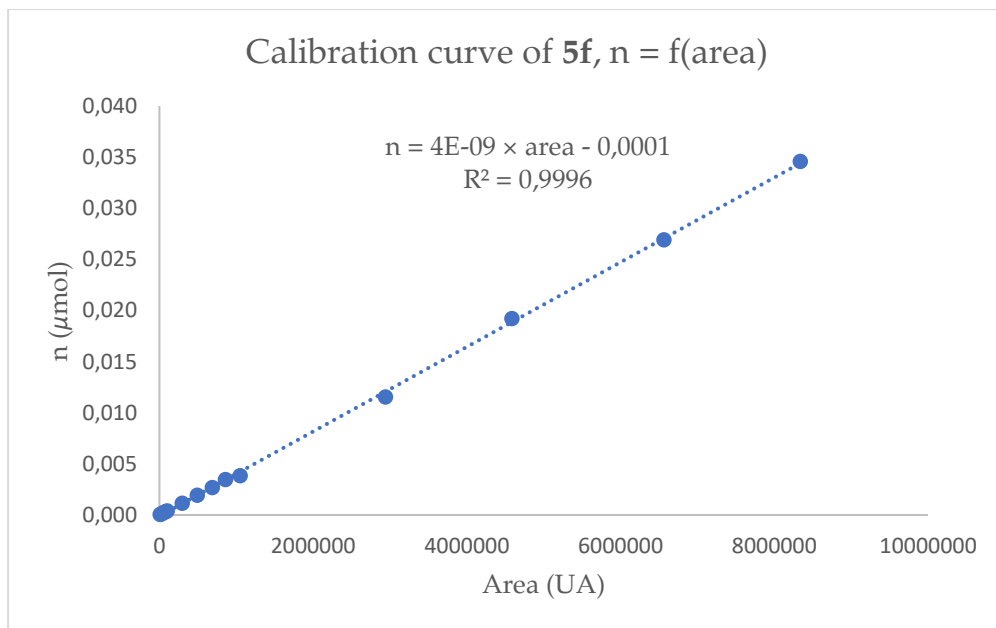


Figure S83. Calibration curve of the difluoromethyl heteroaryl-sulfone **5f** (wavelength: 244 nm).

Table S28. Determination of the molar activity of [¹⁸F]**5f**

Reaction	Activity of the radioactive peak of [¹⁸ F] 5f (GBq)	Area under the peak of 5f (UA) at 244 nm	Amount of 5f (μmol)	Molar activity (GBq·μmol ⁻¹)
1	1.702×10^{-2}	57459	1.378×10^{-4}	124
2	1.193×10^{-2}	57048	1.361×10^{-4}	88
3	1.435×10^{-2}	51785	1.143×10^{-4}	126
Molar activity (GBq·μmol⁻¹) ± Deviation				113 ± 17

The sulfone [¹⁸F]**5f** was isolated with a molar activity of 113 ± 17 GBq·μmol⁻¹ at the EOS.

5.6. Photocatalytic C-H ¹⁸F-Difluoromethylation of Heteroarenes with the Reagents [¹⁸F]**5a**, [¹⁸F]**5c**, and [¹⁸F]**5f**

The propensity of the reagents [¹⁸F]**5a**, [¹⁸F]**5c**, and [¹⁸F]**5f** to undergo the desired photocatalytic C-H ¹⁸F-difluoromethylation reaction was carried out using 2-amino-9-((2-hydroxyethoxy)methyl)-9H-purin-6-ol (acyclovir, **7e**) as a model substrate. The best conditions for the C-H ¹⁸F-difluoromethylation of the substrate **7e** were:

- **Conditions A:** [¹⁸F]difluoromethyl heteroaryl-sulfone [¹⁸F]**5a** (30-40 MBq), *fac*-Ir^{III}(ppy)₃ (0.05 mol%), residence time (2 min), DMSO (250 μL), 35 °C, blue LED (470 nm, 2 W).

- **Conditions B:** [¹⁸F]difluoromethyl heteroaryl-sulfone [**18F**5c] (30-40 MBq), *fac*-Ir^{III}(ppy)₃ (0.5 mol%), residence time (4 min), DMSO (250 μL), 35 °C, blue LED (470 nm, 2 W).
- **Conditions C:** [¹⁸F]difluoromethyl heteroaryl-sulfone [**18F**5f] (30-40 MBq), *fac*-Ir^{III}(ppy)₃ (0.1 mol%), residence time (2.5 min), DMSO (250 μL), 35 °C, blue LED (470 nm, 2 W).



Figure S84. Instrument used for the C-H ¹⁸F-difluoromethylation reaction of the heteroarenes (FlowStart Evo, FutureChemistry).

5.6.1. Synthesis of [¹⁸F]2-Amino-8-(difluoromethyl)-9-((2-hydroxyethoxy)methyl)-9H-purin-6-ol (**18F**8e)

The implementation of the general procedure 3.2.5. for the C-H ¹⁸F-difluoromethylation of the 2-amino-9-((2-hydroxyethoxy)methyl)-9H-purin-6-ol (acyclovir, **7e**) (4.5 mg, 0.02 mmol) provided the labeled compound [**18F**8e] in 57 ± 7%, 51 ± 7%, and 56 ± 1% RCY, using the reagents [**18F**5a], [**18F**5c], and [**18F**5f], respectively (see the Tables S30-S32 for more details of the RCY determination). The UPLC radio-chromatogram of the crude product [**18F**8e] is depicted in Figure S86. Figure S87 represents the UPLC UV-chromatogram of the non-radioactive reference **8e**.

The RCY of the C-H ¹⁸F-difluoromethylation reactions were determined according to the following equation:

$$RCY (\%) = \frac{\text{radioTLC purity} (\%) \times \text{radioUPLC purity} (\%)}{100}$$

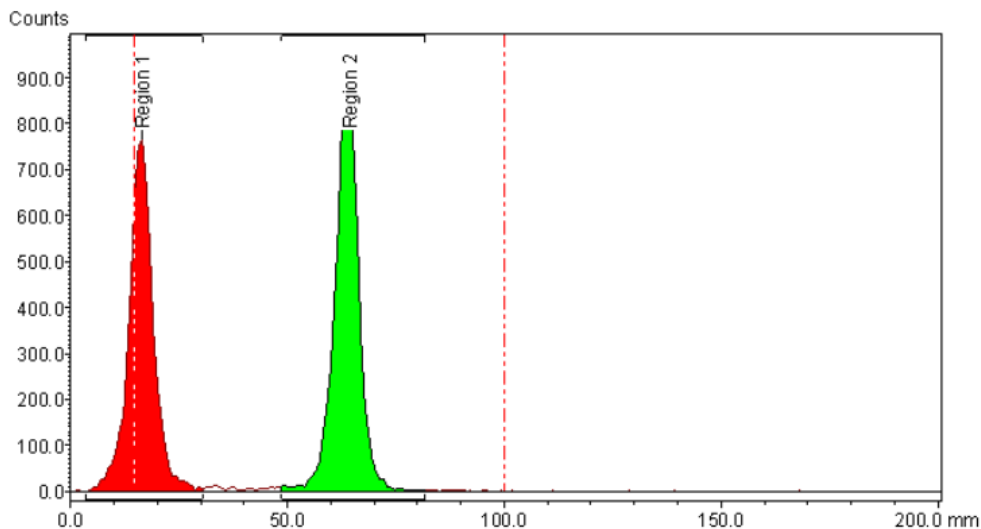


Figure S85. TLC radio-chromatogram of the crude product $[^{18}\text{F}]\mathbf{8e}$ (eluent: methanol).

Table S29. Determination of the radio-TLC purity of the crude product $[^{18}\text{F}]\mathbf{8e}$

Retention factor (R_f , mm)	Ratio (%)
0.02	46 (impurity/by-product)
0.77	54 (desired crude product)

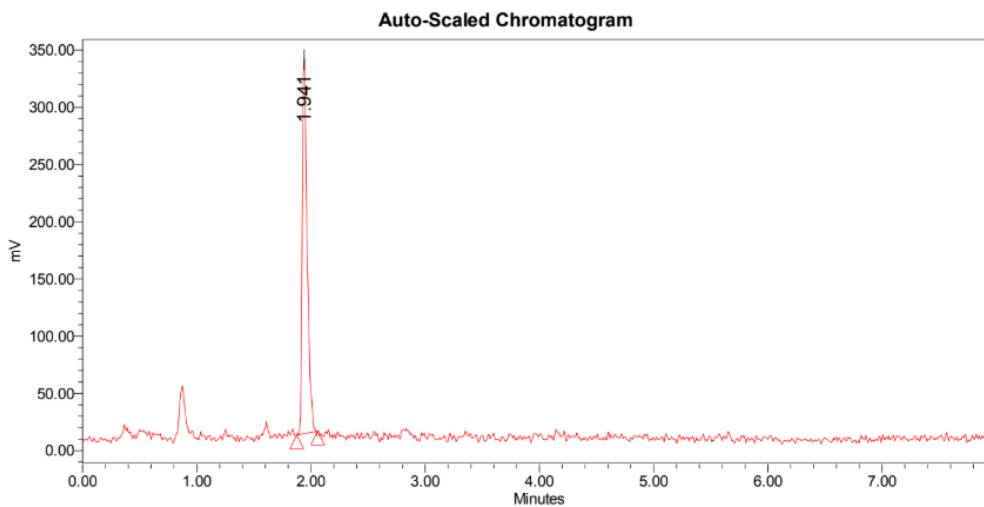


Figure S86. UPLC radio-chromatogram of the crude product $[^{18}\text{F}]\mathbf{8e}$. ACQUITY UPLC[®] CSH C18 column (1.7 μm , 2.1 \times 100 mm); MeCN and HCO₂H/H₂O (0.05%, v/v) in gradient mode at 0.5 mL \cdot min⁻¹ (from 100% HCO₂H/H₂O (0.05%, v/v) to 100% MeCN in 6 min, and from 100% MeCN to 100% HCO₂H/H₂O (0.05%, v/v) in 2 min).

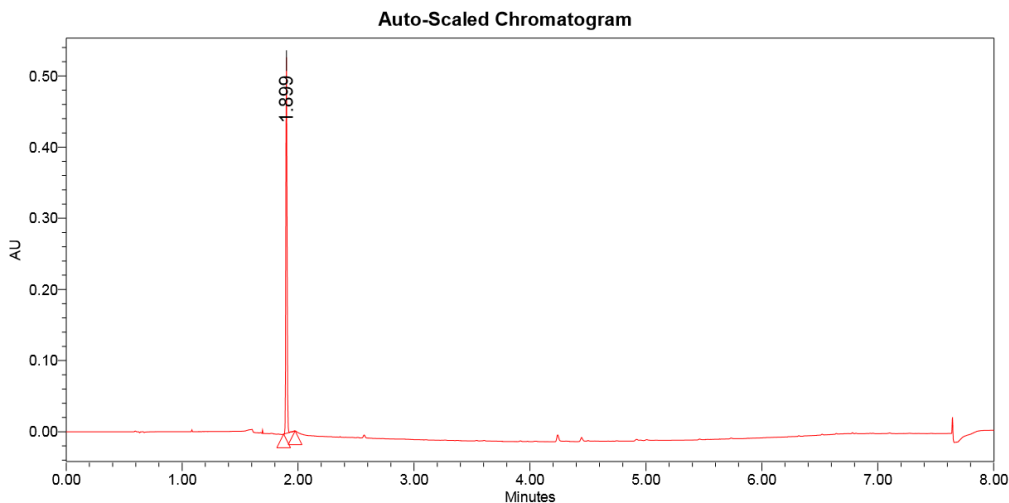


Figure S87. UPLC UV-chromatogram of the authentic reference **8e** (wavelength: 254 nm). ACQUITY UPLC® CSH C18 column (1.7 μm , 2.1 \times 100 mm); MeCN and HCO₂H/H₂O (0.05%, v/v) in gradient mode at 0.5 mL·min⁻¹ (from 100% HCO₂H/H₂O (0.05%, v/v) to 100% MeCN in 6 min, and from 100% MeCN to 100% HCO₂H/H₂O (0.05%, v/v) in 2 min).

$$RCY (\%) = \frac{\text{radioTLC purity} (\%) \times \text{radioUPLC purity} (\%)}{100}$$

$$RCY (\%) = \frac{54 \times 100}{100}$$

$$RCY (\%) = 54 \%$$

Note: In some cases, some peaks at 0.6 and 0.9 min were observed on the radio-UPLC chromatograms. Those two peaks were collected and their radio-TLC purity was analyzed. Since the retention factor corresponding to these peaks is approximately 0, their contribution for the radio-UPLC purity was not taken into consideration. The contribution of these peaks were accounted for the determination of the radio-TLC purity.

Table S30. Determination of the radiochemical yield (%) of the synthesis of [¹⁸F]**8e** using the reagent [¹⁸F]**5a**

Reaction	Radio-TLC purity (%)	Radio-UPLC purity (%)	Radiochemical Yield (%)
1	54	100	54
2	67	100	67
3	51	100	51
Radiochemical Yield (%) \pm Deviation			57 \pm 7

Table S31. Determination of the radiochemical yield (%) of the synthesis of [¹⁸F]8e using the reagent [¹⁸F]5c

Reaction	Radio-TLC purity (%)	Radio-UPLC purity (%)	Radiochemical Yield (%)
1	74	79	58
2	68	57	39
3	63	84	53
4	67	80	54
Radiochemical Yield (%) ± Deviation			51 ± 7

Table S32. Determination of the radiochemical yield (%) of the synthesis of [¹⁸F]8e using the reagent [¹⁸F]5f

Reaction	Radio-TLC purity (%)	Radio-UPLC purity (%)	Radiochemical Yield (%)
1	54	100	54
2	67	100	67
3	51	100	51
Radiochemical Yield (%) ± Deviation			57 ± 7

5.6.2. Synthesis of [¹⁸F]2-(Difluoromethyl)-4-methyl-1*H*-pyrrolo[2,3-*b*]pyridine (**[¹⁸F]8aa**) and [¹⁸F]6-(Difluoromethyl)-4-methyl-1*H*-pyrrolo[2,3-*b*]pyridine (**[¹⁸F]8ab**)

The implementation of the general procedure 3.2.5. for the C-H ¹⁸F-difluoromethylation of the 4-methyl-1*H*-pyrrolo[2,3-*b*]pyridine (2.6 mg, 0.02 mmol) provided the labeled compound [¹⁸F]8aa in 32 ± 1%, 58 ± 3%, and 46 ± 3% RCY, using the reagents [¹⁸F]5a, [¹⁸F]5c, and [¹⁸F]5f, respectively. The labeled compound [¹⁸F]8ab was afforded in 5 ± 1%, 8%, and 7% RCY, using the reagents [¹⁸F]5a, [¹⁸F]5c, and [¹⁸F]5f, respectively (see the Tables S33-S35 for more details of the RCY determination). The UPLC radio-chromatogram of the crude product [¹⁸F]8a is depicted in Figure S88. Figures S89 and S90 represent the UPLC UV-chromatograms of the non-radioactive references **8aa** and **8ab**, respectively.

Table S33. Determination of the radiochemical yield (%) of the synthesis of [¹⁸F]8a using the reagent [¹⁸F]5a

Reaction	Radio-TLC purity (%)	Radio-UPLC purity (%)		Radiochemical Yield (%)	
	a + b	A	b	a	b
1	37	90	10	33	4
2	34	89	11	30	4
3	38	85	15	32	6
Radiochemical Yield (%) ± Deviation				32 ± 1	5 ± 1

Table S34. Determination of the radiochemical yield (%) of the synthesis of [¹⁸F]8a using the reagent [¹⁸F]5c

Reaction	Radio-TLC purity (%)	Radio-UPLC purity (%)		Radiochemical Yield (%)	
	a + b	A	b	a	b
1	67	80	12	54	8
2	76	82	12	62	9
3	76	75	11	57	8
Radiochemical Yield (%) ± Deviation				58 ± 3	8

Table S35. Determination of the radiochemical yield (%) of the synthesis of [¹⁸F]8a using the reagent [¹⁸F]5f

Reaction	Radio-TLC purity (%)	Radio-UPLC purity (%)		Radiochemical Yield (%)	
	a + b	A	b	a	b
1	64	74	11	47	7
2	58	73	10	42	6
3	67	72	10	48	7
Radiochemical Yield (%) ± Deviation				46 ± 3	7

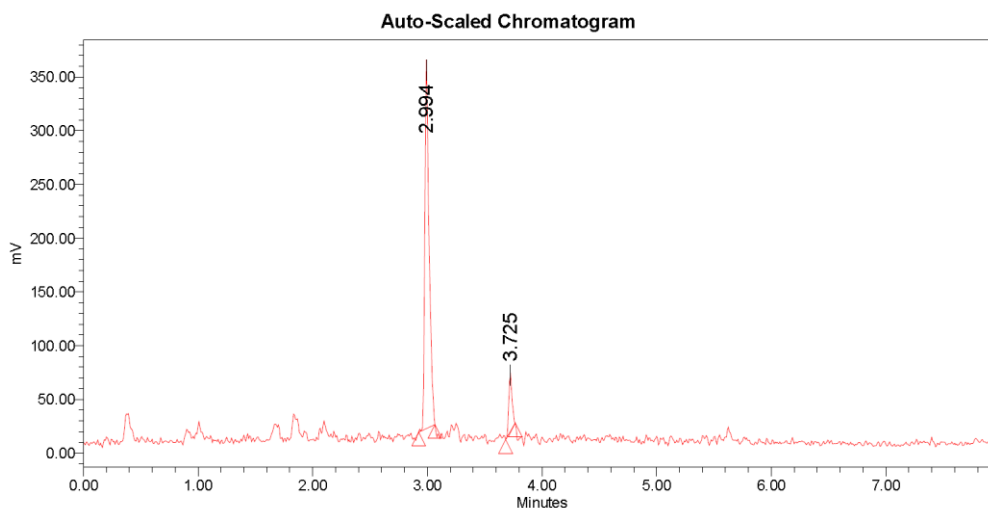


Figure S88. UPLC radio-chromatogram of the crude product [¹⁸F]8a. ACQUITY UPLC® CSH C18 column (1.7 μm, 2.1 × 100 mm); MeCN and HCO₂H/H₂O (0.05%, v/v) in gradient mode at 0.5 mL·min⁻¹ (from 100% HCO₂H/H₂O (0.05%, v/v) to 100% MeCN in 6 min, and from 100% MeCN to 100% HCO₂H/H₂O (0.05%, v/v) in 2 min).

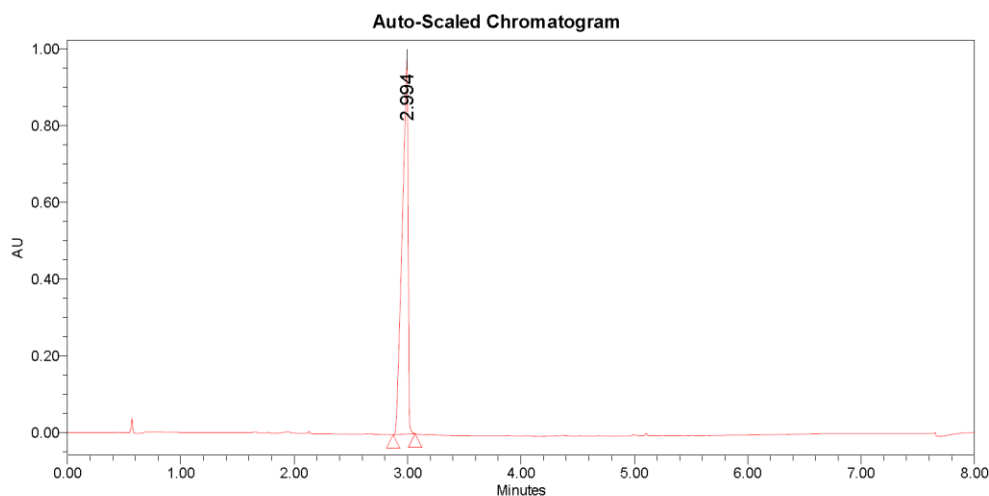


Figure S89. UPLC UV-chromatogram of the authentic reference **8aa** (wavelength: 254 nm). ACQUITY UPLC[®] CSH C18 column (1.7 μm , 2.1 \times 100 mm); MeCN and HCO₂H/H₂O (0.05%, v/v) in gradient mode at 0.5 mL \cdot min⁻¹ (from 100% HCO₂H/H₂O (0.05%, v/v) to 100% MeCN in 6 min, and from 100% MeCN to 100% HCO₂H/H₂O (0.05%, v/v) in 2 min).

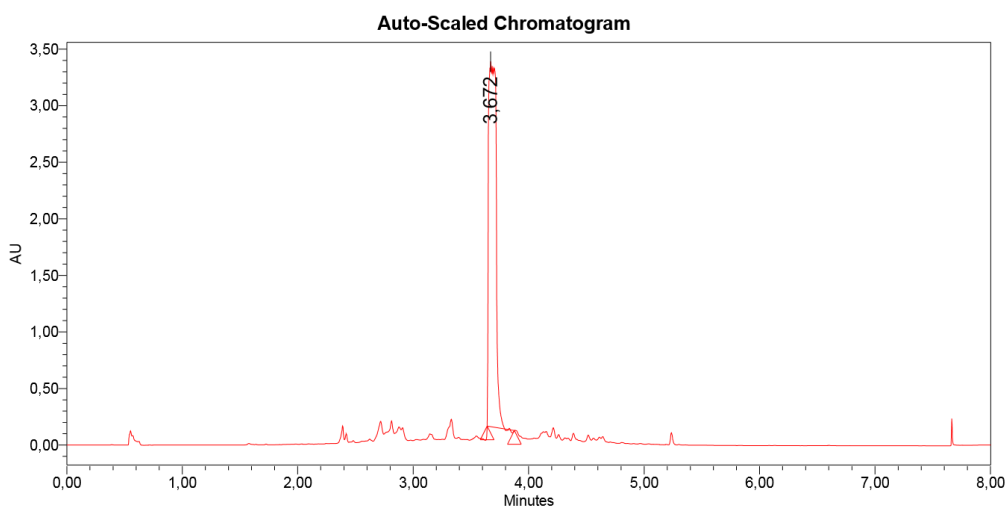


Figure S90. UPLC UV-chromatogram of the authentic reference **8ab** (wavelength: 254 nm). ACQUITY UPLC[®] CSH C18 column (1.7 μm , 2.1 \times 100 mm); MeCN and HCO₂H/H₂O (0.05%, v/v) in gradient mode at 0.5 mL \cdot min⁻¹ (from 100% HCO₂H/H₂O (0.05%, v/v) to 100% MeCN in 6 min, and from 100% MeCN to 100% HCO₂H/H₂O (0.05%, v/v) in 2 min).

5.6.3. Synthesis of [¹⁸F]3-(Difluoromethyl)-6-methyl-1*H*-pyrazolo[3,4-*b*]pyridine (**[¹⁸F]8ba**) and [¹⁸F]4-(Difluoromethyl)-6-methyl-1*H*-pyrazolo[3,4-*b*]pyridine (**[¹⁸F]8bb**)

The implementation of the general procedure 3.2.5. for the C-H ¹⁸F-difluoromethylation of the 6-methyl-1*H*-pyrazolo[3,4-*b*]pyridine (2.7 mg, 0.02 mmol)

provided the labeled compound [¹⁸F]**8aa** in 41 ± 6%, 43 ± 3%, and 41 ± 5% RCY, using the reagents [¹⁸F]**5a**, [¹⁸F]**5c**, and [¹⁸F]**5f**, respectively. The labeled compound [¹⁸F]**8ab** was afforded in 16 ± 1%, 17 ± 3%, and 17 ± 1% RCY, using the reagents [¹⁸F]**5a**, [¹⁸F]**5c**, and [¹⁸F]**5f**, respectively (see the Tables S36-S38 for more details of the RCY determination). The UPLC radio-chromatogram of the crude product [¹⁸F]**8b** is depicted in Figure S91. Figures S92 and S93 represent the UPLC UV-chromatograms of the non-radioactive references **8ba** and **8bb**, respectively.

Table S36. Determination of the radiochemical yield (%) of the synthesis of [¹⁸F]**8b** using the reagent [¹⁸F]**5a**

Reaction	Radio-TLC purity (%)	Radio-UPLC purity (%)		Radiochemical Yield (%)	
	a + b	A	b	a	b
1	53	67	33	36	17
2	67	75	25	50	17
3	55	68	27	37	15
Radiochemical Yield (%) ± Deviation				41 ± 6	16 ± 1

Table S37. Determination of the radiochemical yield (%) of the synthesis of [¹⁸F]**8b** using the reagent [¹⁸F]**5c**

Reaction	Radio-TLC purity (%)	Radio-UPLC purity (%)		Radiochemical Yield (%)	
	a + b	A	b	a	b
1	71	67	22	48	16
2	74	57	28	42	21
3	62	65	22	40	14
Radiochemical Yield (%) ± Deviation				43 ± 3	17 ± 3

Table S38. Determination of the radiochemical yield (%) of the synthesis of [¹⁸F]**8b** using the reagent [¹⁸F]**5f**

Reaction	Radio-TLC purity (%)	Radio-UPLC purity (%)		Radiochemical Yield (%)	
	a + b	A	b	a	b
1	70	50	25	35	18
2	65	61	24	40	16
3	74	63	21	47	16
Radiochemical Yield (%) ± Deviation				41 ± 5	17 ± 1

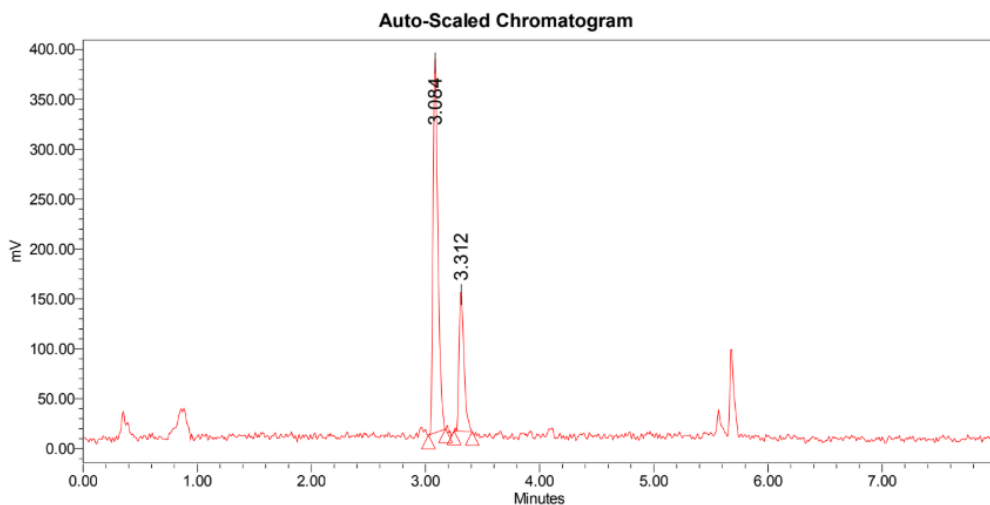


Figure S91. UPLC radio-chromatogram of the crude product [^{18}F]**8b**. ACQUITY UPLC[®] CSH C18 column (1.7 μm , 2.1 \times 100 mm); MeCN and HCO₂H/H₂O (0.05%, v/v) in gradient mode at 0.5 mL·min⁻¹ (from 100% HCO₂H/H₂O (0.05%, v/v) to 100% MeCN in 6 min, and from 100% MeCN to 100% HCO₂H/H₂O (0.05%, v/v) in 2 min).

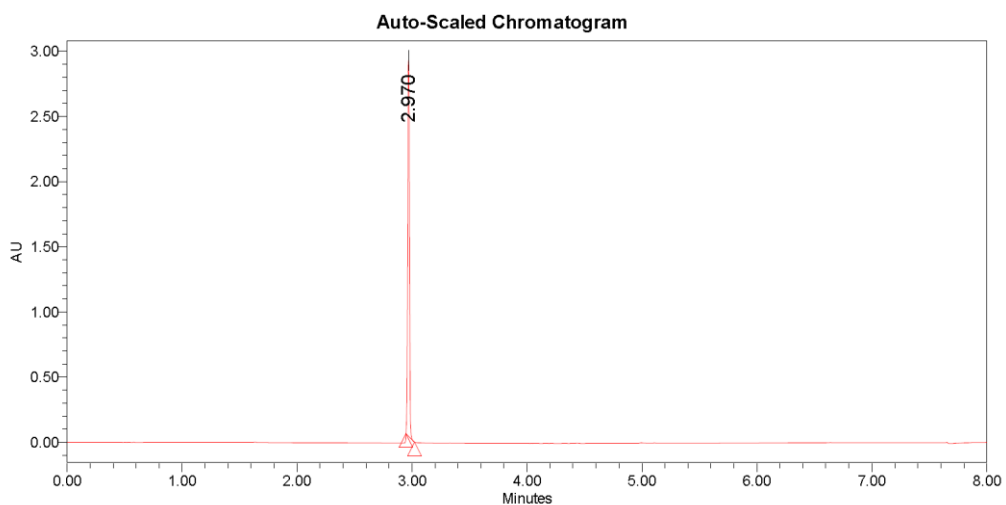


Figure S92. UPLC UV-chromatogram of the authentic reference **8ba** (wavelength: 254 nm). ACQUITY UPLC[®] CSH C18 column (1.7 μm , 2.1 \times 100 mm); MeCN and HCO₂H/H₂O (0.05%, v/v) in gradient mode at 0.5 mL·min⁻¹ (from 100% HCO₂H/H₂O (0.05%, v/v) to 100% MeCN in 6 min, and from 100% MeCN to 100% HCO₂H/H₂O (0.05%, v/v) in 2 min).

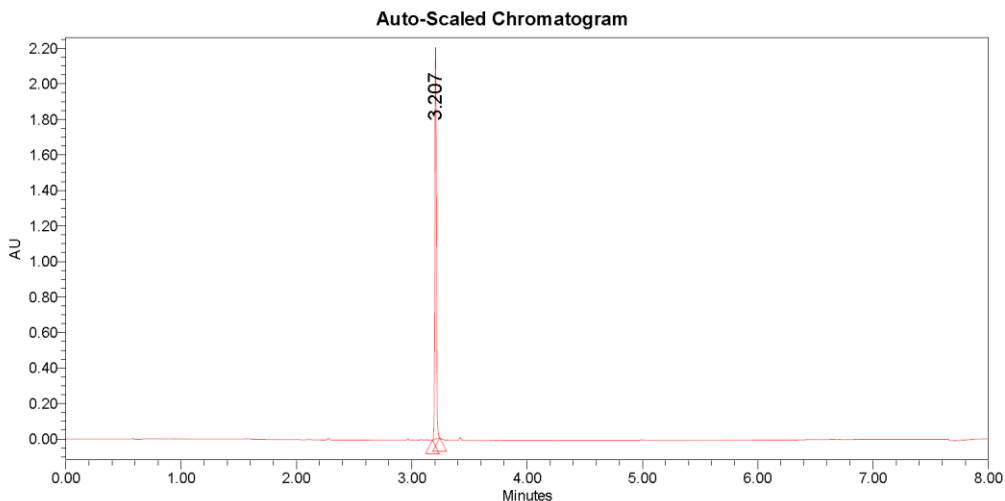


Figure S93. UPLC UV-chromatogram of the authentic reference **8bb** (wavelength: 254 nm). ACQUITY UPLC® CSH C18 column (1.7 μm , 2.1 \times 100 mm); MeCN and HCO₂H/H₂O (0.05%, v/v) in gradient mode at 0.5 mL·min⁻¹ (from 100% HCO₂H/H₂O (0.05%, v/v) to 100% MeCN in 6 min, and from 100% MeCN to 100% HCO₂H/H₂O (0.05%, v/v) in 2 min).

5.6.4. Synthesis of [¹⁸F]4-(Difluoromethyl)-2-methyl-5,8-dihydropyrido[2,3-*d*]pyrimidin-7(6*H*)-one (**[¹⁸F]8c**)

The implementation of the general procedure 3.2.5. for the C-H ¹⁸F-difluoromethylation of the 2-methyl-5,8-dihydropyrido[2,3-*d*]pyrimidin-7(6*H*)-one (3.3 mg, 0.02 mmol) provided the labeled compound **[¹⁸F]8c** in 17 \pm 4%, 13 \pm 3%, and 14% RCY, using the reagents **[¹⁸F]5a**, **[¹⁸F]5c**, and **[¹⁸F]5f**, respectively (see the Tables S39-S41 for more details of the RCY determination). The UPLC radio-chromatogram of the crude product **[¹⁸F]8c** is depicted in Figure S94. Figure S95 represents the UPLC UV-chromatogram of the non-radioactive reference **8c**.

Table S39. Determination of the radiochemical yield (%) of the synthesis of **[¹⁸F]8c** using the reagent **[¹⁸F]5a**

Reaction	Radio-TLC purity (%)	Radio-UPLC purity (%)	Radiochemical Yield (%)
1	38	30	11
2	45	44	20
3	51	41	21
Radiochemical Yield (%) \pm Deviation			17 \pm 4

Table S40. Determination of the radiochemical yield (%) of the synthesis of [¹⁸F]8c using the reagent [¹⁸F]5c

Reaction	Radio-TLC purity (%)	Radio-UPLC purity (%)	Radiochemical Yield (%)
1	57	30	17
2	55	20	11
3	19	52	10
Radiochemical Yield (%) ± Deviation			13 ± 3

Table S41. Determination of the radiochemical yield (%) of the synthesis of [¹⁸F]8c using the reagent [¹⁸F]5f

Reaction	Radio-TLC purity (%)	Radio-UPLC purity (%)	Radiochemical Yield (%)
1	54	25	14
2	43	30	13
3	54	25	14
Radiochemical Yield (%) ± Deviation			14

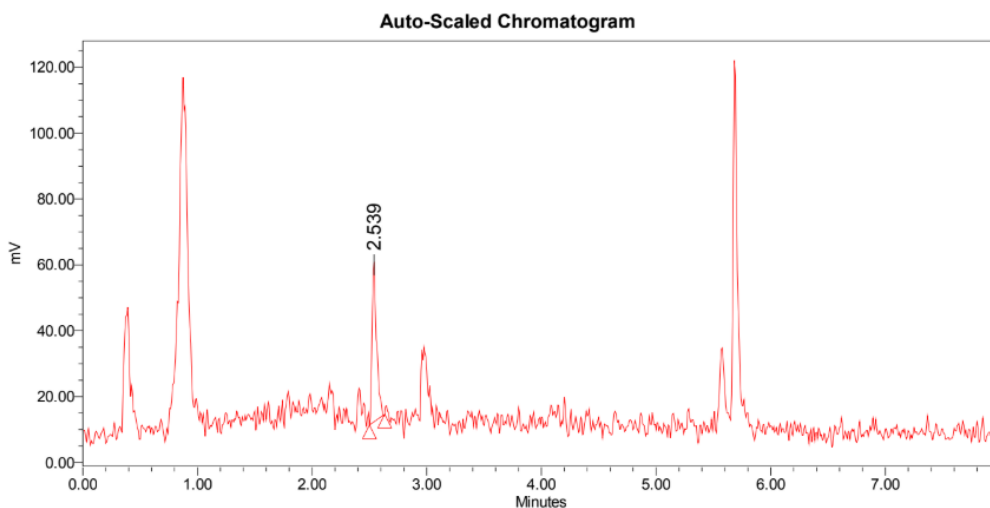


Figure S94. UPLC radio-chromatogram of the crude product [¹⁸F]8c. ACQUITY UPLC® CSH C18 column (1.7 μm, 2.1 × 100 mm); MeCN and HCO₂H/H₂O (0.05%, v/v) in gradient mode at 0.5 mL·min⁻¹ (from 100% HCO₂H/H₂O (0.05%, v/v) to 100% MeCN in 6 min, and from 100% MeCN to 100% HCO₂H/H₂O (0.05%, v/v) in 2 min).

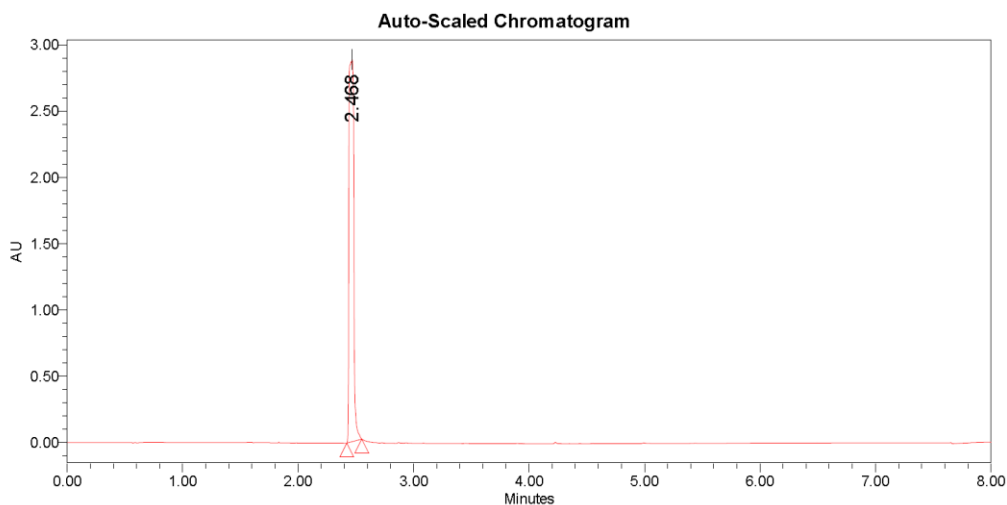


Figure S95. UPLC UV-chromatogram of the authentic reference **8c** (wavelength: 254 nm). ACQUITY UPLC® CSH C18 column (1.7 μm , 2.1 \times 100 mm); MeCN and HCO₂H/H₂O (0.05%, v/v) in gradient mode at 0.5 mL·min⁻¹ (from 100% HCO₂H/H₂O (0.05%, v/v) to 100% MeCN in 6 min, and from 100% MeCN to 100% HCO₂H/H₂O (0.05%, v/v) in 2 min).

5.6.5. Synthesis of [¹⁸F]Ethyl 2-(difluoromethyl)isonicotinate ([¹⁸F]**8da**) and [¹⁸F]Ethyl 3-(difluoromethyl)isonicotinate ([¹⁸F]**8db**)

The implementation of the general procedure 3.2.5. for the C-H ¹⁸F-difluoromethylation of the ethyl isonicotinate (3.0 mg, 0.02 mmol) provided the labeled compound [¹⁸F]**8da** in 19 \pm 7%, 24 \pm 2%, and 36 \pm 4% RCY, using the reagents [¹⁸F]**5a**, [¹⁸F]**5c**, and [¹⁸F]**5f**, respectively. The labeled compound [¹⁸F]**8db** was afforded in 10 \pm 3%, 13 \pm 1%, and 13 \pm 2% RCY, using the reagents [¹⁸F]**5a**, [¹⁸F]**5c**, and [¹⁸F]**5f**, respectively (see the Tables S42-S44 for more details of the RCY determination). The UPLC radio-chromatogram of the crude product [¹⁸F]**8d** is depicted in Figure S96. Figures S97 and S98 represent the UPLC UV-chromatograms of the non-radioactive references **8da** and **8db**, respectively.

Table S42. Determination of the radiochemical yield (%) of the synthesis of [¹⁸F]**8d** using the reagent [¹⁸F]**5a**

Reaction	Radio-TLC purity (%)	Radio-UPLC purity (%)		Radiochemical Yield (%)	
	a + b	a	b	a	b
1	29	42	21	12	6
2	32	51	34	16	11
3	47	61	30	29	14
Radiochemical Yield (%) \pm Deviation				19 \pm 7	10 \pm 3

Table S43. Determination of the radiochemical yield (%) of the synthesis of [¹⁸F]8d using the reagent [¹⁸F]5c

Reaction	Radio-TLC purity (%)	Radio-UPLC purity (%)		Radiochemical Yield (%)	
	a + b	a	b	a	b
1	50	51	25	26	12
2	50	49	24	24	12
3	49	45	30	22	15
Radiochemical Yield (%) ± Deviation				24 ± 2	13 ± 1

Table S44. Determination of the radiochemical yield (%) of the synthesis of [¹⁸F]8d using the reagent [¹⁸F]5f

Reaction	Radio-TLC purity (%)	Radio-UPLC purity (%)		Radiochemical Yield (%)	
	a + b	a	b	a	b
1	62	64	26	40	16
2	53	69	23	37	12
3	45	68	22	31	10
Radiochemical Yield (%) ± Deviation				36 ± 4	13 ± 2

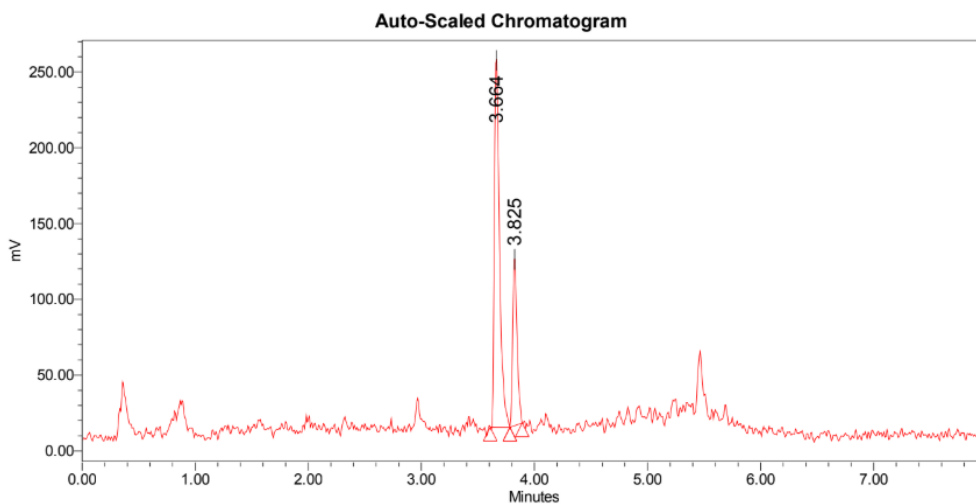


Figure S96. UPLC radio-chromatogram of the crude product [¹⁸F]8d. ACQUITY UPLC® CSH C18 column (1.7 μm, 2.1 × 100 mm); MeCN and HCO₂H/H₂O (0.05%, v/v) in gradient mode at 0.5 mL·min⁻¹ (from 100% HCO₂H/H₂O (0.05%, v/v) to 100% MeCN in 6 min, and from 100% MeCN to 100% HCO₂H/H₂O (0.05%, v/v) in 2 min).

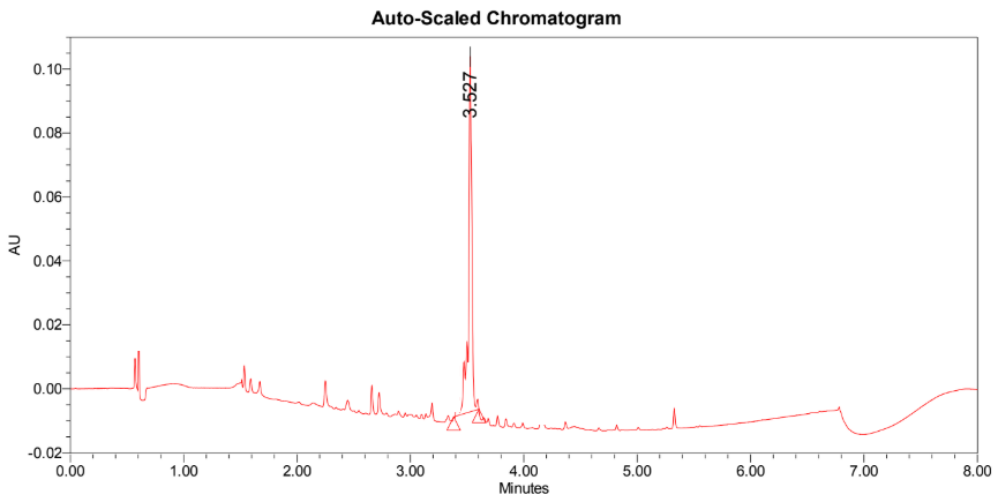


Figure S97. UPLC UV-chromatogram of the authentic reference **8da** (wavelength: 254 nm). ACQUITY UPLC® CSH C18 column (1.7 μm , 2.1 \times 100 mm); MeCN and HCO₂H/H₂O (0.05%, v/v) in gradient mode at 0.5 mL·min⁻¹ (from 100% HCO₂H/H₂O (0.05%, v/v) to 100% MeCN in 6 min, and from 100% MeCN to 100% HCO₂H/H₂O (0.05%, v/v) in 2 min).

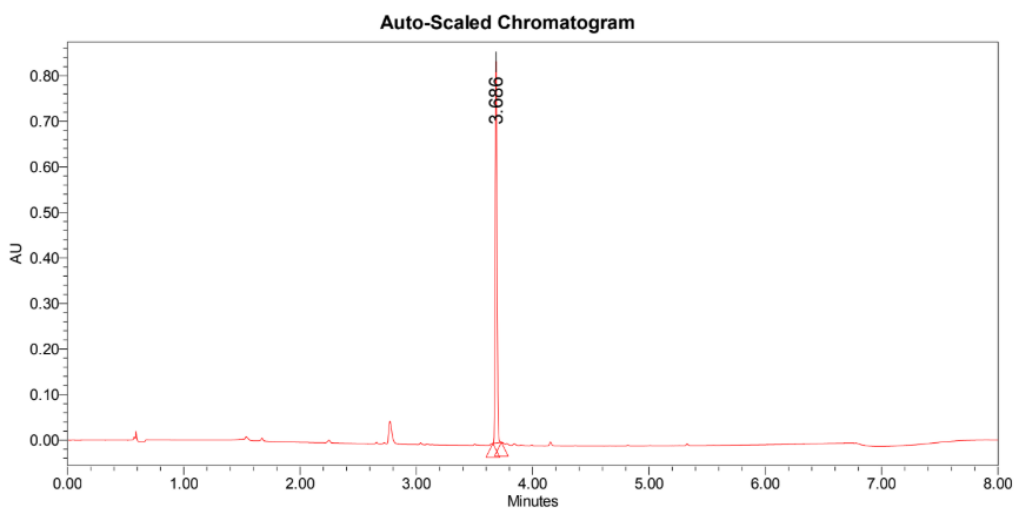


Figure S98. UPLC UV-chromatogram of the authentic reference **8db** (wavelength: 254 nm). ACQUITY UPLC® CSH C18 column (1.7 μm , 2.1 \times 100 mm); MeCN and HCO₂H/H₂O (0.05%, v/v) in gradient mode at 0.5 mL·min⁻¹ (from 100% HCO₂H/H₂O (0.05%, v/v) to 100% MeCN in 6 min, and from 100% MeCN to 100% HCO₂H/H₂O (0.05%, v/v) in 2 min).

5.6.6. Synthesis of [¹⁸F]4-Chloro-2-(difluoromethyl)-*N*-(4,5-dihydro-1*H*-imidazol-2-yl)-6-methoxypyrimidin-5-amine ([¹⁸F]**8f**)

The implementation of the general procedure 3.2.5. for the C-H ¹⁸F-difluoromethylation of the 4-chloro-*N*-(4,5-dihydro-1*H*-imidazol-2-yl)-6-methoxypyrimidin-5-amine (4.6 mg, 0.02 mmol) provided the labeled compound

[¹⁸F]8f in 52 ± 6%, 17 ± 3%, and 60 ± 3% RCY, using the reagents [¹⁸F]5a, [¹⁸F]5c, and [¹⁸F]5f, respectively (see the Tables S45-S47 for more details of the RCY determination). The UPLC radio-chromatogram of the crude product [¹⁸F]8f is depicted in Figure S99. Figure S100 represents the UPLC UV-chromatogram of the non-radioactive reference 8f.

Table S45. Determination of the radiochemical yield (%) of the synthesis of [¹⁸F]8f using the reagents [¹⁸F]5a

Reaction	Radio-TLC purity (%)	Radio-UPLC purity (%)	Radiochemical Yield (%)
1	50	100	50
2	47	100	47
3	60	100	60
Radiochemical Yield (%) ± Deviation			52 ± 6

Table S46. Determination of the radiochemical yield (%) of the synthesis of [¹⁸F]8f using the reagents [¹⁸F]5c

Reaction	Radio-TLC purity (%)	Radio-UPLC purity (%)	Radiochemical Yield (%)
1	67	35	23
2	60	27	16
3	53	26	14
4	64	26	17
5	63	24	15
Radiochemical Yield (%) ± Deviation			17 ± 3

Table S47. Determination of the radiochemical yield (%) of the synthesis of [¹⁸F]8f using the reagents [¹⁸F]5c

Reaction	Radio-TLC purity (%)	Radio-UPLC purity (%)	Radiochemical Yield (%)
1	73	84	61
2	67	83	56
3	78	80	62
Radiochemical Yield (%) ± Deviation			60 ± 3

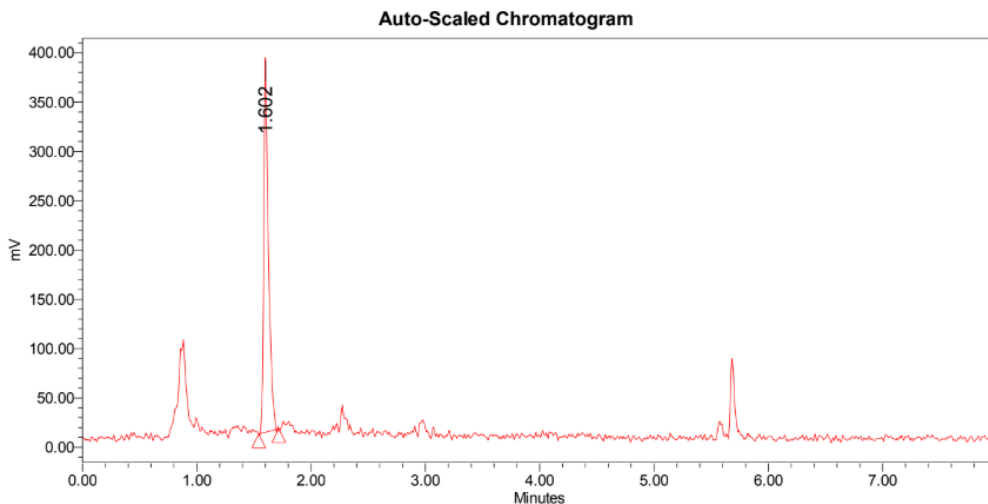


Figure S99. UPLC radio-chromatogram of the crude product [^{18}F]**8f**. ACQUITY UPLC[®] CSH C18 column (1.7 μm , 2.1 \times 100 mm); MeCN and HCO₂H/H₂O (0.05%, v/v) in gradient mode at 0.5 mL·min⁻¹ (from 100% HCO₂H/H₂O (0.05%, v/v) to 100% MeCN in 6 min, and from 100% MeCN to 100% HCO₂H/H₂O (0.05%, v/v) in 2 min).

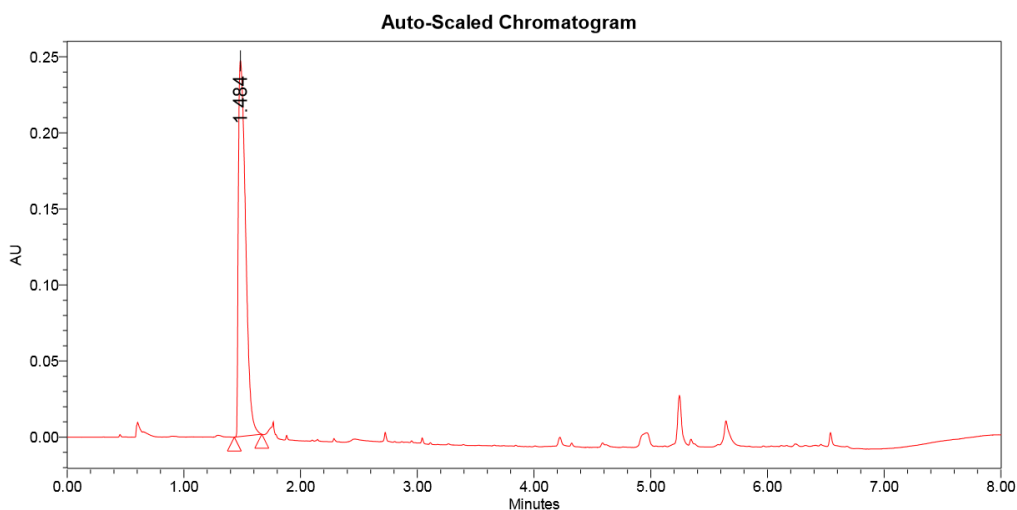


Figure S100. UPLC UV-chromatogram of the authentic reference **8f** (wavelength: 254 nm). ACQUITY UPLC[®] CSH C18 column (1.7 μm , 2.1 \times 100 mm); MeCN and HCO₂H/H₂O (0.05%, v/v) in gradient mode at 0.5 mL·min⁻¹ (from 100% HCO₂H/H₂O (0.05%, v/v) to 100% MeCN in 6 min, and from 100% MeCN to 100% HCO₂H/H₂O (0.05%, v/v) in 2 min).

5.6.7. Synthesis of [^{18}F]**8**-(Difluoromethyl)-3,7-dimethyl-1-(5-oxohexyl)-3,7-dihydro-1*H*-purine-2,6-dione ([^{18}F]**8g**)

The implementation of the general procedure 3.2.5. for the C-H ^{18}F -difluoromethylation of the 3,7-dimethyl-1-(5-oxohexyl)-3,7-dihydro-1*H*-purine-2,6-dione (5.6 mg, 0.02 mmol) provided the labeled compound [^{18}F]**8g** in 52 \pm 6%, 17 \pm 3%,

and $60 \pm 3\%$ RCY, using the reagents [^{18}F]5a, [^{18}F]5c, and [^{18}F]5f, respectively (see the Tables S48-S50 for more details of the RCY determination). The UPLC radio-chromatogram of the crude product [^{18}F]8g is depicted in Figure S101. Figure S102 represents the UPLC UV-chromatogram of the non-radioactive reference 8g.

Table S48. Determination of the radiochemical yield (%) of the synthesis of [^{18}F]8g using the reagents [^{18}F]5a

Reaction	Radio-TLC purity (%)	Radio-UPLC purity (%)	Radiochemical Yield (%)
1	18	100	18
2	23	100	23
3	22	100	22
Radiochemical Yield (%) \pm Deviation			21 \pm 2

Table S49. Determination of the radiochemical yield (%) of the synthesis of [^{18}F]8g using the reagents [^{18}F]5c

Reaction	Radio-TLC purity (%)	Radio-UPLC purity (%)	Radiochemical Yield (%)
1	42	58	24
2	56	62	35
3	61	61	37
4	48	53	25
Radiochemical Yield (%) \pm Deviation			30 \pm 6

Table S50. Determination of the radiochemical yield (%) of the synthesis of [^{18}F]8g using the reagents [^{18}F]5f

Reaction	Radio-TLC purity (%)	Radio-UPLC purity (%)	Radiochemical Yield (%)
1	52	60	31
2	47	82	39
3	42	81	34
Radiochemical Yield (%) \pm Deviation			35 \pm 3

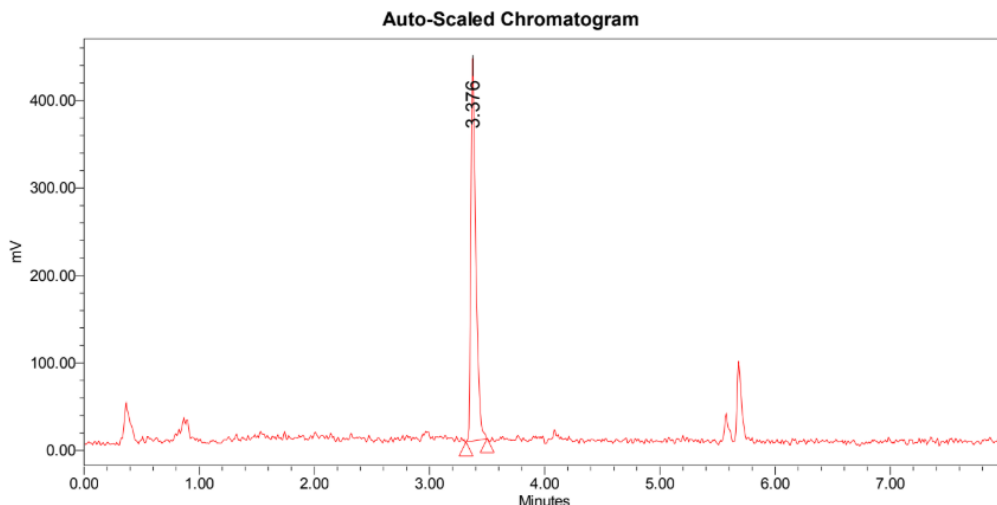


Figure S101. UPLC radio-chromatogram of the crude product [^{18}F]**8g**. ACQUITY UPLC[®] CSH C18 column (1.7 μm , 2.1 \times 100 mm); MeCN and HCO₂H/H₂O (0.05%, v/v) in gradient mode at 0.5 mL·min⁻¹ (from 100% HCO₂H/H₂O (0.05%, v/v) to 100% MeCN in 6 min, and from 100% MeCN to 100% HCO₂H/H₂O (0.05%, v/v) in 2 min).

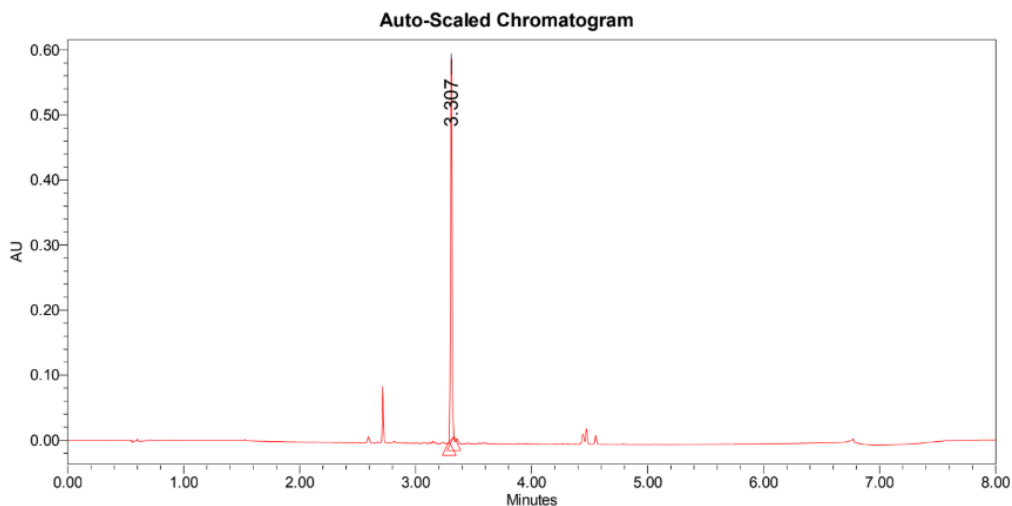


Figure S102. UPLC UV-chromatogram of the authentic reference **8g** (wavelength: 254 nm). ACQUITY UPLC[®] CSH C18 column (1.7 μm , 2.1 \times 100 mm); MeCN and HCO₂H/H₂O (0.05%, v/v) in gradient mode at 0.5 mL·min⁻¹ (from 100% HCO₂H/H₂O (0.05%, v/v) to 100% MeCN in 6 min, and from 100% MeCN to 100% HCO₂H/H₂O (0.05%, v/v) in 2 min).

References

- [1] Le Bars, D. Fluorine-18 and medical imaging: radiopharmaceuticals for positron emission tomography. *J. Fluorine. Chem.* **2006**, *127*, 1488-1493.
- [2] Even-Sapir, E.; Mishani, E.; Flusser, G.; Metser, U. ^{18}F -Fluoride positron emission tomography and positron emission tomography/computed tomography. *Semin. Nucl. Med.* **2007**, *37*, 462-469.

- [3] Banister, S.; Roeda, D.; Dollé, F.; Kassiou, M. Fluorine-18 chemistry for PET: A concise introduction. *Curr. Radiopharm.* **2010**, *3*, 68-80.
- [4] Varlow, C. Szames, D.; Dahl, K.; Bernard-Gauthier, V.; Vasdev, N. Fluorine-18: An untapped resource in inorganic chemistry. *Chem. Commun.* **2018**, *54*, 11835-11842.
- [5] Shukla, A.K.; Kumar, U. Positron emission tomography: An overview. *J. Med. Phys.* **2006**, *31*, 13-21.
- [6] Lin, M.; Shon, I.H.; Lin, P. Positron emission tomography: Current status and future challenges. *Intern. Med. J.* **2010**, *40*, 19-29.
- [7] Vaquero, J.J.; Kinahan, P. Positron emission tomography: Current challenges and opportunities for technological advances in clinical and preclinical imaging systems. *Annu. Rev. Biomed. Eng.* **2015**, *17*, 385-414.
- [8] El-Galaly, T.C.; Gormsen, L.C.; Hutchings, M. PET/CT for staging; Past, present, and future. *Semin. Nucl. Med.* **2018**, *48*, 4-16.
- [9] Miller, P.W.; Long, N.J.; Vilar, R.; Gee, A.D. Synthesis of ^{11}C , ^{18}F , ^{15}O , and ^{13}N radiolabels for positron emission tomography. *Angew. Chem. Int. Ed.* **2008**, *47*, 8998-9033.
- [10] Gu, Y.; Huang, D.; Liu, Z.; Huang, J.; Zeng, W. Labeling strategies with F-18 for positron emission tomography imaging. *Med. Chem.* **2011**, *7*, 334-344.
- [11] Ying, L. ^{18}F -Labeling techniques for positron emission tomography. *Sci. China Chem.* **2013**, *56*, 1682-1692.
- [12] Brooks, A.F.; Topczewski, J.J.; Ichiishi, N.; Sanford, M.S.; Scott, P.J.H. Late-stage ^{18}F fluorination: new solutions to old problems. *Chem. Sci.* **2014**, *5*, 4545-4553.
- [13] Jacobson, O.; Kiesewetter, D.O.; Chen, X. Fluorine-18 radiochemistry, labeling strategies and synthetic routes. *Bioconjugate Chem.* **2015**, *26*, 1-18.
- [14] Preshlock, S.; Tredwell, M.; Gouverneur, V. ^{18}F -Labeling of arenes and heteroarenes for applications in positron emission tomography. *Chem. Rev.* **2016**, *116*, 719-766.
- [15] Van der Born, D.; Pees, A.; Poot, A.J.; Orru, R.V.A.; Windhorst, A.D.; Vugts, D.J. Fluorine-18 labelled building blocks for PET tracer synthesis. *Chem. Soc. Rev.* **2017**, *46*, 4709-4773.
- [16] Krishnan, H.S.; Ma, L.; Vasdev, N.; Liang, S.H. ^{18}F -Labeling of sensitive biomolecules for positron emission tomography. *Chem. Eur. J.* **2017**, *23*, 15553-15577.
- [17] Coenen, H.H.; Ermert, J. ^{18}F -Labeling innovations and their potential for clinical application. *Clin. Transl. Imaging* **2018**, *6*, 169-193.
- [18] Krüll, J.; Heinrich, M.R. ^{18}F Fluorine-labeled pharmaceuticals: direct aromatic fluorination compared to multi-step strategies. *Asian J. Org. Chem.* **2019**, *8*, 576-590.
- [19] Deng, X.; Rong, J.; Wang, L.; Vasdev, N.; Zhang, L.; Josephson, L.; Liang, S.H. Chemistry for positron emission tomography: recent advances in ^{11}C -, ^{18}F -, ^{13}N -, and ^{15}O -labeling reactions. *Angew. Chem. Int. Ed.* **2019**, *58*, 2580-2605.
- [20] Meanwell, N.A. Fluorine and fluorinated motifs in the design and application of bioisosteres for drug design. *J. Med. Chem.* **2018**, *61*, 5822-5880.
- [21] Erickson, J.A.; McLoughlin, J.I. Hydrogen bond donor properties of the difluoromethyl group. *J. Org. Chem.* **1995**, *60*, 1626-1631.

- [22] Zafrani, Y.; Yeffet, D.; Sod-Moriah, G.; Berliner, A.; Amir, D.; Marciano, D.; Gershonov, E.; Saphier, S. Difluoromethyl bioisostere: examining the “lipophilic hydrogen bond donor” concept. *J. Med. Chem.* **2017**, *60*, 797-804.
- [23] Sessler, C.D.; Rahm, M.; Becker, S.; Goldberg, J.M.; Wang, F.; Lippard, S.J. CF₂H, a hydrogen bond donor. *J. Am. Chem. Soc.* **2017**, *139*, 9325-9332.
- [24] Zafrani, Y.; Sod-Mariah, G.; Yeffet, D.; Berliner, A.; Amir, D.; Marciano, D.; Elias, S.; Katalan, S.; Ashkenazi, N.; Madmon, M.; Gershonov, E.; Saphier, S. CF₂H, a functional group-dependent hydrogen-bond donor: is it a more or less lipophilic bioisostere of OH, SH, and CH₃? *J. Med. Chem.* **2019**, *62*, 5628-5637.
- [25] Rong, J.; Ni, C.; Hu, J. Metal-catalyzed direct difluoromethylation reactions. *Asian J. Org. Chem.* **2017**, *6*, 139-152.
- [26] Yerien, D.E.; Barata-Vallejo, S.; Postigo, A. Difluoromethylation reactions of organic compounds. *Chem. Eur. J.* **2017**, *23*, 14676-14701.
- [27] Feng, Z.; Xiao, Y.-L.; Zhang, X. Transition-metal (Cu, Pd, Ni)-catalyzed difluoroalkylation via cross-coupling with difluoroalkyl halides. *Acc. Chem. Res.* **2018**, *51*, 2264-2278.
- [28] Lemos, A.; Lemaire, C.; Luxen, A. Progress in difluoroalkylation of organic substrates by visible light photoredox catalysis. *Adv. Synth. Catal.* **2019**, *361*, 1500-1537.
- [29] Koike, T.; Akita, M. Recent progress in photochemical radical di- and mono-fluoromethylation. *Org. Biomol. Chem.* **2019**, *17*, 5413-5419.
- [30] Levi, N.; Amir, D.; Greshonov, E.; Zafrani, Y. Recent progress on the synthesis of CF₂H-containing derivatives. *Synthesis* **2019**, *51*, 4549-4567.
- [31] Wagner, K.; Kraatz, U.; Kugler, M.; Schrage, H.; Uhr, H. Benzazole derivatives with microbiocidal properties. Ger. Offen. DE 19523447 A1 19970102, 1997.
- [32] Mizuta, S.; Stenhagen, I.S.R.; O'Duill, M.; Wolstenhulme, J.; Kirjavainen, A.K.; Forsback, S.J.; Tredwell, M.; Sandford, G.; Moore, P.R.; Huiban, M.; Luthra, S.K.; Passchier, J.; Solin, O.; Gouverneur, V. Catalytic decarboxylative fluorination for the synthesis of tri- and difluoromethyl arenes. *Org. Lett.* **2013**, *15*, 2648-2651.
- [33] Verhoog, S.; Pfeifer, L.; Khotavivattana, T.; Calderwood, S.; Collier, T.L.; Wheelhouse, K.; Tredwell, M.; Gouverneur, V. Silver-mediated ¹⁸F-labeling of aryl-CF₃ and aryl-CHF₂ with ¹⁸F-fluoride. *Synlett* **2016**, *27*, 25-28.
- [34] Shi, H.; Braun, A.; Wang, L.; Liang, S.H.; Vasdev, N.; Ritter, T. Synthesis of ¹⁸F-difluoromethylarenes from aryl (pseudo) halides. *Angew. Chem. Int. Ed.* **2016**, *55*, 10786-10790.
- [35] Yuan, G.; Wang, F.; Stephenson, N.A.; Wang, L.; Rotstein, B.H.; Vasdev, N.; Tang, P.; Liang, S.H. Metal-free ¹⁸F-labeling of aryl-CF₂H *via* nucleophilic radiofluorination and oxidative C-H activation. *Chem. Commun.* **2017**, *53*, 126-129.
- [36] Sap, J.B.I.; Wilson, T.C.; Kee, C.W.; Straathof, N.J.W.; amEnde, C.W.; Mukherjee, P.; Zhang, L.; Genicot, C.; Gouverneur, V. Synthesis of ¹⁸F-difluoromethylarenes using aryl boronic acids, ethyl bromofluoroacetate and [¹⁸F]fluoride. *Chem. Sci.* **2019**, *10*, 3237-3241.

- [37] Trump, L.; Lemos, A.; Lallemand, B.; Pasau, P.; Mercier, J.; Lemaire, C.; Luxen, A.; Genicot, C. Late-stage ^{18}F -difluoromethyl labeling of *N*-heteroaromatics with high molar activity. *Angew. Chem. Int. Ed.* **2019**, *58*, 13149-13154.
- [38] Trump, L.; Lemos, A.; Jacq, J.; Pasau, P.; Lallemand, B.; Mercier, J.; Genicot, C.; Luxen, A.; Lemaire, C. Development of a general automated flow photoredox ^{18}F -difluoromethylation of *N*-heteroaromatics in an AllInOne synthesizer. *Org. Process Res. Dev.* **2020**, *24*, 734-744.
- [39] Rong, J.; Deng, L.; Tan, P.; Ni, C.; Gu, Y.; Hu, J. Radical fluoroalkylation of isocyanides with fluorinated sulfones by visible-light photoredox catalysis. *Angew. Chem. Int. Ed.* **2016**, *55*, 2743-2747.
- [40] Fu, W.; Han, X.; Zhu, M.; Xu, C.; Wang, Z.; Ji, B.; Hao, X.-Q.; Song, M.-P. Visible-light-mediated radical oxydifluoromethylation of olefinic amides for the synthesis of CF_2H -containing heterocycles. *Chem. Commun.* **2016**, *52*, 13413-13416.
- [41] Zou, G.; Wang, X. Visible-light induced di- and trifluoromethylation of *N*-benzamides with fluorinated sulfones for the synthesis of $\text{CF}_2\text{H}/\text{CF}_3$ -containing isoquinolinediones. *Org. Biomol. Chem.* **2017**, *15*, 8748-8751.
- [42] Zhu, M.; Fu, W.; Wang, Z.; Xu, C.; Ji, B. Visible-light-mediated direct difluoromethylation of alkynoates: synthesis of 3-difluoromethylated coumarins. *Org. Biomol. Chem.* **2017**, *15*, 9057-9060.
- [43] Zhu, M.; Fu, W.; Guo, W.; Tian, Y.; Wang, Z.; Xu, C.; Ji, B. Visible-light-induced radical di- and trifluoromethylation of β , γ -unsaturated oximes: synthesis of di- and trifluoromethylated isoxazolines. *Eur. J. Org. Chem.* **2019**, *2019*, 1614-1619.
- [44] Zhu, M.; You, Q.; Li, R. Synthesis of CF_2H -containing oxindoles *via* photoredox-catalyzed radical difluoromethylation and cyclization of *N*-arylacrylamides. *J. Fluorine Chem.* **2019**, DOI: 10.1016/j.jfluchem.2019.109391.
- [45] Sun, H.; Jiang, Y.; Yang, Y.-S.; Li, Y.-Y.; Li, L.; Wang, W.-X.; Feng, T.; Li, Z.-H.; Liu, J.-K. Synthesis of difluoromethylated 2-oxindoles and quinoline-2,4-diones *via* visible light-induced tandem radical cyclization of *N*-arylacrylamides. *Org. Biomol. Chem.* **2019**, *17*, 6629-6638.
- [46] Arai, Y.; Tomita, R.; Ando, G.; Koike, T.; Akita, M. Oxydifluoromethylation of alkenes by photoredox catalysis: simple synthesis of CF_2H -containing alcohols. *Chem. Eur. J.* **2016**, *22*, 1262-1265.
- [47] Carbonnel, E.; Besset, T.; Poisson, T.; Labar, D.; Pannecoucke, X.; Jubault, P. ^{18}F -Fluoroform: a ^{18}F -trifluoromethylating agent for the synthesis of $\text{SCF}_2^{18}\text{F}$ -aromatic derivatives. *Chem. Commun.* **2017**, *53*, 5706-5709.
- [48] O'Brien, J.J.; Campoli-Richards, D.M. Acyclovir. An updated review of its antiviral activity, pharmacokinetic properties and therapeutic efficacy. *Drugs* **1989**, *37*, 233-309.
- [49] Fenton, C.; Keating, G.M.; Lyseng-Williamson, K.A. Moxonidine. A review of its use in essential hypertension. *Drugs* **2006**, *66*, 477-496.
- [50] Frampton, J.E.; Brogden, R.N. Pentoxifylline (Oxpentifylline). A review of its therapeutic efficacy in the management of peripheral vascular and cerebrovascular disorders. *Drugs Aging* **1995**, *7*, 480-503.

- [51] Sakamoto, R.; Kashiwagi, H.; Marouka, K. The direct C-H difluoromethylation of heteroarenes based on the photolysis of hypervalent iodine(III) reagents that contain difluoroacetoxy ligands. *Org. Lett.* **2017**, *19*, 5126-5129.
- [52] Lemaire, C.; Libert, L.; Franci, X.; Genon, J.-L.; Kuci, S.; Giacomelli, F.; Luxen, A. Automated production at the curie level of no-carrier-added 6-[¹⁸F]fluoro-L-dopa and 2-[¹⁸F]fluoro-L-tyrosine on a FASTlab synthesizer. *J. Label. Compd. Radiopharm.* **2015**, *58*, 281-290.
- [53] Wei, J.; Bao, K.; Wang, Y.; Sheng, R.; Hu, J. Novel usage of 2-BT₂SO₂CF₂H for metal-free electrophilic difluoromethylthiolation of indoles. *Org. Biomol. Chem.* **2020**, *18*, 4556-4559.
- [54] Zhao, Y.C.; Huang, W.Z.; Zhu, L.G.; Hu, J.B. Difluoromethyl 2-Pyridyl Sulfone: A New *gem*-Difluoroolefination Reagent for Aldehydes and Ketones. *Org. Lett.* **2010**, *12*, 1444-1447.
- [55] Habib, S.; Gueyrard, D. Modified Julia Olefination on Sugar-Derived Lactones: Synthesis of Difluoro-*exo*-glycals. *Eur. J. Org. Chem.* **2015**, *2015*, 871-875.
- [56] Liu, X.; Yin, Q.; Yin, J.; Chen, G.H.; Wang, X.; You, Q.D.; Chen, Y.L.; Xiong, B.; Shen, J.K. Highly Stereoselective Nucleophilic Addition of Difluoromethyl-2-pyridyl Sulfone to Sugar Lactones and Efficient Synthesis of Fluorinated 2-Ketoses. *Eur. J. Org. Chem.* **2014**, *2014*, 6150-6154.
- [57] Moschitto, M.J.; Silverman, R.B. Synthesis of (S)-3-Amino-4-(difluoromethylenyl)-cyclopent-1-ene-1-carboxylic Acid (OV329), a Potent Inactivator of γ -Aminobutyric Acid Aminotransferase. *Org. Lett.* **2018**, *20*, 4589-4592.
- [58] Gao, B.; Zhao, Y.C.; Hu, M.Y.; Ni, C.F.; Hu, J.B. *gem*-Difluoroolefination of Diaryl Ketones and Enolizable Aldehydes with Difluoromethyl 2-Pyridyl Sulfone: New Insights into the Julia-Kocienski Reaction. *Chem. Eur. J.* **2014**, *20*, 7803-7810.

Chapter V

General Discussion and Perspectives

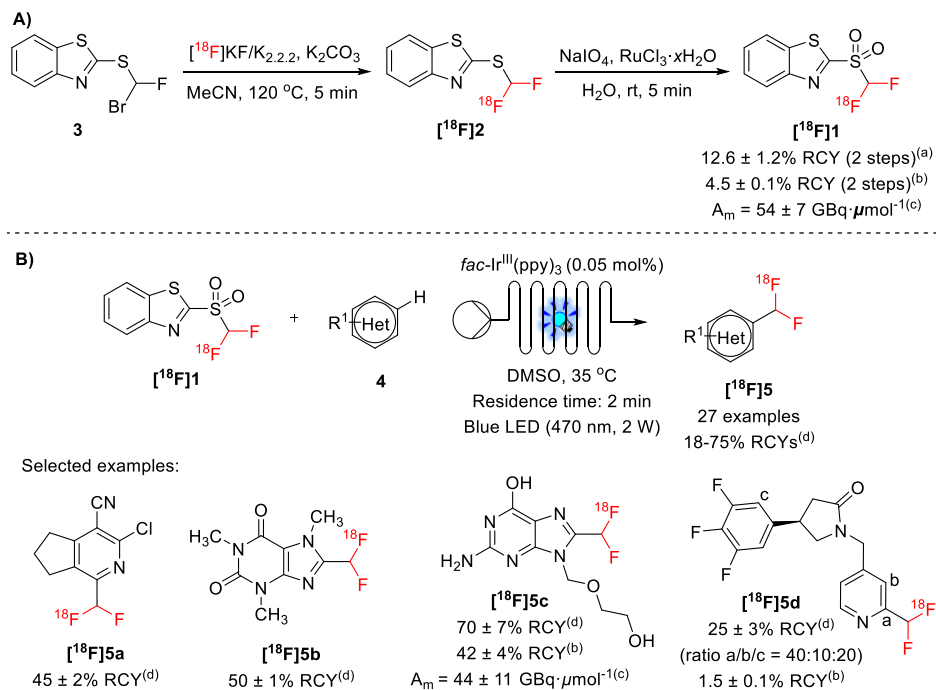
Chapter V

1. General Discussion and Perspectives.....	291
References.....	296

1. General Discussion and Perspectives

The radionuclide fluorine-18 (^{18}F) has been regarded the “radionuclide of choice” for due to its suitable physical and nuclear features for *in vivo* positron emission tomography (PET) imaging in living subjects. Inspired by the great benefits of difluoromethyl (CHF_2) groups in medicinal chemistry and pharmaceutical research, the ^{18}F -labeling of these functional groups has recently gained attention in radiochemistry. The preparation of ^{18}F -labeled CHF_2 -containing compounds has been mainly focused on the late-stage ^{18}F -fluorination of precursors and these methods with the electrophilic reagents or with the cyclotron-produced ^{18}F -fluoride by aliphatic nucleophilic substitution. Furthermore, the resulting ^{18}F -labeled compounds are afforded in low-to-moderate molar activities (up to $22 \text{ GBq} \cdot \mu\text{mol}^{-1}$).

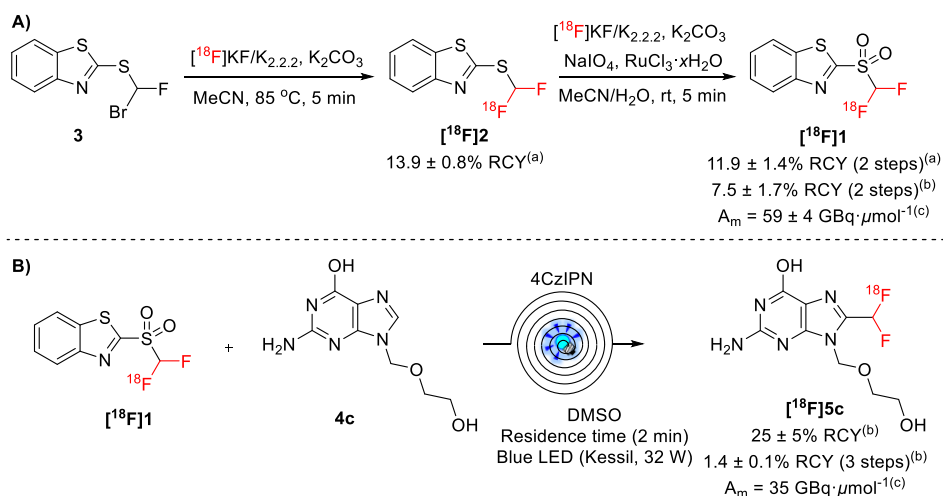
The present thesis focused on the development of a new methodology for the photoredox ^{18}F -difluoromethylation of heteroarenes typically found in medicinal chemistry. In this project, we opted to prepare the ^{18}F -labeled difluoromethyl benzothiazolyl-sulfone (^{18}F **1**) because of their expected photoredox properties [1] and of its potential for nucleophilic ^{18}F -labeling using an adequate precursor. In addition, an efficient separation and isolation of non-ionic ^{18}F -labeled reagents, such as the compound ^{18}F **1**, by semipreparative HPLC is more easily achieved in comparison with other ionic reagents (e.g. Baran reagents). From the investigated synthetic approaches, the two-step methodology involving an initial ^{18}F -labeling of the bromofluoromethyl benzothiazolyl-sulfide (**3**) with ^{18}F -labeled $\text{K}^+/\text{K}_2.2.2$ and concomitant oxidation of the ^{18}F -labeled difluoromethyl benzothiazolyl-sulfone (^{18}F **2**) provided the ^{18}F **1** with the best radiochemical yield (RCY). Under optimal conditions, the cartridge-purified ^{18}F **1** was afforded in $12.6 \pm 1.2\%$ RCY (decay-corrected at the SOS). The radiosynthesis of ^{18}F **1** was fully automated on a GE FASTlabTM synthesizer. After semipreparative HPLC purification and formulation in a preconditioned Sep-Pak[®] C18 Plus Short Cartridge, the ^{18}F **1** was isolated in $4.5 \pm 0.1\%$ RCY (decay-corrected at the SOS) and with a molar activity of $54 \pm 7 \text{ GBq} \cdot \mu\text{mol}^{-1}$ at the EOS (Scheme 1). The employment of this two-step methodology led to an improved molar activity compared to those reported in literature. In 2019, Trump *et al.* demonstrated the effectiveness of the newly synthesized reagent ^{18}F **1** in photoredox C-H ^{18}F -difluoromethylation of a broad scope of *N*-containing heteroarenes, including caffeine derivatives, nucleic bases, nucleosides, and pharmaceutical drugs [2]. This reaction was conducted in continuous-flow using an easy-to-use platform equipped with a $100 \mu\text{L}$ microreactor made from glass and a syringe that continuously pumps the reaction mixture into the microreactor at a given flow rate (FlowStart Evo, FutureChemistry, Nijmegen, The Netherlands).



Scheme 1. (A) Radiosynthesis of the [¹⁸F]difluoromethyl benzothiazolyl-sulfone ([¹⁸F]1). (B) Visible light-induced ¹⁸F-difluoromethylation of heteroarenes (4) with the reagent [¹⁸F]1, under continuous-flow conditions. ^(a)RCY of the isolated products after cartridge purification. ^(b)RCY of the isolated product after HPLC purification. ^(c)Molar activity at the end of the synthesis (EOS). ^(d)RCY determined by radio-TLC and radio-UPLC of the crude product.

Despite the elegance of the photoredox ¹⁸F-difluoromethylation reaction, the described protocol is not compatible with the use of a very high amount of radioactivity. The development of a fully automated ¹⁸F-difluoromethylation methodology in a dedicated module would allow the manipulation of multiple GBq of starting radioactivity while avoiding potential radioprotection issues resulting from the radiation exposure. Radiosynthesis of ¹⁸F-difluoromethyl-bearing radiopharmaceuticals with high level of radioactivity is critical for future human PET applications. This fully automated process would include the two-step radiosynthesis of [¹⁸F]1 and concomitant flow photoredox ¹⁸F-difluoromethylation of the substrates. In the previous work, the synthesis of [¹⁸F]1 at high level of radioactivity was fully automated on a commercial FASTlab™ module from GE Healthcare. The restricted number of free positions on the FASTlab™ cassette (25 valves) and the absence of an integrated HPLC purification system constitute important limitations for the complete automation of the two-step radiosynthesis of [¹⁸F]1 and consecutive ¹⁸F-difluoromethylation methodology. Recently, we developed a general method enabling the fully automated ¹⁸F-difluoromethylation of a *N*-containing heteroarene, the antihypertensive drug acyclovir, on a commercially available AllInOne (AIO) synthesizer from Trasis [3]. The higher number of positions available for the introduction of components for both radiochemical reactions and the existence of an

integrated HPLC purification system led to the selection of this module for the three-step radiosynthesis of ^{18}F -difluoromethyl-containing compounds. The two-step radiosynthesis of $[^{18}\text{F}]\mathbf{1}$ was successfully transposed from the GE FASTlab™ to the AIO module and furnished the cartridge-purified $[^{18}\text{F}]\mathbf{1}$ in $11.9 \pm 1.4\%$ RCY (decay-corrected at the SOS). No significant variation in the RCY was observed when the oxidation was performed in the AIO glass reactor [82.9% RCY (GE FASTlab™) vs. 86.2% RCY (AIO)]. These results suggest that the presence of MeCN, K_2CO_3 , and $\text{K}_{2.2,2}$ has no meaningful impact on the oxidation of $[^{18}\text{F}]\mathbf{1}$. Starting with 165 GBq of $[^{18}\text{F}]$ fluoride, the reagent $[^{18}\text{F}]\mathbf{1}$ was isolated in $7.5 \pm 1.7\%$ RCY (decay-corrected at the SOS) with a molar activity of $59 \pm 4 \text{ GBq}\cdot\mu\text{mol}^{-1}$ [decay-corrected at the end of the bombardment (EOB)], after semi-preparative HPLC purification and reformulation on a SepPak® C18 short cartridge (Scheme 2A). The subsequent flow photoredox ^{18}F -difluoromethylation procedure was performed in a photochemistry reactor consisting of a three-dimensional (3D)-printed with poly(ethylene terephthalate) recovered with a transparent polycarbonate (Lexan) plate and the reaction mixture was irradiated with a 32 W blue LED lamp. The replacement of *fac*- $\text{Ir}^{\text{III}}(\text{ppy})_3$ by the organic photocatalyst 1,2,3,5-tetrakis(carbazol-9-yl)-4,6-dicyanobenzene (4CzIPN) demonstrated to be beneficial for the efficiency of the ^{18}F -difluoromethylation reaction. The purification of the crude product by semipreparative HPLC afforded the $[^{18}\text{F}]$ acyclovir- CHF_2 $[^{18}\text{F}]\mathbf{5c}$ in $25 \pm 5\%$ RCY. Overall, the fully automated three-step radiosynthesis of $[^{18}\text{F}]\mathbf{5c}$ was achieved in $1.4 \pm 0.1\%$ RCY (Scheme 2B). This automated protocol can be implemented for the ^{18}F -difluoromethylation of a wide range of *N*-heteroaromatics typically found in medicinal chemistry.



Scheme 2. Fully automated photoredox ^{18}F -difluoromethylation of acyclovir (**4c**) in an AllInOne synthesizer, under continuous-flow conditions. ^(a)RCY of the isolated products after cartridge purification. ^(b)RCY after HPLC purification. ^(c)Molar activity decay-corrected at the end of bombardment (EOB).

This fully automated ^{18}F -difluoromethylation protocol was further applied to the radiosynthesis of a synaptic vesicle glycoprotein 2A (SV2A) PET tracer. SV2A is the molecular target of the antiepileptic drugs levetiracetam (**6**, Figure 1) [4] and brivaracetam (**7**, Figure 1) [5]. SV2A is widely expressed in the brain and the potential of the potential of SV2A PET tracers such as the ^{11}C UCB-J as biomarkers of synaptic density has been studied in various neurotransmission-related diseases. Despite the favorable pharmacodynamic and pharmacokinetic profiles of UCB-J [6] and the great potential of ^{11}C UCB-J to image the SV2A protein [7-9], the short half-life of carbon-11 (^{11}C , $t_{1/2} = 20.3$ min) may restrict the transportation of the radiotracer over considerable distances and limit its broad applicability as an imaging biomarker. The University of Liège in collaboration with UCB reported the synthesis and evaluation of the first SV2A radiotracer labeled with ^{18}F (^{18}F UCB-H, Figure 1) [10-13]. The half-life of the radionuclide ^{18}F ensures that the radiopharmaceutical can be used in nuclear imaging facilities located apart from its production site. However, the replacement of the ^{11}C -methyl (^{11}C CH $_3$) group by the ^{18}F substituent on the pyridine ring slightly reduced the affinity for SV2A.

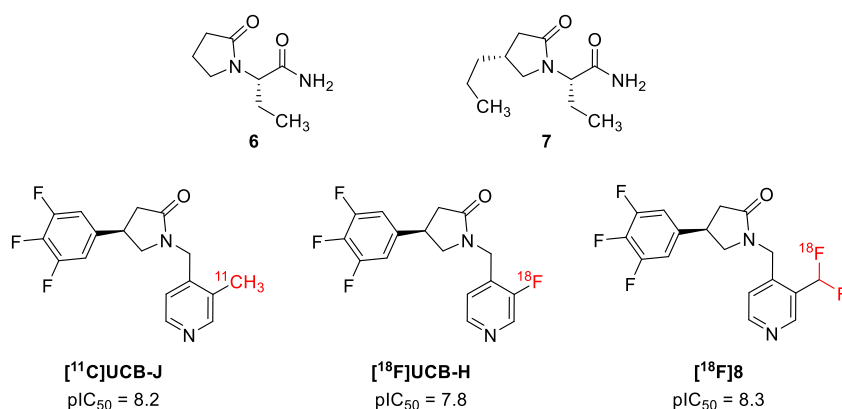
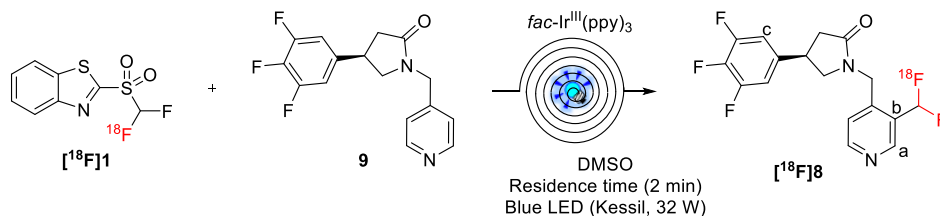


Figure 1. Chemical structures of the levetiracetam (**6**), the brivaracetam (**7**), and the SV2A PET tracers ^{11}C UCB-J, ^{18}F UCB-H, and ^{18}F **8**.

Considering the ^{18}F -difluoromethylation methodology automated on AllInOne module, we intended to prepare a new SV2A PET tracer labeled with a ^{18}F CHF $_2$ group (^{18}F **8**, Figure 1) and to study its potential as a imaging biomarker of SV2A protein. We hypothesized that the introduction of a ^{18}F CHF $_2$ moiety in the pyridine ring would offer a suitable balance between the half-life of ^{18}F and the binding affinity for SV2A. The SV2A PET tracer ^{18}F **8** was synthesized by late-stage insertion of ^{18}F CHF $_2$ moieties in the precursor **9** (Scheme 3). *In vitro* and *in vivo* experiments with SV2A tracer ^{18}F **8** are currently ongoing on University of Liège.



Scheme 3. Photoredox ^{18}F -difluoromethylation of the precursor **9** with the reagent ^{18}F **1**, under continuous-flow conditions.

The principal limitation of the reported ^{18}F -difluoromethylation methodologies resided mainly on the low RCY of two-step radiosynthesis of the reagent ^{18}F **1**. This can be explained by the low reactivity of the brominated precursor **3** toward the ^{18}F -fluorination. The replacement of the bromine substituent to better leaving groups, such as iodine (-I), tosyl (-OTs), or triflyl (-OTf) groups, would afford a set of precursors unsuitable for ^{18}F -labeling, owing to their chemical instability. To address this issue, we synthesized a series of structurally-related ^{18}F [difluoromethyl heteroaryl-sulfones as potential ^{18}F -difluoromethylating reagents in order to understand the effect of certain molecular modifications in the reactivity of the brominated precursors toward ^{18}F -labeling [14]. We found that the introduction of electron-donating groups (EDG) or electron-withdrawing groups (EWG) on the benzothiazolyl ring of the precursors, or the alteration of the original benzothiazolyl ring to other heteroaryl rings did not induce a significant effect on the reactivity of the bromine atom as a leaving group. Employing the same two-step methodology, the HPLC-purified difluoromethyl heteroaryl-sulfones ^{18}F **10**, ^{18}F **11**, and ^{18}F **12** were obtained in $2.9 \pm 0.1\%$, $5.7 \pm 0.5\%$, and $8.0 \pm 0.9\%$ RCYs, respectively. Starting from 125–150 GBq of ^{18}F fluoride, the fully automated radiosynthesis on a FASTlab™ synthesizer (GE Healthcare) allowed the isolated of the ^{18}F **10**, ^{18}F **11**, and ^{18}F **12** with molar activities ranging from 62 to 139 GBq· μmol^{-1} (Figure 2). Taking advantage of the reactivity of ^{18}F **1** as ^{18}F -difluoromethylating reagent, we intended to study of the influence of these structural modifications toward the ^{18}F -difluoromethylation of heteroarenes using the antiherpetic drug acyclovir as a model substrate. Our results showed that the introduction of molecular modifications in the structure of ^{18}F **1** influenced the amount of photocatalyst and the residence time needed to ensure a complete C–H ^{18}F -difluoromethylation process. The photocatalytic C–H ^{18}F -difluoromethylation reaction with the reagents ^{18}F **10**, ^{18}F **11**, and ^{18}F **12** was extended to other heteroarenes of biological relevance.

The great probability of $^{18}\text{F}/^{19}\text{F}$ isotopic exchange still constitutes a major limitation in the preparation of ^{18}F CHF₂-bearing compounds with high molar activity. In this work, the radiosynthesis of ^{18}F [difluoromethyl heteroaryl-sulfones with improved molar activity (54 to 139 GBq· μmol^{-1}) constitutes a great advantage as it may allow the preparation of ^{18}F CHF₂-containing heteroarenes as novel PET ligands with enhanced molar activities. However, the low RCYs of the syntheses of ^{18}F [difluoromethyl heteroaryl-sulfones still restricts the use of these reagents in the GMP production of clinically-relevant radiopharmaceuticals. Furthermore, the

plausible existence of multiple sites for the introduction of $[^{18}\text{F}]\text{CHF}_2$ groups in the (hetero)aryl rings of non-prefunctionalized substrates, as exemplified in the preparation of the SV2A PET tracer $[^{18}\text{F}]\mathbf{8}$, results in a significant decrease of the RCY of the isolated radiopharmaceutical. Alternatively, the employment of prefunctionalized heteroarenes amenable to the ^{18}F -difluoromethylation reaction would minimize the formation of undesired $[^{18}\text{F}]\text{CHF}_2$ -containing structural isomers and potentially contribute to the preparation of the PET radiopharmaceutical with an enhanced RCY.

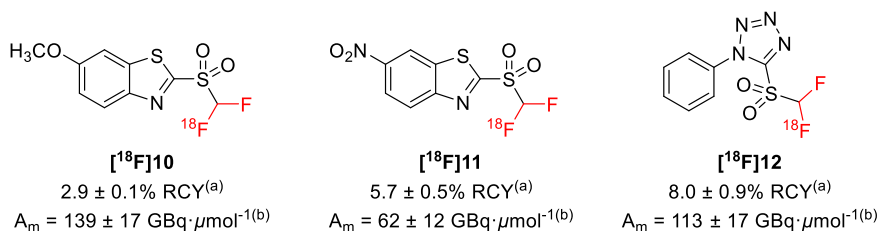


Figure 2. Radiochemical yields and molar activities of the reagents $[^{18}\text{F}]\mathbf{10}$, $[^{18}\text{F}]\mathbf{11}$, and $[^{18}\text{F}]\mathbf{12}$. ^(a)RCY of the isolated products after HPLC purification. ^(b)Molar activities at the EOS.

In non-radioactive chemistry, the reagent difluoromethyl benzothiazolyl-sulfone (2-BT SO_2CHF_2) has been extensively implemented in the difluoromethylation of substrates bearing C=C, C \equiv C, and C \equiv N bonds by visible light photoredox catalysis. The versatility of this reagent in organofluorine chemistry along with the demonstrated synthetic accessibility of $[^{18}\text{F}]\mathbf{1}$ may allow the future applicability of this ^{18}F -difluoromethylating reagent in the radiosynthesis of $[^{18}\text{F}]\text{CHF}_2$ -containing heterocycles of pharmaceutical relevance, including phenanthridines [15], benzoxazines [16], oxazolines [16], isoquinolinediones [17], coumarins [18], isoxazolines [19], and oxindoles [20]. Besides its efficiency in photoredox ^{18}F -difluoromethylation, Hu and co-workers reported for the first time the employment of the 2-BT SO_2CHF_2 in the metal-free insertion of difluoromethylthio (-SCF $_2\text{H}$) groups in indole derivatives [21]. Thus, the reagent $[^{18}\text{F}]\mathbf{1}$ can also be used as ^{18}F -difluoromethylthiolating reagent. Alternatively, the ^{18}F -labeling of the difluoromethyl pyridyl-sulfone (2-Py SO_2CHF_2) should be explored in the future owing to its involvement in numerous reactions in organofluorine chemistry, including the radical difluoromethylation of arylzincs [22] and *N*-arylacrylamides [23], and the Julia-Kocienski difluoroolefination of aldehydes and ketones [24-28].

Overall, we expect that the potential versatility of newly synthesized $[^{18}\text{F}]\text{difluoromethyl heteroaryl-sulfones}$ may contribute to the development of novel radioactive probes for PET imaging with improved molar activities.

References

- [1] Lemos, A.; Lemaire, C.; Luxen, A. Progress in Difluoroalkylation of Organic Substrates by Visible Light Photoredox Catalysis. *Adv. Synth. Catal.* **2019**, *361*, 1500-1537.

- [2] Trump, L.; Lemos, A.; Lallemand, B.; Pasau, P.; Mercier, J.; Lemaire, C.; Luxen, A.; Genicot, C. Late-stage ^{18}F -difluoromethyl labeling of *N*-heteroaromatics with high molar activity. *Angew. Chem. Int. Ed.* **2019**, *58*, 13149–13154.
- [3] Trump, L.; Lemos, A.; Jacq, J.; Pasau, P.; Lallemand, B.; Mercier, J.; Genicot, C.; Luxen, A.; Lemaire, C. Development of a general automated flow photoredox ^{18}F -difluoromethylation of *N*-heteroaromatics in an AllInOne synthesizer. *Org. Process Res. Dev.* **2020**, *24*, 734–744.
- [4] Klitgaard, H.; Verdru, P. Levetiracetam: the first SV2A ligand for the treatment of epilepsy. *Expert Opin. Drug Discov.* **2007**, *2*, 1537–1545.
- [5] Gillard, M.; Fuks, B.; Leclercq, K.; Matagne, A. Binding characteristics of brivaracetam, a selective, high affinity SV2A ligand in rat, mouse and human brain: Relationship to anti-convulsant properties. *Eur. J. Pharmacol.* **2011**, *664*, 36–44.
- [6] Mercier, J.; Archen, L.; Bollu, V.; Carré, V.; Evrard, Y.; Jnoff, E.; Kenda, B.; Lallemand, B.; Michel, P.; Montel, F.; Moureau, F.; Price, N.; Quesnel, Y.; Sauvage, X.; Valade, A.; Provins, L. Discovery of heterocyclic nonacetamide synaptic vesicle protein 2A (SV2A) ligands with single-digit nanomolar potency: Opening avenues towards the first SV2A positron emission tomography (PET) ligands. *ChemMedChem* **2014**, *9*, 693–698.
- [7] Nabulsi, N.B.; Mercier, J.; Holden, D.; Carré, S.; Najafzadeh, S.; Vandergeten, M.-C.; Lin, S.-F.; Deo, A.; Price, N.; Wood, M.; Lara-Jaime, T.; Montel, F.; Laruelle, M.; Carson, R.E.; Hannestad, J.; Huang, Y. Synthesis and preclinical evaluation of ^{11}C -UCB-J as a PET tracer for imaging the synaptic vesicle glycoprotein 2A in the brain. *J. Nucl. Med.* **2016**, *57*, 777–784.
- [8] Mercier, J.; Provins, L.; Valade, A. Discovery and development of SV2A PET tracers: Potential for imaging synaptic density and clinical applications. *Drug Discov. Today Technol.* **2017**, *25*, 45–52.
- [9] Finnema, S.J.; Nabulsi, N.B.; Mercier, J.; Lin, S.-F.; Chen, M.-K.; Matuskey, D.; Gallezot, J.-D.; Henry, S.; Hannestad, J.; Huang, Y.; Carson, R.E. Kinetic evaluation and test-retest reproducibility of ^{11}C UCB-J, a novel radioligand for positron emission tomography imaging of synaptic vesicle glycoprotein 2A in humans. *J. Cereb. Blood Flow Metab.* **2018**, *38*, 2041–2052.
- [10] Warnock, G.I.; Aerts, J.; Bahri, M.A.; Bretin, F.; Lemaire, C.; Giacomelli, F.; Mievis, F.; Mestdagh, N.; Buchanan, T.; Valade, A.; Mercier, J.; Wood, M.; Gillard, M.; Seret, A.; Luxen, A.; Salmon, E.; Plenevaux, A. Evaluation of ^{18}F -UCB-H as a novel PET tracer for synaptic vesicle protein 2A in the brain. *J. Nucl. Med.* **2014**, *55*, 1336–1341.
- [11] Warnier, C.; Lemaire, C.; Becker, G.; Zaragoza, G.; Giacomelli, F.; Aerts, J.; Otabashi, M.; Bahri, M.A.; Mercier, J.; Plenevaux, A.; Luxen, A. Enabling Efficient Positron Emission Tomography (PET) Imaging of Synaptic Vesicle Glycoprotein 2A (SV2A) with a Robust and One-Step Radiosynthesis of a Highly Potent ^{18}F -Labeled Ligand (^{18}F UCB-H). *J. Med. Chem.* **2016**, *59*, 8955–8966.
- [12] Becker, G.; Warnier, C.; Serrano, M.E.; Bahri, M.A.; Mercier, J.; Lemaire, C.; Salmon, E.; Luxen, A.; Plenevaux, A. Pharmacokinetic Characterization of ^{18}F UCB-H PET Radiopharmaceutical in the Rat Brain. *Mol. Pharm.* **2017**, *14*, 2719–2725.

- [13] Bahri, M.A.; Plevenaux, A.; Aerts, J.; Bastin, C.; Becker, G.; Mercier, J.; Valade, A.; Buchanan, T.; Mestdagh, N.; Ledoux, D.; Seret, A.; Luxen, A.; Salmon, E. Measuring brain synaptic vesicle protein 2A with positron emission tomography and [¹⁸F]UCB-H. *Alzheimer's Dement. Transl. Res. Clin. Interv.* **2017**, *3*, 481-486.
- [14] Lemos, A.L.P.; Trump, L.; Lallemand, B.; Pasau, P.; Mercier, J.; Lemaire, C.; Monbaliu, J.-C.; Genicot, C.; Luxen, A. Radical C-H ¹⁸F-Difluoromethylation of Heteroarenes with [¹⁸F]Difluoromethyl Heteroaryl-Sulfones by Visible Light Photoredox Catalysis. *Catalysts* **2020**, *10*, 275.
- [15] Rong, J.; Deng, L.; Tan, P.; Ni, C.; Gu, Y.; Hu, J. Radical fluoroalkylation of isocyanides with fluorinated sulfones by visible-light photoredox catalysis. *Angew. Chem. Int. Ed.* **2016**, *55*, 2743-2747.
- [16] Fu, W.; Han, X.; Zhu, M.; Xu, C.; Wang, Z.; Ji, B.; Hao, X.-Q.; Song, M.-P. Visible-light-mediated radical oxydifluoromethylation of olefinic amides for the synthesis of CF₂H-containing heterocycles. *Chem. Commun.* **2016**, *52*, 13413-13416.
- [17] Zou, G.; Wang, X. Visible-light induced di- and trifluoromethylation of *N*-benzamides with fluorinated sulfones for the synthesis of CF₂H/CF₃-containing isoquinolinediones. *Org. Biomol. Chem.* **2017**, *15*, 8748-8751.
- [18] Zhu, M.; Fu, W.; Wang, Z.; Xu, C.; Ji, B. Visible-light-mediated direct difluoromethylation of alkynoates: Synthesis of 3-difluoromethylated coumarins. *Org. Biomol. Chem.* **2017**, *15*, 9057-9060.
- [19] Zhu, M.; Fu, W.; Guo, W.; Tian, Y.; Wang, Z.; Xu, C.; Ji, B. Visible-light-induced radical di- and trifluoromethylation of β, γ-unsaturated oximes: Synthesis of di- and trifluoromethylated isoxazolines. *Eur. J. Org. Chem.* **2019**, *2019*, 1614-1619.
- [20] Zhu, M.; You, Q.; Li, R. Synthesis of CF₂H-containing oxindoles *via* photoredox-catalyzed radical difluoromethylation and cyclization of *N*-arylacrylamides. *J. Fluorine Chem.* **2019**, DOI: 10.1016/j.jfluchem.2019.109391.
- [21] Wei, J.; Bao, K.; Wang, Y.; Sheng, R.; Hu, J. Novel usage of 2-BT₂SO₂CF₂H for metal-free electrophilic difluoromethylthiolation of indoles. *Org. Biomol. Chem.* **2020**, *18*, 4556-4559.
- [22] Miao, W.J.; Zhao, Y.C.; Ni, C.F.; Gao, B.; Zhang, W.; Hu, J.B. Iron-Catalyzed Difluoromethylation of Arylzincs with Difluoromethyl 2-Pyridyl Sulfone. *J. Am. Chem. Soc.* **2018**, *140*, 880-883.
- [23] Sun, H.; Jiang, Y.; Yang, Y.-S.; Li, Y.-Y.; Li, L.; Wang, W.-X.; Feng, T.; Li, Z.-H.; Liu, J.-K. Synthesis of difluoromethylated 2-oxindoles and quinoline-2,4-dione *via* visible light-induced tandem radical cyclization of *N*-arylacrylamides. *Org. Biomol. Chem.* **2019**, *17*, 6629-6638.
- [24] Zhao, Y.C.; Huang, W.Z.; Zhu, L.G.; Hu, J.B. Difluoromethyl 2-Pyridyl Sulfone: A New *gem*-Difluoroolefination Reagent for Aldehydes and Ketones. *Org. Lett.* **2010**, *12*, 1444-1447.
- [25] Habib, S.; Gueyrard, D. Modified Julia Olefination on Sugar-Derived Lactones: Synthesis of Difluoro-*exo*-glycals. *Eur. J. Org. Chem.* **2015**, *2015*, 871-875.
- [26] Liu, X.; Yin, Q.; Yin, J.; Chen, G.H.; Wang, X.; You, Q.D.; Chen, Y.L.; Xiong, B.; Shen, J.K. Highly Stereoselective Nucleophilic Addition of Difluoromethyl-2-pyridyl

Sulfone to Sugar Lactones and Efficient Synthesis of Fluorinated 2-Ketoses. *Eur. J. Org. Chem.* **2014**, 2014, 6150-6154.

[27] Moschitto, M.J.; Silverman, R.B. Synthesis of (S)-3-Amino-4-(difluoromethylenyl)-cyclopent-1-ene-1-carboxylic Acid (OV329), a Potent Inactivator of γ -Aminobutyric Acid Aminotransferase. *Org. Lett.* **2018**, 20, 4589-4592.

[28] Gao, B.; Zhao, Y.C.; Hu, M.Y.; Ni, C.F.; Hu, J.B. *gem*-Difluoroolefination of Diaryl Ketones and Enolizable Aldehydes with Difluoromethyl 2-Pyridyl Sulfone: New Insights into the Julia–Kocienski Reaction. *Chem. Eur. J.* **2014**, 20, 7803-7810.

LIST OF ABBREVIATIONS

[¹⁸ F]Py-9HF	[¹⁸ F]Pyridinium poly(hydrogen fluoride)
3D	Three-dimensional
ADME	Absorption, distribution, metabolism, and excretion
Ag AchE	<i>Anopheles gambiae</i> acetylcholinesterase
AIO	AllInOne
BHT	2,6-Di- <i>tert</i> -butyl-4-methylphenol
CFL	Compact fluorescent lamp
COC	Cyclic olefin copolymer
COX-2	Cyclooxygenase-2
Cp ₂ Fe	Ferrocene
CRF ₁ R	Corticotropin-releasing factor-1 receptor
DABCO	1,4-Diazabicyclo[2.2.2]octane
DBH	1,3-Dibromo-5,5-dimethylhydantoin
DBU	1,8-Diazabicyclo[5.4.0]undec-7-ene
d.c.	Decay corrected
DCE	1,2-Dichloroethane
DCM	Dichloromethane
DFT	Density functional theory
DIPEA	<i>N,N</i> -Diisopropylethylamine
DMA	Dimethylacetamide
DMF	Dimethylformamide
DMPO	5,5-Dimethyl-1-pyrroline- <i>N</i> -oxide
DMSO	Dimethyl sulfoxide
EOB	End of the bombardment
EOS	End of the synthesis
ESI	Electrospray ionization
ESR	Electron spin resonance
EtOAc	Ethyl acetate
FDA	Food and Drug Administration
GM	Geiger-Muller
HCV NS3	Hepatitis C virus nonstructural protein 3
HPLC	High performance liquid chromatography
HRMS	High resolution mass spectrometry
KIE	Kinetic isotope effect
KSP	Kinesin spindle protein
LED	Light-emitting diode
LFP	Laser flash photolysis
<i>m</i> CPBA	<i>meta</i> -Chloroperoxybenzoic acid
MeCN	Acetonitrile
m.p.	Melting point
n.c.a.	No carrier added

NMP	<i>N</i> -Methyl-2-pyrrolidone
NMR	Nuclear magnetic resonance
OQC	Oxidative quenching cycle
QMA	Quaternary methyl ammonium
PC	Photocatalyst
PDA	Photodiode array
PEG 600	Polyethylene glycol 600
PET	Positron emission tomography
PXX	<i>Peri</i> -xanthenoxanthene
RB	Rose Bengal
RCC	Radiochemical conversion
RCP	Radiochemical purity
RCY	Radiochemical yield
Rh-6G	Rhodamine-6G
RQC	Reductive quenching cycle
SCE	Saturated calomel electrode
SET	Single-electron transfer
SOS	Start of the synthesis
SPE	Solid-phase extraction
SV2A	Synaptic vesicle glycoprotein 2A
TEA	Triethylamine
TEAB	Tetraethylammonium bicarbonate
TEAF	Tetraethylammonium fluoride
TEMPO	2,2,6,6-Tetramethyl-1-piperidinyloxy
TFA	Trifluoroacetic acid
THF	Tetrahydrofuran
TLC	Thin layer chromatography
TMEDA	Tetramethylethylenediamine
TMS	Trimethylsilane
(TMS) ₃ SiH	<i>Tris</i> (trimethylsilyl)silane
TRPV1	Transient receptor potential cation channel subfamily V member 1
UPLC	Ultra performance liquid chromatography
UV	Ultraviolet

SCIENTIFIC ACTIVITY

Publications in peer-reviewed journals

Lemos, A.; Trump, L.; Lallemand, B.; Pasau, P.; Mercier, J.; Lemaire, C.; Monbaliu, J.C.; Genicot, C.; Luxen, A. Radical C-H ¹⁸F-difluoromethylation of heteroarenes with [¹⁸F]difluoromethyl heteroaryl-sulfones by visible light photoredox catalysis. *Catalysts* **2020**, 10(3), 275.

Trump, L.; **Lemos, A.;** Jacq, J.; Lallemand, B.; Pasau, P.; Mercier, J.; Lemaire, C.; Genicot, C.; Luxen, A. Development of a general automated flow photoredox ¹⁸F-difluoromethylation of N-heteroaromatics in an AllInOne synthesizer. *Org. Process Res. Dev.* **2020**, 24(5), 734-744.

Trump, L.; **Lemos, A.;** Lallemand, B.; Pasau, P.; Mercier, J.; Lemaire, C.; Luxen, A.; Genicot, C. Late stage ¹⁸F-difluoromethyl labeling of N-heteroaromatics with high molar activity for PET imaging. *Angew. Chem. Int. Ed.* **2019**, 58(37), 13149-13154.

Lemos, A.; Lemaire, C.; Luxen, A. Progress in difluoroalkylation of organic substrates by visible light photoredox catalysis. *Adv. Synth. Catal.* **2019**, 361(7), 1500-1537.

Poster communications in scientific conferences

Lemos, A.; Trump, L.; Lallemand, B.; Pasau, P.; Mercier, J.; Genicot, C.; Lemaire, C.; Luxen, A. *Radiosynthesis of potential reagents for late-stage ¹⁸F-difluoromethylation of organic substrates.* 24th Workshop of the IIS CED, Bad Soden, Germany, September 19-20, **2019**.

Lemos, A.; Trump, L.; Lallemand, B.; Pasau, P.; Mercier, J.; Genicot, C.; Lemaire, C.; Luxen, A. *Automated radiosynthesis of 2-[¹⁸F]BTSO₂CF₂H in a GE FASTlab synthesizer.* 24th International Symposium on Radiopharmaceutical Sciences, Beijing, China, May 26-31, **2019**.

Honours and awards

The article entitled "Progress in difluoroalkylation of organic substrates by visible light photoredox catalysis" was recognized as one of the most read in *Advanced Synthesis & Catalysis* journal.

